Dissecting cell division in the human pathogen *Staphylococcus aureus*

By

Katarzyna Wacnik, BSc MSc
(Jagiellonian University)

A thesis submitted for the degree of Doctor of Philosophy
April 2016

Department of Molecular Biology and Biotechnology, University of Sheffield, Firth Court, Western Bank, Sheffield, S10 2TN

Summary

Bacterial cell division is a fundamental process mediated by a large collection of proteins, collectively called the divisome. The divisome is responsible for the appropriate synthesis of new cell wall peptidoglycan to produce the septum, allowing the production of two new daughter cells. Although divisome components have been identified, their precise roles are not well understood. Many cell division proteins interact and coordination of information from the cytoplasm, through the membrane, to the peptidoglycan biosynthesis machinery is required. FtsZ is a key cytoplasmic component, which initiates septum formation resulting in new peptidoglycan synthesis via penicillin binding proteins (PBPs).

In *Staphylococcus aureus*, cell division components, including EzrA, have been identified by a bacterial two-hybrid analysis. EzrA, a membrane-associated protein, interacts with both cytoplasmic proteins and those with periplasmic domains. It is therefore proposed to act as an interface between FtsZ in the cytoplasm and PBPs in the membrane forming a scaffold for other cell division components.

In this study, a combination of protein labelling and super-resolution microscopy approaches have been used to study the architecture of the cell division process in *S. aureus*. Conventional wide-field fluorescence microscopy shows EzrA and FtsZ as uniform rings at the division site. Super-resolution fluorescence microscopy of a strain, in which the only copy of EzrA was tagged with a fluorophore, revealed that EzrA does not form a homogenous ring but it is rather a collection of 'patches' distributed at the division site. FtsZ precedes EzrA and also forms heterogeneous structures around the midcell. Unsuccessful attempts were made to investigate the localisation of the essential PBP2 at molecular level using fluorescent proteins or fluorescent derivatives of β-lactams. A model of septum formation in *S. aureus,* in which a decreasing concentration gradient of cell division components wraps around the septum and forms a framework for peptidoglycan synthesis, has been developed.

Acknowledgements

Firstly, I would like to thank my supervisor Prof Simon Foster for giving me the opportunity to carry out my PhD, and for all his guidance and support throughout the project.

I am indebted to Dr Bob Turner and Dr Christa Walther for their contribution to the super-resolution microscopy data acquisition and analysis. I want to thank Dr Stéphane Mesnage for all his life/science advice. I would like to thank many past and present members of the F18 and F25 labs, particularly Beatriz Gonzalez and Joe Kirk who have truly been my friends and companions during my studies.

I would like to thank my family and friends for their continued support, encouragement, understanding and patience.

Finally, I would like to express particular thanks to Bartek for being there no matter what.

Abbreviations

°C	Degree Celsius
~	Approximately
2D	Two dimensional
3D	Three dimensional
a.u.	Arbitrary units
ADA	Azido-D-alanine
ADP	Adenosine diphosphate
AF647	Alexa Fluor 647
Amp	Ampicillin
AP	Alkaline phosphatase
APA	(+)-6-aminopenicillanic acid
APS	Ammonium persulphate
ATP	Adenosine triphosphate
ATPase	Adenosine triphosphate hydrase
attB	Bacterial attachment site
attP	Phage attachment site
A_x	Absorbance at indicated wavelength x (nm)
BCIP	5-bromo-5-chloro-3-indolyl phosphate
BHI	Brain heart infusion
BODIPY-FL	Boron-dipyrromethene
bp	Base pair
BSA	Bovine serum albumin
CFP	Cyan fluorescent protein
CFU	Colony forming units
CHIPS	Chemotaxis inhibitory protein of *S. aureus*
Cm	Chloramphenicol
ConA	Concanavalin A
D	Diameter
D-Ala	D-alanine
D-Glu	D-glutamic acid
D-Ser	D-serine
DAPI	4',6-diamidino-2-phenylindole
dcw	Cell division and cell wall biosynthesis gene cluster
dH_2O	Distilled water
DIBO	Dibenzocyclooctyne
DIG	Digoxigenin
DMSO	Dimethyl sulphoxide
DNA	Deoxyribonucleic acid
DNase	Deoxyribonuclease
dNTP	Deoxyribonucleoside-5'-triphosphate
DTT	Dithiothreitol
ECM	Electron cryotomography
EDTA	Ethylenediamine tetra-acetic acid
EM	Electron multiplying
Ery	Erythromycin
eYFP	Enhanced yellow fluorescent protein
FITC	Fluorescein isothiocyanate
FRAP	Fluorescence recovery after photobleaching
FRET	Förster resonance energy transfer

FWHM	Full-width half maxima
g	Gram
GDP	Guanosine diphosphate
GFP	Green fluorescent protein
Glc*N*Ac	*N*-acetyl glucosamine
GSH	Glutathione
GTP	Guanosine triphosphate
GTPase	Guanosine triphosphate hydrolase
h	Hour
HADA	Hydroxycoumarin 3-amino-D-alanine
HMW	High molecular weight
HPLC	High performance liquid chromatography
HRP	Horseradish peroxidase
IDP	Intrinsically disordered peptide
IgG	Immunoglobulin G
IPTG	Isopropyl beta-D-1-thiogalactopyranoside
Kan	Kanamycin
kb	Kilobase pair
kDa	Kilodalton
KOPS	FtsK orienting polar sequences
kV	Kilovolt
l	Litre
L-Ala	L-alanine
L-Lys	L-lysine
LB	Lysogeny broth
Lin	Lincomycin
LMW	Low molecular weight
M	Molar
Mbp	Megabase
MCS	Multiple cloning site
mEos2	Monomeric Eos2 fluorescent protein
meYFP	Monomeric enhanced yellow fluorescent protein
mg	Milligram
MIC	Minimum inhibitory concentration
min	Minute
ml	Millilitre
mm	Millimetre
mM	Millimolar
MRSA	Methicillin-resistant *Staphylococcus aureus*
MSCRAMMs	Microbial surface components recognising adhesive matrix molecules
Mur*N*Ac	*N*-acetyl muramic acid
mW	Milliwatt
NA	Numerical aperture
NAD	Oxidised nicotinamide adenine dinucleotide
NADH	Reduced nicotinamide adenine dinucleotide
NBS	Noc-binding sequence
NBT	Nitroblue tetrazolium
ng	Nanogram
nm	Nanometre
nM	Nanomolar
NO	Nucleoid occlusion
nt	Nucleotide
OD_{600}	Optical density measure at 600 nm

ori	Origin of replication
PALM	Photoactivated localisation microscopy
PAmCherry1	Photoactivatable monomeric mCherry
PBP	Penicillin binding protein
PBS	Phosphate buffered saline
PCR	Polymerase chain reaction
PDH	Pyruvate dehydrogenase complex
Pen-AF647	APA, Alexa Fluor 647 conjugate
PenG	Penicillin G
PFU	Plague forming unit
POTRA	Polypeptide transport-associated domain
Ppcn	Penicillinase promoter
PSF	Point spread function
PSmOrange	Photoswitchable monomeric Orange protein
Pspac	Spac promoter
Pxyl	Xylose promoter
RBS	Ribosome binding site
rcf	Relative Centrifugal Force
rpm	Revolutions per min
s	Second
SBS	SlmA-DNA binding sequence
SCIN	Staphylococcal complement inhibitor
sdH_2O	Sterile distilled water
SDS	Sodium dodecyl sulphate
SDS-PAGE	Sodium dodecyl sulphate polyacrylamide gel electrophoresis
SEDS	Shape, elongation, division and sporulation family
SERAMs	Secretable expanded repertoire adhesive molecules
SIM	Structured illumination microscopy
SiR	Silicon-rhodamine
Spec	Spectinomycin
SSS	Scalded skin syndrome
STED	Stimulated emission-depletion
STORM	Stochastic optical reconstruction microscopy
Str	Streptomycin
TADA	Tetramethylrhodamine 3-amino-D-alanine
TAE	Tris-acetate EDTA
Taq	Thermostable DNA polymerase derived from *Thermus aquaticus*
TBSI	Tris buffered saline containing a protease inhibitor cocktail
TBST	Tris buffered saline tween
TCA	Citric acid
tdEos2	Tandem dimer Eos2 fluorescent protein
TE	Tris-EDTA (buffer)
TEMED	N,N,N'N'-tetramethyl-ethylenediamine
Tet	Tetracycline
TGase	Transglycosylase
TMDH	Transposon-mediated differential Hybridisation
Tn	Transposon
TPase	Transpeptidase
Tris	Tris (hydroxymethyl) aminomethane
TSS	Toxic shock syndrome
TSST-1	Toxic shock syndrome toxin-1
U	Units (of enzyme activity)
UDP	Uridine diphosphate

UV	Ultra violet
V	Volts
v/v	Volume for volume
Van-AF647	Vancomycin, Alexa Fluor 647 conjugate
VISA	Vancomycin-intermediate *S. aureus*
VRSA	Vancomycin-resistant *S. aureus*
w/v	Weight for volume
WTA	Wall teichoic acid
x	Times
X-Gal	5-bromo-4-chloro-3-indolyl-β-D-galactoside
YFP	Yellow fluorescent protein
µF	Microfarad
µg	Microgram
µl	Microlitre
µm	Micrometre
µM	Micromolar
Φ	Phage
Ω	Ohms

Table of contents

List of figures

List of tables

CHAPTER 1

Introduction

1.1 Bacterial cell division

Cell division is a fundamental process by which a parent cell divides into two daughter cells. In prokaryotes, binary fission is the most common type of cell division. Binary fission consists of two concurrent events, replication and segregation of DNA and cell growth. As the cell increases in size, DNA replication occurs. This is followed by chromosome segregation and septum formation. Finally, the nascent daughter cells split (Errington et al., 2003).

1.2 Regulation of cell division

Bacteria exhibit little variation in their growth rate and cell size under steady state conditions (Chien et al., 2012a). The bacterial cell cycle does not have distinct stages, cell growth, chromosome duplication and segregation often occur simultaneously. In contrast to eukaryotes, prokaryotic cells lack an intracellular organisation in the form of organelles and a complex net of cytoskeleton (Chien et al., 2012a). Therefore binary fission seems to be a simple process that requires little orchestration (Chien et al., 2012a). However, to grow and stay alive bacterial cells have to coordinate the timing of division with cell growth so that the daughter cells are functional replicas of the mother cell with the whole set of genetic material. This indicates that there must exist some mechanisms that regulate temporally and spatially cell division.

1.2.1 Temporal regulation of cell division

It is well known that bacterial cells adjust their sizes and speed of the cell cycle to nutrient availability (Kjeldgaard et al., 1958; Schaechter et al., 1958; Donachie and Begg, 1989). While *Escherichia coli* and *Bacillus subtilis* have to reach a critical ratio of DNA content to the cell length, suggesting that cells are able to sense their size, *Enterococcus hirae* divides at a constant cell volume regardless of chromosome

replication and cell growth rate (Donachie, 1968; Gibson et al., 1983; Donachie and Begg, 1989; Sharpe et al., 1998; Robert et al., 2014). However, no bacterial component(s) sensing cell size to control the cell cycle have been detected so far. Growth and size of *B. subtilis* was shown to depend on UDP-glucose availability. In the absence of PgcA and GtaB, proteins synthesising UDP-glucose, *B. subtilis* forms cells 30% reduced in length (Weart et al., 2007). UgtP is a glucosyltransferase enzyme that utilises UDP-glucose in glucolipid synthesis. Additionally it interacts with FtsZ, the key component of the division machinery, in a UDP-glucose dependent manner. In nutrient rich conditions, which is concomitant with high levels of UDP-glucose, UgtP is concentrated at midcell where it interacts with FtsZ. This inhibits FtsZ oligomerisation and thus allowing cells to increase their size (Weart et al., 2007; Chien et al., 2012b). In nutrient poor conditions UgtP interacts with itself and forms discrete foci distributed along the cell. The foci do not interfere with FtsZ, therefore cell division occurs without delay, however the average cell size is reduced (Weart et al., 2007; Chien et al., 2012b). In *E. coli,* a glucosyltransferase OpgH, a functional homologue of *B. subtilis* UgtP was identified (Hill et al., 2013). OpgH does not share any structural similarity with, and has a different activity to UgtP. It is proposed to function as the UDP-glucose metabolic sensor that coordinates cell size with growth in *E. coli* but through a different mechanism in *B. subtilis* (Hill et al., 2013).

Pyruvate, a final product of glycolysis is another example of a metabolite that controls the cell cycle. *B. subtilis* mutants lacking *pyk*, the gene encoding pyruvate kinase tend to form polar or more than one division septum. However addition of exogenous pyruvate reduces the effect of a *pyk* deletion (Monahan et al., 2014a). Pyruvate is either converted into acetyl-CoA by the pyruvate dehydrogenase complex (PDH), which is then used in the citric acid (TCA) cycle, or it is utilised in fermentation. The E1α subunit of pyruvate dehydrogenase (PDH E1α) was suggested to positively regulate localisation of FtsZ (Monahan et al., 2014a). Distribution of PDH E1α was shown to depend on pyruvate levels. In nutrient rich conditions PDH E1α colocalises with nucleoid, while in the *pyk* mutant it goes to the cell poles. Additionally in the absence of both PDH E1α and EzrA, which is a negative regulator of FtsZ, FtsZ presents abnormal short helix-like structures (Monahan et al., 2014a).

In *Caulobacter crescentus* two proteins, GdhZ and KidO were identified to directly and negatively regulate cell division (Radhakrishnan et al., 2010; Beaufay et al., 2015). GdhZ, is a NAD-dependent glutamate dehydrogenase that catalyses conversion of glutamate to α-ketoglutarate and links the nitrogen cycle with the TCA cycle, while KidO is a bifunctional NAD(H)-binding protein (Radhakrishnan et al., 2010; Beaufay et al., 2015). Both KidO and GdhZ colocalise with FtsZ, synergistically and directly promote FtsZ disassembly in a substrate-dependent manner (Radhakrishnan et al., 2010; Beaufay et al., 2015). Since GdhZ reduces NAD+ to NADH and KidO binds NADH it has been proposed that GdhZ may supply KidO with the coenzyme and KidO in return could stimulate activity of GdhZ (Beaufay et al., 2015). KidO was shown to disrupt lateral interactions of FtsZ protofilaments, which are subsequently depolymerised into monomers by FtsZ GTPase activity increased by GdhZ (Beaufay et al., 2015). Even though deletion of *gdhZ* results in a severe growth defect, the mutation can be complemented by addition of glucose or xylose. This indicates that in *C. crescentus* some other enzymes may be involved in cell division control depending on specific carbon source (Beaufay et al., 2015).

1.2.2 Spatial regulation of cell division

Not only timing but also selection of division site is crucial. Cell division starts with an assembly of FtsZ into a ring-like structure, called the Z-ring (Erickson, 1997; Adams and Errington, 2009). The Z-ring acts as a scaffold that recruits other components involved in the process. FtsZ is the first protein to localise to the division site and therefore its role is to initiate cell division and to mark the septal position (Adams and Errington, 2009). In rod-shaped bacteria such as *E. coli* and *B. subtilis* positioning of the Z-ring at midcell is highly precise with a deviation of ~1% (Trueba, 1982; Yu and Margolin, 1999; Migocki et al., 2002). In *E. coli* the estimated concentration of FtsZ is up to 10 μM, which is ten times higher than its critical concentration of ~1 μM required for polymerisation into protofilaments *in vitro* (Adams and Errington, 2009; Erickson et al., 2010). This indicates that bacteria had to develop mechanisms to control Z-ring assembly spatially and temporally. In this way a cell divides when it has reached a critical size and the division septum is formed in the midcell allowing for generation of equal and fully functional daughter cells (Margolin, 2005).

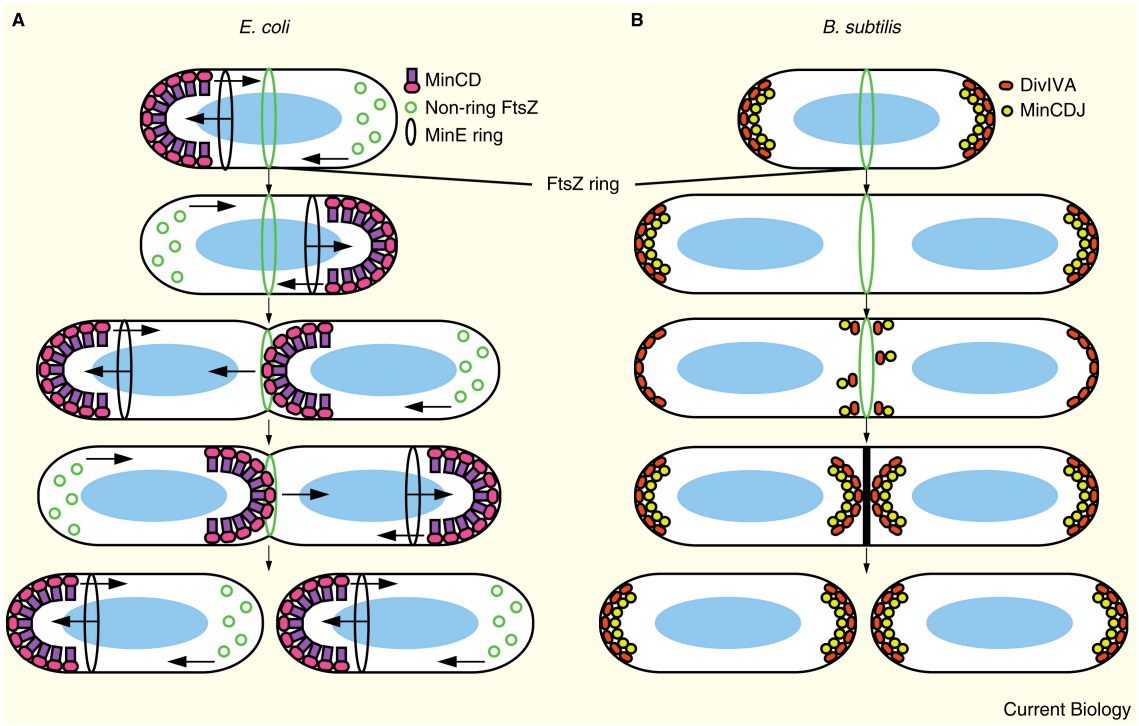

Figure 1.1. Control of division site selection by the Min system

A. In *E. coli*, MinE forms a ring-like structure that oscillates from one cell pole to the other one. When MinE moves toward the complex of MinC and MinD it recognises MinD dimers, stimulates release of MinC from the MinCD complex, which in turn activates the ATPase activity of MinD. MinD hydrolyses ATP to ADP, monomerises and leaves the membrane. Oscillation of MinE establishes a gradient of the MinC protein, with the maximal concentration at the cell poles. The lower concentration of MinC in the midcell allows for the FtsZ ring assembly. Reproduced from (Rowlett and Margolin, 2013).

B. In *B. subtilis,* DivIVA binds to the membrane at the cell poles. It recruits MinCD through MinJ, which acts as a bridging protein between DivIVA and MinCD. The concentration of MinC at the cell poles leaves the midcell free for FtsZ to assemble. Reproduced from (Rowlett and Margolin, 2013).

In rod-shaped organisms, *E. coli* and *B. subtilis* the Min system and nucleoid occlusion are the two major systems involved in the Z-ring positioning.

1.2.2.1 The Min system

The Min system prevents formation of the Z-ring at the cell poles. In *E. coli*, the Min system is composed of MinC, MinD and MinE proteins, while in *B. subtilis* it consists of MinC, MinD and DivIVA (Monahan et al., 2014b; Rowlett and Margolin, 2015a). In both *E. coli* and *B. subtilis* the MinC protein interacts directly with FtsZ destabilising and inhibiting its polymerisation (Hu et al., 1999; Dajkovic et al., 2008). MinC is a modular protein that has two independent domains. The N-terminal domain inhibits polymerisation of FtsZ into protofilaments, whereas the C-terminal domain prevents lateral interactions of FtsZ polymers and interacts with a membrane protein MinD (Hu and Lutkenhaus, 2000; Shiomi and Margolin, 2007; Dajkovic et al., 2008).

In *E. coli,* regulation of FtsZ placement is thought to occur through a gradient of the MinC protein that is established through an oscillation of the Min components from one cell pole to the other (Figure 1.1A) (Hu and Lutkenhaus, 1999; Rowlett and Margolin, 2015a). MinD is a member of the ParA family of ATPases and it binds the cell membrane via its C-terminal membrane targeting sequence and directly interacts with the C-terminus of MinC (de Boer et al., 1991; Hu and Lutkenhaus, 2000, 2003). In the presence of ATP MinD forms dimers and together with MinC forms copolymers that are bound to the membrane (Hu and Lutkenhaus, 2003; Ghosal et al., 2014; Conti et al., 2015). MinE is a small 88 amino-acid protein that has an N-terminal membrane targeting sequence and it forms a ring-like structure that oscillates from side to side (Raskin and de Boer, 1997; Hale et al., 2001; Hsieh et al., 2010; Park et al., 2011). MinE recognises the bound MinD dimer and binds it, which in turn leads to the release of MinC from the MinCD complex. Displacement of MinC triggers the ATPase activity of MinD, which monomerises and leaves the membrane (Raskin and de Boer, 1997; Hale et al., 2001; Hsieh et al., 2010; Park et al., 2011). ADP in MinD is then exchanged with ATP and MinC can be bound again to the membrane through MinD on the opposite side of the cell away from MinE (Hu et al., 2002; Huang et al., 2003; Park et al., 2011). Thus, the oscillation of MinC is driven by a competition with MinE for binding to MinD. This results in accumulation of MinC at the cell poles preventing FtsZ

assembly. The lower MinC concentration at midcell allows for the Z-ring formation (Hu et al., 1999; Hale et al., 2001; Lackner et al., 2003; Ma et al., 2004).

B. subtilis does not have a homologue of MinE and DivIVA acts as a topological factor of MinCD displacement (Lee and Price, 1993; Edwards and Errington, 1997). DivIVA is able to recognise cell curvature and thus to localise to both the cell poles and the cell septum (Edwards and Errington, 1997; Edwards et al., 2000; Lenarcic et al., 2009). After septation DivIVA remains at the native cell poles. DivIVA recruits MinD to the cell poles through another protein MinJ, which acts as a bridging component between DivIVA and MinD (Bramkamp et al., 2008; Patrick and Kearns, 2008). In turn, membrane bound MinD recruits MinC, which inhibits FtsZ (Figure 1.1B) (Bramkamp et al., 2008; Patrick and Kearns, 2008). In contrast to *E. coli*, MinCD do not oscillate in *B. subtilis* (Marston and Errington, 1999). However, fusing MinC with GFP revealed that the fusion relocalises dynamically from an old cell pole to the site of division, suggesting that the Min system not only inhibits FtsZ assembly at the cell poles but also prevents formation of more than one Z-ring at midcell (Gregory et al., 2008).

The Min system proteins are not essential in either *E. coli* or *B. subtilis*. In their absence or when they are not functional a number of cells forming polar septa or more than one septum increases and anucleate minicells are often generated (de Boer et al., 1989). Interestingly, in the absence of MinD overproduced MinC is able to inhibit cell division, which is manifested by formation of long filamentous cells (de Boer et al., 1992a).

1.2.2.2 Nucleoid occlusion

Nucleoid occlusion (NO) inhibits cell division in the vicinity of the chromosome by preventing FtsZ polymerisation into a ring over nucleoid (Figure 1.2). The process of NO is mediated by Noc and SlmA in *B. subtilis* and *E. coli*, respectively (Wu and Errington, 2004; Bernhardt and de Boer, 2005) Noc and SlmA do not have any similarity in a primary sequence and belong to different families of DNA-binding proteins. Noc is a member of the ParB family, whereas SlmA is of the TetR family, although the effect of NO absence is similar in *B. subtilis* and *E. coli* (Sievers et al., 2002; Bernhardt and de Boer, 2005). Neither Noc nor SlmA are essential for cell

division in *B. subtilis* and *E. coli*, respectively, and *noc* and *slmA* mutants form septa over unsegregated nucleoids, which causes bisection of the chromosome (Wu and Errington, 2004; Bernhardt and de Boer, 2005). By contrast, overproduction of Noc leads to cell enlargement and delay or complete inhibition in cell division, while SlmA overproduction blocks Z-ring formation and induces cell filamentation (Wu and Errington, 2004; Bernhardt and de Boer, 2005).

SlmA binds DNA by recognising a 12 bp palindromic sequence called the SlmA-DNA binding sequence (SBS) (Tonthat et al., 2011). There are from 24 to 50 possible SBSs clustered in specific regions on the chromosome in *E. coli* (Cho et al., 2011; Tonthat et al., 2011). SlmA interacts with FtsZ *in vitro* and therefore is proposed to act as an inhibitor of FtsZ polymerisation (Cho et al., 2011). DNA bound SlmA becomes activated and supports disassembly of FtsZ polymers by competing for its C-terminal conserved tail with other FtsZ interacting proteins, such as ZipA (Cho and Bernhardt, 2013; Du and Lutkenhaus, 2014). Interestingly, disassembly of the FtsZ protofilaments was shown to proceed without FtsZ GTPase activity (Cabré et al., 2015). Contrarily, by using transmission electron microscopy it was shown that SlmA did not disrupt assembly of FtsZ polymers, suggesting that SlmA impairs organisation of the FtsZ protofilaments into a higher organisation, the Z-ring (Tonthat et al., 2011, 2013).

Noc is a specific DNA binding protein and fluorescent microscopy imaging of YFP-Noc revealed that the protein localises to the nucleoid (Wu et al., 2009). It recognises a 14 bp palindromic sequence, called the Noc-binding sequence (NBS) and there are about 70 NBSs present on the *B. subtilis* chromosome (Wu et al., 2009). Overexpression of Noc was shown to delay cell division but how Noc effects FtsZ assembly is not well understood (Wu et al., 2009). Noc has an N-terminal amphipathic helix that allows for its membrane binding (Adams et al., 2015). The simultaneous binding of NBSs and the cell membrane are required for Noc full activity and cell division inhibition (Adams et al., 2015). Additionally, Noc is an abundant protein (4,500 to 7,500 molecules per cell) and therefore it has been proposed that its physical presence inhibits FtsZ assembly as it occupies the space between the nucleoid and cell membrane, leaving no room for FtsZ (Wu et al., 2009; Muntel et al., 2014; Adams et al., 2015).

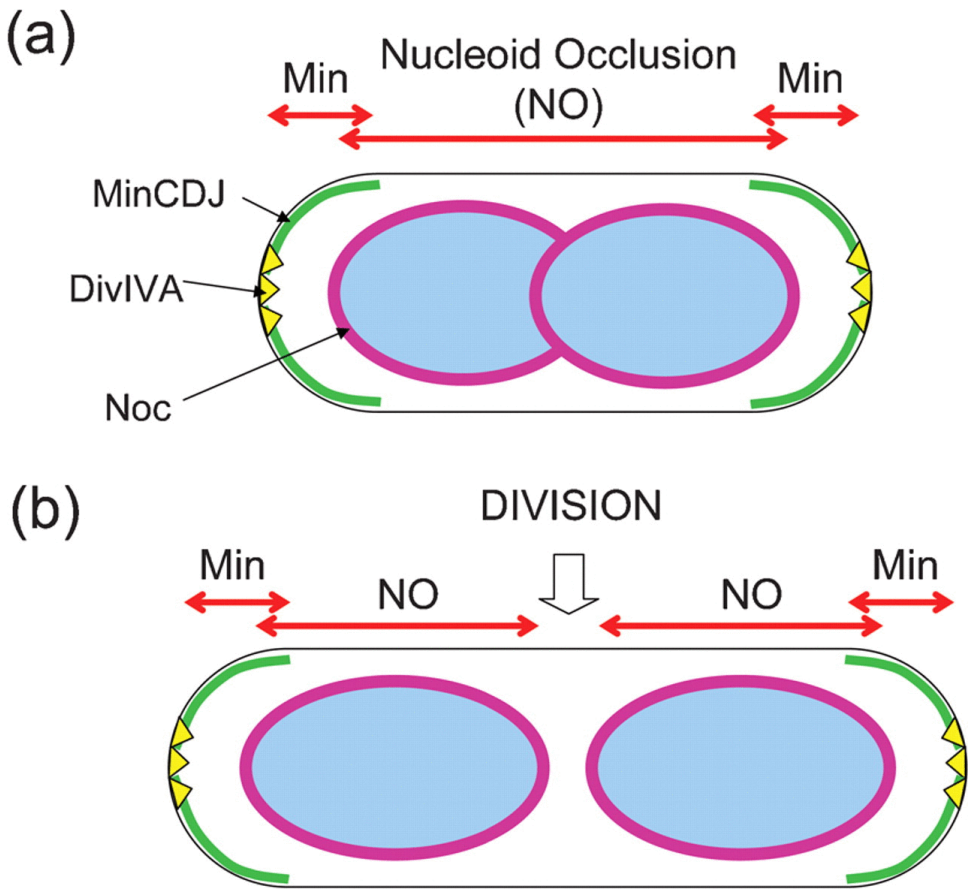

Figure 1.2. Regulation of Z-ring positioning by nucleoid occlusion combined with the Min system in *B. subtilis*

A. Nucleoid occlusion blocks formation of the Z-ring over unsegregated chromosomal DNA, while the Min system accumulates at the cell poles, protecting them from FtsZ assembly. Reproduced from (Errington, 2010).

B. After chromosome segregation the midcell becomes a nucleoid occlusion free zone, where FtsZ can assemble. Reproduced from (Errington, 2010).

1.2.2.3 Alternative mechanisms to the Min system and nucleoid occlusion

The Min system and nucleoid occlusion play an important role in spatial regulation of Z-ring placement. However there is more evidence that they are not the only regulators and other additional systems are present. In *E. coli* and *B. subtilis* depletion of either the Min system or SlmA/Noc does not affect cell viability when cells are grown in minimal medium, nevertheless division is not as efficient as in the wild type cells (Migocki et al., 2002; Wu and Errington, 2004; Bernhardt and de Boer, 2005). Although loss of both Min and NO proteins affects their cell division and viability, *B. subtilis* and *E. coli* are still able to locate the Z-ring at midcell with a higher precision than cells only devoid of the Min system and their growth is partially restored when *ftsZ* is overexpressed (Wu and Errington, 2004; Bernhardt and de Boer, 2005; Bailey et al., 2014). The low importance of the Min system and NO was further supported by using outgrowing spores of a *min noc B. subtilis* mutant, in which the majority of cells (87%) placed the Z-rings with a precision comparable to the wild type (Rodrigues and Harry, 2012). This implies that the role of the Min system and NO is not to pinpoint the midcell but to reduce the number of possible locations to the cell centre (Rodrigues and Harry, 2012). Moreover, not all bacteria have homologues of either the Min system or NO proteins. While *Staphylococcus aureus* encodes analogues of *noc* and *divIVA*, it does not have genes encoding MinC and MinD (Pinho and Errington, 2004; Veiga et al., 2011). *Streptococcus pneumoniae* and *C. crescentus* lack both regulatory systems, indicating that different bacterial species have developed alternatives to the Min system and NO (Nierman et al., 2001; Pinho et al., 2013).

1.2.2.3.1 PomZ

PomZ like MinD, belongs to the ParA ATPase family and is present in the δ-proteobacterium *Myxococcus xanthus* (Treuner-Lange et al., 2013). PomZ was shown to localise in the midcell independently of, and prior to FtsZ and to positively regulate formation of FtsZ rings (Figure 1.3A) (Treuner-Lange et al., 2013). However it is not known how PomZ stimulates FtsZ as these proteins do not interact *in vitro* (Treuner-Lange et al., 2013). Cells lacking PomZ form filamentous cells and minicells. Nevertheless its absence does not effect chromosome replication and segregation,

indicating that PomZ is required for efficient formation and septal placement of the Z-ring (Treuner-Lange et al., 2013).

1.2.2.3.2 SsgAB

Streptomyces coelicolor grows as hyphae and does not have both the Min system and NO. SsgA and SsgB are unique to Actinobacteria and positively regulate formation of the Z-rings (Traag and van Wezel, 2008; Willemse et al., 2011). When *S. coelicolor* starts to form spores, SsgA localises to sporulation septa (Willemse et al., 2011). It recruits a membrane associated protein, SsgB, which in turn recruits FtsZ and tethers it to the membrane (Figure 1.3B) (Willemse et al., 2011). In FtsZ depleted *S. coelicolor* SsgA and SsgB located to the septa, showing that their localisation is FtsZ independent (McCormick et al., 1994; Willemse et al., 2011). SsgB was shown to stimulate FtsZ polymerisation *in vitro* and therefore SsgAB are considered as activators of cell division in *S. coelicolor* (Willemse et al., 2011).

1.2.2.3.3 MipZ

As mentioned above *C. crescentus* has neither the Min system nor NO but encodes MipZ, a protein conserved among α-proteobacteria, which belongs to the same ParA family of ATPases as MinD (Thanbichler and Shapiro, 2006). In contrast to MinD, MipZ interacts with, and directly inhibits, FtsZ assembly by stimulating its GTPase activity (Thanbichler and Shapiro, 2006; Kiekebusch et al., 2012). MipZ forms a complex with ParB, a chromosome partitioning protein that binds the *parS* DNA motif, located close to the origin of replication (*oriC*) (Figure 1.3C) (Thanbichler and Shapiro, 2006). In a cell that has not started the chromosome replication MipZ locates to the cell pole where *oriC* is present, while FtsZ accumulates at the opposite cell pole (Figure 1.3C) (Thanbichler and Shapiro, 2006). Once the chromosome is replicated and is sorted to the opposing cell poles, MipZ follows *oriC* and thus creates a bipolar gradient, restricting localisation of FtsZ to midcell (Figure 1.3C) (Thanbichler and Shapiro, 2006).

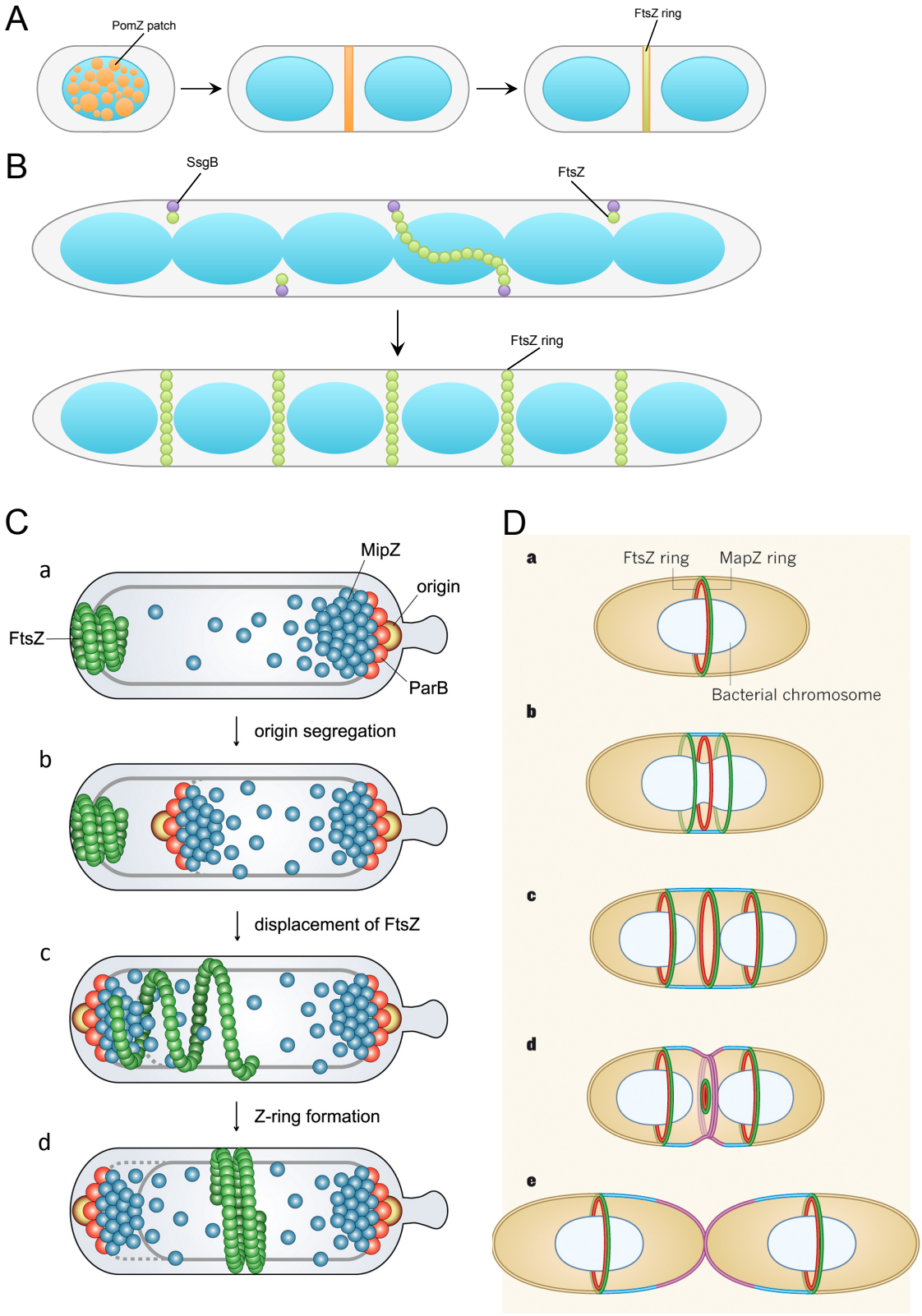

Figure 1.3. Alternative mechanisms of Z-ring positioning

A. In *M. xanthus*, PomZ (yellow) exhibits a patchy localisation pattern prior to division. When the cell starts to divide PomZ localises to the division site and recruits FtsZ (green). Adapted from (Monahan and Harry, 2013).

B. In sporulating *S. coelicolor*, SsgB (purple) localises to division sites via association with SsgA. SggAB recruits and tethers FtsZ (green) to the membrane and FtsZ polymerises into Z-rings. Adapted from (Rowlett and Margolin, 2015b)

C. In *C. crescentus*, MipZ (blue) is an inhibitor of FtsZ (green) assembly. It localises to the cell pole close to the chromosomal origin of replication (*oriC,* yellow) through an association with a DNA binding protein, ParB (red). Since MipZ follows *oriC*, a bipolar gradient is set up upon chromosome replication and segregation to the opposite sites, leaving the midcell as a region where FtsZ can assemble. Reproduced from (Thanbichler and Shapiro, 2006).

D. In *S. pneumoniae,* MapZ (green) localises and recruits FtsZ (red) to midcell. When FtsZ has formed the Z-ring, MapZ splits into two rings that are moved to the next division sites by growing peptidoglycan (blue and pink). Reproduced from (Harry, 2014).

1.2.2.3.4 MapZ/LocZ

A transmembrane protein called either MapZ or LocZ was recently identified in *S. pneumoniae* (Fleurie et al., 2014a; Holečková et al., 2015). MapZ/LocZ depletion leads to disrupted cell morphology, aberrant division septa and minicells, indicating its role in cell division regulation (Fleurie et al., 2014a; Holečková et al., 2015). Indeed MapZ/LocZ was shown to localise to the division site prior to FtsZ (Fleurie et al., 2014a; Holečková et al., 2015). Although cells are still viable and able to divide in its absence, implying non-essentiality of MapZ/LocZ, FtsZ localisation is altered, the Z-rings are tilted or shifted from the midcell (Fleurie et al., 2014a; Holečková et al., 2015). MapZ/LocZ interacts directly with FtsZ through the N-terminal cytoplasmic domain (Fleurie et al., 2014a). Although the N-terminal domain is not required for septal localisation of MapZ/LocZ, it is necessary for proper recruitment of FtsZ to the cell septum (Fleurie et al., 2014a). MapZ/LocZ was suggested to mark future division sites, once the FtsZ ring is established at midcell MapZ/LocZ splits into two rings that gradually move in opposite directions toward next division sites (Figure 1.3D) (Fleurie et al., 2014a; Holečková et al., 2015). Enterococci, lactococci and streptococci have homologues of MapZ/LocZ which do not show any sequence similarity to other proteins, indicating that MapZ/LocZ is an FtsZ positioning regulator unique to ovococci (Fleurie et al., 2014a; Holečková et al., 2015).

1.3 Divisome

Bacterial cell division is mediated by a large collection of proteins that localise to the division site. This complex machinery is called the divisome (Figure 1.4) (Adams and Errington, 2009). In many organisms components potentially involved in cell division have been identified, although their precise roles are not well understood (Adams and Errington, 2009). Most of the proteins are conserved and essential across bacterial species (FtsZ, FtsA), some of them are characteristic to only one group of organisms (ZipA in *E. coli*) and others importance depends on species (EzrA is essential in *S. pneumoniae* and *S. aureus* but not in *B. subtilis*) (Hale and de Boer, 1997; Levin et al., 1999; Thanassi et al., 2002; Adams and Errington, 2009; Steele et al., 2011). Also a number of crucial cell division components differs between bacterial species.

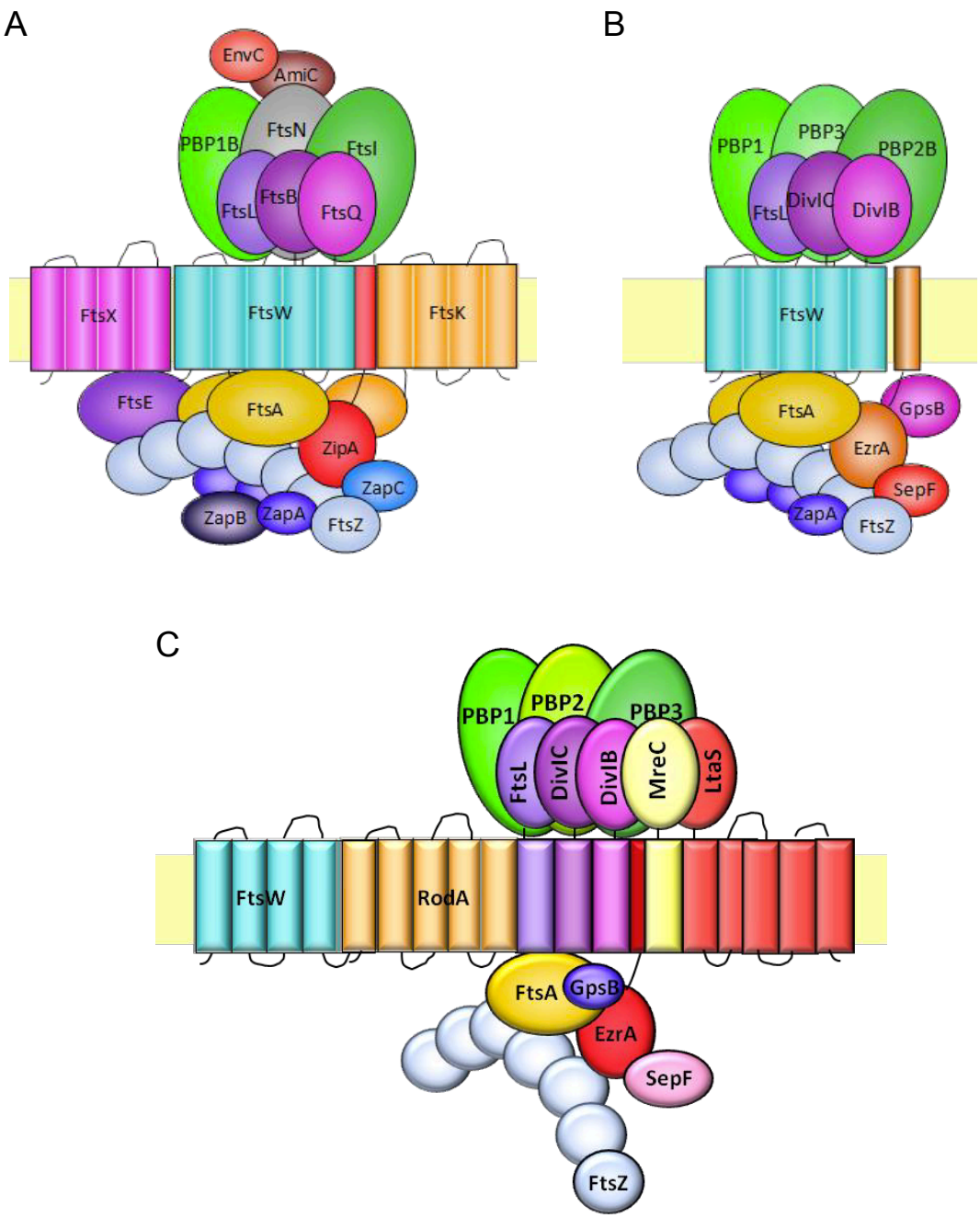

Figure 1.4. Cell division machineries in *Escherichia coli, Bacillus subtilis* and *Staphylococcus aureus* Schematic representation of divisome in *E. coli* (A), *B. subtilis* (B) and *S. aureus* (C). Reproduced from (Bottomley, 2011).

In *S. pneumoniae* six genes were identified as essential (Song et al., 2005), *B. subtilis* and *C. crescentus* have ten crucial genes (Kobayashi et al., 2003; Goley et al., 2011), while *S. aureus* and *E. coli* have at least 11 and 12 essential genes, respectively, associated with cell division (Figure 1.4) (Chaudhuri et al., 2009; Egan and Vollmer, 2013). This variety of cell division components and their divergent significance suggest that different organisms have modified and/or adopted cell division mechanisms to best fit their shapes, growth modes and lifestyles.

1.3.1 FtsZ

FtsZ is an essential and the most critical bacterial cell division protein (Adams and Errington, 2009). It is conserved in almost all bacteria and most Archaea (Erickson, 2007). FtsZ is also found in eukaryotic organelles such as chloroplasts and some mitochondria, which in contrast to bacteria harbour two homologues of the *ftsZ* gene (Stokes and Osteryoung, 2003; Miyagishima et al., 2004)

FtsZ is a cytoplasmic protein that is considered to be the very first protein to localise to the division site, where it assembles into a structure, called the Z-ring (Adams and Errington, 2009). The Z-ring acts as a scaffold that recruits other division proteins, which together with FtsZ coordinate cell division (Bi and Lutkenhaus, 1991). FtsZ is able to localise to the division independently of the other cell division components, it however requires either FtsA or ZipA, which are membrane tethering proteins, for formation of a stable Z-ring (Pichoff and Lutkenhaus, 2002). When both FtsA and ZipA are absent no rings are produced (Pichoff and Lutkenhaus, 2002). *E. coli ftsZ* mutants form filamentous cells and do not present any sign of constriction, which supports the crucial role of FtsZ and indicates that it acts earliest in the division process (Begg and Donachie, 1985; Taschner et al., 1988; Dai and Lutkenhaus, 1991).

FtsZ consists of four domains: a variable N-terminal segment, a highly conserved globular domain, a variable spacer and a C-terminal conserved peptide (Figure 1.5)(Löwe and Amos, 1998; Oliva et al., 2004). The role of the N-terminal segment and the variable spacer are not known (Margolin, 2005). Since the structure of the spacer is not resolvable in crystal structures, it has been proposed to serve as a flexible linker (Erickson et al., 2010). More recently it has been confirmed that the

spacer is an intrinsically disordered peptide (IDP), in which the length but not the sequence conservation play a significant role in FtsZ functionality and ability to assemble (Buske and Levin, 2013; Gardner et al., 2013). Interestingly, the IDP was shown to be crucial in *C. crescentus* and its depletion resulted in severe defects in peptidoglycan synthesis and subsequent cell lysis (Sundararajan et al., 2015). The C-terminal peptide is highly conserved across bacterial species. Even though it is not essential for FtsZ polymerisation its deletion results in a loss of FtsZ function (Ma and Margolin, 1999; Mosyak, 2000; Erickson et al., 2010). FtsZ interacts with other cell division proteins, such as FtsA and ZipA, through its C-terminus and truncation of this domain prevents these interactions (Bi and Lutkenhaus, 1991; Mosyak, 2000; Erickson et al., 2010; Szwedziak et al., 2012). In *S. aureus* FtsZ is a self-interacting protein and the binding site for FtsA is 10 residues in the C-terminal region with Phe376 critical for this interaction (Yan et al., 2000). The globular domain contains two subunits, the N-terminal and the C-terminal globular domains (Figure 1.5), which are connected by a conserved central core helix and have the ability to fold independently of each other (Löwe and Amos, 1998; Oliva et al., 2004; Osawa and Erickson, 2005). The N-terminal globular domain is responsible for GTP binding and hydrolysis, while the C-terminal globular domain contains the synergy loop T7 (Figure 1.5), which is crucial for FtsZ GTPase activity (de Boer et al., 1992b; Scheffers et al., 2002; Erickson et al., 2010).

FtsZ is considered to be a structural tubulin homologue (Erickson, 1997). A three-dimensional structure of FtsZ is similar to the structure of tubulin, despite its limited sequence similarity (Löwe and Amos, 1998). FtsZ, like tubulin, is a self-activating GTPase, it binds GTP and GDP and hydrolyses GTP to GDP (de Boer et al., 1992b; Mukherjee et al., 1993; Mukherjee and Lutkenhaus, 1994). The N-terminal globular domain of FtsZ contains a glycine-rich sequence motif, GGGTGTG, which is homologous to the segment found in tubulin and is important for GTP binding (de Boer et al., 1992b; RayChaudhuri and Park, 1992). Although, FtsZ utilizes GTP to form tubulin-like protofilaments, they do not assemble into microtubules as tubulin does (de Boer et al., 1992b; Mukherjee and Lutkenhaus, 1994; Nogales et al., 1998).

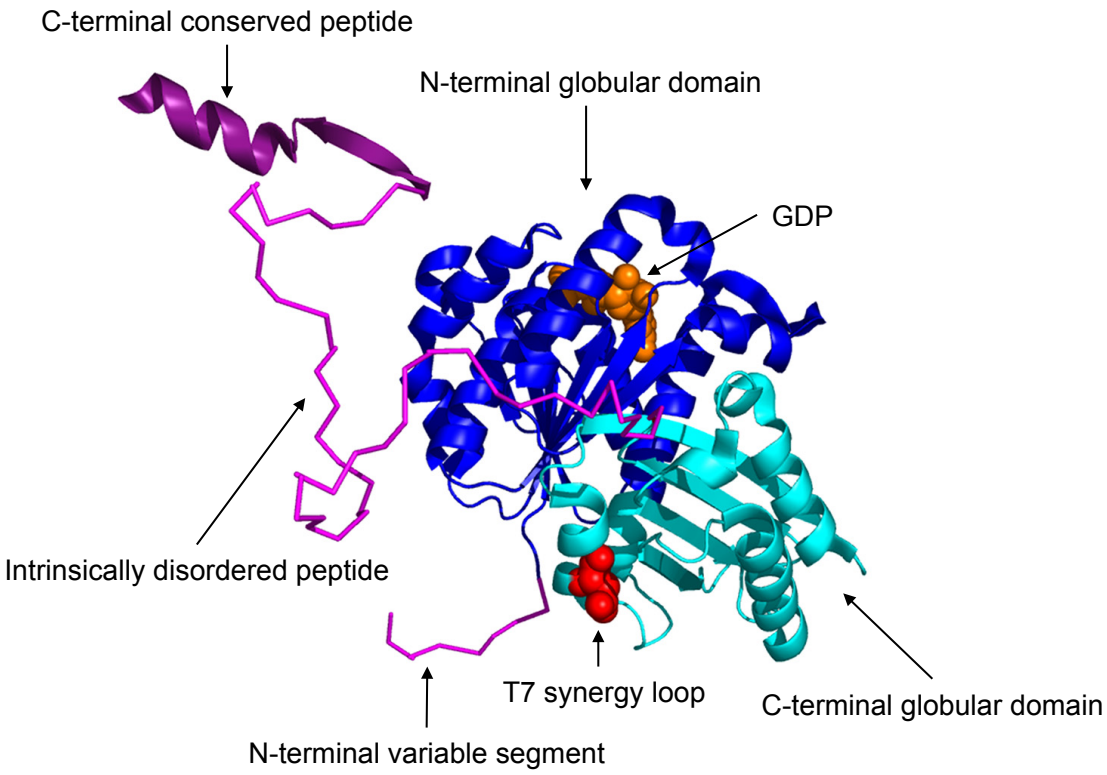

Figure 1.5. Crystal structure of *P. aeruginosa* FtsZ

The globular domain of FtsZ consists of two subdomains: N-terminal (blue) and C-terminal (cyan). The N-terminal globular domain binds GTP/GDP (orange), while the C-terminal globular domain contains the synergy loop T7. A 10 aa N-terminal variable segment, a 50 aa intrinsically disordered linker and a C-terminal conserved peptide are shown in magenta. Adapted from (Erickson et al., 2010).

FtsZ polymerisation is induced by binding of GTP. FtsZ assembles into protofilaments where the synergy loop T7 of one FtsZ monomer makes contact with the GTP binding site of the other FtsZ monomer. The polymerisation therefore induces FtsZ GTPase activity (Mukherjee et al., 2001; Scheffers et al., 2001; Oliva et al., 2004). What is more, GTP hydrolysis is not required for FtsZ assembly as FtsZ polymerisation was observed in the presence of GDP. This suggests that GTP binding and hydrolysis are to facilitate disassembly of the Z-ring and recycling of the FtsZ monomers (Mukherjee and Lutkenhaus, 1994; Erickson et al., 1996; Huecas and Andreu, 2004). *In vitro*, under different experimental conditions FtsZ assembles into single stranded protofilaments and superstructures of minirings, sheets, ribbons and helical tubes (Mukherjee and Lutkenhaus, 1994; Erickson et al., 1996; González et al., 2003; Löwe and Amos, 2005). The *ftsZ* gene was first identified in *E. coli* to be organised in a cluster of genes involved in cell division and cell wall synthesis, called the *dcw* cluster (Lutkenhaus et al., 1980; de la Fuente et al., 2001). Immunoelectron microscopy revealed that FtsZ localises in a ring-like structure near the cell membrane (Bi and Lutkenhaus, 1991). FtsZ localisation in the midcell was also visualised in *E. coli, B. subtilis* and other bacterial species by immunofluorescence microscopy and fluorescent protein fusions with GFP (Levin and Losick, 1996; Ma et al., 1996; Wang and Lutkenhaus, 1996). Fluorescence recovery after photobleaching (FRAP) revealed that the Z-ring is a highly dynamic structure with a half time of recovery 8 and 9 s in *B. subtilis* and *E. coli,* respectively (Anderson et al., 2004). *In vivo*, the Z-ring is proposed to consist of short FtsZ protofilaments (Stricker et al., 2002; Anderson et al., 2004; Chen and Erickson, 2005). This is further supported by electron cryotomography (ECM) which detected individual protofilaments organised into a single and radial layer distributed along the division site in *C. crescentus* (Li et al., 2007; Holden et al., 2014). Photoactivated localisation microscopy (PALM) showed that in *E. coli* FtsZ protofilaments are arranged into loose bundles that are randomly distributed along the cell membrane in longitudinal and radial directions (Fu et al., 2010). The non-continuous structure of the Z-ring was also observed in *C. crescentus* by PALM, which revealed thick and of non-uninform density FtsZ rings (Holden et al., 2014).

Interestingly, FtsZ has been observed to form dynamic helical patterns different to a Z-ring structure in exponentially growing *E. coli, C. crescentus,* vegetatively growing *B. subtilis* cells, and in sporulating *B subtilis* and *S. coelicolor* cells (Wang and

Lutkenhaus, 1996; Ben-Yehuda and Losick, 2002; Thanedar and Margolin, 2004; Grantcharova et al., 2005; Thanbichler and Shapiro, 2006; Peters et al., 2007). Time-lapse microscopy of FtsZ fluorescent fusions showed that these helices were moving along the cell to eventually condensate into the Z-ring in *E. coli* and *B. subtilis* (Thanedar and Margolin, 2004; Peters et al., 2007). In *E. coli* it was suggested that the helical pattern could represent a reservoir for a rapid turnover of FtsZ into the ring (Thanedar and Margolin, 2004).

It is not understood how bacteria constrict the membrane to close the division septum (Margolin, 2005). The FtsZ ring could either be mechanically pushed inwards by growing cross wall or generate a pinching force itself (Margolin, 2005). FtsZ bound to the membrane through either FtsA or amphipathic helix was sufficient for the Z-ring formation and constriction of liposomes *in vitro*, supporting FtsZ ability to provide the force in constriction of the cell membrane (Osawa et al., 2008; Osawa and Erickson, 2013). There are proposed several models for Z ring constriction. The 'sliding' model predicts filaments of FtsZ to be bound by an unidentified motor protein, which slides them past each another, resulting in a reduction in Z ring circumference (Hörger et al., 2008). This model is supported by ECM data which revealed FtsZ filaments organised into a single-layered band of filaments distributed along the cell membrane (Szwedziak et al., 2014). In the 'depolymerisation' model FtsZ protofilaments depolymerise at a membrane anchor site, which results in the Z ring constriction (Bramhill, 1997). Latest research on FtsZ polymerisation on bilayers *in vitro* showed that short FtsZ protofilaments attached to the membrane via FtsA grew at one end and gradually shortened at the other end, supporting an idea that FtsZ protofilaments are remodelled by polymerisation treadmilling dynamics (Loose and Mitchison, 2014) Other studies reported that FtsZ protofilaments can switch from a straight conformation favoured by GTP to a curved conformation favoured by GDP and thus the conformational change could provide force for constriction (Lu et al., 2000; Peters et al., 2007; Li et al., 2013). The 'iterative pinching' model proposes that FtsZ monomers polymerise into straight filaments and bind to the inner membrane. GTP hydrolysis occurs and protofilaments change their conformation from straight to curved, which drives the constriction force (Li et al., 2007).

Quantitative fluorescence analysis showed that only 30-40% of FtsZ molecules form a ring structure while the rest of them is diffused in the cytoplasm (Anderson et al., 2004; Geissler et al., 2007). It has been estimated that a single cell contains from ~6,000 FtsZ molecules in *B. subtilis* to even 15,000 in *E. coli*, which is equal to a 4-10 μM FtsZ concentration in a single cell, while *in vitro* the FtsZ critical concentration for its assembly is around 1 μM (Lu et al., 1998; Feucht et al., 2001; Ishikawa et al., 2006; Erickson et al., 2010). The critical concentration required for FtsZ polymerisation is a few times lower than its cellular concentration, implying that cells have developed a mechanism that regulates the assembly of FtsZ monomers (Mukherjee and Lutkenhaus, 1998; Chen and Erickson, 2005; Erickson et al., 2010). The other proteins involved in cell division have been shown to interact and modulate FtsZ dynamics.

1.3.2 FtsA

FtsA is a membrane-binding cytoplasmic protein widely conserved throughout bacteria, however it is absent from Cyanobacteria and Mycobacteria (Miyagishima et al., 2005; Adams and Errington, 2009; Gola et al., 2015). The *ftsA* gene is often found upstream of the *ftsZ* gene, in the *dcw* gene cluster (Beall et al., 1988; Pichoff and Lutkenhaus, 2005). In *E. coli* FtsA is an essential protein that tethers FtsZ to the cell membrane and localises to the membrane in a FtsZ dependent manner (Addinall and Lutkenhaus, 1996; Hale and de Boer, 1997). FtsA interacts directly with the conserved C-terminus of FtsZ and binds FtsZ to the cell membrane through the C-terminal amphipathic helix (Din et al., 1998; Pichoff and Lutkenhaus, 2005; Szwedziak et al., 2014). The interaction between FtsZ and FtsA was first observed in *E. coli* and *B. subtilis* using the yeast two-hybrid system and later confirmed to occur in other bacterial species, such as *S. aureus* and *S. pneumoniae* (Wang et al., 1997; Karimova et al., 2005; Maggi et al., 2008; Steele et al., 2011). The cellular ratio of FtsZ:FtsA was estimated as 100:1 and 5:1 in *E. coli* and *B. subtilis*, respectively (Dai and Lutkenhaus, 1992; Feucht et al., 2001). Maintenance of the FtsZ:FtsA ratio is critical for correct cell division, as FtsA overproduction or deletion disrupts Z-ring formation, but this effect of FtsA overproduction can be counteracted by overproduction of FtsZ (Wang and Gayda, 1990; Dai and Lutkenhaus, 1992). Interestingly, in *B. subtilis* FtsA is not required for cell viability but its inactivation results in severe growth defect (Beall and Lutkenhaus, 1992).

As a result of its primary sequence homology and biochemical activities, FtsA was predicted as a member of the actin/Hsp70/sugar kinase ATPase superfamily (Bork et al., 1992; Sánchez et al., 1994). The crystal structure of FtsA from *Thermotoga maritime* confirmed that it is a structural homologue of actin (van den Ent and Löwe, 2000). FtsA consists of two domains (1 and 2) that can be divided into two subdomains (1A and 1C, and 2A and 2B) (van den Ent and Löwe, 2000). The 1A, 2A and 2B subdomains form a site for ATP binding (van den Ent and Löwe, 2000). While the 2B subdomain is involved in direct interactions with FtsZ, the 1C domain is crucial for recruitment of another cell division component, FtsN (Pichoff and Lutkenhaus, 2007; Busiek et al., 2012; Szwedziak et al., 2012). FtsA is also required for recruitment of cell division components, such as FtsQ, FtsI and FtsK, and even though *E. coli* has an alternative membrane tethering protein, ZipA, in the absence of FtsA cell division is inhibited, confirming the role of FtsA as an early cell division component (Yu et al., 1998; Weiss et al., 1999; Goehring et al., 2005).

FtsA binds ATP, which is required for its interaction with FtsZ (Sánchez et al., 1994; Beuria et al., 2009; Krupka et al., 2014). Although ATP presence was shown to promote FtsA attachment to the membrane and polymerisation into actin-like protofilaments, no ATPase activity of FtsA was demonstrated (Lara et al., 2005; Szwedziak et al., 2012; Krupka et al., 2014). Interestingly, the ATPase activity was confirmed for FtsA from *B. subtilis* and *Pseudomonas aeruginosa,* however ATP was not required for *B. subtilis* FtsA to assemble into polymers (Feucht et al., 2001; Paradis-Bleau et al., 2005; Singh et al., 2013).

FtsA together with ZipA are essential membrane anchoring proteins required for FtsZ ring stability (Addinall and Lutkenhaus, 1996; Hale and de Boer, 1997). FtsA cannot takeover the role of ZipA but mutations which result in a R286W substitution in FtsA, yielding FtsA*, can bypass requirements for ZipA (Geissler et al., 2003, 2007). This implies that FtsA plays a more important part in FtsZ polymerisation than ZipA (Geissler et al., 2003, 2007). The requirement for ZipA was later shown to be able to be replaced by an L169R FtsZ mutant (FtsZ*) or increased FtsN production (Busiek et al., 2012; Haeusser et al., 2015). The main role of FtsA in arrangement of FtsZ polymers was recently confirmed by dynamics of FtsZ protofilaments on lipid bilayers *in vitro*

(Loose and Mitchison, 2014). FtsA was shown to have a dual role. It attaches FtsZ to the membrane and recruits more readily FtsZ protofilaments than monomers (Loose and Mitchison, 2014). Additionally, FtsZ protofilaments tethered to the membrane by FtsA are constantly remodelled as FtsA can destabilise FtsZ polymers without stimulating its GTPase activity (Loose and Mitchison, 2014). In contrast the FtsZ protofilaments anchored by ZipA are static (Loose and Mitchison, 2014). This indicates that FtsA is not only a passive FtsZ membrane anchor but is also an active modulator of FtsZ polymerisation dynamics (Loose and Mitchison, 2014).

1.3.3 ZipA

ZipA is an FtsZ membrane tethering protein conserved in *E. coli* and other γ-proteobacteria (Hale and de Boer, 1997; RayChaudhuri, 1999). In *E. coli* ZipA is an essential protein (Hale and de Boer, 1997). Its depletion or overproduction results in filamentous cells that do not divide, which is analogous to FtsA overproduction (Wang and Gayda, 1990; Hale and de Boer, 1997). Immunofluorescence and GFP fusions of ZipA revealed that it localises to the midcell, where it forms a ring-like structure (Hale and de Boer, 1997, 1999). Similar to FtsA, its localisation is FtsZ dependent, but does not need FtsA for midcell recruitment (Hale and de Boer, 1999; Liu et al., 1999). Although ZipA depletion does not abolish FtsZ assembly, the efficiency of Z-rings formation, the number of Z-ring per unit of cell mass is reduced, implying that ZipA may be responsible for stabilisation of the FtsZ polymers (Hale and de Boer, 1999).

ZipA is a transmembrane protein. It consists of a short N-terminal membrane helix and a large cytoplasmic C-terminus (Hale and de Boer, 1997; Mosyak, 2000; Moy et al., 2000). The cytoplasmic fragment can be further divided into a Map-Tau repeat, a proline/glutamine rich region and a globular domain (Hale and de Boer, 1997; RayChaudhuri, 1999; Mosyak, 2000; Moy et al., 2000). The globular domain interacts directly with the C-terminal conserved peptide of FtsZ, the same FtsZ fragment as FtsA binds to (Mosyak, 2000; Moy et al., 2000). *In vitro*, the C-terminus of ZipA promotes FtsZ assembly into bundles and sheets (Hale et al., 2000). In contrast to FtsA, which recruits preferably FtsZ protofilaments to the membrane, ZipA can recruit both polymers and monomers, which assemble into protofilaments (Loose and Mitchison, 2014). They remain relatively static when compared to protofilaments anchored to the

membrane by FtsA (Loose and Mitchison, 2014). More recently the interaction between FtsZ and the globular domain of ZipA was shown to be involved in protecting FtsZ from degradation by a ClpXP protease (Pazos et al., 2013). All this suggests that ZipA may have a chaperone like function, which is to stabilise FtsZ protofilaments (Mosyak, 2000; Pazos et al., 2013). Interestingly, *zipA* deletion can be bypassed by the FtsA* mutant (FtsA with a R286W substitution), however it is not able to prevent ClpXP induced degradation of FtsZ (Pazos et al., 2013).

ZipA is required for recruitment of other downstream proteins like FtsK, FtsL, FtsQ and FtsN(Hale and de Boer, 2002). Since ZipA can be replaced by either FtsA* or FtsZ* it has been suggested that ZipA indirectly recruits other cell division components by stabilising the Z-ring (Geissler et al., 2003; Margolin, 2005; Haeusser et al., 2015).

1.3.4 ZapA

ZapA is a small cytoplasmic protein consisting of 85 amino acids (Gueiros-Filho and Losick, 2002). It is widly conserved in Eubacteria and its homologues are found both in *B. subtilis* and *E. coli* (Gueiros-Filho and Losick, 2002). ZapA is not essential in *B. subtilis*, although it becomes crucial when another cell division protein, EzrA is missing or when the levels of FtsZ are depleted (Gueiros-Filho and Losick, 2002). ZapA, similar to other division proteins, localises to the midcell and its localisation depends on the presence of FtsZ (Gueiros-Filho and Losick, 2002). The interaction between FtsZ and ZapA was shown by affinity chromatography experiments and *in vitro* ZapA promotes stability of FtsZ protofilaments and formation of higher ordered structures as bundles and sheets (Gueiros-Filho and Losick, 2002; Anderson et al., 2004; Low et al., 2004; Small et al., 2007; Mohammadi et al., 2011).

The solved crystal structure of ZapA from *Pseudomonas aeruginosa* revealed that ZapA consists of two domains: an N-terminal domain and a long coiled-coil C-terminal domain (Low et al., 2004). *In vitro* ZapA forms an equilibrium of dimers and tetramers but as ZapA concentration increases tetramers are more preferable (Low et al., 2004). Dimerisation of ZapA monomers occurs via the N-terminus of the coiled-coil domains and subsequently an antiparallel tetramer is formed from two parallel dimers (Low et al., 2004). *In vitro* ZapA was shown to interact with FtsZ in a 1:1 molar stoichiometry,

and this ratio is consistent throughout different bacterial species (Low et al., 2004; Small et al., 2007; Mohammadi et al., 2011). The *E. coli* ZapA N-terminus of the coiled-coil domain was shown to be involved in the interaction with FtsZ and this interaction could stabilise FtsZ protofilaments by reducing FtsZ GTPase activity (Low et al., 2004; Mohammadi et al., 2011; Roach et al., 2014).

ZapA interacts with ZapB, another FtsZ polymer stabilising protein (Ebersbach et al., 2008; Galli and Gerdes, 2010). While ZapA is required for ZapB recruitment to the division septum, its overproduction leads to dispersion of ZapB throughout the cytoplasm (Galli and Gerdes, 2010, 2012). Since ZapA was shown to be able to cross-link FtsZ protofilaments, it either promotes lateral interactions between FtsZ polymers itself or by acting as a bridging protein between ZapB and FtsZ (Dajkovic et al., 2010; Galli and Gerdes, 2010, 2012).

1.3.5 ZapB

ZapB is a small cytoplasmic coiled-coil protein identified in *E. coli* and its homologues are found in other γ-proteobacteria (Ebersbach et al., 2008). ZapB localises to the midcell in a ring-like pattern and its septal recruitment is FtsZ and ZapA dependent (Ebersbach et al., 2008; Galli and Gerdes, 2010). Although in *E. coli*, ZapB is not essential, its depletion results in a delay in cell division, an increase of an average cell length and abnormal helix-like FtsZ structure, indicating a ZapB role in stabilisation of Z-rings (Ebersbach et al., 2008).

Bacterial two-hybrid analysis revealed that ZapB interacts with itself, FtsZ and ZapA, however affinity chromatography did not confirm the FtsZ:ZapB interaction (Ebersbach et al., 2008; Galli and Gerdes, 2012). ZapB associates via its N-terminal fragment with the C-terminal coiled-coil domain of ZapA (Galli and Gerdes, 2012).

Early fluorescence studies revealed that ZapB colocalises with, and proceeds FtsZ and ZapA at midcell (Galli and Gerdes, 2010). Recently, high-resolution microscopy (PALM) confirmed that ZapA is sandwiched between FtsZ structures, while ZapB locates the most toward the centre of the cell (Buss et al., 2015). Additionally, ZapB was found to interact with MatP, a DNA-binding protein involved in condensation and

segregation of the chromosomal terminus in *E. coli* (Espéli et al., 2012). Based on microscopy colocalisation studies and protein interactions in two-hybrid system, ZapB and ZapA have been proposed to form a network that connects the cell division machinery and the chromosome to coordinate cell division with chromosome segregation (Buss et al., 2015; Männik et al., 2016).

1.3.6 ZapC, ZapD and ZapE

In recent years additional Zap (Z-associated protein) proteins that are considered as the Z-ring stabilisers were identified in *E. coli* (Durand-Heredia et al., 2011, 2012; Hale et al., 2011; Marteyn et al., 2014).

ZapC is an early cell division protein characterised independently by two research groups at the same time (Durand-Heredia et al., 2011; Hale et al., 2011) It is a non-essential protein which is conserved throughout γ-proteobacteria (Durand-Heredia et al., 2011; Hale et al., 2011). ZapC is a small cytoplasmic protein which localises to midcell and its septal recruitment is FtsZ dependent (Durand-Heredia et al., 2011; Hale et al., 2011). Its recruitment to the site of division does not rely on FtsA, ZipA, ZapA and ZapB, and neither ZapA nor ZapB needs ZapC for proper localisation (Durand-Heredia et al., 2011; Hale et al., 2011; Galli and Gerdes, 2012).

ZapC was shown to interact with FtsZ in the yeast-two hybrid system, and to stabilise FtsZ protofilaments and promote their lateral interactions by decreasing GTPase activity of FtsZ *in vitro* (Durand-Heredia et al., 2011; Hale et al., 2011). More recently the crystal structure of ZapC from *E. coli* was solved and revealed that ZapC consists of two domains, each containing a pocket (Schumacher et al., 2016). Mutagenesis studies showed the C-terminal domain pocket is crucial for interactions with FtsZ (Schumacher et al., 2016). In contrast to other FtsZ interacting proteins such as FtsA and ZipA, ZapC does not bind the C-terminal conserved peptide but the globular domain of FtsZ, presumably the region involved in formation of the GTP binding site (Bhattacharya et al., 2015; Schumacher et al., 2016).

ZapD is an early, non-essential division protein that localises to the midcell in an FtsZ dependent manner in *E. coli* (Durand-Heredia et al., 2012). ZapD binds the FtsZ

C-terminal conserved peptide (Durand-Heredia et al., 2012). Like other Zap proteins, ZapD stabilises FtsZ filaments and stimulates their lateral interactions by reducing FtsZ GTPase activity *in vitro* (Durand-Heredia et al., 2012).

ZapE is an ATPase that is recruited to the midcell at later stages of cell division in *E. coli* (Marteyn et al., 2014). Its role as a late division protein is further supported by its interactions with other late division proteins, such as FtsQ, FtsL, FtsI and FtsN (Marteyn et al., 2014). A pull down assay revealed that ZapE interacts with FtsZ in an ATP independent manner (Marteyn et al., 2014). However this interaction was not confirmed by the bacterial two-hybrid system (Marteyn et al., 2014). Moreover*, in vitro* ZapD promotes FtsZ bundles but they are not stable in the presence of ATP (Marteyn et al., 2014).

1.3.7 SepF

SepF is conserved across Gram-positive bacteria and it was for the first time identified as a cell division protein in *B. subtilis* (Hamoen et al., 2006; Ishikawa et al., 2006). The gene encoding SepF is organised into a gene cluster that is located in the vicinity of the *divIVA* gene and the *dcw* gene cluster, implying its role in cell division (Hamoen et al., 2006; Gola et al., 2015). SepF is not essential in *B. subtilis* and its depletion results in deformed division septa, however it becomes synthetically lethal when another division protein, either FtsA or EzrA is absent (Hamoen et al., 2006; Ishikawa et al., 2006; Gündoğdu et al., 2011). Interestingly, SepF overproduction can complement the deletion of the *ftsA* gene, which is not crucial for *B. subtilis* but results in a severe growth defect (Ishikawa et al., 2006). This indicates that SepF and FtsA can have similar roles in cell division and it is further supported by SepF essentiality in Actinobacteria and Cyanobacteria, represented by *Mycobacterium tuberculosis* and *Synechococcus elongatus*, respectively, which do not harbour any FtsA homologues (Miyagishima et al., 2005; Gola et al., 2015).

In *B. subtilis* SepF requires FtsZ to be recruited to the division site and its localisation does not depend on the late division proteins, FtsL and PBP2B (Hamoen et al., 2006; Ishikawa et al., 2006; Gola et al., 2015). In a yeast two-hybrid system SepF interacts with itself and FtsZ (Hamoen et al., 2006; Ishikawa et al., 2006). *In vitro*, SepF stimulates FtsZ polymerisation and bundling by inhibiting its GTPase activity and also

by decreasing the FtsZ critical concentration (Singh et al., 2008). SepF assembles into 50 nm diameter rings and such rings promote FtsZ bundling into tubulin-like structures (Gündoğdu et al., 2011).

SepF, like FtsA, binds membrane through its N-terminal amphipathic helix and through direct interaction attaches FtsZ to the membrane (Duman et al., 2013). SepF interacts through its C-terminus with the FtsZ C-terminal conserved peptide (Singh et al., 2008; Król et al., 2012). *In vitro*, the self interaction between SepF monomers occurs via the C-terminal β-strands, resulting in a parallel dimers, which through their outside α-helices interact with other dimers to form long polymers (Duman et al., 2013).

1.3.8 EzrA

EzrA was identified and described as an inhibitor of FtsZ assembly in *B. subtilis* (Levin et al., 1999) An *ezrA* null *B. subtilis* mutant had a tendency to form more than one Z-ring and polar rings, suggesting that EzrA was involved in preventing FtsZ assembly in other locations but midcell (Levin et al., 1999; Haeusser et al., 2004). EzrA is considered to control FtsZ assembly by regulating the critical concentration of FtsZ required for polymerisation (Levin et al., 1999; Haeusser et al., 2004; Singh et al., 2007). While *ezrA* deletion results in an increased frequency of Z-rings formation, two-fold overexpression of EzrA delays and inhibits Z-rings formation, which is manifested by filamentous cells (Levin et al., 1999; Haeusser et al., 2004).

EzrA is an membrane associated protein that is found in Gram-positive bacteria with a low GC content, such as *B. subtilis, S. aureus*, *S. pneumoniae* and *Listeria monocytogenes* (Levin et al., 1999; Thanassi et al., 2002; Considine et al., 2011; Steele et al., 2011). In *B. subtilis* EzrA is distributed throughout the cell membrane and is recruited to the cell division where it forms a ring-like structure. In both *B. subtilis* and *S. aureus* it requires FtsZ presence for midcell localisation (Levin et al., 1999; Steele et al., 2011). Although EzrA is visualised as a uniform ring-like structure by conventional fluorescence microscopy, recent studies using structured illumination microscopy (SIM) revealed that EzrA consists of dynamic ‘beads’ distributed around the division site (Strauss et al., 2012).

In vitro studies have shown that EzrA interacts directly with FtsZ and modulates its assembly by two distinct ways. EzrA inhibits polymerisation of FtsZ monomers by reducing their affinity towards GTP, whereas at the polymeric level it destabilises and stimulates FtsZ protofilaments disassembly by enhancing FtsZ GTPase activity (Chung et al., 2007; Singh et al., 2007).

EzrA is composed of a short N-terminal transmembrane domain and a large cytoplasmic coiled-coil C-terminus and is thought to have an analogous topology to *E. coli* ZipA (Levin et al., 1999; Haeusser et al., 2004; Cleverley et al., 2014). The N-terminal membrane-spanning domain can be replaced for other membrane tethers without disrupting the *B. subtilis* phenotype and EzrA localisation (Land et al., 2014). A truncation of the membrane anchor gives the *ezrA* null-like phenotype, as EzrA loses its ability to inhibit formation of Z-rings at cell poles (Haeusser et al., 2004; Land et al., 2014). *In vitro*, an EzrA recombinant protein without the transmembrane domain is able to interact with FtsZ and block its assembly (Haeusser et al., 2004). This indicates that the membrane domain is involved in tethering to the membrane and increasing the local concentration (Haeusser et al., 2004; Land et al., 2014). The C-terminal domain contains a conserved patch of seven residues (IQFGNRF), called the QNR patch (Haeusser et al., 2007). The QNR patch is required for midcell localisation of EzrA but not for FtsZ assembly inhibition (Haeusser et al., 2007). The QNR patch mutants retain their ability to inhibit FtsZ ring formation at cell poles, despite the loss of septal localisation (Haeusser et al., 2007). *In vitro* EzrA still inhibits formation of FtsZ protofilaments in the absence of the QNR patch (Haeusser et al., 2007). EzrA interacts directly with the C-terminus of FtsZ and it is not able to prevent FtsZ assembly when FtsZ is missing its last 16 residues *in vitro* (Singh et al., 2007).

Recently, a crystal structure of *B. subtilis* EzrA cytoplasmic domain has been solved (Cleverley et al., 2014). EzrA is made up of five repeats, each consisting of three anti-parallel helices, and the C-terminal four-helix boundle (Figure 1.6) (Cleverley et al., 2014). The first two repeats of EzrA were shown to interact with FtsZ and inhibit its oligomerisation (Cleverley et al., 2014). Moreover, EzrA was shown to have little effect on FtsZ GTPase activity and its affinity for GTP, indicating that it modulates FtsZ polymerisation through another mechanism than stimulation of GTP binding and hydrolysis by FtsZ (Cleverley et al., 2014).

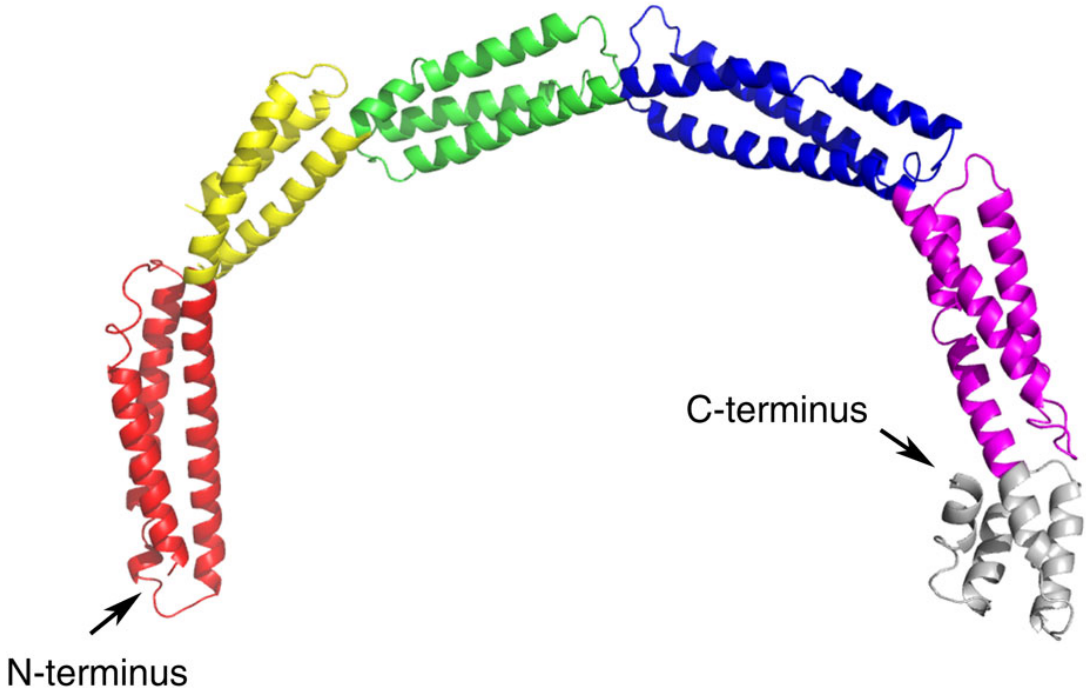

Figure 1.6. Crystal structure of *B. subtilis* EzrA

Ribbon representation of the cytoplasmic domain of EzrA (22-562 aa). EzrA consists of five triple helical bundle repeats coloured from the N- to C-terminus red, yellow, green, blue and magenta, and the C-terminal four-helix boundle coloured grey. The linear head-to-tail arrangement of the triple helical bundles forms an extended structure that bends into a semi-circle. Reproduced from (Cleverley et al., 2014).

More interestingly, the crystal structure revealed that EzrA is a structural homologue of eukaryotic spectrin proteins, which crosslink and stabilise actin protofilaments (Cleverley et al., 2014). EzrA self interacts in a bacterial two-hybrid system (Steele et al., 2011). As a result a model, where an EzrA anti-parallel dimer could form an arch over the membrane, which traps FtsZ polymers between the membrane and the inside curve of the arch, preventing lateral interactions of FtsZ polymers, has been proposed (Claessen et al., 2014). Additionally, EzrA was shown to interact with several cell division components and be required for their septal localisation (Jorge et al., 2011; Steele et al., 2011; Claessen et al., 2014). In both *B. subtilis* and *S. aureus,* EzrA recruits a bifunctional penicillin binding protein, PBP1 and PBP2, respectively (Steele et al., 2011; Claessen et al., 2014). Depletion of EzrA results in a severe growth defect and delocalisation of the peptidoglycan biosynthesis machinery all over the cell surface (Jorge et al., 2011; Steele et al., 2011; Claessen et al., 2014). Although EzrA is not essential in *B. subtilis*, it becomes synthetically lethal when either SepF or GpsB is absent, and it is crucial in *S. aureus*, *S. pneumoniae* and *L. monocytogenes* (Levin et al., 1999; Thanassi et al., 2002; Hamoen et al., 2006; Considine et al., 2011; Steele et al., 2011; Claessen et al., 2014). All this suggests that EzrA may play a positive role in cell division and could act as a scaffold protein and an interface between cytoplasmic cell division components and periplasmic peptidoglycan biosynthetic machinery (Steele et al., 2011; Cleverley et al., 2014).

1.3.9 GpsB

GpsB is a cell division protein conserved in Gram-positive bacteria and it was first identified in *B. subtilis* (Claessen et al., 2008; Tavares et al., 2008; Gamba et al., 2009; Steele et al., 2011; Land et al., 2013; Fleurie et al., 2014b; Rismondo et al., 2015). The *gpsB* gene is located in the vicinity of the *recU* and *ponA* genes encoding the DNA resolvase and a penicillin binding protein, respectively (Tavares et al., 2008). GpsB is considered as a paralogue of DivIVA, the Min system component, since their N-terminal fragments show a high degree of similarity (Claessen et al., 2008; Tavares et al., 2008). Recently the crystal structures of the N-terminal and C-terminal domains of *L. monocytogenes* and *B. subtilis* GpsB were solved (Rismondo et al., 2015). The N-terminus is homologous to the N-terminal membrane interacting domain of DivIVA,

while the conserved C-terminal domain has its unique sequence and is a triple helical bundle (Rismondo et al., 2015).

Whilst in *S. pneumoniae* GpsB can be essential depending on the genetic background and thus its loss is either lethal or results is a severe growth defect, in *B. subtilis* it is synthetically lethal in the presence of either an *ezrA* or *ftsA* mutation (Claessen et al., 2008; Tavares et al., 2008; Land et al., 2013). Fluorescence microscopy studies showed that GpsB localises to the division site. After division it remains at the new cell poles from which it localises laterally to again concentrate at the division septum (Claessen et al., 2008; Tavares et al., 2008; Land et al., 2013). GpsB is recruited to the site through its N-terminal domain when the septum is detectable and also it leaves the division site relatively late (Claessen et al., 2008; Tavares et al., 2008; Land et al., 2013). Its role as a late division protein is further supported by its localisation dependency on both early (FtsZ and FtsA) and late (DivIC and PBP2B) division proteins in *B. subtilis* (Tavares et al., 2008). Additionally, in *B. subtilis* and *S. aureus* GpsB fails to localise to the septum in the absence of EzrA and DivIB (Claessen et al., 2008; Steele et al., 2011; Bottomley et al., 2014).

The loss of both GpsB and EzrA leads to a severe growth defect in *B. subtilis* (Claessen et al., 2008). Cells lacking EzrA and GpsB are prone to lysis which results from disruption of cell wall synthesis; cross wall separation and hydrolysis progresses even when the formation of the septal wall is not completed (Claessen et al., 2008). In a bacterial two-hybrid system GpsB interacts with itself, EzrA, MreC involved in cell elongation and PBP1, a penicillin binding protein involved both in lateral and septal peptidoglycan synthesis in *B. subtilis* (Claessen et al., 2008; Steele et al., 2011). PBP1 presents a similar dynamic pattern of localisation as GpsB. In the absence of EzrA and GpsB, PBP1 is delocalised (Claessen et al., 2008). It has been suggested that EzrA and GpsB may coordinate cell elongation with septation of *B. subtilis* by modulating PBP1 localisation (Claessen et al., 2008). EzrA recruits PBP1 to midcell to form septum, whereas GpsB removes PBP1 from newly formed cell poles so that it can localise along the cell periphery and control lateral cell wall synthesis (Claessen et al., 2008). In *S. pneumoniae* GpsB was also proposed to link cell division and growth through an interaction with EzrA and DivIVA (Land et al., 2013; Fleurie et al., 2014a).

1.3.10 FtsK

FtsK was originally identified as an essential cell division protein in *E. coli* (Begg et al., 1995). It is a highly conserved protein within Eubacteria and its homologue, HerA, is also found in Archaea (Bigot et al., 2007). FtsK is considered as a bifunctional protein that coordinates cell division with chromosome segregation (Liu et al., 1998; Wang et al., 2006; Grainge, 2010; Stouf et al., 2013). In *E. coli,* FtsK-GFP localises to the septum and requires FtsZ, FtsA and ZipA to be recruited, and its presence was shown to be needed for assembly of other cell division components: FtsQ, FtsL and FtsI (Yu et al., 1998; Chen and Beckwith, 2001; Hale and de Boer, 2002).

FtsK is a membrane protein which comprises of three domains: an N-terminal domain with four membrane-spanning segments, a large proline/glutamine-rich linker and an ATP-binding cytoplasmic C-terminus (Dubarry et al., 2010). In *E. coli*, only the N-terminal domain is essential in cell division and sufficient for FtsK localisation to the midcell (Draper et al., 1998; Liu et al., 1998; Yu et al., 1998). FtsK is known to form hexamers (Massey et al., 2006). The interaction between the membrane domains was shown to be involved in oligomerisation of FtsK monomers and to occur independently of the presence of the C-terminal domain (Bisicchia et al., 2013.). The sequence of the linker is not conserved and its length varies between bacterial species (Dubarry et al., 2010). Although the linker is considered to work as a spacer between the N-terminal and C-terminal domains of FtsK, it has been shown to be required for maintaining the *E. coli* wild type phenotype and for the stability of the cytoplasmic domain (Aussel et al., 2002; Bigot et al., 2004; Dubarry et al., 2010). Thus, the linker has been proposed to couple two functions of FtsK in cell division and chromosome segregation (Aussel et al., 2002; Bigot et al., 2004; Dubarry et al., 2010). The C-terminus of FtsK is required for chromosome segregation in *E. coli* (Yu et al., 1998). A truncation of this domain leads to defects in a chromosome segregation and septum placement (Yu et al., 1998). The C-terminal domain of FtsK oligomerises into the hexamer that forms an ATP-dependent DNA translocase (Crozat and Grainge, 2010; Graham et al., 2010; Bisicchia et al., 2013). The cytoplasmic domain shows high sequence similarity to the C-terminal domain of *B. subtilis* SpoIIIE, which translocates DNA to the prespore (Wu and Errington, 1994; Bath et al., 2000; Massey et al., 2006; Cattoni et al., 2014). The FtsK C-terminal domain is composed of three subdomains α, β, and γ (Massey et al.,

2006). Whilst the α an β subdomains form a motor that pumps double-stranded DNA, the γ domain recognises an 8 bp asymmetric sequence, called KOPS (FtsK orienting polar sequences) (Bigot et al., 2006; Massey et al., 2006; Ptacin et al., 2006; Bisicchia et al., 2013). KOPS orientates the direction of DNA translocation and three γ subdomains are required for recognition of a single KOPS (Bigot et al., 2006; Ptacin et al., 2006; Löwe et al., 2008). Additionally, the γ subdomain recruits XerCD recombinases to the *dif* site, which resolves chromosome dimers (Bigot et al., 2004; Grainge et al., 2011; Zawadzki et al., 2013).

FtsK localisation to the division site depends on early division proteins, while its inactivation results in a defect in cell morphology that is similar to cell phenotype caused by defects in peptidoglycan synthesis (Varma et al., 2007; Lesterlin et al., 2008). Furthermore, in the bacterial two-hybrid system FtsK interacts with FtsI (PBP3), which synthesises peptidoglycan at the septum (Di Lallo et al., 2003). Therefore it has been suggested that FtsK may interact with the peptidoglycan synthesis machinery to delay septum closure until DNA has been segregated (Begg et al., 1995; Di Lallo et al., 2003; Lesterlin et al., 2008).

1.3.11 FtsW

FtsW belongs to SEDS (shape, elongation, division and sporulation) family of integral membrane proteins, which are conserved and essential among cell wall-containing bacteria (Ikeda et al., 1989; Henriques et al., 1998). The primary sequence of FtsW has a high degree of similarity to RodA, which is a membrane protein involved in lateral peptidoglycan synthesis in *E. coli,* and SpoVE, which controls peptidoglycan formation during the sporulation process in *B. subtilis* (Ikeda et al., 1989; Henriques et al., 1998).

FtsW is an essential protein for *E. coli* cell division and indispensable in sporulating *S. coelicolor* (Boyle et al., 1997; Mistry et al., 2008). Its depletion results in severe growth defect and frequency of Z-rings formation decreases, suggesting its role in stabilisation of FtsZ polymers (Boyle et al., 1997; Mistry et al., 2008). Moreover, *ftsW* is organised into the *dcw* cluster (Ikeda et al., 1990; Boyle et al., 1997). Similar to other cell division components, FtsW localises to midcell where it is recruited by FtsZ, FtsA, FtsQ and FtsL, and in turn it recruits FtsI (PBP3) (Boyle et al., 1997; Wang et al., 1998;

Mercer and Weiss, 2002). This indicates that FtsW is a late division protein that recruits a peptidoglycan synthesis machinery to midcell and couples cell division with cell wall formation (Mercer and Weiss, 2002). FtsW interacts with FtsL, FtsN and FtsI in two-hybrid systems, and its binding to FtsI was further supported by Förster resonance energy transfer (FRET) and immunoprecipitation experiments (Di Lallo et al., 2003; Karimova et al., 2005; Fraipont et al., 2011).

FtsW is a large membrane protein that is predicted to consist of ten transmembrane-spanning domains, a large periplasmic loop between the transmembrane domains 7 and 8, and N- and C- terminal fragments located in the cytoplasm (Gérard et al., 2002; Lara and Ayala, 2002). Site-directed mutagenesis experiments coupled with fluorescence microscopy visualisation showed that the short periplasmic loop between transmembrane segments 9 and 10 was required for FtsI recruitment to the septum by FtsW (Pastoret et al., 2004). The large periplasmic loop (between membrane domains 7 and 8) might form an interacting site for other peptidoglycan synthesis machinery components, as mutations in this fragment resulted in a cell chaining phenotype and often cell lysis (Pastoret et al., 2004).

Recently, FtsW was proposed to act as a flippase that transports the peptidoglycan precursor, lipid II across the cell membrane in *E. coli* (Mohammadi et al., 2011, 2014). The transmembrane segment 4 was shown to be required for FtsW to flip lipid II *in vitro* (Mohammadi et al., 2011, 2014). Contrarily, another integral membrane protein, MurJ was reported as the *E. coli* flippase (Ruiz, 2008). MurJ membrane topology is similar to FtsW and it has 14 membrane spanning domains (Butler et al., 2013). MurJ is a crucial protein for peptidoglycan synthesis and *E. coli* viability, and its depletion results in accumulation of peptidoglycan precursors in the cytoplasm and cell lysis (Inoue et al., 2008; Ruiz, 2008; Butler et al., 2013).

1.3.12 FtsQ/DivIB

FtsQ is membrane protein essential in *E. coli* (Begg et al., 1980; Carson et al., 1991). In *B. subtilis*, DivIB, a homologue of FtsQ is not required for vegetative cell growth, however it becomes essential at temperatures higher than 37^{o}C and is also crucial for *B. subtilis* and *S. coelicolor* to sporulate (Beall and Lutkenhaus, 1989; Harry et al.,

1993, 1994; McCormick and Losick, 1996). Lately, DivIB was shown to be indispensable in *S. aureus* (Chaudhuri et al., 2009; Bottomley et al., 2014). The *ftsQ/divIB* genes are present in the *dcw* cluster and are conserved across bacterial species (Margolin, 2000; de la Fuente et al., 2001; Real and Henriques, 2006). However they are not found in bacteria lacking a cell wall, implying FtsQ/DivIB role both in cell division and peptidoglycan synthesis (Margolin, 2000; de la Fuente et al., 2001; Real and Henriques, 2006).

In *E. coli* FtsQ is a low abundance protein with only about 22 molecules per cell, whereas in *B. subtilis* there are estimated ~5,000 molecules per cell (Carson et al., 1991; Rowland et al., 1997). Immunofluorescence microscopy revealed that FtsQ localises to the septum in constricting cells (Buddelmeijer et al., 1998). Whilst FtsQ localisation to the division site depends on FtsZ, FtsA, ZipA and FtsK, its presence is required for recruitment of FtsL, FtsB, FtsW, FtsI and FtsN (Addinall et al., 1997; Ghigo et al., 1999; Weiss et al., 1999; Chen and Beckwith, 2001; Hale and de Boer, 2002; Pastoret et al., 2004). In *B. subtilis*, DivIB is recruited to the midcell before septation is visible and remains there throughout the cell division process (Harry and Wake, 1997). Interestingly, in *S. aureus* instead of septal ring-like localisation DivIB forms foci round cell periphery in 'line and dot' patterns (Bottomley et al., 2014). The midcell localisation is rarely observed in *S. aureus,* raising possibility that DivIB septal localisation is transient and its peripheral location marks previous sites of division (Bottomley et al., 2014). Two-hybrid analysis confirmed that FtsQ/DivIB interacts with itself, FtsA, FtsK, FtsL, FtsB/DivIC, FtsW, FtsI, FtsN and EzrA, and it coimmunoprecipitates with FtsQ and FtsB (Di Lallo et al., 2003; Buddelmeijer and Beckwith, 2004; Karimova et al., 2005; Daniel et al., 2006; Steele et al., 2011).

FtsQ/DivIB is a membrane protein that consists of a short N-terminal cytoplasmic domain, a hydrophobic membrane-spanning helix and a large C-terminal periplasmic domain (Carson et al., 1991; Real and Henriques, 2006; Robson and King, 2006; van den Ent et al., 2008). The N-terminal hydrophobic and the transmembrane domains are crucial for the proper localisation of FtsQ/DivIB in the membrane and for recruitment to the septum (Dopazo et al., 1992; Scheffers et al., 2007; Wadsworth et al., 2008). FtsQ reacts with FtsA and FtsK via its N-terminal domain, while the periplasmic region is required for interactions with other cell division proteins (Karimova et al., 2005;

D'Ulisse et al., 2007). Fluorescence and immunofluorescence microscopy revealed that FtsQ with replaced or truncated periplasmic domain does not localise to the division site, implying importance of the C-terminus in FtsQ function in cell division. The periplasmic domain of FtsQ/DivIB comprises three subdomains: α, β and γ (Robson and King, 2006; van den Ent et al., 2008; Masson et al., 2009). The α subdomain contains a POTRA (polypeptide transport-associated) domain which may act as a chaperone preventing FtsQ from degradation (Sánchez-Pulido et al., 2003). The β subdomain is a parallel β-sheet required for FtsL and FtsB binding and other division proteins, whereas the γ subdomain is unstructured and is also involved in interactions with FtsL and FtsB (Goehring et al., 2005; Robson and King, 2006; van den Ent et al., 2008). Mapping of FtsQ sites needed for interaction with FtsB and FtsL revealed that Arg75 in the α subdomain is crucial for binding both FtsL and FtsB, and additionally Ser250 in the β subdomain is a second hot spot for FtsB (van den Berg van Saparoea et al., 2013).

As mentioned above FtsQ/DivIB interacts with FtsB/DivIC and FtsL both *in vitro* and *in vivo* independently of other cell division components. *In vitro* they form a 1:1:1 stoichiometry complex by interactions between their C-terminal domains (Buddelmeijer and Beckwith, 2004; Goehring et al., 2005; Karimova et al., 2005; Noirclerc-Savoye et al., 2005; Daniel et al., 2006; Glas et al., 2015). FtsL and FtsB are able to form a subcomplex when FtsQ is not present but they are not recruited to the septum (Weiss et al., 1999; Robichon et al., 2011). In *B. subtilis*, FtsL and DivIC disappear rapidly in the absence of DivIB, indicating that DivIB is essential for their stability. Furthermore, in the absence of FtsL, assembly of DivIB and DivIC at the division site is inhibited (Daniel et al., 1998; Daniel and Errington, 2000; Robson et al., 2002). Additionally, DivIB has been suggested to negatively regulate DivIC stability, as when FtsL is depleted DivIC is degraded (Daniel et al., 2006). This is not observed when both FtsL and DivIB are absent (Daniel et al., 2006). This implies the importance of association of all three proteins and interdependence in their function and stability.

Using artificial septal targeting experiments it has been revealed that the C-terminal region of DivIB is essential for its interaction with PBP2B in *B. subtilis* (Rowland et al., 2010). Moreover, recent findings showed that in *S. aureus* the β subdomain of DivIB binds peptidoglycan and depletion of DivIB blocks septum completion but not its initiation. Other early division proteins and PBPs are present at midcell, where they

form aberrant rings (Bottomley et al., 2014). Additionally, Liu et al. (2015) and Tsang and Bernhardt (2015) has suggested that FtsN could regulate peptidoglycan synthesis by inducing allosteric changes in the FtsQ(DivIB)/FtsB(DivIC)/FtsL complex, supporting the role of this complex in coordinating peptidoglycan synthesis with cell division (Liu et al., 2015; Tsang and Bernhardt, 2015).

1.3.13 FtsB/DivIC

DivIC is an essential protein for both vegetative growth and sporulation in *B. subtilis* (Levin and Losick, 1994). FtsB is a crucial protein in *E. coli* and *Vibrio cholerae,* and despite its low sequence similarity it is considered as a homologue of *B. subtilis* DivIC (Buddelmeijer et al., 2002). DivIC/FtsB is a small bitopic membrane protein with a C-terminal periplasmic coiled-coil domain, which contains a leucine zipper motif (Katis et al., 1997; Buddelmeijer et al., 2002; Buddelmeijer and Beckwith, 2004; Gonzalez and Beckwith, 2009; LaPointe et al., 2013).

Both FtsB and DivIC localise to the division site, with FtsB dependent on FtsL and FtsQ but not FtsW and FtsI (Katis et al., 1997; Buddelmeijer et al., 2002). The N-terminal periplasmic region containing the leucine zipper motif of FtsB is required for interaction with FtsL, while the extreme C-terminus of the periplasmic domain is essential for interaction with FtsQ (Gonzalez and Beckwith, 2009). FtsB can form a subcomplex with FtsL in the absence of FtsQ, however the FtsBL subcomplex is not recruited to the septum without FtsQ (Weiss et al., 1999; Buddelmeijer and Beckwith, 2004). The interaction between FtsB and FtsL occurs presumably through their transmembrane regions and leucine zipper motifs, and *in vitro* they were shown to form heterodimers and even tetramers (Robichon et al., 2011; Khadria and Senes, 2013). Recent studies showed that the periplasmic domain of FtsB forms a stable complex with periplasmic domains from FtsL and FtsQ in a 1:1:1 stoichiometry (Glas et al., 2015). FtsB forms a subcomplex with FtsQ in the absence of FtsL although with a lower affinity (Glas et al., 2015). Fluorescence microscopy studies revealed that in *E. coli* FtsB is required for septal localisation of FtsL, while in *B. subtilis* DivIC localisation is FtsL dependent, indicating that FtsL and FtsB/DivIC may colocalise to the septum (Katis et al., 1997; Daniel et al., 1998, 2006; Buddelmeijer et al., 2002). Depletion of FtsB affects stability of FtsL and *vice versa*. Lack of FtsL results in degradation of the

FtsB C-terminus and in a rapid decrease in the amount of DivIC (Daniel et al., 1998; Buddelmeijer et al., 2002; Gonzalez and Beckwith, 2009). These findings indicate that FtsB/DivIC and FtsL are mutually dependent for their stability and localisation (Buddelmeijer et al., 2002; Gonzalez and Beckwith, 2009).

Lately, DivIC together with DivIB and FtsL was identified as a peptidoglycan binding protein in *S. aureus* (Kabli, 2013; Bottomley et al., 2014). These findings support a model proposed by Liu et al. (2015), and Tsang and Bernhardt (2015), where FtsQBL form a complex involved in linking peptidoglycan synthesis with the Z-ring (Liu et al., 2015; Tsang and Bernhardt, 2015).

1.3.14 FtsL

FtsL is a membrane protein essential in *E. coli* and *B. subtilis* (Guzman et al., 1992; Daniel et al., 1996). Although the primary sequence of FtsL in *E. coli* differs from FtsL in *B. subtilis*, their genes are located upstream of the *ftsI* gene, which encodes a penicillin binding protein. Their membrane topologies are similar, thus this proteins are considered as homologues (Guzman et al., 1992; Daniel et al., 1996, 1998).

FtsL, as FtsQ and FtsB, is a bitopic protein that consists of a cytoplasmic N-terminus, a single membrane-spanning domain and a periplasmic coiled-coil C-terminus (Guzman et al., 1992; Ghigo and Beckwith, 2000). The C-terminal periplasmic domain contains a leucine zipper motif, which allows FtsL to form unstable dimers *in vitro* (Daniel et al., 1998; Ghigo and Beckwith, 2000). Domain-swapping analysis showed that the cytoplasmic and transmembrane domains are essential for FtsL function, whereas both the transmembrane and periplasmic domains are required for localisation to the septum in *E. coli* (Guzman et al., 1997; Ghigo and Beckwith, 2000). Surprisingly, neither random nor site-specific mutagenesis have indicated essentiality of any domain in *B. subtilis* (Sievers et al., 2002).

FtsL interacts with FtsQ/DivIB, FtsB/DivIC, EzrA, FtsI, FtsW and FtsK in a two-hybrid system. (Di Lallo et al., 2003; Karimova et al., 2005; Daniel et al., 2006; Steele et al., 2011). The transmembrane domain and the leucine zipper-like motif are required for interaction with FtsB, while the cytoplasmic fragment is needed for FtsW recruitment

(Sievers et al., 2002; Gonzalez et al., 2010; Robichon et al., 2011; Khadria and Senes, 2013).

FtsL is a highly unstable protein and is degraded rapidly in the absence of DivIB and FtsB/DivIC (Daniel and Errington, 2000; Buddelmeijer et al., 2002; Robson et al., 2002). Moreover, when FtsL is lacking the amount of FtsB/DivIC decreases due to degradation (Daniel et al., 1998, 2006; Buddelmeijer et al., 2002). This indicates that formation of the whole complex FtsL, FtsB/DivIC and FtsQ/DivIB is necessary so that FtsL and FtsB/DivIC are stable (Daniel et al., 2006). Additionally, FtsL is a substrate for a zinc metalloprotease RasP (YluC), which regulates FtsL turnover by recognising its N-terminal cytoplasmic domain (Bramkamp et al., 2008; Wadenpohl and Bramkamp, 2010). DivIC is able to stabilise FtsL by forming a complex with and thus preventing FtsL from RasP cleavage (Bramkamp et al., 2008; Wadenpohl and Bramkamp, 2010). A model, in which FtsL degradation by RasP stimulates divisome disassembly and inhibits its reassembly, has been proposed (Wadenpohl and Bramkamp, 2010).

S. aureus FtsL, DivIC and DivIB were identified as a novel class of peptidoglycan binding proteins that do not hydrolyse murein. FtsL together with DivIB have been proposed to mark previous planes of division to prevent their reuse (Kabli, 2013; Bottomley et al., 2014).

1.3.15 FtsN

FtsN is an essential division protein in *E. coli* and is recruited to the division site by FtsZ, FtsA, ZipA, FtsQ and FtsI, suggesting that it is one of the latest cell division proteins (Dai et al., 1993; Addinall et al., 1997; Hale and de Boer, 2002). Two-hybrid analysis and affinity chromatography experiments showed that FtsN interacts with other division proteins, such as FtsA, FtsW, FtsI, FtsQ, peptidoglycan transpeptidases PBP1B and PBP3 and with a monofunctional transglycosylase MtgA (Di Lallo et al., 2003; Karimova et al., 2005; Müller et al., 2007; Derouaux et al., 2008; Busiek et al., 2012).

FtsN is a membrane protein with a topology similar to FtsQ (Dai et al., 1993). It comprises a short cytoplasmic N-terminal domain, a single transmembrane domain and a large periplasmic C-terminal domain (Dai et al., 1996). The cytoplasmic domain of

FtsN binds the 1C subdomain of FtsA and the presence of FtsA is needed so that the truncated FtsN, comprising the cytoplasmic and membrane domains, can be recruited to midcell (Busiek et al., 2012; Busiek and Margolin, 2014). What is more, the N-terminus and the membrane domain can be relaced by the N-terminal domain and the first membrane-spanning segment of another protein MalG, and the protein still localises to the septum (Addinall et al., 1997). The C-terminal domain of FtsN consists of a short helical region, a glutamine-rich region and a SPOR domain, which binds peptidoglycan (Dai et al., 1996; Chung et al., 2004; Ursinus et al., 2004; Duncan et al., 2013). The SPOR domain was shown to be sufficient for septal localisation of FtsN and to bind the cross wall in purified sacculi, although this domain is not required for cytogenesis (Gerding et al., 2009; Möll and Thanbichler, 2009; Duncan et al., 2013). SPOR binds long glycan strands and shows reduced affinity toward murein from a triple amidase mutant (Ursinus et al., 2004; Gerding et al., 2009). Furthermore, when all three amidases are absent, FtsN is dispersed throughout the cell membrane, indicating that SPOR requires at least one amidase to bind the septal peptidoglycan (Ursinus et al., 2004; Gerding et al., 2009).

More recently it has been shown that FtsN is recruited to the division site at both early and late stages of septation (Busiek and Margolin, 2014). Fusing the cytoplasmic and membrane fragment of FtsN with GFP (GFP-$FtsN_{Cyto-TM}$) and the SPOR domain with mCherry (mCherry-$FtsN_{SPOR}$) revealed that in the majority of cells these two FtsN parts colocalised (Busiek and Margolin, 2014). In cells without colocalisation GFP-$FtsN_{Cyto-TM}$ was found at the newly formed division site, while mCherry-$FtsN_{SPOR}$ was present at midcell in cells with visible constriction (Busiek and Margolin, 2014). A screen for suppressor mutations that can rescue non-functional FtsN (a mutant of the SPOR domain) identified substitutions in the periplasmic domains of FtsL and FtsB, and in the 1C subdomain of FtsA, implying that both the FtsQLB complex and FtsA are targets of FtsN (Liu et al., 2015; Tsang and Bernhardt, 2015). A model in which FtsN triggers peptidoglycan synthesis at the septum has been suggested (Liu et al., 2015; Tsang and Bernhardt, 2015). In this model FtsA, FtsQLB and FtsI localise to the division site and an ‘off’ confirmation of FtsA and FtsQLB represses the activity of FtsI. Recruitment of FtsN to midcell and its interaction with FtsA in the cytoplasm and FtsQLB in the periplasm switches FtsA and FtsQLB from the ‘off’ to the ‘on’

confirmation, releasing the peptidoglycan synthesis activity of FtsI (Liu et al., 2015; Tsang and Bernhardt, 2015).

1.3.16 FtsEX

Genes for FtsE and FtsX are organised in an operon and these two proteins form a complex, an ABC-type transporter (Gill et al., 1986; de Leeuw et al., 1999). FtsX is an integral membrane protein consisting of four transmembrane domains, which anchors an ATP-binding protein, FtsE to the membrane (Gill et al., 1986; de Leeuw et al., 1999; Arends et al., 2009). FtsE and FtsX are considered as division proteins stabilising Z-rings at low salt concentration and osmotic conditions, as *E. coli* mutants lacking *ftsEX* could be rescued in rich-media (Gill et al., 1986; Schmidt et al., 2004; Reddy, 2007). Moreover FtsEX, like other cell division components, localises to the midcell and requires FtsZ, ZipA and FtsA for recruitment (Schmidt et al., 2004). It does not depend on FtsQ, FtsL or FtsI, suggesting that FtsEX localises after FtsZ, FtsA and ZipA but before other downstream proteins (Schmidt et al., 2004). Furthermore, immunoprecipitation and two-hybrid experiments revealed that FtsE binds FtsZ, while FtsX interacts with FtsA and FtsQ (Karimova et al., 2005; Corbin et al., 2007). FtsX localises to the septum in cells lacking FtsE, indicating that FtsX directs the FtsEX complex to the division site (Arends et al., 2009). In an FtsE mutant with the ATP binding site inactivated the Z-ring formation occurs (Arends et al., 2009). Constriction of the Z-ring is not as efficient as in wild type *E. coli* cells, implying that FtsEX utilises ATP to stimulate the Z-ring constriction (Arends et al., 2009).

More recent studies suggested that although FtsEX does not necessarily need to be involved in cell division it regulates the activity of peptidoglycan hydrolases (Sham et al., 2011, 2013; Yang et al., 2011; Meisner et al., 2013; Bartual et al., 2014; Mavrici et al., 2014). In *E. coli*, peptidoglycan hydrolysis is facilitated by three amidases AmiA, AmiB and AmiC, which activities are controlled by EnvC (Uehara et al., 2010). Both functional, and ATPase defective, FtsEX recruit EnvC to the midcell, although the mutant fails to separate, indicating that the activity of amidases is repressed (Yang et al., 2011). A similar situation was observed in *S. pneumoniae* and *M. tuberculosis,* which did not recruit their peptidoglycan hydrolases, PcsB and RipC, respectively, to the septum upon mutations in *ftsEX* (Sham et al., 2011, 2013; Bartual et al., 2014;

Mavrici et al., 2014). Interestingly, in *B. subtilis* FtsEX was shown to have two functions, in cell elongation and sporulation (Garti-Levi et al., 2008; Meisner et al., 2013). In vegetatively growing *B. subtilis* FtsEX activates ClwO, which cleaves peptide cross bridges in elongating cells and has a coiled-coil domain similar to ones found in PcsB and EnvC (Meisner et al., 2013). Additionally, FtsEX is needed to initiate sporulation in *B. subtilis* (Garti-Levi et al., 2008). In its absence, cells enter sporulation with a delay and place a sporulation septum in the cell centre instead of the cell poles (Garti-Levi et al., 2008). Based on the studies in different bacterial species it has been proposed that FtsEX may couple peptidoglycan hydrolysis and remodelling with cell division machinery by modulating peptidoglycan hydrolyses activities through conformational changes induced by FtsEX ATP binding/hydrolysis (Sham et al., 2011; Yang et al., 2011; Bartual et al., 2014; Mavrici et al., 2014).

1.3.17 Penicillin binding proteins

Penicillin binding proteins (PBPs) are involved in the final steps of peptidoglycan synthesis (Typas et al., 2012; Pinho et al., 2013). PBPs are classified into two main groups of high molecular weight (HMW) and low molecular weight (LMW) PBPs. HMW falls into two classes, A of bifunctional enzymes and B of monofunctional enzymes (Goffin and Ghuysen, 1998; Sauvage et al., 2008). Class A HMW PBPs have an N-terminal cytoplasmic tail, a hydrophobic transmembrane domain and a large periplasmic domain, which can be further subdivided into an N-terminal transglycosylase activity domain and a C-terminal transpeptidase activity domain (Goffin and Ghuysen, 1998; Sauvage et al., 2008). Class B HMW PBPs also have a large periplasmic C-terminus, which C-terminal domain has a transpeptidase activity, while the N-terminal domain has an unknown function (Goffin and Ghuysen, 1998; Sauvage et al., 2008). It has been suggested that the N-terminal domain of HMW PBPs class B could acts as a chaperone required for proper folding of the transpeptidase domain or be involved in interaction with other proteins, including cell division components (Goffin et al., 1996; Höltje, 1998; Sauvage et al., 2008). LMW PBPs usually have either a carboxypeptidase or endopeptidase activity and are often either anchored to the membrane via their C-terminus or are soluble (Sauvage et al., 2008).

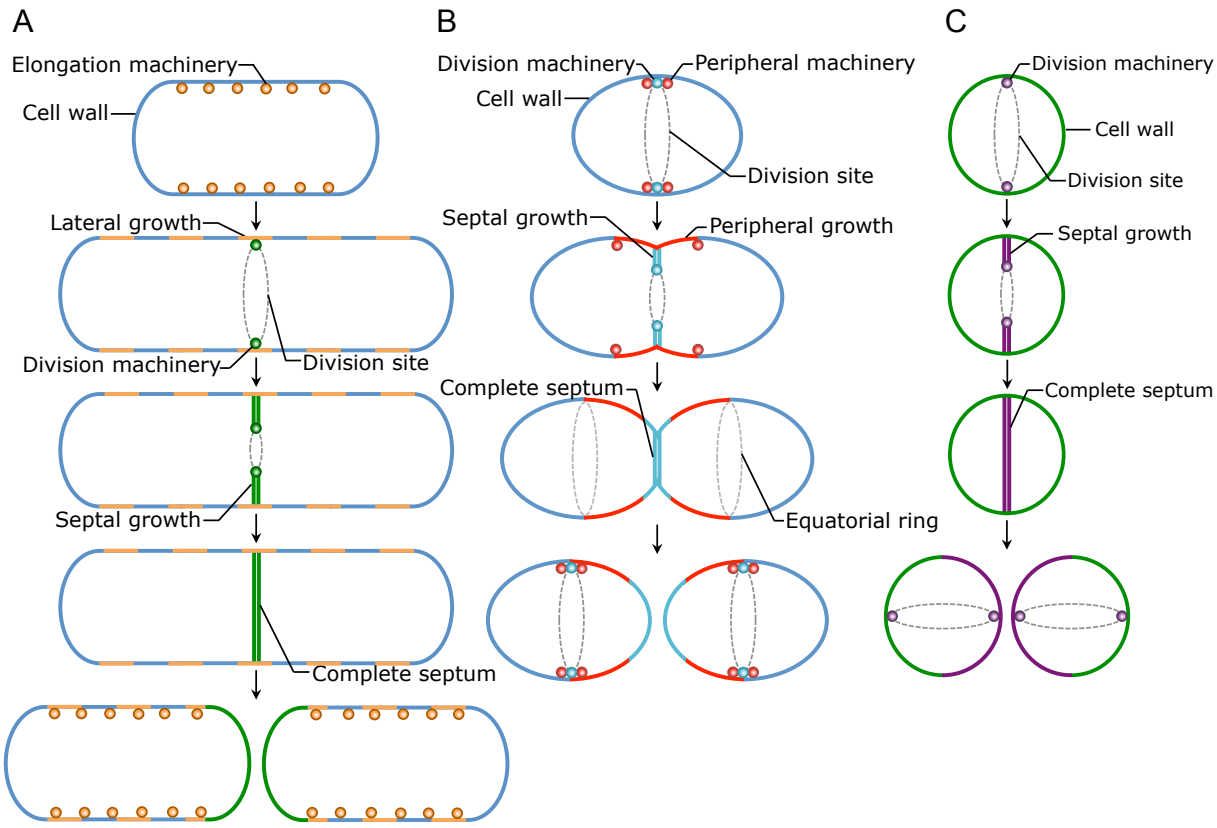

Figure 1.7. Cell wall assembly in Gram-positive rods, ovococci and cocci

A. Schematic representations of cell wall assembly in Gram-positive rod-shaped bacteria (e.g., *B. subtilis*). Rod-shaped bacteria elongate by insertion of peptidoglycan (yellow) within the old cell wall (blue), which is directed by lateral peptidoglycan synthesis machinery (yellow spheres). Cell divides by placing a septum (green) in the midcell, this is driven by a septal peptidoglycan synthesis machinery (green spheres). The daughter cells separate and initiate elongation. Adapted from (Daniel and Errington, 2003).

B. Schematic representations of cell wall assembly in Gram-positive ovococci (e.g., *S. pneumoniae*). Peripheral peptidoglycan (red) synthesis (catalysed by peripheral peptidoglycan synthesis machinery, red spheres) occurs between current and future (equatorial rings) division sites, simultaneously the septal peptidoglycan (light blue) synthesis (catalysed by septal peptidoglycan synthesis machinery, light blue spheres) occurs at the division site. Together peripheral and septal peptidoglycan synthesis modes lead to cell elongation and division. Adapted from (Pinho et al., 2013).

C. Schematic representations of cell wall assembly in Gram-positive cocci (e.g., *S. aureus*). In cocci peptidoglycan is mostly synthesised at the septum (purple) by apparently one peptidoglycan synthesis machinery (purple spheres). The complete septum becomes a new cell wall hemisphere in the daughter cells. Adapted from (Pinho et al., 2013).

The number of PBPs is diverse amongst bacterial species. *B. subtilis* and *E. coli* have 16 and 12 PBPs, respectively, whereas *S. pneumoniae* has 6 and *S. aureus* 4 (Zapun et al., 2008b; Pinho et al., 2013). Bacteria have different shapes and modes of growth, therefore this might be reflected in the amount of PBPs. *B. subtilis* and *E. coli* are rod-shape bacteria and have two modes of growth: elongation and septation (Figure 1.7A) (Zapun et al., 2008b; Typas et al., 2012; Pinho et al., 2013). In ovococcal *S. pneumoniae* cell growth and division are considered to occur concurrently (Figure 1.7B), however it is not understood if one or two separate peptidoglycan biosynthesis machineries drive these processes (Sham et al., 2012; Pinho et al., 2013). *S. aureus* is a coccus and does not elongate, hence the peptidoglycan is thought to be mainly synthesised during division septum formation (Figure 1.7C) (Pinho et al., 2013).

S. aureus encodes PBP2, which is the only PBP that has both transglycosylase and transpeptidase activities, and deletion of this enzyme is lethal to *S. aureus* (Pinho et al., 2001a, 2013). In *S. pneumoniae*, which produces three PBPs classified as HMW PBPs class A, the presence of only one bifunctional PBP, either PBP1A or PBP2A, is essential for viability (Hoskins et al., 1999). Interestingly, in other organisms, such as *B. subtilis, Enterococcus faecalis* and *Enterococcus faecium* none of the class A PBPs is required for cells to survive (McPherson and Popham, 2003; Arbeloa et al., 2004; Rice et al., 2009).

In *E. coli*, two class B HMW PBPs, FtsI (PBP3) and PBP2 are mainly involved in cell division and maintaining cell shape, respectively (Nanninga, 1998). Mutations in PBP2 result in a spherical phenotype, while cells with altered FtsI do not divide and form filaments (Spratt, 1975, 1977). In *B. subtilis*, depletion of the *E. coli* FtsI homologue, PBP2B, blocks cells division, leads to formation of filamentous cells and subsequent cell death (Daniel et al., 1996, 2000). PBP1, a homolog of *E. coli* FtsI, is essential for growth of *S. aureus* (Pereira et al., 2007). The *ftsI* gene is located in the *dcw* cluster of genes encoding cell division and peptidoglycan synthesis proteins (Yanouri et al., 1993; Vicente et al., 1998; Tamames et al., 2001). FtsI is an essential protein for cell division in *E. coli* (Spratt, 1975). Immunofluorescence studies and utilisation of fluorescent protein fusions showed that the localisation of FtsI in the septum occurs at the late stages of division and this depends on FtsZ, FtsA, FtsK, FtsQ, FtsL and FtsW (Weiss et al., 1999; Chen and Beckwith, 2001; Mercer and Weiss, 2002). Two-hybrid analysis

revealed that FtsI interacts directly with FtsA, FtsQ, FtsN and FtsW and its staphylococcal homologue additionally interacts with EzrA, FtsL and DivIC (Di Lallo et al., 2003; Karimova et al., 2005; Steele et al., 2011).

FtsI is a bitopic membrane protein with a short cytoplasmic N-terminal tail, a single transmembrane helix and a large periplasmic C-terminal domain (Bowler and Spratt, 1989; Sauvage et al., 2014). The C-terminus binds peptidoglycan and has a transpeptidase domain of a fold characteristic for this class of PBP (Fraipont et al., 1994; Sauvage et al., 2014). Mutagenesis studies of the non-penicillin binding periplasmic domain, suggested that it may be involved in proper folding of the catalytic domain and in the recruitment of FtsI (Marrec-Fairley et al., 2000). Nevertheless another study showed that the transmembrane helix was sufficient for FtsI localisation to the septal ring (Wissel et al., 2005).

1.4 Peptidoglycan in *Staphylococcus aureus*

Penicillin binding proteins (PBPs) mediate insertion of the new peptidoglycan, the major structural polymer in the cell wall (Scheffers and Pinho, 2005; Typas et al., 2012). The cell wall is an essential bacterial component that maintains the cell integrity and shape, and serves as a barrier and an interface between the bacterium and environment (Scheffers and Pinho, 2005). *S. aureus* is surrounded by a layer of peptidoglycan that is 20-35 nm thick (Vollmer and Seligman, 2010).

Peptidoglycan consists of glycan chains cross-linked via short peptide stems (Vollmer, 2008). The glycan strands are made of alternating *N*-acetylglucosamine (Glc*N*Ac) and *N*-acetylmuramic acid (Mur*N*Ac) units linked by β-1,4 glycosidic bonds (Vollmer, 2008). The composition of the glycan strands is conserved, although their lengths vary between bacterial species (Scheffers and Pinho, 2005). *S. aureus* forms relatively short polymers comprising ~6 disaccharide Glc*N*Ac-Mur*N*Ac units (Vollmer, 2008). In *S. aureus* the peptide stem consists of L-alanine, D-glutamine, L-lysine and a D-alanyl-D-alanine moiety and the pentapeptide is covalently attached to the lactyl group of the Mur*N*Ac residue (Vollmer, 2008; Pinho et al., 2013). The cross-linking of glycan chains occurs between L-Lys at the position 3 on one side chain and D-Ala at the position 4 on the other chain through a pentaglycine bridge (Vollmer, 2008; Pinho et al., 2013).

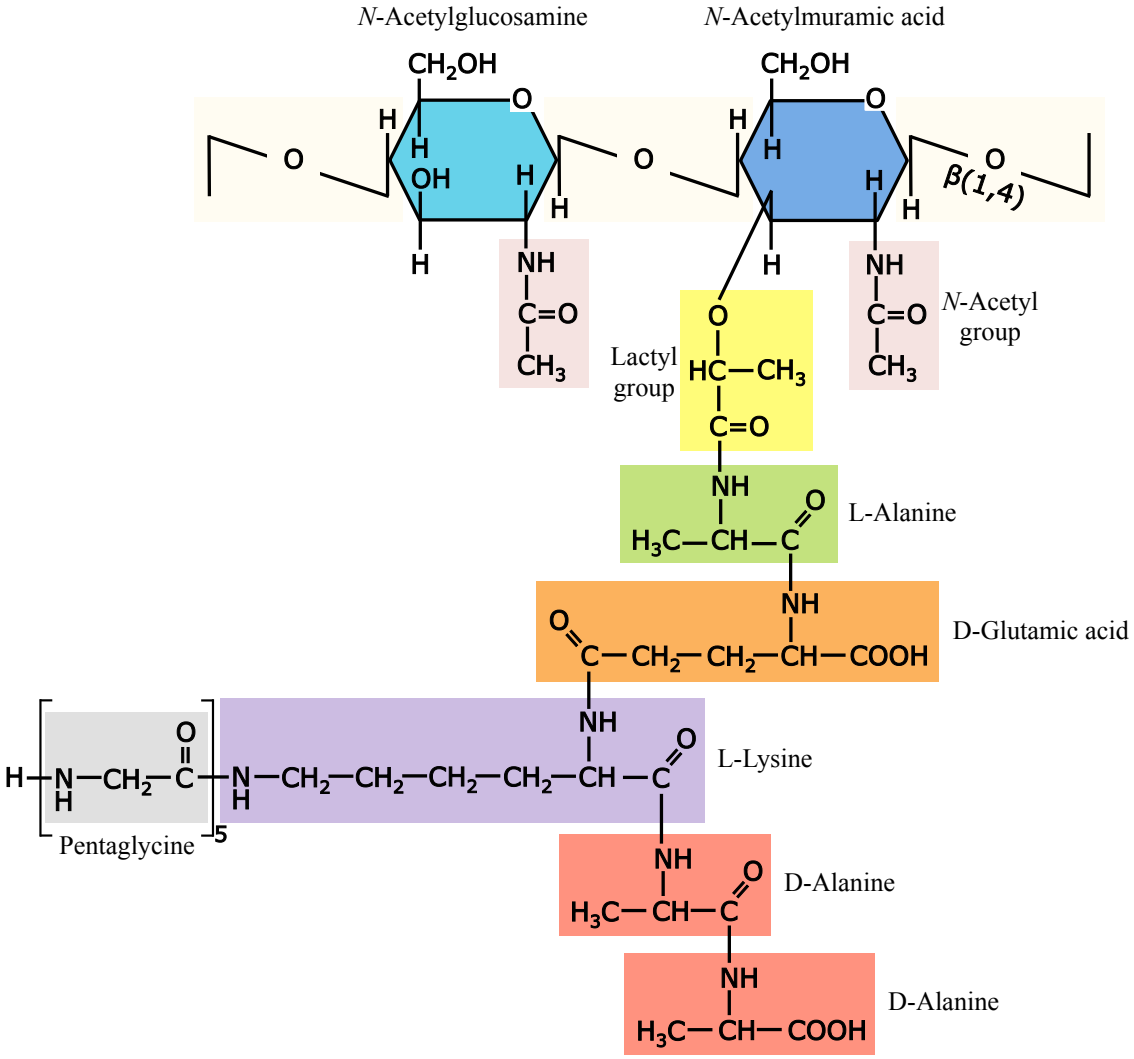

Figure 1.8. The chemical structure of peptidoglycan in *S. aureus*

The figure presents the structure of one peptidoglycan disaccharide pentapeptide. The disaccharide unit is composed of *N*-acetylglucosamine and *N*-acetylmuramic acid residues and the side stem peptide is covalently linked to the glycan polymer via the lactyl group of *N*-acetylmuramic acid. A pentaglycine bridge is attached to L-lysine present at the position 3 on the side chain. Adapted from (Madigan et al., 2002; Fournier and Philpott, 2005)

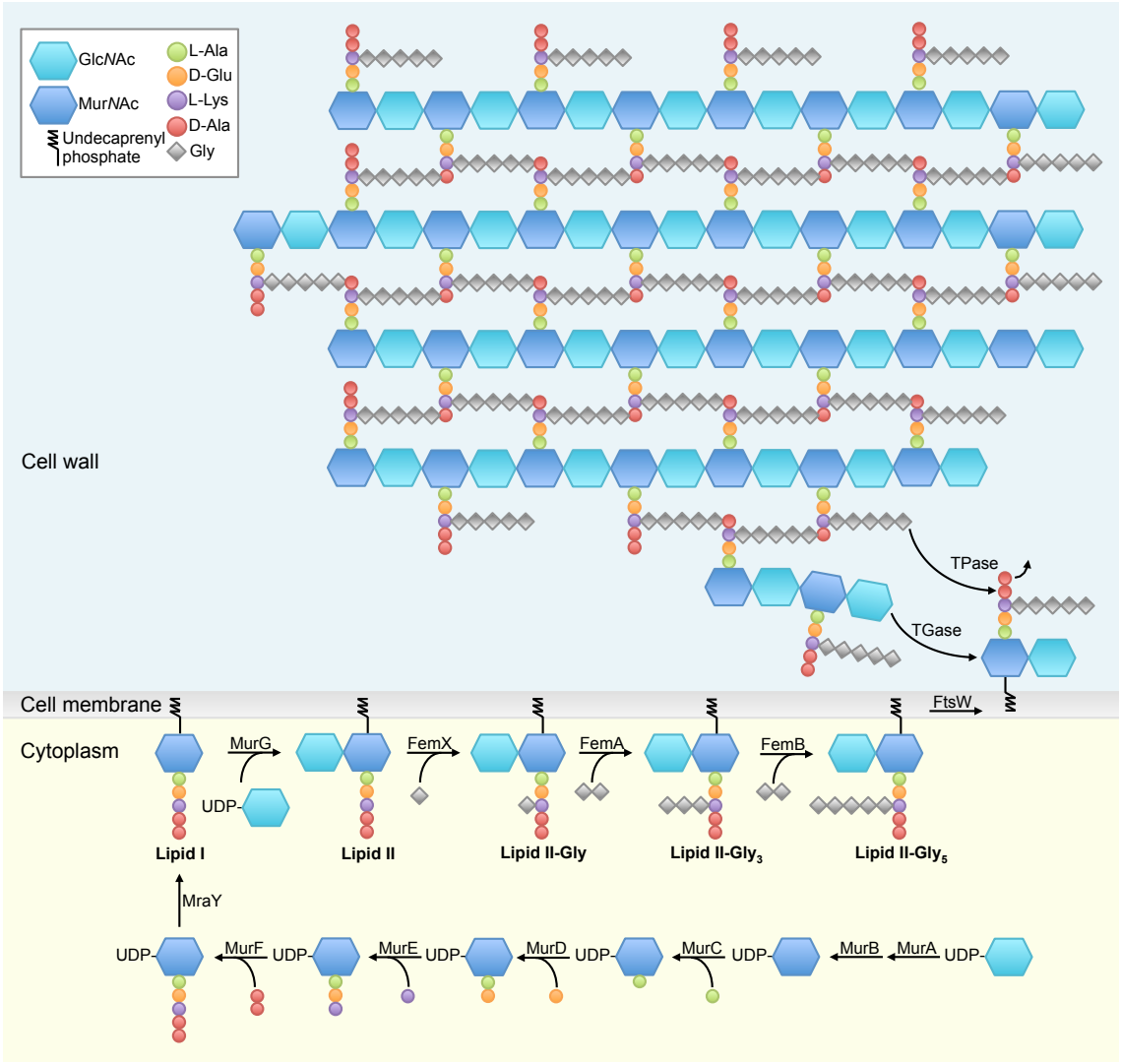

Figure 1.9. Peptidoglycan synthesis in *S. aureus*

The peptidoglycan precursor, lipid II is synthesised on the inner side of the cell membrane, transported across the cell membrane by a flippase (probably FtsW). At the external side of the cell membrane PBPs, which have transglycosylase (TGase) and transpeptidase (TPase) activities, catalyse incorporation of lipid II into nascent peptidoglycan. Adapted from (Typas et al., 2012; Pinho et al., 2013).

A degree of cross-linking is quite high in *S. aureus* since from 74% to 92% of peptidoglycan is cross-linked (Vollmer, 2008). The chemical structure of *S. aureus* peptidoglycan is presented in Figure 1.8.

Peptidoglycan synthesis can be generally described as a process occurring in three steps, each step takes place in a different cell location, summarised in Figure 1.9. In the first step in the cytoplasm, the first peptidoglycan precursor UDP-*N*-acetylglucosamine (UDP-Glc*N*Ac) is synthesised from fructose-6-phosphate. UDP-Glc*N*Ac is converted into UDP-*N*-acetylmuramic acid (UDP-Mur*N*Ac), to which amino acids are subsequently added by Mur ligases, resulting in UDP-Mur*N*Ac-pentapeptide. In the second step, UDP-Mur*N*Ac-pentapeptide is linked to undecaprenyl phosphate, the transport lipid to form lipid I. Glc*N*Ac from UDP-Glc*N*Ac is then added to lipid I leading to lipid II formation. FemABX-like proteins catalyse addition of a pentaglycine bridge to the L-lysine residue, which is in the 3rd position in the side chain. Lipid II is translocated across the cell membrane by the flippase (FtsW). In the last stage penicillin binding proteins (PBPs) catalyse polymerisation of lipid II into nascent peptidoglycan by transglycosylation and transpeptidation reactions (Typas et al., 2012; Pinho et al., 2013).

1.5 Super-resolution microscopy in bacterial cell division studies

Fluorescence microscopy is a widely used tool for visualisation of cell structures, observation of cellular processes and tracking proteins in bacterial cells. The advantage of fluorescence microscopy is that it is a non-invasive method, which allows for specific labelling and thus direct imaging of particular cell components in both live and fixed cells (Fernández-Suárez and Ting, 2008).

For a long time bacterial cells were considered as a mere sac filled with cytosol lacking any organisation, as no defined cytoskeleton structures could be identified by conventional light microscopy or electron microscopy (Coltharp and Xiao, 2012; Rowlett and Margolin, 2015a). Utilisation of immunolabelling and GFP to tag and selectively label bacterial proteins brought breakthroughs in studies on bacterial cell division and revealed that in fact bacterial cells present a high degree of intracellular organisation, similarly to eukaryotic cells (Harry et al., 1995; Webb et al., 1995;

Rowlett and Margolin, 2015a). First fluorescence microscopy imaging of FtsZ, a structural homologue of tubulin, showed that this key protein localises to the cell midcell where it forms a ring-like structure (Harry et al., 1995; Addinall et al., 1996; Ma et al., 1996; Erickson, 1997). Moreover, conventional fluorescence microscopy studies showed that many other cell division components, such as FtsA and ZipA are like FtsZ recruited to the division site and the presence of one component determines localisation of the other one (Addinall and Lutkenhaus, 1996; Hale and de Boer, 1999). It also revealed that roles of protein homologues can vary between different bacterial species, which is manifested by their distinct localisation patterns in different organisms. For example in *B. subtilis* DivIB localises to the midcell, while in *S. aureus* it only transiently locates to the division site and mostly to the cell periphery (Harry and Wake, 1997; Bottomley et al., 2014). Furthermore, fluorescence microscopy was used to study dynamics of cell division components. In *E. coli* FtsZ was found to localise early to the midcell, before any sign of constriction could be observed, and to leave the division site and thus other divisome proteins prior to completion of septum formation (Sun and Margolin, 1998; Söderström et al., 2014). Additionally, it has been shown by FRAP experiments that the Z-ring is not a static structure but highly dynamic with an 8-9 s half time of recovery after photobleaching (Anderson et al., 2004).

Fluorescence microscopy, as any other technique, has its limitations. It is based on light microscopy therefore its resolution is limited to ~200 nm due to the diffraction limit (Fernández-Suárez and Ting, 2008; Coltharp and Xiao, 2012). This means that in conventional fluorescence microscopy two objects located 200 nm apart or less are not resolvable as their point spread functions (PSF) overlap (Fernández-Suárez and Ting, 2008; Coltharp and Xiao, 2012). Many bacterial cells are only 1-5 μm in size and because of the diffraction limit their fine cellular features are not resolvable by conventional fluorescence microscopy (Fernández-Suárez and Ting, 2008). Over the last few years several super-resolution microscopy techniques that circumvent the diffraction limit have been developed and employed to study details of bacterial cell structures.

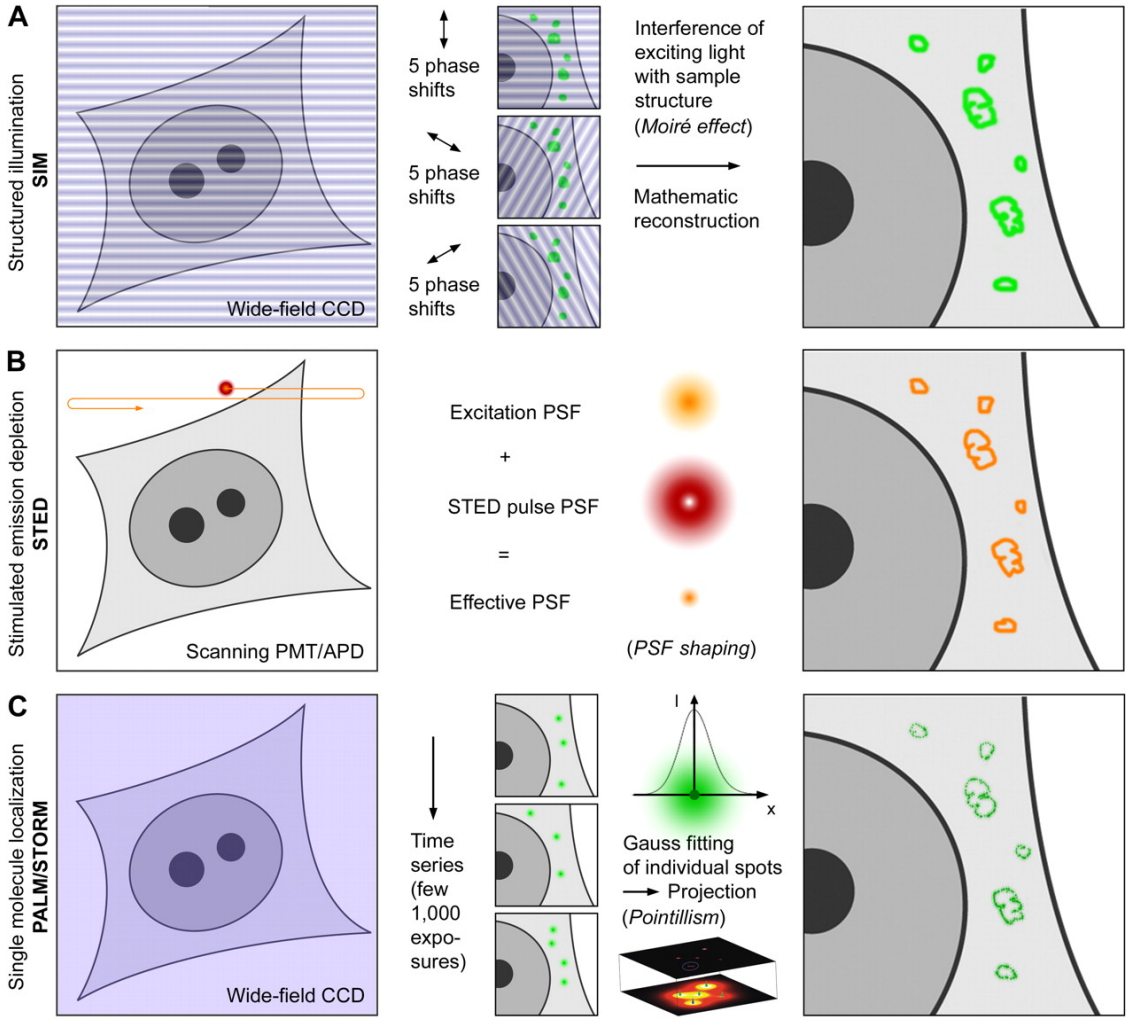

Figure 1.10. Principles of super-resolution microscopy techniques (Reproduced from Schermelleh et al., 2010)

A. In SIM the sample is illuminated through an optical grating, which generates an interface pattern, called moiré fringes. A mathematical reconstruction extracts information about the sample structure.

B. In STED microscopy the sample is scanned by two lasers, excitation and depletion (STED) beams. The first laser beam activates the fluorophores, whereas the second doughnut-shaped one puts the fluorophores from the periphery back to the ground state. Molecules that are in the centre of the illuminated spot stay fluorescent and are imaged.

C. In single-molecule localization microscopy (PALM, STORM) only a small subset of fluorophores is activated allowing for their spatial and temporal separation. Optically resolvable molecules are detected, localised and switched off. The same steps are repeated thousand times and positions of imaged molecules are used to reconstruct an image.

1.5.1 Stimulated emission-depletion microscopy

Stimulated emission-depletion (STED) microscopy is the earliest developed super-resolution technique (Hell and Wichmann, 1994; Coltharp and Xiao, 2012). In STED microscopy high resolution is achieved by narrowing the PSF (Hell and Wichmann, 1994; Fernández-Suárez and Ting, 2008). In this technique two laser beams are used to scan the sample; an excitation laser activates fluorophores, while the depletion (STED) laser, which is a red-shifted doughnut-shaped beam, deactivates fluorescence from molecules located in the periphery of the excited spot. The molecules that are in the centre of the imaged spot remain activated and can be detected (Figure 1.10B) (Hell and Wichmann, 1994; Coltharp and Xiao, 2012). STED microscopy can achieve a resolution of ~35 in all three dimensions, respectively (Klar et al., 2000; Willig et al., 2007; Schmidt et al., 2009) and in specific cases even a lateral resolution of 6 nm has been demonstrated (Rittweger et al., 2009). Resolution of this technique depends on the intensity of the depletion beam laser: the higher laser intensity, the smaller diameter of the PSF, the higher resolution. Therefore resolution of STED microscopy is limited by photostability of utilised fluorophores (Hell and Wichmann, 1994; Fernández-Suárez and Ting, 2008).

STED, in contrast to the other high-resolution methods described below, is a relatively rarely applied microscopy technique in studying bacteria (Coltharp and Xiao, 2012; Tuson and Biteen, 2015). Using immunostaining combined with STED microscopy Jennings et al. (2011) showed that additionally to the midcell Z-ring, FtsZ forms a discontinuous helical structure along the long axis of *B. subtilis* cells (Jennings et al., 2011). In *B. subtilis* MreB filaments were resolved as double helices that span the length of the cell (Grotjohann et al., 2011). Moreover, they were revealed as discontinuous and highly dynamic structures, ~ 3 μm long (Reimold et al., 2013).

1.5.2 Structured-illumination microscopy

In structured illumination microscopy (SIM) a grid pattern is superimposed against the sample, generating an interface pattern, called moiré fringes (Gustafsson, 2000; Coltharp and Xiao, 2012). The information about the sample structure can be calculated as the three patterns: the grid, the sample and the moiré fringes are mathematically

related. If the spatial frequencies of the yielded interface pattern and the grid pattern are known the subdiffraction image of the sample can be extracted by a Fourier transformation (Figure 1.10A) (Gustafsson, 2000; Coltharp and Xiao, 2012). SIM increases resolution to 100 nm and 250 nm in lateral and axial dimensions, respectively (Gustafsson, 2000; MacDonald et al., 2015). The advantage of SIM is that it does not require fluorophores with any special photophysical properties, therefore commonly used fluorescent proteins, such as GFP can be employed (Schermelleh et al., 2010). However the imaging process requires the sample to be illuminated in different spacing and rotation angles of the illumination grid, so that a high-resolution image can be generated. The fluorescent probe is exposed to extensive photobleaching, therefore bright and photostable fluorophores are required (Schermelleh et al., 2010; Coltharp and Xiao, 2012).

SIM is the most often employed microscopy technique in bacterial cell division studies. Using this technique it was shown that while in *B. subtilis* FtsZ is a single ring structure the components of the Min system, DivIVA and MinJ form two rings that flank the Z-ring (Eswaramoorthy et al., 2011). Moreover, fusing FtsZ with GFP revealed that both in *B. subtilis* and *S. aureus* the Z-ring is not a uniform structure but consists of 'beads' heterogeneously distributed around division site (Strauss et al., 2012). Live SIM imaging also confirmed previous observations from FRAP experiments, showing that the FtsZ ring is a very dynamic structure under constant remodelling (Anderson et al., 2004; Strauss et al., 2012). The uneven distribution of FtsZ, FtsA and ZipA was reported in *E. coli* and although these crucial division proteins localise together to the division site, their heterogeneous patterns do not always overlap (Rowlett and Margolin, 2014). Wheeler et al. (2011) by using fluorescently labelled vancomycin showed that *E. faecalis*, *S. pneumoniae* and *Lactococcus lactis* have unique peptidoglycan architecture and even though they are classified to ovococcal bacteria, each species has a distinct mode of peptidoglycan synthesis (Wheeler et al., 2011). 3D-SIM combined with immunostaining and fluorescent fusion proteins revealed that in *S. pneumoniae* PBP1A and PBP2x localise to the division site, where they form rings of a larger diameter than FtsZ and wrap the Z-ring around (Tsui et al., 2014). Additionally, PBP1A and PBP2x were shown to separate at a certain point of the cell cycle, indicating different roles of these PBPs in peptidoglycan synthesis during septum formation (Tsui et al., 2014). Furthermore, 3D-SIM was recently used to characterise localisation of the

newly identified FtsZ positioning regulator, MapZ (Fleurie et al., 2014a). In *S. pneumoniae* MapZ localises to the division site before FtsZ and splits into two equatorial rings that are moved to the next division sites by growing nascent peptidoglycan (Fleurie et al., 2014a).

1.5.3 Single-molecule localisation microscopy

Stochastic optical reconstruction microscopy (STORM), photoactivated localisation microscopy (PALM) and fluorescence photoactivated localisation microscopy (FPALM), although these three methods differ due to the nature of originally used fluorescent probes, they all rely on the same concept of locating positions of single molecules by utilisation of photoswitchable fluorophores that can switch between on (fluorescent) and off (dark) states (Rust et al., 2006; Betzig et al., 2006; Hess et al., 2006). STORM primarily employed organic dyes, such as Cy3 and Cy5, while PALM and FPALM were developed using fluorescent proteins (Rust et al., 2006; Betzig et al., 2006; Hess et al., 2006). The general principle of STORM/PALM is to activate only a small subset of fluorophores at any given time so they become temporally and spatially resolvable. PALM/STORM imaging consists of many imaging cycles and in each cycle single molecules are activated, imaged, localised and switched off. Positions of fluorophores are then used to reconstruct a high-resolution image (Figure 1.10C) (Betzig et al., 2006; Rust et al., 2006; Fernández-Suárez and Ting, 2008). Currently STORM/PALM reaches a spatial resolution of 20 nm and 50 nm in the lateral and axial dimensions, respectively (Betzig et al., 2006; Rust et al., 2006; Fernández-Suárez and Ting, 2008). STORM/PALM relies on photoswitchable fluorophores, which in a light-controllable manner can be activated to a fluorescent state and when their positions has been recorded they turn off or irreversibly photobleach. The STORM/PALM localisation precision depends on the number of collected photons. Therefore the fluorescent probe has to be bright, which is determined by a large quantum yield and a high extinction coefficient (Fernández-Suárez and Ting, 2008). Moreover, the fluorophore should display a high contrast ratio, that is a ratio between the number of photons emitted in the ‘on’ state and the number of photons emitted in the ‘off’ state (Fernández-Suárez and Ting, 2008).

PALM imaging of FtsZ-mEos2 revealed that in *E. coli* the Z-ring is a compressed helical structure composed of a loose bundle of FtsZ protofilaments that randomly overlap with each other along longitudinal and radial directions of the cell (Fu et al., 2010). The non-homogeneous and thick structure of the Z-ring was observed by PALM of FtsZ-Dendra2 in *C. crescentus* (Holden et al., 2014). Additionally, this heterogeneous ring was shown to change its size with the progress of cell division, starting from a ring of ~550 nm in diameter, contracting to a ~350 nm ring and finishing as a 100-200 nm spot at the end of the cell division cycle (Holden et al., 2014). Fusing MreB with eYFP revealed that in *C. crescentus* MreB adopts different spatial structures depending on the stage of cell growth; it has a helical structure in the early stage of the cell cycle and a ring-like structure in the later stages (Biteen et al., 2008). In *B. subtilis*, SpoIIIE, which is an FtsK homologue, translocates DNA through the sporulation septum to formed prespore (Wu and Errington, 1994). PALM of SpoIIIE-tdEos2 showed that the transmembrane domain of SpoIIIE can mediate its localisation to the division site during sporulation and the assembly into the DNA translocating complex occurs in a few steps (Fleming et al., 2010). Recently, STORM accompanied with atomic force microscopy and fluorescence microscopy was applied to develop a novel model of cell wall elongation in Gram-negative bacteria. It was shown that in *E. coli* and *C. crescentus* insertion of peptidoglycan occurs in multiple distinct foci spread over the cell surface (Turner et al., 2013). Finally, PALM colocalisation studies revealed differences in distribution of FtsZ, ZapA and ZapB against the cell membrane and MatP, a chromosome partitioning protein (Buss et al., 2015). The distribution variations indicate that these three proteins may form a network that extends from the membrane to the chromosome to connect and coordinate chromosome segregation with cell division (Buss et al., 2015).

1.6 *Staphylococcus aureus*

Staphylococcus aureus was first identified and characterised in the 19th century by a Scottish surgeon, Sir Alexander Ogston (Archer, 1998). *S. aureus* is a Gram-positive, non-spore forming bacterium of a low GC content (Harris et al., 2002; Baba et al., 2008). It is an apparent spherical coccus, which divides in three orthogonal planes and is ~1 μm in diameter (Tzagoloff and Novick, 1977). It is an opportunistic human and animal pathogen and is a part of the normal flora, found in the nose, respiratory tract and on the skin, although in favourable conditions it can cause disease (Lowy, 1998).

1.6.1 *Staphylococcus aureus* infections

S. aureus is a major cause of nosocomial and community associated infections. It is estimated that from 10% to 20% of the human population are long-term carriers and 30% are transient carriers (Lowy, 1998). *S. aureus* is able to colonise almost all tissues and organs. In favourable circumstances such as a breach of the skin, mucosal barrier or immune deficiency, it can cause a wide range of infections (Archer, 1998). Patients suffering from type I diabetes, cancer, circulatory system diseases, surgical patients and intravenous drug users are at increased risk for staphylococcal diseases (Archer, 1998; Lowy, 1998). *S. aureus* causes minor local skin infections such as boils, acne, scalded skin syndrome (SSS) and serious diseases such as pneumonia, meningitis, sepsis, urinary tract infections, osteomyelitis and endocarditis. SSS, toxic shock syndrome (TSS) and staphylococcal food poisoning result from staphylococcal toxins (Archer, 1998).

The average size of *S. aureus* genome is approximately 2.8 Mbp (Kuroda et al., 2001; Baba et al., 2008). Sequencing of genomes of several *S. aureus* strains revealed that although most of the genome regions are highly conserved there are many sequence regions that vary between staphylococcal strains (Kuroda et al., 2001; Baba et al., 2008). These variable regions often contain antibiotic resistance cassettes and virulence factors that were exogenously acquired through horizontal gene transfer (Kuroda et al., 2001; Baba et al., 2008; Malachowa and DeLeo, 2010; Stefani et al., 2012). This shows that *S. aureus* can relatively easily adapt to changing environmental conditions in order to grow and survive.

1.6.2 *Staphylococcus aureus* virulence factors

S aureus can cause such a broad range of infections due to its ability to produce a vast variety of virulence factors. The coordinated action of virulence factors rather than a single one are responsible for *S. aureus* colonisation and infection abilities (Peacock et al., 2002) The virulence factors include cell-surface components, capsular polysaccharides, toxins, enzymes and superantigens. Expression of the determinants allows *S. aureus* to attach to extracellular matrix and cells, avoid immune system responses, reduce phagocytosis, penetrate tissues and spread infections (Gordon and Lowy, 2008).

S. aureus produces two types of adhesins: microbial surface components recognising adhesive matrix molecules (MSCRAMMs) that are covalently bound to the peptidoglycan and secretable expanded repertoire adhesive molecules (SERAMs). Adhesins promote attachment of bacteria to the extracellular matrix and the cell surface of the host (Clarke and Foster, 2006). Protein A (Spa) belongs to the MSCRAMMs, and despite its adhesion function, is involved in preventing phagocytosis. It inhibits opsonisation and phagocytosis by binding the Fc region of immunoglobulin G (IgG) (Foster, 2005). Chemotaxis inhibitory protein of *S. aureus* (CHIPS) and staphylococcal complement inhibitor (SCIN) evade immune system responses by inhibiting neutrophil recruitment to the site of infection (Foster, 2005). Capsular polysaccharides form a thin layer that covers cells of *S. aureus* clinical isolates and it reduces the uptake of bacteria by neutrophils and supports bacterial survival in neutrophils (Harris et al., 2002; Foster, 2005). *S. aureus* produces several extracellular enzymes, such as nucleases, proteases, lipases, hyaluronidase and collagenase. All of them promote tissue damage and ease *S. aureus* spreading (Lowy, 1998; Foster, 2005). Among numerous toxins produced by *S. aureus* α-toxin is the best characterised one. It forms β-barrel pores in the membrane of a host cell resulting in cell leakage and lysis (Foster, 2005). Toxins, such as toxic shock syndrome toxin-1 (TSST-1), can act as superantigens. The role of superantigens is to non-specifically activate cytokine release by T-cells in order to cause host-mediated tissue damage, and to prevent and avoid immune system response (Lowy, 1998; Foster, 2005).

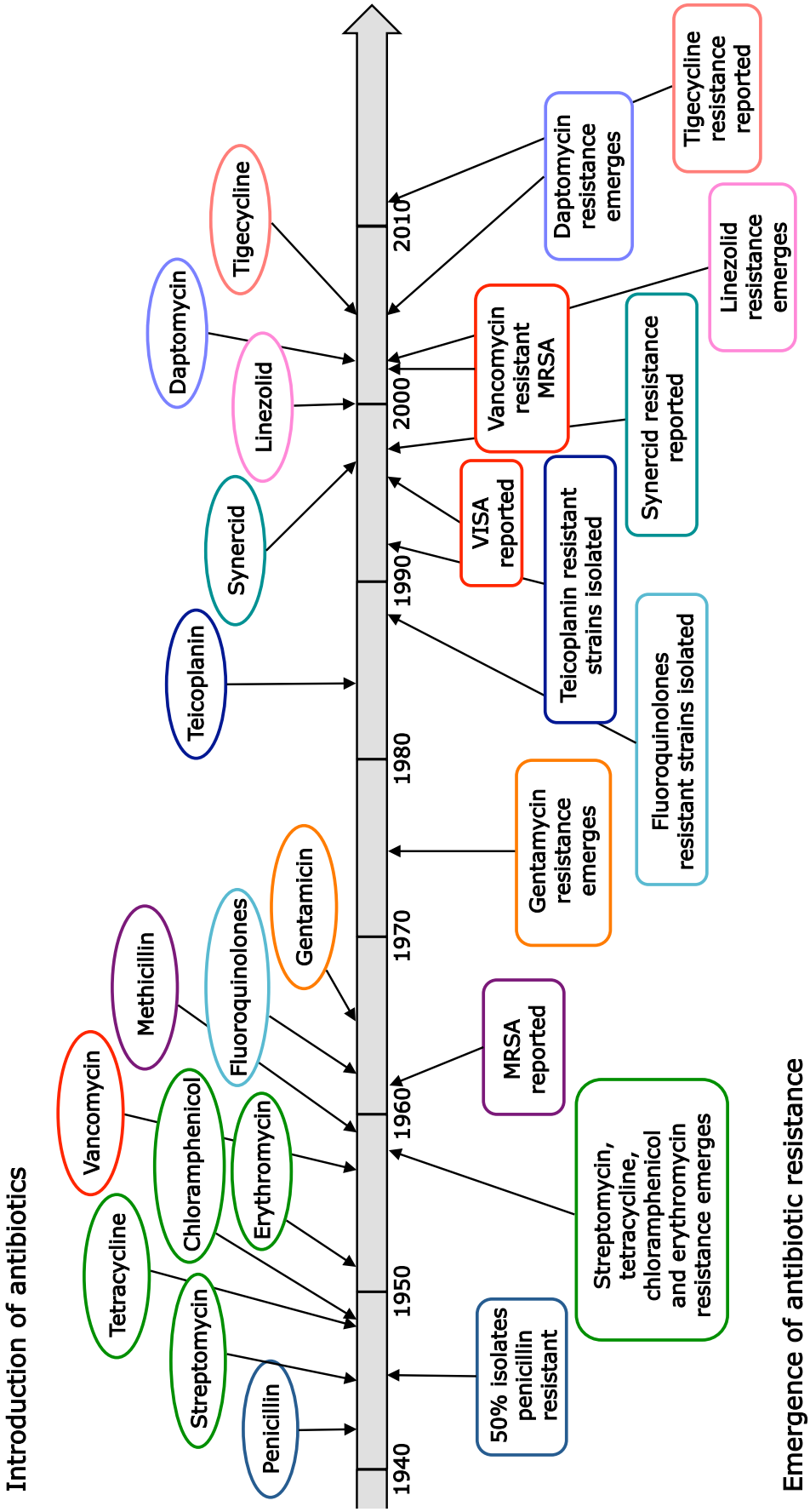

Figure 1.11. Chronology of the introduction of antibiotics and subsequent emergence of resistance in *S. aureus* (Adapted from Bottomley, 2011)

1.6.3 Antibiotic resistance of *Staphylococcus aureus*

Introduction of antibiotics allowed for reduction of mortality caused by *S. aureus* infections, which before the 'antibiotic era' was ~80% (Lowy, 2003; Dancer, 2008). However the *S. aureus* ability to develop and acquire antibiotic resistance mechanisms (Figure 1.11) means it is still a major healthcare issue. Around 30% of patients die due to *S. aureus* infections, similar to the mortality percentage just after penicillin introduction (Lowy, 2003; Dancer, 2008). Strains resistant to penicillin, an inhibitor of penicillin binding proteins, appeared within a few years after incorporation of penicillin into medical practice (Barber and Rozwadowska-Dowzenko, 1948; Lowy, 1998). Currently, more than 95% of clinical isolates have the *blaZ* gene encoding β-lactamase, which hydrolyses and inactivates the penicillin β-lactam ring (Barber and Rozwadowska-Dowzenko, 1948; Lowy, 1998). The same situation occurred for other commonly used antibiotics as tetracycline, erythromycin, chloramphenicol and streptomycin, which inhibit protein synthesis by binding ribosomes (Lacey, 1975; Kohanski et al., 2010). Soon after their introduction in 1950s *S. aureus* resistant strains that had modifications in the ribosomes, could remove antibiotics from the cell by active efflux or deactivate them through acetylation were identified (Lacey, 1975; Bismuth et al., 1990; Warsa et al., 1996; Murray and Shaw, 1997; Nicola et al., 1998). Methicillin is a semi-synthetic β-lactam that was introduced to treat infections caused by penicillin-resistant *S. aureus* in 1961. In the same year reports of methicillin-resistant *S. aureus* (MRSA) isolates were published (Barber, 1961; Lowy, 2003). Nowadays, about 60% of hospital isolates are resistant to methicillin and since late 1990s a new lineage of community-acquired MRSA has become prevalent problem (Rice, 2006; Chambers and DeLeo, 2009). Resistance to methicillin is determined by an additional penicillin binding protein, PBP2A, encoded by *mecA* that *S. aureus* has gained exogenously (Katayama et al., 2000; Lowy, 2003). PBP2A has a lower affinity toward β-lactam antibiotics and can substitute for the transpeptidase activity of PBP2, which is sufficient for *S. aureus* to survive in the presence of the antibiotic (Hartman and Tomasz, 1984; Pinho et al., 2001a; Lim and Strynadka, 2002). Gentamicin and fluoroquinolone were introduced in the 1960-1980s but again resistant strains emerged within a few years after incorporation of these antibiotics into medical practice (Porthouse et al., 1976; Naidoo and Noble, 1978; Schaefler, 1989; Ferrero et al., 1995; Ng et al., 1996). Vancomycin, which is called the last chance drug in a treatment of

MRSA infections, is a glycopeptide antibiotic that prevents peptidoglycan synthesis by binding the D-Ala-D-Ala moiety (Kohanski et al., 2010). It was released in 1958 and only in 1996 the first clinical isolate with reduced susceptibility to vancomycin (vancomycin-intermediate *S. aureus*, VISA) was identified and in 2002 the first vancomycin-resistant *S. aureus* (VRSA) was reported, all of them were also methicillin-resistant (Hiramatsu et al., 1997a; b; Weigel et al., 2003). While VISA emerged due to spontaneous adaptive mutations generated under antibiotic pressure, VRSA acquired the *vanA* gene from vancomycin-resistant *E. faecalis* through inter-species horizontal gene transfer (Sieradzki and Tomasz, 1997; Sievers et al., 2002; Gardete and Tomasz, 2014). VRSA infections are rare and only 14 cases have been reported so far (Gardete and Tomasz, 2014). Soon after the introduction of linezolid, daptomycin, synercid and tigecycline, resistant *S. aureus* have been described (Dowzicky et al., 2000; Tsiodras et al., 2001; Werner et al., 2001; Malbruny et al., 2002; Hayden et al., 2005; Hope et al., 2010). However the majority (>99%) of clinical isolates remain susceptible to these antibiotics (Marty et al., 2006; Gu et al., 2012).

1.6.4 *Staphylococcus aureus* as a cell division model

Increasing antibiotic resistance of *S. aureus* and lack of any anti-staphylococcal vaccine raises a need for the development of alternative anti-staphylococcal compounds. Cell division components are attractive targets of potential drugs since cell division is an essential process and molecules involved in bacterial cell division differ from those found in mammalian cells (Lock and Harry, 2008).

The cell division process has been extensively studied in model organisms such as Gram-negative *E. coli* and Gram-positive *B. subtilis*. Despite great interest in *S. aureus* due to its antibiotic-resistance mechanisms, the cell division process is largely unexplored in this organism. Although *S. aureus* is closely related to *B. subtilis* these two species differ in cell division and peptidoglycan synthesis modes. *B. subtilis* is a rod-shaped bacterium and therefore peptidoglycan synthesis occurs during elongation mode along the lateral cell wall and during cell division in septum formation (Daniel and Errington, 2003). *S. aureus* is a coccus that has only four PBPs and synthesises peptidoglycan mostly at midcell (Pinho and Errington, 2003). Moreover, in conditions of nutrient depletion *B. subtilis* sporulates, while *S. aureus* does not (Carballido-López

and Formstone, 2007). Therefore, it is suggested that *S. aureus* may have a different and simpler mechanism of divisome placement (Steele et al., 2011). Homologues of *B. subtilis* division machinery have been identified in *S. aureus* (Table 1.1), and although many of them were found to be essential in both organisms, some of them, such as EzrA was shown to be crucial only in *S. aureus* (Levin et al., 1999; Chaudhuri et al., 2009; Steele et al., 2011). This indicates that roles of the cell division homologues can vary between different organisms despite the sequence and structural conservation across bacterial species (Steele et al., 2011).

1.7 Aims of this study

Bacterial cell division is a fundamental process mediated by a large collection of proteins, collectively called the divisome. Although divisome components have been identified, their precise roles in *S. aureus* are not well understood. Therefore the aim of this work was to determine the arrangement and dynamics of FtsZ, EzrA and PBPs, the crucial components of the cell division machinery in *S. aureus* in order to develop a cell division model for this coccus. A combination of protein labelling and super-resolution microscopy approaches was used.

	Protein	Essentiality in *B. subtilis*	Essentiality in *S. aureus*
Early division proteins	FtsZ	Essential (Beall and Lutkenhaus, 1991)	Essential (Pinho and Errington, 2003)
	FtsA	Essential - *ftsA* mutants are viable but are defective in division and form filamentous cells, therefore FtsA is classed as essential (Beall and Lutkenhaus, 1992)	Essential (Chaudhuri et al., 2009)
	ZapA	Not essential (Gueiros-Filho and Losick, 2002)	Not essential (Chaudhuri et al., 2009)
	SepF	Not essential (Hamoen et al., 2006)	Essential (Chaudhuri et al., 2009)
	EzrA	Not essential (Levin et al., 1999; Haeusser et al., 2004)	Essential (Steele et al., 2011)
Late division proteins	FtsK	SpoIIIE - FtsK homolog essential for sporulation (Wu and Errington, 1994; Bath et al., 2000)	Essential (Chaudhuri et al., 2009)
	DivIB	Essential at elevated temperatures and for sporulation (Beall and Lutkenhaus, 1989)	Essential (Bottomley et al., 2014)
	DivIC	Essential (Levin and Losick, 1994)	Essential (Chaudhuri et al., 2009; Kabli, 2013)
	FtsL	Essential (Daniel et al., 1998)	Essential (Chaudhuri et al., 2009; Kabli, 2013)
	FtsW	Essential (Kobayashi et al., 2003)	Essential (Chaudhuri et al., 2009)
	GpsB	Not essential (Claessen et al., 2008; Tavares et al., 2008)	Essential (Chaudhuri et al., 2009)
Penicillin binding proteins	Class A PBP	PBP1 - Essential for cell growth and sporulation in divalent cation-deficient media (Murray et al., 1998)	PBP2 – Essential (Pinho et al., 2001a; b)
	Class B PBPs	PBP2B - Essential (Daniel et al., 1996)	PBP1 – Essential (Pereira et al., 2007).
		PBP2A – Not essential; does not have a role in cell division (Murray et al., 1997)	PBP3 - Not essential (Pinho et al., 2000)

Table 1.1 Conservation of cell division proteins between *B. subtilis* and *S. aureus*

CHAPTER 2

Materials and methods

2.1 Media

All media were prepared in distilled water (dH_2O) and sterilised by autoclaving for 20 min at 121°C, 103 kilopascal, unless otherwise stated.

2.1.1 Brain heart infusion (BHI)

Brain heart infusion (Oxoid)	37 g l^{-1}

2.1.2 BHI agar

Brain heart infusion (Oxoid)	37 g l^{-1}

1.5 % (w/v) Oxoid agar No. 1 was added to make BHI agar.

2.1.3 Lysogeny broth (LB)

Yeast extract (Oxoid)	10 g l^{-1}
Tryptone (Oxoid)	5 g l^{-1}
NaCl	5 g l^{-1}

2.1.4 LB agar

Yeast extract (Oxoid)	10 g l^{-1}
Tryptone (Oxoid)	5 g l^{-1}
NaCl	5 g l^{-1}

1.5% (w/v) Oxoid agar No. 1 was added to make LB agar.

2.1.5 LK

Tryptone (Oxoid)	10 g l^{-1}
Yeast extract (Oxoid)	5 g l^{-1}
KCI	7 g l^{-1}

2.1.6 LK agar

Tryptone (Oxoid)	10 g l^{-1}

Yeast extract (Oxoid) 5g l^{-1}

KCI 7 g l^{-1}

1.5 % (w/v) Oxoid agar No. 1 was added to make LK agar.

2.1.7 Baird-Parker agar

Baird-Parker agar base (Oxoid) 63 g l^{-1}

Egg yolk tellurite emulsion (Oxoid) 5% (v/v)

2.1.8 Phage agar

Casamino acids 3 g l^{-1}

Yeast extract (Oxoid) 3 g l^{-1}

NaCl 5.9 g l^{-1}

0.33% (w/v) Oxoid agar No. 1 was added to make phage top agar.

1% (w/v) Oxoid agar No. 1 was added to make phage bottom agar.

2.2 Antibiotics

Antibiotics used in this study are listed in Table 2.1. Stock solutions were filter-sterilised (0.2μm pore size) and stored at -20°C. For use in agar plates, antibiotic stock solutions were added to the media cooled to below 55°C. For use in liquid media, antibiotic stock solutions were added just before use.

Antibiotic	Stock concentration (mg ml^{-1})	*S. aureus* working concentration (μg ml^{-1})	*E. coli* working concentration (μg ml^{-1})	Solvent
Ampicillin (Amp)	100	-	100	dH_2O
Chloramphenicol (Cm)	30	10 or 30	-	95% (v/v) ethanol
Erythromycin (Ery)	5	5	-	95% (v/v) ethanol
Kanamycin (Kan)	50	50	-	dH_2O
Lincomycin (Lin)	25	25	-	50% (v/v) ethanol
Moenomycin	1	0.1-0.5	-	99.8% (v/v) methanol
Penicillin G (PenG)	100	0.01-100	-	dH_2O
Spectinomycin (Spec)	100	250	-	dH_2O
Tetracycline (Tet)	5	0.5 or 5	12.5	50% (v/v) ethanol

Table 2.1. Antibiotic stock solutions and concentrations

2.3 Bacterial strains and plasmids

2.3.1 *Staphylococcus aureus* strains

Staphylococcus aureus strains are listed in Table 2.2. Strains were taken from -80°C Microbank (Pro-lab Diagnostics) stocks. Strains were grown on BHI agar plates containing antibiotics where appropriate to maintain selection of resistance markers. For short-term storage, plates were kept for two weeks at 4°C. For long-term storage, a single colony was stocked in Microbank beads and stored at -80°C.

For liquid cultures, 10 ml medium in a sterile 25 ml universal tube was inoculated with a single colony. Unless otherwise stated, cultures were incubated at 37°C overnight on a rotary shaker at 250 rpm. The overnight culture was used to inoculate fresh medium to an OD_{600} 0.05 and then grown to exponential phase (OD_{600} 0.5-1) at 37°C on a rotary shaker at 250 rpm.

Strain	Relevant genotype/selection markers	Source
RN4220	Restriction deficient transformation recipient	(Kreiswirth et al., 1983)
SH1000	Functional *rsbU+* derivative of 8325-4	(Horsburgh et al., 2002a)
SH1000 *spa::kan* (SJF2978)	SH1000 *spa::kan*; Kan^R	Girbe Buist
SA113 *tarO::erm* (SJF2206)	SA113 *tarO::erm*; Ery^R	Andreas Peschel
SJF1332 (CYL316)	RN4220 pYL112Δ19, a plasmid carrying the L45a integrase gene; Cm^R	(Lee et al., 1991)
VF17	SH1000 pGL485; Cm^R	(Steele et al., 2011)
NE267	JE2 with Tn insertion in *sgtA* (*sgtA::Tn*); Ery^R	(Fey et al., 2013)
NE420	JE2 with Tn insertion in *pbp3* (*pbp3::Tn*); Ery^R	(Fey et al., 2013)
NE596	JE2 with Tn insertion in *mgt* (*mgt::Tn*); Ery^R	(Fey et al., 2013)
NE679	JE2 with Tn insertion in *pbp4* (*pbp4::Tn*); Ery^R	(Fey et al., 2013)
SJF4311 (NE3003)	RN4220 pSPC, a plasmid carrying the SpecR cassette for Tn allelic exchange; $Spec^R$, Cm^R	(Fey et al., 2013)
SJF4313 (NE3005)	RN4220 pTET, a plasmid carrying the TetR cassette for Tn allelic exchange; Tet^R, Cm^R	(Fey et al., 2013)
RNpGM074	RN4220 *geh::ezrA-psmorange*; Kan^R	This study
SJF3963	RN4220 *geh::ezrA-meos2*; Tet^R	This study
SJF4384	RN4220 *geh::ezrA-eyfp*; Kan^R	This study
SJF4385	RN4220 *geh::ezrA-pamcherry1*, Kan^R	This study
SJF4386	SH1000 *geh::ezrA-eyfp*; Kan^R	This study
SJF4387	SH1000 *geh::ezrA-pamcherry1*; Kan^R	This study
RNpOB-ΔezrA	RN4220 pOB-ΔezrA SCO; Ery^R, Tet^R	This study

SJF4388	SH1000 *geh::ezrA-eyfp ΔezrA::tet*; Kan^R, Tet^R	This study
SJF4389	SH1000 *geh::ezrA-pamcherry1 ΔezrA::tet*; Kan^R, Tet^R	This study
SJF4421	SH1000 *pbp3::Tn*; Ery^R	This study
SJF4422	SH1000 *pbp3::spec*; $Spec^R$	This study
SJF4423	SH1000 *pbp3::spec pbp4::Tn*; $Spec^R$, Ery^R	This study
SJF4425	SH1000 *pbp4::Tn*; Ery^R	This study
SJF4430	SH1000 *pbp1::*pMAD-PBP1*; Ery^R, Lin^R	This study
SJF4584	RN4220 *geh::ezrA-meyfp*; Kan^R	This study
SJF4589	SH1000 *pbp1::*pMAD-PBP1* *geh::*Pspac-*pbp1*; Ery^R, Lin^R, Tet^R	This study
SJF4590	SH1000 *pbp1::pbp1** *geh::*Pspac-*pbp1*; Tet^R	This study
SJF4595	SH1000 *pbp2::eyfp-pbp2*	This study
SJF4596	SH1000 *pbp2::eyfp-pbp2* pCQ11-eYFP-PBP2; Ery^R	This study
SJF4597	SH1000 pCQ11-eYFP-PBP2; Ery^R	This study
SJF4598	SH1000 *spa::kan pbp2::eyfp-pbp2*; Kan^R	This study
SJF4599	SH1000 *spa::kan* pCQ11-eYFP-PBP2; Kan^R, Ery^R	This study
SJF4600	SH1000 *spa::kan pbp2::eyfp-pbp2* pCQ11-eYFP-PBP2; Kan^R, Ery^R	This study
SJF4603	SH1000 *geh::ezrA-meyfp*; Kan^R	This study
SJF4604	SH1000 *geh::ezrA-meyfp ΔezrA::tet*; Kan^R, Tet^R	This study
SJF4605	SH1000 pCQ11-FtsZ-SNAP; Ery^R	This study
SJF4628	SH1000 *mgt::Tn*; Ery^R	This study
SJF4629	SH1000 *sgtA::Tn*; Ery^R	This study
SJF4639	SH1000 *geh::ezrA-gfp*; Kan^R	This study
SJF4640	SH1000 *geh::ezrA-gfp ΔezrA::tet*; Kan^R, Tet^R	This study
SJF4641	SH1000 *geh::ezrA-snap*; Kan^R	This study
SJF4642	SH1000 *geh::ezrA-snap ΔezrA::tet*; Kan^R, Tet^R	This study
SJF4643	SH1000 *sgtA::tet*; Tet^R	This study
SJF4644	SH1000 *mgt::Tn sgtA::tet*; Ery^R, Tet^R	This study
SJF4648	RN4220 *geh::ezrA-gfp*; Kan^R	This study
SJF4649	RN4220 *geh::ezrA-snap*; Kan^R	This study
SJF4652	SH1000 *geh::ezrA-eyfp ΔezrA::tet* pCQ11-FtsZ-SNAP; Kan^R, Tet^R, Ery^R	This study
SJF4653	SH1000 *spa::kan* pCQ11-FtsZ-SNAP; Kan^R, Ery^R	This study
SJF4654	SH1000 pCQ11-FtsZ-mEos2; Ery^R	Christa Walther
SJF4655	SH1000 *spa::kan* pCQ11-FtsZ-mEos2; Kan^R, Ery^R	This study
SJF4656	SH1000 *pbp1::pbp1** *geh::*Pspac-*pbp1* pGL485; Tet^R, Cm^R	This study

Table 2.2. *S. aureus* strains used in this study

Cm^R, chloramphenicol resistant; Ery^R, erythromycin resistant; Kan^R, kanamycin resistant; Lin^R, lincomycin resistant; $Spec^R$, spectinomycin resistant; Tet^R, tetracycline resistant; SCO, single crossover.

2.3.2 *Escherichia coli* strains

Escherichia coli strains (Table 2.3) were grown and stored as *S. aureus* strains, using LB broth and agar instead of BHI.

Strain	Relevant genotype/selection markers	Source
Top10	F- *mcrA* Δ(*mrr-hsdRMS-mcrBC*) Φ80*lacZ*Δ*M15* Δ*lacX74 recA1 araD139* Δ(*araleu*)*7697 galU galK rpsL* (Str^R) *endA1 nupG*	Invitrogen
NEB5α	*fhuA2* Δ*(argF-lacZ)U169 phoA glnV44* Φ80 Δ*(lacZ)M15 gyrA96 recA1 relA1 endA1 thi-1 hsdR17*	New England Biolabs
SJF3963	Top10 pKASBAR-EzrA-mEos2; Amp^R	This study
SJF4179	Top10 pGM074; Amp^R	Gareth McVicker
SJF4382	Top10 pKASBAR-EzrA-eYFP; Amp^R	This study
SJF4383	Top10 pKASBAR-EzrA-PAmCherry1; Amp^R	This study

Table 2.3. *E. coli* strains used in this study

Amp^R , ampicillin resistant; Str^R, streptomycin resistant

2.3.3 Plasmids

Plasmids used in the study are listed in Table 2.4. All plasmid DNA was purified using a QIAGEN QIAprep Spin *Miniprep* kit (section 2.9.2).

Plasmid	Relevant genotype/selection markers	Source
pAISH	Tet^R derivative of pMUTIN4; Amp^R (*E. coli*), Tet^R (*S. aureus*)	(Aish, 2003)
pGL485	Cm^R derivative of *E. coli-S. aureus* shuttle vector pMJ8426, containing *E. coli lacI* gene under the control of the constitutive *Bacillus licheniformis* penicillinase promoter (Ppcn); $Spec^R$ (*E. coli*), Cm^R (*S. aureus*)	(Cooper et al., 2009)
pSNAP-tag (T7)-2	*E. coli* expression plasmid carrying the *snap* gene under the control of the T7 promoter; Amp^R (*E. coli*)	New England Biolabs
pMAD	*E. coli-S. aureus* shuttle vector with temperature-sensitive origin of replication in *S. aureus* and constitutively produced thermostable β-galactosidase encoded by *bgaB*; Amp^R (*E. coli*); Ery^R, Lin^R (*S. aureus*)	(Arnaud et al., 2004)
pOB	pGEM3Zf(+) cloning vector containing *ery*; Amp^R (*E. coli*), Ery^R (*S. aureus*)	(Horsburgh et al., 2002b)
pKASBAR	Hybrid vector of pCL84 and pUC18 for integration into *S. aureus* lipase gene (*geh*) encoding the *attP* integration site of L54a phage; Amp^R (*E. coli*), Tet^R (*S. aureus*)	(Bottomley et al., 2014)

pKASBAR-KanR	Kanamycin resistant derivative of pKASBAR; Amp^R (*E. coli*), Kan^R (*S. aureus*)	(Bottomley et al., 2014)
pGM073	pKASBAR containing *ezrA-psmorange* under the putative *ezrA* promoter; Amp^R (*E. coli*), Tet^R (*S. aureus*)	Gareth McVicker
pGM074	pKASBAR-KanR containing *ezrA-psmorange* under the putative *ezrA* promoter; Amp^R (*E. coli*), Kan^R (*S. aureus*)	Gareth McVicker
pGP001	pKASBAR containing *ezrA-gfp* under the putative *ezrA* promoter; Amp^R (*E. coli*), Tet^R (*S. aureus*)	(Poczopko, 2012)
pGP002	pKASBAR containing *ezrA-eyfp* under the putative *ezrA* promoter; Amp^R (*E. coli*), Tet^R (*S. aureus*)	(Poczopko, 2012)
pGP003	pKASBAR containing *ezrA-pamcherry1* under the putative *ezrA* promoter; Amp^R (*E. coli*), Tet^R (*S. aureus*)	(Poczopko, 2012)
pKASBAR-EzrA-GFP	pKASBAR-KanR containing *ezrA-gfp* under the putative *ezrA* promoter; Amp^R (*E. coli*), Kan^R (*S. aureus*)	This study
pKASBAR-EzrA-eYFP	pKASBAR-KanR containing *ezrA-eyfp* under the putative *ezrA* promoter; Amp^R (*E. coli*), Kan^R (*S. aureus*)	This study
pKASBAR-EzrA-mEos2	pKASBAR containing *ezrA-meos2* under the putative *ezrA* promoter; Amp^R (*E. coli*), Tet^R (*S. aureus*)	Katarzyna Wacnik and Bartłomiej Salamaga
pKASBAR-EzrA-meYFP	pKASBAR-KanR containing *ezrA-meyfp* under the putative *ezrA* promoter; Amp^R (*E. coli*), Kan^R (*S. aureus*)	This study
pKASBAR-EzrA-PAmCherry1	pKASBAR-KanR containing *ezrA-pamcherry1* under the putative *ezrA* promoter; Amp^R (*E. coli*), Kan^R (*S. aureus*)	This study
pKASBAR-EzrA-SNAP	pKASBAR-KanR containing *ezrA-snap* under the putative *ezrA* promoter; Amp^R (*E. coli*), Kan^R (*S. aureus*)	This study
pKB-Pspac-PBP1	2.4 kb fragment containing Pspac, RBS and a coding region of *S. aureus pbp1* cloned into *EcoRI* and *BamHI* cut pGM073; Amp^R (*E. coli*), Tet^R (*S. aureus*)	This study
pOB-ΔezrA	pOB containing a 1.5 kb fragment of the upstream region of *S. aureus ezrA* fused in frame to the tetracycline resistance cassette from pAISH and a 1.5 kb fragment of the downstream region of *S. aureus ezrA*; Amp^R (*E. coli*), Ter^R (*E. coli, S. aureus*), Ery^R (*S. aureus*)	This study
pCQ11-FtsZ-SNAP	*E. coli-S. aureus* shuttle vector containing the *lacI* gene and *ftsZ-snap* under Pspac; Amp^R (*E. coli*), Ery^R (*S. aureus*)	Fabien Grein
pCQ11-FtsZ-mEos2	pCQ11-FtsZ-SNAP with *meos2* replacement of *snap*; Amp^R (*E. coli*), Ery^R (*S. aureus*)	Christa Walther

pCQ11-eYFP-PBP2	3 kb fragment containing *S. aureus pbp2* RBS and *eyfp-pbp2* cloned into *NheI* and *AscI* cut pCQ11-FtsZ-SNAP; Amp^R (*E. coli*), Ery^R (*S. aureus*)	This study
pCQ11-PBP1-SNAP	pCQ11-FtsZ-SNAP with RBS and coding region of *S. aureus pbp1* replacement of *ftsZ*; Amp^R (*E. coli*), Ery^R (*S. aureus*)	This study
pMAD-eYFP-PBP2	pMAD containing a 1.1 kb fragment of the upstream region of *S. aureus pbp2* fused in frame to *eyfp* and a 1.1 kb fragment of *S. aureus* 5' *pbp2*; Amp^R (*E. coli*); Ery^R, Lin^R (*S. aureus*)	This study
pMAD-PBP1*	pMAD containing a 0.3 kb fragment of the upstream region of *S. aureus pbp1* and full length *pbp1** (*S. aureus pbp1* with a S314A substitution); Amp^R (*E. coli*); Ery^R, Lin^R (*S. aureus*)	This study

Table 2.4. Plasmids used in this study

Amp^R, ampicillin resistant; Cm^R, chloramphenicol resistant; Ery^R, erythromycin resistant; Kan^R, kanamycin resistant; Lin^R, lincomycin resistant; $Spec^R$, spectinomycin resistant; Tet^R, tetracycline resistant.

2.4 Buffers and solutions

All buffers and solutions were prepared using dH_2O and stored at room temperature. If necessary, solutions were sterilised by autoclaving, unless otherwise stated.

2.4.1 Phage buffer

$MgSO_4$	1 mM
$CaCl_2$	4 mM
Tris-HCl pH 7.8	50 mM
NaCl	0.6% (w/v)
Gelatin	0.1% (w/v)

2.4.2 Phosphate buffered saline (PBS)

NaCl	8 g l^{-1}
Na_2HPO_4	1.4 g l^{-1}
KCl	0.2 g l^{-1}
KH_2PO_4	0.2 g l^{-1}

The pH was adjusted to 7.4 with NaOH.

2.4.3 TAE (50x)

Tris	242 g l^{-1}
Glacial acetic acid	5.7% (v/v)
Na_2EDTA pH 8.0	0.05 M

50x stock solution was diluted 1:50 with dH_2O to produce a 1x TAE working solution.

2.4.4 TBSI

Tris-HCl pH 7.5	50 mM
NaCl	0.1 M

EDTA-free protease cocktail inhibitor (Roche) was dissolved in the buffer following manufacturer's instructions.

2.4.5 Fixative preparation

2.4.5.1 Preparation of 16% (w/v) paraformaldehyde

2.4.5.1.1 100 mM sodium phosphate buffer (pH 7.0)

1 M Na_2HPO_4	57.7 ml
1 M NaH_2PO_4	42.3 ml

The final volume was adjusted to 1 l.

2.4.5.1.2 16% (w/v) paraformaldehyde

100 mM sodium phosphate buffer (pH 7.0)	50 ml
Paraformaldehyde	8 g

The solution was prepared by adding 8 g of paraformaldehyde to 40 ml of 100 mM sodium phosphate buffer (pH 7.0). The solution was heated to 60°C while mixed vigorously. NaOH (≥ 5 M) solution was added drop wise, with heating and vigorous mixing, until the solution cleared. The solution was stored up to 3 months at 4°C.

2.4.5.2 Fixative

16 % (w/v) paraformaldehyde	0.5 ml
PBS	2 ml

2.4.6 SDS-PAGE solutions

2.4.6.1 SDS-PAGE reservoir buffer (10x)

Glycine	144 g l^{-1}
Tris	30.3 g l^{-1}
SDS	10 g l^{-1}

A 1:10 dilution with dH_2O was made to give a 1x SDS-PAGE working buffer.

2.4.6.2 SDS-PAGE loading buffer (5x*)*

Tris-HCl pH 6.8	250 mM
SDS	10% (w/v)
Bromophenol blue	0.5 % (w/v)
Glycerol	50% (v/v)
DTT	0.5 M

2.4.6.3 Coomassie Blue stain

Coomassie Blue	0.1% (w/v)
Methanol	5% (v/v)
Glacial acetic acid	10% (v/v)

2.4.6.4 Coomassie destain

Methanol	5% (v/v)
Glacial acetic acid	10% (v/v)

2.4.7 Western blotting solutions

2.4.7.1 Blotting buffer

Tris	2.4 g l^{-1}
Glycine	11.26 g l^{-1}
Ethanol	20% (v/v)

2.4.7.2 TBST (20x)

Tris	48.4 g l^{-1}
NaCl	20 g l^{-1}
Tween-20	2% (v/v)

The pH was adjusted to 7.6. A 1:20 dilution with dH_2O was made to give a 1x TBST

working solution.

2.4.7.3 Blocking buffer

5% (w/v) dried skimmed milk powder in 1x TBSB.

2.4.8 Southern blotting solutions

2.4.8.1 Depurination solution

HCl	250 mM

2.4.8.2 Denaturation solution

NaOH	0.5 M
NaCl	1.5M

2.4.8.3 Neutralisation solution

Tris	0.5 M
NaCl	1.5 M

The pH was adjusted to 7.5.

2.4.8.4 20x SSC

NaCl	3 M
Sodium citrate	300 mM

The pH was adjusted to 7.0 with 1 M NaOH. 20x SSC was diluted with dH_2O to make 5x, 2x and 0.5x SSC.

2.4.8.5 DIG prehybridisation buffer

SSC	5x
N-lauroylsarcosine	0.1% (w/v)
SDS	0.02% (w/v)
Blocking reagent (Roche)	1% (w/v)

2.4.8.6 ECL prehybridisation buffer

Gold hybridisation buffer (GE Healthcare)	1x
NaCl	0.5 M
Blocking reagent (GE Healthcare)	5% (w/v)

2.4.8.7 2x wash solution

SSC	2x
SDS	0.1% (w/v)

2.4.8.8 0.5x wash solution

SSC	0.5x
SDS	0.1% (w/v)

2.4.8.9 Washing buffer

Maleic acid	0.1 M
NaCl	0.15 M

The pH was adjusted to 7.5 using solid NaOH. The buffer was autocalved and 0.3% (v/v) Tween-20 was added.

2.4.8.10 Maleic acid buffer

Maleic acid	0.1 M
NaCl	0.15 M

The pH was adjusted to 7.5 using solid NaOH.

2.4.8.11 Blocking solution

1% (w/v) blocking reagent (Roche) in maleic acid buffer.

2.4.8.12 Antibody solution

Anti-digoxigenin-AP conjugate (0.2 µl ml^{-1}, Roche) in blocking solution.

2.4.8.13 Detection buffer

Tris	0.1 M
NaCl	0.1 M

The pH was adjusted to 9.5.

2.4.8.14 Colour substrate solution

Detection buffer containing 2% (v/v) NBT/BCIP (Roche).

2.4.8.15 TE buffer

Tris	10 mM
EDTA	1 mM

The pH was adjusted to 8.0.

2.5 Chemicals and enzymes

All chemicals and enzymes were of analytical grade quality and were purchased from Sigma, Fisher Scientific, MP Biomedicals or Roche. All restriction enzymes, ligases, polymerases, Gibson assembly mix, DNase and appropriate buffers were purchased from Fermentas, New England Biolabs or Bioline. Concentrations of stock solutions and storage conditions are shown in Table 2.5.

Stock solution	Concentration	Solvent	Storage
Pen-AF647 ((+)-6-aminopenicillanic acid (APA), Alexa Fluor 647 conjugate; Bryony Cotterell, University of Sheffield)	10 mM	DMSO	- 20°C in dark
Alkyne modified Alexa Fluor 647 (Molecular Probes)	800 µM	DMSO	- 20°C in dark
Ammonium persulfate (APS)	10% (w/v)	dH_2O	- 20°C
ADA (azido-D-alanine, Iris Biotech)	100 mM	DMSO	- 20°C
Bocillin FL (Molecular Probes)	1 mg ml^{-1}	DMSO	- 20°C in dark
Click-iT Alexa Fluor 647 DIBO alkyne (Molecular Probes)	40 mM	DMSO	- 20°C in dark
HADA (hydroxycoumarin 3-amino-D-alanine; Department of Chemistry, University of Sheffield)	100 mM	DMSO	- 20°C in dark
IPTG (isopropyl-β-D-1-thiogalactopyranoside)	1 M	dH_2O	- 20°C
Lysostaphin (Sigma)	5 mg ml^{-1}	20 mM sodium acetate pH 5.2	- 20°C
PC190723 (Calbiochem)	10 mg ml^{-1}	DMSO	- 20°C
SNAP-Cell 647-SiR (New England Biolabs)	1 mM	DMSO	- 20°C in dark
SNAP-Cell TMR-Star (New England Biolabs)	1 mM	DMSO	- 20°C in dark
TADA (tetramethylrhodamine 3-amino-D-alanine; Department of Chemistry, University of Sheffield)	100 mM	DMSO	- 20°C in dark
Van-AF647 (Vancomycin, Alexa Fluor 647 conjugate)	200 µM	1M Tris	- 20°C in dark
X-Gal (5-bromo-4-chloro-3-indolyl-β-D-galactopyranoside)	40 mg ml^{-1}	DMSO	- 20°C in dark

Table 2.5. Chemical stock solutions used in this study.

2.6 Centrifugation

The following centrifuges were used to harvest samples:

- Eppendorf microcentrifuge 5418, capacity up to 18 x 1.5-2ml, maximum speed of 16,783 rcf (14,000 rpm)
- Sigma centrifuge 4K15C, capacity up to 16 x 50 ml, maximum speed of 5,525 rcf (5,100 rpm).
- Avanti High Speed J25I centrifuge, Beckman:
  - JA-25.50, capacity up to 6 x 50 ml, maximum speed of 75,600 rcf (25,000 rpm)
  - JA-10.5, capacity up to 6 x 400 ml; maximum speed of 18,500 rcf (10,000 rpm)

Centrifugation was carried out at room temperature unless otherwise stated.

2.7 Determining bacterial cell density

2.7.1 Spectrophotometric measurement (OD_{600})

In order to quantify the optical density of a bacterial culture, spectrophotometric measurements at 600 nm (OD_{600}) were performed. Measurements were taken using a Biochrom WPA Biowave DNA Life Science spectrophotometer and Semi-micro PS cuvettes (Fisherbrand). If necessary, dilutions of culture samples were made in an appropriate culture medium to give a reading below 0.7.

2.7.2 Direct cell counts (CFU ml^{-1})

Numbers of viable cells numbers in liquid cultures were estimated by direct cell counts. Bacterial samples were serial diluted 1:10 in PBS in triplicate. 10 µl samples of each dilution were spotted onto BHI agar plates. The number of colony forming units per 1 ml of cell culture (CFU ml^{-1}) was estimated after overnight incubation at 37^{o}C.

2.8 Determination of moenomycin A minimal inhibitory concentration (MIC)

The MIC values for moenomycin A were estimated by direct cell counts. An overnight culture was adjusted to an OD_{600} of ~9 and was serial diluted 1:10 in PBS in triplicate. 10 µl of serial dilutions (10^{0} to 10^{-7}) were spotted onto BHI agar plates containing increasing concentrations of moenomycin A (from 0 µg ml^{-1} to 0.5 µg ml^{-1}). Plates were incubated at 37°C for 24-48 h and the number of CFU was counted. CFU ml^{-1} was plotted against the antibiotic concentration, and the MIC was defined as the antibiotic concentration that inhibited the growth of 99.9% of cells.

2.9 DNA purification techniques

2.9.1 Genomic DNA purification

Genomic DNA was isolated and purified using a QIAGEN DNeasy Blood & Tissue kit. 1 ml of an overnight culture of *S. aureus* was spun for 3 min at 16,000 rcf. The cell pellet was resuspended in 190 µl of dH_2O and 10 µl of 5 mg ml^{-1} lysostaphin was added, followed by incubation at 37°C for 1 h. Genomic DNA extraction was then carried out following the manufacturer's instructions.

2.9.2 Plasmid purification

Plasmid purification from *E. coli* was performed using a QIAGEN QIAprep Spin *Miniprep* kit. Manufacturer's instructions were followed.

2.9.3 Gel extraction of DNA

DNA was separated in a 1% (w/v) TAE agarose gel stained with 0.5 µg ml^{-1} ethidium bromide. DNA was visualised using a UV transilluminator. The required band was excised from the gel using a clean scalpel. DNA from the agarose gel slice was then purified using a QIAGEN QIAquick Gel Extraction kit. Manufacturer's instructions were followed.

2.9.4 Purification of PCR products

DNA fragments were purified from PCR reactions using a QIAGEN QIAquick PCR Purification kit. Manufacturer's instructions were followed.

2.9.5 Ethanol precipitation

2.5x volume of 95% (v/v) ethanol and 0.1 volume of 3 M sodium acetate pH 5.2 were added to the purified DNA sample. The sample was incubated at -80°C for 1 h. The sample was spun at 13,000 rcf for 20 min at 4°C. The supernatant was discarded, while the pellet was washed in 1 ml ice cold 70% (v/v) ethanol and centrifuged at 13,000 rcf for 10 min at 4°C. The supernatant was discarded, the pellet was air dried and then resuspended in an appropriate volume of sterile dH_2O (sdH_2O).

2.10 *In vitro* DNA manipulation techniques

2.10.1 Primer design

Primers used for PCR amplification were synthetic oligonucleotides (usually 20-50 nucleotides) that were based on the DNA sequences of *S. aureus* 8325, plasmids or fluorescent proteins. Primers used to amplify DNA fragments used in Gibson assembly were ~50 nucleotides long. Where necessary, suitable restriction sites were introduced at the 5' ends of primers to enable cloning. Additional bases (1-3) were added for efficient restriction digestions at these sites. Primers were synthesised by Eurofins MWG Operon. Primers were resuspended in sdH_2O and stored as 100 µM stocks or 10 µM working solutions at -20°C. Primers used in this study are listed in Table 2.6.

2.10.2 PCR amplification

2.10.2.1 Phusion polymerase

PCR amplification reactions were performed using Phusion High Fidelity Master Mix (Thermo Scientific) where 3'-5' proofreading activity was required. A final reaction volume of 50 µl contained:

Phusion High Fidelity Master Mix (2x)	25 µl
Forward primer (10 µM)	2.5 µl
Reverse primer (10 µM)	2.5 µl
Template DNA	50-100 ng
sdH_2O	up to 50 µl

PCR amplification was carried out in Veriti Thermal Cycler (Applied Biosystems). The lid was pre-heated to 105°C and the following reaction conditions were used:

1 cycle	Initial denaturation	98°C	30 s
30 cycles	Denaturation	98°C	10 s
	Annealing	55-65°C	10 s
	Extension	72°C	15-30 s/kb
1 cycle	Final extension	72°C	3-5 min

Primer	Sequence (5'→3')	Application	Source
ALB135	GGCAGCGGTATCATCAACAGGCTTA	Amplification of *attP* and *tet* on pCL84. Forward primer.	(Bottomley et al., 2014)
ALB136	TTTTTTGCATGCTCCGCATTAAAATCTAGCG	Amplification of *attP* and *tet* on pCL84. The *SphI* site underlined. Reverse primer.	(Bottomley et al., 2014)
kan_for_HindIII	AAAAAAAAGCTTCAGCGAACCATTTGAGG	Amplification of the KanR cassette from pGL433b. The *HindIII* site underlined. Forward primer.	(Bottomley et al., 2014)
kan_rev_HindIII	AAAAAAAAGCTTAATTCCTCGTAGGCGCTCGG	Amplification of *kan* from pGL433b. The *HindIII* site underlined. Reverse primer.	(Bottomley et al., 2014)
eYFP-F	CGGCGCGCCTCAGGTTCAGGTTCAGGTATGGTGAGCAAGGGCGAG	Amplification of *eyfp*. The *AscI* site underlined. Forward primer.	This study
eYFP-R	CGCGGCCGCTTACTTGTACAGCTCGTCCATGCCGAGAGTGATCCCGGC	Amplification of *eyfp*. The *NotI* site underlined. Reverse primer.	This study
PAmCherry-F	GGGCGCGCCTCAGGTTCAGGTTCAGGTATGGTGAGCAAGGGCGAGGAGGATAACATG	Amplification of *pamcherry1*. The *AscI* site underlined. Forward primer.	This study
PAmCherry-R	GGCGGCCGCGATTTAATCTGTATCAGGCTGAAAATCTTCTCTCATCC	Amplification of *pamcherry1*. The *NotI* site underlined. Reverse primer.	This study
pOB-ezrA-up-F	TTTACGTACACTATCTGCAGATGCTTCTCCTCCTAATTTATCATT	Amplification of region upstream of *S. aureus ezrA*. Forward primer.	This study
pOB-ezrA-up-R	ATTCGAGCTCGGTACCCGGGTTTTAAATTAATAAAAAAAACACCCACAATT	Amplification of region upstream of *S. aureus ezrA*. Reverse primer.	This study
pOB-ezrA-down-F	CACTATAGAATACTCAAGCTTACTCCTTAATTTCCTCATAAATGATGA	Amplification of region downstream of *S. aureus ezrA*. Forward primer.	This study
pOB-ezrA-down-R	GGATCAACTTTGGGAGAGAGAAACTAGTATGTAGTTATACTTAAATAATATGAGC	Amplification of region downstream of *S. aureus ezrA*. Reverse primer.	This study

pOB-TetR-F	TAAATTAGGAGGAGAAGCATCTGCAGATAGTGTACGTAAAAAGA	Amplification of *tet* from pAISH1. Forward primer.	This study
pOB-TetR-R	GTATAACTACATACTAGTTTCTCTCTCCCAAAGTTGATCCC	Amplification of *tet* from pAISH1. Reverse primer.	This study
ezrA-up-F	TGATAGAGGGATGAGGATTCGTA	Forward primer upstream of *S. aureus ezrA*.	This study
ezrA-up-R	ATGCTTCTCCTCCTAATTTATCATTAC	Reverse primer upstream of *S. aureus ezrA*.	This study
ezrA-down-R	GTATCTAACAAGCAAGTGATCATAC	Reverse primer downstream of *S. aureus ezrA*.	This study
tet5'-R	CCGTAATGCTATGTTAGCATTACTC	Reverse primer annealing within 5' *tet* region of pAISH1/pOB-ΔezrA.	This study
tet3'-F	GAAAGATGTTCACCAGCTAAGTAC	Forward primer annealing within 3' *tet* region of pAISH1/pOB-ΔezrA.	This study
meYFP-F	CTACCAGTCCAAGCTGAGCAAAGAC	Forward inverse primer to create A206K *eyfp* (*meyfp*). Point mutations to create *meyfp* are underlined.	This study
meYFP-R	CTCAGGTAGTGGTTGTCG	Reverse inverse primer to create A206K *eyfp* (*meyfp*).	This study
GFP-F	CGGCGCGCCTCAGGTTCAGGTTCAGGTATGGCTAGCAAAGGAGAAGAACTTTTCACTGGAGTTGTCCC	Amplification of *gfp*. The *AscI* site underlined. Forward primer.	This study
GFP-R	CGCGGCCGCTTATTTGTAGAGCTCATCCATGCCATGTGTAATCCCAGCAGC	Amplification of *gfp*. The *NotI* site underlined. Reverse primer.	This study
SNAP-F	GGGCGCGCCTCAGGTTCAGGTTCAGGTATGGACAAAGACTGCGAAATGAAGCGCAC	Amplification of *snap*. The *AscI* site underlined. Forward primer.	This study
SNAP-R	CGAATTCTCATTAACCCAGCCCAGGCTTGCCCAGTCTG	Amplification of *snap*. The *EcoRI* site underlined. Reverse primer.	This study
recU-F	CCATGGTACCCGGGAGCTCGAATTCTATCTGTTAAATCAAGTAAATCTAAAAAC	Amplification of region upstream of *S. aureus pbp2*. Forward primer.	This study

recU-R	CCTCGCCCTTGCTAATCATACGCGG TCCTCACTTT	Amplification of region upstream of *S. aureus pbp2*. Reverse primer.	This study
pbp2'-F	GGTGGAGGAGGTTCTGGTGGAGGA GGTTCTATGACGGAAAACAAAGGA TCTTCTCAGCCTAAG	Amplification of *S. aureus* 5' *pbp2*. Forward primer.	This study
pbp2'-R	CCTCGCGTCGGGCGATATCGGATCC TTGTAGAAGCTACCATTATCAAC	Amplification of *S. aureus* 5' *pbp2*. Reverse primer.	This study
eyfp-pbp2-F	GAGGACCGCGTATGATTAGCAAGG GCGAGGAGCTG	Amplification of *eyfp*. Forward primer.	This study
eyfp-pbp2-R	CGGCGCGCCTCAGGTTCAGGTTCAG GTATGGTGAGCAAGGGCGAG	Amplification of *eyfp*. Reverse primer.	This study
pbp2a	ACGATGTAATTTGATCTCATTGAG	Forward primer upstream of *S. aureus recU*.	This study
pbp2d	ACAGCGTCTAAGATGACTATGAG	Reverse primer downstream of *S. aureus pbp2*.	This study
pCQ-eyfp-pbp2-F	AAGGAGATATACATATGGCTAGCA GTGAGGACCGCGTATGA	Amplification of *S. aureus pbp2* RBS and *eyfp-pbp2*. Forward primer.	This study
pCQ-eyfp-pbp2-R	ATTATGCATTTAGAATAGGCGCGCC TTAGTTGAATATACCTGTTAATCCA C	Amplification of *S. aureus pbp2* RBS and *eyfp-pbp2*. Reverse primer.	This study
Tn-PBP3-F	TGATGAAAACATTACAGTGAATG	Forward primer upstream of Tn insertion in *S. aureus pbp3*.	This study
Tn-PBP3-R	GTATCGCCATATGGATATTTTC	Reverse primer downstream of Tn insertion in *S. aureus pbp3*.	This study
PBP4-2	TGACACAGTCACAATGACGAAC	Forward primer upstream of Tn insertion in *S. aureus pbp4*.	This study
PBP4-3	CGTTGGATTGACGAAATGTG	Reverse primer downstream of Tn insertion in *S. aureus pbp4*.	This study
pbp1*5'-F	CCATGGTACCCGGGAGCTCGAATTC AGTATACCGAAGCAACAACCAC	Amplification of *S. aureus* 5' *pbp1* and RBS. Forward primer.	This study

pbp1*5'-R	TTAAATGTTGCTCCAGGCTCGTATG TGTTTTG	Amplification of *S. aureus* 5' *pbp1* and RBS. Point mutation to create *pbp1** (S314A) is underlined. Reverse primer.	This study
pbp1*3'-F	GAGCCTGGAGCAACATTTAAATCAT ATGGGTTA	Amplification of *S. aureus* 3' *pbp1*. Point mutation to create *pbp1** (S314A) is underlined. Forward primer.	This study
pbp1*3'-R	CCTCGCGTCGGGCGATATCGGATCC TTAGTCCGACTTATCCTTGTC	Amplification of *S. aureus* 3' *pbp1*. Reverse primer	This study
up-pbp1-F	AATTACGTGTAGCTGAAATAC	Forward primer upstream of *S. aureus ftsL*.	This study
down-pbp1-R	TTCTATCACAGCATTACTTTAG	Reverse primer downstream of *S. aureus pbp1*.	This study
pCQ-pbp1-F	AGAAGGAGATATACATATGGCTTG AGAACGATAATGTAAAGGTAG	Amplification of *S. aureus pbp1* and RBS. Forward primer.	This study
pCQ-pbp1-R	TTCATTTCGCAATCTTTGTCCATGG AACCTCCTCCACCACTGTCCGACTT ATCCTTGTCAGTTTTACTG	Amplification of *S. aureus pbp1* and RBS. Reverse primer.	This study
pKB-Pspac-pbp1-F	CTATGACCATGATTACGAATTCTTA GTCCGACTTATCCTTG	Amplification of Pspac, RBS and *pbp1*. Forward primer.	This study
pKB-Pspac-pbp1-R	CCTTTTTTTGCCCCGGGATCCGCAA AAAGTTGTTGACTTTATC	Amplification of Pspac, RBS and *pbp1*. Reverse primer.	This study
Tn-mgt-F	ACTCAAACTCAAATGAACATTTTGA G	Forward primer upstream of Tn insertion in *S. aureus mgt.*	This study
Tn-mgt-R	TCTTATTATATTGTTTTTCAACTCGA TGAG	Reverse primer downstream of Tn insertion in *S. aureus mgt.*	This study
Tn-sgtA-F	GGACATGTTAGTTATAAAGGTGTAT TC	Forward primer upstream of Tn insertion in *S. aureus sgtA*.	This study
Tn-sgtA-R	ACTTGATGTTTTAGGGCCTATAATG	Reverse primer downstream of Tn insertion in *S. aureus sgtA*.	This study

Table 2.6. Primers used in this study

2.10.2.2 Taq polymerase

DreamTaq Green Master Mix (Thermo Scientific) was used to perform PCR reactions where accurate amplification was not required. A final reaction volume of 50 µl contained:

DreamTaq Green Master Mix (2x)	25 µl
Forward primer (10 µM)	2.5 µl
Reverse primer (10 µM)	2.5 µl
Template DNA	50-100 ng
sdH_2O	up to 50 µl

PCR amplification was carried out in Veriti Thermal Cycler. The lid was pre-heated to 105°C and the following reaction conditions were used:

1 cycle	Initial denaturation	95^{o}C	1 min
30 cycles	Denaturation	95^{o}C	30 s
	Annealing	50-60^{o}C	30 s
	Extension	72^{o}C	1 min/kb
1 cycle	Final extension	72^{o}C	5-7 min

PCR products were analysed by agarose gel electrophoresis (2.10.7).

2.10.2.3 Colony PCR screening of *E. coli*

The PCR reaction mixture was prepared as described in 2.10.2.2, without the addition of template DNA. Using a sterile pipette tip, a single colony was patched onto a selective agar plate and then introduced into the PCR reaction tube. The PCR reaction was performed as described above.

2.10.3 Restriction endonuclease digestion

Restriction enzymes were purchased from New England Biolabs. Digestion of DNA was performed according to the manufacturer's instructions, using the buffers supplied. The reaction mixtures were incubated at 25^{o}C or 37^{o}C for between 1h and 16 h. If digested DNA was to be used for further manipulation (DNA cloning), it was purified (sections 2.9.3 and 2.9.4).

2.10.4 DNA ligation

Insert and vector DNA were prepared for ligation reaction by restriction endonuclease digestion (section 2.10.3) and purified (sections 2.9.3 and 2.9.4). The ligation reaction was carried out in a 10 µl volume:

Vector DNA	50 ng
Insert	3 fold excess of vector DNA
T4 DNA ligase	0.5 µl (200 U)
T4 DNA ligase buffer (10x)	1 µl
sdH_2O	up to 10 µl

The reaction mix was incubated at 16^{o}C overnight. The ligation products were used to transform competent *E. coli* cells.

2.10.5 Gibson assembly

Inserts were obtained by PCR amplification (section 2.10.2.1). DNA vector was prepared by restriction endonulcease digestion (section 2.10.3). DNA fragments were purified (sections 2.9.3 and 2.9.4). The assembly was performed in a final volume of 10 µl:

Vector DNA	50 ng
Insert	3 fold excess of vector DNA
Gibson Assembly Master Mix (2x)	5 µl
sdH_2O	up to 10 µl

The assembly reaction was performed at 50^{o}C for 1 h. Ligated DNA fragments were used to transform competent *E. coli* cells.

2.10.6 Site directed mutagenesis by inverse PCR

A specific point mutation to a desired DNA sequence was introduced by site directed mutagenesis using inverse PCR and primers designed to introduce the substitution. Purified plasmid containing the desired DNA sequence was used as DNA template. A standard PCR reaction was carried out (section 2.10.2.1) and PCR products were

purified (section 2.9.4). The purified PCR products were digested with *DpnI* to remove the methylated parental DNA. The following components were mixed:

DpnI	2 µl (40 U)
CutSmart buffer (10x)	5 ul
PCR products	43 ul

The reaction was incubated for 2 h at 37^{o}C and *DpnI* treated DNA was purified (section 2.9.4). The following components were then mixed:

Purified *DpnI* treated DNA	25 ng
Quick-Stick Ligase buffer (4x)	2.5 µl
T4 polynucleotide kinase (PNK)	0.5 µl (5 U)
sdH_2O	up to 10 µl

The sample was incubated at 37^{o}C for 30 min. The reaction mix was cooled to room temperature. 0.5 µl of Quick-Stick Ligase was added and the sample was incubated for 15 min at room temperature. The ligation products were used to transform competent *E .coli* cells.

2.10.7 Agarose gel electrophoresis

DNA samples were separated in 1% (w/v) agarose gels stained with 0.5 µg ml^{-1} ethidium bromide, in 1x TAE buffer, unless otherwise stated. Before loading into the wells of the gel, DNA probes were mixed with 6x DNA loading dye (Thermo Scientific) and resolved for 30 min at constant 120 V at room temperature. DNA was visualised using an UV transilluminator at 260 nm and the photograph of the gel was taken using the UVi Tec Digital camera and UVi Doc Gel documentation system. The size of DNA fragments was estimated by comparison with the fragments of a DNA ladder (Table 2.7) that was co-electrophoresed with the samples.

Marker	DNA fragment size (kb)
2-Log DNA ladder (New England Biolabs	10.0
	8.0
	6.0
	5.0
	4.0
	3.0
	2.0
	1.5
	1.2
	1
	0.9
	0.8
	0.6
	0.5
	0.4
	0.3
	0.2
	0.1
GeneRuler 1 kb DNA ladder (Thermo Scientific)	10.0
	8.0
	6.0
	5.0
	4.0
	3.5
	3.0
	2.5
	2.0
	1.5
	1.0
	0.75
	0.5
	0.25
DIG-labelled DNA molecular weight marker III (Roche)	21.226
	5.148
	4.973
	4.268
	3.530
	2.027
	1.904
	1.584
	1.375
	0.947
	0.831
	0.564
	0.125

Table 2.7. DNA fragments used as size markers for agarose gel electrophoresis

2.10.8 DNA sequencing

Plasmids and PCR products were sequenced by either Core Genomic Facility at the University of Sheffield or GATC Biotech. Sequencing results were analysed using SnapGene v.3.0.3.

2.10.9 Determining DNA concentration

DNA concentration in a sample was determined using NanoDrop 3300 fluorospectrometer and operating software v.2.8.0. The blank measurement was taken for 1.5 µl solution used for DNA elution. 1.5 µl of the sample was used to measure DNA concentration at 260 nm.

2.11 Protein analysis

2.11.1 Preparation of whole cell lysate

S. aureus cells were grown in 100 ml BHI to an OD_{600} ~1. Cells were harvested by centrifugation at 5,000 rcf for 10 min at 4^{o}C. The cell pellet was washed two times by resuspension in PBS and centrifugation at 5,000 rcf for 10 min at 4^{o}C. The pellet was resuspended in 0.5 ml of PBS. Cells were added to chilled lysing matrix tubes containing 0.1 mm silica spheres (Lysing Matrix B, MP Biomedicals) and broken using an MP Biomedicals FastPrep 24 Homogeniser in 12 cycles of 30 s, at maximum speed, with 5 minute incubation on ice between cycles. The lysates were cooled on ice for 15 min and the FastPreap beads were allowed to settle. The supernatant was recovered and stored at -20^{o}C until needed.

2.11.2 Preparation of membrane fraction

S. aureus cells were grown in 1 l BHI to an OD_{600} ~1. Cells were harvested by centrufugion at 5,000 rcf for 10 min at 4^{o}C. Cells were washed three times by resuspension in PBPs and centrifugation at 5,000 rcf for 10 min at 4^{o}C. The pellet was resuspended in 3 ml TBSI. Cells were added to chilled lysing matrix tubes containing 0.1 mm silica spheres (Lysing Matrix B, MP Biomedicals) and broken using an MP Biomedicals FastPrep 24 Homogeniser in 12 cycles of 30 s, at maximum speed, with 5 minute incubation on ice between cycles. The supernatant was recovered by centrifugation at 2,000 rcf for 10 min at 4^{o}C. The supernatant was transferred to a 15 ml Falcon tube and any remaining FastPrep beads or unbroken cells were removed by centrifugation at 5,000 rcf for 10 min at 4^{o}C. The supernatant was then spun twice at

15,000 rcf for 10 min at 4°C to sediment cell wall material. The supernatant was transferred to a fresh centrifuge tubes and membranes were sedimented by centrifugation at 70,000 rcf for 60 min at 4°C. The pellet containing the membrane fraction was suspended in PBS and stored at -20°C.

2.11.3 Bradford protein assay

To determine protein concentration, first different concentrations of bovine serum albumin (BSA) were used to prepare a standard curve (Figure 2.1). 0, 1.6, 4, 8 and 12 µg of BSA in 800 µl PBS were transferred into a Semi-micro PS spectrophotometer cuvette (Fisherbrand). 200 µl of Bio-Rad Protein Assay Dye was added to each sample and mixed. After 5 min incubation at room temperature the absorbance at 595 nm (A_{595}) was measured. The sample containing 0 µg of BSA was used to calibrate the spectrophotometer to zero.

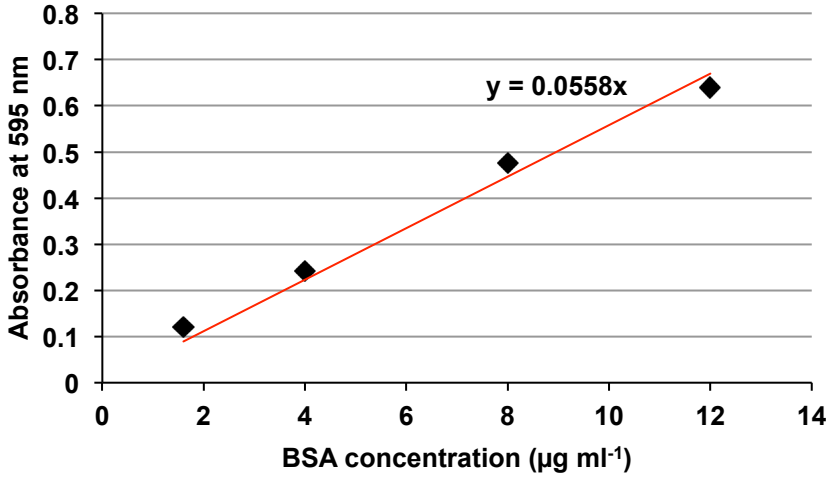

Figure 2.1. Calibration curve for Bradford protein assay

Absorbance at 595 nm of different BSA concentrations. The linear regression line used for estimation of the concentration of protein samples is shown in red. The trend line equation is also presented.

In order to determine concentration of a protein sample, the sample was diluted in PBS to a final volume of 800 µl and transferred into a spectrophotometer cuvette. Next 200 µl of Bio-Rad Protein Assay Dye was added. The mixture was incubated at room temperature for 5 min. After that time the A_{595} was measured and protein concentration was calculated based on the standard curve and a dilution factor.

2.11.4 SDS-PAGE

Cell lysates and membrane fractions were analysed using the Laemmli SDS-PAGE method. A resolving gel was prepared as follows:

SDS-PAGE 10% (w/v) resolving gel:

dH_2O	4 ml
1.5 M Tris-HCl pH 8.8	2.5 ml
10% (w/v) SDS	100 µl
30% (w/v) acrylamide/bis (37.5:1)	3.5 ml
10% (w/v) APS	100 µl
TEMED	20 µl

Ammonium persulfate (APS) and N,N,N'N'-tetramethyl-ethylenediamine (TEMED) were added last to the gel solution. The components were mixed gently and immediately loaded between the glass plates of a gel casting apparatus (Mini-Protean Tetra cell gel slabs, Bio-Rad). A layer of 100% (v/v) isopropanol was pipetted onto the top of the gel to isolate it from the air. Once the gel had set the isopropanol was drained using filter paper. A stacking gel was prepared as follows:

SDS-PAGE 4% (w/v) stacking gel:

dH_2O	3.6 ml
0.5 M Tris-HCl pH 6.8	0.75 ml
10% (w/v) SDS	50 µl
30% (w/v) acrylamide/bis (37.5:1)	0.65 ml
10% (w/v) APS	50 µl
TEMED	20 µl

Stacking gel components were mixed and loaded on top of the resolving gel. A plastic comb was inserted into the gel in order to create sample loading wells. Once the stacking gel had set, the gel was transferred to a Bio-Rad tank and submerged in 1x SDS-PAGE reservoir buffer. A sample was mixed with 5x SDS-PAGE loading buffer, incubated at 100^{o}C for 5 min and an appropriate volume of the sample was loaded into the wells. 5 µl of ColorPlus Prestained Protein Ladder, Broad Range (New England Biolabs) protein size marker was also loaded (Table 2.8). Proteins were separated by

electrophoresis at 100 V until the blue dye front of the sample buffer reached the base of the gel plate.

Protein size marker	Molecular mass (kDa)
ColorPlus Prestained Protein Ladder, Broad Range (New England Biolabs)	250
	150
	100
	80
	60
	50
	40
	30
	25
	20
	15
	10

Table 2.8. Protein size standards

2.11.5 Coomassie staining

After the electrophoresis an SDS-PAGE gel was submerged in Coomassie Blue stain for at least 30 min in order to visualise protein bands. It was then destained in Coomassie destain solution overnight until the background was clear. Molecular sizes of proteins were estimated by comparison to the protein standards of known molecular weight.

2.11.6 Western blotting

Protein samples were separated by SDS-PAGE (section 2.11.4). The gel was equilibrated in blotting buffer for 10 min. Amersham Hybond ECL Nitrocellulose Membrane (GE Healthcare) was cut to the same size as the gel and was equilibrated in blotting buffer for 20 min. Proteins were transferred from the gel to the membrane by wet transfer in ice-cold blotting buffer using the Mini-Protean Tetra cell system (Bio-Rad) at 100 V for 90 min. After the transfer the membrane was rinsed with TBST. The blot was blocked in blocking buffer at room temperature for 1 h with gentle shaking. The membrane was rinsed and washed three times in TBST for 10 min at room temperature. The blot was incubated with primary antibodies diluted in blocking buffer overnight at 4^{o}C with gentle shaking. The primary antibody solution was removed and the membrane was rinsed with TBST and then washed three times for 10 min with TBST to remove unbound primary antibodies. The blot was incubated in blocking buffer containing 1:10,000 horseradish peroxidase (HRP) conjugated goat anti-rat or

anti-rabbit IgG secondary antibodies (Sigma) for 1 h at room temperature with gentle shaking. The membrane was rinsed with TBST and then washed three times for 10 min with TBST to remove unbound antibodies. In the dark room the membrane was drained from TBST. The blot was covered with SuperSignal West Pico Chemiluminescent Substrate (Thermo Scientific) and incubated for 5 min. The blot was drained from the excess substrate, placed between two sheets of plastic and exposed to Amersham Hyperfilm ECL (GE Healthcare). After that the film was developed by submerging it in developer solution and then in fixer solution, and air-dried before scanning.

2.11.7 Gel-based analysis of penicillin binding proteins

The membrane fraction was isolated (section 2.11.2) and the total protein concentration was estimated by Bradford protein assay (section 2.11.3). Approximately, 30 μg of total protein was incubated with 25 μM Bocillin FL or 10 μM Pen-AF647 at 37^{o}C for 10 min. The reaction was stopped by addition of 5x SDS-PAGE loading buffer and incubation at 100^{o}C for 5 min. The proteins were separated by SDS-PAGE. After electrophoresis the gel was soaked in dH_2O and immediately visualised with ChemiDoc MP System (Bio-Rad).

2.11.8 In-gel detection of SNAP-tag fusions

A 1 ml aliquot of cell culture grown to early-exponential phase (OD_{600} ~0.5) was transferred into a microcentrifuge tube. SNAP-Cell TMR-Star was added to a final concentration of 500 nM. Cells were incubated for 1 h at 37^{o}C in order to label SNAP-tag fusion proteins. Cells were washed three times by resuspension in PBS and centrifugation at 10,000 rcf for 1 min at room temperature. Cells were resuspended in PBS containing 200 μg ml^{-1} lysostaphin and 10 U ml^{-1} DNase I, and incubated for 30 min at 37^{o}C. The cell lysate was mixed with 5x SDS-PAGE loading buffer and boiled for 5 min. Proteins were separated by SDS-PAGE. After electrophoresis the gel was soaked in dH_2O and immediately visualised with ChemiDoc MP System (Bio-Rad).

2.12 DNA hybridisation techniques

2.12.1 Preparation of digoxigenin (DIG) labelled probe

2.12.1.1 Labelling of DNA probes with DIG

A method of random primed labelling was used in order to label DNA fragments using a DIG DNA labelling and detection kit (Roche). DNA fragments obtained by PCR amplification were purified (sections 2.9.3 and 2.9.4). Up to 3 µg of DNA in 15µl sdH_2O was denatured at 100^oC for 10 min and immediately chilled on ice for 10 min. The labelling reaction was performer in a final volume of 20 µl:

DNA to be labelled	15 µl
Random hexanucleotide mixture	2 µl
dNTP labelling mixture	2 µl
Klenow enzyme	1 µl

The sample was incubated at 37^oC overnight. The reaction was stopped by incubation at 65^oC for 10 min. DNA was purified (section 2.9.4) and efficiency of DIG labelling was quantified (section 2.21.1.2). The DIG labelled probe was stored at -20^oC.

2.12.1.2 Quantification of DIG labelled DNA probe

The efficiency of DNA sample labelling was determined by comparison to labelled control DNA of known concentration supplied in the DIG DNA labelling and detection kit (Roche). Labelled DNA sample and labelled control DNA were diluted to 1 ng μl^{-1}, according to the expected yield of probe and then serially diluted according to the manufacturer's instructions. 1 µl of each serial dilution was spotted onto Amersham Hybond-N+ nylon membrane (GE Healthcare). The DNA was fixed to the membrane using a UV crosslinker (section 2.12.4) and DIG labelled DNA was detected using AP-conjugated anti-DIG antibody (section 2.4.9.12). Concentration and efficiency of labelling of DNA sample were estimated visually by comparison of the spot intensities of the control and probe dilutions.

2.12.2 Preparation of HRP labelled probe

DNA fragments obtained by PCR amplification were purified (sections 2.9.3 and 2.9.4) and labelled with HRP using an Amersham ECL Direct Nucleic Acid Labelling and Detection System (GE Healthcare). The purified DNA fragments were diluted to a

concentration of 10 ng μl^{-1}. 100 ng of the DNA sample (10 µl of 10 ng μl^{-1} sample) was incubated at 100°C for 5 min. The sample was then incubated on ice for 5 min and spun at 16,000 rcf for 30 s at room temperature. 10 µl of DNA labelling reagent (GE Healthcare) was added to the DNA sample and mixed. 10 µl of glutaraldehyde (GE Healthcare) was added, mixed and spun at 16,000 rcf for 30 s at room temperature. The mix was incubated at 37°C for 10 min and used immediately.

2.12.3 Southern blotting

Genomic DNA was digested by restriction enzymes and then separated by agarose gel electrophoresis for 1 h at constant 120 V at room temperature in 0.8% (w/v) agarose gel (for DIG detection, the gel was not supplemented with ethidium bromide). For DIG detection, DIG-labelled DNA molecular weight marker III (Roche, Table 2.7) was used, while for ECL detection a standard DNA ladder (Table 2.7) was loaded into the gel to estimate the band sizes following development of the blot. The gel was incubated in depurination solution for 10 min and washed in dH_2O. The gel was soaked two times in denaturation buffer for 15 min and rinsed in dH_2O. The gel was neutralised by soaking in neutralisation buffer twice for 15 min. The gel was equilibrated in 20x SSC for 10 min. The DNA was transferred overnight from the gel to a Hybond-N+ Extra nylon membrane by capillary blotting. 20x SSC was used as the transfer buffer.

2.12.4 Fixing DNA to the membrane

DNA was permanently fixed to the Amersham Hybond-N+ nylon membrane with the use of a RPN 2500 UV crosslinker (Amersham) at 70 mJ/cm^2 for 10 s. The membrane was rinsed with dH_2O and air-dried.

2.12.5 Hybridisation for DIG detection

The procedures were performed in a Techne Hybridiser HB-1D in a roller bottle. A membrane was prehybridised for 30 min at 42°C in pre-heated DIG prehybridisation solution (20 ml per 100 cm^2 of membrane). The DIG labelled DNA sample (section 2.12.1) was denatured by boiling for 10 min and then immediately chilled on ice for 10 min. The DIG labelled DNA sample was added to 3.5 ml pre-heated prehybridisation solution to a final probe concentration of 25 ng ml^{-1}. The membrane was then hybridised with the labelled probe for 16 h at 42°C. After incubation the membrane was

washed twice in 2x wash solution for 5 min at room temperature and then washed twice in 0.5x wash solution for 15 min at 68^{o}C.

2.12.6 Hybridisation for ECL detection

The procedures were performed in a Techne Hybridiser HB-1D in a roller bottle. A membrane was prehybridised for 30 min at 42^{o}C in pre-heated ECL prehybridisation solution (12.5 ml per 100 cm^{2} of membrane). 30 µl of HRP labelled probe (section 2.12.2) was added and the membrane was hybridised for 16 h at 42^{o}C. After incubation the membrane was washed with 5x SSC at 42^{o}C for 5 min. The membrane was then washed once for 20 min and twice for 10 min with 0.5x wash solution at 42^{o}C. The blot was washed once with 2x SSC at room temperature.

2.12.7 Immunological detection of DIG labelled DNA

The membrane was washed in washing buffer for 5 min and then blocked for 30 min in 100 ml blocking solution at room temperature. The membrane was transferred to antibody solution (1:5,000 dilution of anti-DIG-AP antibody in blocking solution) and incubated for 30 min at room temperature. The membrane was washed twice for 15 min in washing buffer. The membrane was equilibrated for 2 min in 20 ml detection buffer. The membrane was then incubated in 10 ml colour substrate solution in the dark to allow development of purple bands. After sufficient colour development, the membrane was washed in TE buffer for 5 min in order to stop the reaction. The membrane was air-dried before scanning and stored in the dark.

2.12.8 Detection of HRP labelled DNA

In the dark room the membrane was drained from 2x SSC. The blot was covered with SuperSignal West Pico Chemiluminescent Substrate (Thermo Scientific) and incubated for 2 min. The membrane was drained from the excessive substrate, placed between two sheets of plastic and exposed to Amersham Hyperfilm ECL (GE Healthcare). After that the film was developed by submerging it in developer solution and then in fixer solution, and air-dried before scanning.

2.13 Transformation techniques

2.13.1 Transformation of *E. coli*

2.13.1.1 Transformation of electrocompetent *E. coli* cells

A 50 µl aliquot of *E. coli* Top10 electrocompetent cells (Invitrogen) was defrosted on ice. 1 ng of plasmid DNA or 4 µl of ligation reaction was added to the cells. The mixture was transferred into a pre-chilled 1 mm electroporation cuvette (Bio-Rad). Electroporation was carried out at 1.75 kV, 25 µF and 200 Ω using a GenePulser Xcell Electoporation system (Bio-Rad). Immediately 400 µl LB was added to the cuvette to recover cells. *E. coli* cells were incubated at 37^{o}C with shaking at 250 rpm for 1 h. 100 µl aliquots were spread on selective LB agar plates. The plates were incubated at 37^{o}C until colonies appeared.

2.13.1.2 Transformation of chemically competent *E. coli* cells

A 50 µl aliquot of *E. coli* NEB5α chemically competent cells (New England Biolabs) was defrosted on ice. 1 ng of plasmid DNA or 4 µl of ligation reaction was added to the cells. The mixture was swirled gently and incubated on ice for 30 min. The cells were then incubated at 42^{o}C for 45 s and immediately placed on ice for 5 min. Cells were recovered by addition of 500 µl LB and incubation at 37^{o}C with shaking at 250 rpm for 1 h. 100 µl aliquots were spread on selective LB agar plates. The plates were incubated at 37^{o}C until colonies appeared.

2.13.2 Transformation of *S. aureus*

2.13.2.1 Preparation of *S. aureus* electrocompetent cells

S. aureus was streaked on BHI agar and incubated overnight at 37^{o}C. 400 ml BHI was inoculated with a single colony and cells were grown for 10-12 h at 37^{o}C with shaking at 250 rpm. 400 ml fresh BHI was inoculated with the overnight culture to an OD_{600} 0.1. Cells were incubated for 1-2 h at 37^{o}C with shaking at 250 rpm until they reached an OD_{600} of 0.4-0.6. Cells were divided into 100 ml aliquots and harvested by centrifugation at 5,000 rcf at room temperature for 10 min. Pellets were then washed three times by resuspension in 25 ml sdH_2O and centrifugation at 5,000 rcf for 10 min at room temperature. The pellets were resuspended in 20 ml 10% (v/v) glycerol and centrifuged at 5,000 rcf at room temperature for 10 min. The pellets were combined, resuspended in 10 ml 10% (v/v) glycerol and incubated for 30 min at room temperature. The cells were centrifuged at 5,000 rcf for 10 min at room temperature. The pellet was

resuspended in 500 µl 10% (v/v) glycerol. 50 µl aliquots were pipetted and snap-frozen using liquid nitrogen and stored at -80°C.

2.13.2.2 Transformation of electrocompetent *S. aureus* cells

A 50 µl aliquot of electrocompetent *S. aureus* cells was defrosted at room temperature. 1 µg plasmid DNA was added to cells. The mixture was transferred to a pre-chilled 1 mm electroporation cuvette (Bio-Rad). Electroporation was carried out at 2.3 kV, 25 µF and 100 Ω using a Gene Pulser Xcell Electoporation system (Bio-Rad). Immediately, 1 ml BHI was added to the cuvette to recover *S. aureus* cells after electroporation. Cells were transferred into a 25 ml universal tube and incubated at 37°C for 3 h with shaking at 250 rpm. 200 µl aliquots were spread on selective BHI agar plates and incubated at 37°C until colonies appeared.

2.14 Phage techniques

2.14.1 Bacteriophage

Bacteriophage Φ11 (Mani et al., 1993) was used for phage transduction of *S. aureus*.

2.14.2 Preparation of phage lysate

The *S. aureus* donor strain was grown overnight. 200 µl of the overnight culture was combined with 5 ml of BHI, 5 ml of phage buffer and 100 µl of a phage lysate stock (Φ11). The mixture was incubated at room temperature overnight, until it was clear. The lysate was filter-sterilised (0.2µm pore size) and stored at 4°C.

2.14.3 Determination of phage titre

S. aureus SH1000 was grown overnight at 37°C. 5 ml fresh BHI was inoculated with the overnight culture to an OD_{600} 0.05. Cells were grown at 37°C with shaking at 250 rpm to OD_{600} ~0.5. The phage lysate was serially diluted in phage buffer to 10^{-7}. 100 µl of diluted phage and 50 µl of 1M $CaCl_2$ were added to 400 µl of SH1000 culture. The mixture was incubated at room temperature for 10 min. 5 ml phage top agar was added to the mixture and then a phage bottom agar plate was overlaid with it. Plates were incubated overnight at 37°C. Plagues were counted to determine the phage titre. An expected phage titre (plague forming units per ml, PFU ml^{-1}) was in the range of 10^7 -10^{10} PFU ml^{-1}.

2.14.4 Phage transduction

50 ml LK was inoculated with the *S. aureus* recipient strain and incubated overnight at 37°C, 250 rpm. The overnight culture was centrifuged at room temperature at 5,000 rcf for 10 min. The pellet was resuspended in 3 ml of fresh LK. 500 µl of the recipient strain was mixed with 500 µl of phage lysate, 1 ml of LK and 10 µl of 1 M $CaCl_2$. The mixture was statically incubated at 37°C for 25 min and then with shaking at 250 rpm for 15 min at 37°C. 1 ml of ice-cold 0.02 M sodium citrate was added into the mixture, followed by 5 min incubation on ice. The cells were centrifuged at 5,000 rcf for 10 min 4°C. The resulting pellet was resuspended in 1 ml of 0.02 M sodium citrate and incubated on ice for 45-90 min. 100 µl aliquots were spread on selective LK agar plates containing 0.05% (w/v) sodium citrate. Plates were incubated at 37°C for 24-72 h. Colonies were picked and streaked onto selective BHI agar plates to confirm that they had the correct resistance profile.

2.15 Microscopy imaging

2.15.1 Fixing of cells for microscopy

Cell pellets were resuspended in 0.5 ml PBS. 0.5 ml of freshly prepared fixative (section 2.4.6) was added and cells were incubated for 30 min at room temperature. Fixed cells were washed twice with sdH_2O by centrifugation (16,000 rcf for 1 min at room temperature) and resuspension.

2.15.2 Labelling of nascent peptidoglycan synthesis with HADA

For conventional fluorescence microscopy, a 1 ml aliquot of cells grown to early-exponential phase (OD_{600} ~0.5) was transferred to a microcentrifuge tube. 5 µl of 100 mM HADA was added to a final concentration of 500 µM and cells were incubated for 5 min at 37°C with shaking at 200 rpm. The cells were washed once with PBS by centrifugation (10,000 rcf for 1 min at room temperature) and then fixed.

For SIM visualisation, a 1 ml aliquot of cells grown to early-exponential phase (OD_{600} ~0.5) was incubated with 50 µl of 100 mM HADA for 5 min at 37°C with shaking at 200 rpm. The cells were washed three times with PBS by centrifugation (10,000 rcf for 1 min at room temperature) and resuspension, followed by fixing.

2.15.3 Pulse-chase labelling with TADA and HADA

A 1 ml aliquot of cell culture grown to early-exponential phase (OD_{600} ~0.5) was transferred to a microcentrifuge tube containing 5 µl of 100 mM TADA. Cells were incubated with 500 µM TADA for 30 min or 5 min at 37°C with shaking at 200 rpm. TADA labelled cells were centrifuged (10,000 rcf for 1 min at room temperature) and the pellet was resuspended in 1 ml pre-warmed BHI. 5 µl of 100 mM HADA was added to a final concentration of 500 µM and cells were incubated at 37°C for 5 min with shaking at 200 rpm. The cells were washed once with PBS by centrifugation (10,000 rcf for 1 min at room temperature). The labelled cells were fixed.

2.15.4 Copper (Cu)-click labelling of nascent peptidoglycan synthesis

1 ml of cell culture grown to early exponential phase (OD_{600} ~0.5) was transferred to a microcentrifuge tube. 5 µl of 100 mM azido-D-alanine (ADA) was added to a final concentration of 500 µM and cells were incubated at 37°C for 5 min with shaking at 200 rpm. The cells were washed once with PBS by centrifugation (10,000 rcf for 1 min), followed by fixing. Fixed cells were washed twice in PBS and resuspended in a Click-iT reaction cocktail (Molecular Probes). The Click-iT reaction cocktail contained:

1x Click-iT cell reaction buffer	440 µl
100 mM $CuSO_4$	10 µl
Click-iT cell buffer additive	50 µl
800 µM alkyne modified Alexa Fluor 647	2.5 µl

The cells were incubated with the reaction cocktail for 30 min at room temperature. The 'clicked' cells were washed twice with PBS by centrifugation (10,000 rcf for 1 min) and resuspension.

2.15.5 Copper (Cu)-free 'co-click' labelling of nascent peptidoglycan synthesis

1 ml of cell culture grown to early exponential phase (OD_{600} ~0.5) was transferred to a microcentrifuge tube. 1 µl of 40 mM Click-iT Alexa Fluor 647 DIBO alkyne and 10 µl of 100 mM azido-D-alanine (ADA) were added to a final concentration of 40 µM and 1 mM, respectively. The cells were incubated at 37°C for 5-10 min with shaking at 200 rpm. The 'co-clicked' cells were then washed three times with PBS by centrifugation (10,000 rcf for 1 min) and resuspension, followed by fixing.

2.15.6 Bocillin FL labelling of PBPs

For conventional fluorescence microscopy visualisation, a 1 ml aliquot of cell culture grown to early-exponential phase (OD_{600} ~0.5) was transferred to a microcentrifuge tube. Cells were incubated with 1 μg ml^{-1} Bocillin FL for 5 min at 37°C. Bocillin FL labelled cells were washed twice with PBS by centrifugation (10,000 rcf for 1 min) and resuspension. Cells were then fixed.

For SIM imaging, cells were grown to early-exponential phase (OD_{600} ~0.5) and fixed. 1 ml of cells suspended in PBS was incubated with 10 μg ml^{-1} Bocillin FL for 10 min at room temperature. Bocillin FL labelled cells were washed three times with PBS by centrifugation (16,000 rcf for 1 min) and resuspension.

2.15.7 Penicillin G and Bocillin FL competition assay

1 ml aliquots of cell culture grown to early-exponential phase (OD_{600} ~0.5) were transferred to microcentrifuge tubes. 0-100 μg ml^{-1} Penicillin G (PenG) was added and cells were incubated for 5 min at 37°C with shaking at 200 rpm. Cells were washed by centrifugation at 10,000 rcf for 1 min at room temperature. The cell pellets were resuspended in 1 ml of pre-warmed BHI and 1 μg ml^{-1} Bocillin FL was added. Cells were incubated with for 5 min at 37°C with shaking at 200 rpm. Bocillin FL labelled cells were washed twice with PBS by centrifugation (10,000 rcf for 1 min at room temperature) and resuspension. Cells were then fixed.

2.15.8 Labelling of SNAP fusions

For conventional fluorescence microscopy visualisation, cells producing SNAP fusions were grown to early exponential phase (OD_{600} ~0.5). A 1 ml aliquot of cell culture was transferred to a microcentrifuge tube and a SNAP dye (SNAP-Cell TMR-Star or SNAP-Cell or FtsZ-SNAP 647-SiR) was added to a final concentration of 0.5 or 1 μM. SNAP labelled cells were washed twice with PBS by centrifugation at 10,000 rcf for 1 min and then fixed.

For super-resolution microscopy imaging, a 1 ml aliquot of cell culture grown to early-exponential phase (OD_{600} ~0.5) was incubated with 3 μM SNAP-Cell TMR-Star at 37°C for 10 min. The labelled cells were then spun at 10,000 rcf for 1 min at room temperature. The pellet was resuspended in pre-warmed BHI and cells were grown at

37°C for 10 min with shaking at 200 rpm to remove the excess dye. The cells were washed three times in PBS by centrifugation (10,000 rcf for 1 min) and resuspension, followed by fixing.

2.15.9 Vancomycin labelling of cell wall

Fixed cells were resuspended in 1 ml PBS. 20 µl of 200 µM Vancomycin Alexa Fluor 647 conjugate (Van-AF647) was added to a final concentration of 4 µM and cells were incubated for 30 min at room temperature. The cells were washed twice in PBS by centrifugation (16,000 rcf for 1 min) and resuspension.

2.15.10 Reductive caging of fluorophores

In order to create a photoactivatable fluorescent probe a sample was chemically caged using a reducing agent (Vaughan et al., 2012). Prior to microscopy visualisation, fluorescently labelled and fixed cells were resuspended in PBS containing 10 mM $NaBH_4$. The sample was incubated for 5 min at room temperature. The cells were washed three times with PBS by centrifugation (16,000 rcf for 1 min) and resuspension.

2.15.11 Preparation of samples for fluorescence microscopy

2.15.11.1 Sample preparation for conventional fluorescence microscopy

5 µl of fixed cells was dried onto a poly-L-lysine coated slide (Poly-Prep, Sigma) using nitrogen gas. The slide was washed with dH_2O and dried with nitrogen gas. A coverslip was then mounted with 5 µl PBS and sealed with transparent nail varnish.

2.15.11.2 Coverslip preparation for super-resolution microscopy

A high precision cover glass thickness no 1.5H was cleaned by sonicating in 1 M KOH for 15 min at room temperature. The coverslip was washed with dH_2O. The cover glass was submerged in 0.01% (w/v) poly-L-lysine solution (Sigma) and incubated for 30 min at room temperature. The coverslip was rinsed with dH_2O and dried with nitrogen gas.

2.15.11.3 Sample preparation for structured illumination microscopy (SIM)

3 µl of fixed cells resuspended in HPLC-grade water was dried onto the poly-L-lysine coated coverslip (section 2.15.11.2) with nitrogen gas. The slide was washed with dH_2O and dried with nitrogen gas. 5 µl of SlowFade Gold (Molecular Probes) was placed onto

a Poly-Prep slide (Sigma). The coverslip with the cells was placed on the mounting solution drop and sealed with transparent nail varnish.

2.15.11.4 Sample preparation for stochastic optical reconstruction microscopy (STORM)

3 µl of fixed cells resuspended in HPLC-grade water and 3 µl of 130 nm gold nanoparticles (1:20 dilution HPLC-grade water, Nanopartz) or 100 nm TetraSpeck Microspheres (1:500 dilution in HPLC-grade water, Molecular Probes) were dried onto the poly-L-lysine coated coverslip (section 2.15.11.2) with nitrogen gas. The slide was washed with dH_2O and dried with nitrogen gas. 5 µl of PBS or an imaging buffer (2.15.11.4.2) was placed onto a Poly-Prep slide (Sigma). The coverslip with the cells was placed on the mounting solution drop and sealed with transparent nail varnish.

2.15.11.4.1 STORM dilution buffer

Tris	50 mM
NaCl	10 mM

pH was adjusted to 8.0. The buffer was stored at 4^oC.

2.15.11.4.2 STORM imaging buffers

All STORM imaging buffers were freshly prepared in STORM dilution buffer (section 2.15.11.4.1) prior to microscopy imaging.

GLOX

Glucose	10% (w/v)
Catalase	40 µg ml^{-1}
Glucose oxidase	0.5 mg ml^{-1}

MEA

β-mercaptoethylamine	100 mM

GLOX MEA

Glucose	10% (w/v)
Catalase	40 µg ml^{-1}
Glucose oxidase	0.5 mg ml^{-1}

β-mercaptoethylamine	100 mM

GLOX 50 mM MEA

Glucose	10% (w/v)
Catalase	40 μg ml^{-1}
Glucose oxidase	0.5 mg ml^{-1}
β-mercaptoethylamine	50 mM

GSH

Glutathione	160 mM

2.15.12 Conventional fluorescence microscopy

Fluorescence images were acquired using either a DeltaVision deconvolution microscope (Applied, precision, GE Healthcare) or a Nikon DualCam system (Elipse Ti inverted research microscope). Images obtained by DeltaVision were denconvolved using SoftWoRx v.3.5.1 software. Appropriate filters and wavelengths used for visualisation of fluorophores are listed in Table 2.9. Contrast and brightness adjustment and cell measurements were performed using Fiji (ImageJ 1.49v).

Filter	Nikon DualCam	DeltaVision		Fluorophore(s)
	Excitation wavelength (nm)	Excitation filter/bandpass (nm)	Emission filter/bandpass (nm)	
DAPI	395	360/40	457/50	HADA
FITC	470	492/20	528/38	eYFP, GFP, Bocillin FL, mEos2 (green form)
RD-TR-PE/ TxRED	555	555/28	617/73	TMR-Star, TADA, mEos2 (red form), PAmCherry1 (activated)
Cy5	640	640/20	685/40	Alexa Fluor 647, SiR-647

Table 2.9. Nikon DualCam light wavelengths and DeltaVision filter sets

2.15.13 SIM

3D-SIM was performed using the DeltaVision OMX (GE Healthcare) equipped with a Plan Apo 60x, 1.42 NA oil objective, using 1.514 immersion oil. Laser light was directed through a grating to generate a striped interference pattern on the sample plane. The pattern was shifted through five lateral phases and three angular rotations for each z-section (15 images per z-section). The z-sections were 0.125 µm in depth. The laser lines for visualisation of fluorophores are listed in Table 2.10. The raw data were reconstructed with SoftWoRx v.6.1.3 software. Data analysis was performed using a SIMcheck plugin comprehensive with Fiji. Contrast and brightness were adjusted using Fiji (ImageJ 1.49v).

Excitation laser wavelength (nm)	Emission filters (nm)	Fluorophore(s)
405	436/31	HADA
488	528/48	GFP, eYFP, Bocillin FL
568	609/37	TMR-Star

Table 2.10. DeltaVision OMX laser line details

2.15.14 STORM

2.15.14.1 Homebuilt STORM

Single molecule imaging of eYFP, PAmCherry1 and Alexa Fluor 647 was performed using an Olympus IX71 inverted optical microscope and a 60x, NA 1.4 oil immersion objective, a system described by Robert Turner (Turner et al., 2013). For eYFP imaging a 75 mW, 514 nm laser and a filter cube containing a 514 nm longpass dichroic filter and a 542/27 nm bandpass emission filter were used. To image PAmCherry1 a 50 mW, 405 nm and a 100 mw, 532 nm lasers and a filter cube containing a 570/30 nm longpass dichroic filter and a 620/40 nm bandpass emission filter were used. Alexa Fluor 647 imaging was performed using a 120 mW, 647 nm laser and a filter cube containing a 662 nm longpass dichroic filter and a 676/29 nm bandpass emission filter. A piezoelectric motor (Physik Instrumente) was used to adjust focus. An image expander comprising a 35 mm and 100 mm lens was used to project the image onto a Hamamatsu ImagEM camera set to acquire at 10-50 frames per second. A 1m focal length cylindrical lens was inserted between the image expander lenses to allow for compensation of drift perpendicular to the focal plane (Huang et al., 2008). Focus was maintained by repeatedly localising a fiducial marker (TetraSpeck or gold nanoparticle) and adjusting the objective position using the piezo to maintain a constant ratio of the

fitted full-width half maxima (FWHM) in perpendicular directions. Laser power was adjusted to maximize signal without saturating the charge-coupled device. The camera and piezo were controlled using custom Labview based software (Robert Turner).

Image processing was conducted using methodology as previously described by others (Betzig et al., 2006; Huang et al., 2008). Data were processed by fitting Gaussian functions to individual molecule fluorescence, identified by very clear intrinsic blinks, using Matlab. Drift in the focal plane was corrected retrospectively by tracking a fiducial particle throughout the acquisition sequence and offsetting localisations against its position.

2.15.14.2 N-STORM

Single molecule imaging of mEos2 and Alexa Fluor 647 was performed using a commercial Nikon N-STORM super-resolution system, equipped with Nikon Eclipse Ti-E inverted microscope, a SR Apochromat TIRF 100x 1.49 NA objective and Andor iXon 897 EM-CCD camera (Andor Technology). For 3D-STORM an astigmatic lens was inserted into the light path. A 405 nm laser was used for successive conversion of mEos2 from the green to the red fluorescent state, and the red mEos2 form was excited and read out with a 561 nm laser. Alexa Fluor 647 was imaged using a 647 nm laser. Data were collected at a frame rate of 9.2 ms/frame, with a camera EM gain multiplier value of 300, conversion gain value of 3, without binning for 40,000-80,000 frames until exhaustion of the fluorophore. Data collection and analysis was performed using Nikon NIS-Elements Ar with N-STORM analysis v4.10 software.

CHAPTER 3

Molecular studies on EzrA localisation

The work in this chapter was carried out in collaboration with Robert Turner (STORM) and Christa Walther (N-STORM and SIM)

3.1 Introduction

EzrA is a membrane associated protein involved in cell division in *S. aureus* (Steele et al., 2011). It was first identified as a cell division component in a large bioinformatics search for *B. subtilis* protein homologues in *S. aureus* (Bottomley, 2011; Steele et al., 2011). It was proposed to be a putative essential gene after it was found as one of 351 *S. aureus* genes that were not disrupted by a transposon insertion in a Transposon-Mediated Differential Hybridisation (TMDH) screen (Chaudhuri et al., 2009).

Experimental work carried out in our lab on a conditional *ezrA* mutant has confirmed its crucial role in *S. aureus* viability (Steele et al., 2011). In the absence of EzrA, peptidoglycan synthesis is inhibited, consequently cell division and growth are blocked (Jorge et al., 2011; Steele et al., 2011). Additionally EzrA has been proposed to be involved in the regulation of *S. aureus* cell size since its depletion results in an increase in average cell size (Jorge et al., 2011; Steele et al., 2011). A bacterial two-hybrid investigation of interactions between *S. aureus* proteins showed that EzrA interacts with three distinct groups of cell division components: the cytoplasmic proteins (FtsZ, FtsA, GpsB, SepF), the membrane associated proteins (DivIB, DivIC, FtsL) and proteins involved in peptidoglycan biosynthesis (PBP1, PBP2, PBP3) (Steele et al., 2011; Kent, 2013).

Localisation studies of EzrA using CFP, GFP and mCherry fluorescent fusions revealed that EzrA is recruited to the septum, where similarly to FtsZ, it forms a ring-like structure (Pereira et al., 2010; Steele et al., 2011; Jorge et al., 2011). Additionally, EzrA recruitment to midcell relies on the presence of FtsZ in the cell (Steele et al., 2011). What is more, EzrA is required for the proper localisation of other cell division

components such as GpsB, DivIB and PBP2, suggesting that EzrA acts as a scaffold that recruits other division proteins (Bottomley, 2011; Jorge et al., 2011; Steele et al., 2011).

More recently a crystal structure of *B. subtilis* EzrA has been resolved revealing that EzrA shares structural similarities with spectrin proteins, which in eukaryotic cells are involved in crosslinking and stabilising actin filaments, linking the plasma membrane to the actin cytoskeleton and function as an interface between the membrane and cytoplasm in signal transduction mediation (Cleverley et al., 2014; Machnicka et al., 2014). This finding together with the bacterial two-hybrid analysis results and the fact that EzrA does not have any enzymatic activity led to a hypothesis that EzrA plays a structural function and acts as an interface between cytoplasmic cell division components and the periplasmic peptidoglycan biosynthetic machinery (Steele et al., 2011; Cleverley et al., 2014).

S. aureus is an important human pathogen that has developed strategies to rapidly acquire antibiotic-resistance. As a result of its increasing antibiotic resistance understanding the mechanics of *S. aureus* cell division process may allow for the design of novel antibiotics that specifically target and interfere with cell division. Fluorescence microscopy is an indisputably valuable tool in studying organisation, dynamics and architecture of cellular components. As mentioned above EzrA is an a essential protein for *S. aureus* viability and its localisation, utilising GFP, mCherry and CFP, was successfully studied using widefield fluorescence microscopy and showed that EzrA localises in the mid-cell to form a continuous ring-like structure (Pereira et al., 2010; Jorge et al., 2011; Steele et al., 2011). Due to limitations caused by light diffraction, conventional fluorescence microscopy techniques reach a maximal resolution of ~200 nm. When studying cell processes in such small organisms such as *S. aureus*, which is only 1 μm in diameter and only a few times larger than the maximal resolution traditional microscopy techniques achieve, obtaining detailed information on organisation of cell division components becomes impossible.

Recent advancements in fluorescence microscopy have led to the development of super-resolution techniques that break the light diffraction limit, and thus reach higher resolution (Schermelleh et al., 2010). Lately, a super resolution fluorescence

microscopy technique, called Structured Illumination Microscopy (SIM) has been used to study localisation of EzrA-GFP in *S. aureus* and *B. subtilis* (Strauss et al., 2012). In both organisms EzrA-GFP was shown to be heterogeneously distributed at the future division site (Strauss et al., 2012). A time-lapse analysis of EzrA-GFP in live cells revealed that it is quite dynamic as rapid changes in fluorescence intensity could be observed within the structure formed by EzrA-GFP over a short time (Strauss et al., 2012). Based on these findings a new discontinuous bead-like pattern for EzrA localisation has been proposed (Strauss et al., 2012). Three-dimensional SIM (3D-SIM) can achieve a resolution up to ~100 nm and ~250 nm in lateral and axial dimensions, respectively, which is only a two-fold increase in resolution when compared to the classical microscopy diffraction limit (Schermelleh et al., 2010). Over the last few years other groups of super-resolution microscopy techniques have been developed. Among them, single-molecule super-resolution imaging techniques such as Photoactivated Localisation Microscopy (PALM) or Stochastic Optical Reconstruction Microscopy (STORM) achieve the highest resolution up to ~20 and ~50 nm in the lateral and axial dimensions, respectively (Betzig et al., 2006; Rust et al., 2006). Both STORM and PALM rely on the sequential and stochastic activation and localisation of individual molecules within a specimen. With this strategy a position for every single emitter can theoretically be determined up to a 1-2 nm precision if enough photons are recorded (Gelles et al., 1988). STORM potentially allows for localisation of every single molecule but it has particular requirements. One of them are photoswitchable fluorophores that in a controlled manner can switch between fluorescent and dark states (Dempsey et al., 2011).

Cell components are usually transparent and too small to be observed by light microscopy, that is why several strategies for targeting and labelling subcellular components in order to visualise them using fluorescence microscopy have been developed.

Immunolabelling is one of the most early and extensively used methods in fluorescence microscopy. This technique employs antibodies conjugated with fluorophores to recognise and target specific molecules within a cell (Coons and Kaplan, 1950; Borek, 1961). Immunostaining was successfully used in first localisation studies of FtsZ in *E. coli*, and PBP1 and PBP2 in *S. aureus* (Den Blaauwen et al., 1999; Pinho and

Errington, 2003; Pereira et al., 2007). Immunostaining, in theory, allows for direct and specific targeting of cell components of interest. Also a wide range of available fluorophores potentially gives flexibility in a choice of colour, which is especially important when performing more than one-colour microscopy imaging. Despite the advantages of immunolabelling, an important downside of this technique is the size of an antibody. Antibodies are quite large molecules (~150 kDa) (Janeway et al., 2001). If intracellular structures are studied, permeabilisation of the cell wall and membrane is crucial so that the antibody can get inside the cell. Therefore this method is only useful in fixed and permeabilised cells and is not compatible with live cell imaging. The main concerns when using immunostaining for super-resolution microscopy are the permeabilisation step and the size of an antibody. Permeabilisation can damage and alter the structures inside cells, which can create structural artefacts and lead to wrong conclusions Also the bulky size of the antibody adds an extra distance of 10-20 nm between the fluorescent label and targeted cell component and limits the effective resolution (Bates et al., 2008).

Another group of labels used extensively in fluorescence microscopy are fluorescent proteins. A fluorescent protein is usually produced as a fusion to a protein of interest and therefore acts as its fluorescent reporter. This allows for gene expression studies and tracking protein dynamics, localisation and interactions with other proteins in living organisms in real time. Since its discovery, GFP and its derivatives have been widely employed as reporters for protein localisation studies (Feilmeier et al., 2000; Phillips, 2001). Several fluorescent fusions proteins such as FtsZ-CFP, EzrA-GFP, EzrA-mCherry, GFP-PBP2, PBP4-mCherry and DivIB-GFP were used to investigate localisation of cell division components and to show that the majority of them localise to the midcell in *S. aureus* (Pereira et al., 2010; Jorge et al., 2011; Steele et al., 2011; Bottomley et al., 2014). As fluorescent proteins are produced as fusions and thus every molecule of a protein of interest is tagged, they can be an ideal option for quantification and dynamics studies of cell components. Using a fusion of FtsZ with GFP it was shown that in *E. coli* and *B subtilis* FtsZ is extremely dynamic, with FRAP half recovery time of 8-9 s at the septum (Anderson et al., 2004). Even though fluorescent fusion proteins have revolutionised protein studies such protein engineering carries potential risks. Adding a fluorescent protein to the protein of interest modifies it and this can alter its folding and function. Fluorescent fusion proteins are usually ectopically

produced in the presence of the endogenous protein resulting in protein overproduction (Stadler et al., 2013). Recent findings show that fluorescent tags can disrupt the protein function and its localisation. MreB was believed to form a helical structure in *E. coli* (Shih et al., 2005). ECM however revealed that the helical pattern was an artefact caused by fusing YFP with the N-terminus of MreB. This localisation artefact probably was not caused by the presence of a fluorescent tag by itself, since a fusion where mCherry was inserted into an internal loop of MreB did not form any helical structure (Swulius and Jensen, 2012). What is more, by testing various fusions of Clp proteases it was presented that depending on a fluorescent protein used as a reporter, Clp formed either clusters or was uniformly distributed in *E. coli* cells (Landgraf et al., 2012). Thus when constructing a fluorescent protein fusion it is crucial to make sure that it does not affect the function of the protein of interest and it is produced at wild type levels. This may prevent and eliminate artefacts arising from protein dysfunction and overproduction.

3.1.1 Potential fluorescent proteins for use in *S. aureus* localisation studies

STORM requires fluorophores that have an ability to switch between on and off states in a fashion controlled by light. Fluorescent proteins that are used in STORM can be divided into three groups: photoconvertible (or photoswitchable) fluorescent proteins switch from one emission state to another one following illumination with a specific light; reversibly photoswitchable fluorescent proteins can be repeatedly switched between on and off states with light; photoactivatable fluorescent proteins convert from a dark to a bright fluorescent state upon light irradiation; (Fernández-Suárez and Ting, 2008; Zhuang, 2009). A number of photocontrollable proteins have been developed and successfully incorporated into studies on bacterial structures at super-resolution in recent years (Bates et al., 2008; Subach et al., 2009).

One of the most extensively utilised fluorescent proteins in STORM is monomeric Eos2 (mEos2). This is a photoconvertible protein that upon UV illumination irreversibly converts from a green to a red form (McKinney et al., 2009). In *E. coli* FtsZ-mEos2 was shown to form a helical structure composed of a loose bundle of FtsZ protofilaments that randomly overlap with each other along longitudinal and radial directions of the cell (Fu et al., 2010). ZapA and ZapB fusions with mEos2 revealed that even though

both proteins localise to the midcell they do not share structural similarities in *E. coli* (Buss et al., 2015).

The other protein, whose development was specifically dedicated for STORM needs, is a photoswitchable monomeric Orange (PSmOrange) fluorescent protein. PSmOrange in its initial state is orange and after illumination with blue-green light switches to far-red. It is one of few far-red fluorescent proteins reported to be STORM-compatible to date (Subach et al., 2011).

Blinking enhanced YFP (eYFP) is a yellow derivative of GFP and is one of the first-reported STORM-compatible fluorescent proteins. eYFP is made to blink reversibly by first bleaching with 514 nm light and reactivating its fluorescence with a 407 nm laser. Fusing MreB with eYFP revealed that in *Caulobacter crescentus* MreB adopts different spatial structures depending on the stage of cell growth. eYFP-MreB was shown to adopt a helical structure in the early stage of the cell cycle and a ring-like structure in the late stages (Biteen et al., 2008).

Photoactivatable monomeric mCherry 1 (PAmCherry1) represents a group of photoactivatable fluorescent proteins. This red monomeric fluorescent protein is a derivative of mCherry, in which 10 amino acid substitutions were introduced to create the photoactivatable protein. In contrast to mCherry, PAmCherry1 is not fluorescent unless it is irreversibly photoactivated with ultraviolet light (Subach et al., 2009). Recently PAmCherry1 has been successfully employed in studying localisation of PBP4 in *S. aureus* in PALM (Monteiro et al., 2015). Apart from localisation studies, PAmCherry1 was found useful in quantifying dynamics of DNA polymerase I and ligase binding rates to DNA in *E. coli,* showing that only ~3% of DNA polymerase I and ligase molecules are active in replication and repair of DNA (Uphoff et al., 2013).

PAmCherry1 and eYFP seem to be valuable fluorescent proteins for two-colour PALM/STORM. Two-colour single-molecule localisation microscopy of CreS-eYFP and PopZ-PAmCherry1 in *C. crescentus* has demonstrated that PAmCherry1 and eYFP are a good pair of fluorescent proteins for two-colour imaging since they have different emission spectra (Gahlmann et al., 2013).

Previous studies have shown that EzrA can be successfully fused to fluorescent proteins, such as GFP or mCherry, and visualised using conventional fluorescence microscopy (Steele et al., 2011; Jorge et al., 2011). EzrA localisation, in contrast to other *S. aureus* cell division proteins, has been quite well studied and there are many EzrA molecules in the cell (10,000 to 20,000 estimated EzrA molecules per *B. subtilis* cell (Haeusser et al., 2004). For these reasons EzrA seemed to be an ideal candidate for development of STORM-compatible fluorescent fusions of *S. aureus* cell division components. Based on literature reports mEos2, PSmOrange, eYFP and PAmCherry1 were chosen to construct EzrA fluorescent fusions that could be employed in STORM.

3.1.2 Aims of this chapter

- Development of STORM-compatible fluorescent fusions of EzrA
- Construction of *S. aureus* strains producing functional EzrA fluorescent fusions
- Localisation of EzrA using super-resolution microscopy

3.2 Results

3.2.1 Screen for STORM-compatible EzrA fluorescent fusions

pKASBAR (Figure 3.1) is a shuttle vector that was constructed by amplifying a fragment containing an *attP* phage attachment site and a tetracycline resistance cassette from pCL84 using primers ALB135 and ALB136 and inserting it into pUC18 using *SphI* and *EcoRI* cut sites (Bottomley et al., 2014). pKASBAR-KanR (Figure 3.2) is a derivative of pKASBAR in which the tetracycline cassette was replaced by a kanamycin resistance cassette that was amplified from pGL433b (Wheeler et al., 2015) using primers kan_for_HindIII and kan_rev_HindIII, digested with *HindIII* and cloned into *HindIII* cut pKASBAR (Bottomley et al., 2014). Integration of pKASBAR and its derivatives into the *S. aureus* chromosome is based on the site-specific recombination system of the bacteriophage L54a (Lee et al., 1991). pKASBAR cannot replicate in *S. aureus*, but it can integrate into the bacterial chromosome via the *attP* attachment site present in the plasmid and the bacterial *attB* attachment site present in the 3' region of the lipase gene (*geh*). Recombination occurs in the presence of bacteriophage integrase, whose gene is expressed constitutively from the plasmid pYL112Δ19 (Lee et al., 1991). Integration of the plasmid results in a loss of lipase activity (Lee and Iandolo, 1986).

EzA is a membrane associated protein predicted to consist of a short N-terminal trans-membrane domain and a large C-terminal cytoplasmic domain that contains five coiled-coil domains (Steele et al., 2011). Based on information on its structure C-terminal fluorescent fusions of EzrA where designed.

pKASBAR-EzrA-mEos2 (Figure 3.3A) was constructed prior to this study in collaboration with Bartłomiej Salamaga (University of Sheffield). pKASBAR-EzrA-mEos2 is a pKASBAR derivative that carries *ezrA-meos2* under the control of a putative *ezrA* promoter (Appendix I). In pKASBAR-EzrA-mEos2, *ezrA* and *meos2* are joined by a 12 amino-acid (SRPRSGSGSGSG) spacer. The *ezrA-meos2* fragment, encoding the putative *ezrA* promoter and *ezrA* linked to *meos2* was synthesised by the GeneArt Gene Synthesis service (Life Technologies), digested with *BamHI* and *EcoRI* and inserted into pKASBAR linearised with the same restriction enzymes, resulting in pKASBAR-EzrA-mEos2 (Figure 3.3A).

pGM074 (Figure 3.3B; Gareth McVicker, unpublished) is a pKASBAR-KanR derivative carrying *ezrA-psmorange* under the control of a putative *ezrA* promoter (Appendix I). The *ezrA-psmorange* fragment encoding EzrA and PSmOrange as a translational fusion flanked by multiple cloning sites (MSCI and MSCII) was synthesised by the GeneArt Gene Synthesis service (Life Technologies) and cloned into pKASBAR-KanR using *BamHI* and *EcoRI* sites (Figure 3.3B). In pGM074, *ezrA* and *psmorange* are joined by a 15 amino-acid (SGSGSGGRASGSGSG) linker.

Both in pKASBAR-EzrA-mEos2 and pGM074 the putative *ezrA* promoter (141 nt fragment upstream of *ezrA*) and the *ezrA* gene sequences were based on the available DNA sequence of *S. aureus* NCTC 8325 (SAOUHSC) but corrected for the errors that have been identified in revised sequencing of the SAOUHSC genome. The differences were identified in single nucleotide residues and resulted in Phe54Ser and Thr73Asn substitutions in the original sequence (Table 3.1) (Berscheid et al., 2012).

Position of the nucleotide in SAOUHSC genome	Nucleotide in database	Resequenced nucleotide	Impact of correction
1733515	G	T	T73N
1733572	A	G	F54S

Table 3.1. Errors detected in the *ezrA* sequence of *Staphylococcus aureus* NCTC 8325
Adapted from (Berscheid et al., 2012).

In order to create EzrA-eYFP and EzrA-PAmCherry1 fusions the *eyfp* and the *pamcherry1* genes (Appendix I) were amplified from pG002 and pG003 plasmids (Poczopko, 2012) using eYFP-F and eYFP-R, and PAmCherry-F and PAmCherry-R primer pairs, respectively. Purified PCR products were digested with *AscI* and *NotI* and ligated into pGM074, which was digested with the same enzymes (Figure 3.4A and 3.5A). The ligation products were transformed into *E. coli* TOP10 electrocompetent cells and selected on LB ampicillin (100 μg ml^{-1}) plates. Positive clones were verified by plasmid extraction, restriction digestion with *EcoRI* and *BamHI* and confirmed to contain the correct DNA band sizes by electrophoresis on a 1% (w/v) agarose gel (Figure 3.4B and 3.5B). Plasmids were sequenced by the University of Sheffield Core Genomics Facility to check for the introduction of errors during PCR. The resulting plasmids did not contain any substitutions or mutations within the *eyfp* and the

pamcherry1 genes. A vector carrying *ezrA-eyfp* was named pKASBAR-EzrA-eYFP (Figure 3.4A), while a vector with *ezrA-pamcherry1* was named pKASBAR-EzrA-PAmCherry1 (Figure 3.5A). In both vectors EzrA and a fluorescent protein were linked with a 15 amino-acid (SGSGSGGRASGSGSG) linker.

In order to check if the fluorescent fusions were produced in *E. coli* and therefore had the correct photophysical properties SJF3963 (*E. coli* Top10 pKASBAR-EzrA-mEos2), SJF4179 (*E. coli* Top10 pGM074), SJF4383 (*E. coli* Top10 pKASBAR-EzrA-PAmCherry1) and SJF4382 (*E. coli* Top10 pKASBAR-EzrA-eYFP) were imaged using conventional fluorescence microscopy. All fluorescent fusions were found to be produced in *E. coli*. Both EzrA-PAmCherry1 and EzrA-eYFP were produced at high levels and localised mainly to the cell poles (Figure 3.6B and C). EzrA-mEos2 was produced by the *E. coli* cells and presented the excepted photophysical activities; it photoconverted from green to red after irradiation with UV light (figure 3.6A). Nevertheless EzrA-mEos2 fluorescence was observed in a few cells in the population and both the green and the red forms gave quite a poor fluorescent signal. Even though EzrA-PSmOrange was produced in some of the SJF4179 cells and was fluorescent when activated with a 555 nm wavelength, it did not photoswitch to a far-red form upon illumination with blue-green light (Figure 3.6B).

The ability to produce EzrA fluorescent fusions in *E. coli* suggested that the *ezrA* promoter shares some similarities to *E. coli* promoters and thus was recognised by *E. coli* gene expression systems. The fusions were not only produced and fluorescent but also presented some level of activity in *E. coli* as slightly elongated cells were observed when examined by microscopy (Figure 3.6). Extremely long SJF4383 cells were often found (data not shown) indicating that EzrA-PAmCherry1 might interact and interfere with cell division machinery of *E. coli*.

Fusing a fluorescent protein to a protein of interest can result in misfolding, loss of function and incorrect localisation. As EzrA is an *S. aureus* protein and does not have any homologues in *E. coli*, all designed fusion proteins had to be checked in a system in which EzrA is an endogenous cell component.

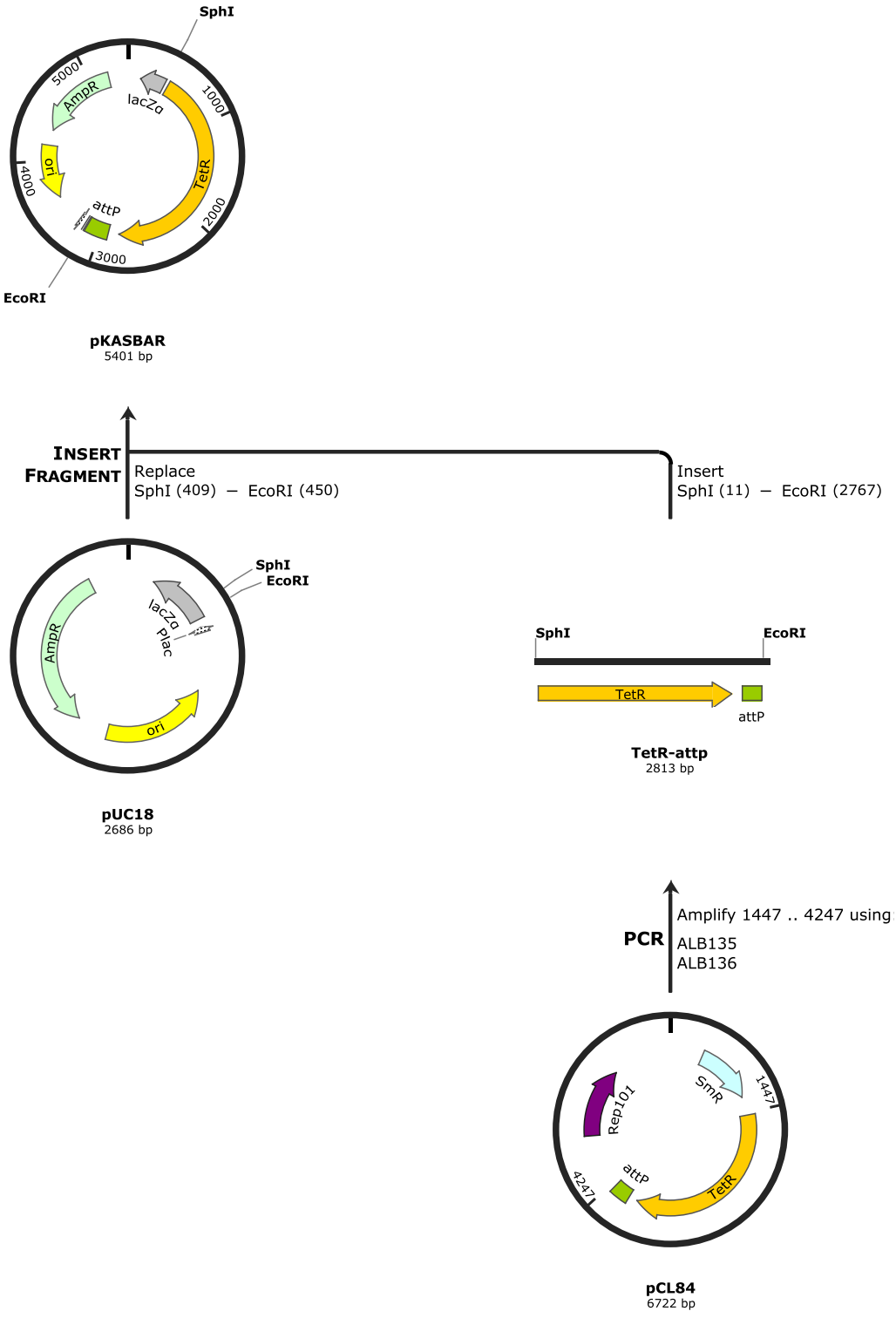

Figure 3.1. Construction of the integration plasmid pKASBAR

The TetR-attP fragment containing *attP* and a tetracycline resistance cassette was PCR amplified from pCL84 using ABL135 and ABL136 primers and ligated into the pUC18 plasmid using *SphI* and *EcoRI* sites, resulting in pKASBAR (Bottomley et al., 2014). pKASBAR comprises the high-copy-number ColE1 origin of replication (*ori*), LacZα fragment for β-galactosidase (*lacZα*) and an ampicillin resistance (AmpR) cassette from pUC18, and an *attP* phage attachment site and a tetracycline resistance (TetR) cassette from pCL84.

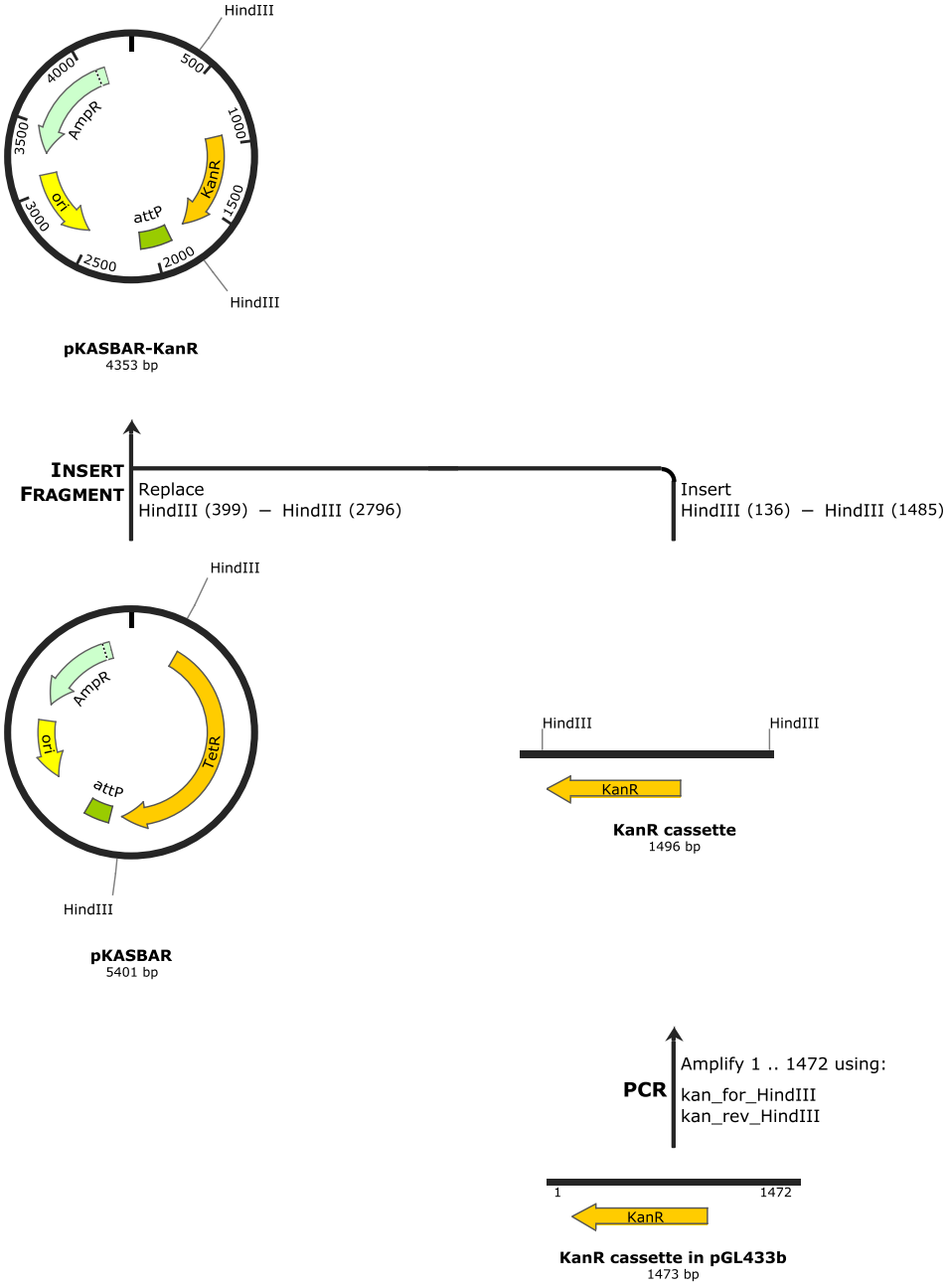

Figure 3.2. Construction of pKASBAR-KanR

The kanamycin resistance (KanR) cassette was PCR amplified from pGL433b using kan_for_HindIII and kan_rev_HindIII primers. The tetracycline resistance (TetR) cassette in pKASBAR was removed and replaced with the KanR cassette by *HindIII* digestion and ligation (Bottomley et al., 2014).

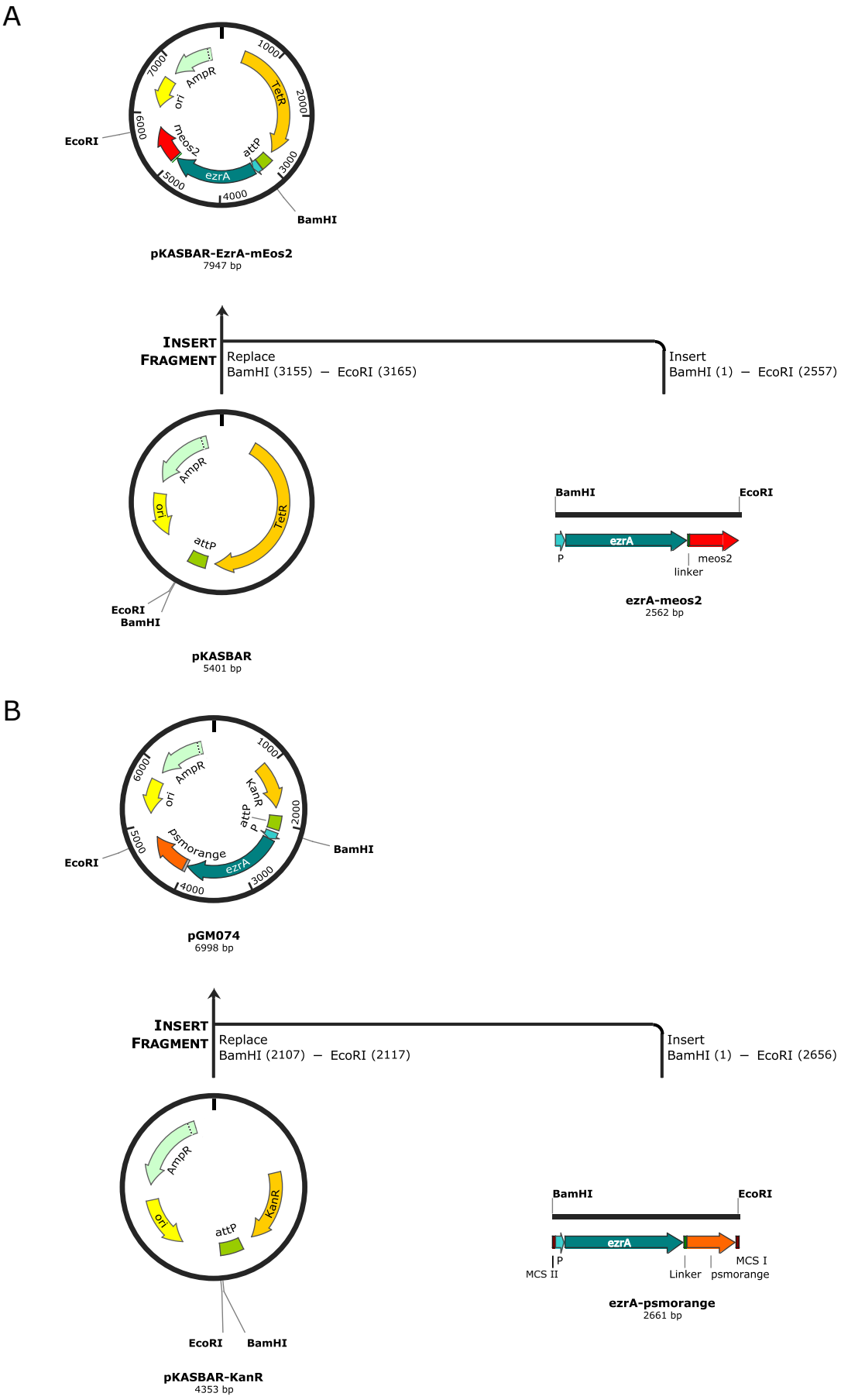

Figure 3.3. Construction of pKASBAR-EzrA-mEos2 and pGM074

A. The *ezrA-meos2* fragment carrying the putative *ezrA* promoter (P), the full length *ezrA* gene joined with the *meos2* gene by a 12 amino-acid linker was ligated into pKASBAR using *BamHI* and *EcoRI* cut sites, creating pKASBAR-EzrA-mEos2. This was carried out in collaboration with Bartłomiej Salamaga (University of Sheffield).

B. The *ezrA-psmorange* fragment flanked by multiple cloning sites (MSCI and MCS II), carrying the putative *ezrA* promoter (P) and the full length *ezrA* gene joined to the *psmorange* gene by a 15 amino-acid linker was digested and ligated into pKASBAR-KanR using *EcoRI* and *BamHI* sites, creating pGM074 (Gareth McVicker, unpublished).

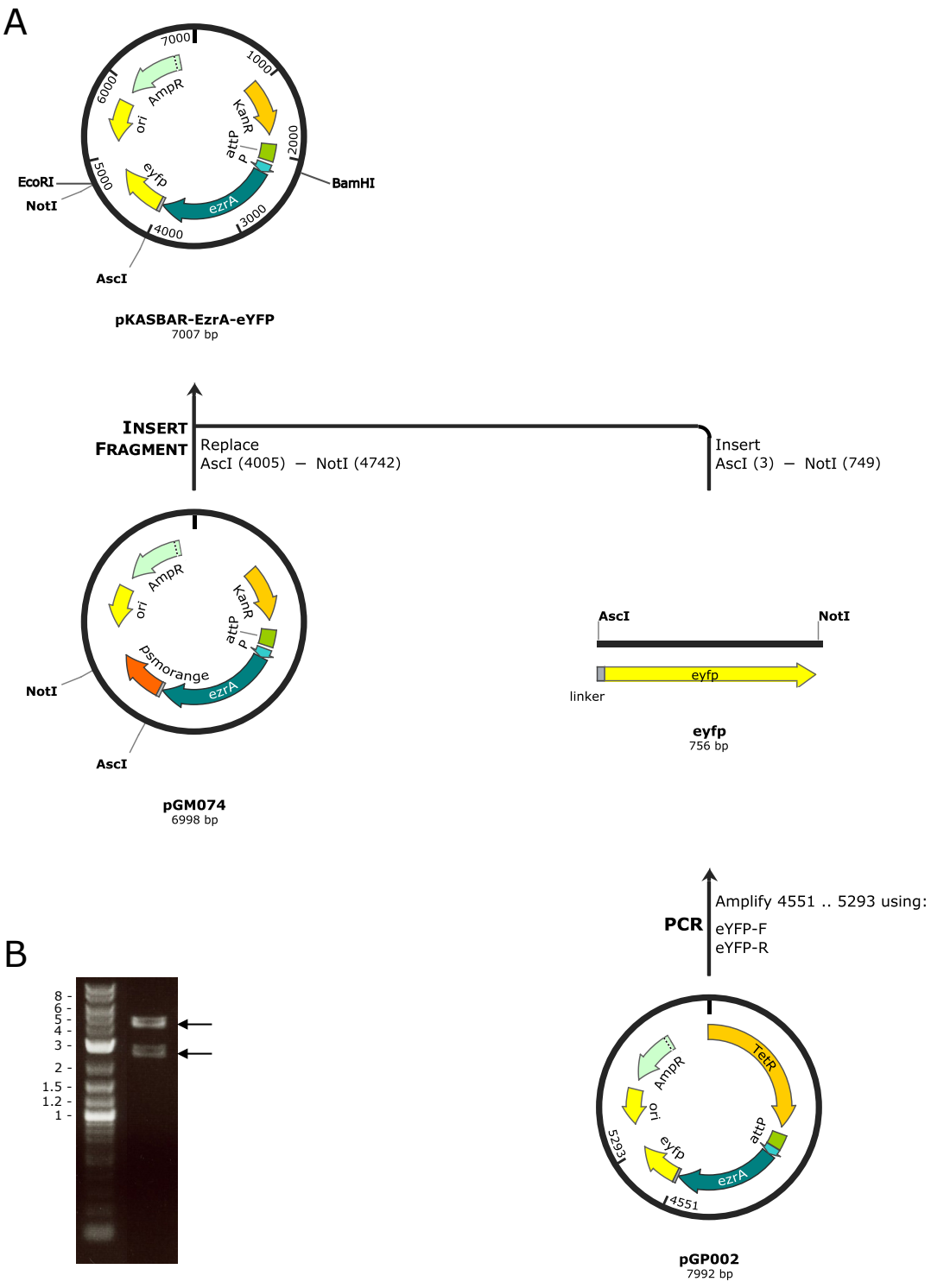

Figure 3.4. Construction of pKASBAR-EzrA-eYFP

A. The *eyfp* gene was PCR amplified from pGP002 using eYFP-F and eYFP-R primers, digested with *AscI* and *NotI* enzymes and ligated into pGM074 cut with the same enzymes, resulting in pKASBAR-EzrA-eYFP.

B. Restriction enzyme digest of pKASBAR-EzrA-eYFP with *EcoRI* and *BamHI*. The expected DNA band sizes of 4.3 kb and 2.6 kb are indicated with black arrows. Sizes of a DNA ladder are shown in kb.

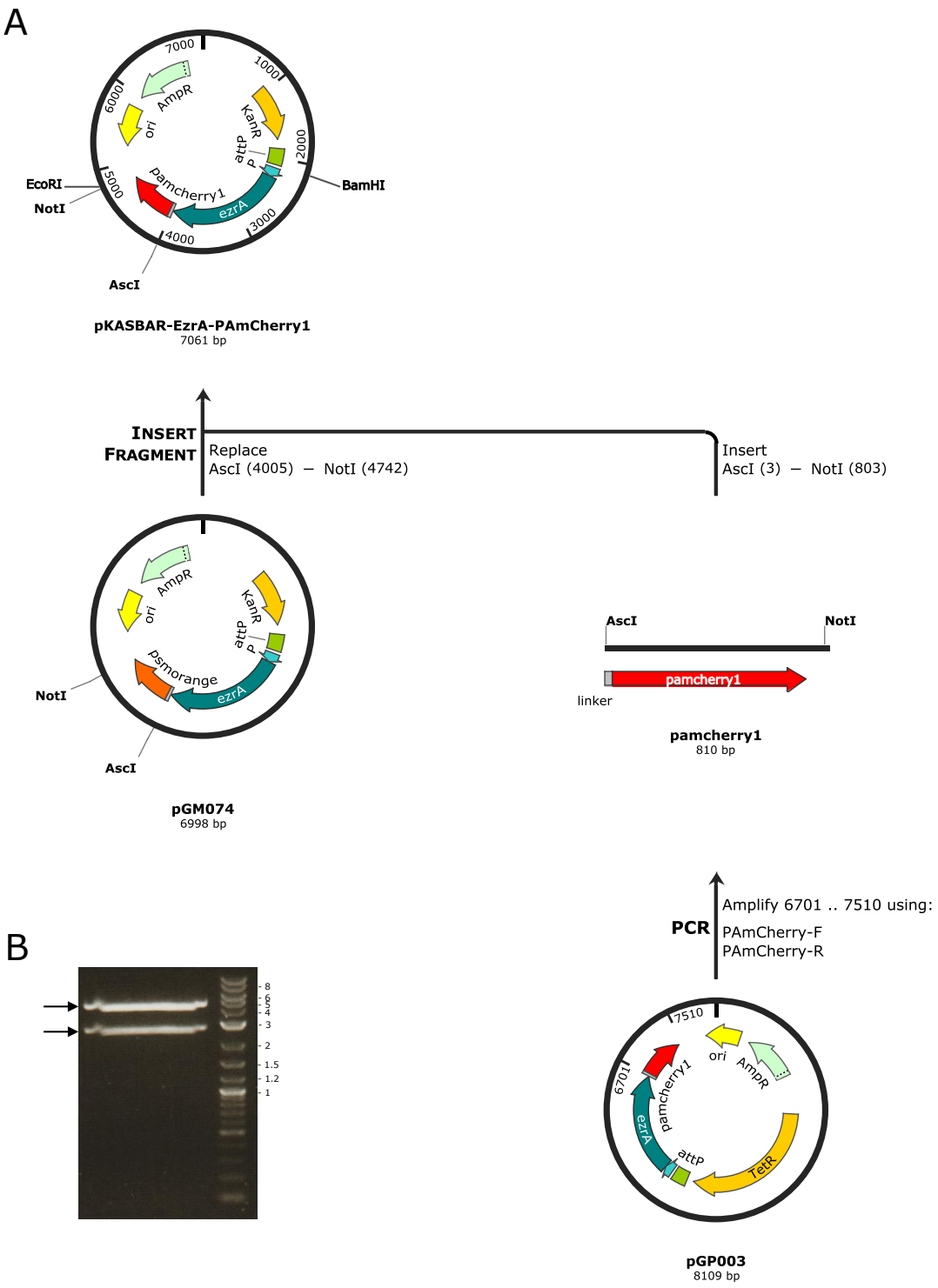

Figure 3.5. Construction of pKASBAR-EzrA-PAmCherry1

A. The *pamcherry1* gene was PCR amplified from pGP003 using PAmCherry-F and PAmCherry-R primers, digested with *AscI* and *NotI* enzymes and ligated into pGM074 cut with the same enzymes, resulting in pKASBAR-EzrA-PAmCherry1.

B. Restriction enzyme digest of pKASBAR-EzrA-PAmCherry1 with *EcoRI* and *BamHI*. The expected DNA band sizes of 4.3 kb and 2.6 kb are indicated with black arrows. Sizes of a DNA ladder are shown in kb.

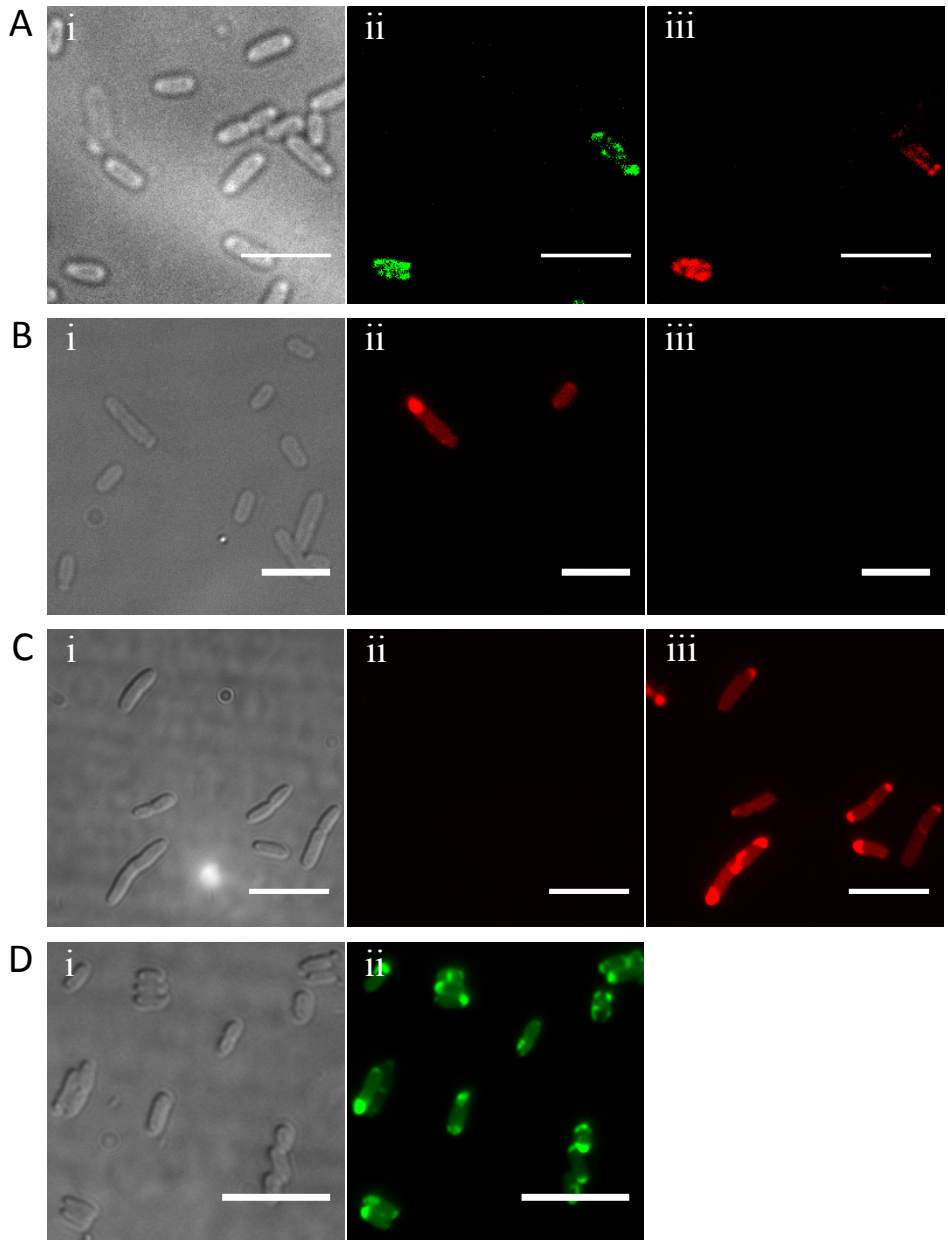

Figure 3.6. Fluorescence imaging of *E. coli* producing EzrA fluorescent fusions

A. EzrA-mEos2 is produced in SJF3963 (*E. coli* Top10 pKASBAR-EzrA-mEos2) but not by all the cells present in a field of view (i, brightfield). EzrA-mEos2 has the expected physical properties and converts from a green (ii) to a red (iii) form upon UV illumination. Scale bars 5 μm.

B. EzrA-PSmOrange is produced in SJF4179 (*E. coli* Top10 pGM074) but only by a few cells present in a field of view (i, brightfield). EzrA-PSmOrange is fluorescent in orange (ii) but does not convert into far-red (iii) when illuminated with blue-green light. Scale bars 5 μm.

C. EzrA-PAmCherry1 is produced by all SJF4383 (*E. coli* Top10 pKASBAR-EzrA-PAmCherry1) cells captured in brightfield (i). The cells are not fluorescent before photoactivation (ii) but become red (iii) after irradiation with UV light. The same contrast was adjusted for the ii and iii images. Scale bars 5 μm.

D. EzrA-eYFP is produced by SJF4382 (*E. coli* Top10 pKASBAR-EzrA-eYFP; i, brightfield) and all cells in the population are fluorescent (ii). Scale bars 5 μm.

In order to test EzrA fluorescent fusions in *S. aureus* pKASBAR-EzrA-mEos2, pGM074, pKASBAR-EzrA-eYFP and pKASBAR-EzrA-PAmCherry1 were transformed into electrocompetent SJF1332 (*S. aureus* RN4220 pYL112Δ19). The cells transformed with pKASBAR-EzrA-mEos2 were selected on BHI tetracycline (5 μg ml^{-1}) plates, whereas the cells transformed with pGM074, pKASBAR-EzrA-eYFP and pKASBAR-EzrA-PAmCherry1 on kanamycin (50 μg ml^{-1}) plates. As integration of pKASBAR and its derivatives into the *S. aureus* chromosome occurs via site-specific recombination within the lipase gene (*geh*), the cells grown after transformation were tested on Baird-Parker plates. The positive control, SJF1332 produced a zone of precipitation around colonies, while the transformants showed a loss of lipase activity indicating correct integration of the plasmids into the chromosome at the *geh* gene (Figure 3.7A and B). Additionally the presence of the *eyfp* and the *pamcherry1* genes in the chromosome of transformants was confirmed by PCR on extracted genomic DNA using primer pairs eYFP-F and eYFP-R, and PAmCherry-F and PAmCherry-R (Figure 3.7C).

The resulting strains SJF3963 (*S. aureus* RN4220 *geh::ezrA-meos2*), RNpGM074 (*S. aureus* RN4220 *geh::ezrA-psmorange*), SJF4384 (*S. aureus* RN4220 *geh::ezrA-eyfp*) and SJF4385 (*S. aureus* RN4220 *geh::ezrA-pamcherry1*) were grown to exponential phase and fixed cells were visualised by fluorescence microscopy. Among all tested EzrA fluorescent fusions only EzrA-eYFP and EzrA-PAmCherry1 were produced and demonstrated the EzrA septal localisation in SJF4384 and SJF4385, respectively (Figure 3.8C and D). The localisation patterns of EzrA-eYFP and EzrA-PAmCherry1 were similar to the one previously reported (Steele et al., 2011). Although both fusions were quite bright, EzrA-PAmCherry1 seemed to give a dimmer signal than EzrA-eYFP. Both eYFP and PAmCherry1 belong to the same family of GFP derived proteins; yet they have different photophysical properties. PAmCherry1, in contrast to eYFP, requires a photoactivation step to become bright. EzrA-mEos2 gave very weak green and red fluorescence emissions thus making it impossible to observe EzrA localisation or to show if mEos2 was photoconvertible in SJF3963 (Figure 3.8A). Similarly to EzrA-mEos2, EzrA-PSmOrange was found to be neither fluorescent in orange nor to photoconvert to far-red, so that EzrA localisation could not be visualised in RNpGM074 (Figure 3.8B).

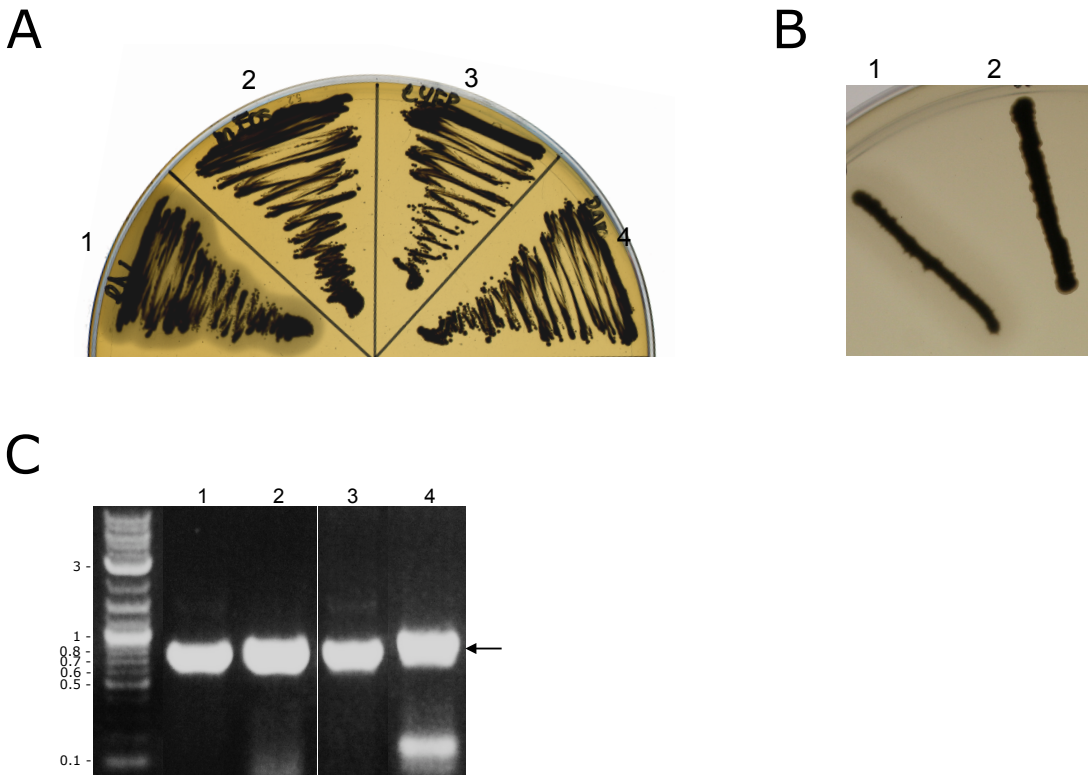

Figure 3.7. Confirmation of correct integration of pKASBAR-EzrA-mEos2, pGM074, pKASBAR-EzrA-eYFP and pKASBAR-EzrA-PAmCherry1 into the *S. aureus* chromosome

A. SJF1332 (1) and SJF3963 (*S. aureus* RN4220 *geh::ezrA-meos2*) (2), SJF4384 (*S. aureus* RN4220 *geh::ezrA-eyfp*) (3), and SJF4385 (*S. aureus* RN4220 *geh::ezrA-pamcherry1*) (4) were plated on Baird-Parker agar. A loss of lipid hydrolysis confirmed the plasmid integration within the *geh* gene.

B. Disruption of lipase production due to correct integration of pGM074 was confirmed by plating SJF1332 (1) and RNpGM074 (*S. aureus* RN4220 *geh::ezrA-psmorange*) (2) on a Baird-Parker agar.

C. Integration of pKASBAR-EzrA-eYFP and pKASBAR-EzrA-PAmCherry1 into the *S. aureus* chromosome was confirmed by PCR amplification on genomic DNA of *S. aureus* RN4220 *geh::ezrA-eyfp* (SJF4384, lane 3) and *S. aureus* RN4220 *geh::ezrA-pamcherry1* (SJF4385, lane 4) using primers eYFP-F and eYFP-R, and PAmCherry-F and PAmCherry-R, respectively. Plasmids pKASBAR-EzrA-eYFP (lane 1) and pKASBAR-EzrA-PAmCherry1 (lane 2) were used as positive controls of PCR. The expected bands of ~750 bp are indicated with a black arrow. Sizes of a DNA ladder are shown in kb.

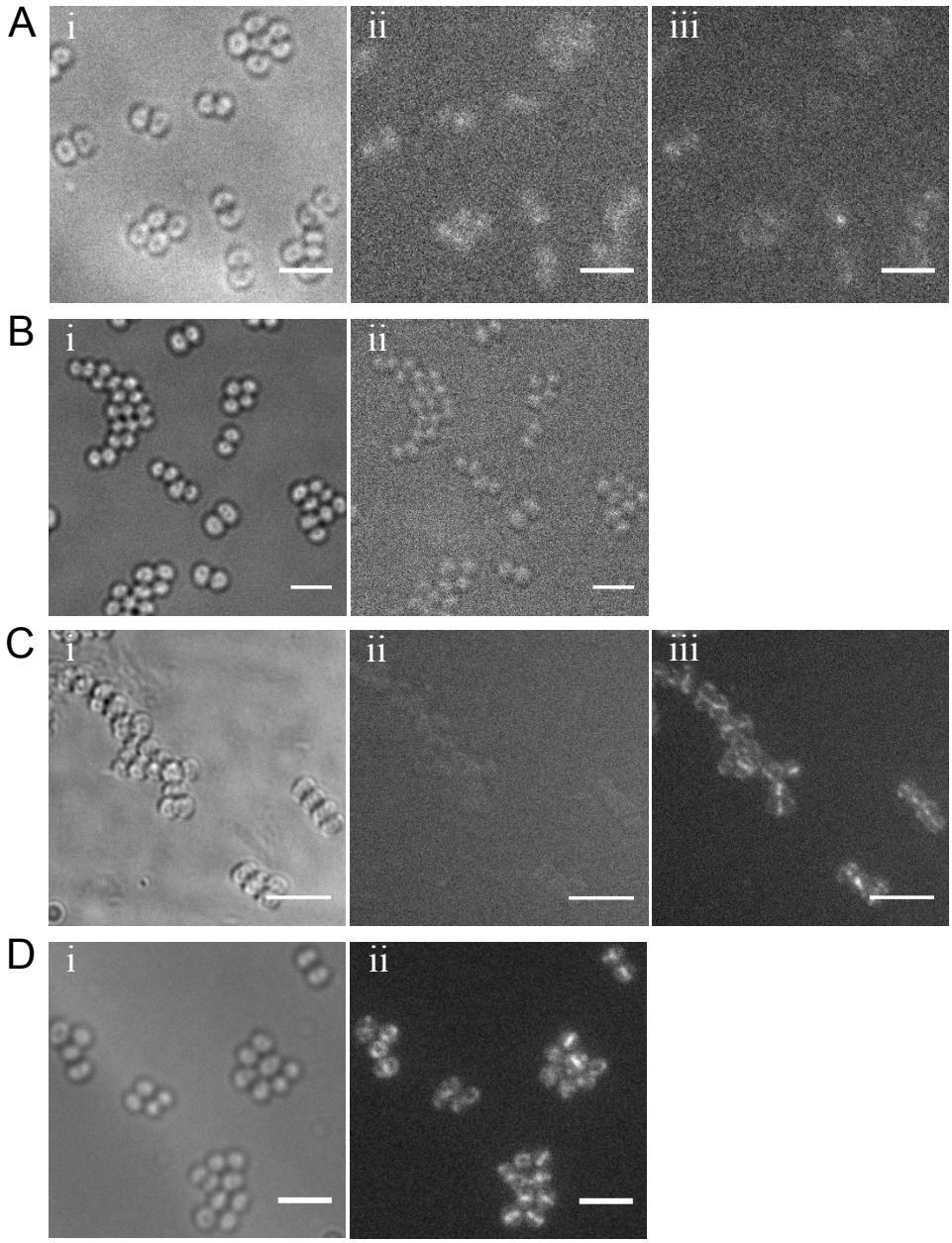

Figure 3.8. Fluorescence imaging of EzrA fluorescent fusions in *S. aureus* RN4220

A. In SJF3963 (*S. aureus* RN4220 *geh::ezrA-moes2*) EzrA-mEos2 is poorly produced and does not form any pattern of localisation characteristic for EzrA. Cells carrying *ezrA-meos2* visible in brightfield (i), are weakly fluorescent both in green (ii) and after illumination with UV light in red (iii). Scale bars 3 μm.

B. None of the RNpGM074 (*S. aureus* RN4220 *geh::ezrA-psmorange*) cells (i, brightfield) is orange fluorescent (ii) or photoswitches to far-red (data not shown). Scale bars 3 μm.

C. EzrA-PAmCherry1 is produced in SJF4385 (*S. aureus* RN4220 *geh::ezrA-pamcherry1*). Cells captured in brightfield (i) produce EzrA-PAmCherry1 that is photoactivatable, converts from a dark state (ii) a red fluorescent form (iii) upon UV irradiation, and has the expected septal localisation. Scale bars 3 μm.

D. In all SJF4384 (*S. aureus* RN4220 *geh::ezrA-eyfp*) cells (i, brightfield) EzrA-eYFP is fluorescent and localises to the septum (ii). Scale bars 3 μm.

Insertion of EzrA fluorescent fusion into the chromosome supplied *S. aureus* with an additional copy of the *ezrA* gene. In the presence of both *ezrA* copies, that is the native and the extra *ezrA* copy in the *geh* locus, EzrA-eYFP and EzrA-PAmCherry1 were produced and localised to the septa as expected. EzrA is an essential protein for *S. aureus*, therefore it was crucial to exclude that the proper localisation of these fluorescent fusions was caused by a masking effect of the native EzrA protein. Since EzrA-eYFP and EzrA-PAmCherry1 were the only two of four tested EzrA fluorescent proteins that were both fluorescent and had the expected localisation pattern. *S. aureus* strains in which either the *ezrA-eyfp* or the *ezrA-pemcherry1* gene was the only copy of *ezrA* present in the genome were constructed to investigate functionality of EzrA fusions.

3.2.2 Construction of *S. aureus* strains in which the only copy of EzrA is tagged with a fluorescent protein

Analysis of the downstream region of the *ezrA* gene showed that a terminator is present after *ezrA,* thus polar effects of *ezrA* transcription on downstream genes is unlikely (Fairclough, 2009). EzrA has been shown to be a crucial protein as depletion of *ezrA* affects an average cell size and viability of *S. aureus* (Jorge et al., 2011; Steele et al., 2011). Therefore creation of a mutant strain in which either *ezrA-eyfp* or *ezrA-pamcherry1* is the only copy of *ezrA* present in *S. aureus* should allow to test the functionality of the EzrA-eYFP and EzrA-PAmCherry1 fusion proteins. Deletion of the native *ezrA* gene was performed in the presence of a copy of either *ezrA-eyfp* or *ezrA-pamcherry1* placed under the control of the native *ezrA* promoter introduced into the *S. aureus* genome within the lipase encoding gene locus.

A pOB vector was chosen to construct *S. aureus* strains with a marked deletion of *ezrA*. Under antibiotic selection this non-replicating, suicide plasmid integrates into the chromosome via single crossover recombination, which occurs between the target sequence and a homologous sequence provided on the plasmid (Horsburgh et al., 2002b).

3.2.2.1 Construction of an *ezrA* deletion vector

In order to delete the native *ezrA* gene from the *S. aureus* genome, an *S. aureus* suicide vector containing a deletion cassette was constructed. Primers pOB-ezrA-up-F and pOB-ezrA-up-R, and pOB-ezrA-down-F and pOB-ezrA-down-R were designed to amplify 1.5 kb upstream (up) and downstream (down) regions of the *ezrA* gene from *S. aureus* SH1000 genomic DNA, respectively (Figure 3.9A). The up fragment covered a region from -1500 bp to -1 bp upstream of the *ezrA* start codon and the down fragment covered a region from 1 bp to 1497 bp downstream of the *ezrA* stop codon (Figure 3.9A). Primers pOB-TetR-F and pOB-TetR-R where used to amplify a 2.1 kb fragment containing the tetracycline resistance (TetR) cassette form pAISH (Aish, 2003) (Figure 3.9C). The primers were designed to incorporate 20 bp overhanging sequences complementary to the end of the other DNA fragment. The PCR products were resolved on a 1% (w/v) agarose gel (Figure 3.9B) and purified. The purified DNA fragments together with pOB, which was linearised by sequential digestion with *SmaI* and *HindIII*, were joined by Gibson assembly (Figure 3.9C). The assembly products were used to transform electrocompetent *E. coli* Top10 cells. Transformants were selected on LB plates containing tetracycline (12.5 μg ml^{-1}). One positive clone was identified by plasmid extraction, restriction digestion with *EcoRI* and *HindIII* and confirmed to contain the correct DNA band sizes by electrophoresis on a 1% (w/v) agarose gel (Figure 3.9D). The plasmid was sequenced by the University of Sheffield Core Genomics Facility to check for the introduction of mutations during the cloning steps. The resulting plasmid carrying the *ezrA* deletion cassette (up-TetR-down) was called pOB-ΔezrA (Figure 3.9C).

3.2.2.2 Construction of *ezrA* deletion *S. aureus* strains

In order to determine functionality of EzrA-eYFP and EzrA-PAmCherry1, SJF4384 (*S. aureus* RN4220 *geh::ezrA-eyfp*) and SJF4385 (*S. aureus* RN4220 *geh::ezrA-pamcherry1*) were lysed with Φ11 and the chromosomal regions that contained *ezrA-eyfp* and *ezrA-pamcherry1* were transferred into SH1000 cells by phage transduction. The resulting strains SJF4386 (*S. aureus* SH1000 *geh::ezrA-eyfp*) and SJF4387 (*S. aureus* SH1000 *geh::ezrA-pamcherry1*) were tested for a loss of lipase activity and verified by PCR using primers eYFP-F and eYFP-R, and PAmCherry-F

and PAmCherry-R (data not shown). When cells were examined by fluorescence microscopy they were fluorescent and EzrA fusions presented septal localisation (Figure 3.10).

pOB-ΔezrA was transformed into electrocompetent *S. aureus* RN4220 with selection on BHI erythromycin (5 μg ml^{-1}) and tetracycline (5 μg ml^{-1}) plates. As pOB-ΔezrA carried DNA fragments homologous to the regions upstream (up) and downstream (down) of the *ezrA* gene integration of the plasmid into the *S. aureus* chromosome could occur through either the up or the down region via a single crossover recombination event (Figure 3.11A). The downstream integration of pOB-ΔezrA into *S. aureus* RN4220 that created RNpOB-ΔezrA (*S. aureus* RN4220 with integrated pOB-ΔezrA) was confirmed by PCR using primers ezrA-up-F and tet5'-R, and ezrA-down-R and tet3'-F (Figure 3.11B). RNpOB-ΔezrA was lysed with Φ11 and the chromosomal fragment containing the deletion cassette was transferred into SJF4386 and SJF4387 via phage transduction with selection using tetracycline (5 μg ml^{-1}) and kanamycin (50 μg ml^{-1}). Clones, in which the double crossover recombination event (Figure 3.11) resulted in replacement of *ezrA* by the tetracycline resistance cassette (*ΔezrA::tet*) were screened for a tetracycline-resistant and erythromycin-sensitive phenotype. The percentage of clones that were resistant to tetracycline but erythromycin sensitive was ~8% (7 out of 85 screened clones) for cells carrying *ezrA-eyfp* and ~5% (11 out of 186 tested clones) for cells with the *ezrA-pamcherry1* gene.

Putative positive clones, SJF4388 (*S. aureus* SH1000 *geh::ezrA-eyfp ΔezrA::tet*) and SJF4389 (*S. aureus* SH1000 *geh::ezrA-pamcherry1 ΔezrA::tet*) were verified by PCR. Genomic DNA was extracted from SJF4388 and SJF4389, and the *ezrA* region was amplified using primers ezrA-up-F and ezrA-down-R (Figure 3.12A). SJF4388 and SJF4389 showed DNA bands of the expected sizes (Figure 3.12B and C). Knowing that there is a restriction site for *HindIII* within the *ezrA* gene and the TetR cassette is not cut by *HindIII*, the same PCR products were analysed by restriction digestion using *HindIII*. SJF4388 and SJF4389 showed a band of 5 kb corresponding to an uncut PCR product, whereas *S. aureus* SH1000, SJF4384 and SJF4385 gave the expected digestion product of 2.4 kb (Figure 3.12D and E).

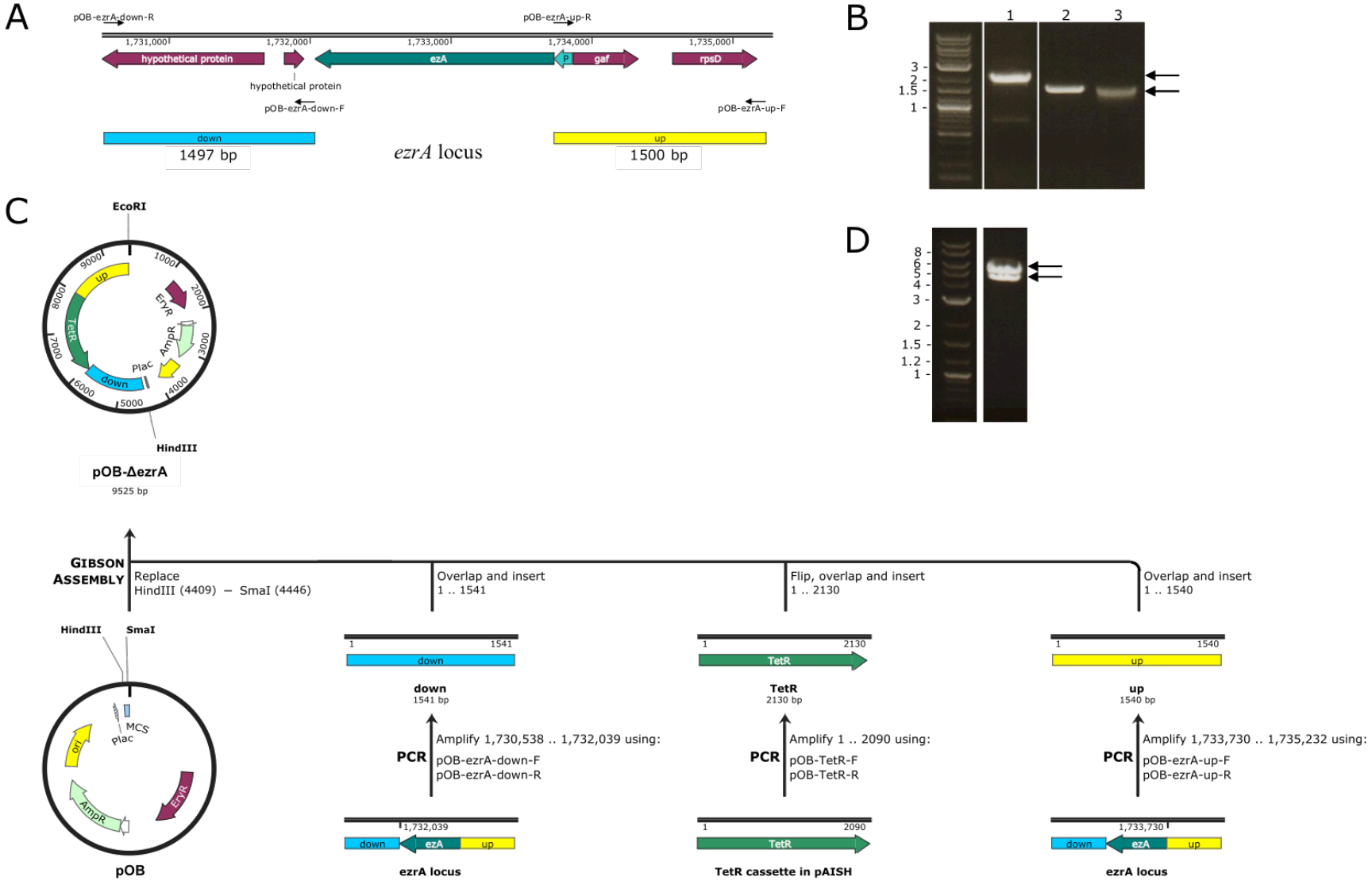
A
pOB-ezrA-down-R
pOB-ezrA-up-R
1,731,000
1,732,000
1,733,000
1,734,000
1,735,000
hypothetical protein
hypothetical protein
ezA
P
gaf
rpsD
pOB-ezrA-down-F
pOB-ezrA-up-F
down
1497 bp
ezrA locus
up
1500 bp
B
1
2
3
3
2
1.5
1
C
EcoRI
9000
1000
2000
3000
4000
5000
6000
7000
8000
up
EtvR
AmpR
Plac
down
TetR
HindIII
pOB-ΔezrA
9525 bp
D
8
6
5
4
3
2
1.5
1.2
1
GIBSON ASSEMBLY
Replace
HindIII (4409) – SmaI (4446)
Overlap and insert
1 .. 1541
Flip, overlap and insert
1 .. 2130
Overlap and insert
1 .. 1540
HindIII
SmaI
MCS
Plac
ori
AmpR
EtvR
pOB
1
1541
down
down
1541 bp
1
2130
TetR
TetR
2130 bp
1
1540
up
up
1540 bp
PCR
Amplify 1,730,538 .. 1,732,039 using:
pOB-ezrA-down-F
pOB-ezrA-down-R
PCR
Amplify 1 .. 2090 using:
pOB-TetR-F
pOB-TetR-R
PCR
Amplify 1,733,730 .. 1,735,232 using:
pOB-ezrA-up-F
pOB-ezrA-up-R
1,732,039
down
ezA
up
ezrA locus
1
2090
TetR
TetR cassette in pAISH
1,733,730
down
ezA
up
ezrA locus

Figure 3.9. Construction of the *ezrA* deletion vector, pOB-ΔezrA

A. Chromosome region of *ezrA* in *S. aureus*. The locations of pOB-ezrA-up-F, pOB-ezrA-up-R, pOB-ezrA-down-F and pOB-ezrA-down-R annealing sites to allow amplification of ~1.5 kb flanking regions of the *ezrA* gene (up and down) are indicated.

B. 1% (w/v) TAE agarose gel showing products of PCR amplification of the tetracycline-resistance cassette (1), the fragment upstream (up) of *ezrA* (2) and the fragment downstream (down) of *ezrA* (3). The expected DNA fragments of 2.1 kb and 1.5 kb are indicated with black arrows. Sizes of a DNA ladder are shown in kb.

C. Diagrammatic representation of pOB-ΔezrA construction. A 1.5 kb fragment (up) covering a region from -1500 bp to -1 bp upstream of the *ezrA* start codon and ~1.5 kb fragment (down) covering region from 1 bp to 1497 bp downstream (down) of the *ezrA* stop codon were PCR amplified from *S. aureus* SH1000 genomic DNA using primers pOB-ezrA-up-F and pOB-ezrA-up-R, and pOB-ezrA-down-F and pOB-ezrA-down-R, respectively. A 2.1 kb fragment (TetR) containing the tetracycline resistance cassette was PCR amplified form pAISH using primers pOB-TetR-R and pOB-TetR-R. The up, TetR and down fragments were joined with *SmaI* and *HindIII* linearised pOB by Gibson assembly. The resulting plasmid, pOB-ΔezrA comprises the high-copy-number ColE1 origin of replication (*ori*), ampicillin resistance (AmpR), tetracycline resistance (TetR) and erythromycin resistance (EryR) cassettes and the *ezrA* up and down regions.

D. Restriction enzyme digest of pOB-ΔezrA with *EcoRI* and *HindIII*. The expected DNA band sizes of 5.1 kb and 4.4 kb are indicated with black arrows. Sizes of a DNA ladder are shown in kb.

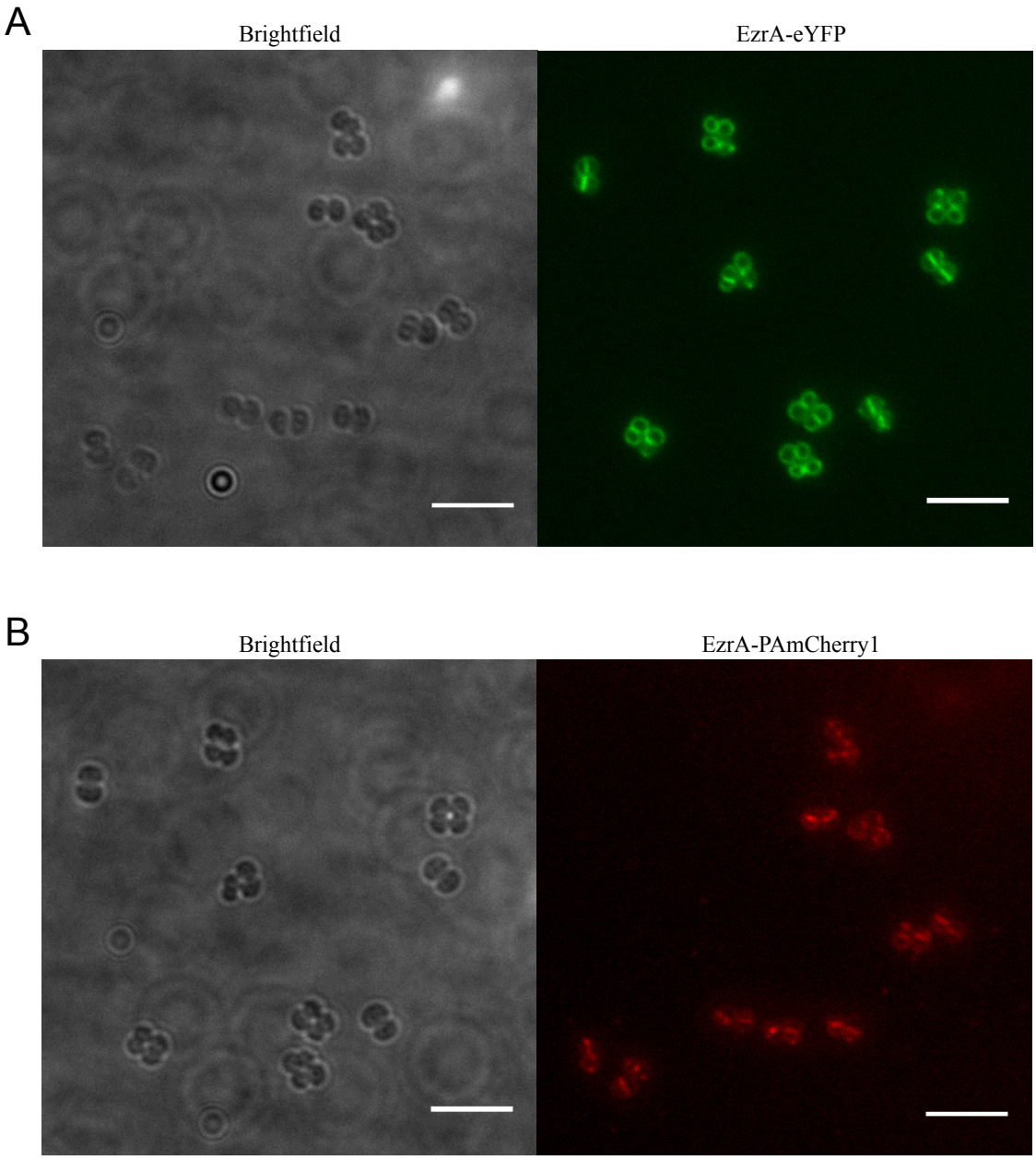

Figure 3. 10. EzrA-eYFP and EzrA-PAmCherry1 are fluorescent and localise to the septa in SJF4386 and SJF4387

A. In SJF4386 (*S. aureus* SH1000 *geh::ezrA-eyfp*) in the presence of the native EzrA protein, EzrA-eYFP localises to the septum. The fluorescence image of EzrA-eYFP is a maximum intensity projection of z-stack images acquired at 200 nm z-intervals. Scale bars 5 μm.

B. In the presence of the native EzrA protein, EzrA-PAmCherry1 localises to the septum in SJF4387 (*S. aureus* SH1000 *geh::ezrA-pamcherry1*). The fluorescence image of EzrA-PAmCherry1 is a maximum intensity maximum intensity projection of z-stack images acquired at 200 nm z-intervals. Scale bars 5 μm.

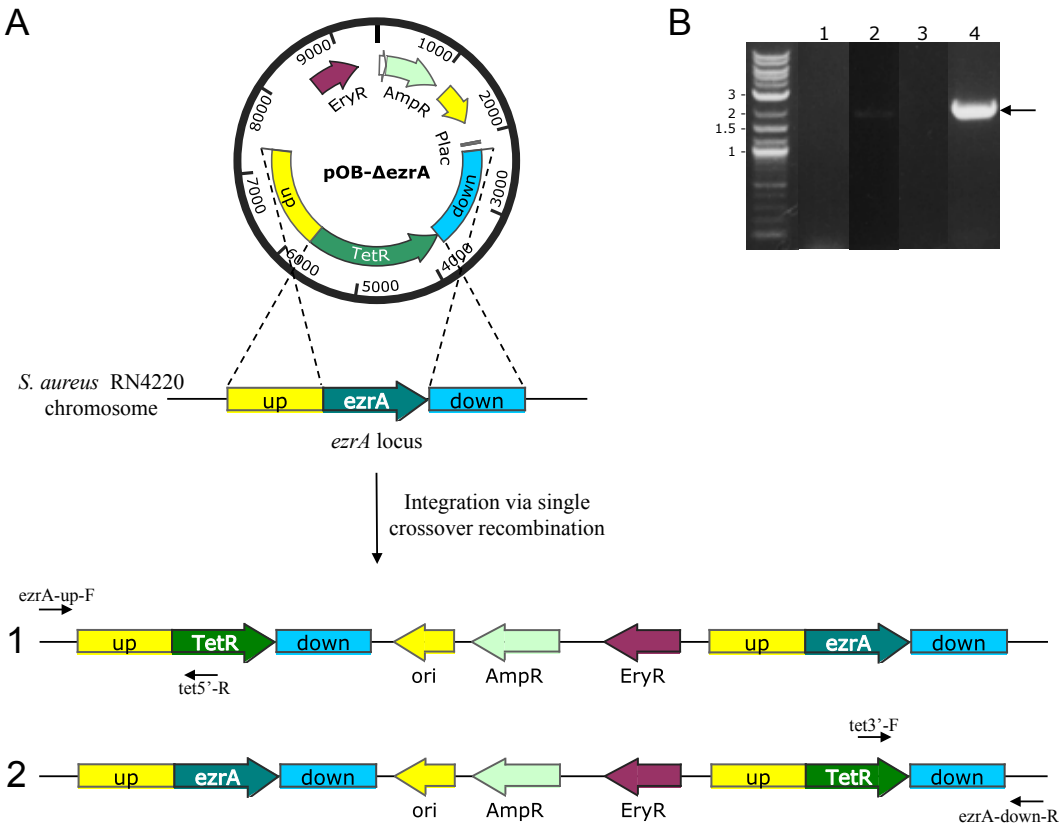

Figure 3.11. Homologous recombination of pOB-ΔezrA into the *S. aureus* RN4220 chromosome

A. Diagrammatic representation of the likely recombination outcomes of pOB-ΔezrA in the *S. aureus* RN4220 chromosome. A single crossover recombination event occurs via either the upstream region (1) or the downstream region (2). Annealing sites of primer pairs ezrA-up-F and tet5'-R, and tet3'-F and ezrA-down-R used to screen for the site of plasmid integration are indicated. Not to scale.

B. The site of pOB-ΔezrA integration into *S. aureus* RN4220 chromosome, which resulted in RNpOB-ΔezrA, was determined by PCR using the primer pairs ezrA-up-F and tet5'-R (upstream integration), and tet3'-F and ezrA-down-R (downstream integration). No product or a faint band was observed for primers ezrA-up-F and tet5'-R (lane 3) and a product of 2 kb (indicated with a black arrow was obtained for primers tet3'-F and ezrA-down-R (lane 4), indicating that the plasmid integration occurred via the downstream region. As expected, *S. aureus* RN4220 genomic DNA, which was used as a PCR negative control, did not give any product for either pair of primers (lanes 1 and 2). Sizes of a DNA ladder are shown in kb.

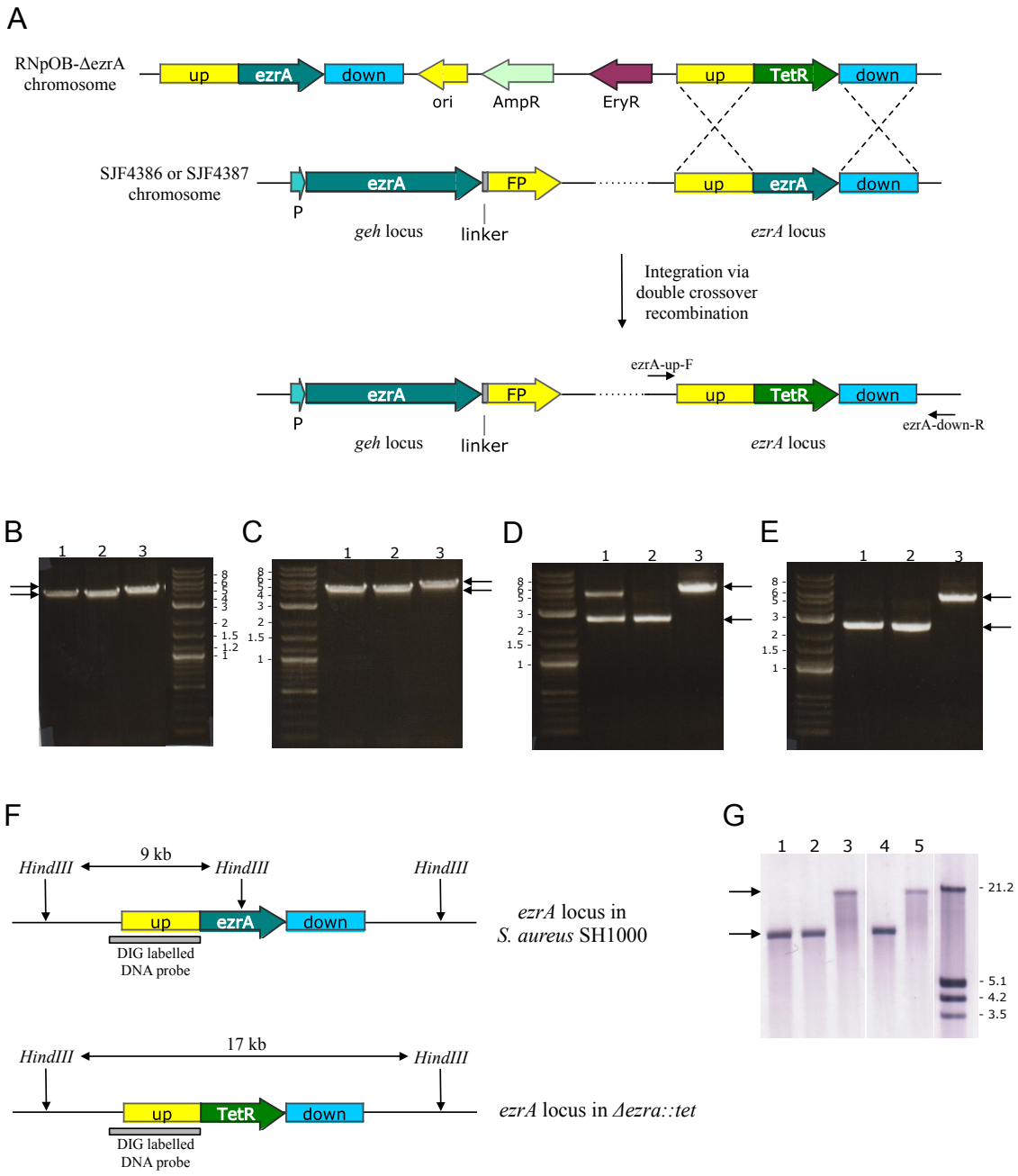

Figure 3.12. Construction of the marked deletion of *ezrA* (*ΔezrA::tet*) in SJF4386 and SJF4387

A. Diagrammatic representation of a double crossover event that leads to replacement of the native *ezrA* gene with the TetR cassette in SJF4386 (*S. aureus* SH1000 *geh::ezrA-eyfp*) and SJF4387 (*S. aureus* SH1000 *geh::ezrA-pamcherry1*). ezrA-FP represents either an *ezrA-eyfp* or an *ezrA-pamcherry1* gene. Annealing sites of primers ezrA-up-F and ezrA-down-R used to confirm the marked deletion of *ezrA* (*ΔezrA::tet*) are indicated. Not to scale.

B. Replacement of *ezrA* for the TetR cassette in SJF4388 (*S. aureus* SH1000 *geh::ezrA-eyfp ΔezrA::tet*) was confirmed by PCR on genomic DNA using primers ezrA-up-F and ezrA-down-R. A product of 4.8 kb that corresponds to the wild type *ezrA* locus and a product of 5.3 kb confirming the *ΔezrA::tet* mutation were obtained for SH1000 and SJF4386 (*S. aureus* SH1000 *geh::ezrA-eyfp*) (lanes 1 and 2),

and SJF4388 (lane 3), respectively. The PCR products are indicated with black arrows. Sizes of a DNA ladder are shown in kb.

C. Replacement of *ezrA* for the TetR cassette in SJF4389 (*S. aureus* SH1000 *geh::ezrA-pamcherry1 ΔezrA::tet*) was confirmed by PCR on genomic DNA using the primer pairs ezrA-up-F and ezrA-down-R. A product of 4.8 kb that corresponds to the wild type *ezrA* locus and a product of 5.3 kb confirming the *ΔezrA::tet* mutation were obtained for SH1000 and SJF4387 (*S. aureus* SH1000 *geh::ezrA-pamcherry1*) (lanes 1 and 2), and SJF4389 (lane 3), respectively. The PCR products are indicated with black arrows. Sizes of a DNA ladder are shown in kb.

D. DNA fragments (from B), which were obtained by PCR amplification of genomic DNA of SH1000 and SJF4386 (*S. aureus* SH1000 *geh::ezrA-eyfp*), using primers ezrA-up-F and ezrA-down-R, are cut by *HindIII* (lanes 1 and 2), whereas the PCR product obtained for SJF4388 (*S. aureus* SH1000 *geh::ezrA-eyfp ΔezrA::tet*) using the same primer pair is not cut by *HindIII* (lane 3). The expected DNA fragments of 2.4 kb and 5.3 kb are indicated with black arrows. A DNA fragment of 4.8 kb in lane 1 corresponds to a not fully cut PCR product. Sizes of a DNA ladder are shown in kb.

E. DNA fragments (from C), which were obtained by PCR amplification of genomic DNA of SH1000 and SJF4387 (*S. aureus* SH1000 *geh::ezrA-pamcherry1*), using primers ezrA-up-F and ezrA-down-R, are cut by *HindIII* (lanes 1 and 2), whereas the PCR product obtained for SJF4389 (*S. aureus* SH1000 *geh::ezrA-pamcherry1 ΔezrA::tet*) using the same primer pair is not cut by *HindIII* (lane 3). The expected DNA fragments of 2.4 kb and 5.3 kb are indicated with black arrows. Sizes of a DNA ladder are shown in kb.

F. Diagrammatic representation of relevant *HindIII* restriction sites in the genome of SH1000 and the *ΔezrA::tet* derivatives: SJF4388 (*S. aureus* SH1000 *geh::ezrA-eyfp ΔezrA::tet*) and SJF4389 (*S. aureus* SH1000 *geh::ezrA-pamcherry1 ΔezrA::tet*). Hybridising sites of the probe and the expected sizes of the DNA fragments bound by the probe during Southern blot analysis are indicated. Not to scale.

G. Southern blot analysis of SJF4388 (*S. aureus* SH1000 *geh::ezrA-eyfp ΔezrA::tet*) and SJF4389 (*S. aureus* SH1000 *geh::ezrA-pamcherry1 ΔezrA::tet*). Genomic DNA was isolated from SH1000 (lane 1), SJF4386 (*S. aureus* SH1000 *geh::ezrA-eyfp*) (lane 2), SJF4387 (*S. aureus* SH1000 *geh::ezrA-pamcherry1*) (lane 4), SJF4388 (lane 3) and SJF4389 (lane 5), digested with *HindIII* and probed with a digoxygenin (DIG)-labelled 1645 bp DNA probe. A DNA band of 9 kb indicates the *ezrA* presence, while 17 kb DNA band confirms the TetR cassette integration at the *ezrA* locus (indicated with black arrows). Sizes of a DNA ladder are shown in kb.

SJF4388 (*S. aureus* SH1000 *geh::ezrA-eyfp ΔezrA::tet*) and SJF4389 (*S. aureus* SH1000 *geh::ezrA-pamcherry1 ΔezrA::tet*) were further analysed by Southern hybridisation. Genomic DNA from *S. aureus* SH1000, SJF4386, SJF4387, SJF4388 and SJF4389 was isolated, digested with *HindIII* and separated by 0.8% (w/v) agarose gel electrophoresis. Genomic DNA fragments were blotted onto a positively charged nylon membrane and probed with a 1645 bp DNA fragment, corresponding to the upstream region of *ezrA* (covering a region from -1645 bp to -1 bp upstream from the *ezrA* start codon), which had been amplified using primers ezrA-up-F and ezrA-up-R and labelled with digoxigenin (DIG). Southern blot results showed that in SJF4388 and SJF4389 the native *ezrA* gene was replaced by the TetR cassette resulting in an expected hybridising band of ~17 kb, whilst *S. aureus* SH1000, SJF4386 and SJF4387 DNA gave hybridising bands of ~9 kb (Figure 3.12F and G).

PCR analysis and Southern blot hybridisation showed SJF4388 (*S. aureus* SH1000 *geh::ezrA-eyfp ΔezrA::tet*) and SJF4389 (*S. aureus* SH1000 *geh::ezrA-pamcherry1 ΔezrA::tet*) to be genetically as expected. Although SJF4388 and SJF4389 were found to be viable when the only copy of EzrA present in the cell was tagged with either eYFP or PAmCherry1, insufficient EzrA production or its deletion can alter cell viability, growth and morphology (Jorge et al., 2011; Steele et al., 2011).

To investigate their morphology, SJF4388 (*S. aureus* SH1000 *geh::ezrA-eyfp ΔezrA::tet*) and SJF4389 (*S. aureus* SH1000 *geh::ezrA-pamcherry1 ΔezrA::tet*) were grown to exponential phase and viewed by fluorescence microscopy. Both in SJF4388 and SJF4389 the fusion proteins localised to the septa. The localisation pattern in SJF4388 was comparable to the EzrA-eYFP localisation in SJF4386 (Figures 3.10A and 3.13A). Similarly, EzrA-PAmCherry1 in SJF4389 gave the same pattern of localisation as in SJF4387 (Figures 3.10B and 3.10B). Moreover, no changes in the fluorescence signal distribution between the strains carrying one copy of *ezrA*, SJF4388 and SJF4389, and those carrying two copies of *ezrA*, that is the native *ezrA* gene and the fusion, SJF4286 and SJF4387, were observed. This demonstrates that the septal localisation of EzrA-eYFP and EzrA-PAmCherrry1 observed in SJF4386 and SJF4387, respectively, was not an artefact caused by the presence of the functional native protein.

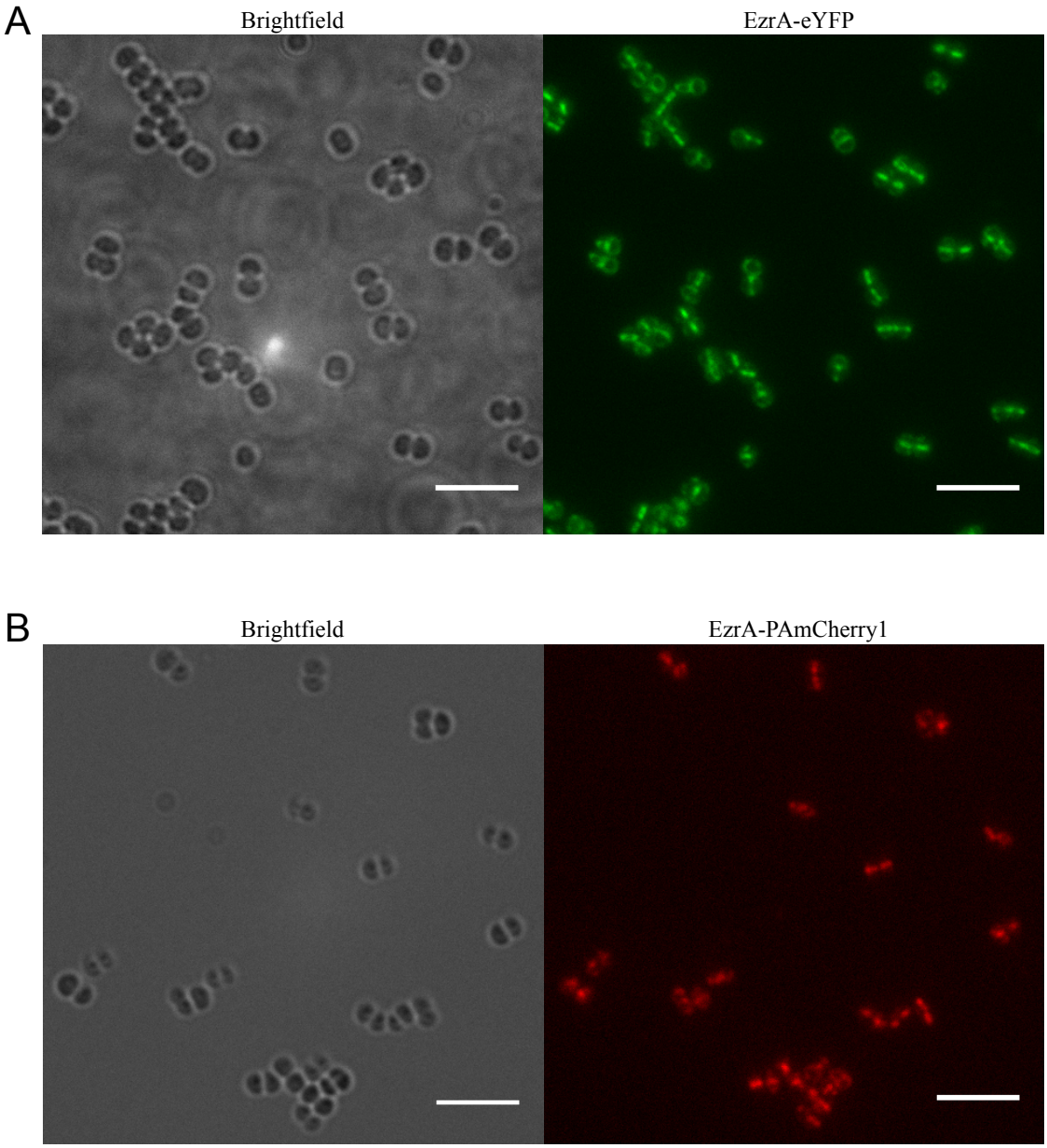

Figure 3.13. EzrA-eYFP and EzrA-PAmCherry1 localise to the septa in the absence of native EzrA

A. In SJF4388 (*S. aureus* SH1000 *geh::ezrA-eyfp ΔezrA::tet*) EzrA-eYFP septal localisation is not altered by the lack of the native EzrA protein and it forms a ring-like structure, similar to the localisation pattern in SJF4386. The fluorescence image of EzrA-eYFP is a maximum intensity projection of z-stack images acquired at 200 nm z-intervals. Scale bars 5 µm.

B. In SJF4389 (*S. aureus* SH1000 *geh::ezrA-pamcherry1 ΔezrA::tet*) EzrA-PAmCherry1 septal localisation is not altered by the lack of the native EzrA protein and it forms a ring-like structure, similar to the localisation pattern in SJF4387. The fluorescence image of EzrA-PAmCherry1 is a maximum intensity projection of z-stack images acquired at 200 nm z-intervals. Scale bars 5 µm.

SJF4388 (*S. aureus* SH1000 *geh::ezrA-eyfp ΔezrA::tet*) and SJF4389 (*S. aureus* SH1000 *geh::ezrA-pamcherry1 ΔezrA::tet*) did not show any severe growth defect on solid media. In order to test if EzrA-eYFP and EzrA-PAmCherry1 could complement the absence of native EzrA, growth of SJF4388 and SJF4389 was compared against the growth of the parental *S. aureus* SH1000 strain in liquid media. SH1000, SJF4388 and SJF4389 were grown overnight in BHI media containing appropriate antibiotics. These cultures were used to inoculate 50 ml of prewarmed BHI to an OD_{600} 0.01 and growth of the cultures was checked by optical density measurements. No differences were observed between *S. aureus* SH1000 and SJF4388 or SJF4389 (Figure 3.14A and B) suggesting that the growth of the mutant strains was not affected by the lack of native *ezrA* when either *ezrA-eyfp* or *ezrA-pamcherry1* was present.

Morphology of SJF4388 and SJF4389 was further examined by measurements of cell diameter. SJF4388 and SJF4389 did not display any altered cell sizes and their average cell diameter of 0.89 ± 0.12 μm was similar to the size of *S. aureus* SH1000 (0.9 ± 0.11 μm) (Figure 3.14C).

Western blot analysis was performed to check for the correct size and stability of fluorescent fusions of EzrA. Whole cell lysates of SJF4386 and SJF4388 grown to exponential phase (OD_{600} ~1) were probed with rabbit anti-GFP antibodies at a 1:1000 dilution. A band of ~90 kDa, which corresponds to the expected size of EzrA-eYFP, was detected in both strains. No additional bands were observed suggesting that the EzrA-eYFP fusion was stable and was not degraded (Figure 3.14D). A faint band of ~50 kDa was detected in *S. aureus* SH1000 but its size matches the molecular weight of Protein A that binds the Fc region of immunoglobulins. When the whole cell lysates of SJF4387 and SJF4389 were analysed with rat serum raised against the mCherry-HisTag protein, the expected band of ~90 kDa likely representing EzrA-PAmCherry1 was observed for both strains (Figure 3.14E). As a result of non-specific reactivity of the rat serum with other components of the cell lysates it was difficult to determine if the EzrA-PAmCherry1 fusion was stable. Interestingly, western blot analysis showed that the levels of EzrA-eYFP and EzrA-PAmCherry1 are comparable between SJF4386 and SJF4387, and their *ΔezrA::tet* derivative strains, SJF4388 and SJF4389, respectively. Due to the lack of anti-EzrA antibodies it was not possible to analyse if the EzrA fluorescent proteins were produced at the same level as native EzrA in SH1000.

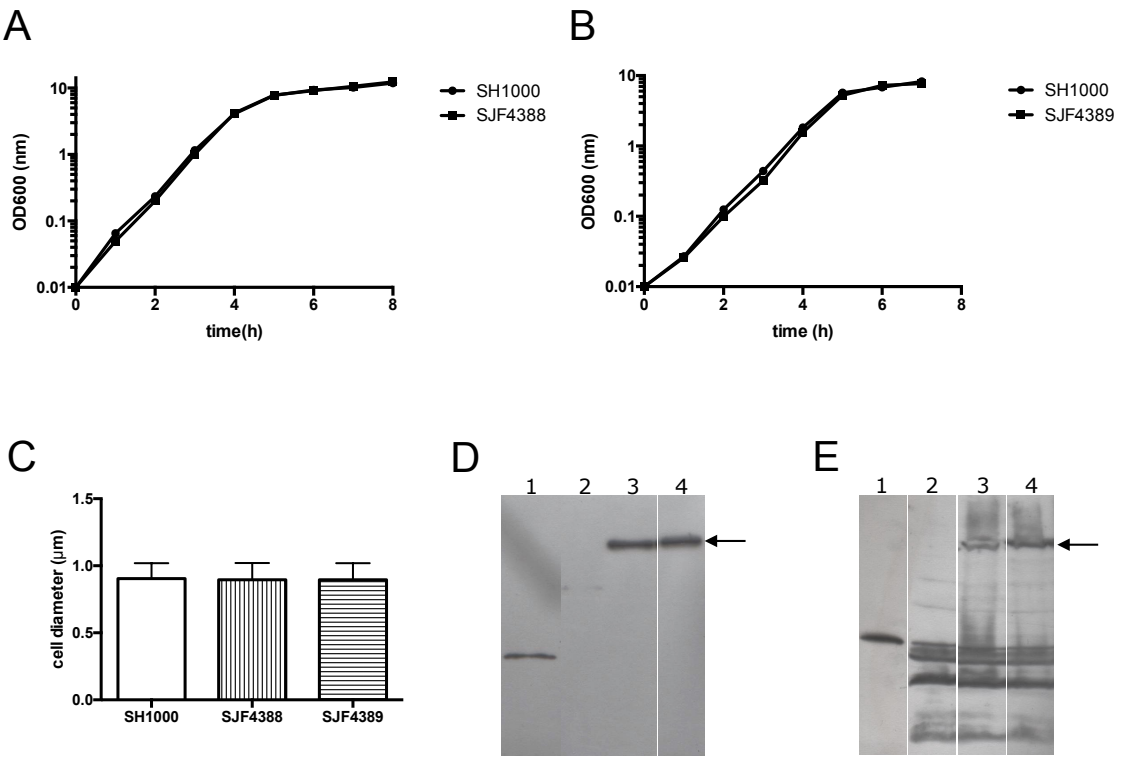

Figure 3.14. EzrA-eYFP and EzrA-PAmCherry1 are functional in *S. aureus*

A. Growth of SJF4388 (*S. aureus* SH1000 *geh::ezrA-eyfp ΔezrA::tet*) was compared against the wild type SH1000 strain. SJF4388 generation time (~27 min) was comparable to the generation time of SH1000 (~27 min).

B. Growth of SJF4389 (*S. aureus* SH1000 *geh::ezrA-pamcherry1 ΔezrA::tet*) was compared against the SH1000. The generation times of SJF4389 and SH1000 are comparable, ~30.5 min and ~29.5 min, respectively.

C. Bars represent the mean value of cell diameters for *S. aureus* SH1000 (n=435), SJF4388 (*S. aureus* SH1000 *geh::ezrA-eyfp ΔezrA::tet*) (n=447) and SJF4389 (*S. aureus* SH1000 *geh::ezrA-pamcherry1 ΔezrA::tet*) (n=359). Error bars represent standard deviation of the mean. Measurements were made using Fiji analysis software.

D. Western blot analysis of whole cell lysates of *S. aureus* SH1000 (lane 2), SJF4386 (*S. aureus* SH1000 *geh::ezrA-eyfp*) (lane 3) and SJF4388 (*S. aureus* SH1000 *geh::ezrA-eyfp ΔezrA::tet*) (lane 4). GFP-HisTag (lane 1; kindly provided by Stéphane Mesnage, University of Sheffield) was used as a positive control. The blot was probed with rabbit anti-GFP antibodies at a 1:1000 dilution. Bands detected at ~90 kDa are indicated with a black arrow.

E. Western blot analysis of whole cell lysates of *S. aureus* SH1000 (lane 2), SJF4387 (*S. aureus* SH1000 *geh::ezrA-pamcherry1*) (lane 3) and SJF4389 (*S. aureus* SH1000 *geh::ezrA-pamcherry1 ΔezrA::tet*) (lane 4). A recombinant mCherry-HisTag protein (lane 1; kindly provided by Stéphane Mesnage, University of Sheffield) was used as a positive control. The blot was probed with rat serum raised against mCherry HisTag at a dilution of 1:1000. Bands detected at ~90 kDa are indicated with a black arrow.

In the absence of the native EzrA protein SJF4388 and SJF4389 could grow, their generation times and the average cell diameters were comparable to *S. aureus* SH1000. Fluorescent proteins produced by these strains presented the midcell localisation pattern as expected for EzrA and no degradation products where detected for EzrA-eYFP in the western blot analysis. This suggested that EzrA-eYFP and EzrA-PAmCherry1 were functional and able to compensate for the lack of the native *ezrA* gene in *S. aureus.*

3.2.3 EzrA localisation using single-molecule localisation microscopy

Conventional fluorescence microscopy depicts EzrA as a uniform ring at the division site. However, because of the light-diffraction limit its spatial organisation is unclear. Super-resolution microscopy, STORM was applied to investigate the localisation of this important cell division component beyond the diffraction limit.

3.2.3.1 EzrA-PAmCherry1 localisation by STORM

In order to examine localisation of EzrA-PAmCherry1 *S. aureus*, firstly a sample of SJF4389 (*S. aureus* SH1000 *geh::ezrA-pamcherry1 ΔezrA::tet*) was used to test if EzrA-PAmCherry1 was photoswitchable in the STORM experimental set-up. SJF4389 was grown to early-exponential phase, fixed, attached to a poly-L-lysine covered coverslip, alongside 103 nm gold nanoparticles (Nanopartz) and mounted in PBS. The sample was illuminated with 405 nm light in order to photoactivate EzrA-PAmCherry1, while red fluorescence of PAmCherry1 was excited continuously with a 532 nm laser. Single blinks associated with cells were observed, suggesting that the EzrA-PAmCherry1 fusion was photoswitchable, controllable with light and could be used in super-resolution imaging of EzrA localisation (Figure 3. 15).

Unfortunately, despite several attempts, visualisation and localisation EzrA-PAmCherry1 in *S. aureus* in STORM was not successful. The reconstruction images obtained from recorded fluorophores positions showed EzrA-PAmCherry1 distributed uniformly within the cell (Figure 3.16A). The uniform signal distribution was not expected for a membrane associated protein. Furthermore this was contradictory to images obtained with conventional fluorescence microscopy, which clearly depicted that EzrA-PAmCherry1 was recruited to the midcell in *S. aureus*.

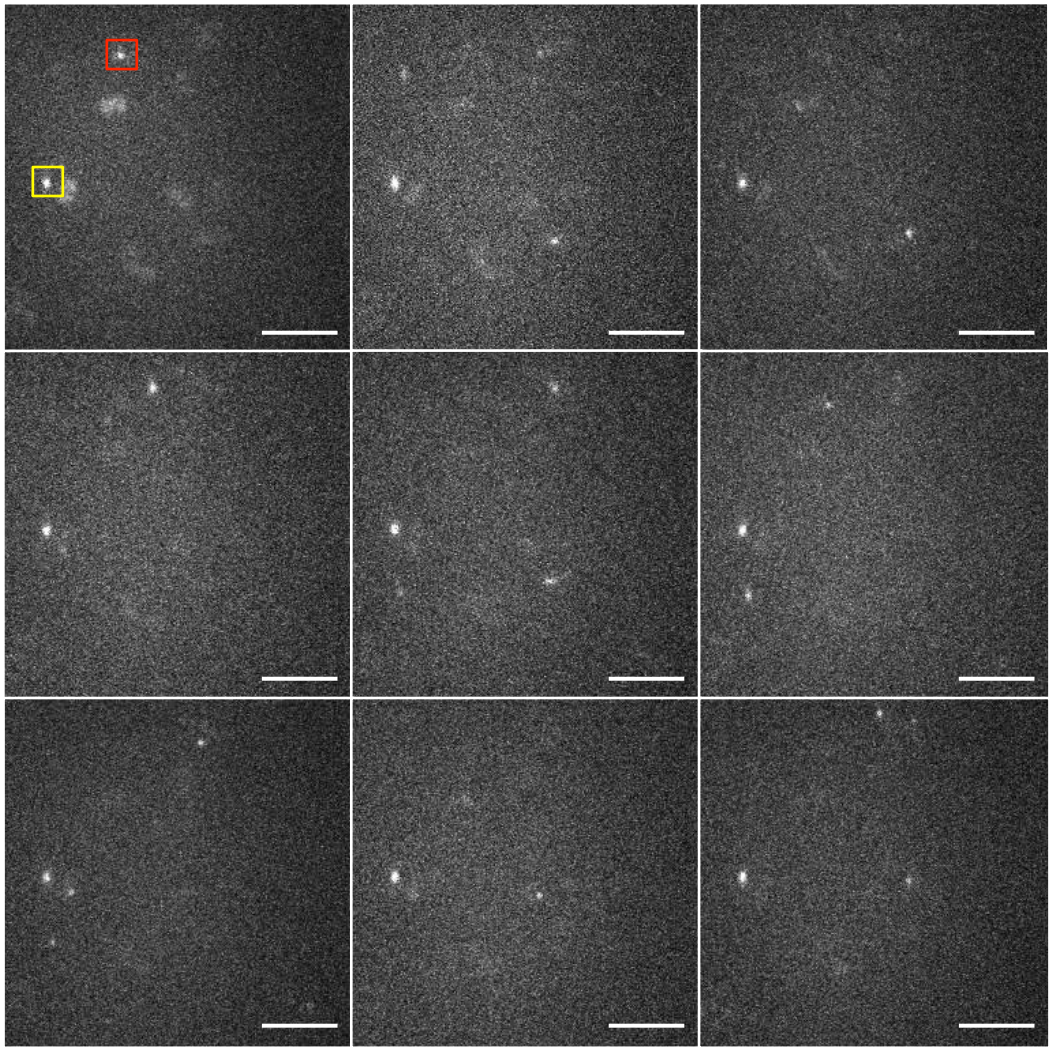

Figure 3.15. Single frame images of SJF4389 (*S. aureus* SH1000 *geh::ezrA-pamcherry1 ΔezrA::tet*) showing the stochastic fluorescence (blinking) of individual EzrA-PAmCherry1 molecules.

A gold nanoparticle (boxed in yellow) was used to maintain focus, a representative blink emitted by a single EzrA-PAmCherry1 molecule is marked in red. Scale bars 5 µm.

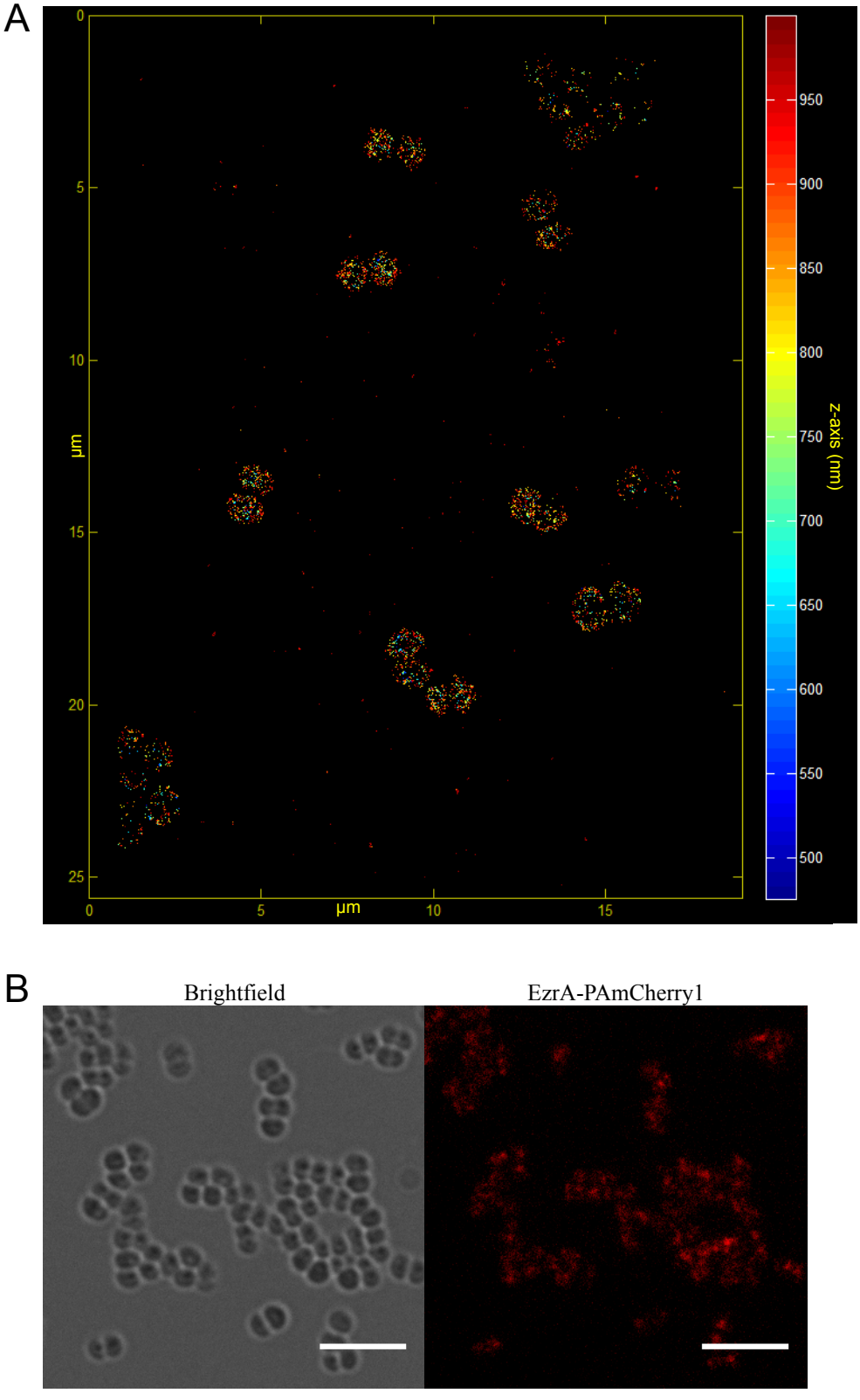

Figure 3.16. EzrA-PAmCherry1 localisation viewed by 3-D STORM and conventional fluorescence microscopy

A. SJF4389 (*S. aureus* SH1000 *geh::ezrA-pamcherry1 ΔezrA::tet*) was examined by STORM. The reconstruction of recorded fluorescent signals shows EzrA-PAmCherry1 to be homogeneously distributed across the cell. Imaging performed in PBS. The colour scale represents the z-axis.

B. EzrA-PAmCherry1 is not a consistent fluorescent fusion in SJF4389. Scale bars 5 µm.

STORM resolution relies on the number of detected photons and a high signal-to-noise ratio (Dempsey et al., 2011). The low intensity of blinks emitted by EzrA-PAmCherry1, relatively quick photobleaching and high background noise were the potential problems that were identified. Steps to find optimal conditions for EzrA-PAmCherry1 single-localisation were taken. Different laser intensities and buffers containing either an oxygen scavenger or a thiol or both, which are the standard buffer conditions applied in STORM imaging studies and which allow to control on and off states of fluorophores, and therefore enhancing their photostability and controlled photoswitching abilities (Dempsey et al., 2011), were employed. They did not however bring any improvements. It was also noticed that SJF4389 (*S. aureus* SH1000 *geh::ezrA-pamcherry1 ΔezrA::tet*) was not a stable strain. Even though it was shown to carry the sequence for *ezrA-pamcherry1*, when rechecked by PCR (data not shown), on many occasions SJF4389 was not fluorescent and even if it was it did not display the EzrA characteristic ring-like structure when examined by conventional fluorescence microscopy (Figure 3.16B). EzrA-PamCherry1 is a fusion protein and although western blot analysis showed that the protein was produced, any degradation could not be excluded because of non-specific cross-reactivity of the rat serum with other *S. aureus* proteins. Therefore, possible strain instability could explain why the difficulties encountered during experiments on EzrA-PAmCherry1 imaging in STORM were not solved. As SJF4389 was not consistent and did not give reproducible results, no further work on optimising imaging conditions for EzrA-PAmCherry1 was performed.

3.2.3.2 EzrA-eYFP localisation by STORM

EzrA-eYFP was shown to be functional in SJF4388 (*S. aureus* SH1000 *geh::ezrA-eyfp ΔezrA::tet*) and was used to resolve localisation of EzrA at super-resolution.

SJF4388 was grown to early-exponential phase. Fixed cells and 100 nm TetraSpeck Microspheres (Molecular Probes) were attached to a poly-L-lysine coated coverslip and mounted in PBS. SJF4388 was imaged using STORM. A 514 nm light wavelength was used to reduce fluorescence of EzrA-eYFP to single-molecule events and the same excitation light was used to image active molecules. Although it has been reported that a 407 nm laser could be used to reactivate the eYFP molecules from the dark state (Biteen et al., 2008), this reactivation step was omitted as it did not improve the

blinking performance of EzrA-eYFP but rather led to permanent bleaching of molecules within a few minutes. Since in the course of time of data acquisition the number of active fluorophores declined and TetraSpecks, which were utilized as fiduciary markers for drift correction, photobleached, up to 8,000 frames per one region of interest were recorded. The fluorescent signal emitted by EzrA-eYFP molecules was then used to reconstruct high-resolution images. Reconstruction of events recorded in 3D-STORM imaging showed that EzrA-eYFP could be successfully used in super-resolution imaging (Figure 3.17A).

STORM did not only provide improvement in microscopic resolution but also brought new insights into EzrA distribution in *S. aureus*. The STORM reconstruction data showed that EzrA-eYFP localised to the site of division in *S. aureus*. Interestingly, the pattern formed by EzrA-eYFP at the midcell was not as uniform as in diffraction-limited microscopy. STORM data revealed that EzrA was heterogeneously distributed at midcell. This non-uniform distribution of EzrA was observed as a collection of 'patches' around division site (Figure 3.17B i-v). In addition to the septal localisation of EzrA-eYFP, a peripheral signal could be observed in many cells (Figure 3.17B vi-xv). The off-septal localisation of EzrA-eYFP seemed to depend on and change with the stage of cell division as different distributions of the fluorescent signal could be observed in individual cells (Figure 3.17B). What is more, the STORM images showed that there was no defined pattern for EzrA-eYFP distribution and it formed not very distinct structures of 'patches' varying in size. These 'patchy' structures measured from ~80 to ~150 nm in width, with the average width of ~100 nm. This finding was quite surprising for a membrane associated protein, as the EzrA-eYFP 'patches' were found to be larger than the width of the membrane, which is ~5 nm (Suganuma, 1961).

Most of the STORM-compatible fluorescent proteins have been shown to exhibit switching behaviour in standard physiological buffers. However, in STORM buffers containing oxygen scavengers and reducing agents are used to improve the photostability and switching abilities of fluorophores (Dempsey et al., 2011). Although EzrA-eYFP showed intrinsic blinking properties under PBS buffering conditions, it bleached relatively quickly probably due to photodamage caused by excitation lasers used in data acquisition. Thus a GLOX MEA buffer that contains both an oxygen scavenger (glucose oxidase, catalase, glucose) and a primary thiol

(β-mercaptoethylamine) was tested for EzrA-eYFP. SJF4388 was grown to early-exponential phase, fixed, mounted in GLOX MEA and imaged by STORM. When GLOX MEA was used a change in photostability of EzrA-eYFP could be observed. EzrA-eYFP blinked longer and the acquisition of data was usually halted not by protein photobleaching but by photodegradation of fluorescent beads, which were used to keep the focus and for drift correction. What is more important, the reconstruction of STORM data revealed the 'patchy' distribution of EzrA-eYFP, similar to the pattern obtained in STORM imaging performed in PBS (Figure 3.18).

EzrA-eYFP retained its blinking properties in GLOX MEA. This is an advantage in making two-colour STORM image of EzrA-eYFP in combination with synthetic dyes, such as Alexa Fluor 647.

3.2.3.3 Do the EzrA-eYFP 'patches' result from eYFP dimers?

Protein localisation studies strongly rely on properties of selected fluorescent proteins. When examining cell components at a molecular level, it is crucial that the chosen labelling method is not intrusive and does not disrupt structure, localisation and function of studied molecules. Fluorescent proteins have been shown to have a tendency to oligomerise and can be responsible for a clustering effect (Zacharias et al., 2002; Landgraf et al., 2012). Utilisation of various fluorescent tags may help to validate localisation results of a protein. Unfortunately, among all screened STORM-compatible fluorescent fusions of EzrA only EzrA-eYFP was found to be both functional and stable in *S. aureus* and suitable for STORM localisation experiments. EzrA has been reported to interact with itself in bacterial two-hybrid system and to form anti-parallel dimers in crystal structures (Steele et al., 2011; Cleverley et al., 2014). Thus, it was important to determine if the heterogeneous distribution of EzrA-eYFP in *S. aureus* could be caused by eYFP oligomerisation.

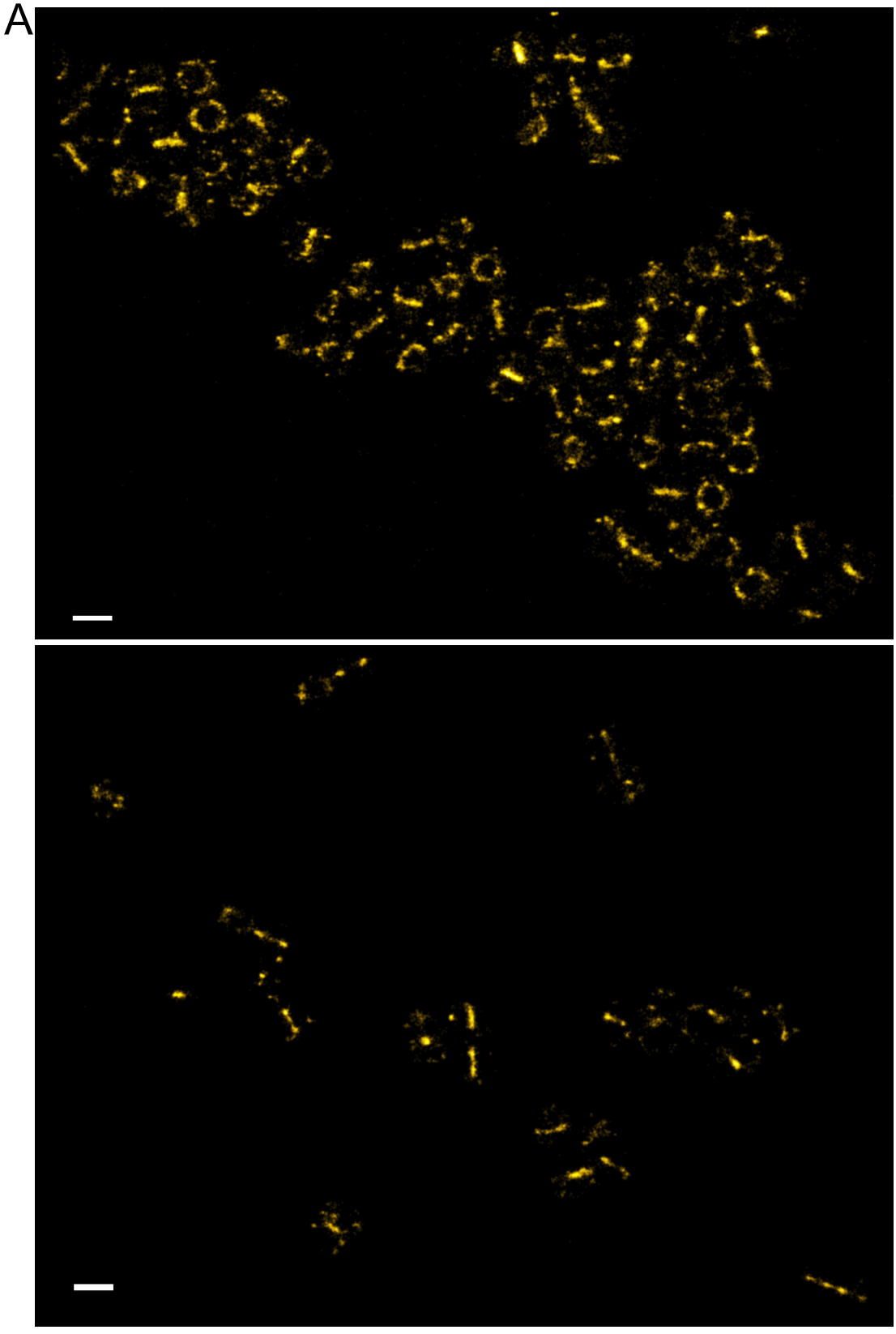
A

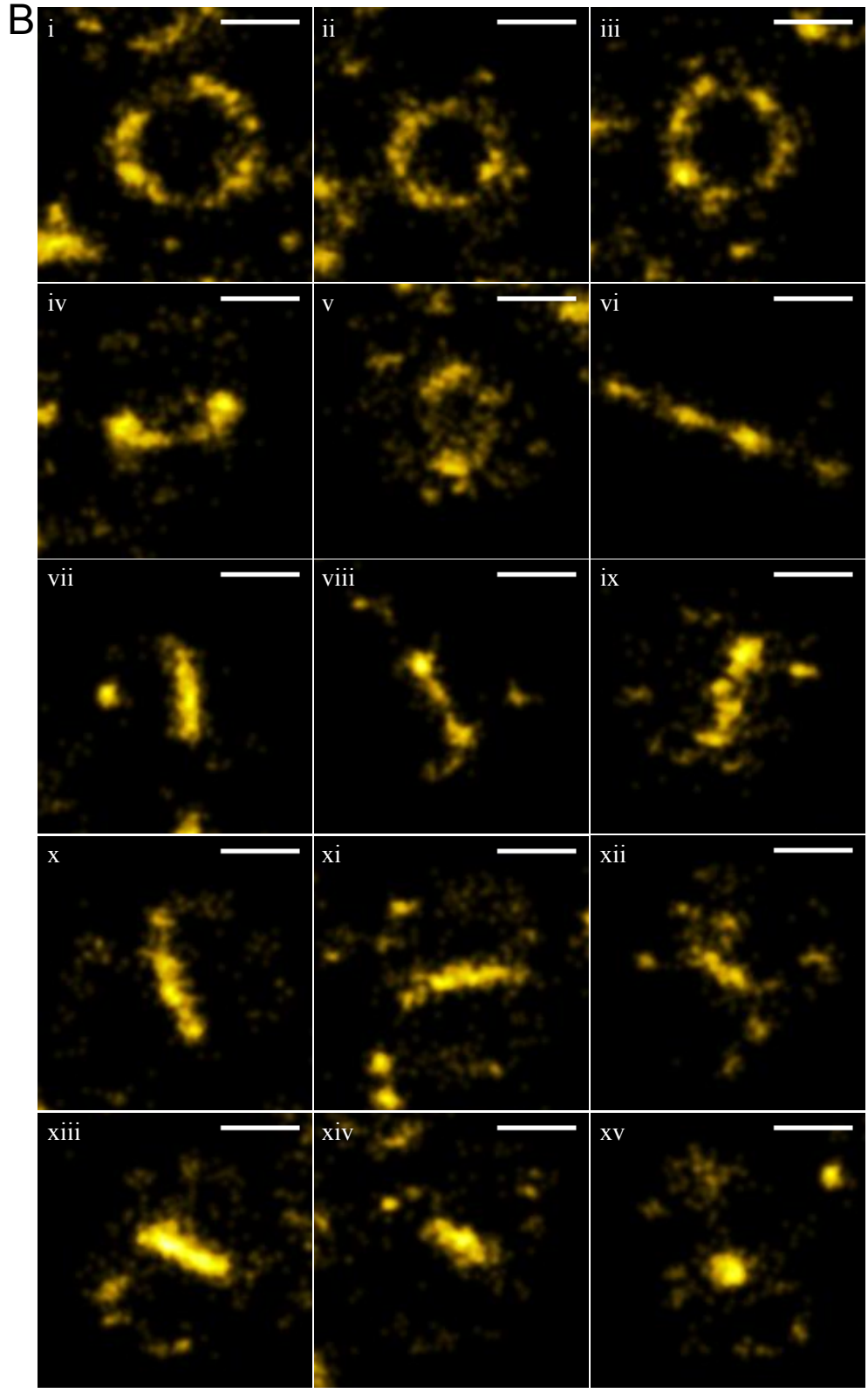

Figure 3. 17. EzrA-eYFP localisation by STORM

A. EzrA-eYFP localisation in SJF4388 (*S. aureus* SH1000 *geh::ezrA-eyfp ΔezrA::tet*) by STORM. Imaging performed in PBS. The reconstructions present EzrA-eYFP locations recorded in 3D and projected to 2D images. Scale bars 1 μm.

B. Individual cells from (A) selected to highlight EzrA-eYFP localisation. Scale bars 500 nm.

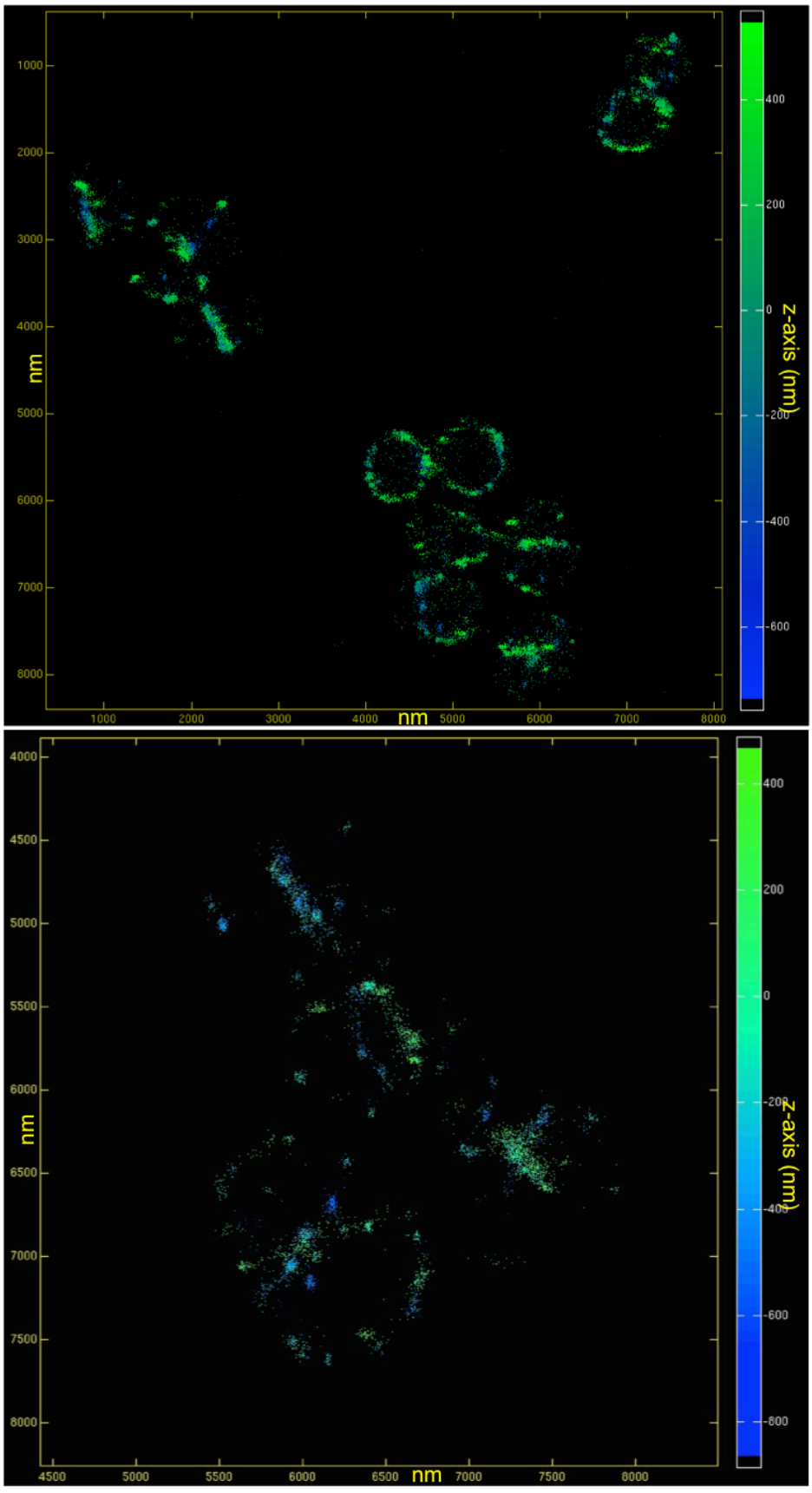

Figure 3.18. EzrA-eYFP localisation by 3D-STORM

3D-STORM images of EzrA-eYFP localisation in SJF4388 (*S. aureus* SH1000 *geh::ezrA-eyfp ΔezrA::tet*). Imaging performed in GLOX MEA. The colour scale represents the z-axis.

3.2.3.3.1 Construction of an *S. aureus* strain in which the only copy of EzrA is tagged with monomeric eYFP

In order to exclude eYFP dimers being responsible for the 'patchy' localisation of EzrA-eYFP, an *S. aureus* strain producing EzrA fused to monomeric eYFP (meYFP) was constructed. It has been previously reported that hydrophobic amino acid residues Ala206, Lys221 and Phe223 are involved in dimerization of GFP and its derivatives, and one of three mutations, A206K, L221K or F223R, is sufficient to prevent formation of dimers (Zacharias et al., 2002). The A206K mutation is the most effective and often incorporated substitution in creating monomeric GFPs (von Stetten et al., 2012), therefore a site directed mutagenesis was employed to change the hydrophobic Ala206 for a positively charged Lys in eYFP.

The whole pKASBAR-EzrA-eYFP plasmid was amplified using primers meYFP-F and meYFP-R (primer meYFP-F incorporated the desired mutations at the Ala206 site) by inverse PCR. The PCR products were digested with *DpnI* to remove methylated DNA, the 5' ends of DNA were phosphorylated with kinase and DNA was circularised using ligase (Figure 3.19A). The ligation products were transformed into chemically competent *E. coli* NEB5α and selected on LB ampicillin (100 μg ml^{-1}) plates. Positive clones were screened by colony PCR using eYFP-F and eYFP-R primers and verified by plasmid extraction, restriction digestion with *Bpu1102I* and *BamHI* and confirmed to contain the correct DNA band sizes by electrophoresis on a 1% (w/v) agarose gel (Figure 3.19B). Plasmids were sequenced by GATC Biotech to check for the introduction of substitutions during PCR. The resulting pKASBAR-EzrA-meYFP plasmid (Figure 3.19A) contained the substitutions designed within the *eyfp* that generated monomeric *eyfp* (*meyfp*, Appendix I).

pKASBAR-EzrA-meYFP was transformed into the electrocompetent SJF1332 cells. The correct integration of the plasmid into the *S. aureus* chromosome was confirmed by loss of the lipase activity by plating SJF4584 (*S. aureus* RN4220 *geh::ezrA-meyfp*) on Baird-Parker medium (data not shown). SJF4584 was lysed with Φ11 and the chromosomal region containing *ezrA-meyfp* was moved into *S. aureus* SH1000 by phage transduction. The resulting strain SJF4603 (*S. aureus* SH1000 *geh::ezrA-meyfp*) did not hydrolyse lipids when grown on Baird-Parker medium indicating that recombination

occurred properly at the *geh* gene region (Figure 3.20A). In order to delete the native *ezrA* gene in SJF4603 (*S. aureus* SH1000 *geh::ezrA-meyfp*), SJF4603 was transduced with a Φ11 lysate from SJF4388 (*S. aureus* SH1000 *geh::ezrA-eyfp ΔezrA::tet*) and selected using kanamycin (50 μg ml^{-1}) and tetracycline (5 μg ml^{-1}). The marked deletion of native *ezrA* in SJF4604 (*S. aureus* SH1000 *geh::ezrA-meyfp ΔezrA::tet*) was confirmed by PCR on extracted genomic DNA using primers ezrA-up-F and ezrA-down-R and further analysed by Southern blot hybridisation as previously described (section 3.2.3.2), except that an ECL detection method was used (Figure 3.20B and C). PCR and Southern blot results confirmed SJF4604 to have the right genotype.

The functionality of the EzrA-meYFP protein was verified by growth experiments. SH1000, SJF4388 and SJF4604 were grown overnight in BHI media with appropriate antibiotics and 50 ml of BHI was inoculated with the overnight cultures to a starting OD_{600} of 0.001. Growth of the cultures was measured by optical density every hour. SJF4604 showed no growth defect since it grew with the similar rate to *S. aureus* SH1000 and SJF4388 (Figure 3.20D) Measurements of an average cell diameter revealed that SJF4604 formed cells of comparable sizes to SH1000 and SJF4388, showing that cells did not have any altered phenotype (Figure 3.20E). In order to check if EzrA-meYFP was produced and stable whole cell lysates of SJF4604 were probed with anti-GFP antibodies at a dilution of 1:1000 in western blot analysis. An expected band of ~90 kDa was detected, with no additional products, which would indicate protein degradation, were detected. This suggests that EzrA-meYFP was stable (Figure 3.20F). Furthermore, the intensity of the band obtained for EzrA-meYFP was equivalent to the signal for EzrA-eYFP showing that in SJF4604 EzrA-meYFP is produced at the same level as EzrA-eYFP in SJF4388. (Figure 3.20F).

Although the A206K mutation has been shown to not affect spectroscopic proprieties in other fluorescent protein, single mutations in fluorescent proteins can lead to changes in their photophysical or folding abilities (Zacharias et al., 2002; Zhang et al., 2002). In order to exclude such a possibility SJF4604 was grown to early-exponential phase, fixed and examined by fluorescence microscopy. EzrA-meYFP showed the septal localisation, similar to the pattern of localisation of EzrA-eYFP in SJF4388. What is more important, EzrA-meYFP was found to be as bright as EzrA-eYFP indicating that despite the introduced substitution the spectral properties of the fluorescent protein were not altered.

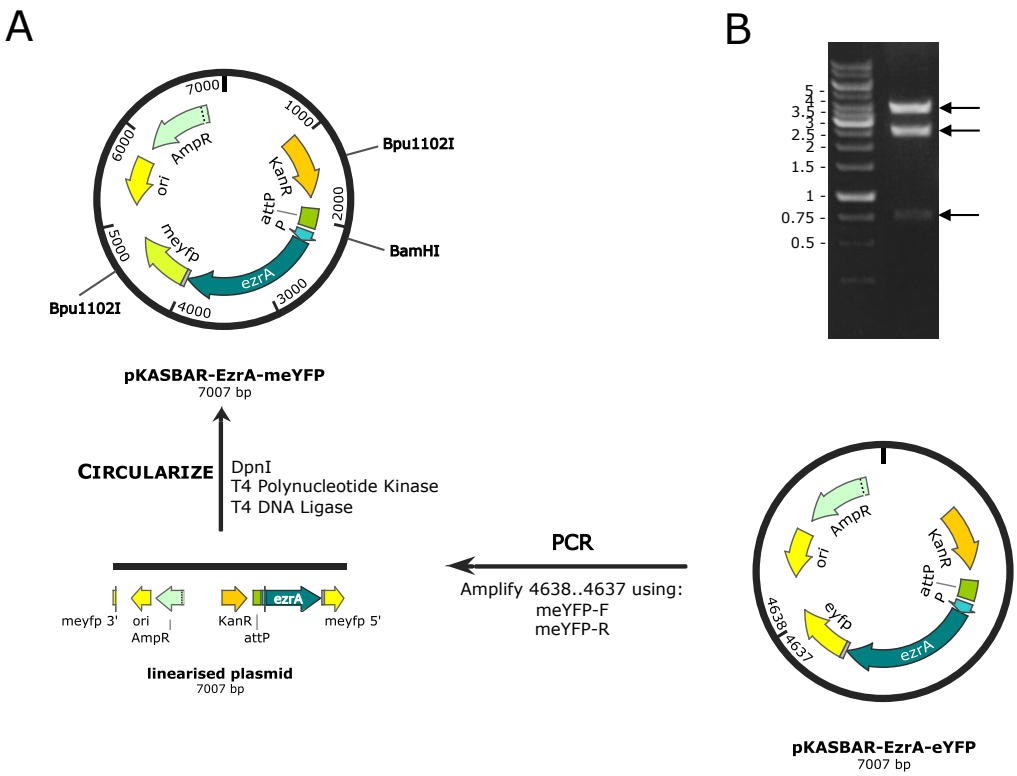

Figure 3.19. Construction of pKASBAR-EzrA-meYFP

A. The whole pKASBAR-EzrA-eYFP plasmid was PCR amplified using primers meYFP-F and meYFP-R. The PCR product (linearised plasmid) was digested with *DpnI* and re-circularised by treatment with T4 polynucleotide kinase and T4 DNA ligase, resulting in pKASBAR-EzrA-meYFP.

B. Restriction enzyme digest of pKASBAR-EzrA-meYFP with *BamHI* and *Bpu1102I*. The expected DNA band sizes of 3.7 kb, 2.5 kb and 0.76 kb are indicated with black arrows. Sizes of a DNA ladder are shown in kb.

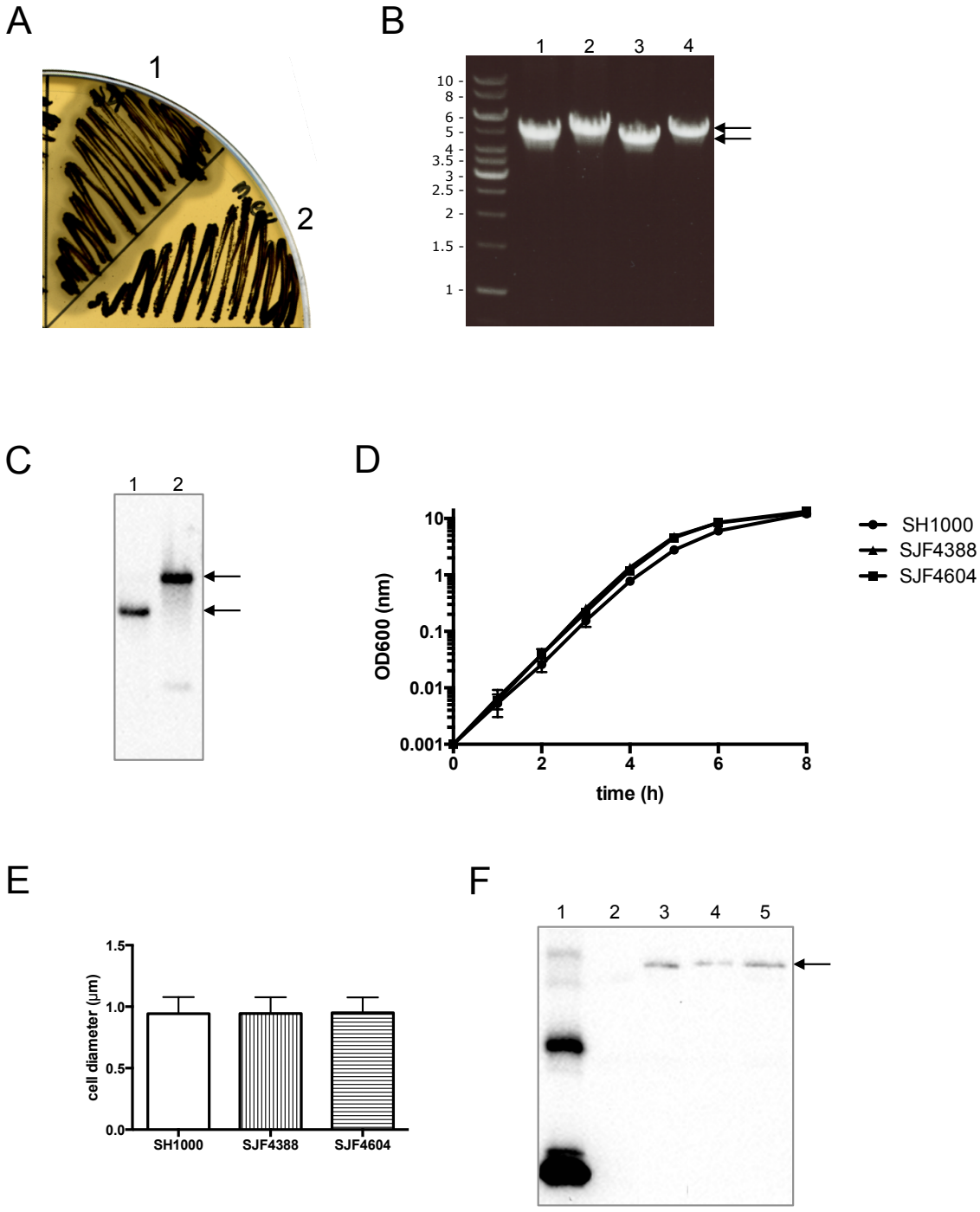

Figure 3.20. Construction of functional EzrA-meYFP

A. Disruption of lipase production confirms presence of *ezrA-meyfp* within the *geh* gene in SJF4603 (*S. aureus* SH1000 *geh::ezrA-meyfp*). In contrast to *S. aureus* SH1000 (1), SJF4603 (2) does not form a zone of precipitation around colonies.

B. Replacement of *ezrA* with the TetR cassette was confirmed by PCR on genomic DNA using primers ezrA-up-F and ezrA-down-R. Similarly to SJF4388 (*S. aureus* SH1000 *geh::ezrA-eyfp ΔezrA::tet*) (lane 2), SJF4604 (*S. aureus* SH1000 *geh::ezrA-meyfp ΔezrA::tet*) (lane 4) gave a product of 5.3 kb confirming the *ΔezrA::tet* mutation, whereas SJF4603 (*S. aureus* SH1000 *geh::ezrA-meyfp*) (lane 3)

and SJF4386 (*S. aureus* SH1000 *geh::ezrA-eyfp*) (lane 1) showed the expected bands of 4.8 kb that indicates the presence of *ezrA* at its native locus. The PCR products are indicated with black arrows. Sizes of a DNA ladder are shown in kb.

C. Deletion of *ezrA* in SJF4604 (*S. aureus* SH1000 *geh::ezrA-meyfp ΔezrA::tet*) was confirmed by Southern blot analysis. Genomic DNA from SJF4603 (*S. aureus* SH1000 *geh::ezrA-meyfp*) (lane 1) and SJF4604 (lane 2) was isolated, digested with *HindIII* and probed with a 1645 bp probe labelled with peroxidase. DNA bands corresponding to approximately 9 kb and 17 kb are indicated with black arrows. Sizes of a DNA ladder are shown in kb.

D. The generation time of SJF4604 (*S. aureus* SH1000 *geh::ezrA-meyfp ΔezrA::tet*) (~25 min) is comparable to SH1000 and SJF4388 (*S. aureus* SH1000 *geh::ezrA-eyfp ΔezrA::tet*) generation times (~26 min and ~25 min, respectively). Cell cultures were grown from an OD_{600} 0.001 and the optical density of the cultures was measured every hour. Bacterial cultures were prepared in triplicate and error bars represent standard deviation from the mean.

E. SJF4604 (*S. aureus* SH1000 *geh::ezrA-meyfp ΔezrA::tet*) forms cells of the similar size as SH1000 and SJF4388 (*S. aureus* SH1000 *geh::ezrA-eyfp ΔezrA::tet*). Bars represent the mean value of cell diameters for *S. aureus* SH1000 (0.94 ± 0.13 µm, n=535), SJF4388 (0.94 ± 0.13 µm, n=412) and SJF4604 (0.95 ± 0.13 µm, n=321). Error bars represent standard deviation of the mean. Measurements were made using the Fiji program.

F. Whole cell lysates of SH1000 (lane 2) SJF4388 (lane 3) (*S. aureus* SH1000 *geh::ezrA-eyfp ΔezrA::tet*), SJF4603 (*S. aureus* SH1000 *geh::ezrA-meyfp*) (lane 4) and SJF4604 (*S. aureus* SH1000 *geh::ezrA-meyfp ΔezrA::tet*) (lane 5), and a recombinant GFP-HisTag protein (lane 1) were probed with anti-GFP antibodies at a 1:1000 dilution. Bands detected at ~90 kDa are indicated with a black arrow.

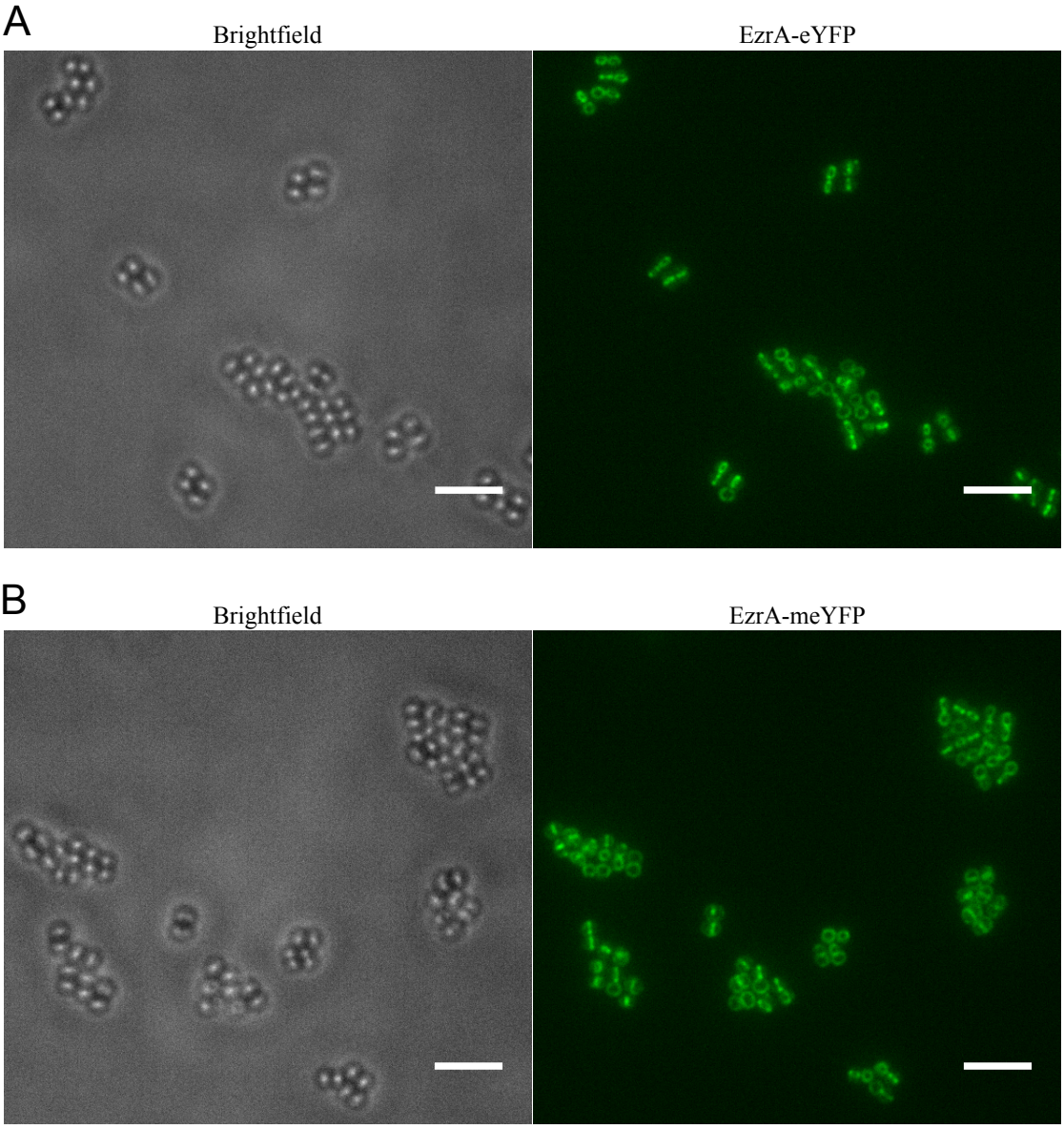

Figure 3.21. EzrA-meYFP is bright and localises to the septum in *S. aureus*

A. EzrA-eYFP localisation in SJF4388 (*S. aureus* SH1000 *geh::ezrA-eyfp ΔezrA::tet*) by fluorescence microscopy. The fluorescence images are a maximum intensity projection of z-stack images acquired at 200 nm z-intervals. Scale bars 5 μm.

B. In SJF4604 (*S. aureus* SH1000 *geh::ezrA-meyfp ΔezrA::tet*), EzrA-meYFP similarly to EzrA-eYFP in SJF4388 is recruited to the septum where it forms a ring-like structure. The fluorescence images are maximum intensity projections of z-stack images acquired at 200 nm z-intervals. Scale bars 5 μm.

3.2.3.3.2 EzrA-meYFP localisation by STORM

STORM imaging of EzrA-eYFP suggested that EzrA might form a heterogeneous pattern. To ensure that this non-uniform distribution was not caused by dimerization of eYFP, a monomeric variant of this fluorescent protein was prepared. In conventional fluorescence microscopy EzrA-eYFP and EzrA-meYFP did not show any differences in terms of localisation and fluorescence intensities.

EzrA-eYFP and EzrA-meYFP were imaged at super-resolution and patterns formed by these two fluorescent fusions were compared. SJF4388 (*S. aureus* SH1000 *geh::ezrA-eyfp ΔezrA::tet*) and SJF4604 (*S. aureus* SH1000 *geh::ezrA-meyfp ΔezrA::tet*) were grown to early-exponential phase and fixed. Cells were mounted in the GLOX MEA buffer and visualised in STORM. The reconstruction data revealed that both EzrA-eYFP and EzrA-meYFP were heterogeneously distributed around division site and this non-uniform distribution pattern was comparable. In contrast to EzrA-eYFP, EzrA-meYFP was however found to give more events associated with the cell cytoplasm than EzrA-eYFP did (Figure 3.22). Despite the additional cytoplasmic signal the EzrA-meYFP molecules formed membrane associated structures of a thickness comparable to EzrA-eYFP structure and wider than the width of the cell membrane.

Although both EzrA-eYFP and EzrA-meYFP were shown to be stable by western blot analysis, small variations in sample preparation that could affect protein stability and the final result of microscopic visualisation were possible. Nevertheless the EzrA 'patches' were observed to be formed in both samples, suggesting that the potential eYFP oligomerisation was not the major cause of EzrA heterogeneous distribution in *S. aureus*.

3.2.4 EzrA localisation using structured illumination microscopy

STORM provides the highest spatial resolution among fluorescence microscopy techniques developed to date. As a result of it requirements for photoswitchable fluorophores and a narrow range of available STORM-compatible fluorophores application of STORM to study biological samples becomes extremely limited.

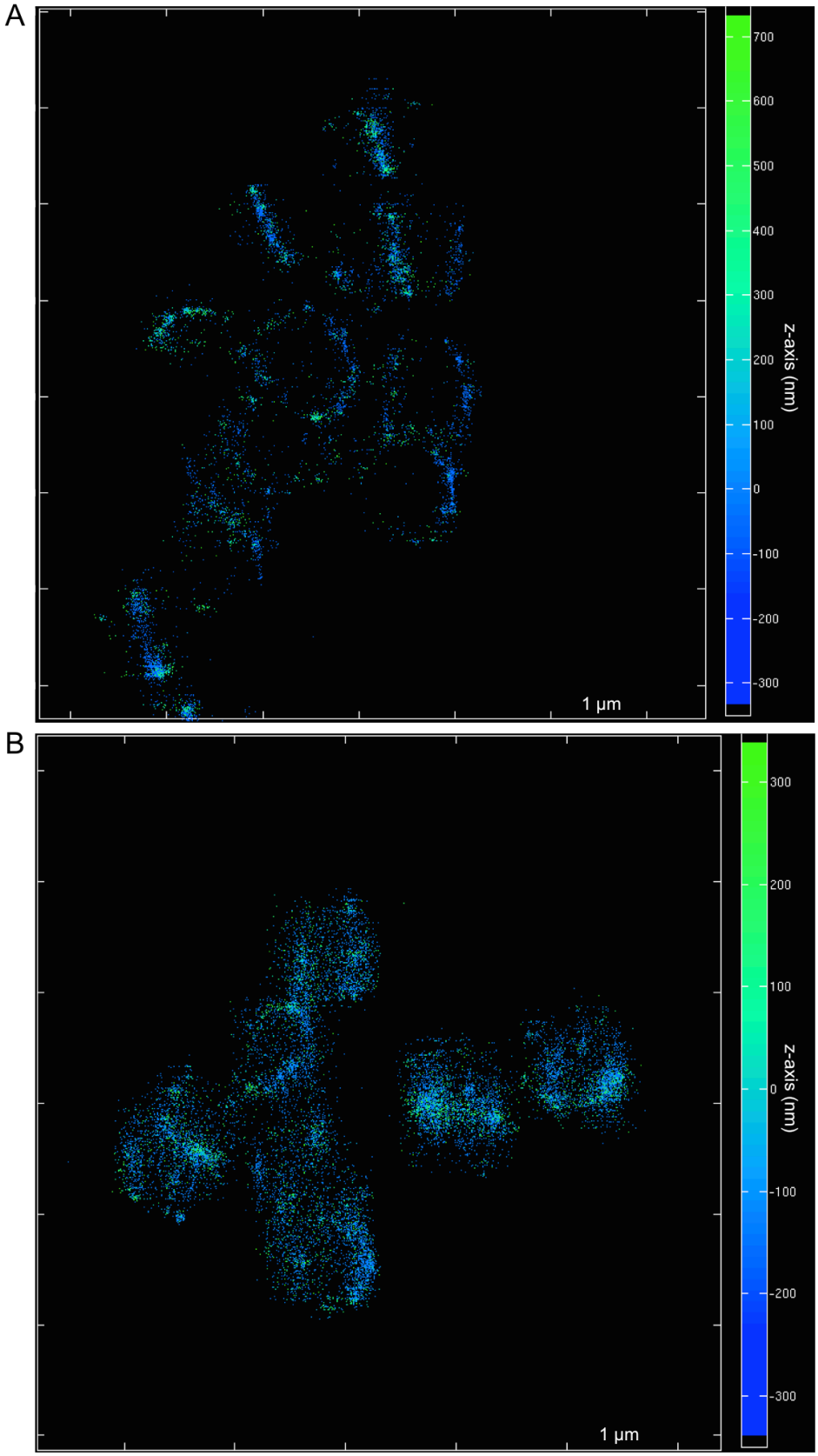

Figure 3.22. EzrA-eYFP and EzrA-meYFP localisation by 3D-STORM

3D-STORM localisation images of EzA-eYFP in SJF4388 (*S. aureus* SH1000 *geh::ezrA-eyfp ΔezrA::tet*) (A) and EzrA-meYFP in SJF4604(*S. aureus* SH1000 *geh::ezrA-meyfp ΔezrA::tet*) (B). Imaging performed in GLOX MEA. The colour scale represents the z-axis.

Structured Illumination Microscopy (SIM) is another super-resolution microscopy technique in which illumination patterns are applied to a fluorescent sample to extract information with a sub-diffraction-limited resolution, that is 100 nm and 250 nm in lateral and axial dimensions, respectively. The main advantage of SIM is that it potentially allows for utilisation of any fluorescent label that has been developed and used in conventional fluorescence microscopy (Schermelleh et al., 2010). GFP is the first isolated and the most often employed fluorescent protein in conventional fluorescence microscopy. Recently GFP and its derivatives have been shown to be useful for SIM and applied in localisation and structural studies of bacterial cell division components. 3-D SIM imaging of FtsZ-GFP, DivIVA-GFP and MinJ-YFP showed that in *B. subtilis* FtsZ forms a single-ring structure, while DivIVA and MinJ form double-rings that flank division sites (Eswaramoorthy et al., 2011).

Localisation of EzrA labelled with various fluorescent tags was investigated in SIM.

3.2.4.1 Localisation of EzrA-eYFP and EzrA-meYFP by SIM

The pattern of localisation of EzrA-eYFP and EzrA-meYFP was visualised in SIM. SJF4388 (*S. aureus* SH1000 *geh::ezrA-eyfp ΔezrA::tet*) and SJF4604 (*S. aureus* SH1000 *geh::ezrA-meyfp ΔezrA::tet*) were grown to early-exponential phase and fixed. Cells were mounted in SlowFade Gold (Molecular Probes) to prevent the sample from photobleaching. When EzrA-eYFP and EzrA-meYFP were visualised in 3D-SIM (Figure 3.23 Ai and Bi) it quickly became apparent that the fluorescent proteins fused to EzrA were not bright enough to allow for EzrA localisation in SIM. EzrA is a membrane associated protein and during cell division is recruited to the septum being observed as a line across a cell or a ring around a division site dependent on cell orientation. Before each SIM data acquisition a snap shot of the region of interest for EzrA-eYFP/EzrA-meYFP in conventional wide-field fluorescence microscopy was taken. These images showed that EzrA was recruited to septa both in SJF4388 and SJF4604 (Figure 3.23 Aii and Bii). Algorithms used to reconstruct SIM data allow for detection of features that are not clearly visible in conventional fluorescence microscopy, for example suggesting that in a dividing SJF4388 cell an additional off-septal localisation of EzrA-eYFP could be present (Figure 3.23Aiii-vi). However most of the cells imaged in SIM showed the fluorescent signal associated with the cell

surface/membrane. Such a signal was not present in conventional fluorescence microscopy of the same region of interest. Figure 23.Biii shows a dividing SJF4604 cell. The profile of fluorescence intensity measured across the plane of cell division suggested that EzrA-meYFP was mainly localised to the septum as the highest grey values of fluorescent signal were mainly associated with the midcell (Figure 3.23Biv). The SIM reconstruction showed an opposite result for the same cell; the highest fluorescence values were for regions associated with cell periphery and less with the division site (Figure 3.23Bv-vi). SIM requires bright and stable fluorophores and eYFP/meYFP were found to fade immediately during exposure cycles. Additionally background fluorescence associated with SJF4388 and SJF4604 cells could be observed. This signal possibly masked or added up to the final eYFP/meYFP fluorescent signal or made up a new structure, which was then picked up by algorithms and used to reconstruct a SIM image (Figure 3.23Aiii-iv and Biii-iv). A low contrast-to-noise ratio caused by sample bleaching and background fluorescence could be a source of artefacts and contributed to the SIM reconstruction that did not bring any information on EzrA localisation pattern in *S. aureus.*

3.2.4.2 Localisation of EzrA-GFP and EzrA-SNAP by SIM

EzrA-eYFP and EzrA-meYFP were shown to be suitable fluorescent fusion proteins to study EzrA localisation in single-molecule localisation microscopy. However because of their photophysical properties, eYFP and meYFP were not bright enough fluorescent labels that could be utilised in SIM studies. Among fluorescent proteins GFP is the most often employed genetically encoded fluorophore and has been successfully incorporated in localisation studies of bacterial components (Eswaramoorthy et al., 2011). Organic dyes are known to be more photostable and brighter than fluorescent proteins. The SNAP-tag system allows utilising synthetic dyes to stain cellular components, which are generally more favourable in microscopy studies. Two EzrA fusions, EzrA-GFP and EzrA-SNAP were chosen to investigate structures formed by EzrA in SIM.

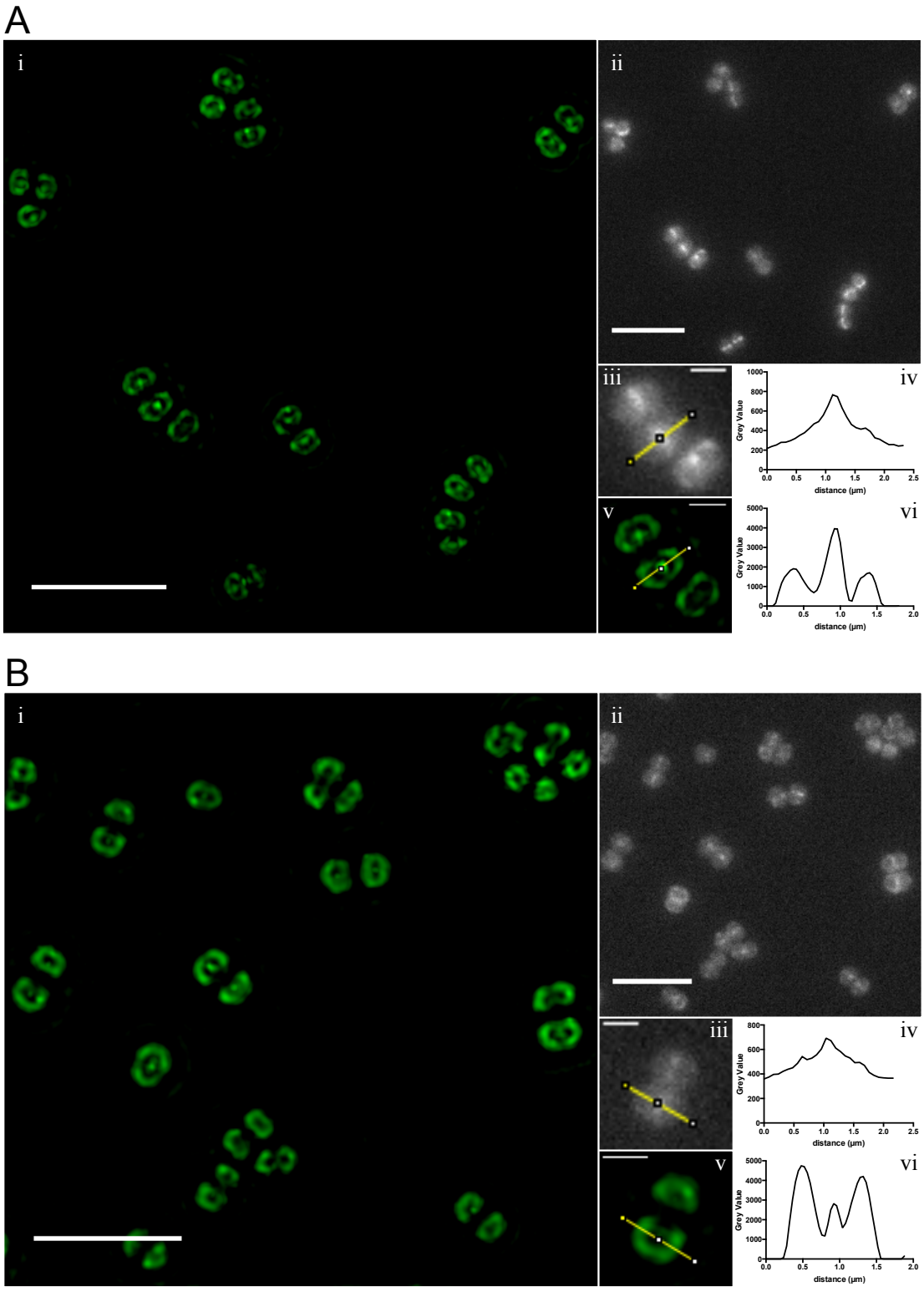

Figure 3.23. EzrA-eYFP and EzrA-meYFP by 3D-SIM

SJF4388 (*S. aureus* SH1000 *geh::ezrA-eyfp ΔezrA::tet*) (A) and SJF4604 (*S. aureus* SH1000 *geh::ezrA-meyfp ΔezrA::tet*) (B) were visualised using 3D-SIM (i) and conventional fluorescence microscopy (ii). Individual cells imaged by conventional fluorescence microscopy (iii) and 3D-SIM (v) were selected and profiles of fluorescence intensity measured across yellow lines within the images iii and v are presented in iv and vi, respectively. Scale bars 5 µm in i and ii, and 1 µm iii and v.

3.2.4.2.1 Construction of *S. aureus* strains in which the only copy of EzrA is tagged with either GFP or SNAP

Even though an *S. aureus* strain, in which EzrA-GFP is the only functional copy of EzrA present in the cell, was available, this strain was constructed via a homologous recombination of a pMUTIN derivative within the *ezrA* gene (Steele et al., 2011) and varied genetically too far from SJF4388 and SJF4604.

The SNAP-tag is a 20 kDa engineered protein of a human DNA repair enzyme, O^6-alkylguanine-DNA-alkyltransferase that reacts irreversibly with O^6-benzylguanine derivatives (Keppler et al., 2003; Gautier et al., 2008). The SNAP-tag can be potentially fused to any protein and covalently labelled with any fluorophore conjuncted to a benzyl group. The advantage of this method is that it allows for using different fluorescent dye substrates for one tag. Utilisation of organic dyes in the SNAP-tag system is another positive aspect of this labelling method. Synthetic probes usually have a higher quantum yield, so that they are brighter and more stable than fluorescent proteins. *S. aureus* strains that were either GFP or SNAP equivalents of SJF4388 and SJF4604 were constructed.

The pGP003 plasmid (Poczopko, 2012) was digested with *AscI* and *NotI* enzymes and the *gfp* gene (Appendix I) was ligated into pGM074 (Gareth McVicker, unpublished) cut with the same enzymes (Figure 3.24A). Primers SNAP-F and SNAP-R were used to PCR amplify the *snap-tag* gene from pSNAP-tag (T7)-2 (New England Biolabs). The PCR products were ligated into pGM074 using *EcoRI* and *AscI* cut sites (Figure 3.25A). The ligation products were transformed into electrocompetent *E. coli* Top10 cells and transformants were selected on LB ampicillin (100 μg ml^{-1}) plates. Clones carrying the *gfp* and the *snap* genes were screened by colony PCR using primer pairs GFP-F and GFP-R, and SNAP-F and SNAP-R, respectively. The clones identified as positive were confirmed by plasmid extraction, and restriction digestion with *EcoRI* and *BamHI* and analysis on a 1% (w/v) agarose gel showed correct DNA fragments (Figures 3.24B and 3.25B). Plasmids were sequenced by GATC Biotech and the resulting plasmids pKASBAR-EzrA-GFP and pKASBAR-EzrA-SNAP (Figures 3.24A and 3.25A) did not contain any substitutions.

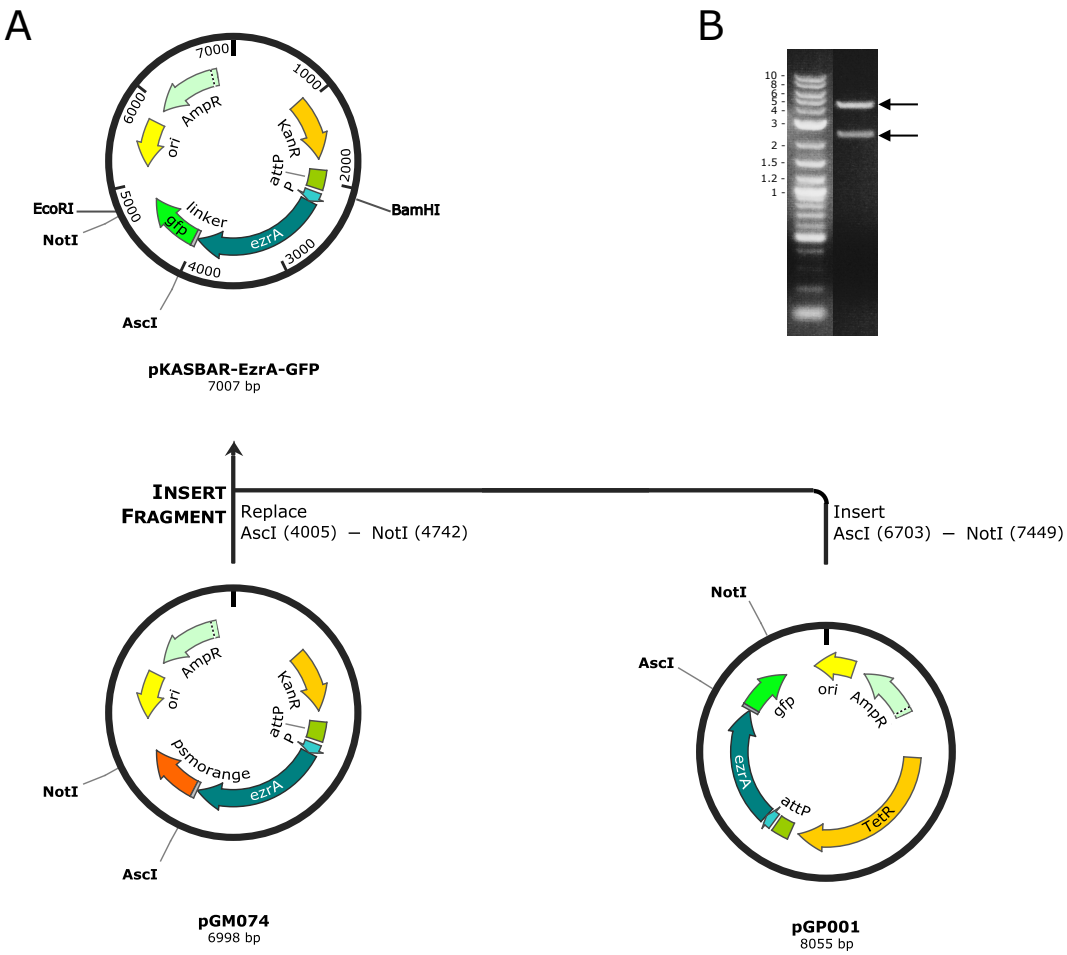

Figure 3.24. Construction of pKASBAR-EzrA-GFP

A. pGP003 was digested with *AscI* and *NotI* enzymes and the *gfp* gene was ligated into pGM074 cut with the same enzymes, resulting in pKASBAR-EzrA-GFP.

B. Restriction enzyme digest of pKASBAR-EzrA-GFP with *EcoRI* and *BamHI*. The expected DNA band sizes of 4.3 kb and 2.4 kb are indicated with black arrows. Sizes of DNA are ladder shown in kb.

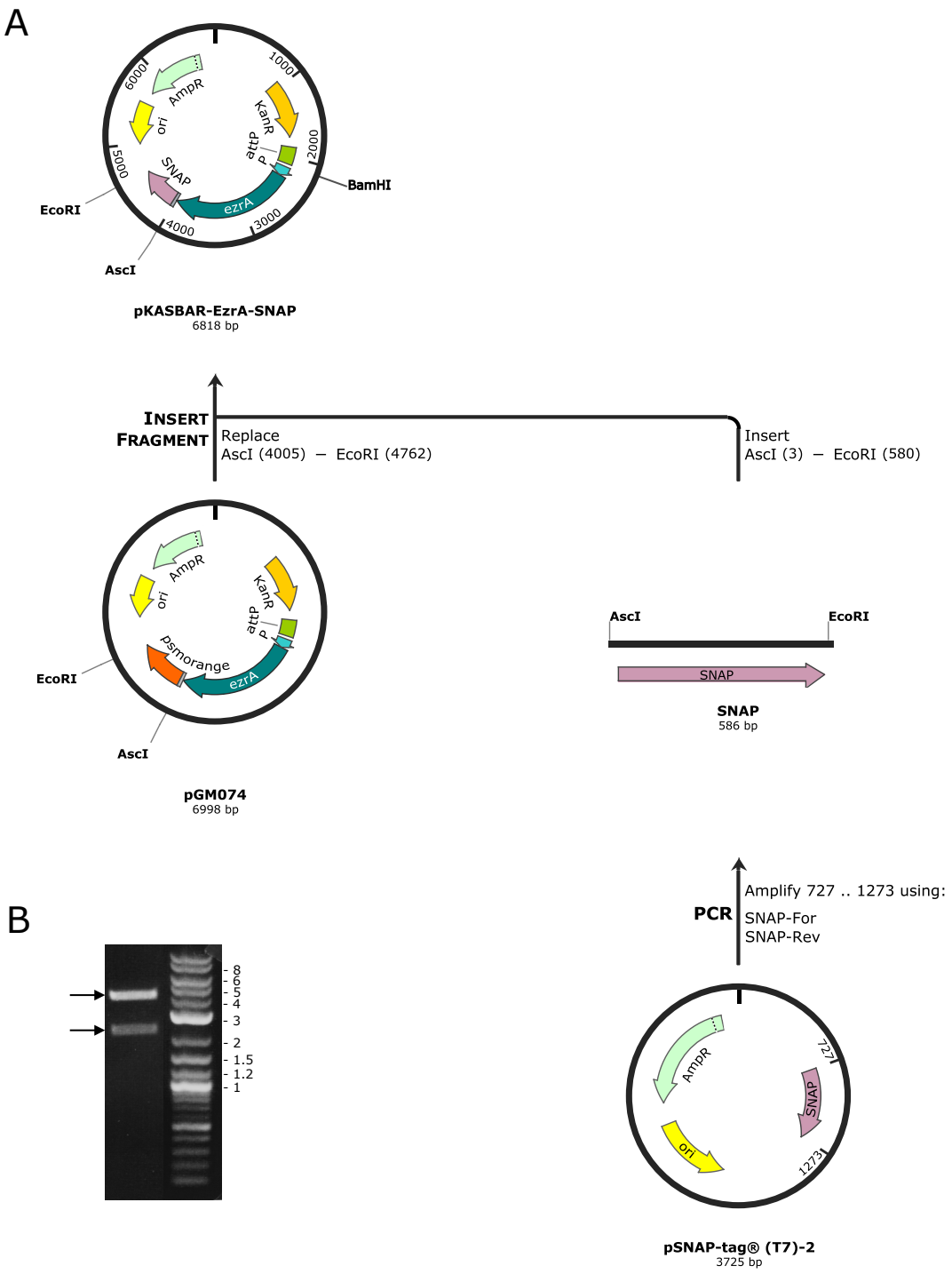

Figure 3.25. Construction of pKASBAR-EzrA-SNAP

A. The *snap* gene was PCR amplified from pSNAP-tag (T7)-2, digested with *AscI* and *NotI* enzymes and ligated into pGM074 cut with the same enzymes, resulting in pKASBAR-EzrA-SNAP.

B. Restriction enzyme digest of pKASBAR-EzrA-SNAP with *EcoRI* and *BamHI*. The expected DNA band sizes of 4.3 kb and 2.5 kb are indicated with black arrows. Sizes of a DNA ladder are shown in kb.

pKASBAR-EzrA-GFP and pKASBAR-EzrA-SNAP were transformed into electrocompetent SJF1332 creating SJF4648 (*S aureus* RN4220 *geh::ezrA-gfp*) and SJF4649 (*S aureus* RN4220 *geh::ezrA-snap*). Integration of the plasmids was confirmed by plating SJF4648 and SHF4649 on Baird-Parker media (data not shown). The chromosomal regions containing integrated plasmids where then moved to *S. aureus* SH1000 by phage transduction. Disruption of lipase activity was confirmed in the resulting SJF4639 (*S aureus* SH1000 *geh::ezrA-gfp*) and SJF4641 (*S aureus* SH1000 *geh::ezrA-snap*) strains (Figure 3.26A). SJF4639 and SJF4641 were examined by fluorescence microscopy for the proper localisation of the fusion proteins. SJF4639 and SJF4641 were grown to early-exponential phase, SJF4649 was labelled with SNAP-Cell TMR-Star (New England Biolabs), which is a red fluorescent dye that labels the SNAP-tag, and cells were fixed with paraformaldehyde. In the presence of native EzrA EzrA-GFP and EzrA-SNAP TMR-Star showed the characteristic ring-like pattern (Figure 3.26B and C).

In order to delete the copy of the native *ezrA* gene, SJF4639 and SJF4641 were transduced with a Φ11 lysate from SJF4388 (*S. aureus* SH1000 *geh::ezrA-eyfp ΔezrA::tet*) and selected using kanamycin (50 μg ml^{-1}) and tetracycline (5 μg ml^{-1}). Phage transduction of SJF4639 was not efficient and resulted only in seven clones, suggesting that the incorporated *ΔezrA::tet* mutation could be not well complemented by EzrA-GFP. Therefore all seven clones were first examined using fluorescence microscopy to find if they had the wild type phenotype and produced the fluorescent protein. Only one clone, SJF4640 (*S. aureus* SH1000 *geh::ezrA-gfp ΔezrA::tet*) formed cells which morphology was comparable to the wild type SH1000 strain and showed the correct EzrA localisation (Figure 3.27A). In the rest of the tested clones, even though the majority of the cells looked wild type, cells with severe morphological defect could be observed in every field of view. These cells were enlarged and had EzrA-GFP localisation altered (Figure 3.27B). When the *ΔezrA::tet* derivative of SJF4641, SJF4642 (*S. aureus* SH1000 *geh::ezrA-snap ΔezrA::tet*) was viewed by fluorescence microscopy, in all cells EzrA-SNAP stained with SNAP-Cell TMR-Star showed the characteristic EzrA ring-like structure (Figure 3.28). SJF4640 and SJF4642 were then confirmed to be genetically correct by PCR on extracted genomic DNA using primers ezrA-up-F and ezrA-down-R and by Southern blot hybridisation using the ECL detection method (Figure 3.29A and B).

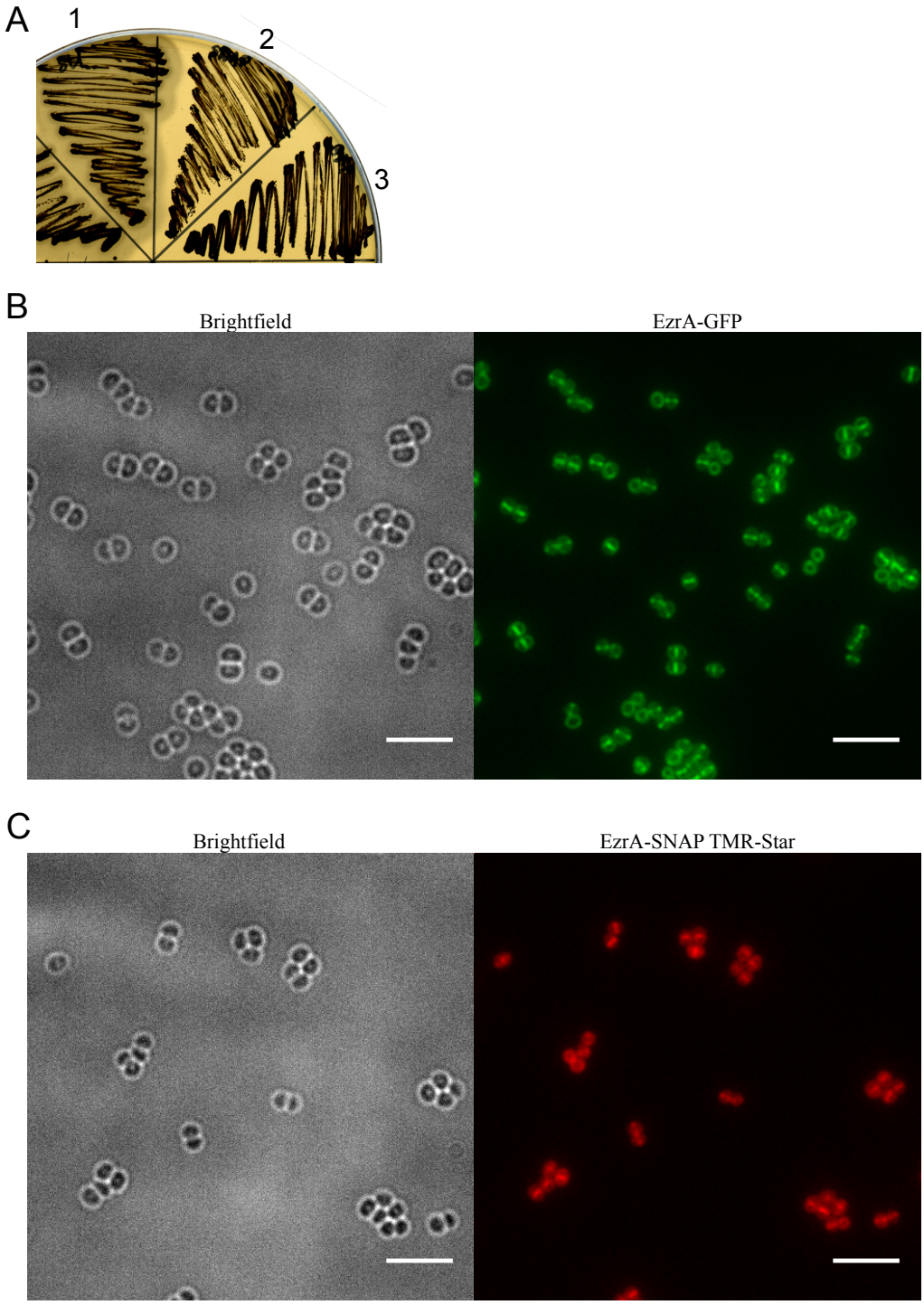

Figure 3.26. Confirmation of EzrA-GFP and EzrA-SNAP in SJF4639 and SJF4641

A. Correct integration of pKASBAR-EzrA-GFP and pKASBAR-EzrA-SNAP into the chromosome was confirmed by plating *S. aureus* SH1000 (1), SJF4641 (*S. aureus* SH1000 *geh::ezrA-snap*) (2) and SJF4639 (*S. aureus* SH1000 *geh::ezrA-gfp*) (3) onto a Baird-Parker medium. Disruption of lipase production confirms presence of the plasmids at the *geh* locus.

B. In SJF4639 (*S. aureus* SH1000 *geh::ezrA-gfp*) EzrA-GFP localises to the septa and presents the characteristic ring-like pattern. Scale bars 5 µm.

C. In SJF4641 (*S. aureus* SH1000 *geh::ezrA-snap*) EzrA-SNAP labelled with SNAP-Cell TMR-Star shows the same pattern of localisation as other EzrA fluorescent fusions. Scale bars 5 µm

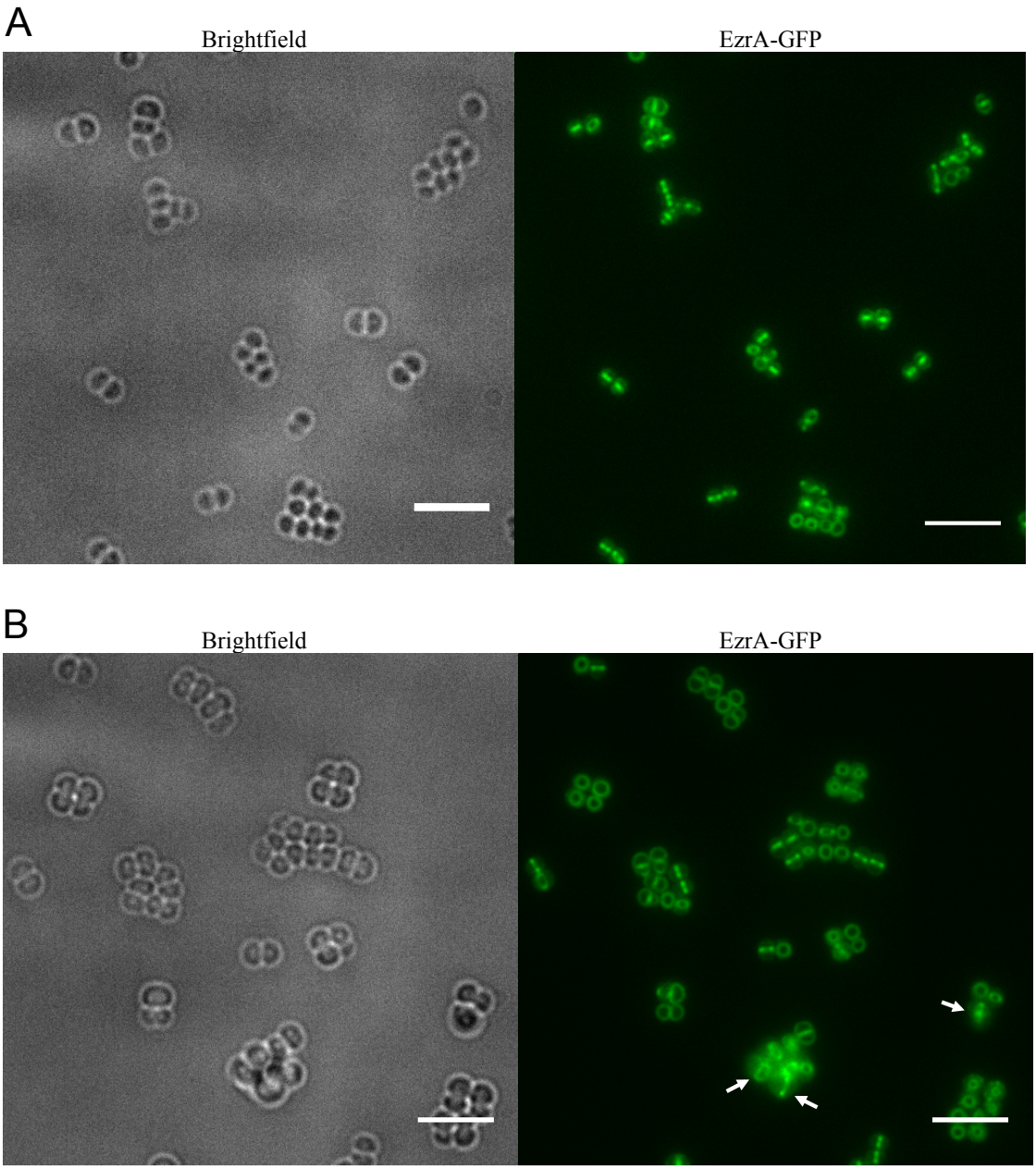

Figure 3.27. Morphology of *S. aureus* and localisation of EzrA-GFP in the absence of the native copy of *ezrA*

A. SJF4640 (*S. aureus* SH1000 *geh::ezrA-gfp ΔezrA::tet*) forms cells of wild type morphology and EzrA-GFP shows expected localisation. Scale bars 5 μm.

B. A representative clone producing EzrA-GFP in the absence of native EzrA but forming cells with abnormal morphology and EzrA-GFP localisation (indicated with white arrows). Scale bars 5 μm.

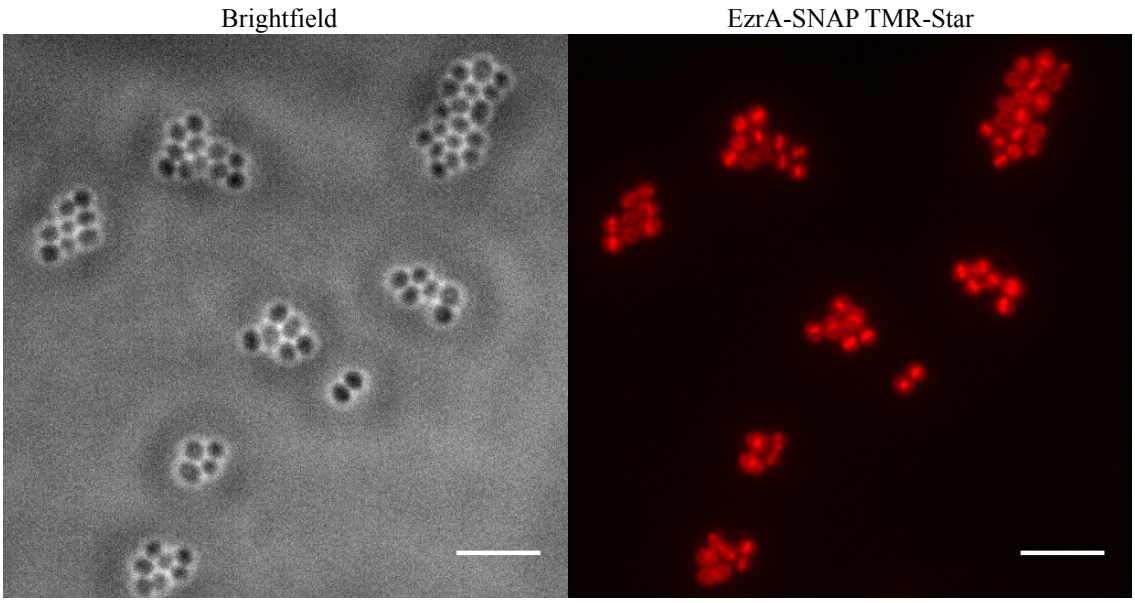

Figure 3.28. Localisation of EzrA-SNAP in SJF4642

In SJF4642 (*S. aureus* SH1000 *geh::ezrA-snap ΔezrA::tet*) EzrA-SNAP stained with SNAP-Cell TMR-Star presents the characteristic EzrA septal localisation. Scale bars 5 µm.

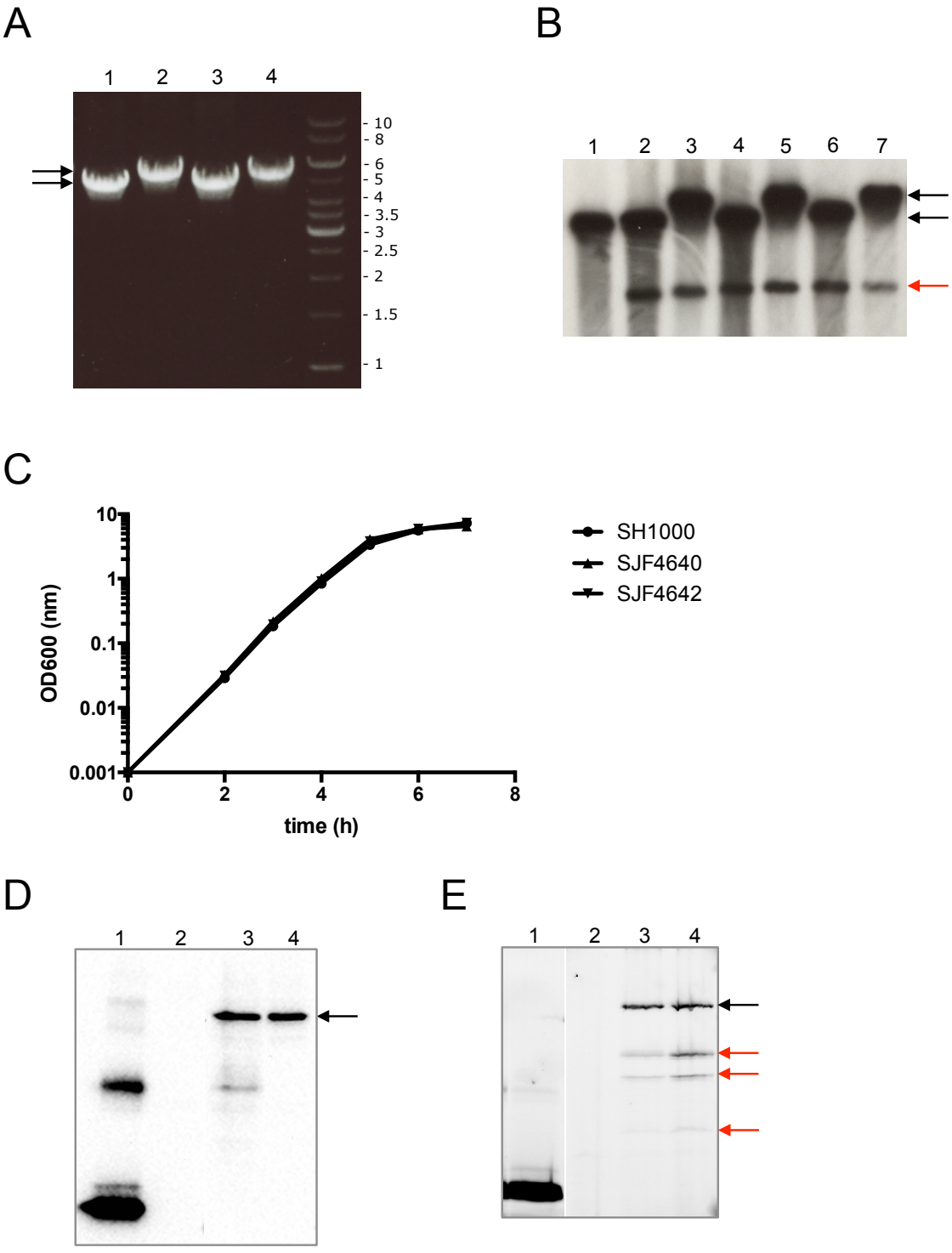

Figure 3.29. Confirmation of EzrA-GFP and EzrA-SNAP functionality in *S. aureus*

A. Products of PCR amplification of the *ezrA* region using primers ezrA-up-F and ezrA-down-R indicate presence of the TetR cassette in the *ezrA* locus in SJF4640 (*S. aureus* SH1000 *geh::ezrA-gfp ΔezrA::tet*) and SJF4642 (*S. aureus* SH1000 *geh::ezrA-snap ΔezrA::tet*) (lanes 2 and 4, respectively), and the *ezrA* presence at its native locus in SJF4639 (*S. aureus* SH1000 *geh::ezrA-gfp*) (lane 1) and SJF4641 (*S. aureus* SH1000 *geh::ezrA-snap*) (lane 3). The expected PCR products are indicated with black arrows. Sizes of a DNA ladder are shown in kb.

B. Southern blot hybridisation confirms *ezrA* deletion in SJF4640 (*S. aureus* SH1000 *geh::ezrA-gfp ΔezrA::tet*) and SJF4642 (*S. aureus* SH1000 *geh::ezrA-snap ΔezrA::tet*). Genomic DNA was isolated from SH1000 (lane 1), SJF4386 (*S. aureus* SH1000 *geh::ezrA-eyfp*) (lane 2), SJF4388 (*S. aureus* SH1000 *geh::ezrA-eyfp ΔezrA::tet*) (lane 3), SJF4639 (*S. aureus* SH1000 *geh::ezrA-gfp*) (lane 4), SJF4640 (lane 5), SJF4641 (*S. aureus* SH1000 *geh::ezrA-snap*) (lane 6) and SJF4642 (lane7), digested with *HindIII* and probed with a 1645 bp probe labelled with peroxidase. DNA bands corresponding to approximately 9 kb and 17 kb are indicated with black arrows. An extra band that likely corresponds to the *ezrA* promoter at the *geh* locus is indicated with a red arrow. Sizes of a DNA ladder shown in kb.

C. *S. aureus* SH1000, SJF4640 (*S. aureus* SH1000 *geh::ezrA-gfp ΔezrA::tet*) and SJF4642 (*S. aureus* SH1000 *geh::ezrA-snap ΔezrA::tet*) were grown overnight in BHI media with appropriate antibiotics. These cultures were used to inoculate 50 ml of BHI to an OD_{600} of 0.001. Optical density of cell cultures was measured every hour. All three strains grew with the same rate (generation time ~25 min). Cell cultures were grown in triplicate and error bars represent standard deviation from the mean.

D. Whole cell lysates of SH1000 (lane 2), SJF4639 (lane 3) and SJF4640 (lane 4), and a recombinant GFP-HisTag protein (lane 1) were probed with anti-GFP antibodies at a 1:1000 dilution. Bands detected at ~90 kDa are indicated with a black arrow.

E. SH1000 (lane 2), SJF4641 (lane 3) and SJF4642 (lane 4) were grown to early exponential phase and labelled with SNAP-Cell TMR-Star. The whole cell lysates were run in a 10% (w/v) SDS-PAGE gel and visualised by fluorescence detection. A purified SNAP-tag protein (kindly provided by Joe Kirk, University of Sheffield) labelled with SNAP-Cell TMR-Star was used as a positive control (lane 1). Bands detected at ~90 kDa, which likely represent EzrA-SNAP, are indicated with a black arrow, the additional bands of approximately 40, 50 and 60 kDa are indicated with red arrows.

The functionality of EzrA-GFP and EzrA-SNAP was tested by growth experiments. Growth of SJF4640 and SJF4642 was compared against SH1000 and the doubling times of all three strains were the same (~25 min, Figure 3.29C). The stability of the EzrA-GFP was examined by western blot analysis. A whole cell lysate of SJF4640 was probed with anti-GFP at a dilution of 1:1000. A band of ~90 kDa was identified which correlated to the expected molecular weight of full length EzrA-GFP (Figure 3.29D). The size and stability of EzrA-SNAP was verified by SDS-PAGE and in-gel fluorescence visualisation of whole cell extracts from SJF4642 labelled with SNAP-Cell TMR-Star. A band of ~90 kDa was detected, which likely represented EzrA-SNAP. Additional bands of ~40 kDa, ~50 kDa and ~60 kDa were detected and probably were products of EzrA-SNAP degradation (Figure 3.29E).

The above results indicated that EzrA-GFP and EzrA-SNAP in SJF4640 and SJF4642 were functional and able to complement the native *ezrA* depletion.

3.2.4.2.2 EzrA-GFP and EzrA-SNAP TMR-Star by SIM

Localisation of EzrA-GFP and EzrA-SNAP was visualised in 3D-SIM. SJF4640 (*S. aureus* SH1000 *geh::ezrA-gfp ΔezrA::tet*) and SJF4642 (*S. aureus* SH1000 *geh::ezrA-snap ΔezrA::tet*) were grown to early-exponential phase and fixed. SJF4642 additionally was labelled with SNAP-Cell TMR-Star before fixation. Cells were mounted in an antifade reagent, SlowFade Gold.

GFP and TMR-Star were found to be more stable and bright fluorophores than eYFP/meYFP and allowed for visualisation of EzrA in SIM. The data generated from 3D-SIM imaging of EzrA-GFP and EzrA-SNAP TMR-Star showed the characteristic septal localisation of EzrA (Figures 3.30A and 3.31A). The patterns formed by these two fusions were comparable when visualised by conventional fluorescence microscopy (Figure 3.27A and 3.28) and the 3D-SIM images confirmed this observation. In contrast to conventional fluorescence microscopy, which depicts EzrA-GFP and EzrA-SNAP TMR-Star as uniform rings, SIM data showed the fusion proteins heterogeneously distributed around division site. In order to visualise this, individual cells imaged by conventional fluorescence microscopy and 3D-SIM were selected and surface profiles of fluorescence intensity distribution of laterally placed rings were generated (Figures 3.30B and C, 3.31B and C).

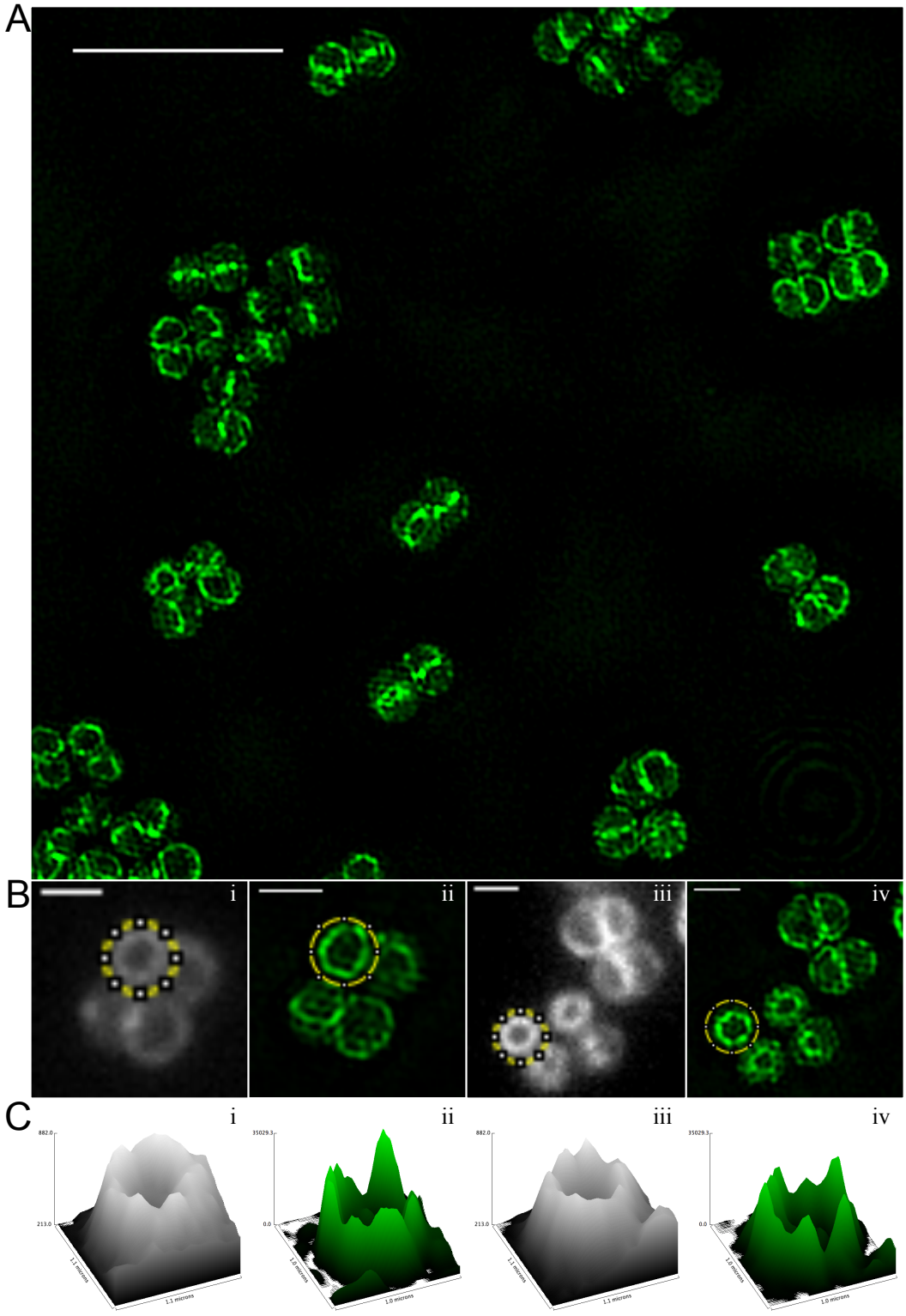

Figure 3.30. EzrA-GFP localisation by 3D-SIM

A. EzrA-GFP in SJF4640 (*S. aureus* SH1000 *geh::ezrA-gfp ΔezrA::tet*) was visualised in 3D-SIM. Scale bars 5 µm.

B. Individual SJF4640 cells visualised with both conventional fluorescence microscopy (i and iii) and 3D-SIM (ii and iv), respectively, are highlighted. Scale bars 1 µm.

C. Surface plots show distribution of fluorescence intensity in EzrA-GFP rings oriented in the lateral plane. Each intensity plot represents a ring highlighted in yellow in the image shown above.

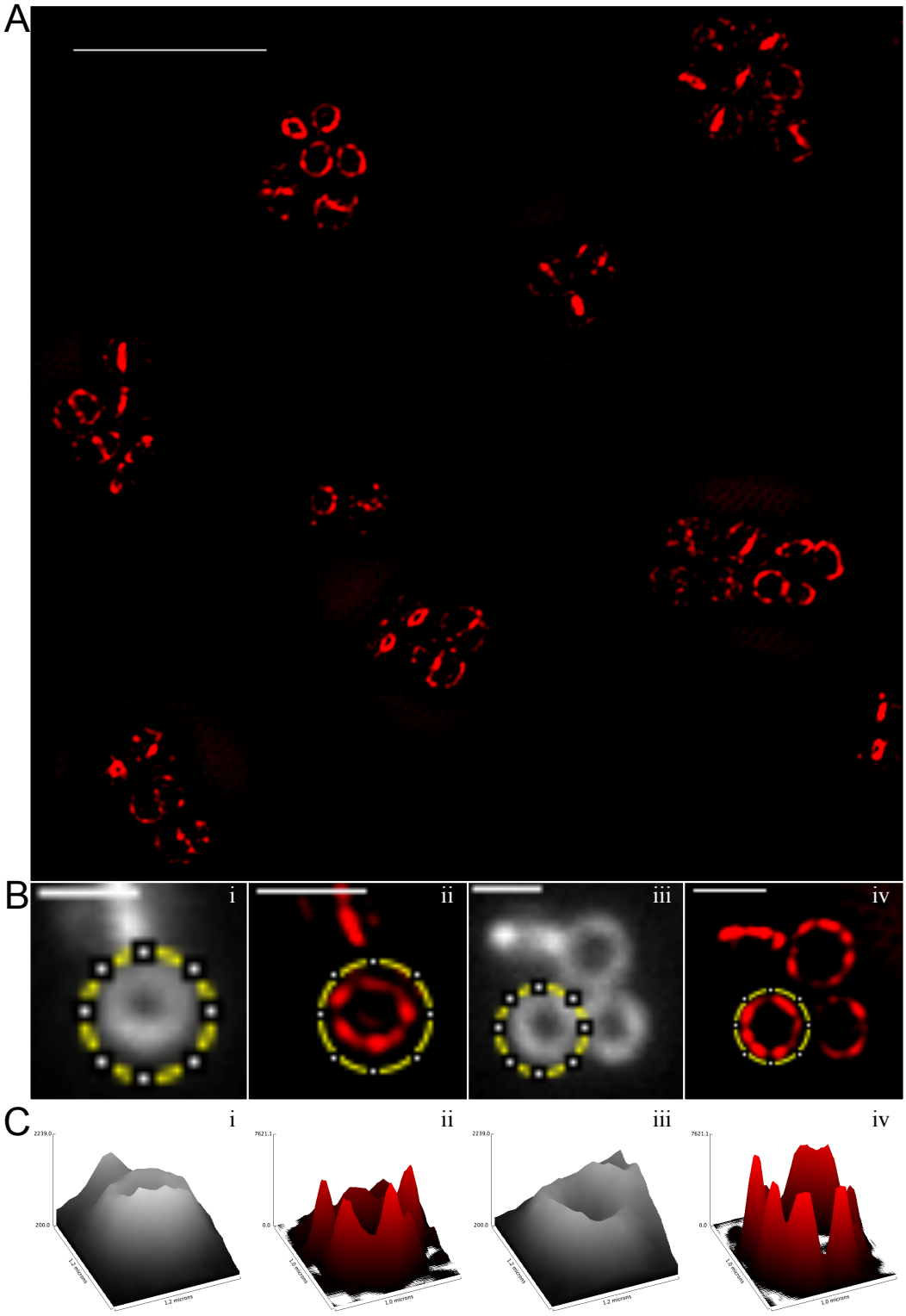

Figure 3.31. EzrA-SNAP TMR-Star localisation by 3D-SIM

A. In SJF4642 (*S. aureus* SH1000 *geh::ezrA-snap ΔezrA::tet*) EzrA-SNAP was labelled with SNAP-Cell TMR-Star and visualised in 3D-SIM. Scale bars 5 µm.

B. Individual SJF4642 cells visualised with both conventional fluorescence microscopy (i and iii) and 3D-SIM (ii and iv), respectively, are highlighted. Scale bars 1 µm.

C. Surface plots show distribution of fluorescence intensity in EzrA-SNAP rings oriented in the lateral plane. Each intensity plot represents a ring highlighted in yellow in the image shown above.

The surface profiles of EzrA rings in conventional fluorescence microscopy showed not much variation in distribution of a fluorescent signal within one ring (Figures 3.30Bi, iii and Ci, iii and 3.31Bi, iii and Ci, iii). When the same structures were visualised in SIM and their intensities were plotted, clear non-uniform distribution of EzrA was revealed (Figures 3.30Bii, iv and Cii, iv and 3.31Bii, iv and Cii, iv). This data showed that EzrA was not homogeneously distributed, but there were regions of EzrA concentration in rings, presented as distinct peaks. What is more, this heterogeneous distribution was not influenced by a type of a fluorophore used to visualise EzrA. The similar patterns were observed when either GFP or SNAP TMR-Star were used as fluorescent tags. This was also supported by the sizes of rings formed by EzrA-GFP and EzrA-SNAP TMR-Star, as rings for both fusions were ~200 nm wide. The almost identical localisation pattern of EzrA-GFP and EzrA-SNAP indicated that the heterogeneous EzrA distribution was not caused by the tags fused to it. However the reconstruction process could incorporated these patterns (Appendix II).

3.2.5 EzrA-SNAP TMR-Star localisation by STORM

STORM imaging of EzrA-eYFP and EzrA-meYFP revealed that EzrA does not form a uniform structure but it is rather a heterogeneous number of 'patches'. As mentioned previously fusing EzrA with other STORM-compatible fluorescent proteins was not successful. However in order to confirm that localisation pattern observed for EzrA another approach of EzrA labelling was needed to be used.

In SJF4642 (*S. aureus* SH1000 *geh::ezrA-snap ΔezrA::tet*), SNAP was fused to the C-terminus of EzrA. As the C-terminal SNAP-tag was located in the cytoplasm, a cell permeable dye was required to label the EzrA-SNAP fusion. There are very few available SNAP dyes that can cross the cell membrane and stain intracellular components. One of them, SNAP-Cell TMR-Star was reported to be suitable for STORM analyses of cellular structures in eukaryotic cells (Klein et al., 2011). Therefore, this dye was chosen to localise EzrA-SNAP in STORM and to verify the structures generated by EzrA-eYFP and EzrA-meYFP. As a result of problems described in section 4.2.1.3 a method called reductive caging that creates photoactivatable fluorophores was introduced. In this method a reducing agent, $NaBH_4$ is used to convert a fluorophore into a reduced (caged) form and such a reduced dye is

activated into a bright form upon UV illumination (Vaughan et al., 2012).

To check the effectiveness of caging reaction and how it influenced the fluorophore SJF4642 labelled with TMR-Star and reduced with $NaBH_4$ was first viewed by conventional fluorescence microscopy. The fluorescence images of EzrA-SNAP TMR-Star uncaged, caged or caged but illuminated with UV light appeared to show no difference between one another (Figure 3.32A). Nevertheless, an attempt to visualise caged EzrA-SNAP TMR-Star by STORM was made.

In order to examine EzrA-SNAP localisation by N-STORM SJF4642 was grown to early-exponential phase, labelled with SNAP-Cell TMR-Star and fixed. The cells were reduced with $NaBH_4$ and mounted in GLOX MEA. EzrA-SNAP TMR-Star was imaged with 561 nm excitation and the fluorescent signal was reactivated by illumination at 405 nm. Single blinks emitted by TMR-Star were used to reconstruct STORM images. The 2D-STORM images showed that TMR-Star could be utilised in STORM imaging of EzrA-SNAP (Figure 3.33). The high-resolution pattern obtained for EzrA-SNAP TMR-Star was in agreement with localisation pattern of EzrA in conventional fluorescence microscopy. In both microscopy techniques the fluorescent signal was associated with cell septa and cell membrane (Figures 3.32 and 3.33). STORM data of EzrA-SNAP TMR-Star confirmed that EzrA formed a heterogeneous 'patches' around the division site. The width of these 'patches' varied from ~150 to ~300 nm. The STORM data acquired for EzrA-SNAP TMR-Star suggested that EzrA-SNAP structures were two times larger than EzrA-eYFP 'patches'. Furthermore, a signal associated not only with the septa and cell membrane but the cytoplasm could be observed in many cells. TMR-Star is an organic dye that recognises SNAP and does not need to bind the tag to become fluorescent. The cytoplasmic signal could therefore come from the dye that did not react covalently with the SNAP-tag but was not washed out properly. The other explanation could be instability of the EzrA-SNAP fusion. An in-gel based fluorescence analysis of SJF4643 stained with SNAP-Cell TMR-Star showed that EzrA-SNAP might not be stable (Figure 3.29E) and degraded EzrA-SNAP could contribute to the cytoplasmic signal.
The SNAP-tag system combined with TMR-Star was shown to be a promising alternative labelling method to eYFP for EzrA super-resolution localisation studies. Due to time limits, further experiments confirming TMR-Star STORM-compatibility and utility were not carried out.

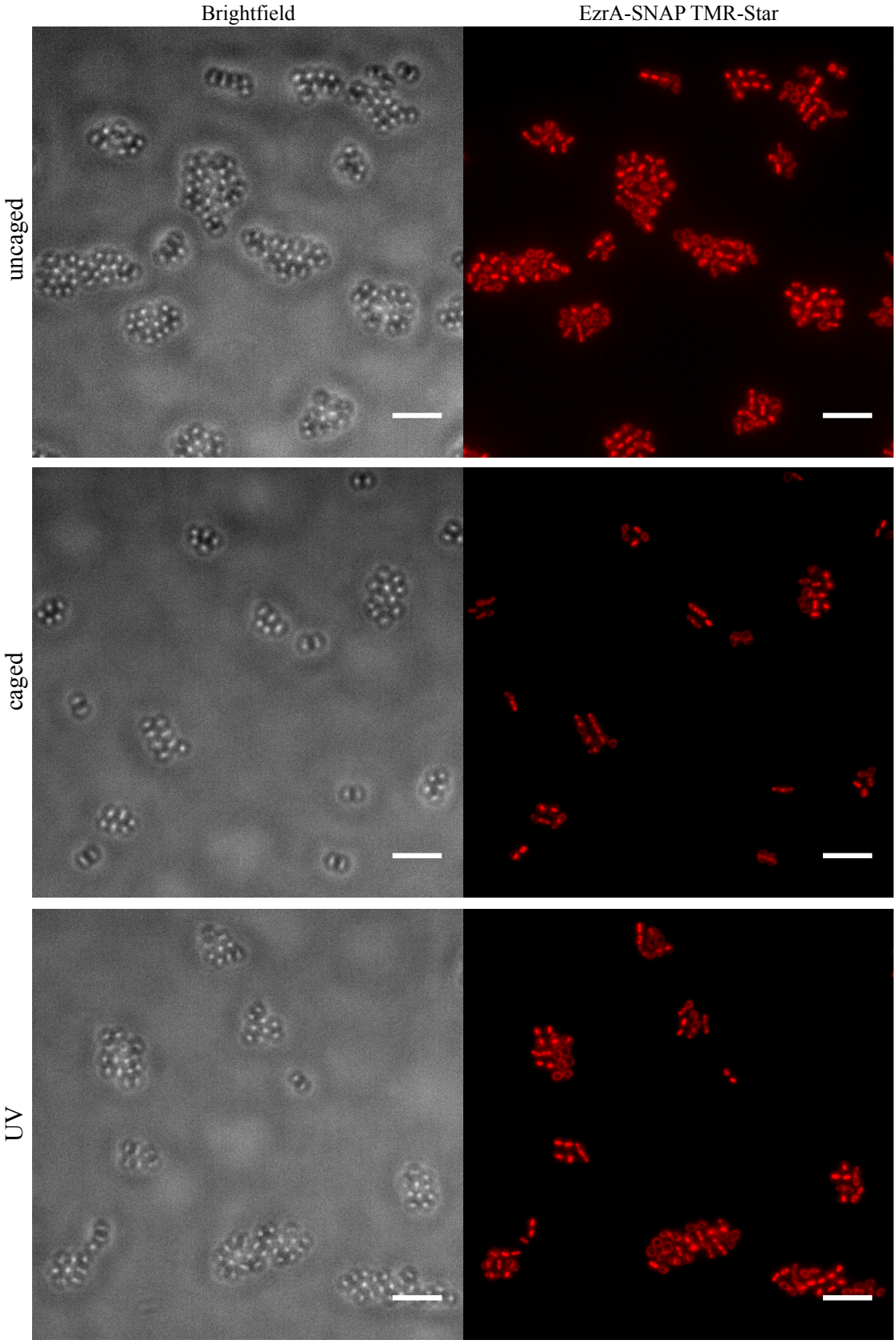

Figure 3.32. Reductive caging of TMR-Star

Initial fluorescence of SJF4642 (*S. aureus* SH1000 *geh::ezrA-snap ΔezrA::tet*) labelled with SNAP-Cell TMR-Star (uncaged), fluorescence signal after $NaBH_4$ treatment (caged) and after reduction with $NaBH_4$ and UV illumination (UV). Scale bars 5 µm.

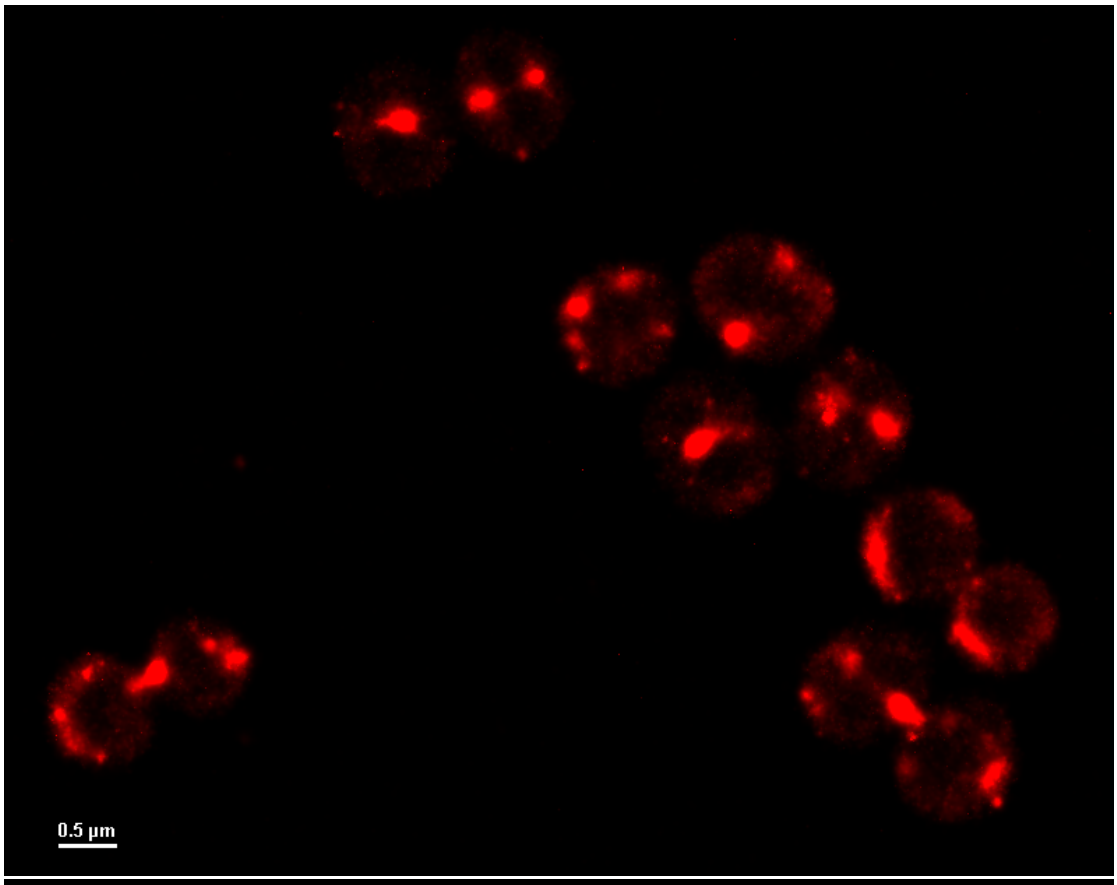
0.5 µm

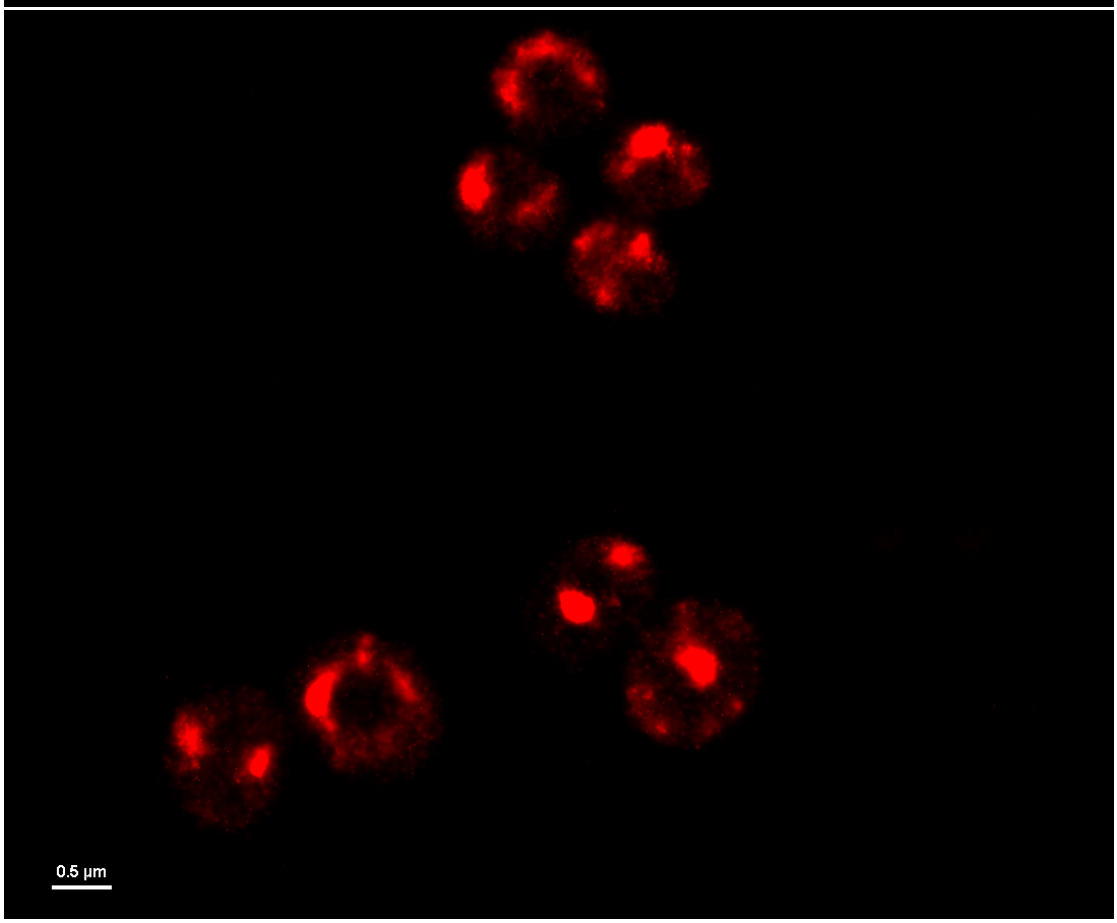
0.5 µm

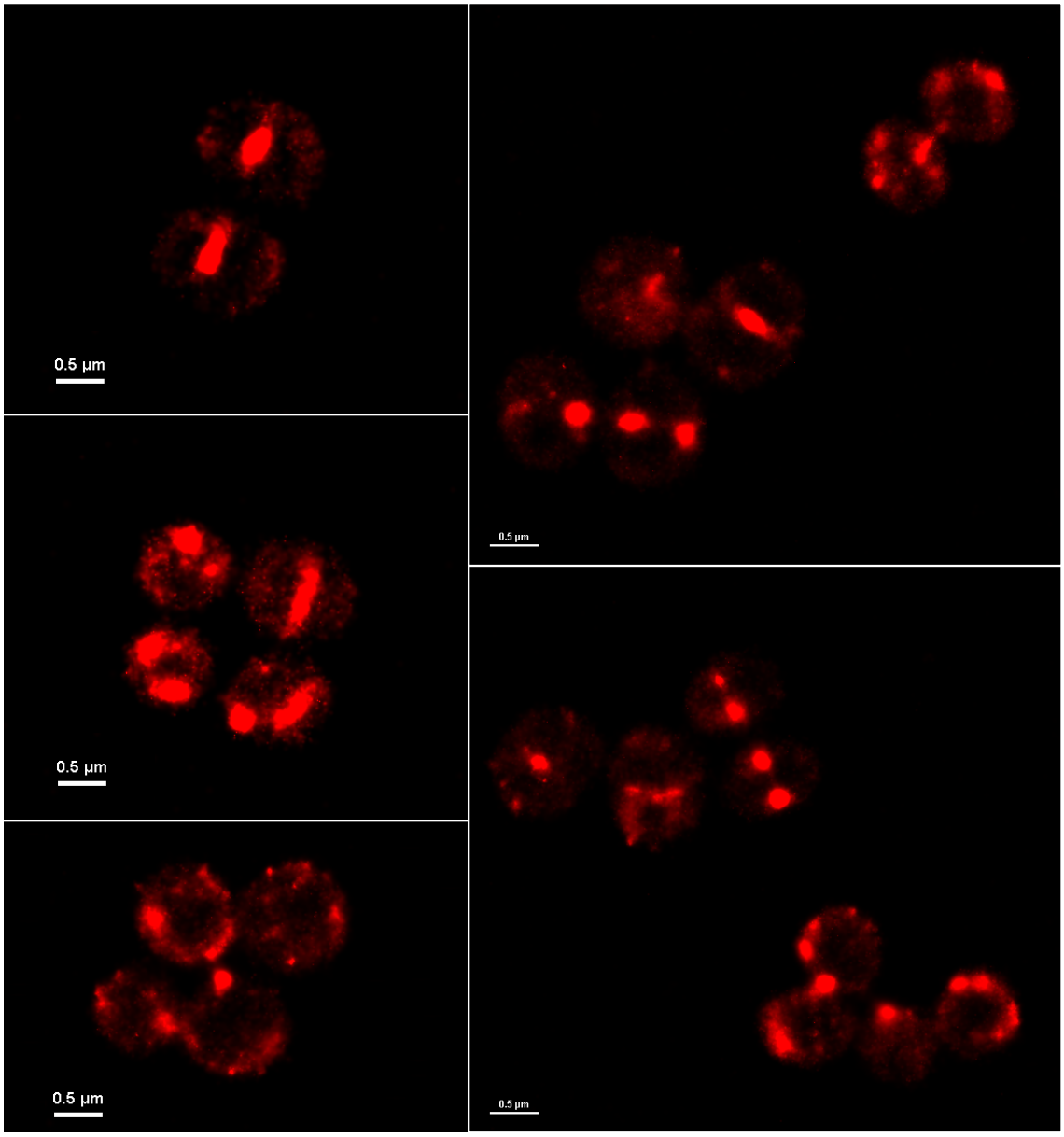

Figure 3.33. EzrA-SNAP TMR-Star localisation by 2D-STORM

EzrA-SNAP in SJF4642 (*S. aureus* SH1000 *geh::ezrA-snap ΔezrA::tet*) was labelled with SNAP-Cell TMR-Star. $NaBH_4$ reduced cells were visualised by 2D-STORM. Imaging performed in GLOX MEA.

3.3 Discussion

Previous work carried out in the lab identified EzrA as an essential *S. aureus* cell division component. Studies on EzrA localisation by conventional fluorescence microscopy showed that it is recruited to the septum where it forms a ring-like structure during cell division (Steele et al., 2011). The aim of the study described in this chapter was to identify fluorescent proteins that could be used in the *S. aureus* system to study EzrA localisation in super-resolution. This study demonstrates for the first time utilisation of the STORM technique to obtain detailed information on the EzrA localisation structure in *S. aureus*.

EzrA is an abundant protein, in *B. subtilis* there are predicted from 10,000 to 20,000 EzrA molecules per cell, which makes it relatively an easy target to visualise by fluorescence microscopy (Haeusser et al., 2004). As mentioned before, EzrA was successfully fused to GFP and its septal and uniform localisation was demonstrated with standard fluorescence microscopy approaches (Steele et al., 2011). Conventional microscopy is however limited by light diffraction and detailed visualisation of bacterial components is constricted. More recently, Strauss et al. (2012) studied EzrA-GFP localisation in *S. aureus* using 3D-SIM and suggested that EzrA similarly to other cell division components, that is FtsZ and PBP2, forms a non-uniform ring. Based on observations from SIM experiments a new model in which EzrA localises in a bead-like pattern was proposed. In this model an EzrA ring consists of around 13 ‘beads’ and each ‘bead’ measures around 200 nm in length. The ‘beads’ are heterogeneously distributed thus the ring is not continuous and at least one gap within a Z-ring is observed (Strauss et al., 2012).

In this study two high-resolution microscopy techniques were employed to visualise EzrA localisation in *S. aureus*, SIM and STORM. The data obtained with SIM suggest that EzrA indeed does not form a uniform ring like structure. The regions of higher fluorescent signal concentration were observed that one could interpret as ‘beads’ (Figures 3.30 and 3.31). The other technique used to elucidate EzrA localisation, STORM provides the highest resolution among all available fluorescence microscopy techniques, thus allows to look into fine sample features in even more detail than other super-resolution microscopy techniques, including SIM. Whilst the heterogeneous

distribution of EzrA was observed, STORM did not confirm that EzrA forms distinct 'beads'. Instead 'patchy' distribution of EzrA molecules was revealed. This 'patchy' distribution is characterised by no regular or defined arrangement of EzrA molecules. EzrA seems to be randomly, but with some regions of a local concentration, dispersed around the division site.

One of the questions raised during this study was: how does the method used to label EzrA affect its localisation? In order to avoid building up conclusions about EzrA localisation based on one protein fusion, a range of fluorescent proteins with different photophysical properties were tested: mEos2, PSmOrange, PAmCherry1 and eYFP. All four EzrA fluorescent fusions placed under the putative *ezrA* promoter were produced by *E. coli* (Figure 3.6). This was not expected, as EzrA does not have any orthologues in *E. coli* but this was not surprising either. The predicted putative *ezrA* promoter TATAAT sequence at -10 region is identical to the -10 conserved sequence recognised by *E. coli* RNA polymerase $E\sigma^A$. Furthermore, *S. aureus* is closely related to another Gram-positive bacterium, *B. subtilis* and promoters from *B. subtilis* were shown to work well in *E. coli* (Voskuil and Chambliss, 1998). Thus *E. coli* was a useful preliminary organism for testing EzrA fluorescent fusions that allowed at an early stage for verification if the particular fluorescent protein when fused to EzrA had the correct spectral properties. At the *E. coli* cell stage only the EzrA-PSmOrange fusion was found to not have the right photophysical properties, it was fluorescent in orange but did not convert to far-red upon blue-green light illumination (Figure 3.6B). Surprisingly, EzrA fluorescent fusions were more readily produced and fluorescent in *E. coli* than in *S. aureus*. Only EzrA-eYFP and EzrA-PAmCherry1 were produced, fluorescent and had the expected localisation in *S. aureus* (Figure 3.8). Lack of fluorescent signals from EzrA-mEos2 and EzrA-PSmOrange could be explained by lack of expression of these two fusions in *S. aureus*. However this seems to be unlikely as other EzrA fusions, EzrA-eYFP, EzrA-GFP or EzrA-SNAP were all produced by *S. aureus* strains that are otherwise isogenic with *S. aureus* carrying *ezrA-meos2* or *ezrA-psmorange* genes (Figures 3.13 and 3.26B and C). This indicates that the selected sequence of the putative *ezrA* promoter is correct and regulates production of the EzrA fusion proteins. Misfolding and instability of one of the fusion components and protein degradation are a more probable explanation why no fluorescent signal was detected for EzrA-mEos2 and EzrA-PSmOrange in *S. aureus.* Whilst mEos2 is one of the most often employed

fluorescent proteins for STORM studies of bacterial components, to date PSmOrange has only been shown to be produced and fluorescent in mammalian system by a group which developed this fluorophore (Subach et al., 2011).

Initial work on EzrA-PAmCherry1 suggested that this fluorescent fusion could be utilised in localisation studies of EzrA as it was fluorescent and could complement the knock-out of the native *ezrA* gene (Figure 3.14). Nevertheless, this fusion protein was not consistent, that is cells often were not fluorescent or did not show the expected EzrA localisation (Figure 3.16B). Western blot analysis showed that EzrA-PAmCherry1 was produced in *S. aureus* however the used detection method did not allow the exclusion of protein degradation (Figure 3.14E). It is possible that *S. aureus* cells did not favour this particular type of a fusion since recently another research group has reported usage of a PBP4-PAmCherry1fusion to observe localisation of PBP4 in *S. aureus* by PALM (Monteiro et al., 2015). This publication indicates that PAmCherry1 can be produced and fluorescent in *S. aureus* but it does not show if the protein fused to PAmCherry1 is functional as PBP4 is not an essential protein and its depletion does not impair growth and viability of *S. aureus* (Wyke et al., 1981).

EzrA-eYFP was the only STORM-compatible fluorescent fusion of EzrA that was both functional and stable (Figures 3.13 and 3.13). Utilisation of EzrA-eYFP led to reconstruction of a heterologous and 'patchy' distribution of this protein in *S. aureus* (Figures 3.17 and 3.18). Recently a similar buffer system to GLOX MEA, which was used in this study, was published to be optimal in eYFP imaging by another research group (Jusuk et al., 2015), supporting the choice of buffering conditions for EzrA-eYFP STORM localisation experiments. Correct selection of buffers in one aspect when localising fluorophores in super-resolution, another are the physical properties of the chosen fluorophore. eYFP was the only STORM-compatible fluorescent protein that worked well when fused to EzrA. Because of the lack of other STORM-compatible EzrA fluorescent fusions and reported tendency of fluorescent proteins to low-affinity oligomerisation (Zacharias et al., 2002) a monomeric variant of eYFP was constructed. This together with SNAP-tagged EzrA ($NaBH_4$ caged EzrA-SNAP TMR-Star) verifies and confirms that EzrA is heterogeneously localised in *S. aureus* and the non-uniform distribution of EzrA-eYFP in STORM is not a result of possible oligomeric interactions of eYFP (Figures 3.19 and 3.33).

This work also presents how the right choice of a fluorescent marker can influence the final results and conclusions. For example eYFP/meYFP fits requirements of STORM but due to its rapid photobleaching it is not useful in SIM imaging and is the source of localisation artefacts (Figure 3.23). Not only fluorophores and imaging conditions but the microscopy technique, its requirements and limitations can lead to errors.

In SIM fluorophores that are resistant to photobleaching are required since 15 images per z-stack (three imaging angles, five images per angle) are acquired in order to reconstruct a high-resolution image. Thus the sample is exposed to extensive photobleaching, each exposure produces less fluorescent signal that can be detected, which consequently results in a low signal-to-noise ratio and affects the quality of the reconstruction. A hexagonal pattern also called 'honeycomb', which is a characteristic for samples with a poor signal-to-noise ratio, is visible in SIM images of EzrA-GFP, less for EzrA-SNAP TMR-Star (Figures 3.30. and 3.31). This highlights artefacts that deteriorate the quality of obtained 3D-SIM images for EzrA-GFP and EzrA-SNAP TMR-Star.

STORM, as its name indicates, relies on stochastic excitation of single fluorophores. In a stochastic process molecules are randomly activated and every single molecule has the same probability to be turned on (Rust et al., 2006). Therefore the overall distribution of imaged EzrA molecules is believed to be representative. STORM reconstruction data are however limited in several ways. STORM resolution depends on number of photons emitted by a molecule and background fluorescence – the more detected photons and the minimal background noise, the position of the emitter can be determined with a higher precision (Fernández-Suárez and Ting, 2008). Moreover, the number of recorded events can be another limiting factor. Unless the underlying structure of the studied sample is known, it is difficult to determine whether the amount of collected events is sufficient. If there are not enough of them then a full image of the sample cannot be formed and the final structure can arise from under-sampling. Additionally, in order to localise molecules with super-resolution they have to be well separated. When imaging samples of a high fluorophore density a large number of imaging cycles have to be recorded so that a considerable proportion of spatially and temporally separated emitters can be detected, their localisations determined and used to reconstruct a high-resolution image (Geissbuehler et al., 2011).

The simulation in Figure 3.34 prepared by Dr Robert Turner (University of Sheffield) shows a hypothetical spatial distribution of fluorescent molecules in cells, which are 1 μm in diameter, imaged by STORM. 90 randomly distributed molecules are constrained into a ring with a radius of 500 nm, 10 molecules are distributed between the septum and the cell surface. STORM resolution is based on localisation precision and the simulation illustrates how the final reconstruction images change qualitatively as localisation precision is reduced. Therefore the representation of the nature of the sample differs depending on resolution of reconstructed images (Figure 3.34.). This simulation also emphasises how much uncertainty is in the reconstructed images of EzrA especially when its underlying structure is unknown and its localisation cannot be verified by comparison to other well-defined structures.

STORM data show EzrA as a heterogeneous structure but it does not confirm its 'beady' pattern obtained from SIM localisation studies presented in this study and by Strauss et al. (2012). As eYFP is a fluorophore that can reversibly photoswitch between on and off states the STORM images are only a qualitative but not quantitative representation of EzrA distribution in *S. aureus*. Additionally, STORM data suggest that not all EzrA-eYFP molecules localise to the septa during cell division. In *B. subtilis* EzrA is distributed through the cell membrane and concentrates in the midcell during cell division. The off-septal EzrA is considered to be responsible for preventing formation of the FtsZ ring in any other places than septum (Levin et al., 1999). *S. aureus* divides sequentially in orthogonal planes and the peripheral EzrA molecules might be the protein that remains and marks the previous plane to prevent reuse. On the other hand, the off-septal signal may be EzrA that has left the current division site to localise to, and mark, the next division plane. However, in order to be able to determine this, EzrA needs to be set in a context of other cell division and structural components.

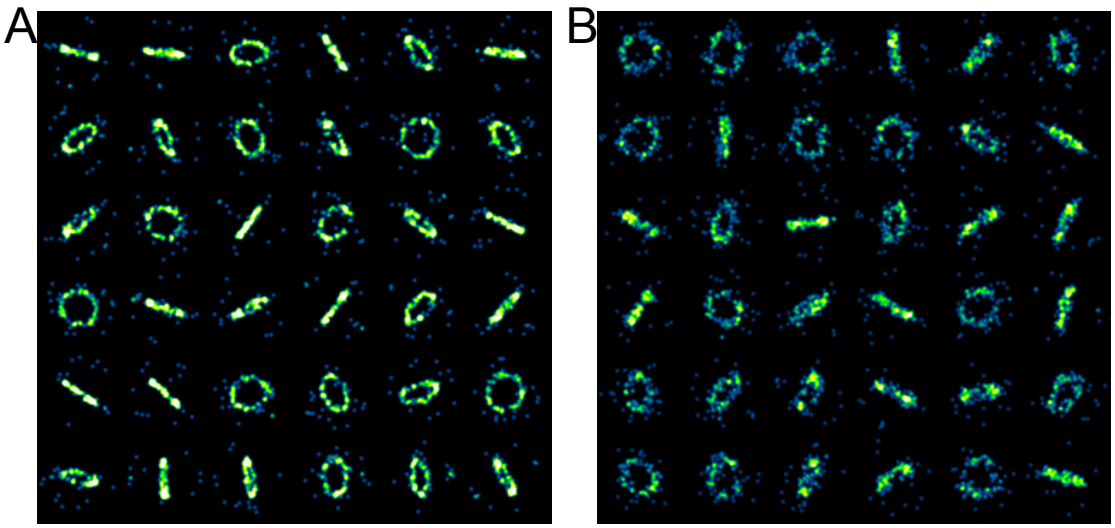

Figure 3.34. STORM simulation of fluorescent molecules forming a ring-like structure at high (A) and low (B) resolution

CHAPTER 4

Colocalisation of EzrA with other cell division components

The work in this chapter was carried out in collaboration with Robert Turner (STORM) and Christa Walther (N-STORM and SIM)

4.1 Introduction

FtsZ, a structural homologue of eukaryotic tubulin, is a highly conserved key component of the cell division process in many bacterial species (Adams and Errington, 2009). It is considered to be the first protein that localises to the division site where it polymerises into a Z-ring like structure (Bi and Lutkenhaus, 1991). The Z-ring acts as a scaffold that recruits other cell division components to the site of division. FtsZ together with the other components, collectively called the divisome, mediate cell division (Adams and Errington, 2009). In rod-shaped bacteria such as *E. coli* and *B. subtilis*, which during vegetative growth divide symmetrically, the division septum is precisely placed at midcell, with a deviation of ~1% off the cell midpoint (Trueba, 1982), so that two equal daughter cells are generated. In these two model organisms the Min system and nucleoid occlusion (NO) regulate positioning of the Z-ring (Yu and Margolin, 1999; Monahan et al., 2014b). They both act as negative regulators as they inhibit polymerisation of FtsZ into the Z-ring in other places but midcell and its assembly over unreplicated and unsegregated chromosomes (Yu and Margolin, 1999; Monahan et al., 2014b). However neither the Min system nor NO are essential in *E. coli* and *B. subtilis.* Recently it has been shown that *B. subtilis* mutants lacking both systems, although less efficiently than the wild type cells, still form the Z-ring precisely in the cell centre (Bernhardt and de Boer, 2005; Migocki et al., 2002; Rodrigues and Harry, 2012). This suggests that there may exist some other cell component that identifies the division site at midcell. The Min system and NO have been therefore proposed to be involved in efficient selection of the site of division by reducing the number of possible Z-ring formation positions to the cell centre by inhibiting FtsZ polymerisation in other places, such as the cell poles (Rodrigues and Harry, 2012). This is further supported by the fact that many bacterial species do not have either the Min system, or NO, or both (Margolin, 2005; Harry et al., 2006).

S. aureus is a coccus that divides sequentially in three perpendicular planes (Tzagoloff and Novick, 1977). Although *S. aureus* carries a homologue of DivIVA, which is a part of the Min system in *B. subtilis*, it does not contain other Min proteins (Pinho and Errington, 2004). Additionally, deletion of the *divIVA* gene does not impair cell viability or morphology (Pinho and Errington, 2004). *S. aureus* however encodes a homologue of *B. subtilis* nucleoid occlusion protein, Noc (Veiga et al., 2011). As the cytoplasmic space of *S. aureus* is largely occupied by nucleoid, NO must play a crucial role in determination of Z-ring placement (Veiga et al., 2011). Indeed it has been shown that in *noc* depleted *S. aureus* cells, FtsZ assembles on top of the non-segregated chromosome and the Z-ring is delocalised, that is it does not polymerise in orthogonal planes and multiply rings are often observed (Veiga et al., 2011). Event though the role of NO is to ensure that FtsZ does not assemble over the chromosomal DNA, this process does not however seem to be sufficient to direct *S. aureus* sequential division on orthogonal planes (Pinho et al., 2013).

Cell wall features called 'piecrusts' have been proposed to carry epigenetic information about previous division planes in *S. aureus* (Turner et al., 2010). Atomic force microscopy of purified *S. aureus* cell wall revealed a thick band of peptidoglycan material, a 'piecrust' around the midcell. This band is retained as 'ribs' after subsequential divisions, indicating that the local differences in peptidoglycan architecture may be recognised and used as division site selection 'signposts' (Figure 4.1) (Turner et al., 2010).

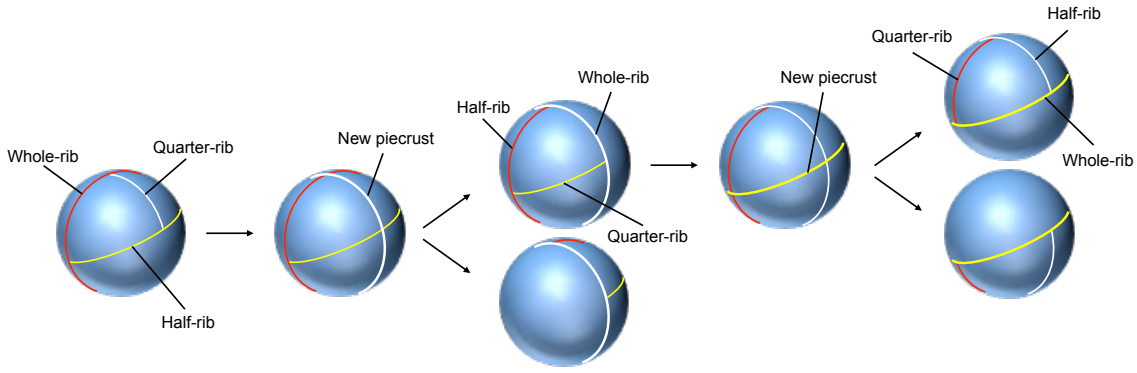

Figure 4.1. Schematic representation of localisation of 'piecrust' and 'rib' features and their inheritance during *S. aureus* cell division

S. aureus forms a new 'piecrust' in the orthogonal plane of the 'quarter-rib'. The cell divides and the new 'piecrust', 'whole-rib' and 'half-rib' are resolved as a new 'whole-rib', 'half-rib' and a new 'quarter-rib', respectively, in the daughter cells. The new 'quarter-rib' acts a 'signpost' for the next division plane. Adapted from (Turner et al., 2010).

Other cell wall components, such as wall teichoic acids (WTAs) have been suggested to be involved in regulation of midcell selection (Atilano et al., 2010; Schlag et al., 2010; Kent, 2013). Nevertheless, the presence of WTAs in the septum of *S. aureus* is controversial. One of the studies where Concanavalin A (ConA is a lectin that binds to teichoic acids) was used to stain WTAs showed that WTAs were present throughout the whole cell surface except for the septum (Schlag et al., 2010). On the contrary, localisation studies on *S. aureus* TarO (TagO), which is the first protein of the WTAs biosynthesis pathway, showed that this enzyme localises to the septum (Atilano et al., 2010). More recent research performed in our lab has shown that TarO together with other proteins involved in WTAs maturation interact with *S. aureus* divisome components that have been shown to localise at midcell in *S. aureus*, implying that WTAs may be synthesised in the septum since their biosynthesis machinery is present there (Kent, 2013). Moreover, septal binding of ConA could be observed in both whole cells and sacculi of broken *S. aureus* cells but the distribution of ConA was not uniform across the cell surface, indicating that WTAs may not be present on 'piecrust' and 'rib' features (Kent, 2013).

Lately, a cell division protein DivIB has been suggested to link selection of plane division to 'piecrust' features (Bottomley et al., 2014). DivIB does not form a typical septal localisation pattern but it is distributed as peripheral foci and hemispheres in *S. aureus*. It binds peptidoglycan but its affinity toward this polymer decreases when WTAs are present (Bottomley et al., 2014). Thus DivIB may be directed to 'piecrust' and 'rib' features, and mark previous division planes as they are the only accessible peptidoglycan structures free of WTAs (Bottomley, 2011; Kent, 2013).

Nevertheless, the role of cell wall architecture has been questioned by the most recently published data on *S. aureus* cell shape dynamics. It has been shown that *S. aureus* is not spherical during the whole cell cycle but elongates and increases in its volume before division (Zhou et al., 2015; Monteiro et al., 2015). Additionally, the division septum was found to constitute from 25% to 33% of the new daughter cell surface instead of 50% as previously assumed, suggesting that the 'piecrust' and 'rib' features are not retained at midcell and therefore may not act as topological 'signposts' directly marking the next placement site of division septum (Zhou et al., 2015; Monteiro et al., 2015; Seligman and Pincus, 1987; Pinho and Errington, 2003; Turner et al., 2010)

The mechanism by which *S. aureus* selects the correct division site still remains unknown. As mentioned before in *S. aureus* FtsZ is the first know protein that localises to the division site and recruits other cell division components prior to cell division. Among them EzrA is a protein that localises quite early to the division site (Jorge et al., 2011). In *B. subtilis* it may act as an additional regulator of FtsZ assembly as it prevents formation of Z-rings at the cell poles (Levin et al., 1999). In *S. aureus* EzrA is an essential cell division component but its precise role is not well understood (Steele et al., 2011). EzrA was shown to interact with almost all identified cell division components in *S. aureus* and therefore it is proposed to act as a scaffold that recruits other cell division components and mediates between FtsZ and the peptidoglycan biosynthetic machinery (Steele et al., 2011). Indeed, in *S. aureus* penicillin binding proteins (PBPs) 1, 2 and 4 were shown to localise to the septum (Pinho and Errington, 2003; Pereira et al., 2007; Monteiro et al., 2015). Additionally, PBP2 localisation to the midcell was revealed to depend on the presence ot its substrate, lipid II (Pinho and Errington, 2005). This suggests that enzymes involved in lipid II synthesis are also recruited to the sites of peptidoglycan synthesis, that is midcell in *S. aureus* (Typas et al., 2012). In *E. coli* lipid II is translocated from the cytoplasm to the periplasm by a flippase, which is either FtsW or MurJ or both (Mohammadi et al., 2011; Sham et al., 2014). *S. aureus* encodes homologues of both proteins, of which both are considered to be essential (Chaudhuri et al., 2009; Huber et al., 2009). Additionally in *E. coli* FtsW was shown to localise to the septum and to recruit another cell division component, PBP3 (Wang et al., 1998; Fraipont et al., 2011; Mohammadi et al., 2014).

For a long time *S. aureus* was considered to synthesise peptidoglycan mainly at the division septum and therefore growth and expansion of the daughter cells would result from reshaping of the septal disc (Pinho and Errington, 2003; Turner et al., 2010). Lately it has been shown that during growth prior to division *S. aureus* slightly elongates which in consequence results in a prolate shape instead of coccal one (Monteiro et al., 2015). Moreover, reshaping of peptidoglycan in the septum has been proposed to be driven by a coordinated action of glucosaminidases, which modify long peptidoglycan chains and make the peptidoglycan more flexible and coupled with the turgor pressure, daughter cells resolve and grow (Zhou et al., 2015; Wheeler et al., 2015).

Bacterial growth and division involves production of a new cell wall (Scheffers and Pinho, 2005). Peptidoglycan is the major cell wall component (Scheffers and Pinho, 2005). As described in Chapter 1, peptidoglycan has three production phases. First one is associated with cytoplasmic construction of peptidoglycan building blocks. In the second one, the lipid linked intermediate is flipped across the membrane to be finally incorporated into the existing cell wall. The last stage is mediated by penicillin binding proteins (PBPs) which have transpeptidase and transglycosylase activities (Typas et al., 2012). Growth in rod-shaped bacteria involves two different peptidoglycan synthetic apparatuses (Daniel and Errington, 2003). In *S. aureus* this process is apparently directed by one machine (Pinho and Errington, 2005; Pinho et al., 2013). Peptidoglycan synthesis is guided by an agglomeration of cell division components that span from the cytoplasm, through the membrane, to the periplasm (Adams and Errington, 2009; Steele et al., 2011). The periplasmic components include peptidoglycan biosynthesis machinery elements, PBPs (Sauvage et al., 2008; Pinho et al., 2013). In *S. aureus* EzrA has been proposed to interact with both cytoplasmic and periplasmic components to coordinate cytokinesis with peptidoglycan synthesis (Steele et al., 2011). In order to understand the molecular interplay during *S. aureus* growth and division EzrA has to be set in the context of other cellular components.

4.1.1 Aims of this chapter

- Colocalisation of EzrA and FtsZ at super-resolution
- Colocalisation of EzrA and newly synthesised peptidoglycan at super-resolution

4.2 Results

4.2.1 Colocalisation of EzrA with FtsZ

In both *B. subtilis* and *S. aureus* EzrA colocalises with FtsZ at the division site and its localisation is FtsZ dependent (Levin et al., 1999; Steele et al., 2011). In *ftsZ* conditional mutants of *B. subtilis* and *S. aureus,* in the absence of inducer, EzrA midcell localisation is disrupted (Levin et al., 1999; Steele et al., 2011). In *B. subtilis* EzrA is considered to have two distinct roles. It acts as a negative regulator of FtsZ assembly at cell poles but it also has a positive role in maintaining FtsZ dynamics, that is assembly and disassembly of the FtsZ Z-ring at midcell (Levin et al., 1999; Haeusser et al., 2004). In *S. aureus* depletion of EzrA results in mislocalisation of FtsZ in only 7% cells in the population (Jorge et al., 2011). Additionally, EzrA was not observed to be present in other cell locations except for the septum, suggesting that in *S. aureus* EzrA is only responsible for modulating FtsZ dynamics but not inhibiting it polymerisation anywhere else but cell centre (Jorge et al., 2011). However STORM microscopy of EzrA localisation revealed that EzrA molecules are present in the peripheral cell membrane of *S. aureus* cells undergoing cell division (Chapter 3), indicating that EzrA may have a role in efficient selection of a division site in this coccus. Therefore colocalisation of EzrA with the first cell division protein, FtsZ was chosen for investigation by super-resolution microscopy.

4.2.1.1 Construction of an *S. aureus* FtsZ-SNAP strain

In order to study EzrA and FtsZ localisations in *S. aureus* an FtsZ fusion that is STORM-compatible and which emission spectra do not overlap with the eYFP fluorophore was constructed. The SNAP-tag system using SNAP-Cell TMR-Star (New England Biolabs), which is a cell permeable derivative of a red 6-carboxytetramethylrhodamine dye, was successfully used in STORM imaging of eukaryotic cell components (Klein et al., 2011). Therefore, an FtsZ-SNAP stained with SNAP-Cell TMR-Star combined with EzrA fused to eYFP were selected for two-colour labelling and microscopy imaging of *S. aureus* cell division components.

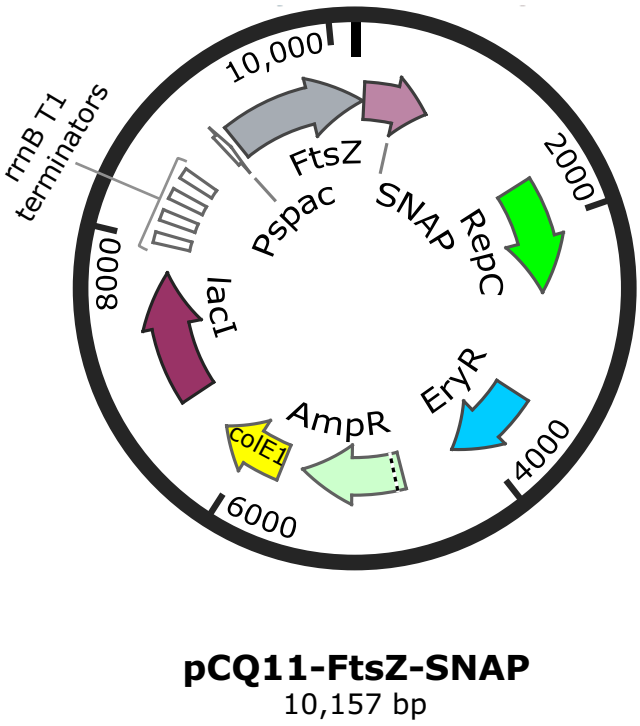

Figure 4.2. Map of the FtsZ-SNAP expression plasmid, pCQ11-FtsZ-SNAP

pCQ11-FtsZ-SNAP is an *E. coli-S. aureus* shuttle vector. pCQ11-FtsZ-SNAP comprises the high-copy-number ColE1 origin of replication, the staphylococcal origin of replication from pT181 (RepC), the *lacI* gene, four transcription terminators T1 from the *E. coli rrnB* gene, the ampicillin resistance (AmpR) and the erythromycin resistance (EryR) cassettes, and the *ftsZ-snap* fusion placed under the control of the Pspac promoter.

First an *S. aureus* strain expressing an ectopic *ftsZ-snap* fusion was constructed. Electrocompetent *S. aureus* RN4220 cells were transformed with a pCQ11-FtsZ-SNAP plasmid (Fabien Grein, University of Bonn, unpublished). pCQ11-FtsZ-SNAP is a shuttle vector that replicates both in *E. coli* and *S. aureus*. In pCQ11-FtsZ-SNAP the *ftsZ* and the *snap* genes were linked with a short three amino-acid linker (EFP) and the fusion expression was controlled by the Pspac promoter (Figure 4.2). The plasmid was subsequently transferred into *S. aureus* SH1000 by phage transduction using erythromycin (5 μg ml^{-1}) for selection, resulting in the SJF4605 (*S. aureus* SH1000 pCQ11-FtsZ-SNAP) strain.

4.2.1.2 Determination of the optimal IPTG and SNAP-Cell TMR-Star concentrations and labelling time

In SJF4605 (*S. aureus* SH1000 pCQ11-FtsZ-SNAP), *ftsZ-snap* was ectopically expressed from the pCQ11-FtsZ-SNAP plasmid. The *ftsZ-snap* fusion was placed under the IPTG inducible Pspac promoter and to visualise FtsZ-SNAP it had to be labelled with a probe that was recognised by the SNAP-tag.

First the optimal concentration of IPTG was determined. SJF4605 was grown to early-exponential phase in BHI in the presence of erythromycin (5 μg ml^{-1}) and different IPTG concentrations: 0, 10, 50, 100, 500 and 1000 μM. Cells were labelled with 3 μM SNAP-Cell TMR-Star for 30 min at 37^{o}C (the concentration and time were as recommended by the manufacturer) and fixed with paraformaldehyde. *S. aureus* SH1000 grown in the absence of IPTG stained with SNAP-Cell TMR-Star acted as a negative control of the labelling specificity. The cell morphology and FtsZ-SNAP TMR-Star localisation were examined by fluorescence microscopy. In SH1000 and SJF4605 grown in the absence of IPTG a weak fluorescent signal was observed across the whole cell (Figure 4.3Ai and ii). This signal was likely emitted by the dye that was incorporated into the cells but did not bind the SNAP-tag and was not efficiently washed out. In SJF4605 grown without IPTG FtsZ-SNAP localisation could not be visualised, suggesting that expression of the *ftsZ-snap* gene was repressed in the absence of inducer, and if the Pspac promoter was leaky, the level of FtsZ-SNAP production was not sufficient to be detected by the used labelling method. The characteristic FtsZ ring-like pattern was observed for cells grown in the presence of

IPTG (Figure 4.3Aiii-vi). SJF4605, in which FtsZ-SNAP production was induced with either 50 μM or 100 μM IPTG, formed cells of uniform sizes and the midcell localisation of FtsZ, similar to the one previously published, could be seen in the majority of the cells (Figure 4.3Aiii and iv) (Pinho and Errington, 2005; Liew et al., 2011). Sporadically a cell with two parallel or 'V' shaped septa could be found when induced with 100 μM IPTG (Figure 4.17H). When SJF4605 was grown in the presence of either 500 μM or 1000 μM IPTG cells with abnormal morphology could be often observed. These cells were enlarged and did not present the typical ring-like pattern but FtsZ-SNAP was either mislocalised or only an intensive fluorescent signal across the whole cell was observed (Figure 4.3Av and vi). In SJF4605, FtsZ-SNAP was produced in the presence of the native FtsZ copy, therefore any additional overproduction of FtsZ could be a source of growth defects. The observed effect of FtsZ overproduction on *S. aureus* morphology was consistent with the results published for *S. aureus* in which high levels of FtsZ-GFP led to the fusion protein delocalisation, a cell size increase and a cell lysis (Liew et al., 2011).

The stability of FtsZ-SNAP and how IPTG titration influences its levels were checked by western blot analysis. In order to reduce cross-reactivity of antibodies with *S. aureus* Protein A, which binds the Fc region of immunoglobulins, the pCQ11-FtsZ-SNAP plasmid was transduced into *S. aureus* SH1000 *spa::kan* in which the *spa* gene encoding Protein A was replaced with a kanamycin resistance cassette (Girbe Buist, unpublished). Whole cell lysates of the resulting strain SJF4653 (*S. aureus* SH1000 *spa::kan* pCQ11-FtsZ-SNAP) grown in the presence of erythromycin (5 μg ml^{-1}) and 0, 50, 100, 500 and 1000 μM IPTG were probed with rabbit anti-FtsZ and rabbit anti-SNAP antibodies at 1:1000 dilutions (Figure 4.3B and D). Bands of ~50 kDa, likely representing FtsZ, were detected for all cell lysates from SJF4653 by the anti-FtsZ antibodies (Figure 4.3B). The 50 kDa band was higher then predicted molecular weight of 41 kDa for FtsZ, however this shift was previously reported by Victoria Fairclough (2009). Additionally, bands of ~60 kDa, corresponding to the expected size of the FtsZ-SNAP fusion, were detected in lysates from SJF4653 grown in the presence of 50, 100, 500 and 1000 μM IPTG when probed with both the anti-FtsZ and the anti-SNAP antibodies (Figure 4.3B and D).

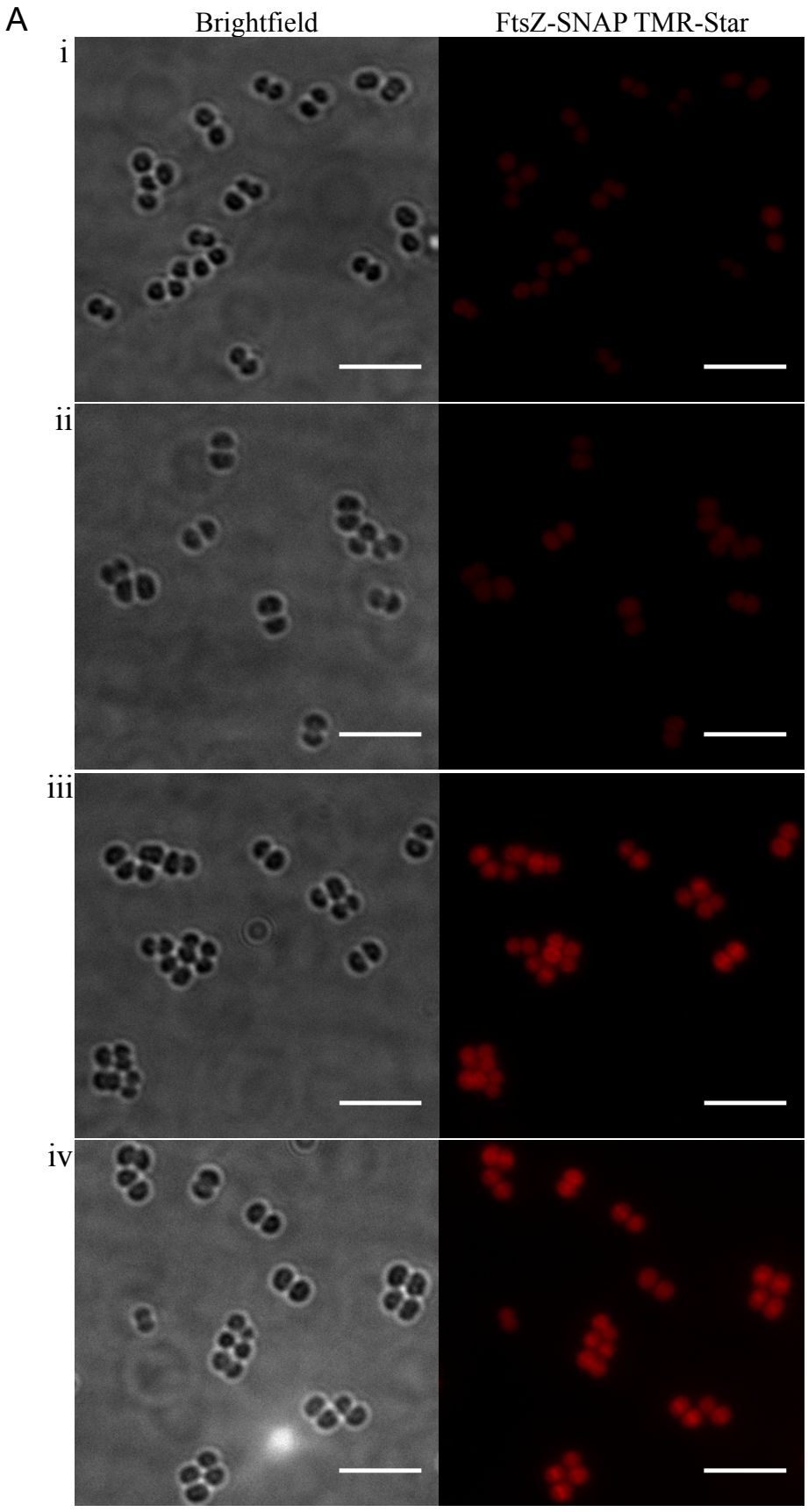
A
Brightfield
FtsZ-SNAP TMR-Star
i
ii
iii
iv

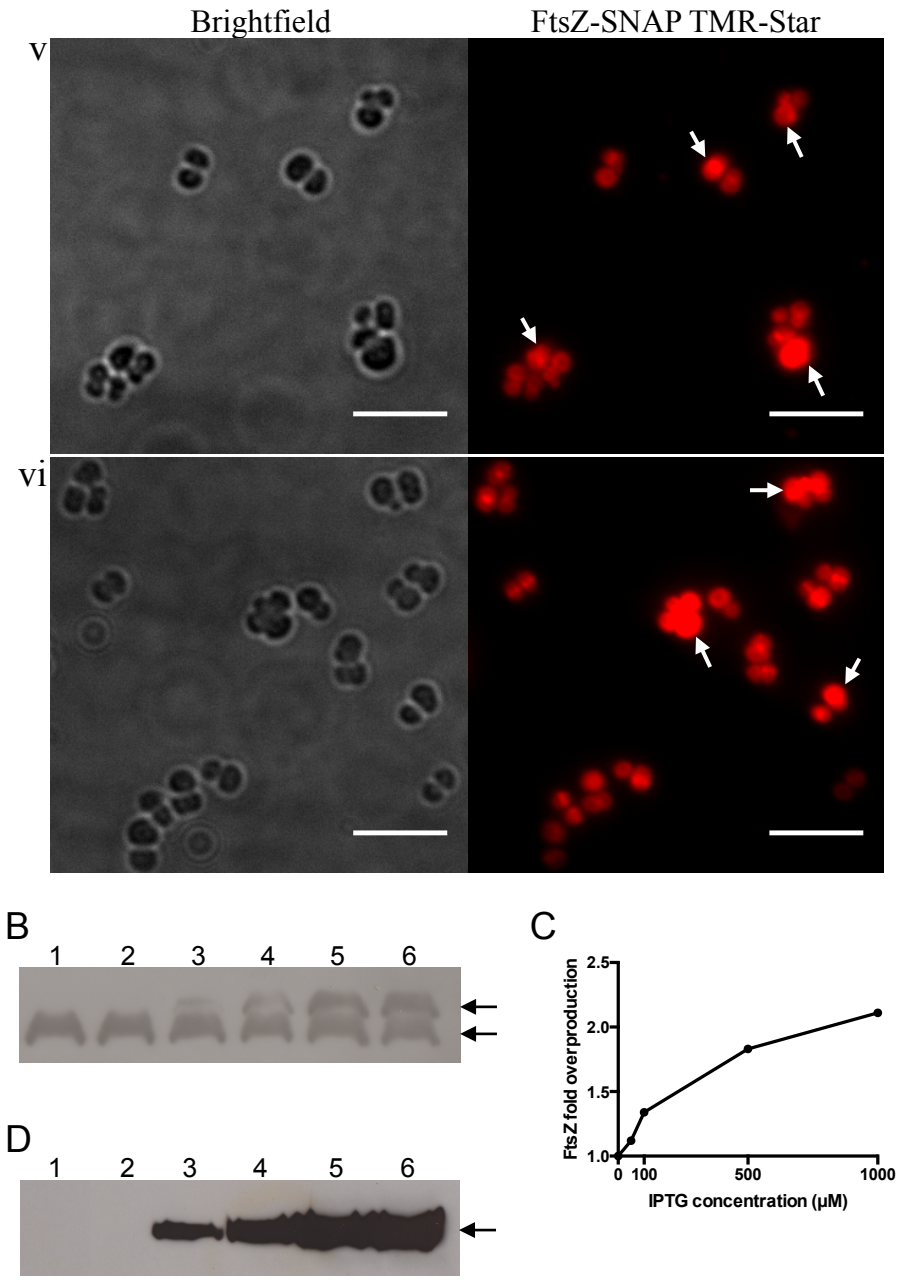

Figure 4.3. FtsZ-SNAP localisation and production in *S. aureus*

A. SH1000 (i) and SJF4605 (*S. aureus* SH1000 pCQ11-FtsZ-SNAP) grown in the presence of 0 μM (ii), 50 μM (iii), 100 μM (iv), 500 μM (v) and 1000 μM (vi) IPTG were labelled with 3 μM SNAP-Cell TMR-Star for 30 min at 37°C. The fluorescence images are maximum intensity projections of z-stack images acquired at 200 nm z-intervals. The same contrast was adjusted to the fluorescence images. White arrows indicate cells with abnormal morphology and FtsZ-SNAP TMR-Star localisation. Scale bars 5 μm.

B. Quantitative immunoblot showing levels of FtsZ and FtsZ–SNAP production in *S. aureus* SH1000 *spa::kan* (1) and SJF4653 (*S. aureus* SH1000 *spa::kan* pCQ11-FtsZ-SNAP) grown in 0 μM (2), 50 μM (3), 100 μM (4), 500 μM (5) and 1000 μM (6) IPTG. Whole cell lysates were probed with

anti-FtsZ antibodies at a dilution of 1:1000. Bands detected at ~50 kDa (FtsZ) and ~ 60 kDa (FtsZ-SNAP) are indicated with black arrows.

C. Fold overproduction of FtsZ represents the ratio of FtsZ total level (native FtsZ and FtsZ-SNAP) to the native FtsZ level in SJF4653 (SH1000 *spa::kan* pCQ11-FtsZ-SNAP) grown in varying IPTG concentrations. The FtsZ levels were calculated using the western blot in (B).

D. Whole cell lysates of SH1000 *spa::kan* (1) and SJF4653 (SH1000 *spa::kan* pCQ11-FtsZ-SNAP) grown in grown in 0 μM (2), 50 μM (3), 100 μM (4), 500 μM (5) and 1000 μM (6) IPTG were probed with anti-SNAP antibodies at a dilution of 1:1000. Bands detected at ~ 60 kDa that likely represent FtsZ-SNAP are indicated with a black arrow.

The results from western blot analysis were in agreement with microscopy data and showed that in the absence of IPTG FtsZ-SNAP either was not produced or its levels were too low to be detected by the anti-FtsZ and the anti-SNAP antibodies (Figure 4.3B and D). FtsZ-SNAP production was IPTG dependent and increased with the higher inducer concentrations. In SJF4653 grown in 50 and 100 μM IPTG the levels of FtsZ-SNAP were about 12% and 34% of the native FtsZ level (Figure 4.3C). At 500 and 1000 μM IPTG concentrations the total FtsZ levels increased about twofold, that is FtsZ-SNAP comprised 83% and 111% of the native FtsZ levels, respectively (Figure 4.3C). This two times higher levels of FtsZ (native FtsZ and FtsZ-SNAP) may explain severe morphological changes observed for SJF4605 cells grown in the presence of 500-1000 μM IPTG (Figure 4.3A). Based on above results the 50 μM IPTG concentration was used in the further work.

The optimal SNAP-Cell TMR-Star concentration and labelling time were determined. SJF4605 was grown in the presence of 50 μM IPTG and erythromycin (5 μg ml^{-1}). When they reached early-exponential phase, cells were incubated in varying SNAP-Cell TMR-Star concentrations: 0.1 μM, 0.2 μM, 0.5 μM, 1 μM, 2 uM and 3 μM for 30 min at 37^{o}C. Cell were fixed with paraformaldehyde and examined by fluorescence microscopy. The characteristic FtsZ pattern could be observed in the cells for which a 0.2 μM SNAP-Cell TMR-Star concentration and above were used for labelling (Figure 4.4Aii-vi). Cells labelled with 0.1 μM SNAP-Cell TMR-Star gave only a weak fluorescent signal and therefore the Z-ring like pattern was not evident and difficult to observe (Figure 4.4Ai). The 0.5 μM concentration of SNAP-Cell TMR-Star was found to be optimal for FtsZ-SNAP labelling (Figure 4.4Aiii). It gave a strong signal so that the FtsZ-SNAP localisation features could be easily detected. The higher dye concentrations did not improve the quality of the fluorescence images but often resulted in cells oversaturated in the fluorescent signal (Figure 4.4Av and vi). Poorly labelled cells could be observed for every tested SNAP-Cell TMR-Star concentration and its higher concentrations did reduce the proportion of cells with weak fluorescent signals.

Shorter than 30 min labelling times were tested. It was found that 5 min and 10 min incubation with 0.5 μM SNAP-Cell TMR-Star was sufficient for the SNAP-tag to reveal the characteristic ring-like pattern of FtsZ-SNAP (Figure 4.4B).

In SJF4605 labelled with SNAP-Cell TMR-Star the midcell localisation of FtsZ-SNAP was observed but also an additional cytoplasmic signal could be detected. A quantitative fluorescence analysis revealed that only about 30% of FtsZ molecules is incorporated into the Z-ring in *B. subtilis* and *E. coli* (Anderson et al., 2004). Thus in SJF4605 the cytoplasmic signal could come from free non-polymerised FtsZ-SNAP monomers. However to visualise FtsZ-SNAP, SJF4605 had to be stained with an organic fluorophore, which cells did not synthesise and it had to be delivered across the cell wall and membrane. SNAP-Cell TMR-Star labelling of SH1000 showed that some amount of the excess dye remained in cells giving a non-specific fluorescent signal (Figure 4.3Ai). Therefore an additional washing step of SJF4605 labelled with SNAP-Cell TMR-Star was added in order to try to remove the free substrate and to reduce the cytoplasmic signal. SJF4605 labelled for 5 min with 0.5 μM SNAP-Cell TMR-Star was grown in fresh BHI at 37^{o}C for 0, 10, 20 and 30 min before being fixed with paraformaldehyde and examined by fluorescence microscopy. No difference between cells stained with the SNAP dye and those stained and grown in BHI after labelling could be observed (Figure 4.4C). The fluorescent signal was comparable for all washing times, suggesting that the cytoplasmic signal came from the FtsZ-SNAP TMR-Star molecules which were not involved in formation of the Z-ring. This experiment also showed that FtsZ-SNAP was a stable fusion confirming the results obtained by western blot analysis (Figure 4.3B and D).

Deconvolution is a method in which algorithms are applied in order to increase the signal-to-noise ratio and thus to increase image resolution. When SJF4605 was labelled with SNAP-Cell TMR-Star at optimal conditions (50 μM IPTG to induce FtsZ-SNAP production and incubated with 0.5 μM SNAP-Cell TMR-Star at 37^{o}C for 5 min) both the Z-ring like pattern and cytoplasmic signal were observed (Figure 4.4Di, raw). When the images were deconvolved the FtsZ-SNAP TMR-Star septal localisation was well defined whereas the cytoplasmic signal was much weaker but not completely lost (Figure 4.4Di, deconvolved and ii). Deconvolution revealed or highlighted additional features of FtsZ-SNAP localisation that were not obvious and probably too subtle to be observed in the raw images. A very faint membrane associated signal associated with the cell periphery was observed in SJF4605 undergoing division (Figure 4.4Dii, deconvolved).

A

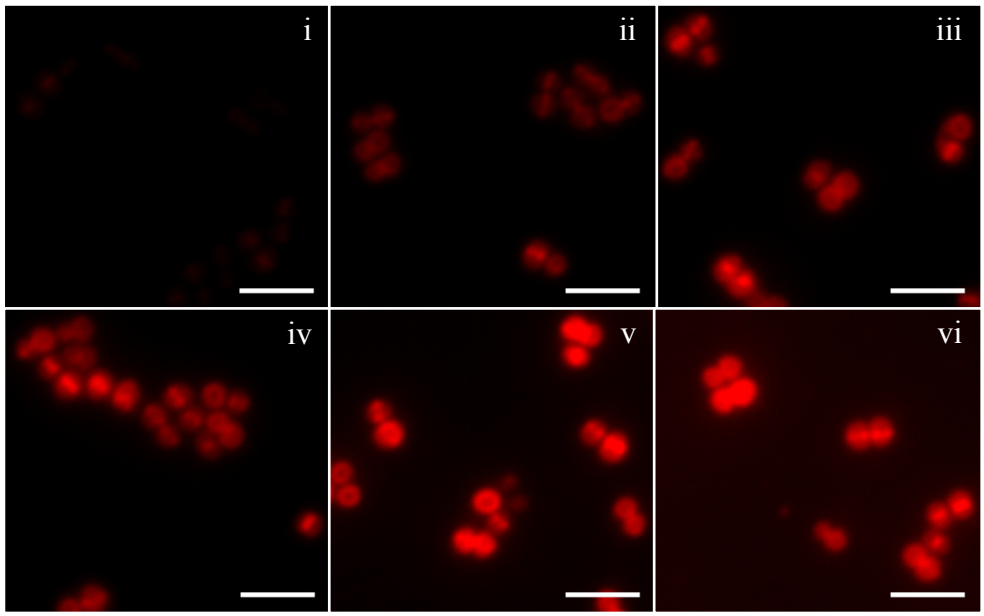

B

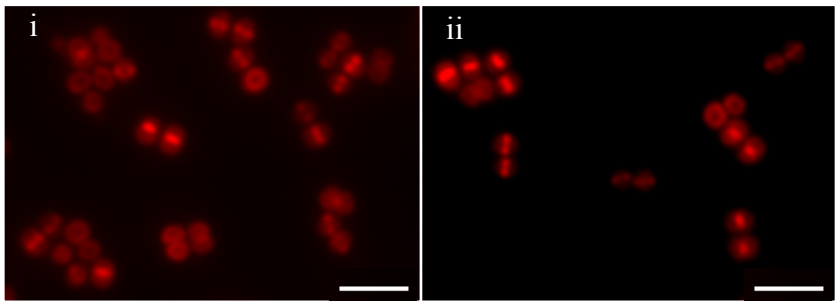

C

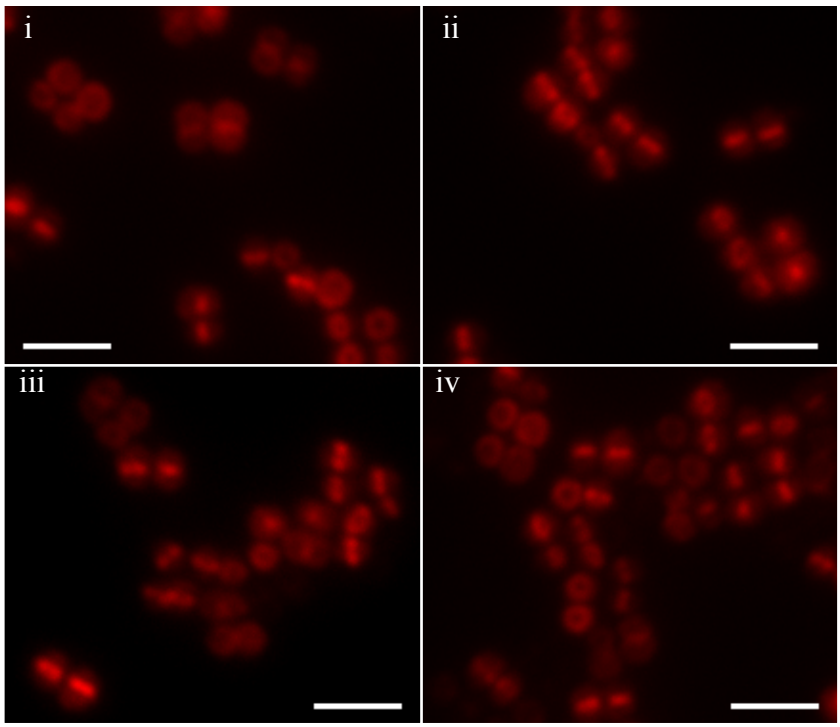

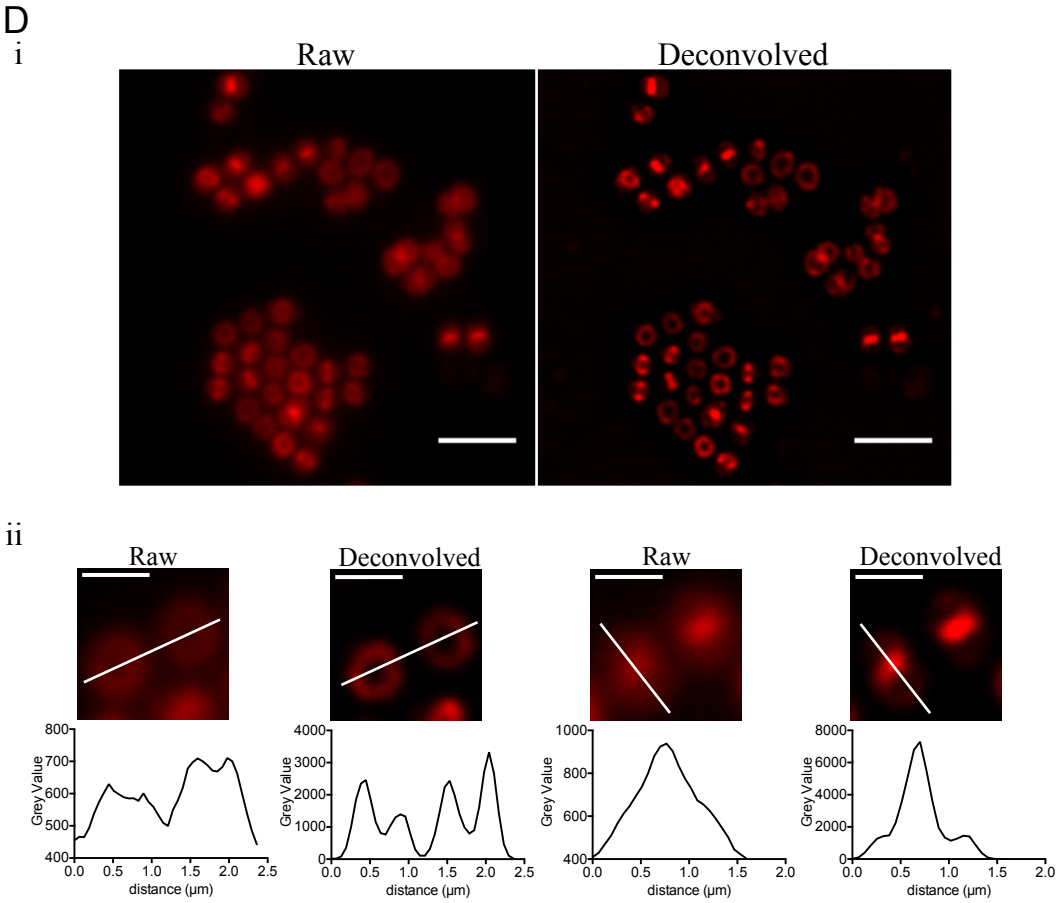

Figure 4.4. Determination of FtsZ-SNAP optimal labelling conditions

A. SJF4605 (*S. aureus* SH1000 pCQ11-FtsZ-SNAP) was incubated with 0.1 µM (i), 0.2 µM (ii), 0.5 µM (iii), 1 µM (iv), 2 µM (v) and 3 µM (vi) SNAP-Cell TMR-Star at 37°C for 30 min. The images are maximum intensity projections of z-stack images acquired at 200 nm z-intervals. The same contrast was adjusted to the images. Scale bars 3 µm.

B. FtsZ-SNAP in SJF4605 (*S. aureus* SH1000 pCQ11-FtsZ-SNAP) was labelled with 0.5 µM SNAP-Cell TMR-Star for 5 min (i) and 10 min (ii) min at 37°C. The images are maximum intensity projections of z-stack images acquired at 200 nm z-intervals. The same contrast was adjusted to the images. Scale bars 3 µm.

C. In SJF4605 (*S. aureus* SH1000 pCQ11-FtsZ-SNAP) FtsZ-SNAP was labelled with 0.5 µM SNAP-Cell TMR-Star for 5 min at 37°C and then incubated for 0 min (i), 10 min (ii), 20 min (iii) and 30 min (iv) in BHI at 37°C to wash out the excess dye. The images are maximum intensity projections of z-stack images acquired at 200 nm z-intervals. The same contrast was adjusted to the images. Scale bars 3 µm.

D. (i) Comparison of raw and deconvolved images of SJF4605 (*S. aureus* SH1000 pCQ11-FtsZ-SNAP) labelled with SNAP-Cell TMR-Star at optimal conditions (0.5 µM dye for 5 min at 37°C, no extra washing step in BHI). The images are maximum intensity projections of z-stack images acquired at 200 nm z-intervals. The same contrast was adjusted to the images. Scale bars 3 µm.

(ii) Individual cells from (i) are highlighted to reveal the FtsZ-SNAP TMR-Star pattern. The profiles present the distribution of the fluorescence signal (Grey Value) measured along the yellow lines across the individual cells in the images above. Scale bars 1 µm

4.2.1.3 FtsZ-SNAP localisation by STORM

In order to look into FtsZ-SNAP localisation at super-resolution SJF4605 (*S. aureus* SH1000 pCQ11-FtsZ-SNAP) was grown to early-exponential phase, labelled with SNAP-Cell TMR-Star as optimised in section 4.2.1.2 and fixed with paraformaldehyde. Unfortunately several attempts to image FtsZ-SNAP TMR-Star were not successful. Different mounting buffers such as GLOX (0.5 mg ml^{-1} glucose oxidase, 40 μg ml^{-1} catalase, 10% (w/v) glucose), MEA (100 mM β-mercaptoethylamine), GLOX MEA or GSH (160 mM glutathione) were tested. Although the GSH buffer helped to improve imaging conditions, that is acquire more isolated blinks than in the other buffering conditions, the reconstructed data for all screened buffers showed FtsZ-SNAP TMR-Star distributed across the whole cell (data not shown). This was not in agreement with data obtained with diffraction limited microscopy, which presented FtsZ-SNAP TMR-Star to be mainly septaly localised.

The STORM imaging process consists of many cycles, in each cycle (acquisition frame) a small subset of fluorescent molecules is activated, detected and localised. The positions of identified fluorophores are then used to reconstruct a high-resolution image. The other observed problem associated with FtsZ-SNAP TMR-Star STORM imaging was that the localisation pattern of the fusion protein seemed not to be stable over the time of the STORM data acquisition, even though fixed cells were used. This is demonstrated in Figure 4.5. An average of first 200 raw frames collected during STORM imaging showed that at the beginning of the imaging FtsZ-SNAP TMR-Star had a clear midcell localisation (Figure 4.5A). An average of the last 10000 raw frames however did not give the similar localisation pattern any more and the fluorescent signal became dispersed (Figure 4.5A). During STORM data acquisition the fluorescent signal subsequently drops due to photodamage caused by excitation lasers, however the localisation pattern of fluorescently labelled structures is expected to stay unchanged in fixed samples. The dispersed fluorescent signal could be explained by suboptimal imaging conditions (laser power, buffering conditions) and thus the fluorescent signal emitted by TMR-Star could be masked by some auto-fluorescent signal. The other explanation could be instability of the fluorophore, which might have detached from the protein during the imaging process and was freely floating in the cell.

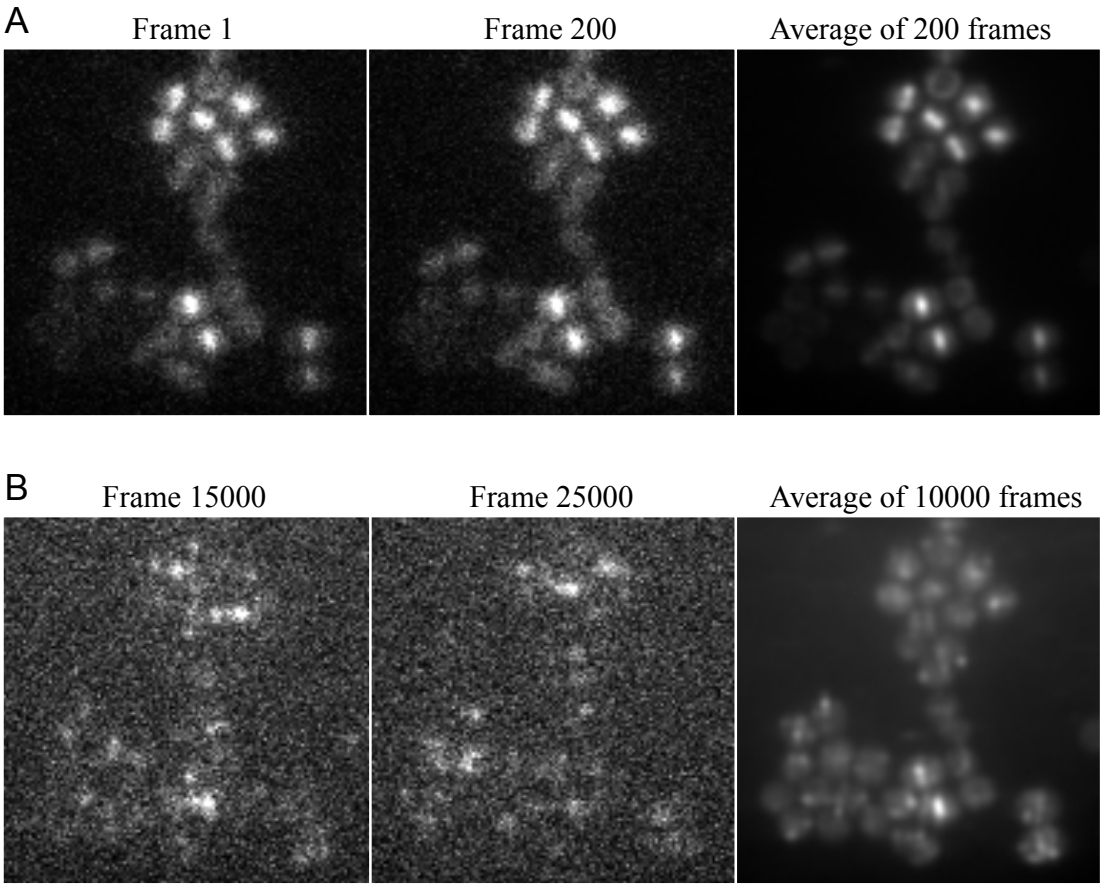

Figure 4.5. FtsZ-SNAP TMR-Star fluorescent signal and pattern formed during over the time of STORM data acquisition

A. FtsZ-SNAP TMR-Star forms the characteristic pattern which is visible in frames 1 and 200. An average of the first 200 out of 25,000 collected frames shows the same localisation features.

B. Fluorescent signal emitted by FtsZ-SNAP TMR-Star in frames 15,000 and 25,000. An average of the last 10,000 out of 25,000 collected frames does not show the same localisation pattern as the average of first 200 frames shown in (A).

The SNAP-Cell TMR-Star substrate did not allow one to obtain super-resolution information on FtsZ-SNAP localisation. SNAP-Cell 505-Star, which is a 6-carboxyrhodamine 110 derivative was reported as a STORM-compatible dye suitable for protein labelling inside cells (Klein et al., 2011). However there is an overlap between eYFP and 505-Star excitation and emission spectra and these fluorophores are not a good pair for two-colour microscopy. A new near-infrared silicone-rhodamine (6-carboxy-tetramethylsiliconrhodamine, SiR) substrate was developed and showed to pass trough the cell membrane and to have blinking properties (Lukinavičius et al., 2013). Therefore a SiR benzylguanine derivative (SNAP-Cell 647-SiR) was tested.

SJF4605 (*S. aureus* SH1000 pCQ11-FtsZ-SNAP) was grown in 50 μM IPTG and erythromycin (5 $\mu g\, ml^{-1}$) to early-exponential phase, labelled with 1 μM SNAP-Cell 647-SiR for 5 min at 37^{o}C and fixed with paraformaldehyde. Cells were first examined by conventional fluorescence microscopy. Similar to FtsZ-SNAP labelled with SNAP-Cell TMR-Star, FtsZ-SNAP 647-SiR showed the Z-ring like pattern in SJF4605 (Figure 4.6A, raw). When the fluorescence microscopy images were deconvolved the features, such as FtsZ-SNAP 647-SiR midcell localisation were well defined, peripheral membrane signals highlighted and the cytoplasmic signals reduced (Figure 4.6A, deconvolved). SJF4605 labelled with SNAP-Cell 647-SiR was also imaged by N-STORM. Despite several attempts, 647-SiR did not allow the localisation of FtsZ-SNAP at super-resolution. Instead of septal localisation the reconstruction data presented FtsZ-SNAP 647-SiR distributed not evenly but in a form of fluorescent signals dispersed inside the cells (Figure 4.6B), which was not in agreement with the fluorescent pattern obtained by conventional fluorescence microscopy (Figure 4.6A).

Later reductive caging (Vaughan et al., 2012) was tested and shown to be a promising method in imaging proteins labelled with TMR-Star (Chapter 3, section 3.2.5). However because of time constraints this method was not tested and optimised for FtsZ-SNAP.

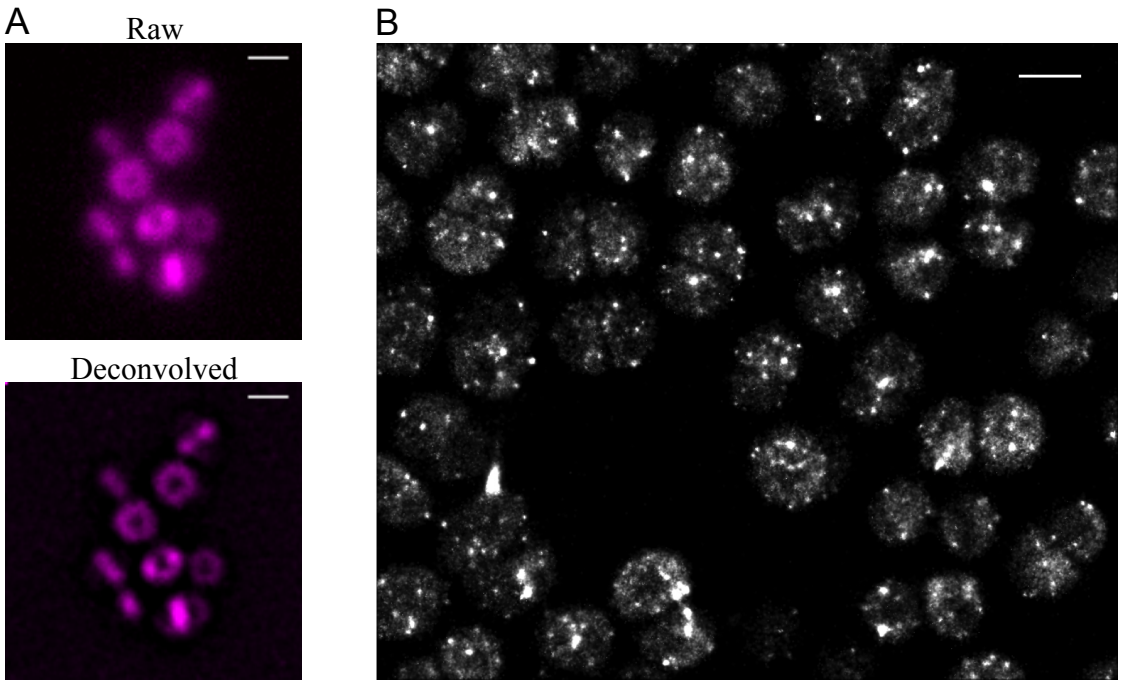

Figure 4.6. FtsZ-SNAP 647-SiR visualisation by conventional fluorescence microscopy and 2D N-STORM

A. In SJF4605 (*S. aureus* SH1000 pCQ11-FtsZ-SNAP) labelled with 1 μM SNAP-Cell 647-SiR FtsZ-SNAP is localised to the midcell. The raw and deconvolved images are shown. The images are maximum intensity projections of z-stack images acquired at 200 nm z-intervals. Scale bars 1 μm.

B. SJF4605 (*S. aureus* SH1000 pCQ11-FtsZ-SNAP) labelled with 1 μM SNAP-Cell 647-SiR was examined by 2D N-STORM. The reconstruction data show FtsZ-SNAP 647-SiR forming clumps distributed across the cell. The scale bar 1 μm.

4.2.1.4 Colocalisation of EzrA and FtsZ

In order to colocalise EzrA and FtsZ an *S. aureus* strain producing EzrA-eYFP and FtsZ-SNAP was constructed. SJF4388 (*S. aureus* SH1000 *geh::ezrA-eyfp ΔezrA::tet*) was transduced with a Φ11 lysate from SJF4605 (*S. aureus* SH1000 pCQ11-FtsZ-SNAP) with selection using kanamycin (50 μg ml^{-1}) and erythromycin (5 μg ml^{-1}). The resulting strain SJF4652 (*S. aureus* SH1000 *geh::ezrA-eyfp ΔezrA::tet* pCQ11-FtsZ-SNAP) coproduced EzrA-eYFP an FtsZ-SNAP.

Localisation of EzrA-eYFP and FtsZ-SNAP was visualised by conventional fluorescence microscopy. SJF4652 was grown in BHI in the presence of erythromycin (5 μg ml^{-1}) and 50 μM IPTG to induce FtsZ-SNAP production. When it reached early-exponential phase cells were labelled with 0.5 μM SNAP-Cell TMR-Star for 5 min at 37^{o}C, fixed with paraformaldehyde and examined with by deconvolution microscopy. As expected EzrA-eYFP and FtsZ-SNAP TMR-Star were found to colocalises during cell division in *S. aureus* (Figure 4.7A). A closer inspection of their localisation patterns showed that EzrA-eYFP accompanied FtsZ-SNAP at every step of division (Figure 4.7B). When FtsZ-SNAP TMR-Star was at a division site and was observed as two dots, EzrA-eYFP was also was seen as two spots (Figure 4.7Bi-v). At this stage of the cell cycle some off-septal signal could be observed for both FtsZ-SNAP TMR-Star and EzrA-eYFP (Figure 4.7Bi-v). This peripheral signal was well defined in deconvolved images (Figure 4.7A) and was in agreement with STORM data on EzrA-eYFP localisation (Figure 3.17B). In cells finishing division FtsZ-SNAP TMR-Star and EzrA-eYFP displayed strong signals both at the current plane of division and associated with peripheral membrane at a presumptive new orthogonal plane of division (Figure 4.7Bvi-viii). Even though these two components appeared at the same locations in *S. aureus* during the cell division cycle (Figure 4.7Bi-x), examination of distribution of fluorescence intensities of EzrA-eYFP and FtsZ-SNAP TMR-Star revealed that their intensity profiles overlapped but not overlaid. There was a subtle shift between EzrA and FtsZ intensity profiles (Figure 4.7B). The peaks of the FtsZ-SNAP TMR-Star maximal fluorescence intensity were distributed in between maxima of EzrA-eYFP fluorescence intensities (Figure 4.7B). The difference between the distance of EzrA-eYFP peaks (*a*) and FtsZ-SNAP TMR-Star peaks (*b*) varied from 64 nm to 200 nm, ~130 nm on average (Figure 4.7C).

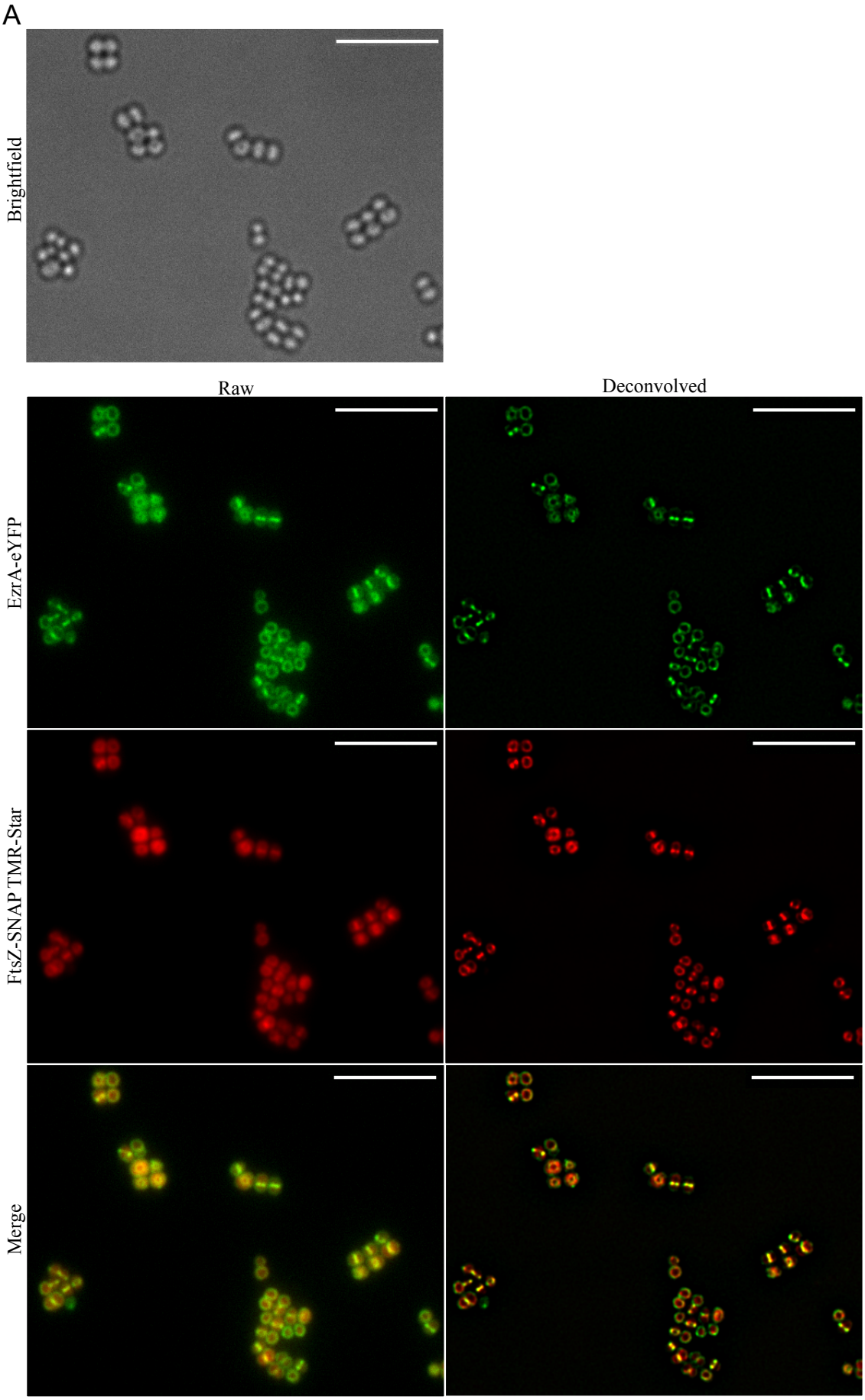
A
Brightfield
Raw
Deconvolved
EzrA-eYFP
FtsZ-SNAP TMR-Star
Merge

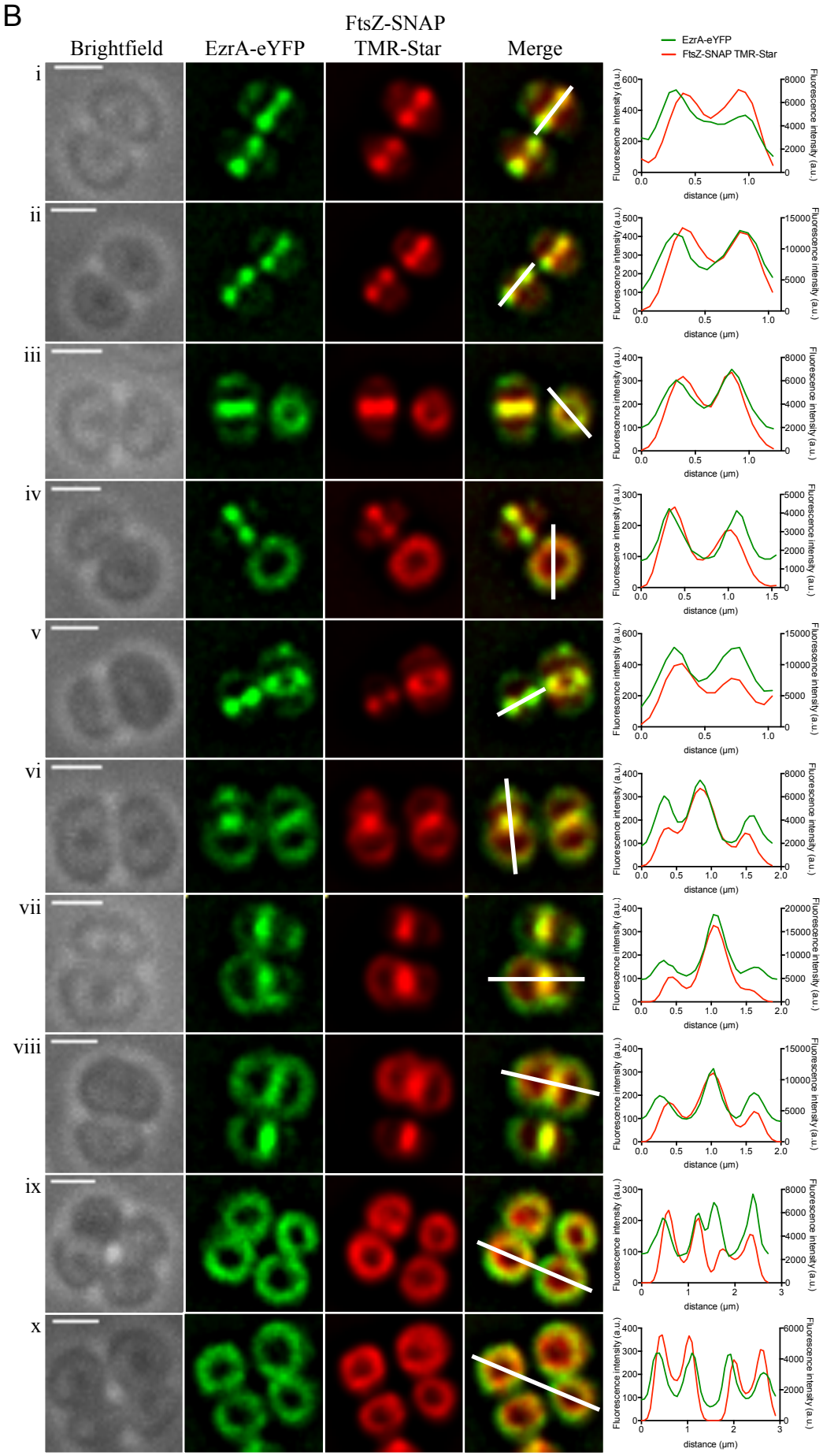
B
Brightfield
EzrA-eYFP
FtsZ-SNAP TMR-Star
Merge
EzrA-eYFP
FtsZ-SNAP TMR-Star
i
ii
iii
iv
v
vi
vii
viii
ix
x
Fluorescence intensity (a.u.)
distance (µm)

C

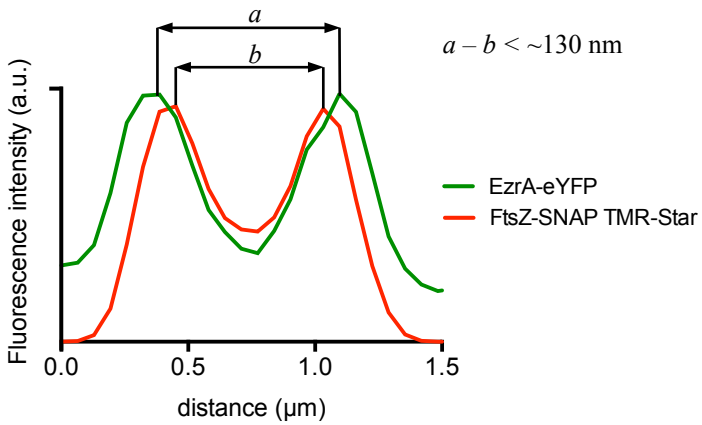

Figure 4.7. Colocalisation of EzrA-eYFP and FtsZ-SNAP TMR-Star

A. SJF4652 (*S. aureus* SH1000 *geh::ezrA-eyfp ΔezrA::tet* pCQ11-FtsZ-SNAP) grown in the presence of 50 µM IPTG and erythromycin (5 µg ml^{-1}) was labelled with 0.5 µM SNAP-Cell TMR-Star when it reached early-exponential phase. Cells were examined by fluorescence microscopy. In SJF4652 EzrA-eYFP and FtsZ-SNAP TMR-Star are localised to the site of division. The raw and deconvolved images are shown. The fluorescence images are maximum intensity projections of z-stack images acquired at 200 nm z-intervals. Scale bars 5 µm.

B. Individual SJF4652 (*S. aureus* SH1000 *geh::ezrA-eyfp ΔezrA::tet* pCQ11-FtsZ-SNAP) cells selected to highlight EzrA-eYFP and FtsZ-SNAP TMR-Star localisations. The diagrams show fluorescence intensity profiles of EzrA-eYFP (green) and FtsZ-SNAP TMR-Star (red) in arbitrary units (a.u.) measured along the white lines across the individual cells in the merged images. In each diagram the right y-axis presents EzrA-eYFP fluorescence intensity, while the left one FtsZ-SNAP TMR-Star intensity. The images of individual cells at different stages of the cell cycle are maximum intensity projections of deconvolved z-stack images acquired at 200 nm z-intervals (i-x). Scale bars 1 µm.

C. A representative image fluorescence intensity profile of EzrA-eYFP and FtsZ-SNAP TMR-Star in SJF4652 (*S. aureus* SH1000 *geh::ezrA-eyfp ΔezrA::tet* pCQ11-FtsZ-SNAP). The distance between EzrA-eYFP peaks is indicated in *a*, while *b* presents the distance between FtsZ-SNAP TMR-Star peaks. The difference between *a* and *b* is on average lower than ~130 nm (n=13).

This short shift between EzrA-eYFP and FtsZ-SNAP TMR-Star intensity profiles suggested that FtsZ may go slightly ahead of EzrA. In *S. aureus* EzrA was shown to interact with FtsZ in the bacterial two-hybrid analysis (Steele et al., 2011) therefore these two proteins are expected to be in close proximity. EzrA-eYFP and FtsZ-SNAP TMR-Star appeared to overlap and the distance separating their features was estimated to be shorter than the light diffraction limit (Figure 4.7). Due to the limits of conventional fluorescence microscopy a degree of FtsZ and EzrA separation could not be determined. STORM is the only fluorescence microscopy technique that reaches a resolution below 100 nm, which is also below the distance of EzrA and FtsZ calculated from the fluorescence image profiles (Figure 4.7C). However FtsZ-SNAP labelled with either SNAP-Cell TMR-Star or SNAP-Cell 647-SiR was not successfully visualised in STORM and thus two-colour STORM imaging of EzrA-eYFP and FtsZ-SNAP in *S. aureus* was not possible to perform.

4.2.2 Colocalisation of EzrA and newly synthesised peptidoglycan

In *S. aureus* EzrA interacts both with cytoplasmic and membrane components of the divisome. EzrA depletion results in hindrance of peptidoglycan synthesis. This indicates that in *S. aureus* EzrA may act as an interface between cytoplasmic division components and peptidoglycan synthesis machinery (Steele et al., 2011).

As a result of the EzrA role in peptidoglycan synthesis in *S. aureus* its localisation compared to the product of divisome activity, nascent peptidoglycan was studied. D-alanine (D-Ala) is a unique amino-acid to bacteria and is incorporated into positions 4^{th} and 5^{th} of the stem peptide during peptidoglycan biosynthesis (Figure 1.9) (Typas et al., 2012; Pinho et al., 2013). Recently fluorescent D-Ala derivatives have been developed and shown to be useful probes for marking sites of active cell wall synthesis in different bacterial species (Kuru et al., 2012).

4.2.2.1 EzrA-eYFP and newly synthesised peptidoglycan localisation using conventional fluorescence microscopy

In order to study localisation of EzrA-eYFP in the context of the product of the division machinery, sites of newly incorporated peptidoglycan in SJF4388 (*S. aureus* SH1000 *geh::ezrA-eyfp ΔezrA::tet*) were labelled with HADA. HADA is a blue fluorescent derivative of D-Ala covalently attached to 7-hydroxycoumarin 3-carboxylic acid. SJF4388 grown to early-exponential phase was labelled with 500 μM HADA for 5 min at 37^{o}C. Fixed cells were visualised using deconvolution microscopy.

Similar to previous studies on vancomycin labelled *S. aureus* (Pinho and Errington, 2005; Turner et al., 2010) peptidoglycan synthesis, marked by HADA incorporation, was observed mainly at the cell septum (Figure 4.8A). EzrA-eYFP and HADA were observed to localise to the same cell locations where they formed similar patterns (Figure 4.8A). Closer inspection of individual cells revealed that EzrA-eYFP is accompanied by HADA both at early stages when cells initiate division septa (Figure 4.8Bi-v), during septum constriction (Figure 4.8Bvi-x) and when cells split into two daughter cells (Figure 4.8xi-xii). EzrA-eYFP and HADA could be observed not only at the sides where the septum was actively produced but also in the other cell parts associated with cell periphery (Figure 4.8Bi-x). Peptidoglycan incorporation in other parts than division septa was in agreement with the recent publication on changes in the cell shape during the division cycle (Monteiro et al., 2015) and studies performed in our laboratory on peptidoglycan dynamics in *S. aureus* (Victoria Lund, unpublished). The off-septal EzrA-eYFP was found in cells undergoing division by STORM imaging (Figure 3.17), indicating that the subtle peripheral signal was not an artefact incorporated into images after the deconvolution step (Figure 4.8B). The colocalisation of EzrA-eYFP and HADA at other than septal sites was verified by linear profiles of fluorescence intensities measured across selected cells (Figure 4.8Ci-ii). Comparison of distribution of EzrA-eYFP and HADA maximal fluorescence peaks showed that in the septum, EzrA went slightly ahead of newly synthesised peptidoglycan (Figure 4.8C). This small variation in their positions was not surprising as EzrA is a membrane associated protein and the eYFP tag in the EzrA fluorescent fusion was located in the cytoplasm, whereas peptidoglycan is a part of the cell wall, the outermost layer of the cell envelope in *S. aureus*. Additionally the cell membrane is a source of a physical

boundary that incorporates a distance between components located inside and outside of the cell membrane. Furthermore, fluorescence intensity profiles showed that peripheral signals from EzrA-eYFP and HADA overlapped (Figure 4.8Ci-ii). There was no obvious shift between EzrA-eYFP and HADA peaks as in plot profiles measured for these components localised in the septa (Figure 4.8C). The peripheral signal displayed by EzrA-eYFP and HADA may correspond to EzrA and thus the peptidoglycan biosynthesis machinery localising to the new division site before the current cell cycle is finished.

In order to check if the off-septal EzrA-eYFP signal came from either the new or old plane of division SJF4388 (*S. aureus* SH1000 *geh::ezrA-eyfp ΔezrA::tet*) was pulse-chase labelled with two fluorescent D-alanines, HADA and TADA. TADA is a red analogue of HADA, a fluorescent tetramethylrhodamine derivative of D-Ala.

SJF4388 (*S. aureus* SH1000 *geh::ezrA-eyfp ΔezrA::tet*) was grown to early-exponential phase. Cells were incubated with 500 μM TADA for approximately one generation time (30 min) at 37^{o}C to label the cell contour. TADA was removed by centrifugation and cells were grown with 500 μM HADA for 5 min at 37^{o}C to mark sites of nascent peptidoglycan incorporation. Fixed cells were imaged by deconvolution microscopy. HADA mainly labelled septa where the peptidoglycan synthesis mostly occurs during the cell growth of *S. aureus*, TADA was present both all over the cell wall and in division septa (Figure 4.9Ai). As expected EzrA-eYFP localised to the same sites where new peptidoglycan was produced (4.9Ai). A strong signal from TADA could be observed between two separating daughter cells (Figure 4.9Aii-viii). This signal indicated sites where TADA was incorporated during the 30 min incubation time, before switching to HADA, and it was distributed on the plane perpendicular to the most current division site (indicated by EzrA-eYFP), thus likely marking the last plane of cell division. In agreement with the previous observations EzrA-eYFP was located at midcell but also gave a fine peripheral signal accompanied by both TADA and HADA (Figure 4.9Aiv-vii). This off-septal EzrA-eYFP fluorescence was on a plane perpendicular to the previous and current division planes, indicating that EzrA may go to the next division plane before the ongoing formation of septal wall and division are completed.

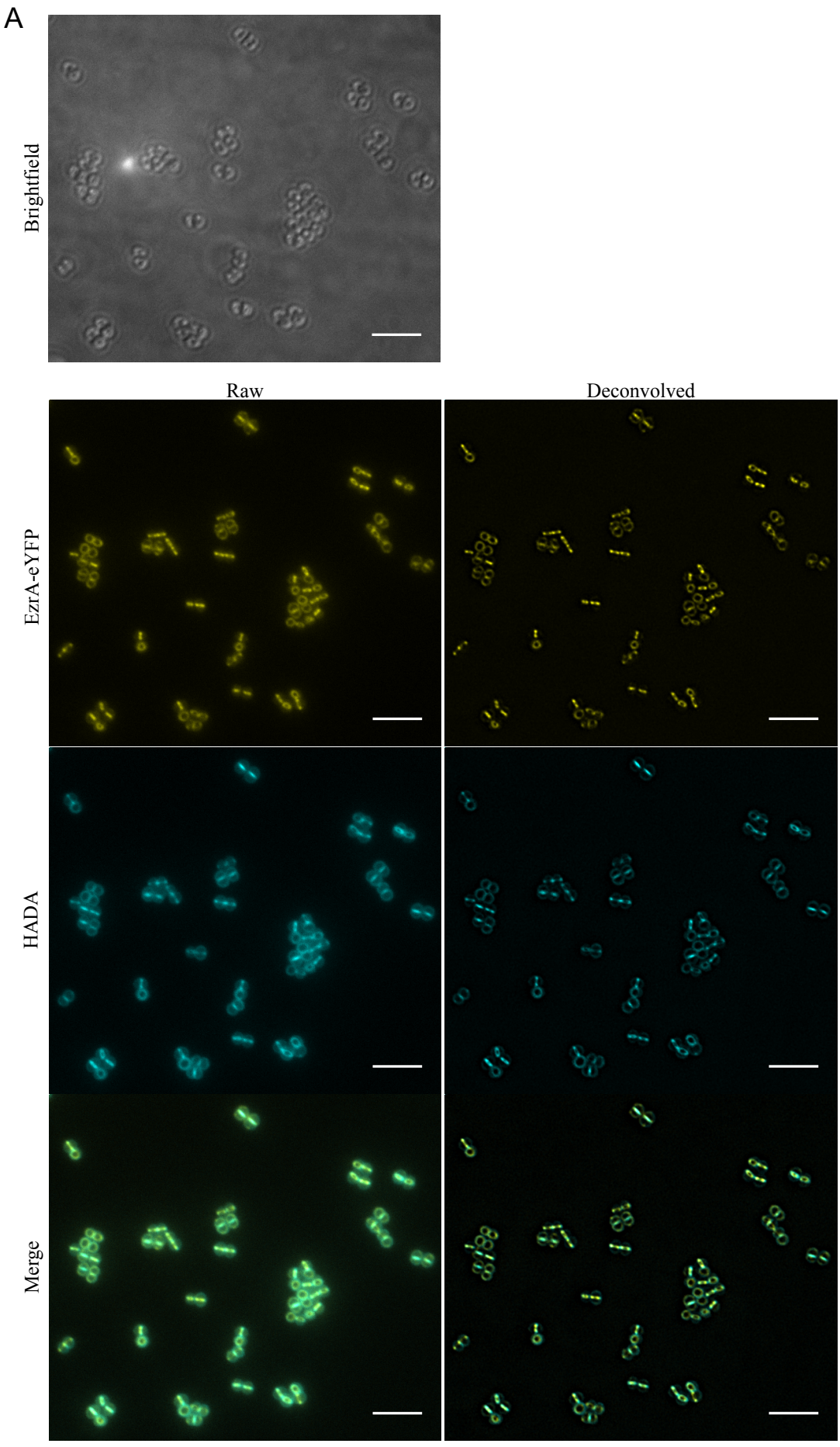
A
Brightfield
Raw
Deconvolved
EzrA-eYFP
HADA
Merge

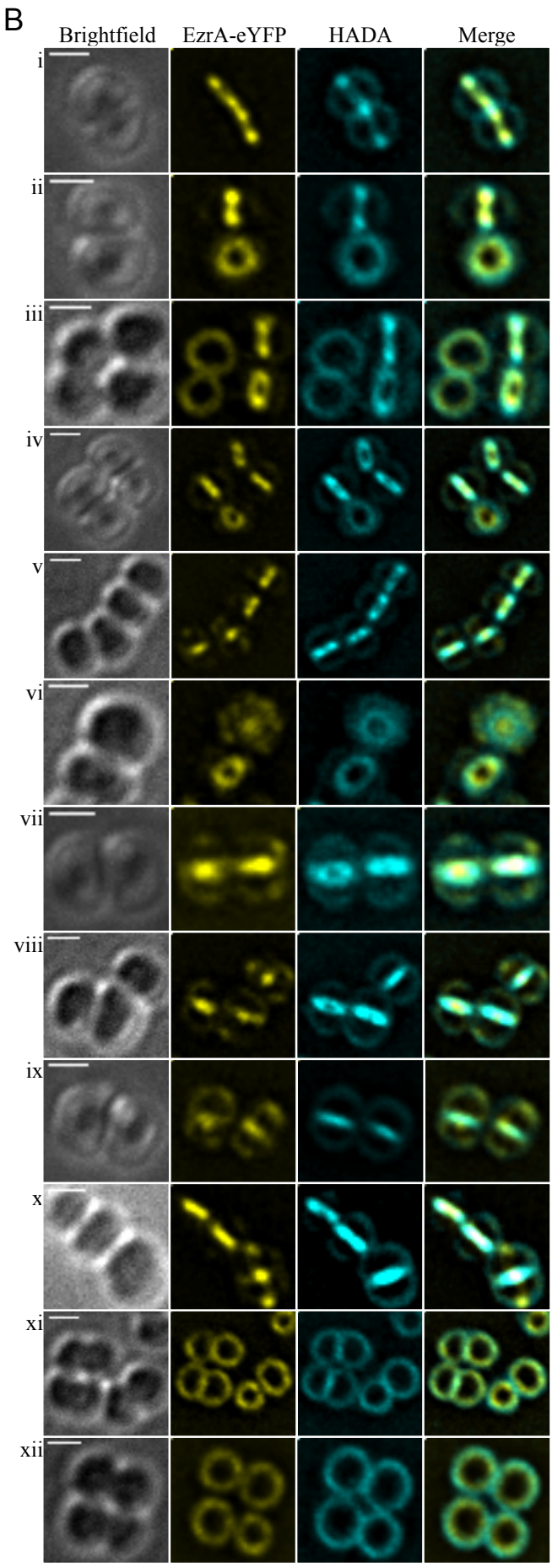
B
Brightfield
EzrA-eYFP
HADA
Merge
i
ii
iii
iv
v
vi
vii
viii
ix
x
xi
xii

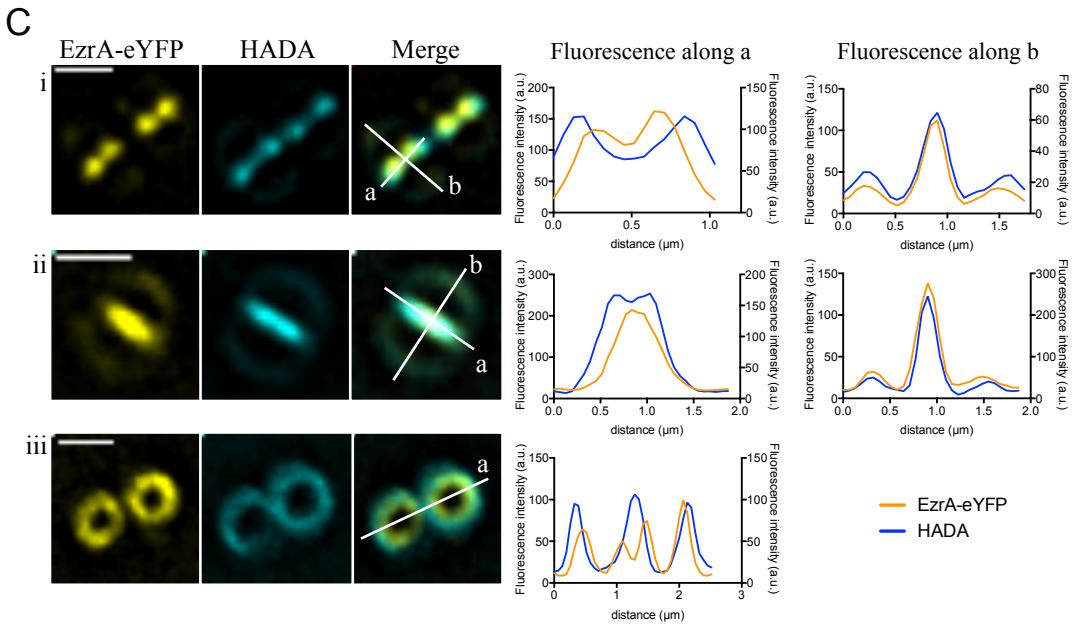

Figure 4.8. Colocalisation of EzrA-eYFP and newly synthesised peptidoglycan (5 min incubation time with HADA)

A. SJF4388 (*S. aureus* SH1000 *geh::ezrA-eyfp ΔezrA::tet*) grown to early-exponential phase was labelled with 500 μM HADA for 5 min at 37°C. Fixed cells were examined by fluorescence microscopy. HADA gives fluorescent signal mainly associated with division septa and together with EzrA-eYFP are localised to the same cell sites. The raw and deconvolved images are shown. The fluorescence images are maximum intensity projections of z-stack images acquired at 200 nm z-intervals. Scale bars 5 μm.

B. Individual SJF4388 (*S. aureus* SH1000 *geh::ezrA-eyfp ΔezrA::tet*) cells labelled with HADA selected to highlight localisation of EzrA-eYFP and sites of new peptidoglycan incorporation. The fluorescence images of cells at different stages of the cell cycle are maximum intensity projections of deconvolved z-stack images acquired at 200 nm z-intervals (i-xii). Scale bars 1 μm.

C. The linear profiles represent fluorescence intensities of EzrA-eYFP (yellow) and HADA (blue) in arbitrary units (a.u.) measured along the white lines across the individual cells in the merged images In each diagram the right y-axis presents EzrA-eYFP fluorescence intensities, while the left one HADA intensities. The images of individual SJF4388 (*S. aureus* SH1000 *geh::ezrA-eyfp ΔezrA::tet*) cells labelled with HADA, as described in (A) are maximum intensity projections of deconvolved z-stack images acquired at 200 nm z-intervals (i-iii). Scale bars 1 μm.

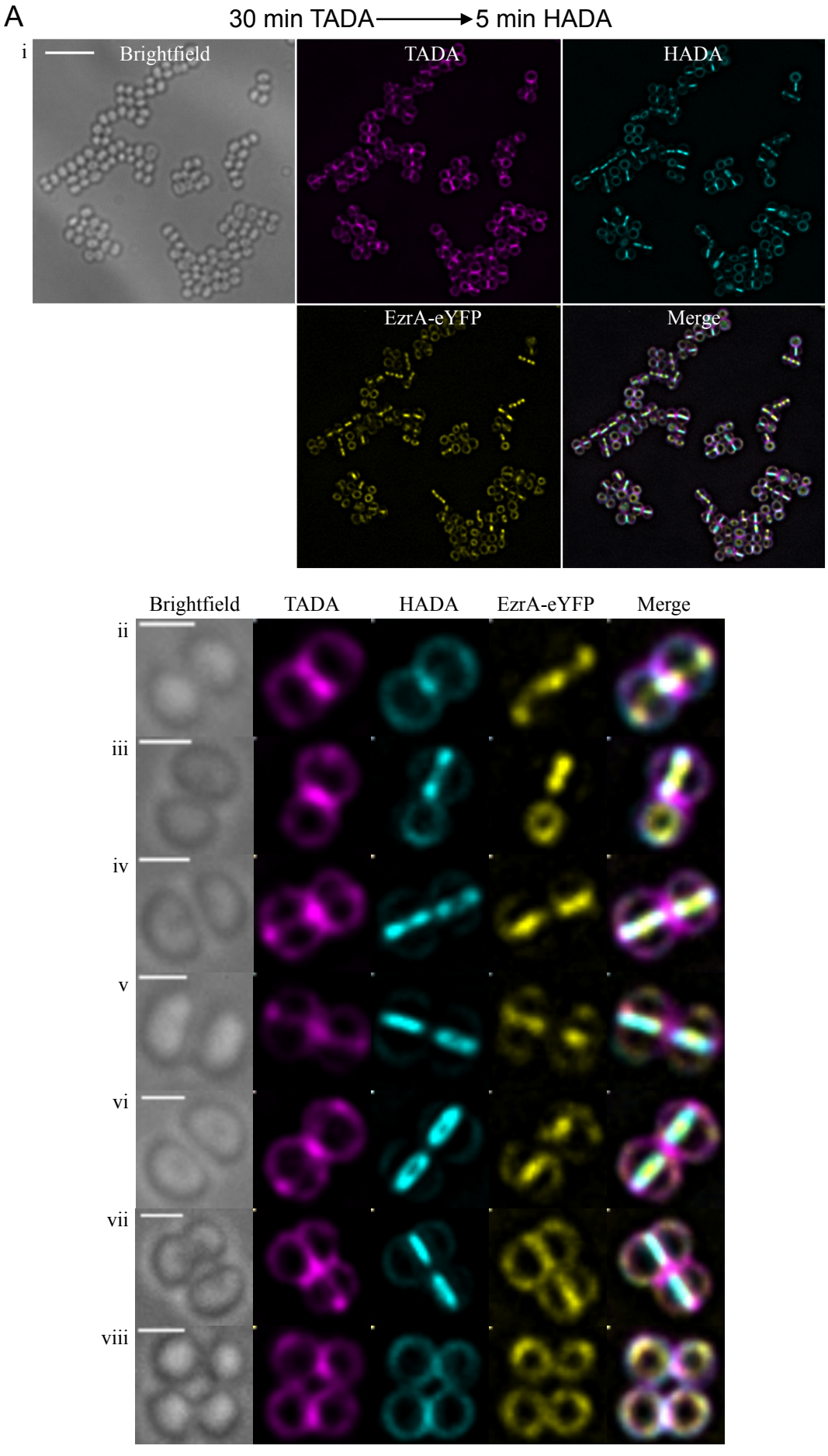
A
30 min TADA
5 min HADA
i
Brightfield
TADA
HADA
EzrA-eYFP
Merge
Brightfield
TADA
HADA
EzrA-eYFP
Merge
ii
iii
iv
v
vi
vii
viii

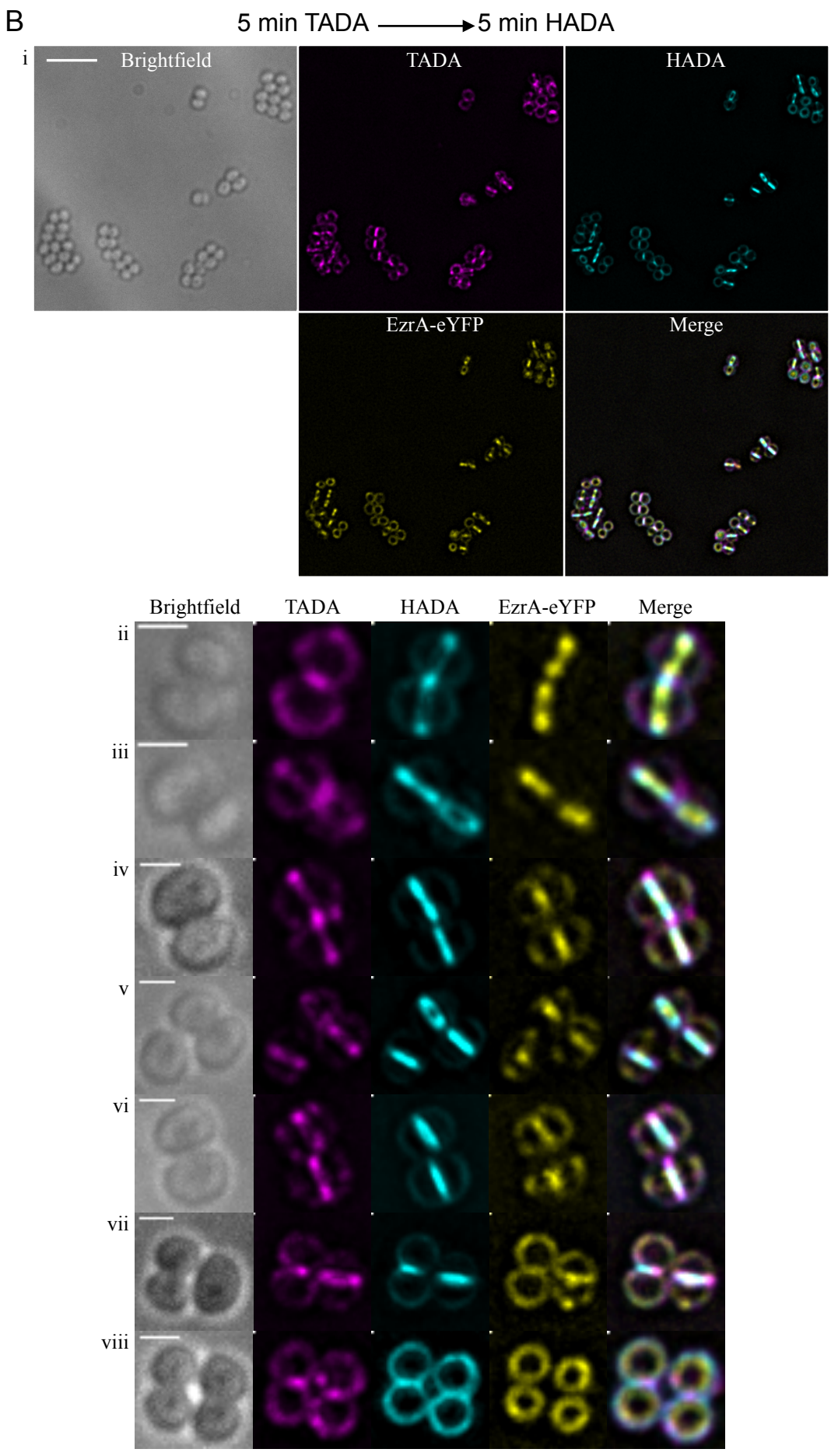
B
5 min TADA
5 min HADA
i
Brightfield
TADA
HADA
EzrA-eYFP
Merge
Brightfield
TADA
HADA
EzrA-eYFP
Merge
ii
iii
iv
v
vi
vii
viii

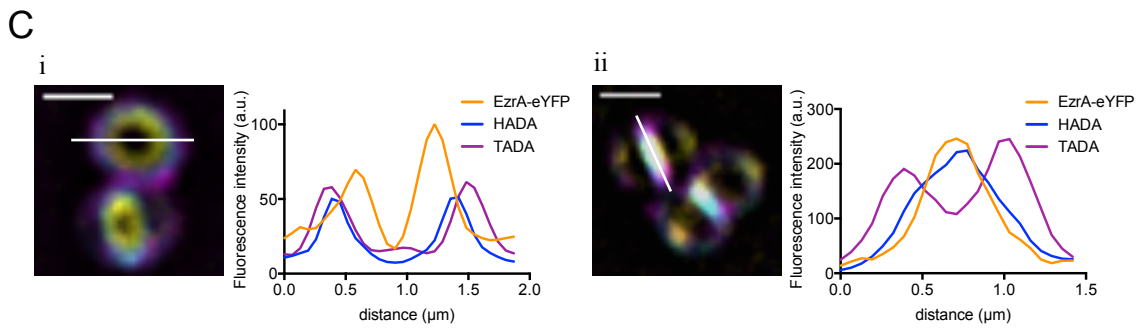

Figure 4.9. Pulse-chase labelling of *S. aureus* with TADA and HADA

A. (i) SJF4388 (*S. aureus* SH1000 *geh::ezrA-eyfp ΔezrA::tet*) was grown in the presence of 500 μM TADA for 30 min (one generation time) to label the cell contour, washed by centrifugation and incubated with 500 μM HADA for 5 min to label nascent peptidoglycan synthesis. Fixed cells were examined by fluorescence microscopy. The fluorescence images are maximum intensity projections of deconvolved z-stack images acquired at 200 nm z-intervals. Scale bars 5 μm.

(ii-viii) Selected individual cells at different stages of the cell cycle. The images are maximum intensity projections of deconvolved z-stack images acquired at 200 nm z-intervals. Scale bars 1 μm.

B. (i) SJF4388 (*S. aureus* SH1000 *geh::ezrA-eyfp ΔezrA::tet*) grown to early-exponential phase was pulsed with 500 μM TADA for 5 min, washed by centrifugation and followed by a 5 min pulse of 500 μM HADA. Fixed cells were examined by fluorescence microscopy. The fluorescence images are maximum intensity projections of deconvolved z-stack images acquired at 200 nm z-intervals. Scale bars 5 μm.

(ii-viii) Selected individual SJF4388 cells at different stages of the cell cycle. The images are maximum intensity maximum intensity projections of z-stack images acquired at 200 nm z-intervals. Scale bars 1 μm.

C. The linear profiles represent fluorescence intensities of EzrA-eYFP (yellow), HADA (blue) and TADA (magenta) in arbitrary units (a.u.) measured along the white lines across the individual cells in the merged images. The images are maximum intensity projections of deconvolved z-stack images acquired at 200 nm z-intervals of SJF4388 labelled with TADA for 5 min and then with HADA for 5 min. Scale bars 1 μm.

SJF4388 (*S. aureus* SH1000 *geh::ezrA-eyfp ΔezrA::tet*) labelling with short pulses of TADA and HADA showed similar dependence between EzrA and newly synthesised peptidoglycan (Figure 4.9B). SJF4388 grown to early-exponential phase was labelled with 500 μM TADA for 5 min, washed by centrifugation and incubated with 500 μM HADA for the next 5 min. Fixed cells were examined by fluorescence microscopy. Both TADA and HADA labelled mainly cell septa and they both exhibited subtle peripheral fluorescence (Figure 4.9Bii-viii). Whilst TADA gave the outermost signal, HADA was located between TADA and EzrA-eYFP showing the sequential incorporation of peptidoglycan at the septum during cell division (Figure 4.9C). This sequence of the fluorescent signals positions (TADA→HADA→EzrA-eYFP) indicated that EzrA might lead the peptidoglycan biosynthesis machinery.

4.2.2.2 Colocalisation of EzrA and newly synthesised peptidoglycan using SIM

In order to visualise localisation of EzrA versus newly synthesised peptidoglycan at higher resolution SJF4640 (*S. aureus* SH1000 *geh::ezrA-gfp ΔezrA::tet*) and SJF4642 (*S. aureus* SH1000 *geh::ezrA-snap ΔezrA::tet*) labelled with HADA were imaged by 3D-SIM.

SJF4642 was grown to early-exponential phase and incubated with 3 μM SNAP-Cell TMR-Star min at 37^{o}C for 10 min. Cells were then grown in fresh BHI for 10 min at 37^{o}C to wash out the excess dye. This was followed by 5 min incubation with 5 mM HADA at 37^{o}C and fixation. Similarly, when SJF460 reached early-exponential phase it was labelled with 5 mM HADA at 37^{o}C for 5 min and then fixed with paraformaldehyde. 3D-SIM imaging gave an obvious increase in resolution revealing subtle peptidoglycan features that were not visible in images obtained by conventional fluorescence microscopy (Figures 4.10 an 4.11). EzrA-GFP and EzrA-SNAP TMR-Star formed heterogeneous rings surrounded by a ring of peptidoglycan material (Figures 4.10 an 4.11). The SIM data highlighted how the size of EzrA rings changed with septum formation progression. Additionally, in cells in which septum was closing but its formation was not fully completed both EzrA-GFP and EzrA-SNAP TMR-Star could be seen in planes perpendicular to the current plane of division (Figures 4.10iv-vii and 4.11iv-vi). Interestingly, EzrA presumably located to the next division plane was not always accompanied by a signal from HADA (Figure 4.11 iv-vi).

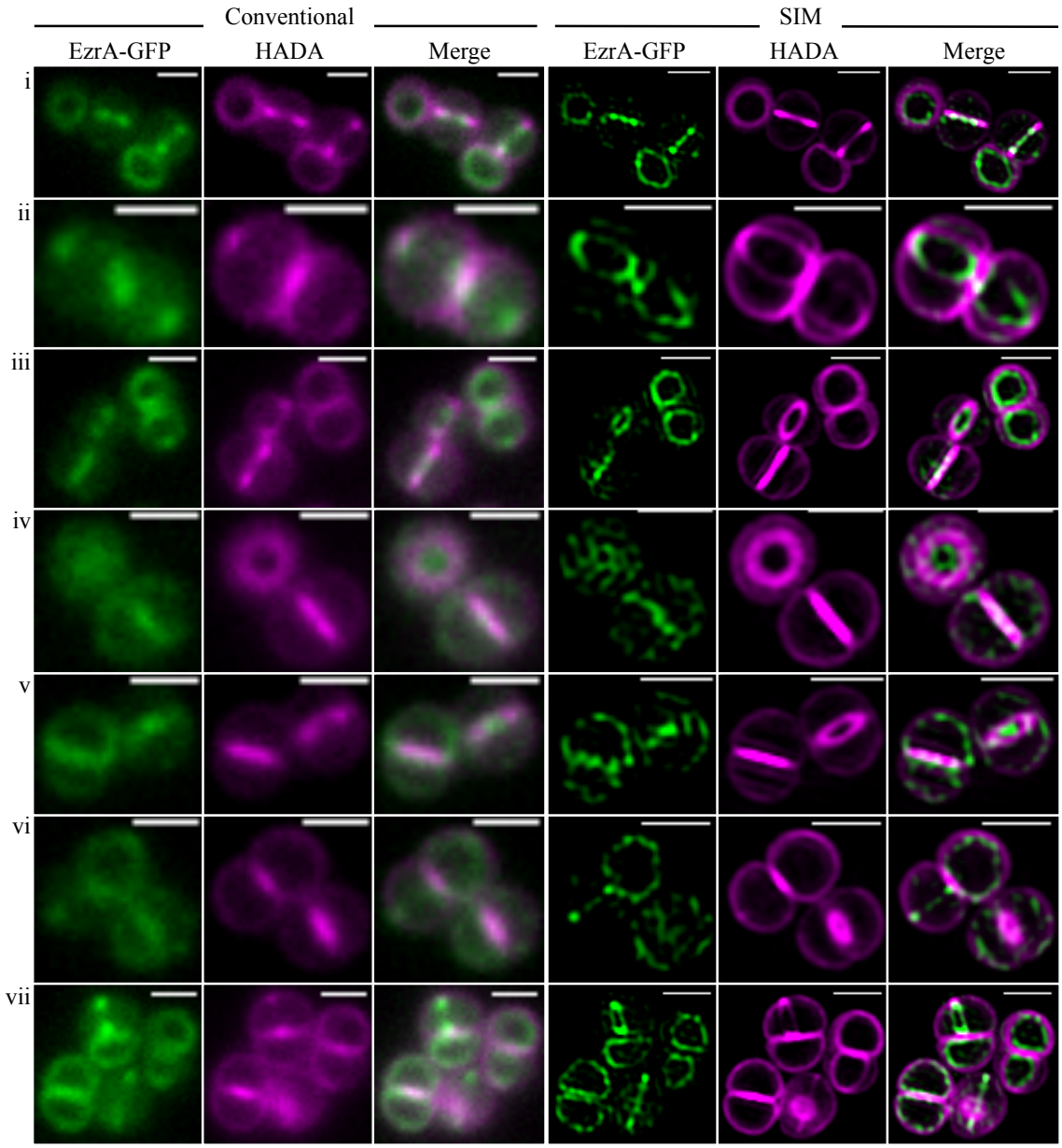

Figure 4.10. Colocalisation of EzrA-GFP and newly synthesised peptidoglycan (HADA) by conventional microscopy and SIM

SJF4640 (*S. aureus* SH1000 *geh::ezrA-gfp ΔezrA::tet*) grown to early-exponential phase was labelled with 5 mM HADA at 37^{o}C for 5 min and fixed. Images present a comparison between conventional fluorescence microscopy and SIM images of selected cells (i-vii). Scale bars 1 μm.

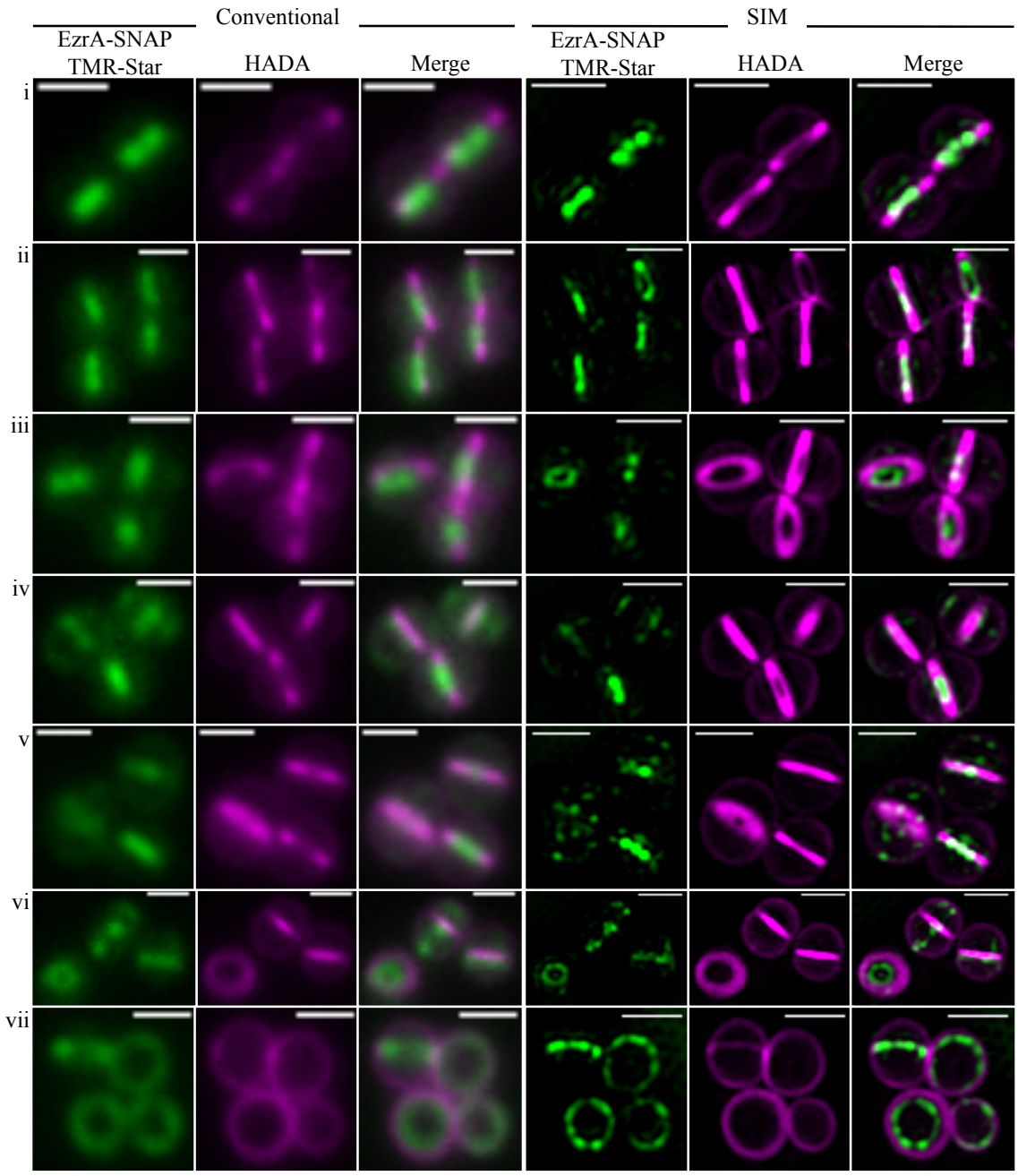

Figure 4.11. Colocalisation of EzrA-SNAP TMR-Star and newly synthesised peptidoglycan (HADA) by conventional microscopy and SIM

SJF4642 (*S. aureus* SH1000 *geh::ezrA-snap ΔezrA::tet*) was grown to early-exponential phase. Cells were labelled with 3 μM SNAP-Cell TMR-Star at 37°C for 15 min, followed by 5 min incubation with 5 mM HADA at 37°C and fixation with paraformaldehyde. Images present a comparison between conventional fluorescence microscopy and SIM images of selected cells (i-vii). Scale bars 1 μm.

This suggested that the often observed peripheral peptidoglycan incorporation was not simply a consequence of the activity of divisome components at the new site of division but due to other mechanisms such as peptidoglycan remodelling or an exchange of peptidoglycan building blocks. The most recent research on *S. aureus* cell size changes suggested that *S. aureus* increases in size before dividing (Monteiro et al., 2015; Zhou et al., 2015) and thus the off-septal HADA may mark sites of lateral peptidoglycan incorporation so that a cell can enlarge. SIM allowed for EzrA and nascent peptidoglycan synthesis colocalisation in more detail than conventional fluorescence microscopy. However the acquired data and the final images could be a result of artefacts arising from sample photobleaching and thus a low signal-to-noise ratio (Appendix II).

4.2.2.3 Colocalisation of EzrA and newly synthesised peptidoglycan by STORM

SIM imaging did give new information on EzrA localisation against newly synthesised peptidoglycan. Therefore these two bacterial components were visualised by STORM. HADA however is not compatible with STORM and could not be used in single-molecule localisation microscopy. No STORM-compatible D-Ala derivatives were available. This required an alternative method for peptidoglycan labelling. In click chemistry two substrates, an azide and an alkyne are covalently linked in a copper (Cu)-catalysed reaction of cycloaddition. The azide moiety is rare in natural biomolecules and therefore the azide-alkyne coupling is considered to be highly specific (Breinbauer and Köhn, 2003). Click chemistry was employed to label an azide-modified D-Ala (ADA) incorporated into nascent peptidoglycan with a STORM compatible alkyne modified Alexa Fluor 647.

SJF4388 (*S. aureus* SH1000 *geh::ezrA-eyfp ΔezrA::tet*) grown to early-exponential phase was incubated with 500 μM ADA for 5 min at 37^{o}C. Cells were fixed with paraformaldehyde. Click chemistry was then used to attach 4 μM Alexa Fluor 647 alkyne to the azide group present in ADA incorporated into peptidoglycan. The reaction was performed at room temperature for 30 min as described in section 2.15.4. The click chemistry approach allowed the labelling of nascent peptidoglycan incorporation and gave a pattern comparable to a 5 min pulse with HADA (Figure 4.12B). However it turned out that this labelling method could not be used together with fluorescent

proteins as it quenched EzrA-eYFP fluorescence (4.12B). EzrA-eYFP, which was initially fluorescent (Figure 4.12A), did not emit any signal post-click reaction (Figure 4.12B). Extinction of eYFP fluorescence was probably caused by the damaging effect of the Cu catalyst used in the reaction. Therefore an alternative method for peptidoglycan staining was required. In copper (Cu)-free click chemistry a DIBO alkyne reagent, which reacts with azide-modified molecules in the absence of the Cu catalyst, is utilised and thus the toxic copper catalyst can be eliminated. SJF4388 incubated with 500 μM ADA was fixed and incubated 20 μM Click-iT Alexa Fluor 647 DIBO alkyne in PBS at room temperature for 30 min. Although Cu-free click chemistry did not harm EzrA-eYFP fluorescence and the characteristic septal localisation pattern could be observed in some cells, the majority of the cells presented a fluorescent signal spread across the whole cell (Figure 4.12C). These cells were saturated in fluorescence and the surrounding cells with the septal pattern appeared poorly labelled (Figure 4.12C). Neither additional washing steps nor reduction of the dye concentration helped to reduce the non-septal signal (data not shown). Alexa Fluor 647 is a large, negatively charged probe that is not cell permeable (Lukinavičius et al., 2013) and when live SJF4388 cells were incubated with only Click-iT Alexa Fluor 647 DIBO alkyne followed by fixation, they did not give any signal from Alexa Fluor 647 (Figure 4.12D). This suggested that the fixation step was responsible for the cell membrane permeabilisation allowing the Alexa Fluor 647 DIBO substrate to get into the cells. In SJF4388 grown without ADA, fixed and incubated with the fluorescent substrate a strong fluorescent signal associated with the cell cytoplasm was observed in many cells (Figure 4.12E). This showed that the cytoplasmic fluorescence was due to non-specific Alexa Fluor 647 DIBO alkyne incorporation upon cell fixation and permeabilisation, as no septal or cell surface associated signal could be observed in cells grown without the reaction partner for alkyne (Figure 4.12E). Cu-free click chemistry was shown to not be toxic for live cells (Liechti et al., 2014), thus labelling procedure was performed on live cells. Cell division is a dynamic process and one generation time lasts ~25 min in *S. aureus*. Since 5 min HADA labelling was shown to be sufficient to observe nascent peptidoglycan incorporation a 5 min Cu-free 'co-click' chemistry was tested. When SJF4388 reached early-exponential phase it was incubated simultaneously with both 1 mM ADA and 40 μM Click-iT Alexa Fluor 647 DIBO alkyne for 5 min at 37^{o}C and then fixed with paraformaldehyde.

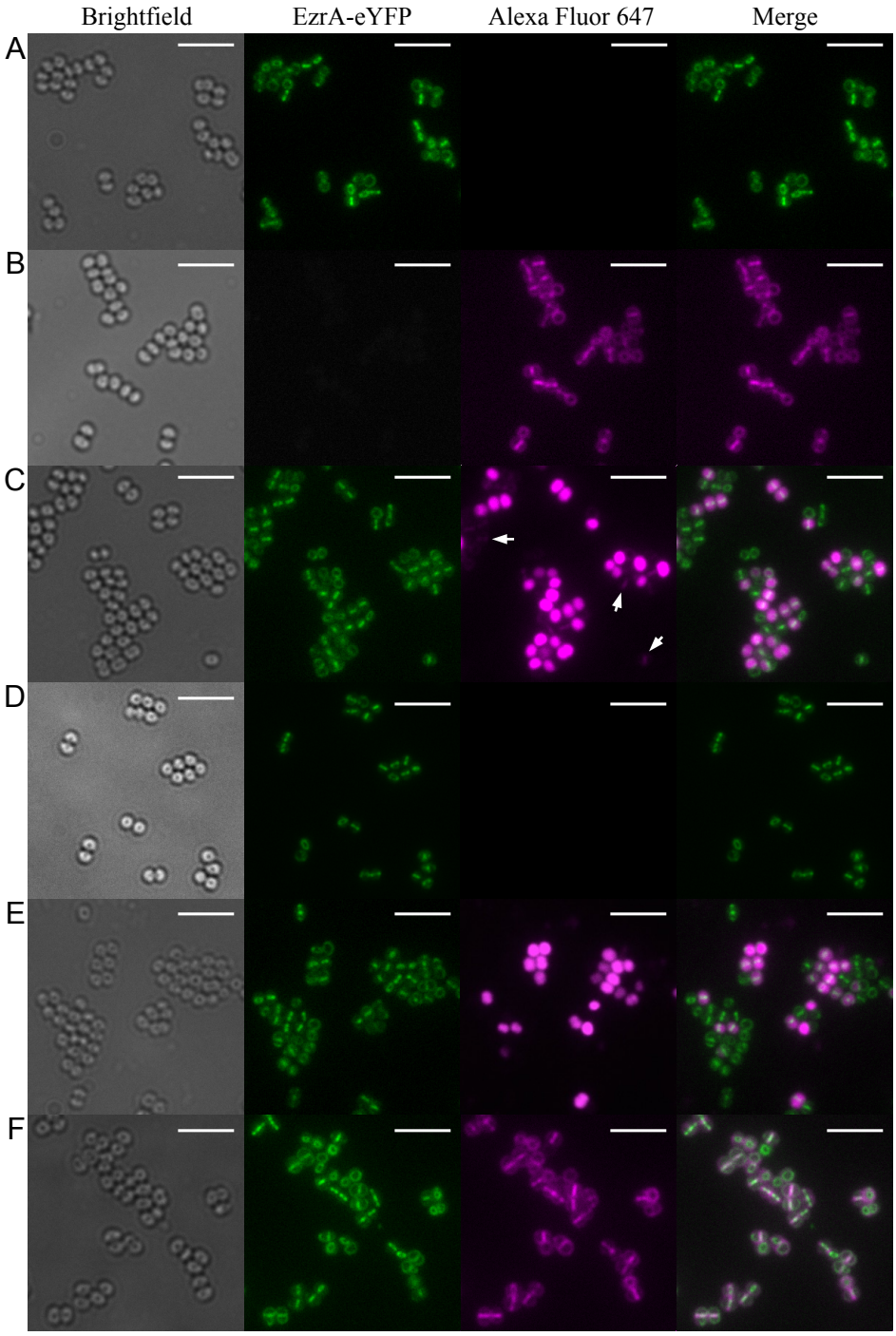

Figure 4.12. Optimisation of peptidoglycan labelling using click chemistry

A. In SJF4388 (*S. aureus* SH1000 *geh::ezrA-eyfp ΔezrA::tet*) EzrA-eYFP is fluorescent.

B. SJF4388 (*S. aureus* SH1000 *geh::ezrA-eyfp ΔezrA::tet*) was grown with 500 μM ADA for 5 min. Fixed cells were 'clicked' with 4 μM alkyne-modified Alexa Fluor 647 at room temperature for 30 min. Cu-catalysed click chemistry revealed sites of peptidoglycan incorporation however it led to EzrA-eYFP fluorescence extinction.

C. SJF4388 (*S. aureus* SH1000 *geh::ezrA-eyfp ΔezrA::tet*) was grown with 500 μM ADA for 5 min, fixed and 'clicked' with 20 μM Click-iT Alexa Fluor 647 DIBO alkyne at room temperature for 30 min. Cu-free click chemistry did not quench EzrA-eYFP fluorescence. Labelling with Cu-free click

chemistry revealed the characteristic septal localisation pattern in some cells (selected cells indicated with white arrows), however in many cells strong and non-specific cytoplasmic signal was present.

D. SJF4388 (*S. aureus* SH1000 *geh::ezrA-eyfp ΔezrA::tet*) grown to early-exponential phase was incubated with 20 μM Click-iT Alexa Fluor 647 DIBO alkyne at 37°C for 30 min and then fixed. Cells did not show any signal from Alexa Fluor 647.

E. SJF4388 (*S. aureus* SH1000 *geh::ezrA-eyfp ΔezrA::tet*) grown to early-exponential phase was fixed and incubated with 20 μM Click-iT Alexa Fluor 647 DIBO alkyne at 37°C for 30 min. In some cells cytoplasmic signal from Alexa Fluor 647 was present.

F. SJF4388 (*S. aureus* SH1000 *geh::ezrA-eyfp ΔezrA::tet*) grown to early-exponential phase was incubated at the same time with 1 mM ADA and 40 μM Click-iT Alexa Fluor 647 DIBO alkyne at 37°C for 5 min. In cells labelled via Cu-free 'co-click' chemistry Alexa Fluor 647 presented signal associated with division septa.

The fluorescence images are maximum intensity projections of z-stack images acquired at 200 nm z-intervals. Scale bars 5 μm.

The characteristic septal pattern for newly synthesised peptidoglycan and no signal associated with the cytoplasm could be observed, showing that the Cu-free 'co-click' chemistry could be used in short-time labelling of nascent peptidoglycan synthesis in cells producing fluorescent proteins (Figure 4.12F).

Having two STORM-compatible fluorophores, Alexa Fluor 647 and eYFP labelling two distinct cell components, single-molecule super-resolution imaging of EzrA and newly synthesised peptidoglycan was performed. Alexa Fluor 647 was shown to work most efficiently in buffers containing both an oxygen scavenging system (GLOX) and a primary thiol (MEA) (Dempsey et al., 2011) and GLOX MEA buffering system did not impair EzrA-eYFP blinking properties (Section 3.2.4.2) making two-colour STORM imaging possible. Nascent peptidoglycan synthesis was labelled by Cu-free 'co-click' chemistry in SJF4388 grown to early exponential phase. Cells were fixed, mounted in GLOX MEA buffer and imaged by 3D-STORM. Fluorophores were detected sequentially. First EzrA-eYFP was imaged using a 514 nm laser and filters dedicated to eYFP. Then the filter set was changed and a 647 nm laser was used to collect data for Alexa Fluor 647. About 10,000 frames were collected for each fluorophore and used for a reconstruction. The fiduciary markers (100 nm TetraSpecks) were used to align images from the two channels.

When peptidoglycan was labelled with Cu-free 'co-click' chemistry non-homologues distribution of EzrA-eYFP was still observed in SJF4388, indicating that the used peptidoglycan labelling method did not perturb localisation of the fusion protein that could be detected at a molecular level (Figure 4.13A). Cu-free 'co-click' labelling revealed non-uniform and 'patchy' distribution of nascent peptidoglycan surrounding EzrA-eYFP 'patches' (Figure 4.13B and C). The 'patchy' peptidoglycan distribution was however not completely consistent with the labelling pattern obtained by utilisation of Cu-catalysed click chemistry (Victoria Lund, unpublished), indicting that Cu-free 'co-click' chemistry was a less efficient method of peptidoglycan labelling. Despite this, similarly to deconvolution microscopy and SIM images of EzrA-eYFP and HADA, EzrA-eYFP was shown to localise ahead of newly synthesised peptidoglycan, suggesting that EzrA 'patches' may direct peptidoglycan synthesis.

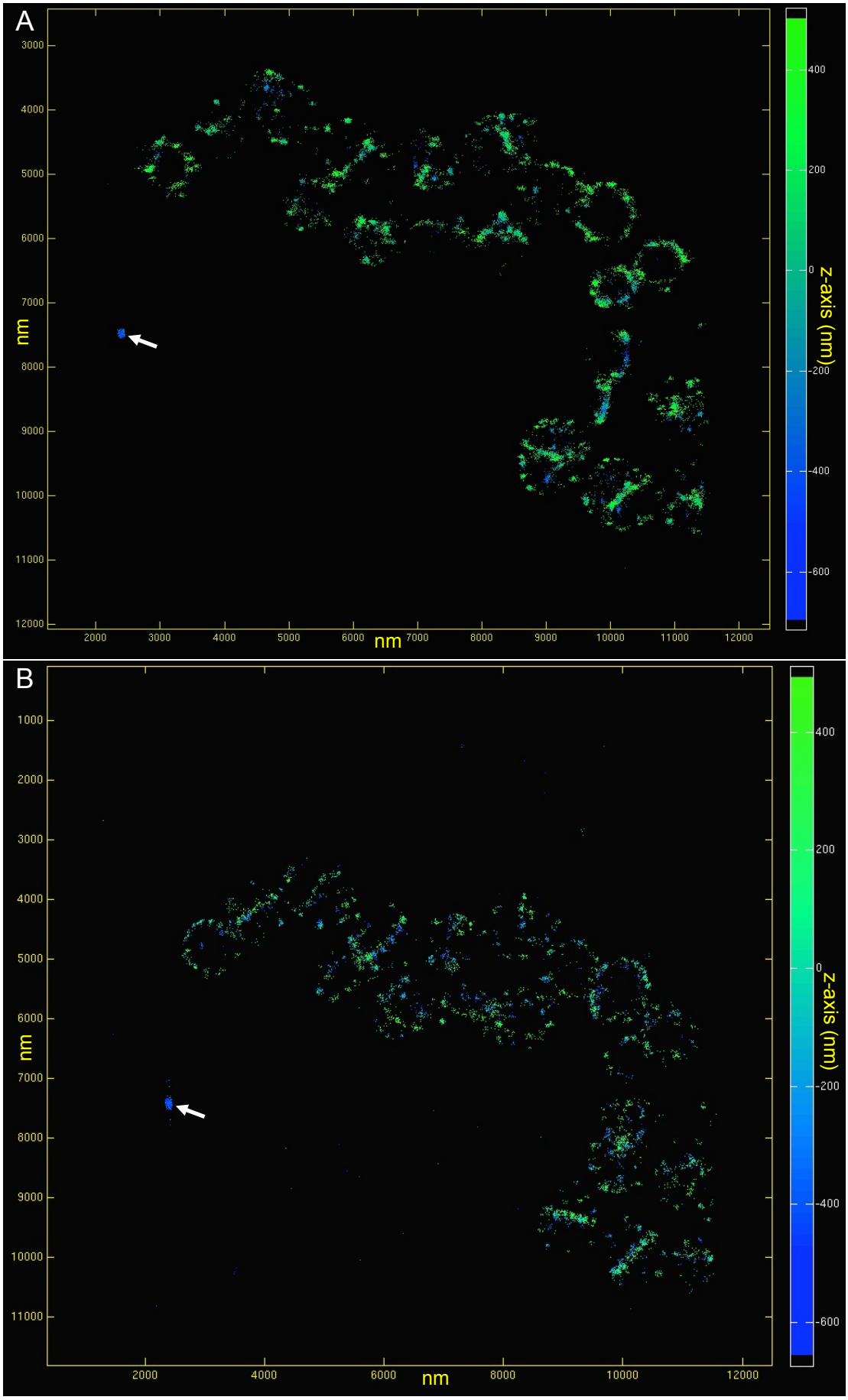
A
3000
4000
5000
6000
7000
8000
9000
10000
11000
12000
nm
2000
3000
4000
5000
6000
7000
8000
9000
10000
11000
12000
nm
400
200
0
-200
-400
-600
z-axis (nm)
B
1000
2000
3000
4000
5000
6000
7000
8000
9000
10000
11000
nm
2000
4000
6000
8000
10000
12000
nm
400
200
0
-200
-400
-600
z-axis (nm)

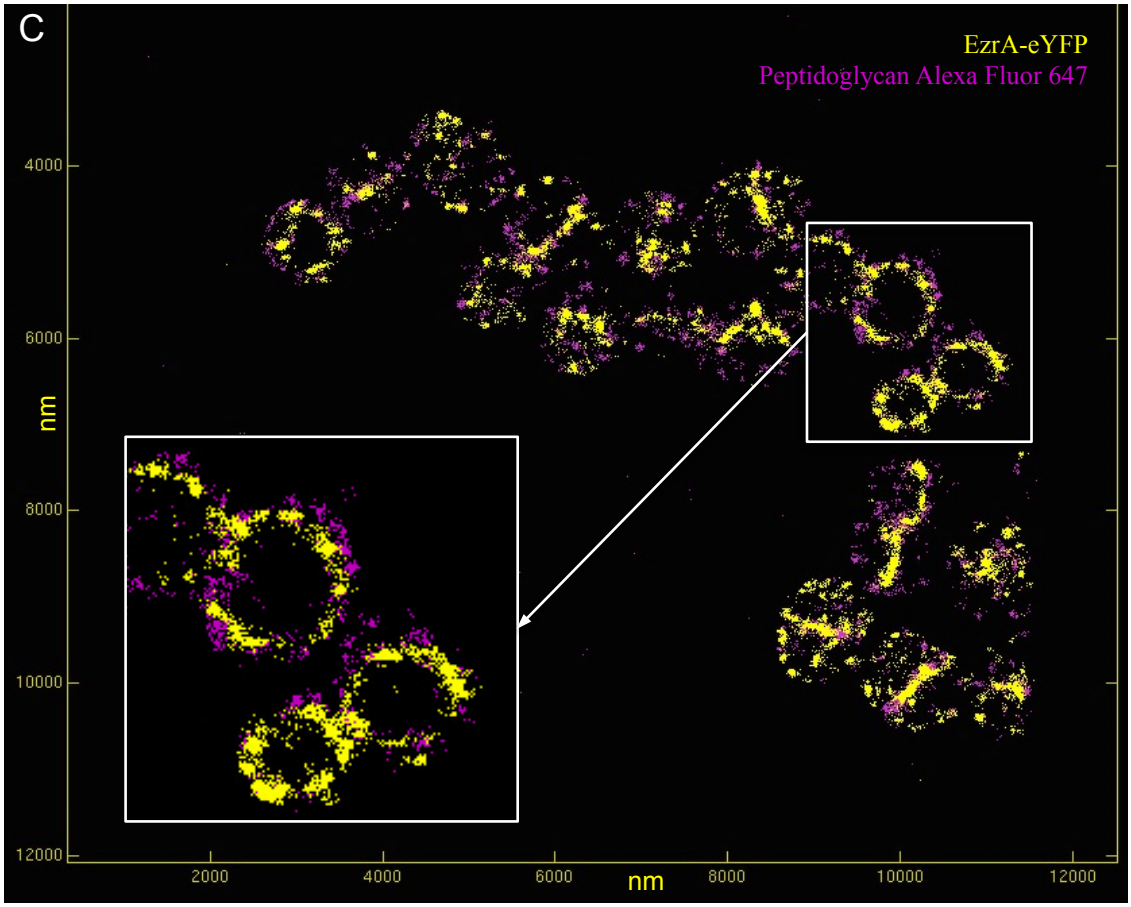

Figure 4.13. Two-colour 3D-STORM imaging of EzrA-eYFP and newly synthesised peptidoglycan in *S. aureus*

A. 3D-STORM reconstruction images of EzrA-eYFP localisation in SJF4388 (*S. aureus* SH1000 *geh::ezrA-eyfp ΔezrA::tet*). Imaging performed in GLOX MEA. The colour scale represents the z-axis. A white arrow indicates localisation of a fiduciary marker (a fluorescent bead).

B. 3D-STORM imaging of newly synthesised peptidoglycan in SJF4388 (*S. aureus* SH1000 *geh::ezrA-eyfp ΔezrA::tet*). Nascent peptidoglycan synthesis was labelled by 5 min Cu-free 'co-click' chemistry (1 mM ADA and 40 µM Click-iT Alexa Fluor 647 DIBO alkyne). A white arrow indicates localisation of a fiduciary marker (a fluorescent bead).

C. Merge of EzrA-eYFP (yellow) and nascent peptidoglycan (magenta) localisations from A and B. Representative cells marked in white are shown enlarged.

4.2.3 Localisation of FtsZ by super-resolution microscopy

Imaging of the FtsZ-SNAP fusion was not successful in revealing FtsZ localisation at the molecular level. Monomeric Eos2 (mEos2) is one of the most often utilised fluorescent proteins in bacterial components localisation studies (Fu et al., 2010; Wang et al., 2011; Buss et al., 2015; Schneider et al., 2015). A C-terminal fusion of FtsZ with mEos2 was employed in super-resolution imaging of FtsZ in *E. coli* (Fu et al., 2010). There is a high FtsZ conservation throughout bacterial species (Adams and Errington, 2009) and even though the EzrA-mEos2 fluorescent protein was not produced in *S. aureus* (Section 3.2.1), an *S. aureus* strain producing FtsZ-mEos2 was constructed.

4.2.3.1 Construction of an *S. aureus* FtsZ-mEos2 strain

pCQ11-FtsZ-mEos2 (Figure 4.14A) is a derivative of the pCQ11-FtsZ-SNAP shuttle vector, in which an *ftsZ-meos2* gene was placed under the control of the Pspac promoter. The pCQ11-FtsZ-mEos2 plasmid was designed by Dr Christa Walther (University of Sheffield), whereas the linker (EFPMGSGGGGS) and the *meos2* insert were synthesised and inserted in-frame with the *ftsZ* gene in the place of the *snap* gene in pCQ11-FtsZ-SNAP by the GeneArt Gene Synthesis service (Life Technologies). pCQ11-FtsZ-mEos2 was transformed into electorcompetent *S. aureus* RN4220 cells and then transferred into *S. aureus* SH1000 by phage transduction, with selection using erythromycin (5 $\mu g\ ml^{-1}$). The resulting SJF4654 (*S. aureus* SH1000 pCQ11-FtsZ-mEos2) strain was tested for FtsZ-mEos2 production.

SJF4654 was grown in the presence of erythromycin (5 $\mu g\ ml^{-1}$) and 1 mM IPTG to induce FtsZ-mEos2 production. When cells reached early-exponential phase, they were fixed and viewed by fluorescence microscopy. In SJF4654, FtsZ-mEos2 was produced and presented the characteristic midcell localisation (Figure 4.14B), similar to the data obtained for FtsZ-SNAP (section 4.2.1). FtsZ-mEos2 had the expected photophysical properties, it switched from a green state to a red one upon UV illumination (Figure 4.14B). Induction with 1 mM IPTG resulted in FtsZ-mEos2 levels that could be easily visualised by fluorescence microscopy, however enlarged cells, saturated with fluorescence and mislocalised FtsZ-mEos2 could be often observed (Figure 4.14B).

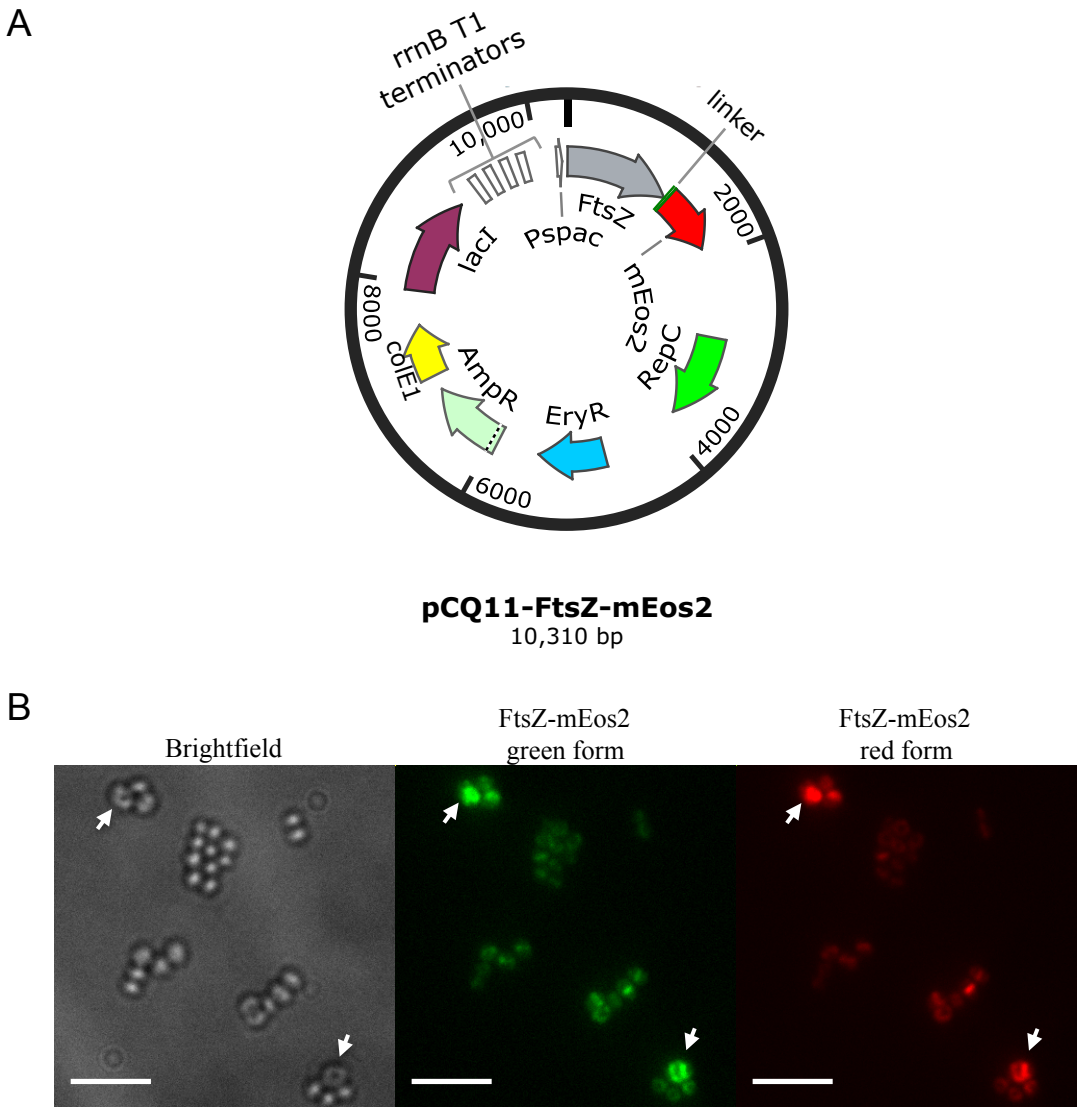

Figure 4.14. Construction of an *S. aureus* strain producing FtsZ-mEos2

A. Map of the FtsZ-mEos2 expression plasmid, pCQ11-FtsZ-mEos2. pCQ11-FtsZ-mEos2 is an *E. coli-S. aureus* shuttle vector. It comprises the high-copy-number ColE1 origin of replication, the staphylococcal origin of replication from pT181 (RepC), the *lacI* gene, four transcription terminators T1 from the *E. coli rrnB* gene, the ampicillin resistance (AmpR) and the erythromycin resistance (EryR) cassettes, and the *ftsZ-meos2* fusion joined by a 10 amino-acid linker, placed under the control of the Pspac promoter.

B. In SJF4654 (*S. aureus* SH1000 pCQ11-FtsZ-mEos2) FtsZ-mEos2 is produced, has the ring-like localisation pattern and converts from a green form to a red one after irradiation with UV light. SJF4654 was grown in the presence of 1 mM IPTG to induce FtsZ-mEos2 production. Some cells showed morphological changes due to FtsZ overproduction: cell enlargement and FtsZ-mEos2 delocalisation (cells indicated with white arrows). The fluorescence images are maximum intensity projections of z-stack images acquired at 200 nm z-intervals. Scale bars 5 μm.

In SJF4654, *ftsZ-meos2* was ectopically expressed from the plasmid in the presence of the native FtsZ protein and any additional FtsZ could lead to altered cell morphology. A similar observation, that is an increase in *S. aureus* cell size and FtsZ fusion delocalisation, were previously observed for FtsZ-SNAP and FtsZ-GFP high levels (section 4.2.1.2; Liew et al., 2011).

The optimal concentration of IPTG that allowed for sufficient FtsZ-mEos2 production for microscopy visualisation that did not alter cell morphology was determined. SJF4654 (*S. aureus* SH1000 pCQ11-FtsZ-mEos2) was grown in BHI in the presence of erythromycin (5 μg ml^{-1}) and different IPTG concentrations: 0, 5, 10, 20, 50, 100, 200 and 1000 μM to early-exponential phase. *S. aureus* SH1000 wild type grown in the absence of IPTG was used as a control of autofluorescence. Fixed cells were examined for FtsZ-mEos2 green emission by fluorescence microscopy. In SH1000 and SJF4654 grown in 0, 5 and 10 μM IPTG a weak fluorescent signal distributed across the whole cell could be observed (Figure 4.15Ai-iv). This was likely cell autofluorescence. When SJF4654 was incubated with 20 and 50 μM IPTG an increase in signal associated with cell could be seen but the FtsZ-mEos2 localisation pattern was poorly defined and the emitted signal was still quite weak (Figure 4.15Av-vi). The characteristic FtsZ ring-like pattern was observed for cells grown in the presence of 100 μM IPTG and above (Figure 4.14Avii-ix). Whilst in the presence of 100 and 200 μM IPTG cells had uniform size and FtsZ-mEos2 showed the midcell localisation, 1 mM IPTG resulted in a strong fluorescent signal but enlarged cells with delocalised FtsZ-mEos2 could be found (Figure 4.15Aix).

As FtsZ-mEos2 was produced ectopically in the presence of native FtsZ, its stability and levels in varying IPTG concentrations were checked by western blot analysis. The pCQ11-FtsZ-mEos2 plasmid was transduced into *S. aureus* SH1000 *spa::kan* to reduce the cross-reactivity of antibodies with *S. aureus* Protein A. The resulting SJF4655 (*S. aureus* SH1000 *spa::kan* pCQ11-FtsZ-mEos2) strain was grown in the presence of erythromycin (5 μg ml^{-1}) and 0, 10, 20, 50, 100, 200 and 1000 μM IPTG. Whole cell lysates were probed with rabbit anti-FtsZ antibodies at a 1:1000 dilution. (Figure 4.15B). Bands of ~50 kDa were detected in all cell lysates and likely represented native FtsZ. In SJF4655 grown in 50, 100, 200 and 1000 μM IPTG bands of ~70 kDa, which correlated to the expected size of FtsZ-mEos2, were detected (Figure 4.15B).

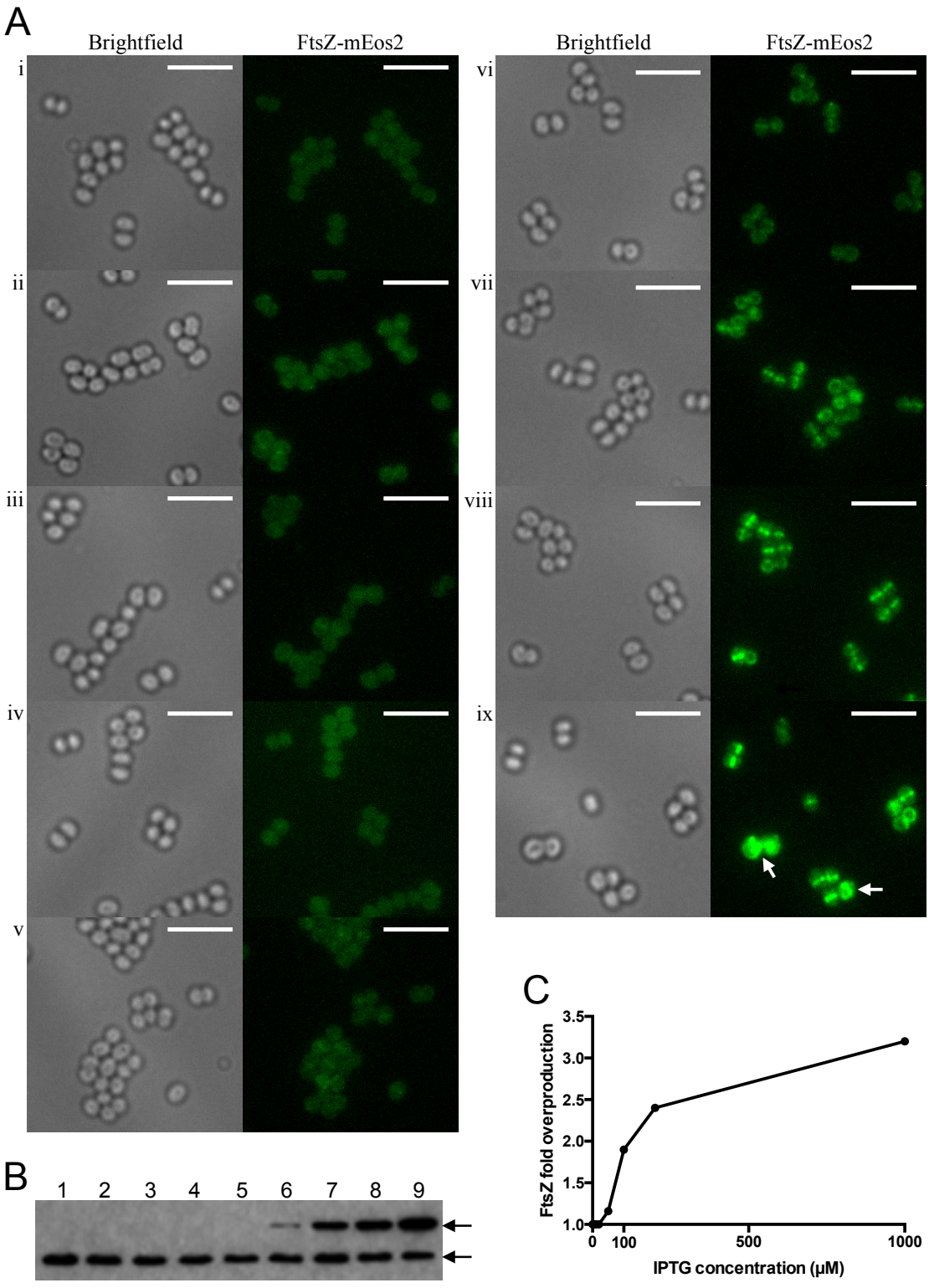

Figure 4.15. Optimisation of IPTG concentrations for FtsZ-mEos2 production in *S. aureus*

A. SH1000 (i) and SJF4654 (*S. aureus* SH1000 pCQ11-FtsZ-mEos2) grown in the presence of 0 μM (ii), 5 μM (iii), 10 μM (iv), 20 μM (v), 50 μM (vi), 100 μM (vii), 200 μM (viii) and 1000 μM (ix) IPTG were imaged by fluorescence microscopy. White arrows indicate cells with disrupted morphology and mislocalised FtsZ-mEos2. The fluorescence images are maximum intensity

projections of z-stack images acquired at 200 nm z-intervals. The same contrast was adjusted to the fluorescence images. Scale bars 5 μm.

B. Quantitative immunoblot showing levels of FtsZ and FtsZ-mEos2 production in *S. aureus* SH1000 *spa::kan* (1) and SJF4655 (*S. aureus* SH1000 *spa::kan* pCQ11-FtsZ-mEos2) grown in 0 μM (2), 5 μM (3), 10 μM (4), 20 μM (5), 50 μM (6), 100 μM (7), 200 μM (8) and 1000 μM (9) IPTG. Whole cell lysates were probed with anti-FtsZ antibodies at a dilution of 1:1000. Bands detected at ~50 kDa (FtsZ) and ~ 70 kDa (FtsZ-mEos2) are indicated with black arrows.

C. Fold overproduction of FtsZ represents the ratio of an FtsZ total level (native FtsZ and FtsZ-SNAP) to the native FtsZ level in SJF4655 (*S. aureus* SH1000 *spa::kan* pCQ11-FtsZ-mEos2) grown in varying IPTG concentrations. The FtsZ levels were calculated using western blot in (B).

No additional products that could indicate protein instability were found. Consistent with the fluorescence microscopy data, the western blot analysis showed that FtZ-mEos2 either was not produced in the absence of IPTG or at low concentrations or its levels were not sufficient to be detected by the used methods. Microscopy imaging and data obtained from the western blot showed that FtsZ-mEos2 production was IPTG dependent and increased with the higher concentrations of the inducer. In SJF4655 grown in 50 μM IPTG the FtsZ-mEos2 level was 16% of the native FtsZ level and increased to 90% in the presence of 100 μM IPTG (Figure 4.15C). At 200 and 1000 μM IPTG concentrations the total FtsZ levels rose about 2.4 and 3.2 fold, respectively (Figure 4.15C). The 100 μM IPTG concentration gave the most optimal results. Almost twofold production of FtsZ (100% of native FtsZ and 90% of FtsZ-mEos2) meant that every second FtsZ molecule in the cell was the fusion protein but it did not lead to detectable morphological changes of *S. aureus* and allowed for microscopy visualisation of FtsZ-mEos2.

4.2.3.2 FtsZ-mEos2 localisation by STORM

Localisation of FtsZ-mEos2 was visualised by super-resolution microscopy. SJF4654 (*S. aureus* SH1000 pCQ11-FtsZ-mEos2) was grown to early-exponential phase in the presence of erythromycin (5 μg ml^{-1}) and 100 μM IPTG and was fixed with paraformaldehyde. mEos2 is usually employed in PALM imaging as it spontaneously blinks and does not require any special imaging conditions, thus standard physiological buffers as PBS are sufficient as mounting media (McKinney et al., 2009; Schneider et al., 2015). However mEos2 was also shown to perform well when mounted in a buffer containing a reducing agent and an oxygen scavenger making this protein suitable for STORM experiments (Endesfelder et al., 2011). Therefore SJF4654 was mounted in GLOX 50 mM MEA (50 mM instead of standard 100 mM β-mercaptoethylamine was used, optimised by Christa Walther). Positions of FtsZ-mEos2 molecules were recorded by 2D N-STORM. Two lasers were used simultaneously to image FtsZ-mEos2. A 405 nm laser acted as an activation wavelength switching FtsZ-mEos2 molecules from a green state to a red one, while a 561 nm light was used to excite and read out FtsZ-mEos2 red fluorescence. STORM images obtained from the reconstruction of the recorded data revealed that, similar to EzrA, FtsZ did not form uniform rings and was heterogeneously distributed around division site (Figure 4.16).

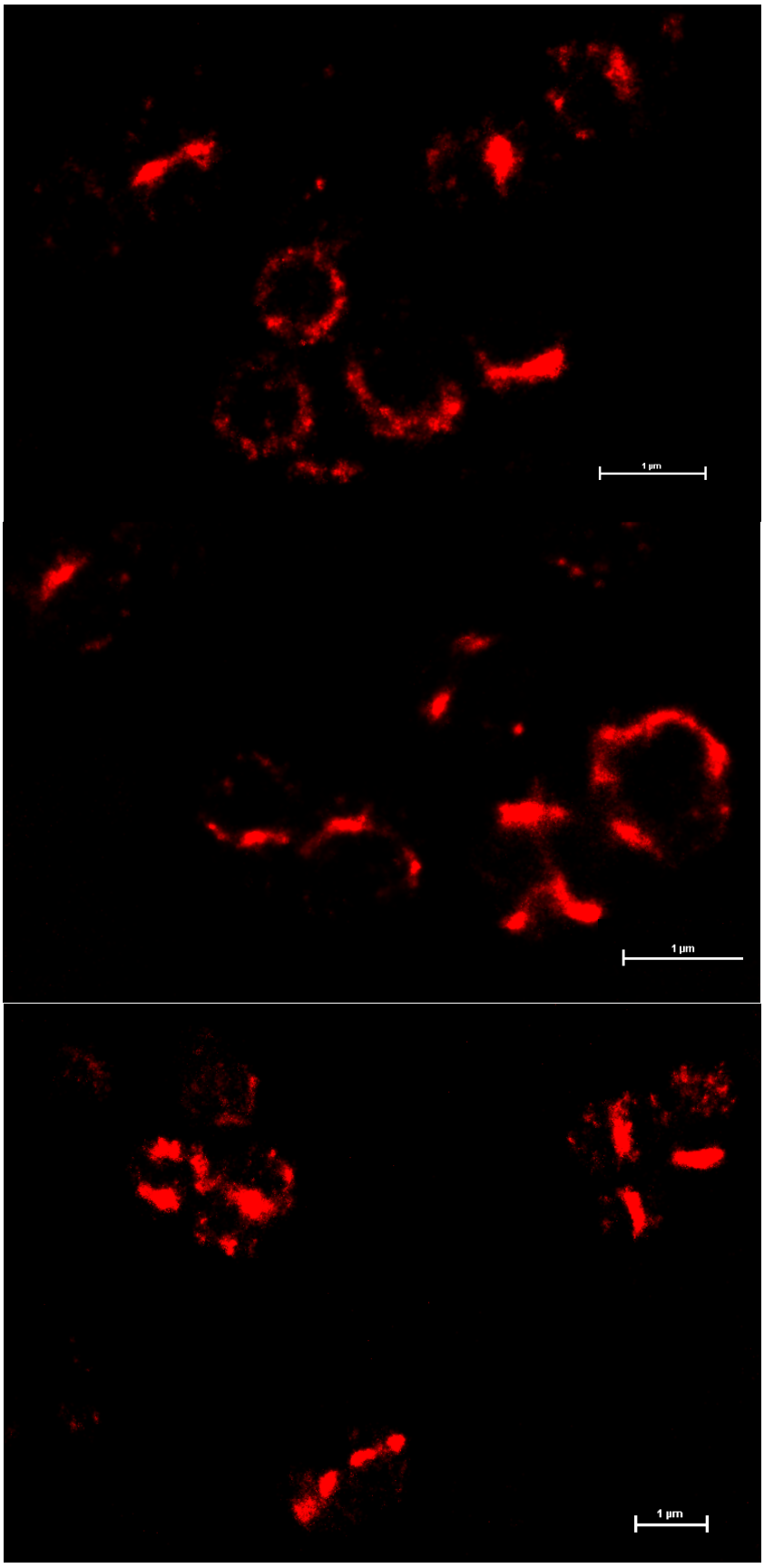

Figure 4.16. N-STORM imaging of FtsZ-mEos2

SJF4654 (*S. aureus* SH1000 pCQ11-FtsZ-mEos2) was induced with 100 µM IPTG and FtsZ-mEos2 was imaged by 2D N-STORM. Imaging was performed in GLOX 50 mM MEA.

4.2.3.3 Colocalisation of FtsZ with peptidoglycan and PBPs

FtsZ is the first protein that localises to the division site and recruits other components of the divisome (Adams and Errington, 2009). The collective action of division components guides the synthesis of new cell wall (Typas et al., 2012). Peptidoglycan is the major structural polymer in the cell wall and the insertion of new material is mediated by penicillin binding proteins (PBPs) (Typas et al., 2012; Pinho et al., 2013). Therefore FtsZ, the first protein recruited to the midcell was juxtaposed with peptidoglycan, the outcome of divisome activity.

SJF4654 (*S. aureus* SH1000 pCQ11-FtsZ-mEos2) was grown in the presence of 100 μM IPTG and erythromycin (5 μg ml^{-1}). When cells reached early-exponential phase they were labelled with 500 μM HADA to mark sites of peptidoglycan synthesis, fixed and imaged by fluorescence microscopy. As expected both FtsZ-mEos2 and newly synthesised peptidoglycan were found to localise to the division site and FtsZ was observed to precede HADA in formation of division septa (Figure 4.17A). HADA does not blink and cannot be used in single-molecule localisation microscopy. Thus in SJF4654 nascent peptidoglycan incorporation was labelled by click chemistry. 10 min Cu-free 'co-click' chemistry using 1 mM ADA and 40 μM Click-iT Alexa Fluor 647 DIBO alkyne was found to give comparable results to 5 min HADA labelling of SJF4654. The colocalisation pattern of FtsZ-mEos2 and nascent peptidoglycan synthesis labelled by Cu-free 'co-click' chemistry was similarly to the one in HADA labelled SJF4654 cells (Figure 4.17A and B). Furthermore, the Cu-free 'co-click' reaction did not led to extinction of FtsZ-mEos2 fluorescence (Figure 4.17B). Usage of a fluorescent conjugate of vancomycin is another way of labelling peptidoglycan. Vancomycin is a glycopeptide antibiotic that binds D-Ala-D-Ala residues present in the uncross-linked stem peptide of the peptidoglycan precursor (Figure 4.2) (Reynolds, 1989). When SJF4654 was grown to early-exponential phase it was fixed and incubated with 4 μM vancomycin Alexa Fluor 647 conjugate (Van-AF647) for 30 min at room temperature. Van-AF647 labelled relatively uniformly cell surface and cell septa (Figure 4.17C). This was expected since in *S. aureus* both old and new cell walls contain D-Ala-D-Ala residues, and nascent peptidoglycan that is mostly present in a division septum is not more abundant in these two terminal residues (de Jonge et al., 1992).

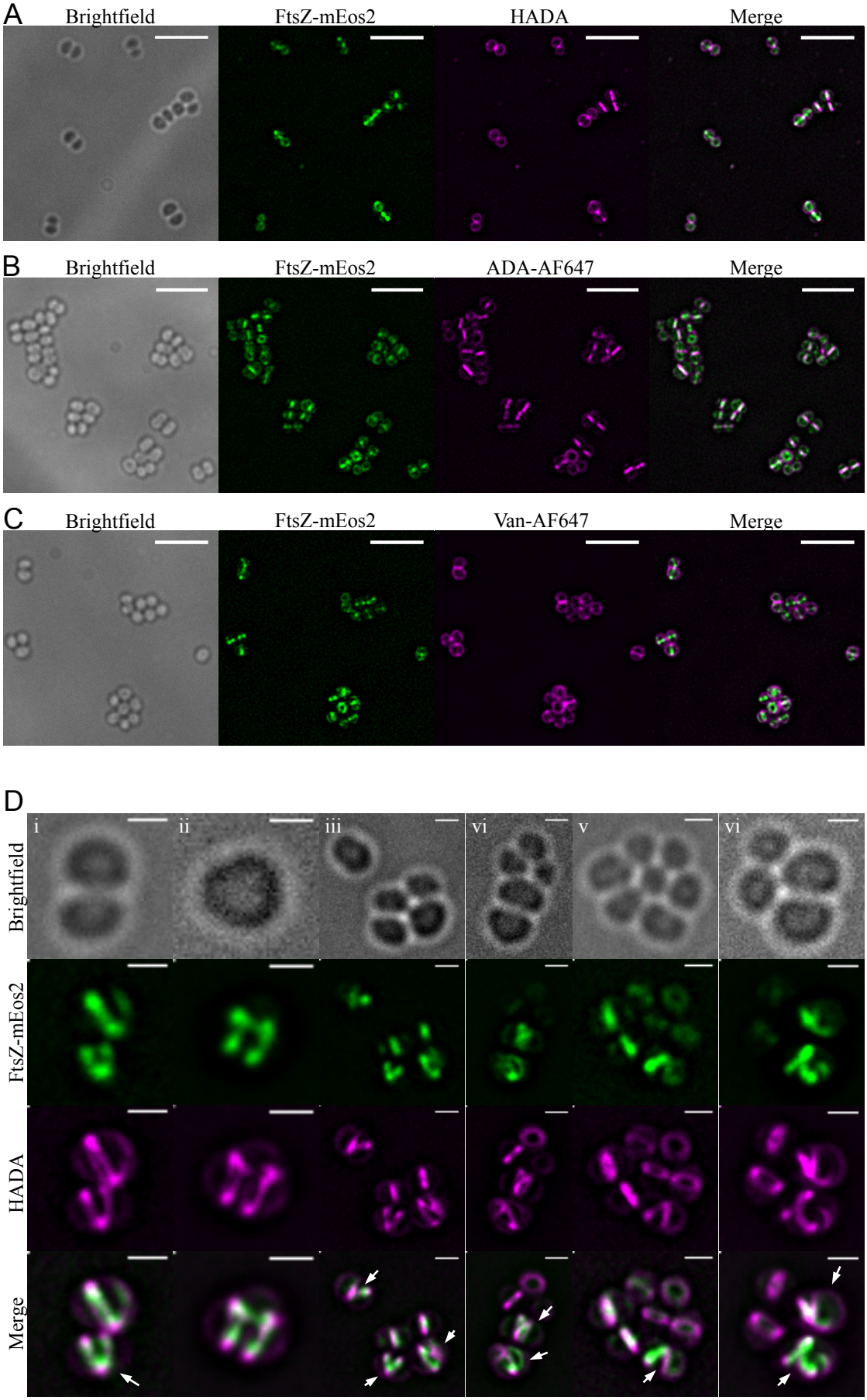
A
Brightfield
FtsZ-mEos2
HADA
Merge
B
Brightfield
FtsZ-mEos2
ADA-AF647
Merge
C
Brightfield
FtsZ-mEos2
Van-AF647
Merge
D
i
ii
iii
vi
v
vi
Brightfield
FtsZ-mEos2
HADA
Merge

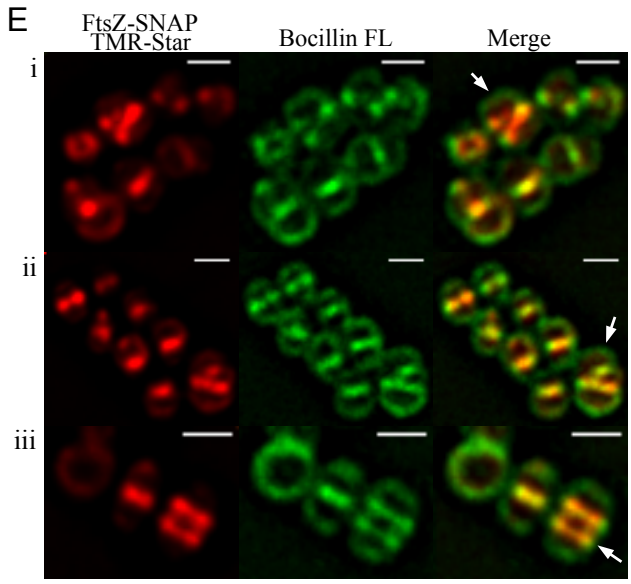

Figure 4.17. FtsZ colocalisation with either peptidoglycan or PBPs imaged by conventional microscopy

A. SJF4654 (*S. aureus* SH1000 pCQ11-FtsZ-mEos2) grown in the presence of 100 μM IPTG was pulsed with 500 μM HADA for 5 min. The fluorescence images are maximum intensity projections of deconvolved z-stack images acquired at 200 nm z-intervals. Scale bars 5 μm.

B. In SJF4654 (*S. aureus* SH1000 pCQ11-FtsZ-mEos2) induced with 100 μM IPTG nascent peptidoglycan incorporation was labelled by 10 min Cu-free 'co-click' chemistry using 1 mM ADA and 40 μM Click-iT Alexa Fluor 647 DIBO alkyne. The fluorescence images are maximum intensity projections of deconvolved z-stack images acquired at 200 nm z-intervals. Scale bars 5 μm.

C. SJF4654 (*S. aureus* SH1000 pCQ11-FtsZ-mEos2) grown in the presence of 100 μM IPTG was fixed and incubated with vancomycin Van-AF647 to label the cell contour. The fluorescence images are maximum intensity projections of deconvolved z-stack images acquired at 200 nm z-intervals. Scale bars 5 μm.

D. SJF4654 (*S. aureus* SH1000 pCQ11-FtsZ-mEos2) grown in the presence of 1 mM IPTG was pulsed with 500 μM HADA for 5 min. White arrows indicate cells with abnormal morphology in images containing more than one cell. The fluorescence images are maximum intensity projections of deconvolved z-stack images acquired at 200 nm z-intervals. Scale bars 1 μm.

E. SJF4605 (*S. aureus* SH1000 pCQ11-FtsZ-SNAP) grown in the presence of 100 μM IPTG, was incubated with 500 nM SNAP-Cell TMR-Star to label FtsZ-SNAP, washed by centrifugation and stained with 1 μg ml^{-1} Bocillin FL for 5 min. Cells with abnormal morphology are indicated with white arrows. The fluorescence images are maximum intensity projections of deconvolved z-stack images acquired at 200 nm z-intervals. Scale bars 1 μm.

Growth of SJF4654 (*S. aureus* SH1000 pCQ11-FtsZ-mEos2) in the presence of 1 mM IPTG disrupted *S. aureus* cell morphology, as cells were found enlarged and FtsZ-mEos2 delocalised (Figure 4.15Aix). FtsZ is thought to act as a scaffold for other cell division components (Adams and Errington, 2009), thus the effect of FtsZ mislocalisation on other cell components was investigated. SJF4654 was grown in the presence of erythromycin (5 μg ml^{-1}) and 1 mM IPTG, to induce a three-fold increase of FtsZ levels in a cell. Cells were labelled with 500 μM HADA, fixed and visualised by fluorescence microscopy. FtsZ-mEos2 was observed to be followed by newly synthesised peptidoglycan both in wild type looking cells and those with disrupted morphology (Figure 4.17D). The HADA pattern correlated with that of FtsZ-mEos2, for example in cells in which FtsZ formed 'V' shaped or double septa, HADA adopted the similar localisation pattern (Figure 4.17D). A similar effect of FtsZ localisation on other cell division proteins was observed in Bocillin FL labelled cells. Bocillin is a green fluorescent derivative of penicillin V and binds penicillin binding proteins (PBPs) (Zhao et al., 1999). PBPs catalyse the final stages of peptidoglycan synthesis (Typas et al., 2012; Pinho et al., 2013). SJF4605 (*S. aureus* SH1000 pCQ11-FtsZ-SNAP) was grown in the presence of 100 μM IPTG, which resulted in minor morphological defects. When SJF4605 reached early-exponential phase cells were incubated with 500 nM SNAP-Cell TMR-Star to label FtsZ-SNAP, washed by centrifugation and PBPs were stained with 1 μg ml^{-1} Bocillin FL (Molecular Probes) for 5 min. Fluorescence microscopy revealed that FtsZ-SNAP TMR-Star and Bocillin FL labelled PBPs colocalised even when cells formed abnormal shaped septa (Figure 4.17E). Altogether, the above results showed FtsZ importance in marking division site and directing other cell division components in *S. aureus*.

Localisation of FtsZ-mEos2 compared to peptidoglycan synthesis was investigated by N-STORM. In SJF4654 (*S. aureus* SH1000 pCQ11-FtsZ-mEos2) induced with 100 μM IPTG either the whole cell wall was labelled with Van-AF647 to highlight the cell contour or nascent peptidoglycan synthesis was 'co-clicked' with 1 mM ADA and 40 μM Click-iT Alexa Fluor 647 DIBO alkyne for 10 min. Fixed cells were mounted in GLOX 50 mM MEA. Positions of cell structures marked by mEos2 and Alexa Fluor 647 were recorded by 3D N-STORM. A 561 nm and a 647 nm laser were used as FtsZ-mEos2 and Alexa Fluor 647 excitation lasers, respectively. A 405 nm laser acted as an activation laser, photoconverting FtsZ-mEos2 molecules from the green to the red

fluorescent form, and activating Alexa Fluor 647 molecules from a dark state to a bright fluorescent state. FtsZ-mEos2 and Alexa Fluor 647 were periodically activated, detected, localised and bleached with a sequence of lasers 405/561 nm and 647 nm.

As expected from the conventional fluorescence microscopy Van-AF647 uniformly labelled the cell wall, whereas for ADA 'co-clicked' with Alexa Fluor 647 more events associated with cell septa rather the cell periphery were detected (Figures 4.18 and 4.19). Dual-colour STORM imaging showed that FtsZ-mEos2 formed non-uniform structures, often large foci marking the nascent septum inside the surrounding mother cell wall (Figure 4.18i and iii). FtsZ-mEos2 was observed to precede peptidoglycan synthesis (Figure 4.19). In cells in which formation of division septa was just initiated FtsZ-mEos2 was present as a broad focus ahead of the leading edge of a division septum (Figures 4.18i-iii and 4.19iii). In the later stage of cell division FtsZ-mEos2 formed a thick ring/line along division site accompanied by peptidoglycan material closing over it (Figures 4.18 and 4.19). In cells which were finishing division and splitting into daughter cells, the fusion could be observed focused in the next division plane, perpendicular to the previous one (Figure 4.18i and iii, 4.19i). Moreover, FtsZ-mEos2 was not exclusive to the division septum but was present both in the cytoplasm and the peripheral cell membrane (Figures 4.18 and 4.19).

4.2.4 Colocalisation of FtsZ, EzrA and newly synthesised peptidoglycan in *S. aureus*

Colocalisation studies on dual labelled cells showed that FtsZ-SNAP TMR-Star and EzrA-eYFP localised to the same cell region but their fluorescent signals were slightly offset with FtsZ-SNAP TMR-Star rings observed inside EzrA-eYFP rings (Section 4.2.1.4). Although EzrA follows FtsZ, EzrA was shown to precede nascent peptidoglycan in two-colour conventional fluorescence and super-resolution microscopy (Section 4.2.2). In order to visualise the localisation order of FtsZ, EzrA and newly synthesised peptidoglycan triple labelling was used.

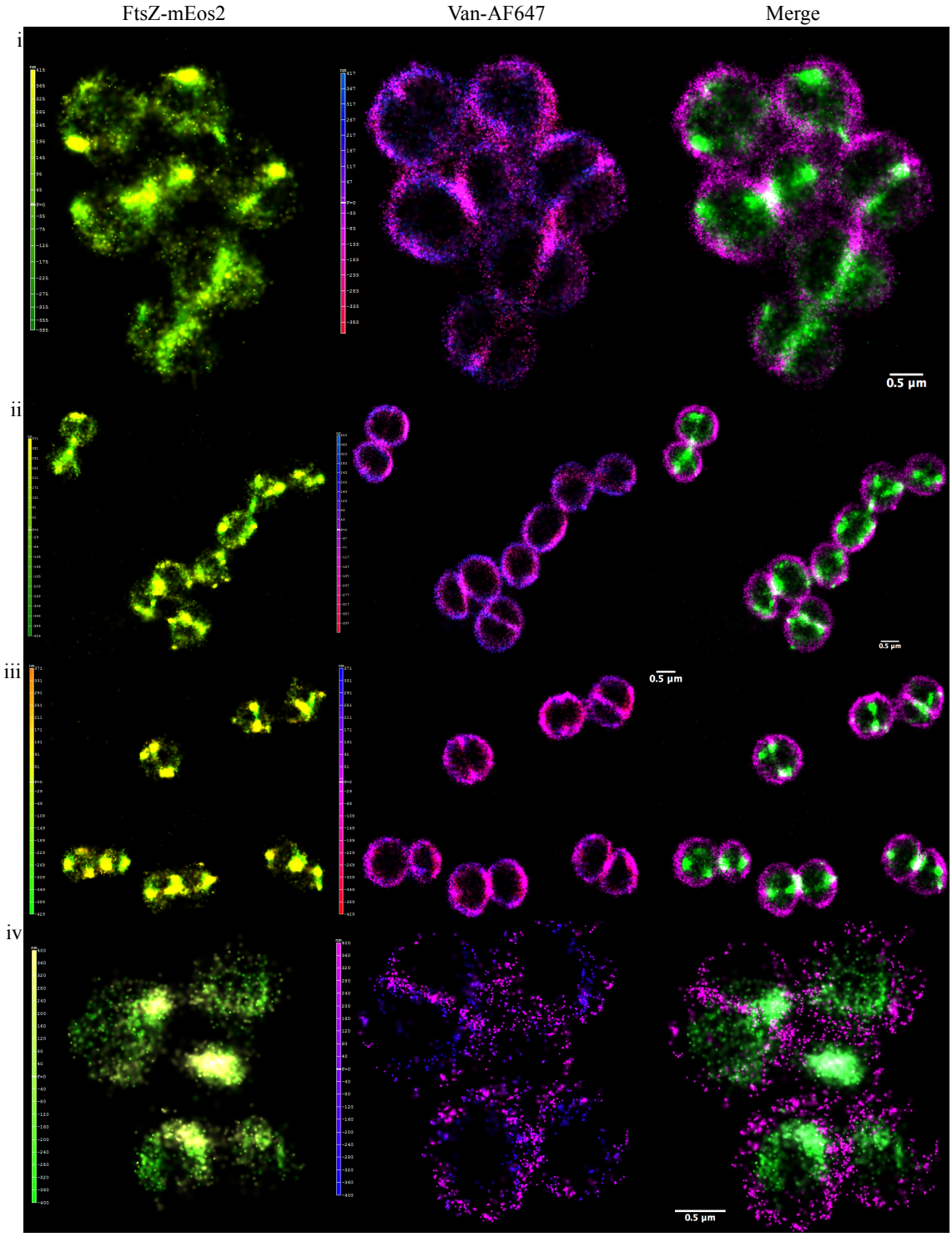

Figure 4.18. Colocalisation of FtsZ-mEos2 and peptidoglycan by 3D N-STORM

SJF4654 (*S. aureus* SH1000 pCQ11-FtsZ-mEos2) grown in the presence of 100 µM IPTG was labelled with Van-AF647. Imaging was performed in GLOX 50 mM MEA. The colour scales in the images of FtsZ-mEos2 and Van-AF647 represent the z-axis. 3D images of single channels were merged into 2D images and green represents FtsZ-mEos2, while magenta Van-AF647. White emerges when two colours overlay and at least one of them is of high intensity.

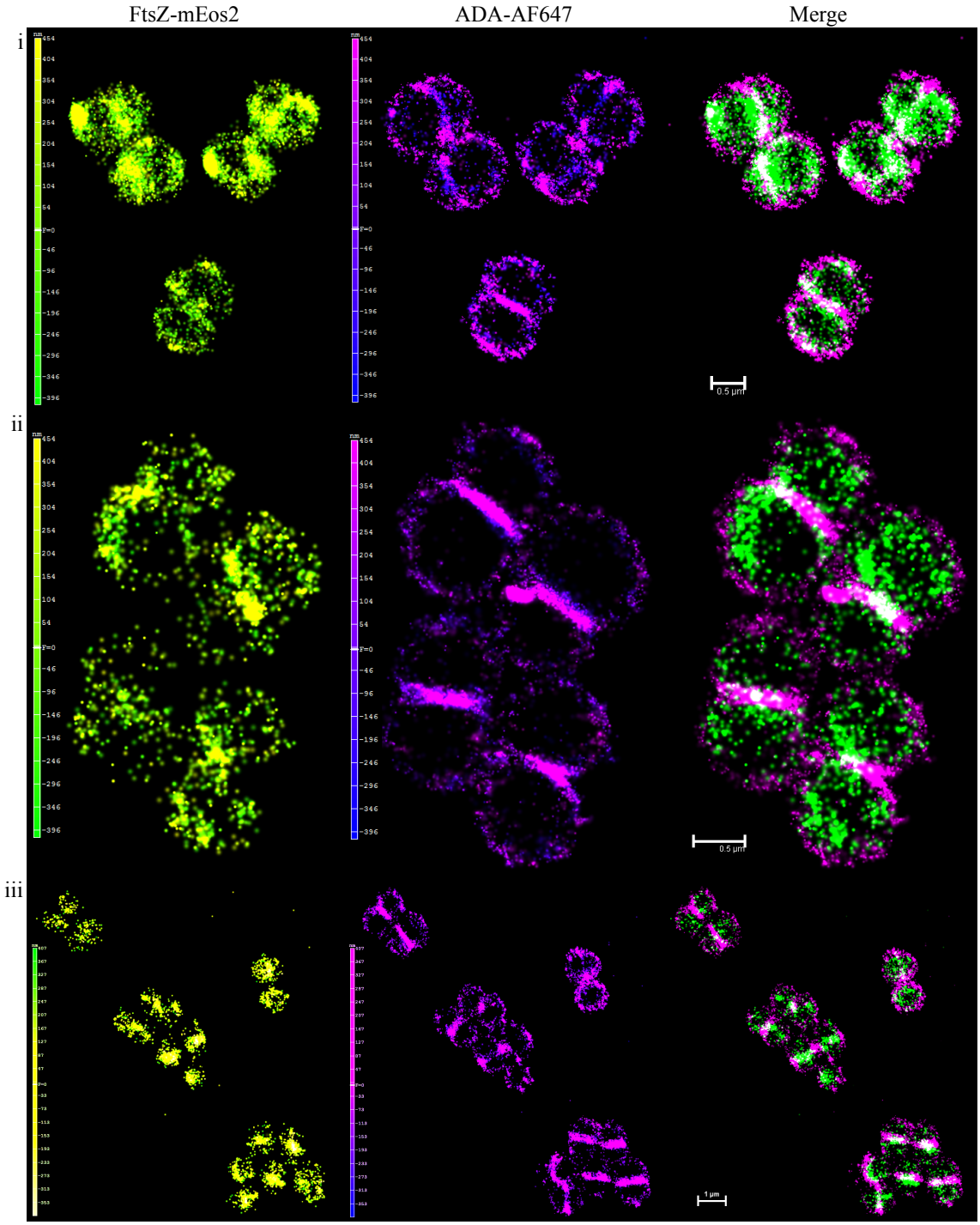

Figure 4.19. Colocalisation of FtsZ-mEos2 and newly synthesised peptidoglycan by 3D N-STORM
SJF4654 (*S. aureus* SH1000 pCQ11-FtsZ-mEos2) was grown in the presence of 100 µM IPTG to induce FtsZ-mEos2 production. Cells were labelled by clicking ADA to Alexa Fluor 647 DIBO alkyne (ADA-AF647) in 10 min 'co-click' chemistry. Imaging was performed in GLOX 50 mM MEA. The colour scales in the images of FtsZ-mEos2 and ADA-AF647 represent the z-axis. 3D images of single channels were merged into 2D images and green represents FtsZ-mEos2, while magenta ADA-AF647. White emerges when two colours overlay and at least one of them is of high intensity.

SJF4652 (*S. aureus* SH1000 *geh::ezrA-eyfp ΔezrA::tet* pCQ11-FtsZ-SNAP) was grown in the presence of erythromycin (5 μg ml^{-1}) and 50 μM IPTG to induce FtsZ-SNAP production. Simultaneous incubation with SNAP-Cell TMR-Star and HADA was found to result in TMR-Star signal dispersed across the whole cell (data not shown) and therefore cells where sequentially labelled with SNAP-Cell TMR-Star and HADA. When SJF4652 reached early-exponential phase it was labelled with 500 nM SNAP-Cell TMR-Star for 5 min. Cells were washed by centrifugation and grown for next 5 min in the presence of 500 μM HADA. Fixed cells were examined by fluorescence microscopy. As expected all three cell division components were observed to be present in the same cell locations where they formed similar localisation patterns (Figure 4.20A). Closer inspection of single cells revealed that the fluorescent signals from the individual components were close to each other but did not overlay completely (Figure 4.20B). EzrA-eYFP followed FtsZ-SNAP TMR-Star, both at early and late stages of septum formation (Figure 4.20B). The nascent peptidoglycan synthesis slightly lagged behind EzrA-eYFP and FtsZ-SNAP TMR-Star. (Figure 4.20B). The colocalisation of FtsZ-SNAP TMR-Star, EzrA-eYFP and HADA was verified by linear profiles of fluorescence intensities measured across selected cells (Figure 4.20C). Comparison of distribution of maximal fluorescence peaks for these three components showed that at the septum FtsZ slightly preceded EzrA and they both were enclosed within HADA outermost peaks. The sequence of distribution of fluorescent signals (HADA→EzrA-eYFP→FtsZ-SNAP TMR-Star) indicated that there exists a localisation hierarchy of cell division components during septum formation.

4.2.5 Colocalisation of EzrA, PBPs and newly synthesised peptidoglycan in *S. aureus*

Newly synthesised peptidoglycan was shown to lag behind EzrA-eYFP during septum formation (Section 4.2.2). While EzrA is a part of divisome which directs cell wall formation during division of *S. aureus*, peptidoglycan is the major cell wall component (Steele et al., 2011; Typas et al., 2012). Fluorescent labelling of EzrA marked the localisation of the divisome, whereas HADA gave an indication about the site of active peptidoglycan synthesis (Section 4.2.2). However these dual-colour studies did not show localisation of penicillin binding proteins (PBPs) that are directly required for peptidoglycan synthesis (Typas et al., 2012; Pinho et al., 2013).

A

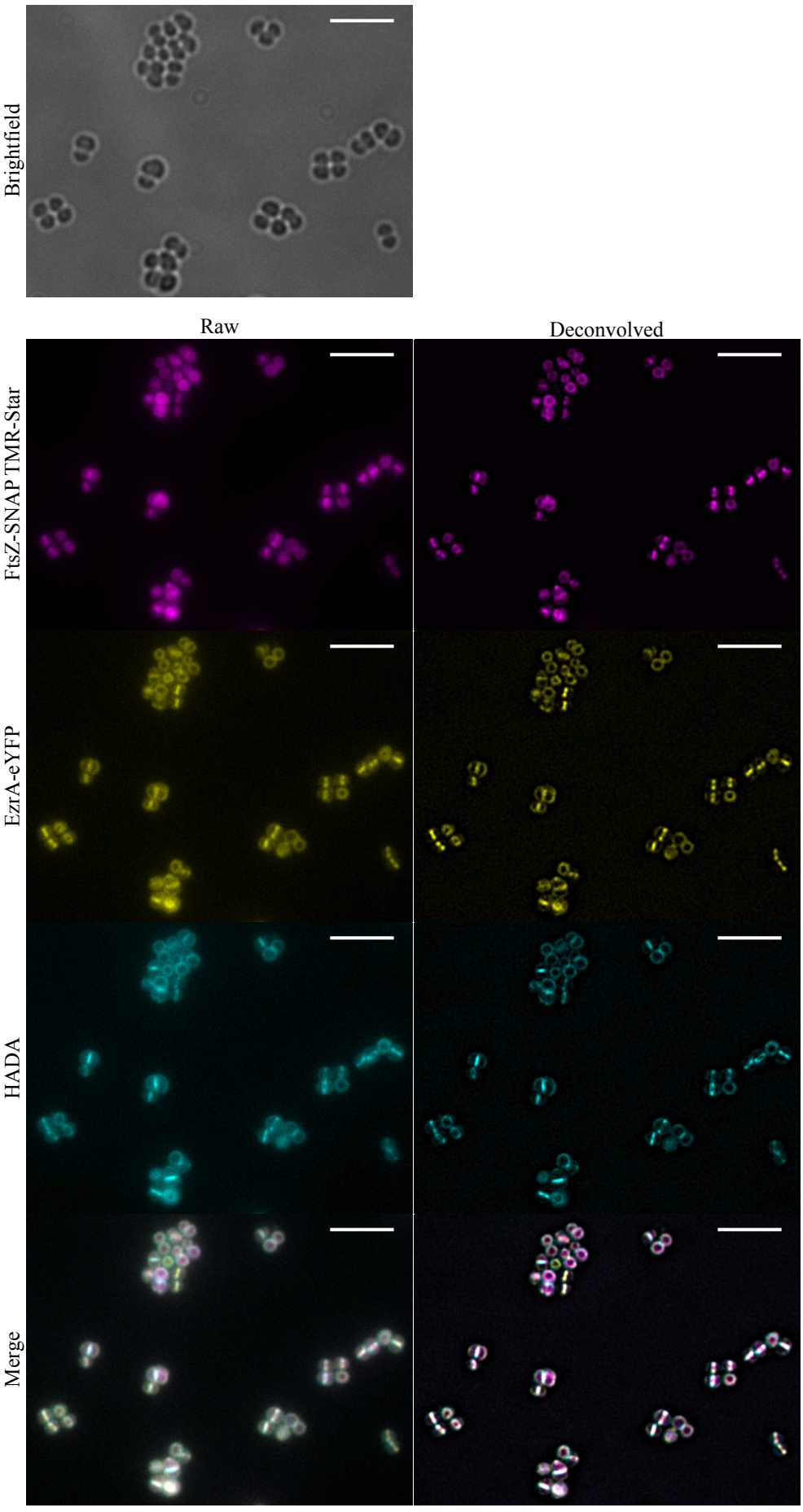
Brightfield
Raw
Deconvolved
FtsZ-SNAP TMR-Star
EzrA-eYFP
HADA
Merge

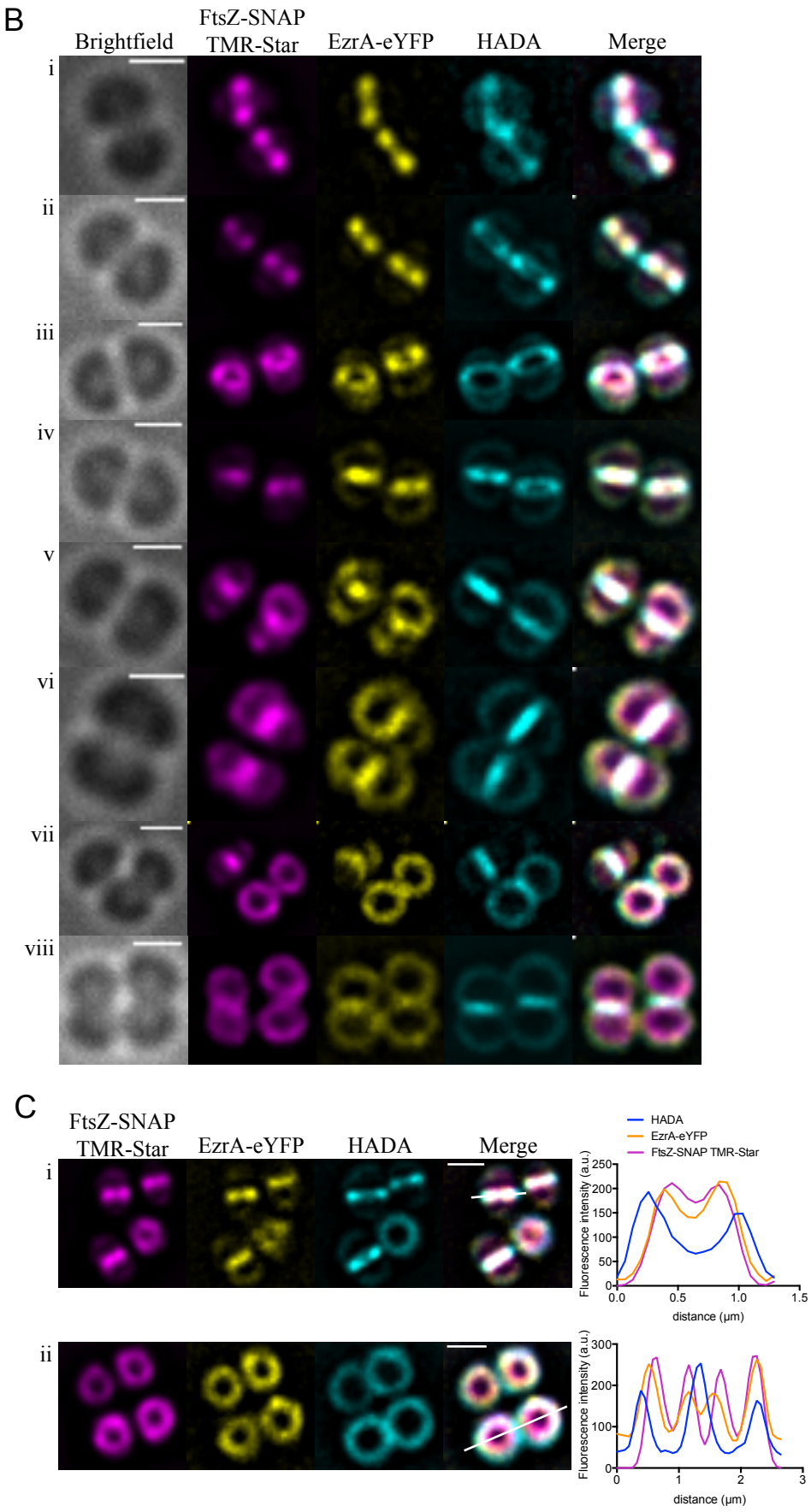

Figure 4.20. Colocalisation of FtsZ, EzrA and newly synthesised peptidoglycan in *S. aureus* by conventional fluorescence microscopy

A. SJF4652 (*S. aureus* SH1000 *geh::ezrA-eyfp ΔezrA::tet* pCQ11-FtsZ-SNAP) grown in the presence of 50 μM IPTG to early-exponential phase was labelled with 500 nM SNAP-Cell TMR-Star for 5 min, washed by centrifugation and incubated with 500 μM HADA for 5 min. Fixed cells were examined by deconvolution microscopy. The raw and deconvolved images are shown. The fluorescence images are maximum intensity projections of z-stack images acquired at 200 nm z-intervals. Scale bars 5 μm.

B. Individual SJF4652 (*S. aureus* SH1000 *geh::ezrA-eyfp ΔezrA::tet* pCQ11-FtsZ-SNAP) cells labelled with SNAP-Cell TMR-Star and HADA were selected to highlight localisation of FtsZ-SNAP TMR-Star, EzrA-eYFP and sites of new peptidoglycan incorporation. The fluorescence images of cells at different stages of the cell cycle are maximum intensity projections of deconvolved z-stack images acquired at 200 nm z-intervals (i-viii). Scale bars 1 μm.

C. The linear profiles represent fluorescence intensities of HADA (blue), EzrA-eYFP (yellow) and FtsZ-SNAP TMR-Star (magenta) in arbitrary units (a.u.) measured along the white lines across the individual cells in the merged images. The images are maximum intensity projections of deconvolved z-stack images acquired at 200 nm z-intervals of SJF4652 (*S. aureus* SH1000 *geh::ezrA-eyfp ΔezrA::tet* pCQ11-FtsZ-SNAP) labelled as described in (A). Scale bars 1 μm.

Bocillin FL labels distribution of all PBPs (section 4.2.3.3). EzrA, PBPs and nascent peptidoglycan synthesis were labelled to visualise their juxtaposition by conventional fluorescence microscopy and SIM.

SJF4642 (*S. aureus* SH1000 *geh::ezrA-snap ΔezrA::tet*) was grown to early-exponential phase, labelled with 1 μM SNAP-Cell TMR-Star for 5 min, washed by centrifugation and incubated with 500 μM HADA for 5 min. Fixed cells were labelled with 1 μg ml^{-1} Bocillin FL at room temperature for 10 min and examined by fluorescence microscopy. Microscopy visualisation revealed that although Bocillin FL bound to the midcell it also labelled the whole surface (Figure 4.21A). In cells undergoing cell division septally located EzrA-SNAP TMR-Star was accompanied by midcell fluorescent signals from Bocillin FL and HADA (Figure 4.21B). Comparison of distribution of EzrA-SNAP TMR-Star, Bocillin FL and HADA fluorescent signals in selected dividing cells showed that EzrA-SNAP TMR-Star was located innermost within the septal plane (Figure 4.21C). Even though Bocillin FL and HADA gave more septally peripheral signals in respect to EzrA-SNAP TMR-Star, and their peaks appeared largely overlapped, Bocillin FL fluorescence intensity profile was slightly shifted towards EzrA-SNAP TMR-Star peaks (Figure 4.21C).

Triple labelled SJF4642 (*S. aureus* SH1000 *geh::ezrA-snap ΔezrA::tet*) was imaged by high-resolution microscopy. SJF4642 was grown to early-exponential phase and 3 μM SNAP-Cell TMR-Star was added for 10 min. The excess dye was washed out by cell centrifugation and growth in fresh BHI for 10 min. Cells were then incubated with 5 mM HADA for 5 min. Fixed cells were labelled with 10 μg ml^{-1} Bocillin FL at room temperature for 10 min and examined by 3D-SIM.

Although SIM reconstruction data gave improvement in resolution it did not bring new information on EzrA, PBP and nascent peptidoglycan synthesis colocalisation different from that provided by conventional fluorescence microscopy. This was evident when the same field of view was imaged both by conventional microscopy and SIM, and the obtained data were compared (Figure 4.22). Similarly, as previously described conventional fluorescence microscopy and deconvolved images depicted EzrA-SNAP TMR-Star as uniform rings, whereas SIM data showed the fusion heterogeneously distributed around the division site (Figure 4.22).

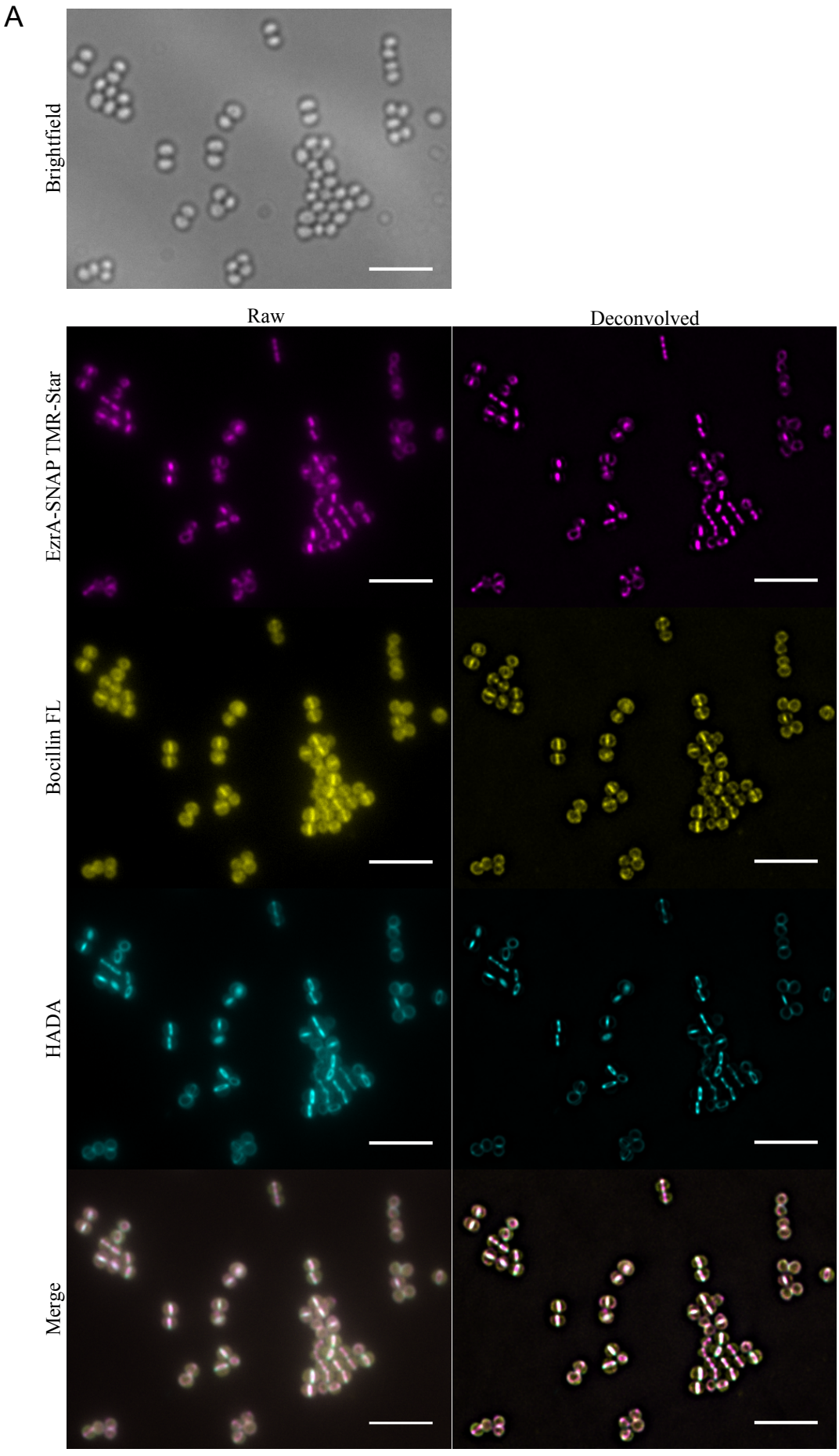
A
Brightfield
Raw
Deconvolved
EzrA-SNAP TMR-Star
Bocillin FL
HADA
Merge

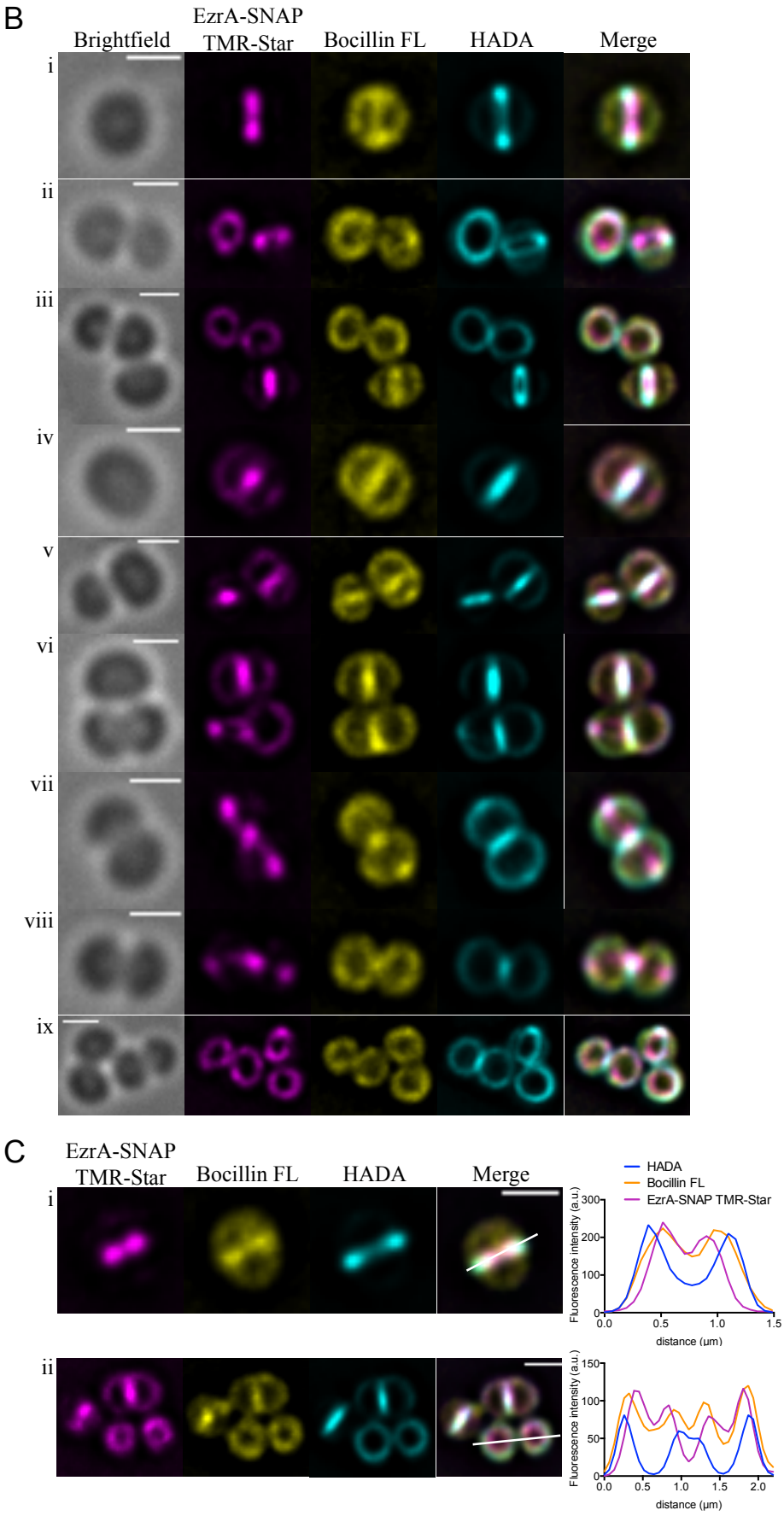

Figure 4.21. Colocalisation of EzrA, PBPs and newly synthesised peptidoglycan by conventional fluorescence microscopy

A. SJF4642 (*S. aureus* SH1000 *geh::ezrA-snap ΔezrA::tet*) grown to early-exponential phase was labelled with 1 μM SNAP-Cell TMR-Star for 5 min, washed by centrifugation and incubated with 500 μM HADA for 5 min. Fixed cells were labelled 1 μg ml^{-1} Bocillin FL at room temperature for 10 min and examined by deconvolution microscopy. The raw and deconvolved images are shown. The fluorescence images are maximum intensity projections of z-stack images acquired at 200 nm z-intervals. Scale bars 5 μm.

B. Individual SJF4642 (*S. aureus* SH1000 *geh::ezrA-snap ΔezrA::tet*) cells labelled with SNAP-Cell TMR-Star , HADA and Bocillin FL were selected to highlight localisation of EzrA-SNAP TMR-Star, PBPs and sites of new peptidoglycan incorporation. The fluorescence images of cells at different stages of the cell cycle are maximum intensity projections of deconvolved z-stack images acquired at 200 nm z-intervals (i-ix). Scale bars 1 μm.

C. The linear profiles represent fluorescence intensities of HADA (blue), Bocillin FL (yellow) and EzrA-SNAP TMR-Star (magenta) in arbitrary units (a.u.) measured along the white lines across the individual cells in the merged images. The images are maximum intensity projections of deconvolved z-stack images acquired at 200 nm z-intervals of SJF4642 (*S. aureus* SH1000 *geh::ezrA-snap ΔezrA::tet*) labelled as described in (A). Scale bars 1 μm.

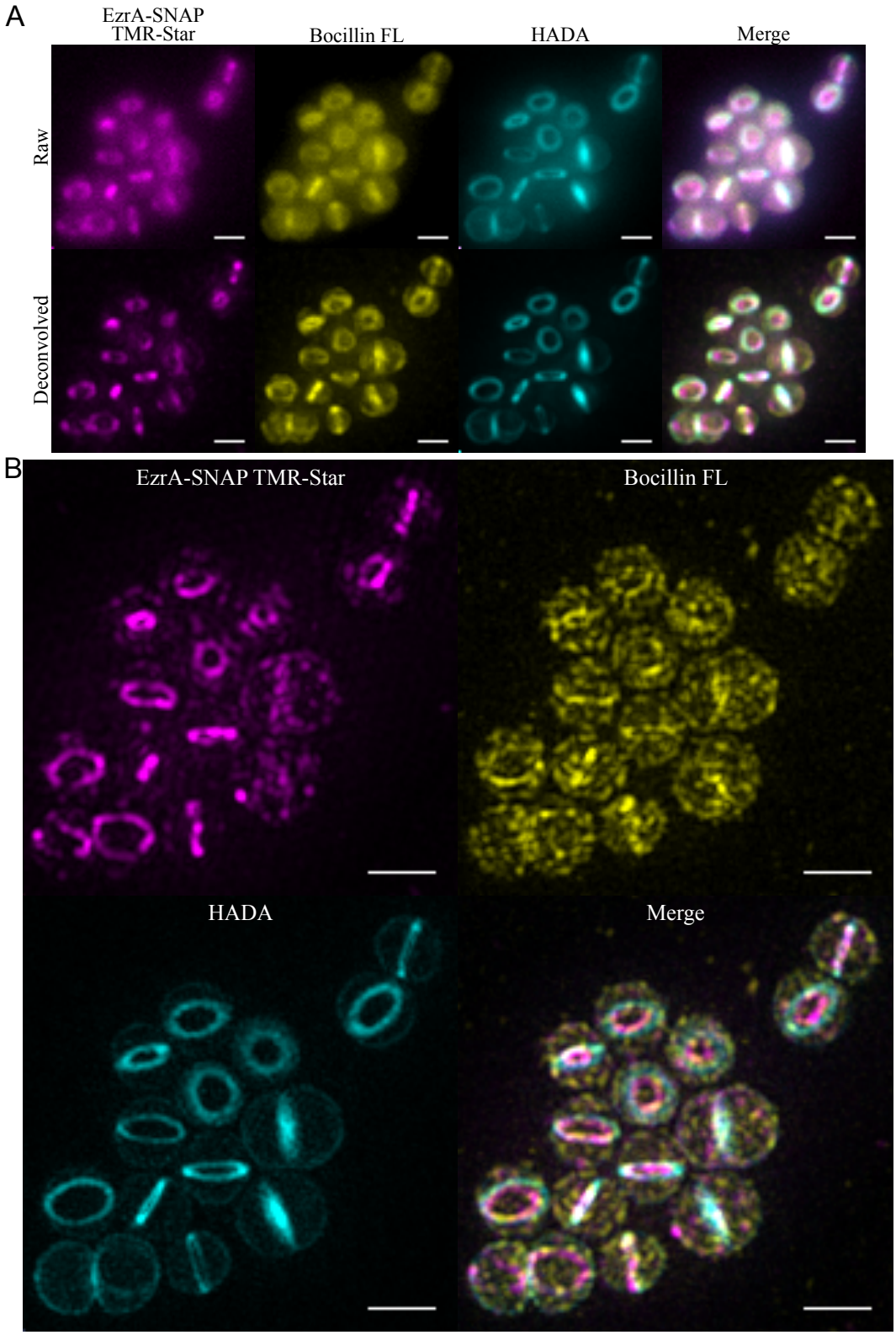

Figure 4.22. Colocalisation of EzrA, PBPs and newly synthesised peptidoglycan by SIM

SJF4642 (*S. aureus* SH1000 *geh::ezrA-snap ΔezrA::tet* grown to early-exponential was labelled with SNAP-Cell TMR-Star and HADA. Fixed cells were labelled with Bocillin. Data obtained by conventional fluorescence microscopy, raw and deconvolved images (A) and by SIM (B) for the same field of view are presented. Fluorescence images are maximum intensity projections of z-stacks acquired at 125 nm z-intervals. Scale bars 1 μm.

Surprisingly, Bocillin FL, which uniformly labelled cell septa and gave less strong but apparent and uniform surface signal by conventional fluorescence microscopy, was revealed to be distributed in a form of coarse grains around the cell surface by SIM (Figure 4.22). Additionally, Bocillin FL labelling at the septum was largely lost following SIM reconstruction, resulting in subtle contrast between midcell and surface features (Figure 4.22). This made the juxtaposition of EzrA, PBPs and HADA at high-resolution difficult to present and analyse due to technical constraints resulting from the loss of information on PBPs localisation. Also a poor signal-to-noise ratio was associated with all three fluorophores. The final image possibly contains artefacts incorporated during the reconstruction process (Appendix II).

4.2.6 Effect of PC190723 on EzrA and nascent peptidoglycan localisation

EzrA colocalises with FtsZ to the nascent division site and its midcell localisation has been shown to be FtsZ dependent (Steele et al., 2011). FtsZ depleted cells are enlarged as the cell wall synthesis machinery is active but dispersed around the cell (Pinho and Errington, 2003; Steele et al., 2011). PC190723 is a 3-methoxybenzamide derivative that inhibits bacterial cell division by stabilising FtsZ polymers (Haydon et al., 2008). PC190723 decreases the FtsZ critical concentration required for its polymerisation, interferes with the FtsZ GTPase activity and thus prevents disassembly of FtsZ polymers into monomers (Haydon et al., 2008; Elsen et al., 2012). This FtsZ inhibitor has been proposed to be a functional homologue of taxol (Haydon et al., 2008). The PC19073 binding site on FtsZ was mapped to an analogous position to that taxol bound to tubulin (Haydon et al., 2008). The effect of PC19072 on EzrA and peptidoglycan synthesis was tested.

SJF4388 (*S. aureus* SH1000 *geh::ezrA-eyfp ΔezrA::tet*) was grown to early-exponential phase. PC190723 at a concentration of 10 μg ml^{-1}, which is 10 times higher than the MIC reported for *S. aureus* (Haydon et al., 2008), was added to the cell culture. At each time point 1 ml of the culture was removed and grown with 500 μM HADA at 37^{o}C for 5 min. Fixed cells were examined by fluorescence microscopy. Initially, before the PC190723 addition, EzrA-eYFP formed uniform rings and together with HADA was present at the septum (Figure 4.23A, control). Immediately just after inhibitor addition to the cell culture EzrA-eYFP was found to be dispersed in some cells (~19% cells)

(Figure 4.23A, 0 min and Bii). In such cells EzrA-eYFP did not form a continuous ring. No effect however on peptidoglycan incorporation was observed (Figure 4.23A, 0 min and Biii). Further incubation with PC190723 resulted in a larger proportion of cells with partially dissipated EzrA-eYFP localisation (Figure 4.23A, 5-10 min and Bii). Additionally, cells with EzrA-eYFP distributed across the cell membrane started to appear (Figure 4.23A, 5-10 min). What is more, at 5-10 min time points cells with disrupted peptidoglycan incorporation emerged (Figure 4.23Biii). In these cells HADA accompanied aberrant EzrA-eYFP localisation (Figure 4.23A, 5-10 min). Longer incubation with PC190723 led to enlarged cells with EzrA-eYFP foci distributed around the cell membrane and peptidoglycan dispersed over the cell surface (Figure 4.23A, 15-25 min and Bi). Nevertheless cells with septal HADA incorporation could be still observed until the 25 min time point (Figure 4.23). After one generation time (approximately 25 min) the majority of cells were enlarged with EzrA-eYFP and HADA located around the cell membrane/surface (Figure 4.23A, 25 min and Bi). Sporadically cells showing EzrA-eYFP and HADA septal-like patterns could be found among 'swollen' cells (Figure 4.23A, 30-45 min). Prolonged incubation resulted in bacterial cell death (Figure 4.23, 60-120 min). Only enlarged cells were present after 60 min incubation time (Figure 23.Bi). At this time point cells with no signal from HADA were observed and the amount of such cells increased with the incubation time (Figure 4.23A, 60-120 min). Lack of HADA incorporation indicated inhibition of peptidoglycan synthesis. Furthermore, cells that were no longer spherical, probably due to cell lysis, were present (Figure 4.23A, 60-120 min). Interestingly, in many cells both with and without active HADA incorporation, EzrA-eYFP not only was concentrated at the cell membrane but also it gave amorphous fluorescent aggregates associated with the cell cytoplasm (Figure 4.23A, 90-120 min). Two-hour exposure to PC190723 resulted in EzrA-eYFP delocalisation and dispersed peptidoglycan synthesis, enlarged cell size and cell lysis. This effect of PC190723 was found to be analogous to the consequences of FtsZ depletion in *S. aureus* (Pinho and Errington, 2003; Steele et al., 2011). PC19073 rapidly interfered with EzrA-eYFP localisation and later disrupted peptidoglycan synthesis.

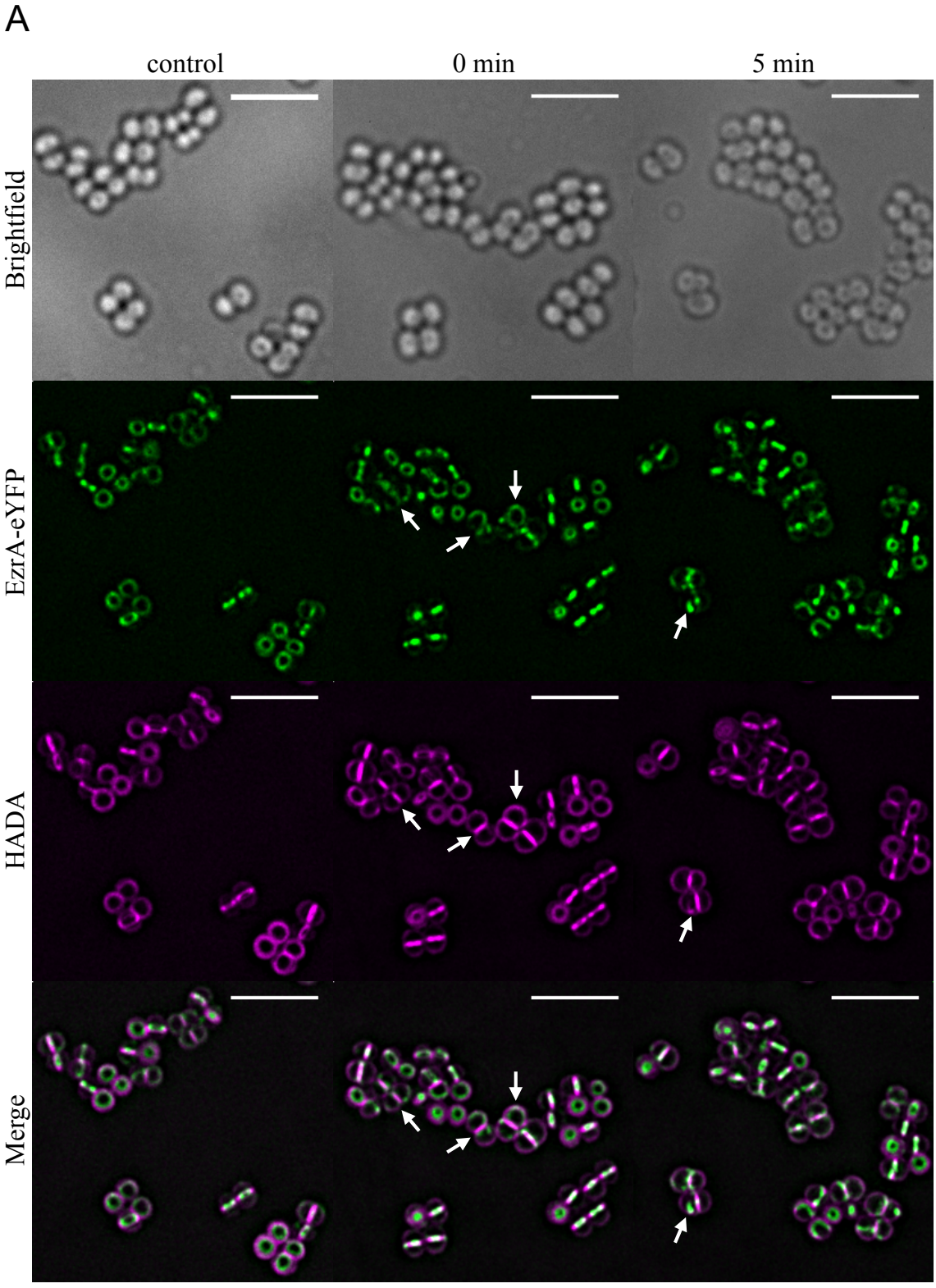
A
control
0 min
5 min
Brightfield
EzrA-eYFP
HADA
Merge

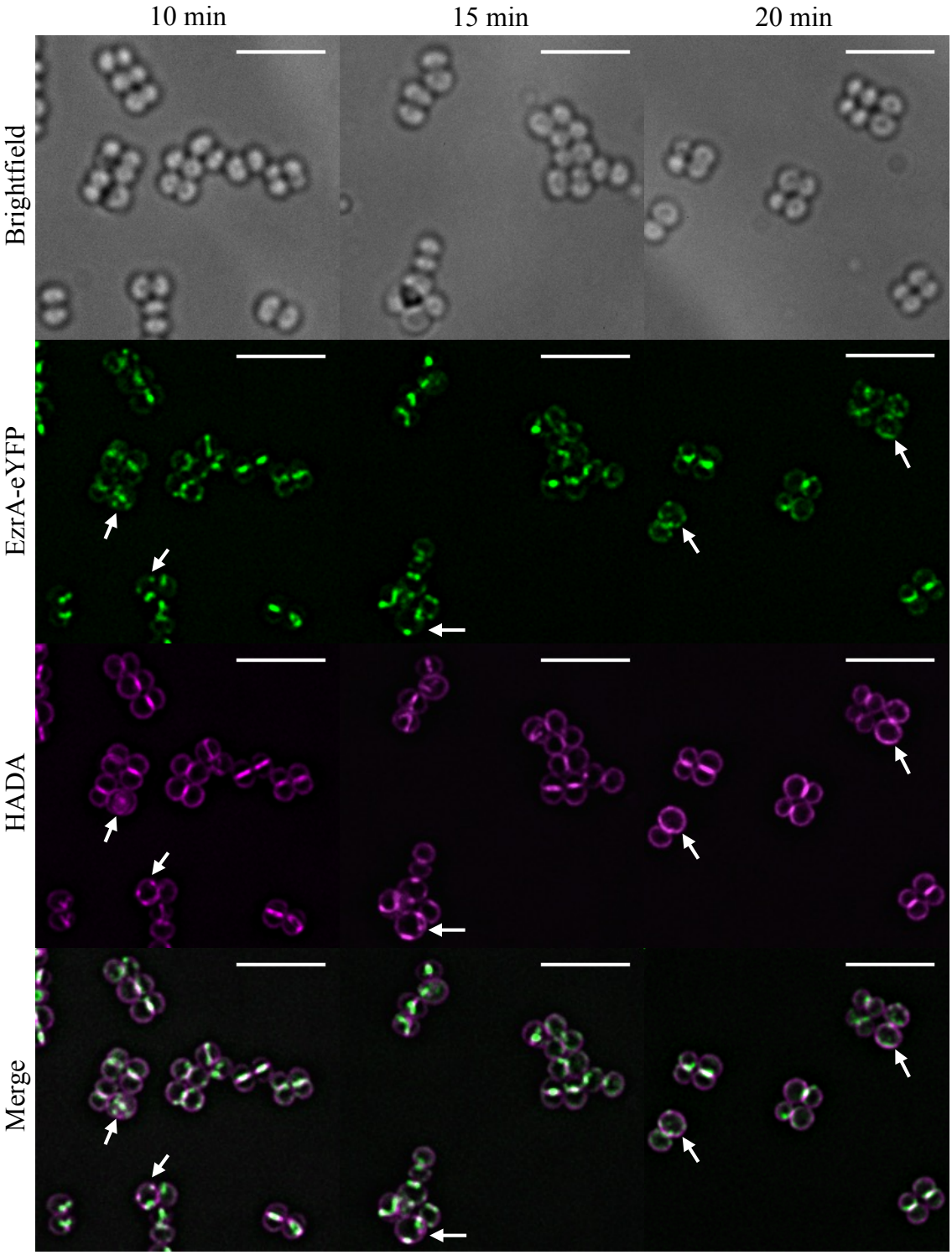
10 min
15 min
20 min
Brightfield
EzrA-eYFP
HADA
Merge

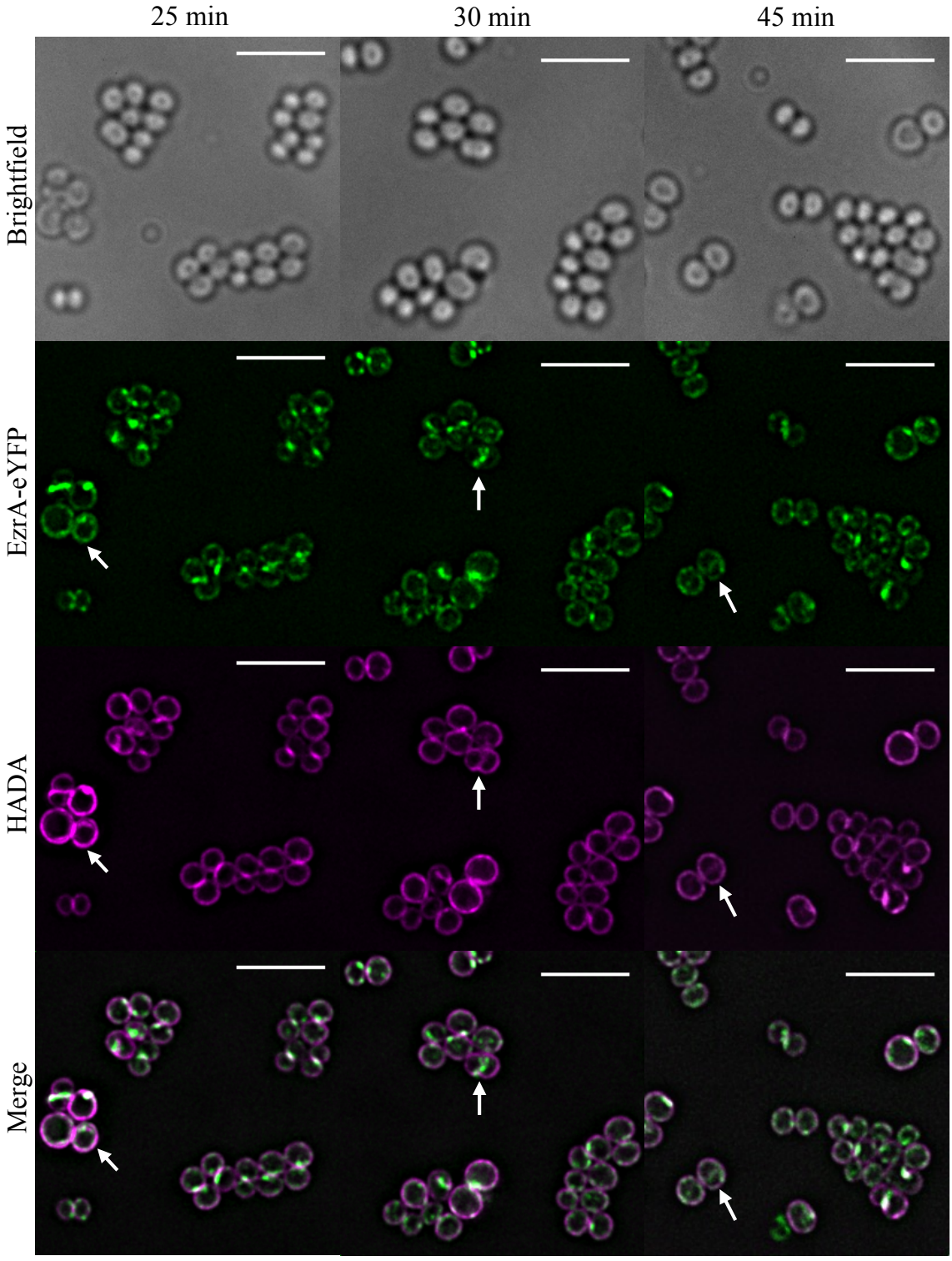
25 min
30 min
45 min
Brightfield
EzrA-eYFP
HADA
Merge

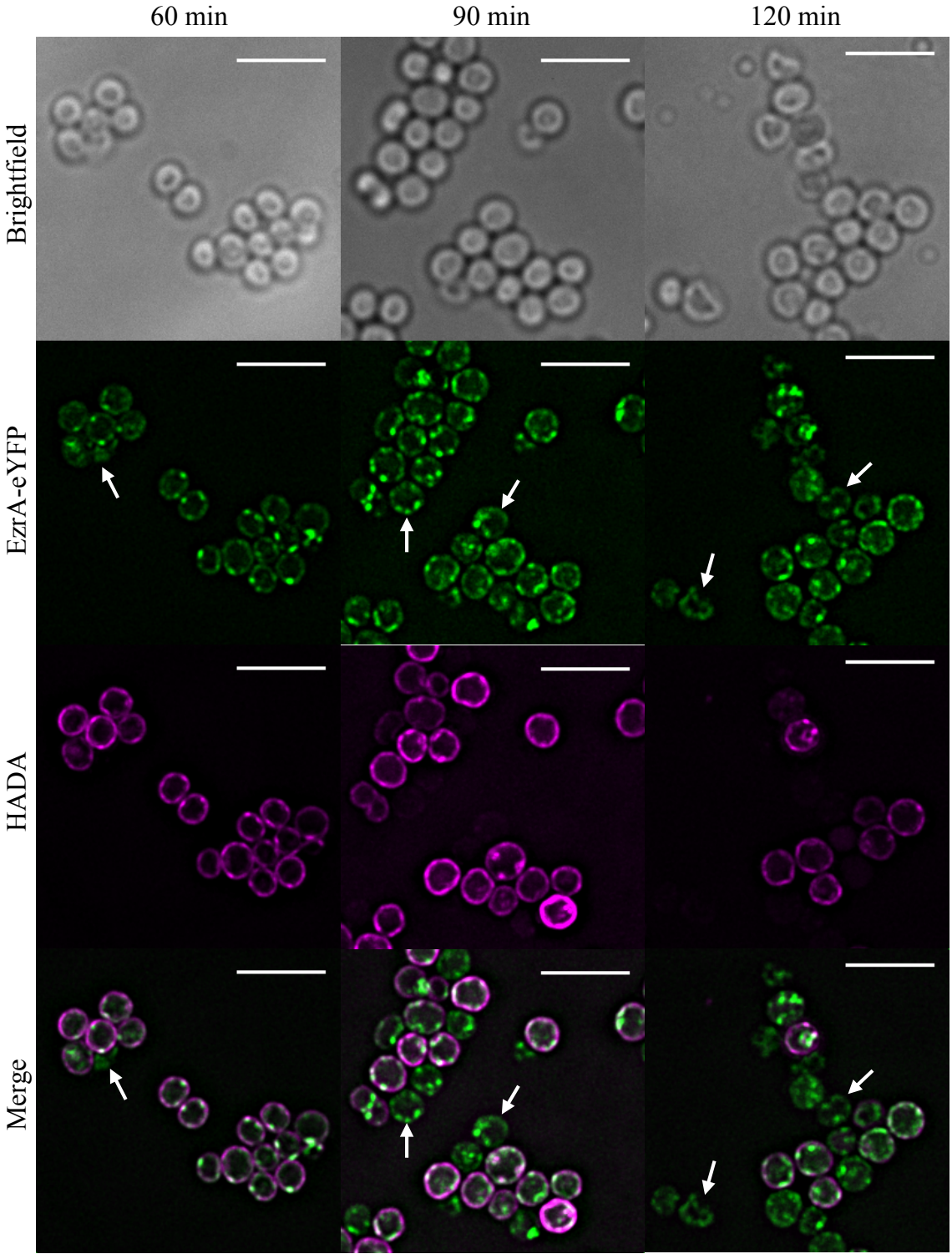
60 min
90 min
120 min
Brightfield
EzrA-eYFP
HADA
Merge

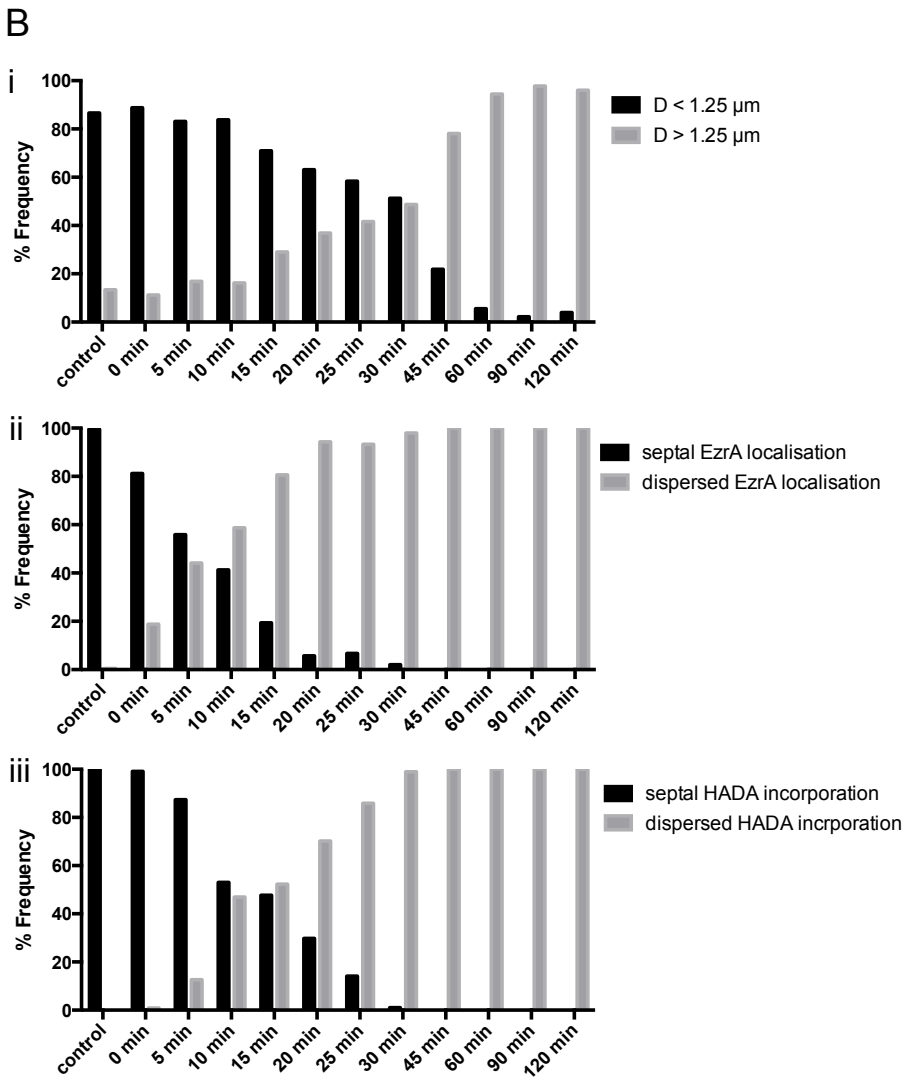

Figure 4.23. Effect of PC190723, the FtsZ inhibitor on EzrA localisation and peptidoglycan synthesis in *S. aureus*

A. SJF4388 (*S. aureus* SH1000 *geh::ezrA-eyfp ΔezrA::tet*) was grown to early-exponential phase and PC190723 (10 µg ml^{-1}) was added. At each time point (indicated in min) 1 ml of culture was removed and incubated with 500 µM HADA at 37^{o}C for 5 min, fixed and examined by fluorescence microscopy. The control is SJF4388 grown without the FtsZ inhibitor labelled with HADA. Cells indicated with white arrows: 0 min, EzrA-eYFP is dispersed with no effect on peptidoglycan incorporation; 5-10 min delocalised EzrA-eYFP is accompanied by nascent peptidoglycan incorporation; 15-25 min, enlarged cells with EzrA-eYFP foci distributed around cell membrane; 30-45 min, cells with septal-like EzrA-eYFP and HADA localisation; 60-120 min; lysed or enlarged cells with inhibited peptidoglycan synthesis. Fluorescence images are maximum intensity projections of deconvolved z-stack images acquired at 200 nm z-intervals. The same contrast was adjusted for EzrA-eYFP, HADA images were treated in the same manner. Scale bars 5 µm.

B. Frequency of cellular phenotypes of SJF4388 (*S. aureus* SH1000 *geh::ezrA-eyfp ΔezrA::tet*) grown in the presence of 10 µg ml^{-1} PC190723 and labelled with HADA as described in (B). Cells were grouped based on their diameter (D) (i), EzrA localisation (ii) and HADA incorporation (iii). At least 100 cells were measured for each time point.

4.3 Discussion

In this chapter an attempt to localise EzrA in a context of cell division proteins and structural components in *S. aureus* was made. EzrA interacts with cytoplasmic (FtsZ), membrane (DivIB) and peptidoglycan biosynthetic (PPB1, PBP2) proteins and that is why EzrA has been proposed to act as a protein framework between other cell division components (Steele et al., 2011). Since in *S. aureus* no homologues of MapZ, which in *Streptococcus pneumoniae* locates to the septa before FtsZ (Fleurie et al., 2014a; Holečková et al., 2015), are predicted to be present in *S. aureus,* FtsZ remains the first known cell division component that localises to the division site. As a result of FtsZ and EzrA interaction, revealed in a bacterial two-hybrid analysis, and mutual dependence - FtsZ depletion leads to EzrA delocalisation and vice versa (Steele et al., 2011; Jorge et al., 2011), colocalisation of these two crucial components was investigated.

FtsZ is an essential protein and since FtsZ fluorescent fusions have been shown to not be completely functional and be able to fully substitute for the native protein, except for the FtsZ-GFP fusion in *B. subtilis* (Ma et al., 1996; Osawa and Erickson, 2005; Strauss et al., 2012) an *S. aureus* strain, in which an FtsZ fusion is produced in a controllable manner in the presence of the endogenous FtsZ protein, was constructed. EzrA-eYFP was the only fully functional, and compatible with STORM, fluorescent fusion of EzrA (Chapter 3). In order to be able to colocalise it with FtsZ, an FtsZ fluorescent protein with emission spectra that did not overlap with eYFP fluorescence was designed. Since the experience with EzrA showed that some of its fluorescent fusions were not produced (mEos2, PSmOrange), and others were not stable (PAmCherry1), an alternative method to fluorescent proteins, the SNAP-tag technique, was chosen for FtsZ labelling. The advantage of the SNAP-tag is that it is a small protein of ~18 kDa and it gives a free choice of fluorophores, which means that one tag can be stained with different dyes (Keppler et al., 2003; Gautier et al., 2008). Furthermore, commercially available dyes for SNAP labelling, TMR-Star and SiR, were reported to be cell permeable, which is important as FtsZ is in the cytoplasm, and to have photophysical properties making them suitable for single-molecule localisation-microscopy studies (Klein et al., 2011; Lukinavičius et al., 2013). FtsZ-SNAP was produced in *S. aureus* and when labelled with either SNAP-Cell TMR-Star or SNAP-Cell 647-SiR it showed

the expected ring-like pattern (Figures 4.3A and 4.7B). Additionally, 50 μM IPTG was enough to produce relatively a low but sufficient number of FtsZ-SNAP molecules (FtsZ-SNAP levels comprised 16% of native FtsZ levels), which could be easily visualised by conventional fluorescence microscopy and more importantly did not disrupt cell morphology (Figure 4.3). Unfortunately, several attempts to image FtsZ-SNAP in STORM, using either TMR-Star or 647-SiR as fluorescent reporters, finished with no success. STORM reconstructions showed FtsZ-SNAP aggregates dispersed throughout the cell (Figures 4.5 and 4.6B). This was not in agreement with data from conventional fluorescence microscopy and indicated that either the imaging conditions (SNAP dyes concentrations, buffering conditions, lasers powers) were not optimal or the FtsZ-SNAP-fluorophore conjugate was not stable. Western blot analysis showed that FtsZ-SNAP was not degraded (Figure 4.3B and D), therefore the dispersed signal obtained in STORM reconstructions might result from an unstable covalent bond formed between FtsZ-SNAP and a SNAP substrate. The covalent bond might have broken upon illumination with a laser and the detached fluorophore was freely floating in the cell cytoplasm. What is more, STORM reconstructions suggested formation of aggregates in cells producing FtsZ-SNAP (Figure 4.6B). Such clumps were not however observed in images from diffraction limited microscopy, suggesting that the aggregates could be artefacts incorporated into the final image during the data processing and reconstruction steps.

Failure to image FtsZ-SNAP by STORM led to development of another STORM compatible fluorescent fusion of FtsZ, FtsZ-mEos2. FtsZ is a conserved protein between bacterial species (Adams and Errington, 2009) and FtsZ-mEos2 was successfully employed to reveal helical conformations of the Z-ring in *E. coli* (Fu et al., 2010). An *S. aureus* strain producing FtsZ-mEos2, analogues to the *S. aureus* FtsZ-SNAP strain, was constructed. In this strain induction with an optimal concentration of 100 μM IPTG for microscopy visualisation resulted in FtsZ-mEos2 levels comparable to the native FtsZ levels (Figure 4.14). This means that FtsZ-mEos2 was every second FtsZ molecule in a cell and there were twice as many FtsZ molecules than in the wild type strain. This FtsZ overproduction did not however alter cell morphology (Figure 4.14A), the effect of FtsZ overproduction reported for *S. aureus* (Liew et al., 2011). In *S. aureus* FtsZ-mEos2 formed a Z-ring (Figure 4.14), suggesting that the fusion was partly functional as it mimicked the localisation pattern of native

FtsZ obtained by immunofluorescence (Steele et al., 2011). Imaging at super-resolution showed that not all FtsZ-mEos2 molecules were recruited to the division site as they were also present in the cytoplasm and the peripheral membrane (Figures 4.18 and 4.19). This was not surprising as calculations from quantitative fluorescence imaging of FtsZ-GFP in *E. coli* and *B. subtilis* suggested that about one third of FtsZ molecules were incorporated into the Z-ring (Anderson et al., 2004; Geissler et al., 2007). What is more, STORM showed that FtsZ-mEos2 formed heterogeneous rings (Figure 4.16). Two-colour microscopy of FtsZ and peptidoglycan synthesis revealed that FtsZ formed wide structures preceding peptidoglycan and large foci marking the nascent septum inside the surrounding cell wall (Figures 4.18 and 4.19). Localisation of FtsZ in *S. aureus* and *B. subtilis* was previously studied using another high-resolution microscopy technique, 3D-SIM where a bead-like model of the FtsZ ring was proposed (Strauss et al., 2012). In this model the Z-ring is composed of ~12 FtsZ 'beads' – regions of high FtsZ density, implying discontinuous ring structures (Strauss et al., 2012). Such a bead-like pattern was not however reported in another study, in which the same microscopy technique was used to visualise single rings of FtsZ-GFP and double-ring structures of DivIVA-GFP in *B. subtilis* (Eswaramoorthy et al., 2011). Although STORM, which reaches a higher resolution than SIM, did not confirm presence of well-defined FtsZ clusters, it supported non-uniform distribution of FtsZ in the ring. The pattern obtained for FtsZ-mEos2 in *S. aureus* resembles the one for FtsZ in *Caulobacter crescentus*. PALM imaging of FtsZ-Dendra2 in *C. crescentus* showed that FtsZ formed thick and non-uninform density rings (Holden et al., 2014). Two models of FtsZ organisation in bacterial species have been proposed. In a 'lateral interaction' model either a single continuous ring or FtsZ protofilaments wrap the inner surface of the cell membrane or FtsZ polymers form a compressed helix stabilised by lateral interactions (Milam et al., 2012). In a 'patchy band' model the FtsZ ring consists of short FtsZ protofilaments that are loosely arranged along the division site resulting in a discontinuous band. (Holden et al., 2014) This model is supported by electron cryotomography (ECM), which showed a single and radial layer of short FtsZ polymers distributed along the division site in *C. crescentus* (Li et al., 2007; Holden et al., 2014). *S. aureus* STORM data on FtsZ-mEos2 correlates closely with FtsZ-Dendra2 in *C. crescentus* by PALM (Holden et al., 2014) and supports the 'patchy band' model of FtsZ organisation in *S. aureus*. The question that arises here is how accurate a presentation of the native FtsZ structure is FtsZ-mEos2? FtsZ-mEos2 levels were close

to levels of native FtsZ, did nor perturb cell morphology and gave similar localisation pattern to FtsZ-GFP and FtsZ-CFP in conventional fluorescence microscopy (Jorge et al., 2011; Liew et al., 2011). However the fact that FtsZ-mEos2 was every second FtsZ molecule present in a cell does not mean that the fusion was every second FtsZ molecule incorporated into the Z-ring. Heterogeneous distribution of FtsZ could be thus a representation of heterogeneous incorporation of the fluorescent protein rather than representing a general non-uniform distribution of FtsZ.

As no STORM data for FtsZ-SNAP were obtained, two-colour STORM of EzrA-eYFP and FtsZ-SNAP was not possible. Although eYFP and mEos2 were suggested as a possible compatible pair of fluorophores in single-molecule localisation-microscopy (Wang et al., 2011), none of the available STORM instruments (homebuilt or commercial) had a set up that would allow for imaging of both EzrA-eYFP and FtsZ-mEos2. Conventional fluorescence microscopy of EzrA-eYFP and FtsZ-SNAP TMR-Star showed that the proteins localised together to the same location (Figure 4.6A and B). EzrA-eYFP could be observed on the outer surface of the FtsZ rings and spots during all stages of the cell cycle, which in combination with previous publications supports the EzrA role as an FtsZ membrane tethering protein (Steele et al., 2011; Cleverley et al., 2014). The recently solved crystal structure of *B. subtilis* EzrA cytoplasmic fragment revealed that EzrA consists of triple-helical repeats and is a structural homologue of eukaryotic spectrin, a protein involved in actin filament stabilisation and linking the cytoskeleton to membrane proteins (Cleverley et al., 2014). Based on the EzrA crystal structure and biochemical assays, which identified which EzrA repeats are responsible for EzrA interaction with FtsZ, a model in which EzrA forms an arch that traps FtsZ polymers between the curve and the cell membrane, so that FtsZ polymers are positioned close to the membrane but their lateral interactions are prevented, was suggested (Cleverley et al., 2014). Colocalisation of EzrA-eYFP and FtsZ-SNAP TMR-Star in *S. aureus* showed that FtsZ rings were closed inside EzrA rings, indicating that FtsZ is located further away from the membrane than EzrA (Figure 4.6 B and C). Therefore a model in which FtsZ interacts with EzrA but binds on the outside of the EzrA arch (Cleverley et al., 2014) is more favourable.

Two- and three-colour microscopy of EzrA and peptidoglycan labelled with fluorescent derivatives of D-Ala (HADA and TADA) showed that EzrA and nascent peptidoglycan

were closely positioned during all stages of the cell cycle (Figures 4.8 and 4.9). EzrA rings appeared to be inside septal peptidoglycan rings (Figures 4.8 and 4.9), which was expected since the cell membrane serves as a boundary and incorporates a physical distance between EzrA, a membrane associated protein, to which a cytoplasmic C-terminus a fluorescent tag was attached, and proteins involved in peptidoglycan synthesis located on the outside of the cell membrane. SIM and STORM of EzrA and nascent peptidoglycan synthesis confirmed the juxtaposition of EzrA 'patches' and newly synthesised peptidoglycan (Figures 4.10, 4.11 and 4.13), suggesting that peptidoglycan synthesis may by directed from EzrA 'patches'. Pulse-chase labelling of peptidoglycan revealed that the off-septal signal from EzrA is placed on a plane perpendicular to the current and the previous division planes (Figure 4.9). Additionally, FtsZ was also observed to give a peripheral signal (Figures 4.4D, 4.18-20) and since it was found accompanied by EzrA (Figures 4.6 and 4.20), these two proteins may localise together and mark the future plane of division. Interestingly, neither EzrA nor FtsZ were showed to completely leave the site of a closing septal disc (Figure 4.6 and 4.20), indicating that remaining EzrA and FtsZ molecules may be directly incorporated from the old septum to the new EzrA and FtsZ rings formed at the next division plane. Utilisation of Bocillin FL revealed that peptidoglycan synthesis occurred in close proximity to penicillin binding proteins (PBPs) (Figure 4.21). Bocillin FL however is not selective for one particular PBP and therefore it did not distinguish specific PBPs. Bocillin FL labelled not only septal features but also gave a peripheral signal, suggesting that not all PBPs are recruited to the division septum (Figure 4.21). This off-septal signal was most likely from PBP4, which was recently shown to be present both in the septa and the peripheral cell wall by visualisation of a PAmCherry1 fusion by PALM (Monteiro et al., 2015). Localisation studies of crucial cell division and structural components in *S. aureus* revealed that they colocalised to the division site and the sequence of their fluorescent signals suggests their hierarchical organisation and localisation (peptidoglycan→PBPs→EzrA→FtsZ) to the division site (Figures 4.20 and 4.21). This indicates that in *S. aureus* cell division components are arranged into a protein network that extends from the cytoplasm through the cell membrane to the periplasm. The sequence of proteins localisation in division septa correlated with their interactions exhibited in a bacterial two-hybrid screen (Steele et al., 2011). FtsZ showed interactions only with EzrA and FtsA, whereas EzrA reacted with both cytoplasmic proteins (FtsZ, SepF) and almost all membrane proteins (DivIB, DivIC, FtsL, PBP1,

PBP2, PBP3) (Steele et al., 2011). In cells, in which FtsZ overproduction led to aberrant cell morphology, peptidoglycan incorporation correlated with the pattern of mislocalised FtsZ (4.17D). This confirmed the role of FtsZ in marking division sites. Moreover, this showed that if the interactions between FtsZ and the peptidoglycan biosynthesis machinery are maintained, presumably through the EzrA linker, they are sufficient for FtsZ to guide cell wall synthesis in any direction. In cells lacking FtsZ the peptidoglycan synthesis machinery is active and still produces new peptidoglycan (Pinho and Errington, 2003). However due to FtsZ depletion and lack of its guidance the synthesis machinery is dispersed around the cell membrane, randomly incorporating peptidoglycan which results in cell enlargement but no division septa are formed (Pinho and Errington, 2003). In the experiment, where PC190723 the FtsZ inhibitor was added, an analogous effect to FtsZ depletion was observed. PC190723 immediately disrupted formation of division septa in cells, which were finishing division and their daughter cells were entering a next division cycle (Figure 4.23). This was manifested by mislocalised EzrA, or EzrA absent from its presumptive division plane. Interestingly, PC190723 did not interrupt EzrA localisation in cells, which were actively dividing (Figure 4.23). After approximately one generation time, EzrA formed foci distributed around cell membrane (Figure 4.23). Furthermore, analogously to FtsZ depletion, stabilization of FtsZ polymers by PC190723 resulted in a switch from the directed to a random peptidoglycan synthesis, peptidoglycan incorporation was dispersed all over the cell surface and cells were enlarged (Figure 4.23). FtsZ, which is trapped in protofilaments stabilised by PC190723, cannot disassociate, be recycled and returned to the pool of free FtsZ monomers. The fact that 30-40% of FtsZ available in the cytoplasm is involved in formation of the Z-ring (Anderson et al., 2004; Geissler et al., 2007) indicates that there must be some critical concentration which has to be reached so that FtsZ can polymerise. The FtsZ inhibitor leads to the similar effect as FtsZ depletion, the pool of available FtsZ subunits is reduced and their amount is not enough for the Z-ring to be formed.

CHAPTER 5

Localisation of penicillin binding proteins in *S. aureus*

The work in this chapter was carried out in collaboration with Robert Turner (STORM)

5.1 Introduction

In bacteria cell growth and division are strictly coordinated with peptidoglycan synthesis. The rod-shaped bacteria, *B. subtilis* and *E. coli* have two modes of peptidoglycan synthesis, lateral and septal, and thus two separate types of cell wall synthesis machineries are responsible for cell elongation and cell division (Zapun et al., 2008b). *S. aureus* is considered to produce nascent peptidoglycan mostly at the division septum and therefore the process of growth and cell division is probably determined by one type of peptidoglycan biosynthetic machinery (Pinho and Errington, 2003; Pinho et al., 2013). Penicillin binding proteins (PBPs) are membrane-associated enzymes, which catalyse the last stages of peptidoglycan synthesis (Typas et al., 2012; Pinho et al., 2013). They mediate insertion of new peptidoglycan building blocks into existing peptidoglycan through their transglycosylation and transpeptidation activities. In the transglycosylation reaction peptidoglycan monomers (lipid II) are polymerised into long glycan chains, which are then cross-linked via a transpeptidation reaction (Scheffers and Pinho, 2005; Typas et al., 2012). In contrast to other organisms, such as *B. subtilis* and *E. coli,* which have 16 and 12 PBPs, respectively, *S. aureus* has only 4 PBPs and hence is regarded as a minimalist PBP system and a model organism for cell wall synthesis (Zapun et al., 2008b; Pinho et al., 2013). In *S. aureus* PBP2 is the only high molecular weight (HMW) class A PBP. It is bifunctional having both of transglycosylase and transpeptidase activities (Murakami et al., 1994; Goffin and Ghuysen, 1998; Pinho et al., 2001b). PBP1 and PBP3 belong to HMW class B PBPs exhibiting transpeptidase activity, whereas PBP4 is classified as a low molecular weight (LMW) PBP being a monofunctional transpeptidase (Zapun et al., 2008b; Pinho et al., 2013).

PBP2 is essential for growth and cell division of *S. aureus* (Pinho et al., 2001a). Immunofluorescence of PBP2 and fusing GFP to its N-terminus showed that PBP2

localises to the division site and its localisation is dependent on both FtsZ and EzrA (Pinho and Errington, 2003, 2005; Steele et al., 2011). In the absence of either FtsZ or EzrA, PBP2 is not recruited to the division site but is dispersed all over the cell membrane (Pinho and Errington, 2003; Steele et al., 2011). Interestingly, PBP2 not only requires FtsZ and EzrA for septal localisation but also its transpeptidation substrate (Pinho and Errington, 2005). D-cycloserine inhibits formation of a D-Ala-D-Ala dipeptide, which comprises two terminal residues of the stem peptide of a peptidoglycan building block (Neuhaus and Lynch, 1964; Lambert and Neuhaus, 1972; Typas et al., 2012). The D-Ala-D-Ala bond is involved in cross-linking a D-Ala residue present in the 4th position of one pentapeptide, via a pentaglycine bridge, to the L-Lys residue in the 3rd position on another pentapeptide (Scheffers and Pinho, 2005; Typas et al., 2012; Pinho et al., 2013). Addition of D-cycloserine results in formation and accumulation of a peptidoglycan precursor lacking two last D-Ala residues (Sieradzki and Tomasz, 1997). In the presence of D-cyloserine, GFP-PBP2 was dispersed all over cell surface, similarly to the absence of FtsZ or EzrA (Pinho and Errington, 2003, 2005; Steele et al., 2011). Studies on a crystal structure of the periplasmic PBP2 fragment revealed that it has two lobes, a C-terminal transpeptidase domain and an N-terminal transglycosylase domain linked by a short β-rich spacer (Figure 5.1) (Lovering et al., 2007). The transpeptidase domain was found to have a structural homology to the transpeptidase domain of PBP1A from *S. pneumoniae.* Its active site has the characteristic SXXK, (S/Y)X(N/C), and (K/H)(T/S)G motifs (Lovering et al., 2007). The transglycosylase domain was shown to be primarily α-helical and to possess two segments, a globular 'head' and a small 'jaw' (Figure 5.1) (Lovering et al., 2007). The 'head' subdomain precedes the β-rich linker, has a structural similarity to bacteriophage λ lysozyme and contains the first putative catalytic residue, Glu114. The 'jaw', which is situated beneath the 'head' and might be partly submerged in the membrane, contains the second putative catalytic residue, Glu171 (Figure 5.1) (Lovering et al., 2007). The transglycosylase domain of *S. aureus* PBP2 has five motifs typical for the mono- and bifunctional peptidoglycan transglycosylases. Motifs I and III possess the catalytic residues, Glu114 and Glu171, motifs IV and V are involved in maintaining the structure of the transglycosylase domain, while motif II is responsible for substrate recognition (Lovering et al., 2007).

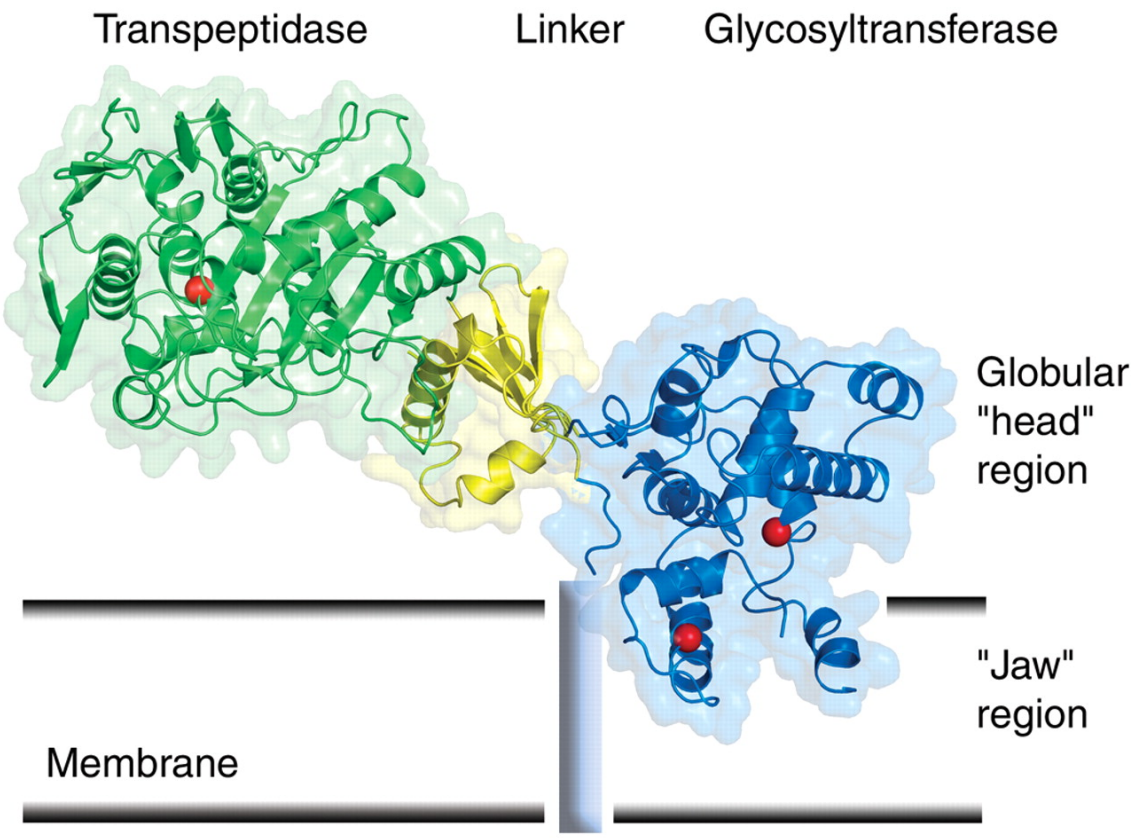

Figure 5.1. Crystal structure of *S. aureus* PBP2

The N-terminal transglycosylase domain (blue) consists of two subdomains, a globular 'head' and a partly membrane buried 'jaw'. The C-terminal transpeptidase domain (green) is linked to the transglycosylase domain by the short β-rich fragment (yellow). The catalytic glutamic acids for the transglycosylase domain and the catalytic serine of the transpeptidase domain are represented by red spheres. The transmembrane domain is shown as a blue rectangle. Reproduced from (Lovering et al., 2007).

PBP1 is a monofunctional transpeptidase that is a crucial for growth and cell division of *S. aureus* (Wada and Watanabe, 1998; Pereira et al., 2007). *S. aureus* PBP1 shows a high degree of sequence similarity to PBP3, an essential cell division enzyme in *E. coli* (Pereira et al., 2007). Consistent with its function and homology to *E. coli* PBP3, *pbp1* is organised in a cluster of divisome and cell wall synthesis (*dcw*) genes together *with mraZ, mraW, ftsL, mraY, murD divIB, ftsA* and *ftsZ* genes (Pucci et al., 1997). Immunofluorescence microscopy revealed that PBP1 localises to the division septum and its depletion results in enlarged cells with incomplete septa, indicating its role in septum formation (Pereira et al., 2007, 2009). It has been suggested that the essential role of PBP1 in cell division does not depend on transpeptidase activity but its physical presence, as mutants producing inactive PBP1 were viable and non-functional PBP1 localised to the septum (Pereira et al., 2009).

PBP4 is the only *S. aureus* PBP classified as a LMW PBP. Biochemical studies showed that PBP4 could work as a carboxypeptidase, a transpeptidase and a β-lactamase (Kozarich and Strominger, 1978; Navratna et al., 2010). The crystal structure of PBP4 revealed that its N-terminal domain has a transpeptidase- and a β-lactamase-like fold and the C-terminal all β-sheet domain resembling D,D-carboxypeptidases found in other organisms (Navratna et al., 2010). More recently it has been shown that PBP4 primarily acts as a transpeptidase *in vivo* and *in vitro* (Qiao et al., 2014). This is further supported by genetic studies, which showed that although PBP4 is not essential, its deletion results in decreased cross-linking and stiffness of peptidoglycan, whereas PBP4 overproduction leads to greater resistance to β-lactams (Wyke et al., 1981; Henze and Berger-Bächi, 1996; Memmi et al., 2008; Loskill et al., 2014). PBP4 is recruited to the division site by an unknown wall teichoic acid (WTA) synthesis intermediate, as in the absence of TarO (TagO), the first protein of the WTA biosynthesis pathway, PBP4 is dispersed throughout the cell membrane (Atilano et al., 2010). PBP4 did not interact with TarO in a bacterial two-hybrid system. Also inactive but still division site localised TarO, was not sufficient to recruit PBP4 to the septum, indicating a role of WTA synthesis in temporal and spatial regulation of PBP4 localisation (Atilano et al., 2010). Additionally, localisation of PBP4-PAmCherry1 in super-resolution revealed that not all PBP4 molecules were localised to the division septa but a significant number was present in the membrane periphery (Monteiro et al., 2015). This suggests that PBP4 may not only be involved in peptidoglycan synthesis during septum formation, but in

remodelling of peripheral peptidoglycan, which was suggested based on observations that PBP4 efficiently exchanges a terminal D-Ala for an exogenous D-Ser (Qiao et al., 2014; Monteiro et al., 2015).

PBP3 is a second monofunctional transpeptidase in *S. aureus* (Yoshida et al., 2012). It was shown to interact with *S. aureus* essential cell membrane components: EzrA, DivIB, DivIC and PBP2, indicating its role in cell division (Steele et al., 2011). PBP3 itself is not a crucial enzyme and its role and localisation in *S. aureus* remain unknown (Pinho et al., 2000, 2013).

Methicillin-resistant *S. aureus* (MRSA) possesses an extra exogenously acquired PBP, PBP2A (Hartman and Tomasz, 1984). PBP2A is a HMW class B PBP and has reduced affinity towards β-lactam antibiotics (Hartman and Tomasz, 1984; Pinho et al., 2001a). In MRSA, PBP2A is able to take over PBP2 transpeptidase activity but not its transglycosylase function (Pinho et al., 2001a; b). MRSA was shown to grow when PBP2 was depleted, indicating that when there is no antibiotic pressure PBP2A is able to replace PBP2 (Pinho et al., 2001a). However in the absence of PBP2 or when its transglycosylase domain was inactivated MRSA showed reduced resistance to β-lactams, implying that the cooperative action of PBP2 and PBP2A is required for cell survival in the presence of β-lactams (Pinho et al., 1997, 2001b). In MRSA in the presence of oxacillin PBP2 is still recruited to the septum, suggesting that PBP2A interactions maintain septal localisation of PBP2 (Pinho and Errington, 2005). Interestingly, even though PBP2A was shown to be able to replace the transpeptidase activity of PBP2 in MRSA, it cannot mimic the function of PBP1, which possesses only a single transpeptidase domain, as MRSA loses its viability upon depletion of PBP1 (Pereira et al., 2007).

PBP2 is not the only protein that has a transglycosylase activity in *S. aureus*. SgtA and Mgt (SgtB) are membrane bound non-penicillin binding monofunctional transglycosylases (Park and Matsuhashi, 1984; Wang et al., 2001; Heaslet et al., 2009; Reed et al., 2011). Neither Mgt nor SgtA are crucial for cell viability, however in the absence of PBP2 transglycosylase activity, the transglycosylase activity of Mgt, but not SgtA, becomes essential (Reed et al., 2011). Both proteins were shown to interact with

each other and PBP1, PBP2 and PBP2A, supporting their role in peptidoglycan polymerisation in *S. aureus* (Reed et al., 2011).

5.1.1 Aims of this chapter

- Localisation of PBP2 at super-resolution

5.2 Results

5.2.1 Localisation of eYFP-PBP2 in *S. aureus*

PBP2 is one of two essential PBPs and the only bifunctional PBP in *S. aureus* (Pinho et al., 2001a; b; Pereira et al., 2007). Previous studies using either immunostaining or a GFP-PBP2 fusion showed that PBP2 localised mainly to the midcell in *S. aureus* (Pinho and Errington, 2003, 2005). The strain producing the fluorescent fusion of PBP2 was merodiploid, which means that it had two copies of the *pbp2* gene, both placed at the *pbp2* locus with the native *pbp2* copy controlled by its native promoter(s) and *gfp-pbp2* placed under the control of the Pxyl promoter (Pinho and Errington, 2005). Single-molecule localisation-microscopy allows for localisation of every single molecule and inadequate labelling, such as using a translational fusion of a protein of interest produced in the presence of an unlabelled endogenous protein, can be a potential source of artefacts. More recently, the GFP-PBP2 fusion was shown to be functional in the MRSA background (Tan et al., 2012). In the presence of an extra PBP, that is PBP2A, GFP-PBP2 localised to the division septum and oxacillin-treated cells did not show any phenotype when the wild type PBP2 was absent (Tan et al., 2012). An *S. aureus* strain, in which the only copy of PBP2 is fused to STORM-compatible eYFP, was constructed.

5.2.1.1 Construction of an *S. aureus* strain in which the only copy of PBP2 is tagged with eYFP

pMAD is a shuttle vector that can be used for allelic exchange in Gram-positive bacteria, such as *B. subtilis*, *Listeria monocytogenes*, and *S. aureus* (Arnaud et al., 2004). The pMAD vector contains pE194, the thermosensitive origin of replication, and it encodes β-galactosidase, which allows for blue/white screening of transformants on plates containing X-Gal (5-bromo-4-chloro-3-indolyl-β-D-galactopyranoside) (Arnaud et al., 2004). Recombination between a target sequence and a homologous sequence carried by the vector occurs in a two-step strategy. Transformation of *S. aureus* with the vector at the permissive temperature results in dark blue colonies. pE194 is thermosensitive and growth at high temperatures (above 30^{o}C) leads to plasmid integration into the chromosome via a single crossover event, resulting in light blue colonies. After plasmid transformation (dark blue colonies) and integration (light blue

colonies), growth at low temperature (30^{o}C and below) leads to a second recombination event - plasmid resolution. Cells that have lost the plasmid form white colonies and these cells are screened for putative mutations (Arnaud et al., 2004). The pMAD system was chosen to construct an *S. aureus* strain, in which the native *pbp2* gene was replaced by an *eyfp-pbp2* fusion.

In *S. aureus* the *pbp2* gene is organised in an operon and can be either co-transcribed with *recU* from the P1 promoter, which is located upstream of *recU*, or alone from the P2 promoter located within the coding sequence of the *recU* gene (Figure 5.2A) (Pinho et al., 1998). The last four nucleotides of *recU* overlap *pbp2* (Figure 5.2B) (Pinho et al., 1998). A 1068 bp fragment (up-recU) covering a region from -390 bp to -1 bp upstream of the *recU* gene, a full copy of the *recU* coding sequence and the P1 and P2 promoters, and a 1062 bp fragment (pbp2') containing the 5′ region (1-1062 bp) of the *pbp2* gene, were amplified from the *S. aureus* SH1000 chromosome by PCR using primer pairs recU-F and recU-R, and pbp2'-F and pbp2'-R, respectively (Figure 5.2B). The *eyfp* gene was PCR amplified from the pKASBAR-EzrA-eYFP plasmid (section 3.2.1) using primers eyfp-pbp2-F and eyfp-pbp2-R (Figure 5.2C). A sequence encoding a 12 amino-acid linker (TSGGGGSGGGGS) was introduced between the *eyfp* and the *pbp2* genes by the eyfp-pbp2-R and pbp2'-F primers (Figure 5.2C). The last four nucleotides of the *recU* gene are ATGA, while the *eyfp* sequence starts ATGGTG. In order to keep the *recU* stop codon and the start codon for the *eyfp-pbp2* fusion within the ORFs overlap, point mutations: G to A, and G to T at positions 4 and 6 of the *eyfp* gene, resulting in Val2Ile substitution, were introduced by the eyfp-pbp2-F and recU-R primers. The PCR products were resolved on a 1% (w/v) agarose gel (Figure 5.2D) and the purified DNA fragments were joined with pMAD cut with *EcoRI* and *BamHI*, by Gibson assembly (Figure 5.2C). The assembly products were used to transform electrocompetent *E. coli* Top10 cells. Transformants were selected at 28°C on LB plates containing ampicillin (100 μg ml^{-1}). Positive clones were verified by plasmid extraction, restriction digestion with *PstI* and confirmed to contain the correct DNA band sizes by electrophoresis on a 1% (w/v) agarose gel (Figure 5.2E). Plasmids were sequenced by GATC Biotech to check for the introduction of mutations during the cloning steps. The resulting vector, pMAD-eYFP-PBP2 (Figure 5.2C) had the expected sequence.

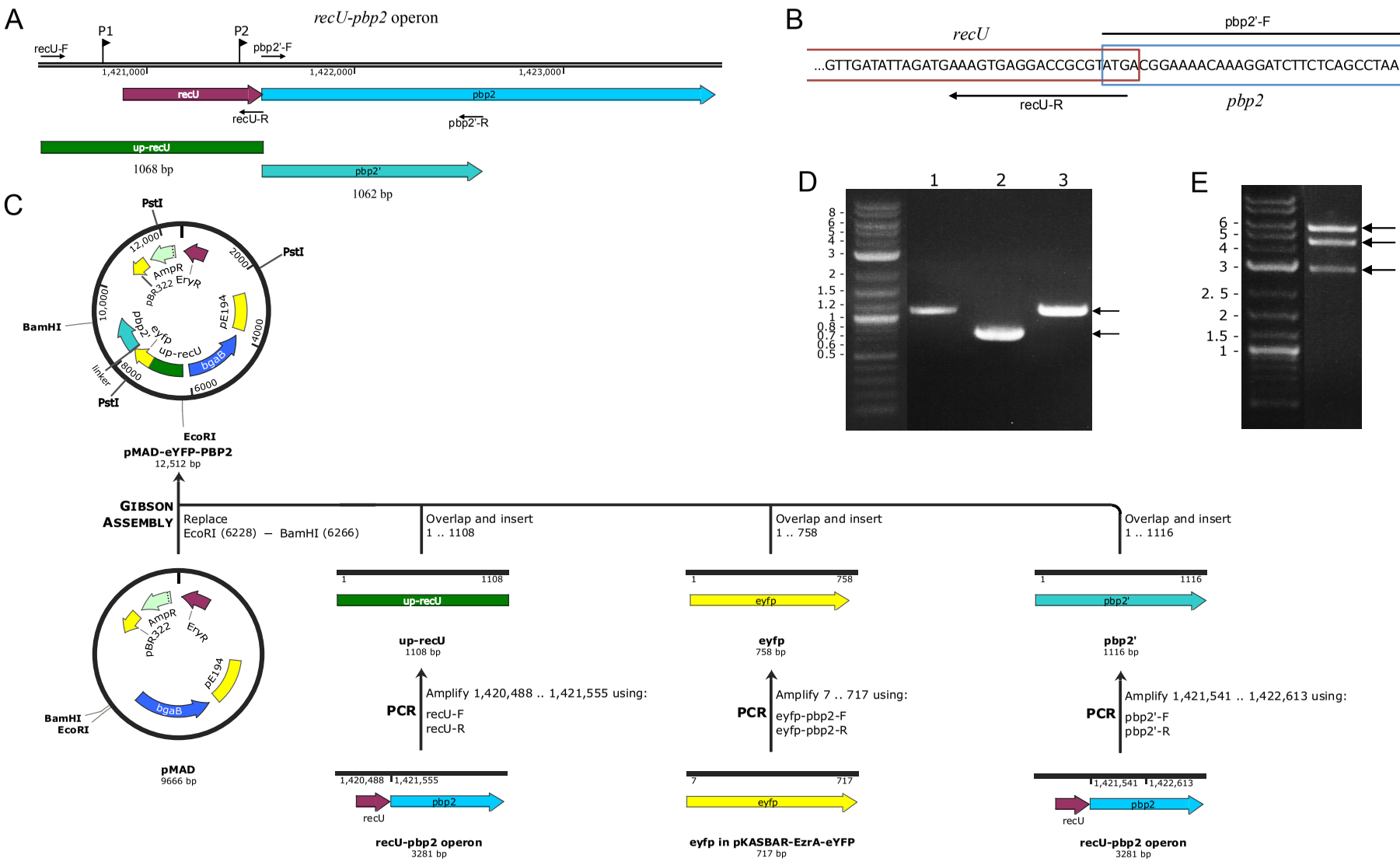
A
recU-pbp2 operon
recU-F
P1
P2
pbp2'-F
1,421,000
1,422,000
1,423,000
recU
pbp2
recU-R
pbp2'-R
up-recU
1068 bp
pbp2'
1062 bp
B
recU
pbp2'-F
...GTTGATATTAGATGAAAGTGAGGACCGCGTATGACGGAAAACAAAGGATCTTCTCAGCCTAAG...
recU-R
pbp2
C
PstI
12,000
2000
PstI
AmpR
pBR322
EryR
BamHI
10,000
pE194
4000
pbp2'
eyfp
up-recU
bgaB
linker
8000
6000
PstI
EcoRI
pMAD-eYFP-PBP2
12,512 bp
D
1
2
3
8
6
5
4
3
2
1.5
1.2
1
0.8
0.7
0.6
0.5
E
6
5
4
3
2. 5
2
1.5
1
GIBSON ASSEMBLY
Replace
EcoRI (6228) – BamHI (6266)
Overlap and insert
1 .. 1108
Overlap and insert
1 .. 758
Overlap and insert
1 .. 1116
pMAD
9666 bp
BamHI
EcoRI
1
1108
up-recU
up-recU
1108 bp
1
758
eyfp
eyfp
758 bp
1
1116
pbp2'
pbp2'
1116 bp
PCR
Amplify 1,420,488 .. 1,421,555 using:
recU-F
recU-R
PCR
Amplify 7 .. 717 using:
eyfp-pbp2-F
eyfp-pbp2-R
PCR
Amplify 1,421,541 .. 1,422,613 using:
pbp2'-F
pbp2'-R
1,420,488
1,421,555
pbp2
recU
recU-pbp2 operon
3281 bp
7
717
eyfp
eyfp in pKASBAR-EzrA-eYFP
717 bp
1,421,541
1,422,613
pbp2
recU
recU-pbp2 operon
3281 bp

Figure 5.2. Construction of pMAD-eYFP-PBP2, a vector for allelic replacement of *pbp2* with *eyfp-pbp2*

A. Schematic representation of the chromosome region of *pbp2* in *S. aureus*. In *S. aureus pbp2* is a part of the *rec-pbp2* operon and is transcribed together with *recU* or alone from the P1 or the P2 promoter, respectively. The locations of recU-F, recU-R, pbp2'-F and pbp2'-R annealing sites allowing for amplification of ~1 kb fragments (up-recU and pbp2') are indicated.

B. Nucleotide sequence of the 3' end of the *recU* gene (indicated with a red box) and the 5' fragment of the *pbp2* gene (in a blue box). Sites of recU-R and pbp2'-F annealing to the *S. aureus* chromosome are indicated.

C. Diagrammatic representation of pMAD-eYFP-PBP2 construction. A ~ 1 kb fragment (up-recU) covering the *recU* gene and the region from -1 bp to -390 bp upstream of the *recU* gene and two *pbp2* promoters, P1 and P2, and a ~1 kb fragment (pbp2') covering the 5' fragment (1-1068 bp) of the *pbp2* gene were PCR amplified from *S. aureus* SH1000 genomic DNA using primers recU-F and recU-R, and pbp2'-F and pbp2'-R, respectively. The *eyfp* gene was PCR amplified from the pKASBAR-EzrA-eYFP plasmid using eyfp-pbp2-F and eyfp-pbp2-R primers. Primers eyfp-pbp2-F and pbp2'-R were designed to incorporate point mutations resulting in a Val2Ile substitution in the *eyfp* gene. The up-recU, eyfp and pbp2' fragments were joined with *BamHI* and *EcoRI* cut pMAD by Gibson assembly. The resulting pMAD-eYFP-PBP2 vector comprises *E. coli* pBR322 origin of replication (pBR322), staphylococcal pE194 thermosensitive origin of replication (pE194), *bgaB* gene encoding a thermostable β-galactosidase from *Bacillus stearothermophilus* (BgaB), ampicillin resistance (AmpR) and erythromycin resistance (EryR) cassettes and the up-recU-eyfp-pbp2' fragment for homologous recombination of *pbp2*. The *eyfp* gene and the 5' end of the *pbp2* gene are linked by a 12-amino acid linker.

D. 1% (w/v) TAE agarose gel showing products of PCR amplification of the up-recU fragment (1), the *eyfp* gene (2) and the pbp2' fragment (3). The expected DNA fragments of ~ 1 kb and ~0.7 kb are indicated with black arrows. Sizes of a DNA ladder are shown in kb. The products of the PCR reaction were used in the Gibson assembly (C).

E. Restriction enzyme analysis of the pMAD-eYFP-PBP2 plasmid with *PstI*. The expected DNA bands of 5.4 kb, 4.3 kb and 2.8 kb are indicated with black arrows. Sizes of a DNA ladder are shown in kb.

pMAD-eYFP-PBP2 was transformed into electrocompetent *S. aureus* RN4220 with selection on BHI plates containing erythromycin (5 μg ml^{-1}), lincomycin (25 μg ml^{-1}) and X-Gal (80 μg ml^{-1}) at 28°C. All colonies were dark blue, indicating successful transformation. The plasmid was subsequently moved into SH1000 by phage transduction. Transformants were selected at 28°C on plates containing erythromycin (5 μg ml^{-1}), lincomycin (25 μg ml^{-1}) and X-Gal (80 μg ml^{-1}). One dark blue colony was grown overnight in BHI erythromycin (5 μg ml^{-1}) and lincomycin (25 μg ml^{-1}) at 42°C to initiate a single crossover event (Figure 5.3A). The overnight culture was serially diluted and plated on BHI plates containing erythromycin (5 μg ml^{-1}), lincomycin (25 μg ml^{-1}) and X-Gal (80 μg ml^{-1}) and cells were incubated at 42°C overnight. To allow a double crossover event to occur (Figure 5.3A), a light blue colony, which was likely a single crossover recombinant, was grown in BHI without any antibiotic at 28°C overnight. The culture was serially diluted and plated on BHI containing X-Gal (80 μg ml^{-1}) and incubated overnight at 42°C. White colonies were tested for erythromycin sensitivity. Successful replacement of *pbp2* by *eyfp-pbp2* was confirmed in ten (~14%) out of 72 screened clones by PCR on genomic DNA using primer pairs eYFP-F and eYFP-R, and pbp2a and pbp2d (Figure 5.3B and C) and sequencing of the PCR products amplified using pbp2a and pbp2d primers.

The mutants were examined by fluorescence microscopy. Microscopy imaging revealed that all ten clones had a morphology defect, they formed cells of smaller size than SH1000 wild type (Figure 5.4A). When tested for the localisation of the fusion protein, fluorescence across the whole cell with slightly enhanced signal associated with cell membrane and presumptive cell septa was observed (Figure 5.4A). However the intensity of the detected fluorescent signals was comparable to autofluorescence emitted by SH1000, which did not carry any genes encoding fluorescent reporters (Figure 5.4A). One representative clone, in which the *eyfp-pbp2* gene was located in the *pbp2* native chromosomal locus, under the control of P1 and P2 promoters, was named SJF4595 (*S. aureus* SH1000 *pbp2::eyfp-pbp2*).

The difference in sizes between the mutant and the wild type strain was easily visible when cells were viewed by light microscopy (Figure 5.4A). Measurements of cell sizes showed that SJF4595 formed cells of 0.80 ± 0.09 μm in diameter, which was smaller than 0.95 ± 0.13 μm for *S. aureus* SH1000 (Figure 5.4B).

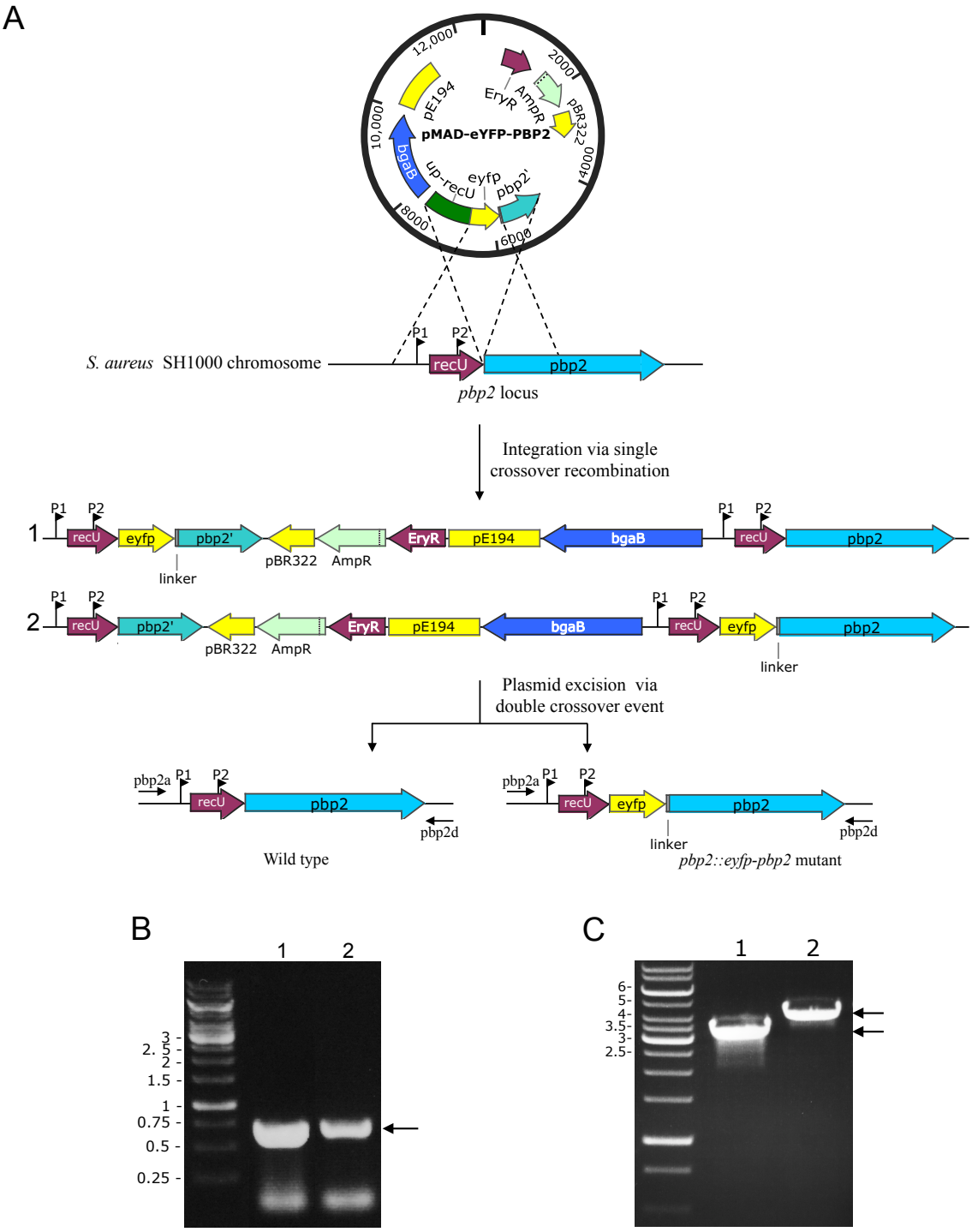

Figure 5.3. Homologous recombination of pMAD-eYFP-PBP2 into the *S. aureus* chromosome

A. Diagrammatic representation of the likely recombination outcomes of pMAD-eYFP-PBP2 into the *S. aureus* SH1000 chromosome. A single crossover can occur through either the upstream region of *pbp2* (1) or the 5' region of *pbp2* (2). The double crossover event can either recreate the wild type *pbp2* locus or creates the mutant strain SJF4595 (*S. aureus* SH1000 *pbp2::eyfp-pbp2*). Annealing sites of primers pbp2a and pbp2d used to confirm the homologous recombination are indicated. Not to scale.

B. Replacement of *pbp2* for *eyfp-pbp2* was confirmed by PCR using eYFP-F and eYFP-R primers. A ~0.7 kb product that corresponds to the expected size of the *eyfp* gene was obtained for pMAD-eYFP-PBP2 (lane 1) and genomic DNA extracted from SJF4595 (*S. aureus* SH1000 *pbp2::eyfp-pbp2*) (lane 2). The expected PCR products are indicated with black arrows. Sizes of a DNA ladder are shown in kb.

C. Replacement of *pbp2* for *eyfp-pbp2* was confirmed by PCR using pbp2a and pbp2d primers. A product of ~3.5 kb that corresponds to the wild type *pbp2* locus was obtained for *S. aureus* SH1000 genomic DNA (lane 1), while a product of ~4 kb obtained for genomic DNA of SJF4595 (*S. aureus* SH1000 *pbp2::eyfp-pbp2*) (lane 2) indicates the presence of the *eyfp-pbp2* gene in the *pbp2* native locus. The expected DNA bands of 3.5 kb and 4 kb are indicated with black arrows. Sizes of a DNA ladder are shown in kb.

In order to test if SJF4595 also had a growth defect, its growth in liquid medium was compared to SH1000. SH1000 and SJF4595 were grown overnight in BHI and were inoculated into 50 ml prewarmed BHI to an OD_{600} of 0.001. Optical density measurements and colony forming unit (CFU) counts showed that SJF4595 had a slower growth rate than the wild type strain (Figure 5.4C and D). While the SH1000 doubling time was approximately 29 min and 25 min, calculated from OD_{600} measurements and CFU counts, respectively, SJF4595 was ~42 min (OD_{600}) and ~33 min (CFU) (Figure 5.4C and D).

PCR analysis and sequencing of the *pbp2* locus confirmed replacement of native *pbp2* with the *eyfp-pbp2* fusion. SJF4595 had the expected genotype but it did not have the wild type phenotype and was poorly fluorescent when examined by fluorescence microscopy. The observed phenotype (reduced cell size) was however different from the one reported for the conditional *S. aureus pbp2* strain, in which PBP2 depletion led to an increase in cell size and multiple division septa (Pinho et al., 2001a). Moreover SJF4595 was alive, suggesting that the eYFP-PBP2 fusion was produced in this strain. Therefore SJF4595 was tested for eYFP-PBP2 production by a fluorescent penicillin derivative binding assay (Figure 5.4C). Penicillins are β-lactam antibiotics that bind and inhibit the transpeptidase domain of PBPs (Zapun et al., 2008a) and fluorescent penicillin derivatives can be used as reporters for detection of PBPs in a cell. Bocillin FL (Molecular Probes) is a commercially available penicillin V with a BODIPY FL dye attached. Pen-AF647 is a (+)-6-aminopenicillanic acid (APA) derivative conjugated with Alexa Fluor 647, synthesised by Bryony Cotterell (University of Sheffield). The membrane fractions of SH1000 and SJF4595 grown to exponential phase (OD_{600} ~1) were prepared, 30 μg of total protein was incubated with 25 μM Bocillin FL or 10 μM Pen-AF647 at 37^{o}C for 10 min and proteins were resolved on a 10% (w/v) SDS-PAGE gel. A band of ~100 kDa, which likely represented eYFP-PBP2, was detected in the membrane protein fraction from SJF4595 both by Bocillin FL and Pen-AF647 (Figure 5.4C). Comparison of the intensity of the signal of the eYFP-PBP2 band in SJF4595 against the intensity of the signal detected from PBP2 in SH1000 revealed that eYFP-PBP2 levels were approximately 20 times lower in the mutant strain than in SH1000 (Figure 5.4C). Whilst Bocillin FL labelling of PBPs showed that the mutant strain did not produce native PBP2, a band of the same intensity as the 100 kDa product and of the comparable size (~80kDa) to wild type PBP2 was

detected in SJF4595 by Pen-AF647 (Figure 5.4C). In SJF4595 *eyfp-pbp2* was the only copy of *pbp2* and therefore the 80 kDa band could represent a product of eYFP-PBP2 degradation. Additionally, the reduced fluorescent signal from eYFP-PBP2, when compared to PBP2 in SH1000, indicated that in SJF4595 eYFP-PBP2 was either produced in lower amounts or had lower affinity for fluorescent penicillins.

Western blot analysis using anti-PBP2 and anti-GFP antibodies was performed to examine the total amount and stability of eYFP-PBP2 and to test if the 80 kDa band identified in SJF4595 by the penicillin assay was recognised as PBP2 by the anti-PBP2 antibodies. To avoid the cross-reactivity of antibodies with *S. aureus* Protein A, SJF4595 was transduced with a Φ11 lysate from *S. aureus* SH1000 *spa::kan.* Transformants were selected using kanamycin (50 μg ml^{-1}) and the resulting strain was named SJF4598 (*S. aureus* SH1000 *spa::kan pbp2::eyfp-pbp2*). Membrane fractions of SJF4598 and SH1000 *spa::kan* grown to exponential phase (OD_{600} ~1) were probed with rabbit anti-GFP and anti-PBP2 antibodies at 1:1000 dilution (Figure 5.4D and E). A band of ~100 kDa, which corresponded to the expected size of eYFP-PBP2, was detected in SJF4598 by both the anti-GFP and anti-PBP2 antibodies (Figure 5.4D and E). An additional band of ~ 80 kD was observed for SJF4598 membrane proteins probed with the anti-PBP2 antibodies (Figure 5.4D). This band was of the same intensity as the band for eYFP-PBP2 (~100 kDa) and of the same size as the band corresponding to native PBP2 in SH1000 *spa::kan* (Figure 5.4D). Western blot analysis using the anti-GFP antibodies revealed an additional band of ~ 50 kDa, however this band was detected both in SH1000 *spa::kan* and SJF4598 (Figure E), indicating that it was not a product of eYFP-PBP2 degradation but probably a product of unspecific cross-reactivity of the antibodies with other bacterial proteins. SJF4598 did not have a gene for native *pbp2* and presence of two bands of ~100 kDa and ~80 kDa suggested that YFP-PBP2 might be processed by truncation of its N-terminal eYFP tag to a form of the same size as the wild type PBP2.

All above results suggested that eYFP-PBP2 was produced in the absence of the native PBP2 protein but at much reduced levels. This was sufficient for cells to stay alive but not enough for cells to retain the wild type phenotype.

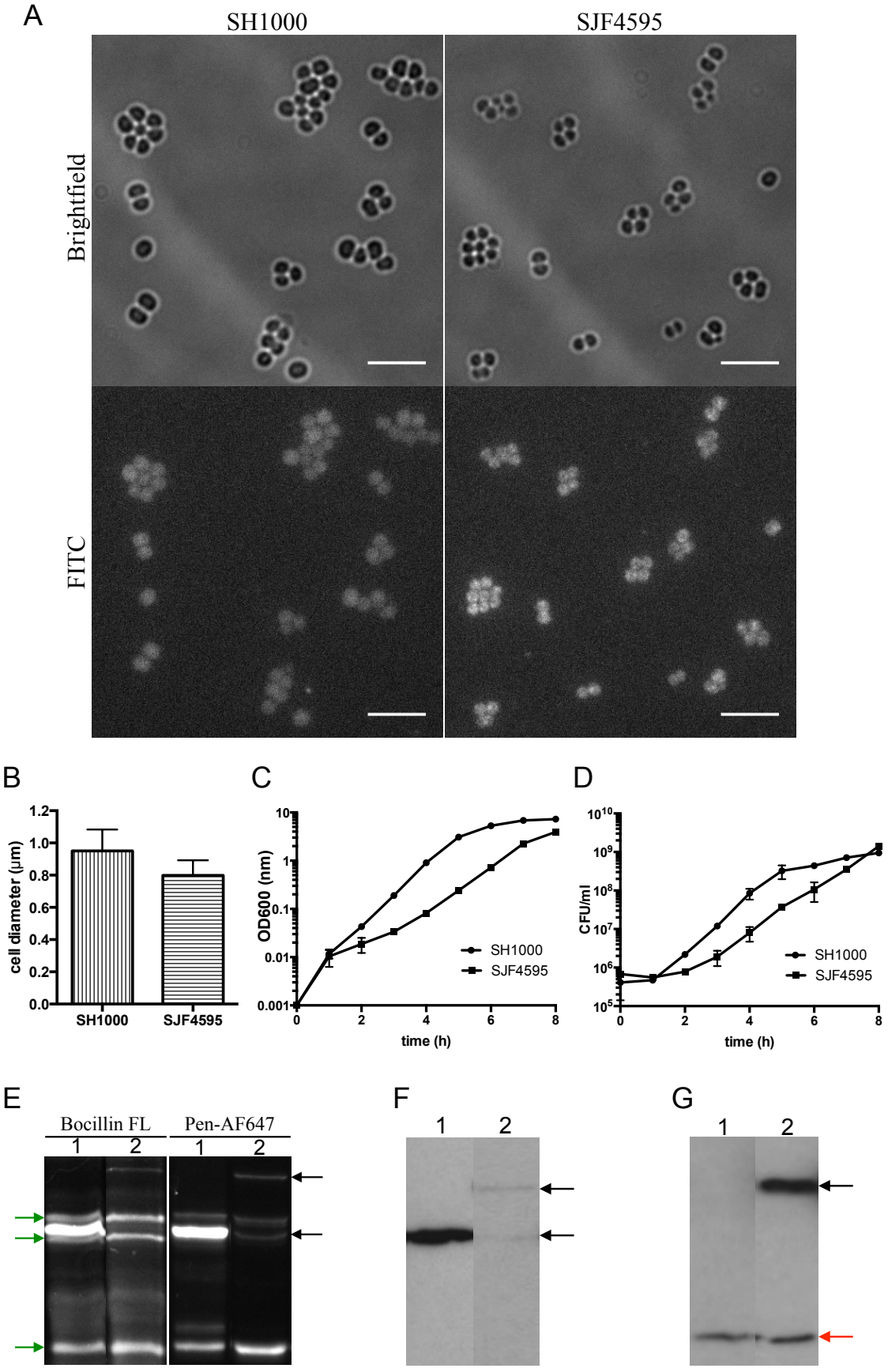

Figure 5.4. Characterisation of eYFP-PBP2 in *S. aureus*

A. Morphology of eYFP-PBP2 *S. aureus* cells. SJF4595 (*S. aureus* SH1000 *pbp2::eyfp-pbp2*) forms cells of smaller sizes than the wild type *S. aureus* SH1000 strain. In SJF4595 eYFP-PBP2 gives a

fluorescent signal associated both with the cell membrane, midcell and the cytoplasm. SH1000 was imaged the same way as SJF4585 by fluorescence microscopy using the FITC filter. The fluorescentce images are maximum intensity projections of z-stack images acquired at 200 nm z-intervals. The same contrast was adjusted to the fluorescence images. Scale bars 5 μm.

B. SJF4595 (*S. aureus* SH1000 *pbp2::eyfp-pbp2*) forms smaller cells than SH1000. Bars represent the mean value of cell diameters for SH1000 (0.95 ± 0.13 μm, n=621) and SJF4595 (0.80 ± 0.09 μm, n=634). Error bars represent standard deviation of the mean. Measurements were made using the Fiji program.

C. Growth of SJF4595 (*S. aureus* SH1000 *pbp2::eyfp-pbp2*) was compared to SH1000 by optical density measurements. Cell cultures were grown from an OD_{600} of 0.001 and the optical density was measured every hour. Bacterial cultures were prepared in triplicate and the error bars represent standard deviation from the mean.

D. Growth of SJF4595 (*S. aureus* SH1000 *pbp2::eyfp-pbp2*) was determined by CFU counts. Its growth was compared against to SH1000. Bacterial cultures were prepared in triplicate and the error bars represent standard deviation from the mean.

E. Analysis of penicillin binding protein (PBPs) profile in SJF4595 (*S. aureus* SH1000 *pbp2::eyfp-pbp2*) by Bocillin FL and Pen-AF647 labelling. Membrane fractions of SH1000 (lane 1) and SJF4595 (lane 2) were prepared and 30 μg of total protein was labelled with 25 μM Bocillin FL or 10 μM Pen-AF647 at 37^{o}C for 10 min. The labelled membrane fractions were resolved by 10% (w/v) SDS-PAGE. Bands of ~80 kDa and ~100 kDa likely representing PBP2 and eYFP-PBP2, respectively, are indicated with black arrows. The green arrows indicate bands correlating to PBP1, PBP3 and PBP4 (top to bottom, respectively).

F. Membrane fractions (~30 μg protein) of *S. aureus* SH1000 *spa::kan* (lane 1) and SJF4598 (*S. aureus* SH1000 *spa::kan pbp2::eyfp-pbp2*) (lane 2) were probed with anti-PBP2 antibodies at a 1:1000 dilution. Bands of ~80 kDa and ~100 kDa, corresponding to wild type PBP2 and the eYFP-PBP2 fusion, respectively, are indicated with black arrows.

G. Membrane fractions (~30 μg protein) of *S. aureus* SH1000 *spa::kan* (lane 1) and SJF4598 (*S. aureus* SH1000 *spa::kan pbp2::eyfp-pbp2*) (lane 2) were probed with anti-GFP antibodies at a dilution of 1:1000. A band detected at ~100 kDa (eYFP-PBP2) is indicated with a black arrow. Additional bands of ~ 50 kDa are indicated with a red arrow.

5.2.1.2 Complementation of *S. aureus pbp2::eyfp-pbp2*

SJF4595 (*S. aureus* SH1000 *pbp2::eyfp-pbp2*) was constructed to localise PBP2 in *S. aureus*. However this strain had a growth defect, likely resulting from a low level of eYFP-PBP2. Attempts to restore the growth of the *pbp2::eyfp-pbp2* mutant were made via introduction of extra copies of the *eyfp-pbp2* gene .

A multi-copy plasmid carrying *eyfp-pbp2* under the control of the Pspac promoter was constructed. The putative *pbp2* ribosome binding site (RBS) (Figure 5.5A) together with full length *eyfp-pbp2* was amplified from SJF4595 (*S. aureus* SH1000 *pbp2::eyfp-pbp2*) genomic DNA using pCQ-eyfp-pbp2-F and pCQ-eyfp-pbp2-R primers (Figure 5.5B). The PCR products were joined with *NheI* and *AscI* digested pCQ11-FtsZ-SNAP by Gibson assembly (Figure 5.5B). The assembly products were transformed into chemically competent *E. coli* NEB5α cells and selected on LB ampicillin (100 μg ml^{-1}) plates. Positive clones were verified by plasmid extraction, restriction digestion with *EcoRI* and confirmed to contain the correct DNA band sizes by electrophoresis on a 1% (w/v) agarose gel (Figure 5.5C). Plasmids were sequenced by GATC Biotech to check for the introduction of substitutions during the PCR step. The resulting pCQ11-eYFP-PBP2 plasmid (Figure 5.5B) did not contain any substitutions. pCQ11-eYFP-PBP2 was transferred into electrocompetent *S. aureus* RN4220 cells with selection on BHI plates containing erythromycin (5 μg ml^{-1}) and lincomycin (25 μg ml^{-1}). The plasmid was subsequently moved into *S. aureus* SH1000 and SJF4595 by phage transduction, with selection using erythromycin (5 μg ml^{-1}) and lincomycin (25 μg ml^{-1}). The resulting SJF4597 (*S. aureus* SH1000 pCQ11-eYFP-PBP2) strain had a wild type copy of *pbp2* at its native locus and ectopic *eyfp-pbp2* placed under the Pspac promoter on the plasmid, while SJF4596 (*S. aureus* SH1000 *pbp2::eyfp-pbp2* pCQ11-eYFP-PBP2) had *eyfp-pbp2* at the *pbp2* locus and also the plasmid.

Morphology of SJF4596 was examined by fluorescence microscopy. As in SJF4596 (*S. aureus* SH1000 *pbp2::eyfp-pbp2* pCQ11-eYFP-PBP2) plasmid encoded *eyfp-pbp2* was placed under the control of the Pspac promoter, cells were grown in BHI supplemented with erythromycin (5 μg ml^{-1}) and with or without 1 mM IPTG.

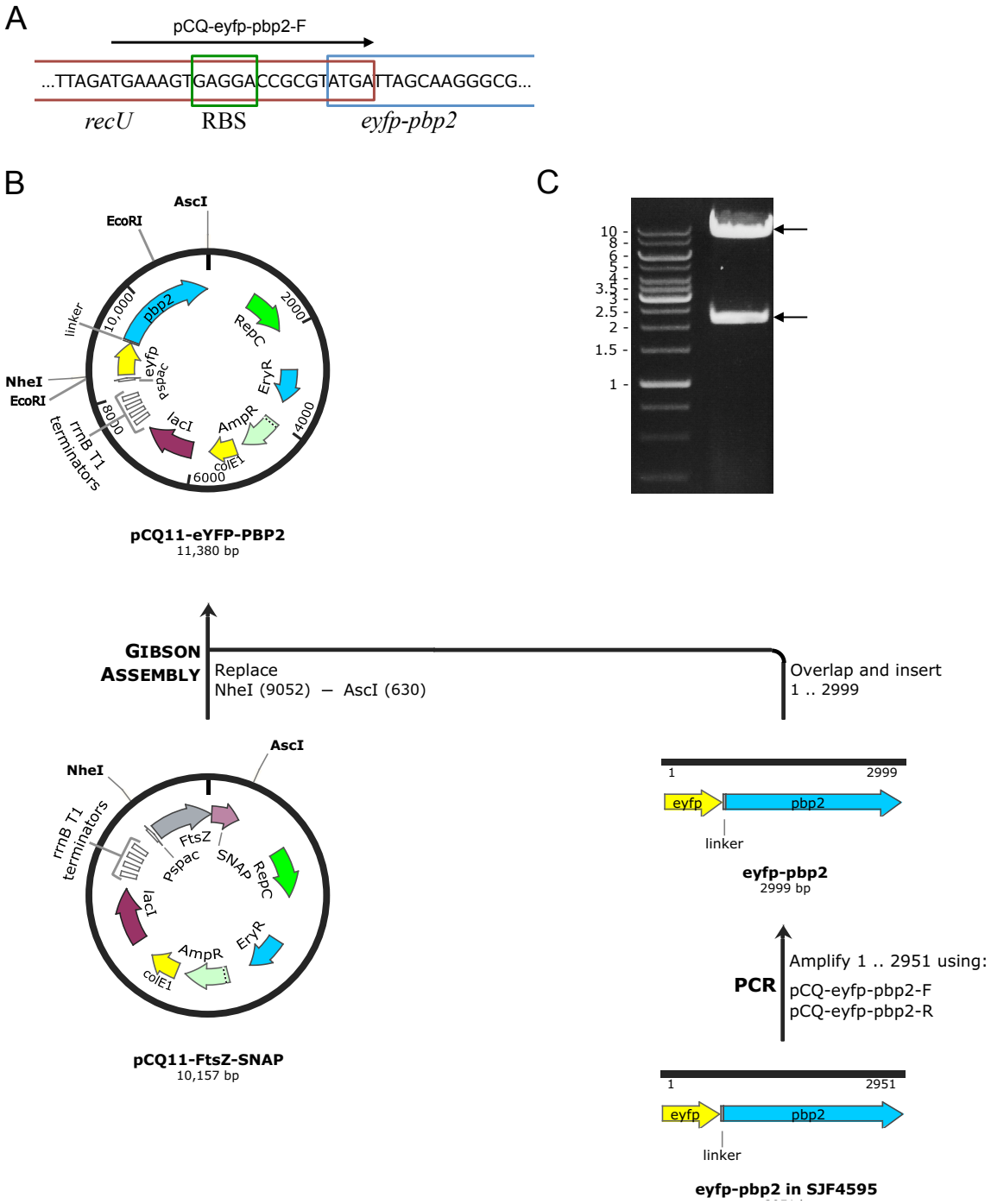

Figure 5.5. Construction of pCQ11-eYFP-PBP2

A. The chromosomal region of *eyfp-pbp2* in SJF4595 (*S. aureus* SH1000 *pbp2::eyfp-pbp2*). Nucleotide sequence of the 3' end of the *recU* gene is indicated with a red box, the 5' fragment of the *eyfp-pbp2* gene is in a blue box and the putative ribosome binding site (RBS) is highlighted in a green box. The annealing site of the pCQ11-eyfp-pbp2 primer to the SJF4595 chromosome is indicated.

B. The putative RBS and the full length *eyfp-pbp2* gene was PCR amplified from the genomic DNA of SJF4595 (*S. aureus* SH1000 *pbp2::eyfp-pbp2*) using pCQ-eyfp-pbp2-F and pCQ-eyfp-pbp2-R primers. The PCR product was cloned into *NheI* and *AscI* cut pCQ11-FtsZ-SNAP by Gibson assembly, resulting in pCQ11-eYFP-PBP2. The pCQ11-eYFP-PBP2 plasmid comprises the

high-copy-number ColE1 origin of replication, the staphylococcal origin of replication form pT181 (RepC), the *lacI* gene, four transcription terminators T1 from the *E. coli rrnB* gene, the ampicillin resistance (AmpR) and the erythromycin resistance (EryR) cassettes, and putative *pbp2* RBS with the full length *eyfp-pbp2* fusion joined by a 12 amino-acid linker, placed under the control of the Pspac promoter.

C. Restriction enzyme digest of pCQ11-eYFP-PBP2 with *EcoRI*. The expected DNA bands of 9 kb and 2.3 kb are indicated with black arrows. Sizes of a DNA ladder are shown in kb.

Interestingly, SJF4596 gave comparable levels of fluorescence regardless of the inducer concentration (Figure 5.6D and E). Cells grown either in the presence or absence of 1 mM IPTG were fluorescent and showed both septal and peripheral localisation of eYFP-PBP2 (Figure 5.6D and E). Addition of plasmid born *eyfp-pbp2* restored morphology of SJF4596, as it no longer formed cells of reduced sizes and poor fluorescence as SJF4595 (*S. aureus* SH1000 *pbp2::eyfp-pbp2*) (Figure 5.6B) and its phenotype resembled SH1000 (Figure 5.6A). SJF4596 cells grown either with or without inducer had a morphology comparable to SH1000 cells, although cells with increased sizes could be often observed (Figure 5.6D and E). Such cells emitted a bright fluorescent signal most likely due to altered expression of *eyfp-pbp2* from the Pspac promoter. The fact that SJF4596 did not required IPTG to produce eYFP-PBP2 indicated that the Pspac promoter was leaky. Interestingly, when SJF4597 (*S. aureus* SH1000 pCQ11-eYFP-PBP2) grown in the presence of erythromycin (5 μg ml^{-1}) and 1 mM IPTG was viewed by fluorescence microscopy it was found to be not fluorescent (Figure 5.6C). Occasionally a few cells in a field of view were fluorescent, however a signal dispersed across the whole cell could be observed in such cells (Figure 5.6C).

Measurements of cell sizes showed that in the absence of IPTG, SJF4596 had an average diameter comparable to SH1000, whilst incubation in 1 mM IPTG resulted in cell with slightly increased diameters (Figure 5.7A). Comparison of cells size distribution of SH1000 and SJF4596 grown in the presence and absence of IPTG revealed that even though the same proportion of cells showed cell diameter of 0.9-1 μm (~60% of cells), SJF4596 grown with 1 mM IPTG a had larger tendency to form cells with a cell diameter >1 μm than SH1000 or SJF4596 incubated without the inducer (Figure 5.7B).

In order to test SJF4596 growth morphology, its growth was compared to growth of SH1000 and SJF4595 (*S. aureus* SH1000 *pbp2::eyfp-pbp2*) strains in liquid media. SH1000, SJF4595 and SJF4596 were grown overnight in BHI supplemented with appropriate antibiotics. The overnight cultures were used to inoculate 50 ml of prewarmed BHI to an OD_{600} 0.001 and growth of SJF4596 in the presence or absence of 1 mM IPTG was measured by optical density (Figure 5.7C). No difference was seen between SJF4596 grown with IPTG and SJF4596 grown without IPTG.

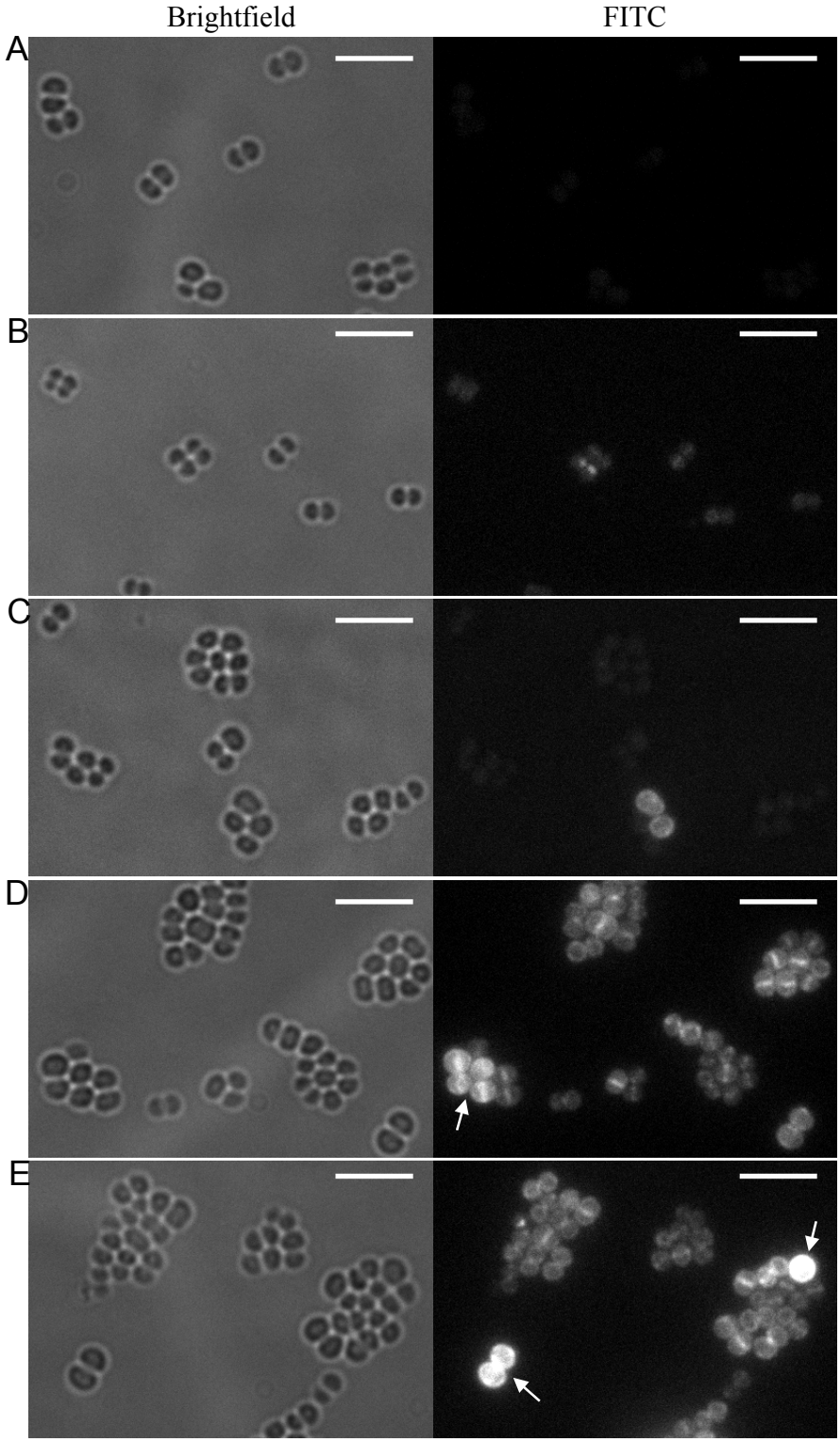

Figure 5.6. Localisation of eYFP-PBP2 and morphology of complemented *S. aureus pbp2::eyfp-pbp2*
Morphology and localisation of eYFP-PBP2 in SJF4596 (*S. aureus* SH1000 *pbp2::eyfp-pbp2* pCQ11-eYFP-PBP2) grown in the absence (D) and presence (E) of 1 mM IPTG. SH1000 (A) and SJF4595 (*S. aureus* SH1000 *pbp2::eyfp-pbp2*) (B) grown in BHI, and SJF4597 (*S. aureus* SH1000 *pbp2::eyfp-pbp2*) grown in 1 mM IPTG (C) were also imaged. White arrows indicate abnormal enlarged cells. The fluorescence images are maximum intensity projections of z-stack images acquired at 200 nm z-intervals. The same contrast was used for all the fluorescence images. Scale bars 5 μm.

The doubling time of SJF4596 was ~28 min, regardless of inducer presence and its growth rate was comparable to SH1000 (~25 min) (Figure 5.7C). SJF4596 needed less time to double than SJF4595 (~34 min), indicating that introduction of the plasmid associated *eyfp-pbp2* allowed SJF4596 growth to be similar to SH1000.

Microscopy imaging showed that in the absence or presence of IPTG, SJF4596 gave comparable fluorescent signals, suggesting that similar amounts of eYFP-PBP2 were produced independently of the inducer. Therefore levels of eYFP-PBP2 in SJF4596 grown with and without IPTG were tested by gel-based analysis of PBPs labelled with fluorescent penicillin. Pen-AF647 was found to have higher sensitivity and give less background noise than Bocillin FL (Figure 5.4E), hence membrane fractions (30 µg protein) from SJF4596 grown with and without 1 mM IPTG were labelled with 10 µM Pen-AF647 at 37^{o}C for 10 min and resolved on a 10% (w/v) SDS-PAGE gel (Figure 5.7D). Penicillin labelling of PBPs confirmed that in SJF4596 eYFP-PBP (~100 kDa band) was produced at a higher level than in SJF4595 (*S. aureus* SH1000 *pbp2::eyfp-pbp2*) and its production was not IPTG dependent (Figure 5.7D). In SJF4597 (*S. aureus* SH1000 pCQ11-eYFP-PBP2), grown in the presence of 1 mM IPTG, the eYFP-PBP2 protein was found at the similar level as eYFP-PBP2 in SJF4595 (~5% of wild type PBP2 levels). The low level of eYFP-PBP2 in SJF4597 may explain the poor fluorescent signal when cells were viewed by fluorescence microscopy (Figure 5.6C). Interestingly, in SJF4596 the amount of eYFP-PBP2 was approximately five times higher than the amount of the fusion protein in SJF4597 grown in the same conditions (presence of 1 mM IPTG) (Figure 5.7D). As it was previously shown for SJF4595, an additional band of ~80 kDa, which was of the same size as native PBP2 in the wild type, was detected for SJF4596 grown both in the absence or presence of IPTG (Figure 5.7D). Whilst the intensities of the 80 kDa and 100 kDa bands were comparable in SJF4595, the 80 kDa product was about four times more intensive than the 100 kDa band in SJF4596. This suggested that eYFP-PBP2 might be unstable and processed to a form of a similar size as native PBP2 in the wild type SH1000 strain. Nevertheless, the total amount of PBP2 (eYFP-PBP2 plus processed form) was ~ 85% of the native PBP2 levels in SH1000.

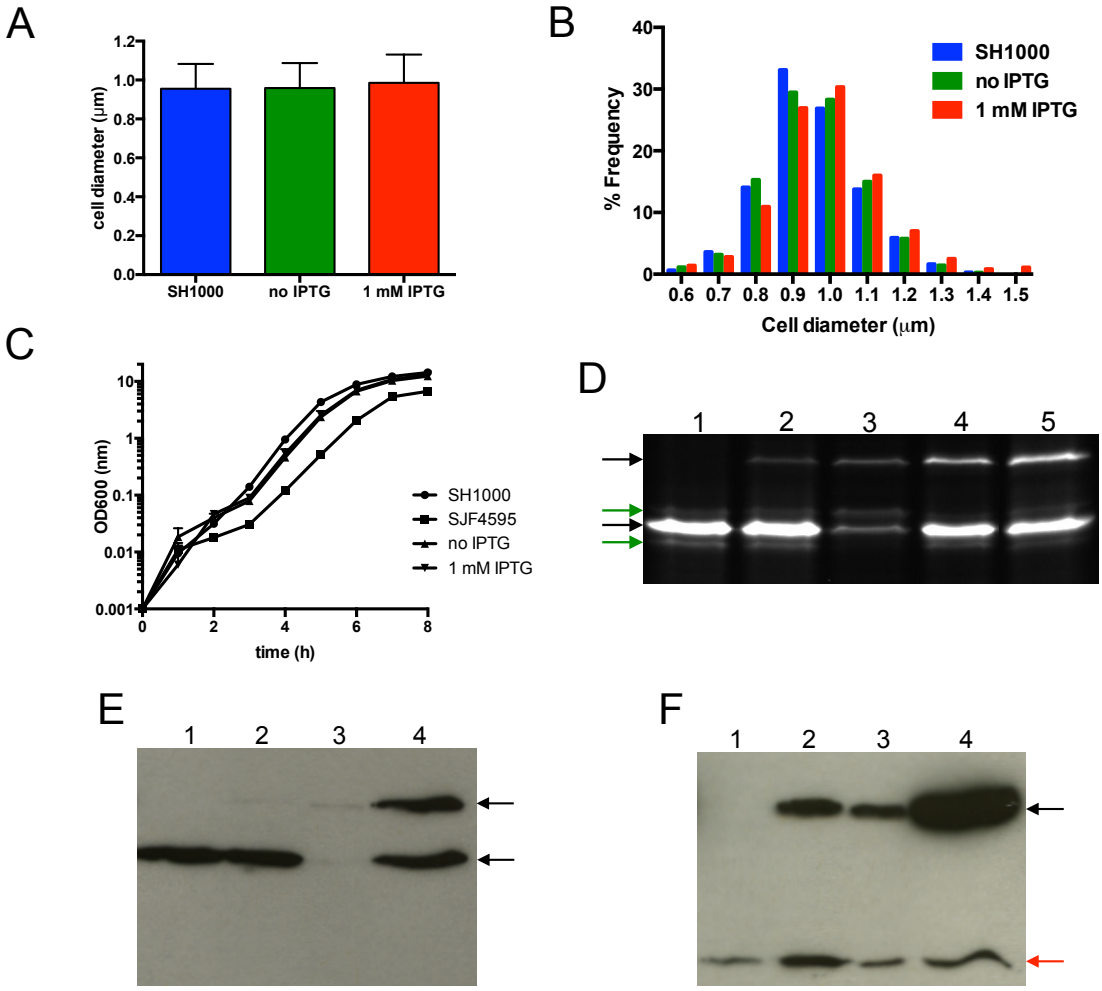

Figure 5.7. Characterisation of complemented *S. aureus pbp2::eyfp-pbp2*

A. Bars represent the mean value of cell diameters for *S. aureus* SH1000 (0.96 ± 0.13 µm, n=305) and SJF4596 (*S. aureus* SH1000 *pbp2::eyfp-pbp2* pCQ11-eYFP-PBP2) grown in the absence (no IPTG, 0.96 ± 0.13 µm, n=346) and presence of 1 mM IPTG (1 mM IPTG, 0.99 ± 0.15 µm, n=356). Error bars represent standard deviation of the mean. Measurements were made using the Fiji program.

B. Histogram showing the distribution of cell diameters of *S. aureus* SH1000 (n=305) and SJF4596 (*S. aureus* SH1000 *pbp2::eyfp-pbp2* pCQ11-eYFP-PBP2) grown without (no IPTG, n=346) and with (1 mM, n=356) 1 mM IPTG. Measurements were made using the Fiji program.

C. Growth of SJF4596 (*S. aureus* SH1000 *pbp2::eyfp-pbp2* pCQ11-eYFP-PBP2) in the absence (no IPTG) and presence (1 mM IPTG) of inducer was measured by optical density. Bacterial cultures were prepared in triplicate and the error bars represent standard deviation from the mean.

D. Analysis of penicillin binding protein (PBPs) profile in SJF4596 (*S. aureus* SH1000 *pbp2::eyfp-pbp2* pCQ11-eYFP-PBP2) by Pen-AF647 labelling. The membrane fractions (30 µg protein) of SH1000 (lane 1), SJF4597 (*S. aureus* SH1000 pCQ11-eYFP-PBP2) grown with 1 mM IPTG (lane 2), SJF4595 (*S. aureus* SH1000 *pbp2::eyfp-pbp2*) (lane 3) and SJF4596 grown in the absence (lane 4) and presence (lane 5) of 1 mM IPTG were labelled with 10 µM Pen-AF647 at 37°C for 10 min. Bands of ~80 kDa and ~100 kDa likely representing PBP2 and eYFP-PBP2, respectively, are indicated with black arrows. The green arrows indicate bands correlating to PBP1 and PBP3.

E. Membrane fractions (~30 μg protein) of *S. aureus* SH1000 *spa::kan* (lane 1), SJF4599 (*S. aureus* SH1000 *spa::kan* pCQ11-eYFP-PBP2) grown with 1 mM IPTG (lane 2), SJF4598 (*S. aureus* SH1000 *spa::kan pbp2::eyfp-pbp2*) (lane 3) and SJF4600 (*S. aureus* SH1000 *spa::kan pbp2::eyfp-pbp2* pCQ11-eYFP-PBP2) grown in 1 mM IPTG (lane 4) were probed with anti-PBP2 antibodies at a 1:1000 dilution. Bands of ~80 kDa and ~100 kDa, corresponding to PBP2 and eYFP-PBP2, respectively, are indicated with black arrows.

F. Membrane fractions (~30 μg protein) of *S. aureus* SH1000 *spa::kan* (lane 1), SJF4599 (*S. aureus* SH1000 *spa::kan* pCQ11-eYFP-PBP2) grown with 1 mM IPTG (lane 2), SJF4598 (*S. aureus* SH1000 *spa::kan pbp2::eyfp-pbp2*) (lane 3) and SJF4600 (*S. aureus* SH1000 *spa::kan pbp2::eyfp-pbp2* pCQ11-eYFP-PBP2) grown in 1 mM IPTG (lane 4) were probed with anti-GFP antibodies at a dilution of 1:1000. A band detected at ~100 kDa (eYFP-PBP2) is indicated with a black arrow. Additional bands of ~ 50 kDa are indicated with a red arrow.

Western blot analysis using anti-PBP2 and anti-GFP antibodies confirmed the results obtained by the penicillin binding assay. To avoid the cross-reactivity of antibodies with *S. aureus* Protein A, SJF4596 (*S. aureus* SH1000 *pbp2::eyfp-pbp2* pCQ11-eYFP-PBP2) and SJF4597 (*S. aureus* SH1000 pCQ11-eYFP-PBP2) were transduced with a Φ11 lysate from *S. aureus* SH1000 *spa::kan*, with selection using kanamycin (50 μg ml^{-1}). The resulting strains were named SJF4600 (*S. aureus* SH1000 *spa::kan pbp2::eyfp-pbp2* pCQ11-eYFP-PBP2) and SJF4599 (*S. aureus* SH1000 *spa::kan* pCQ11-eYFP-PBP2). When SJF4599 grown in the presence of 1 mM IPTG and SJF4598 (*S. aureus* SH1000 *spa::kan pbp2::eyfp-pbp2*) were probed with the anti-PBP2 and anti-GFP antibodies they showed comparable levels of eYFP-PBP2 (~100 kDa band) (Figure 5.7E and F). The amounts of eYFP-PBP2 and its processed form (~80 kDa band) were proportionally the same (Figure 5.7E). Since IPTG seemed not to affect eYFP-PBP2 production in SJF4696, and the control SJF4599 strain was grown in the presence of the inducer, only SJF4600 grown with 1 mM IPTG was probed with the antibodies and showed an increased level of the fusion protein when compared to SJF4598 and SJF4599 (Figure 5.7E and F). Furthermore, detection with the anti-PBP2 antibodies showed that the amounts of eYFP-PBP2 and the 80 kDa protein were equivalent in SJF4600 (Figure 5.7E), which was in contrast to the data obtained for Pen-AF647 labelled PBPs. Interestingly the 80 kDa band was only detected by the anti-PBP2 antibodies but not by the anti-GFP antibodies, indicating that this protein did not have the eYFP tag. Additional bands of ~ 50 kDa were detected in all membrane preparations by the anti-GFP antibodies (Figure 5.7F), and likely represented a product of unspecific cross-reactivity of the antibodies.

The results from the penicillin assay and western blot analysis suggested that PBP2 fused to eYFP was unstable and/or non-functional and was processed to a wild type like PBP2 form, which was of the same size as native PBP2. This truncated protein was then likely functional and able to restore the wild type growth of the *pbp2::eyfp-pbp2* mutants.

Addition of the plasmid born *eyfp-pbp2* in SJF4596 (*S. aureus* SH1000 *pbp2::eyfp-pbp2* pCQ11-eYFP-PBP2) restored growth and morphology. Even though in SJF4596 eYFP-PBP2 was found not to be stable, it suggested that the fusion was able to

complement *pbp2*. PBPs are involved in peptidoglycan synthesis and HADA is a fluorescent D-amino acid that is incorporated during peptidoglycan synthesis (Kuru et al., 2012). It can be used for marking sites of active peptidoglycan production, and hence can be used as an indicator of a location of PBPs that are actively involved in the process of building nascent peptidoglycan. eYFP-PBP2 was presumed to not be fully functional, therefore SJF4596 grown to early-exponential phase in BHI erythromycin (5 μg ml^{-1}) was labelled with 500 μM HADA for 5 min and fixed cells were imaged by fluorescence microscopy. When fluorescence of HADA incorporated by SJF4596 was compared to SH1000 pulsed with HADA, no difference in the intensity of signal could be observed (Figure 5.8). Both the parental strain and the mutant gave fluorescent signals associated mainly with the cell septa and less the off-septal regions (Figure 5.8). Interestingly, in cells in which eYFP-PBP2 was observed to give a relatively high fluorescent signal both from the midcell and cell periphery, the off-septal label was not accompanied by an equal off-septal signal from HADA (Figure 5.8B). In most of the cells, even in enlarged ones with eYFP-PBP2 dispersed around the cell membrane, HADA was unaffected and it was still incorporated in the cross wall (Figure 5.8B). This indicated that eYFP-PBP2 was either not fully functional, it was not able to recognise a substrate containing HADA or that HADA incorporation is not primarily via PBP2.

5.2.1.3 Localisation of eYFP-PBP2 by STORM

SJF4596 (*S. aureus* SH1000 *pbp2::eyfp-pbp2* pCQ11-eYFP-PBP2) was alive and had morphology close to that of SH1000. Although eYFP-PBP2 was processed to a shorter form this did not show that the localisation pattern of eYFP-PBP2 was perturbed. Therefore eYFP-PBP2 localisation was studied by STORM.

SJF4596 was grown to early-exponential phase in the presence of erythromycin (5 μg ml^{-1}), fixed with paraformaldehyde and mounted in GLOX MEA buffer. A 514 nm light wavelength was used to activate and localise single eYFP-PBP2 molecules. eYFP-PBP2 did not blink well, it emitted a weak fluorescent signal and the events were not well isolated. Changes in laser powers or buffering conditions for just MEA or GLOX did not bring any improvements in the blinking performance of eYFP-PBP2.

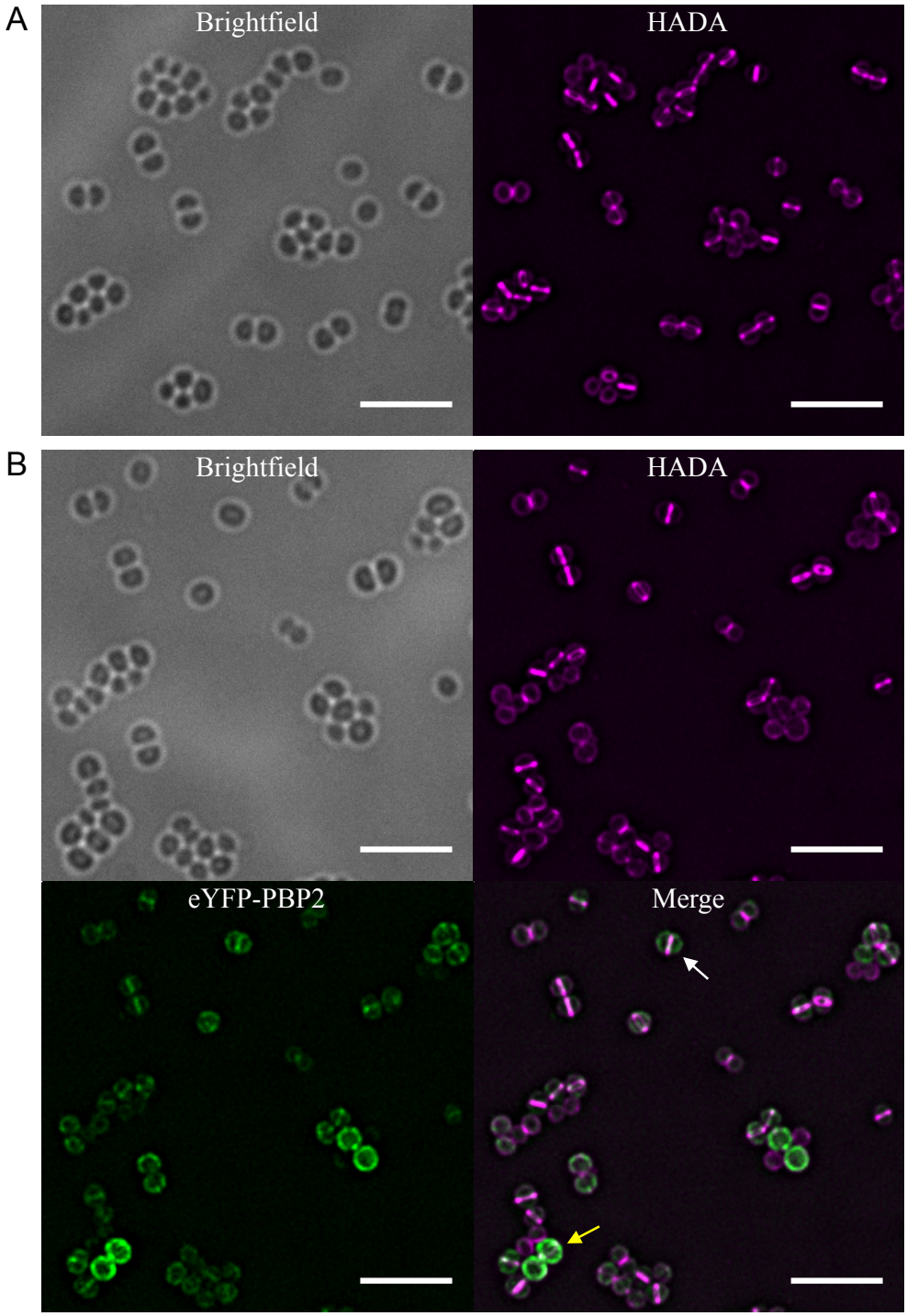

Figure 5.8. HADA incorporation in SJF4596

A. SH1000 labelled for 5 min with 500 µM HADA. The fluorescence image is a maximum intensity projection of deconvolved z-stack images acquired at 200 nm z-intervals. Scale bars 5 µm.

B. In SJF4596 (*S. aureus* SH1000 *pbp2::eyfp-pbp2* pCQ11-eYFP-PBP2) HADA is incorporated into cell septa, similar to SH1000 (A). A cell, in which high peripheral eYFP-PBP2 signal is not accompanied by increased off-septal HADA incorporation is indicated by a white arrow. A yellow arrow indicates a cell in which HADA is incorporated into the cell septum, while eYFP-PBP2 is dispersed all around the cell membrane. The fluorescence images are maximum intensity projections of deconvolved z-stack images acquired at 200 nm z-intervals. Scale bars 5 µm.

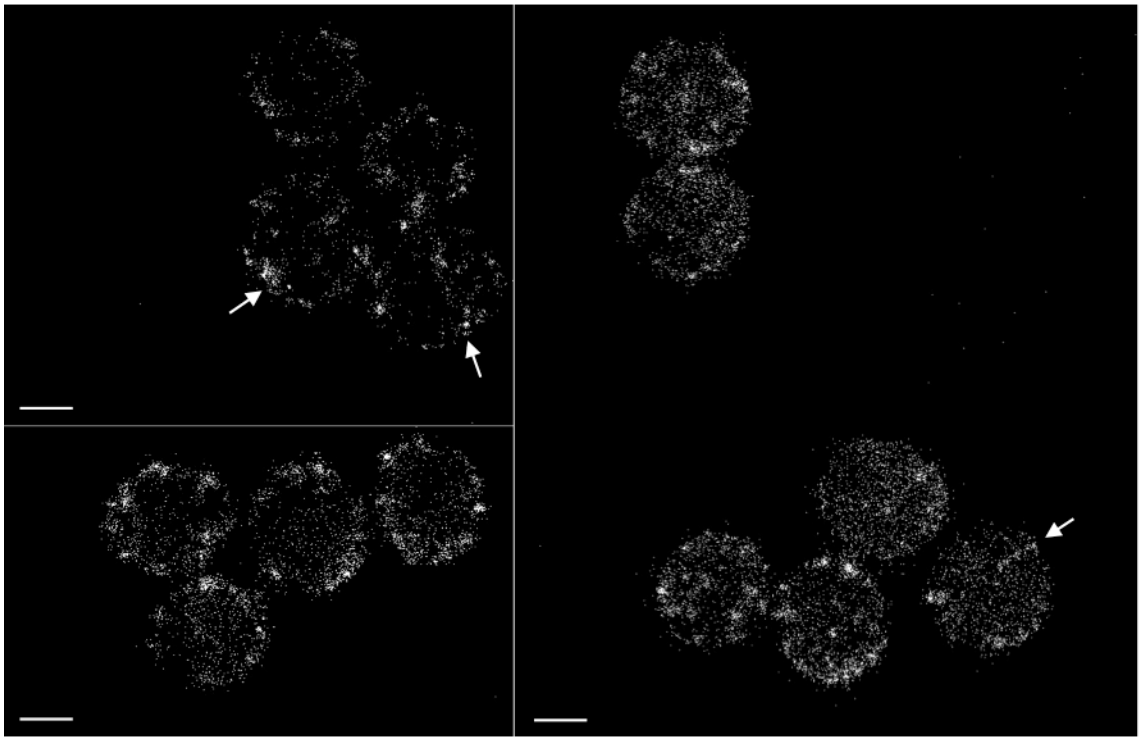

Figure 5.9. eYFP-PBP2 localisation by STORM

eYFP-PBP2 localisation in SJF4596 (*S. aureus* SH1000 *pbp2::eyfp-pbp2* pCQ11-eYFP-PBP2) by STORM. Imaging performed in GLOX MEA. White arrows indicate cells with the fusion protein located in the presumptive cell septa. The reconstructions present eYFP-PBP2 locations recorded in 3D and projected to 2D images. Scale bars 500 nm.

Reconstruction of recorded positions of the fluorophore showed eYFP-PBP2 to be randomly located, with some regions of a higher molecule concentration at the cell membrane, dispersed across the whole cell (Figure 5.9). In a few cells eYFP-PBP2 could be seen localised to the presumptive division septa, however the number or recorded events was comparable to blinks associated with cell periphery (Figure 5.9).

There are estimated about 450 PBP2 molecules per cell in *S. aureus* (Pucci and Dougherty, 2002). PBP2 is not an abundant protein when compared to 10,000-20,000 molecules of predicted EzrA in *B. subtilis* cells (Haeusser et al., 2004). The relatively low amount of PBP2 molecules and instability of eYFP-PBP2 may explain the quality of the obtained STORM data.

5.2.2 Removal of PBPs in *S. aureus*

Fluorescent proteins are one of the ways to tag PBPs. eYFP-PBP2 was unstable in the absence of native PBP2 and therefore the localisation studies could not solely rely on this fluorescent fusion. Thus an alternative method for PBP2 labelling was required. Immunostaining is one of the ways to stain a protein of interest and has been previously used to study PBP1 and PBP2 localisations in *S. aureus* (Pinho and Errington, 2003; Pereira et al., 2007). Immunostaining is however impractical in terms of super-resolution microscopy localisation. Antibodies are large molecules (~150 kDa) (Janeway et al., 2001), therefore they add an extra distance between a fluorophore and a target protein and can alter the precision of localisation. Moreover, PBPs are membrane associated proteins with large periplasmic domains (Goffin and Ghuysen, 1998) and a gentle treatment with lysostaphin, which can destroy cellular integrity, is required so that antibodies can go through the *S. aureus* peptidoglycan layer and bind PBPs. In *S. aureus* all PBPs have the transpeptidase activity (Pinho et al., 2013) and β-lactam antibiotics mimic the structure of D-Ala-D-Ala residues, the substrate for the transpeptidase and bind irreversibly the active site of PBPs (Zapun et al., 2008a). The fluorescent derivatives of penicillins, such as Bocillin FL can be used to label and detect PBPs present in the cell (Zhao et al., 1999). Although penicillin is selective against PBPs, however it recognises all PBPs and does not have high selective affinity for one particular PBP. In order to label only PBP2 in *S. aureus* the pool of other PBPs had to be reduced. PBP3 and PBP4 are not essential and they can be removed without

affecting cell phenotype (Pinho et al., 2013). PBP1 and PBP2 are crucial but it has been suggested that the physical presence, not the transpeptidase activity of PBP1, is required (Pinho et al., 2001a; Pereira et al., 2007, 2009). Therefore attempts to construct an *S. aureus* strain, in which PBP3 and PBP4 were not produced and the PBP1 transpeptidase domain was inactivated, were made.

5.2.2.1 Construction of an *S. aureus pbp3 pbp4* mutant

As mentioned above, PBP3 and PBP4 are not essential enzymes for *S. aureus* growth and division. Mutants of *pbp3* and *pbp4* are available in the Nebraska Transposon Mutant Library of *S. aureus* JE2 (Fey et al., 2013). Both in NE420 (*S. aureus* JE2 *pbp3::Tn*) and NE679 (*S. aureus* JE2 *pbp4::Tn*) the transposon (Tn) is inserted in the 5' end of the *pbp3* or *pbp4* gene interrupting them, resulting in their inactivation.

The chromosomal regions containing the Tn insertions were transferred from NE420 and NE679 into *S. aureus* SH1000 by Φ11 transduction, with selection using erythromycin (5 μg ml^{-1}), resulting in SJF4421 (*S. aureus* SH1000 *pbp3::Tn*) and SJF4425 (*S. aureus* SH1000 *pbp4::Tn*). Tn carries an erythromycin resistance cassette and in order to construct a double *pbp3 pbp4* mutant the erythromycin cassette in one of the single mutants had to be exchanged for another resistance marker. In SJF4421 the erythromycin cassette was swapped for the spectinomycin resistance (SpecR) cassette. SJF4421 was transduced with a phage lysate from SJF4311 (*S. aureus* RN4220 pSPC). In SJF4311 a thermosensitive pSPC plasmid (Figure 5.10A) carries the SpecR cassette flanked by ~500 bp fragments (Tn up and Tn down) that are homologous to the 5' and 3' ends of the Tn, allowing for its allelic exchange. Transformants were selected using chloramphenicol (10 μg ml^{-1}) and spectinomycin (250 μg ml^{-1}) at 28°C. A single colony was streaked on a BHI chloramphenicol (10 μg ml^{-1}) and spectinomycin (250 μg ml^{-1}) plate and incubated overnight at 42°C to initiate a single crossover event. A large colony, which was likely a single crossover recombinant, was grown in BHI at 28°C to initiate a double crossover event (Figure 5.10A). After four passages the cell culture was serially diluted, plated on BHI containing spectinomycin (250 μg ml^{-1}) and incubated at 37°C overnight. The colonies were tested for spectinomycin resistance and erythromycin sensitivity. A clone, which was spectinomycin resistant but no longer grew on erythromycin, was named SJF4422 (*S. aureus* SH1000 *pbp3::spec*).

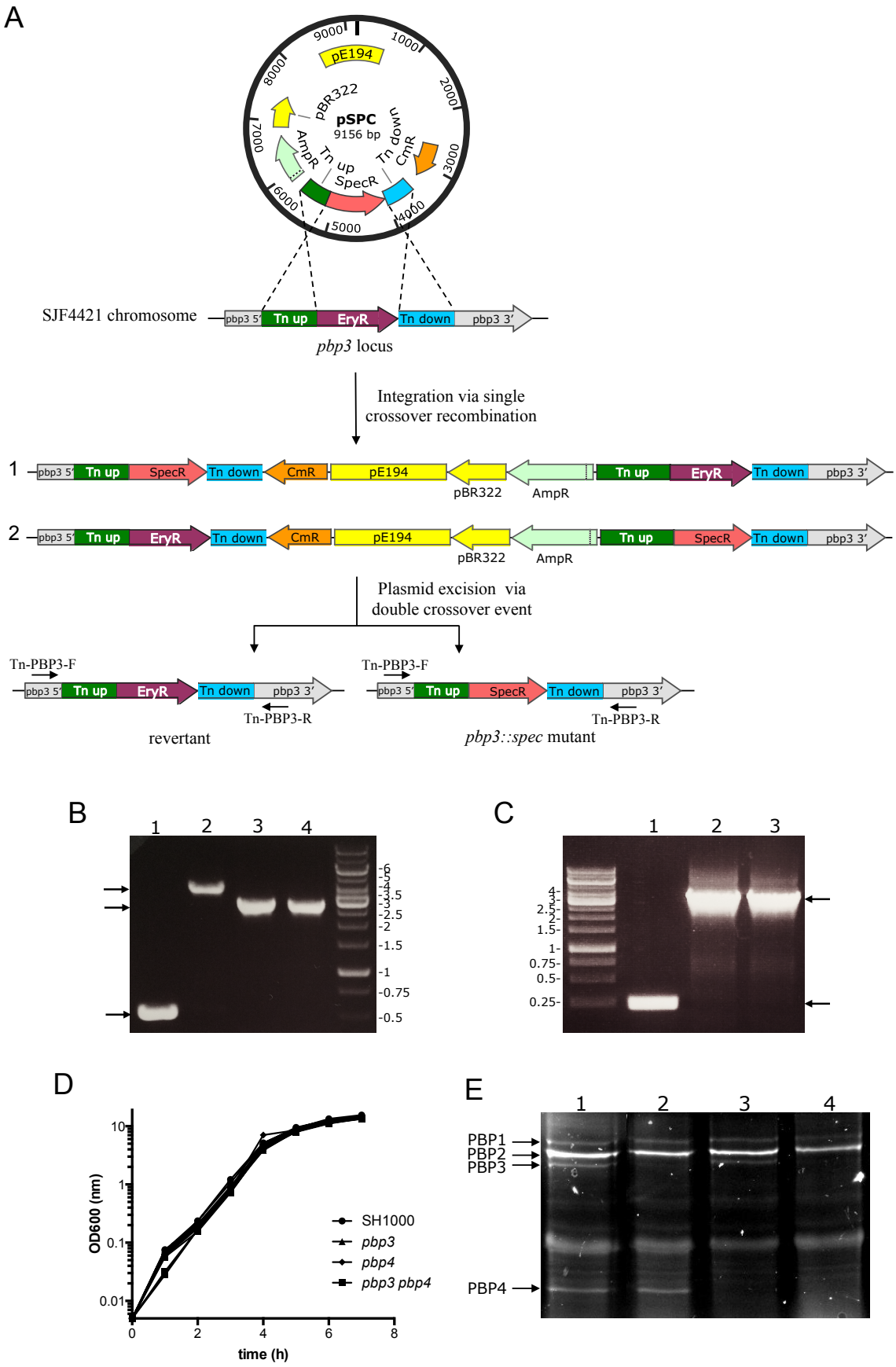

Figure 5.10. Construction of an *S. aureus pbp3 pbp4* mutant

A. Map of the pSPC plasmid used for allelic exchange of the transposon for the spectynomycin cassette within the *pbp3* gene and diagrammatic representation of the likely recombination outcomes. pSPC comprises the high-copy-number pBR322 origin of replication (pBR322), the staphylococcal thermosensitive origin of replication form pE194 (pE194), the ampicillin resistance (AmpR), the chloramphenicol resistance (CmR) and spectinomycin resistance (SpecR) cassettes, and the ~500 bp fragments homologous to the 5' and 3' ends of the transposon (Tn up and Tn down). A single crossover event can occur through either the Tn up (1) or the Tn down (2) fragment of the transposon (Tn up-EryR-Tn down). After the double crossover event either the former genotype is regained (revertant) or the mutant strain SJF4422 (*S. aureus* SH1000 *pbp3::spec*) is created. Annealing sites of primers Tn-PBP3-F and Tn-PBP3-R used to confirm replacement of the Tn for the spectinomycin resistance cassette are indicated. Not to scale.

B. Replacement of Tn for the spectinomycin resistance (SpecR) cassette in the *pbp3* gene was confirmed by PCR of extracted genomic DNA using Tn-PBP3-F and Tn-PBP3-R primers. Tn-PBP3-F and Tn-PBP3-R anneal ~250 bp upstream and ~ 250 bp downstream of the Tn/SpecR cassette insertion site in the *pbp3* gene, respectively. 1, SH1000; 2, SJF4421 (*S. aureus* SH1000 *pbp3::Tn*); 3, SJF4422 (*S. aureus* SH1000 *pbp3::spec*); 4, SJF4423 (*S. aureus* SH1000 *pbp3::spec pbp4::Tn*). The expected DNA fragments of 0.5 kb, 2.7 kb and 3.7 kb are indicated with black arrows. Sizes of a DNA ladder are shown in kb.

C. Insertion of the Tn within the *pbp4* gene was confirmed by PCR using PBP4-2 and PBP4-3 primers on extracted genomic DNA. PBP4-2 and PBP4-3 primers anneal ~70 bp upstream and ~ 180 bp downstream of the Tn insertion site in the *pbp4* gene, respectively. 1, SH1000; 2, SJF4425 (*S. aureus* SH1000 *pbp4::Tn*); 3, SJF4423 (*S. aureus* SH1000 *pbp3::spec pbp4::Tn*). The expected DNA fragments of 0.25 kb and 3.5 kb are indicated with black arrows. Sizes of a DNA ladder are shown in kb.

D. Growth of: *pbp3*, SJF4422 (*S. aureus* SH1000 *pbp3::spec*); *pbp4*, SJF4425 (*S. aureus* SH1000 *pbp4::Tn*); *pbp3 pbp4*, SJF4423 (*S. aureus* SH1000 *pbp3::spec pbp4::Tn*) was measured by optical density. The doubling times of the mutants were similar to SH1000 and lasted ~25 min. Bacterial cultures were prepared in triplicate and the error bars represent standard deviation from the mean.

E. Analysis of penicillin binding protein (PBPs) profiles in SJF4422 (*S. aureus* SH1000 *pbp3::spec*), SJF4425 (*S. aureus* SH1000 *pbp4::Tn*) and SJF4423 (*S. aureus* SH1000 *pbp3::spec pbp4::Tn*) by Bocillin FL labelling. The membrane fractions (30 μg protein) of SH1000 (lane 1), SJF4422 (lane 2), SJF4425 (lane 3) and SJF4423 (lane 4) were labelled with 25μM Bocillin FL at 37^{o}C for 10 min. Bands identified as PBP1, PBP2, PBP3 and PP4 are indicated.

SJF4422 was subsequently transduced with a phage lysate from SJF4425 (*S. aureus* SH1000 *pbp4::Tn*), with selection using spectinomycin (250 μg ml^{-1}) and erythromycin (5 μg ml^{-1}), resulting in the SJF4423 (*S. aureus* SH1000 *pbp3::spec pbp4::Tn*) strain. Interruption of the *pbp3* and *pbp4* genes in SJF4422, SJF4425 and SJF4423 by insertion of the Tn or the SpecR cassette was confirmed by PCR on extracted genomic DNA using primer pairs Tn-PBP3-F and Tn-PBP3-R, and PBP4-2 and PBP4-3 (Figure 5.10B and C). Tn-PBP3-F and Tn-PBP3-R annealed ~250 bp upstream and ~ 250 bp downstream of the Tn/SpecR cassette insertion site, respectively, in the *pbp3* gene, while PBP4-2 and PBP4-3 were positioned ~70 bp and ~ 180 bp, respectively, away from the Tn insertion within the *pbp4* gene.

PBP3 and PBP4 are not essential for growth and division of *S. aureus* (Pinho et al., 2013). SJF4422 (*S. aureus* SH1000 *pbp3::spec*), SJF4425 (*S. aureus* SH1000 *pbp4::Tn*) and SJF4423 (*S. aureus* SH1000 *pbp3::spec pbp4::Tn*) were confirmed to not exhibit any growth defect when their growth in liquid media was examined by optical density measurements (Figure 5.10D). All mutants grew with the same rate of ~25 min as the wild type strain (Figure 5.10D), showing that together PBP3 and PBP4 were not essential in *S. aureus*. SJF4423 had wild type growth when two essential PBPs, PBP1 and PBP2 were only present. This was also in agreement with results reported by another research group (Reed et al., 2015).

The profiles of PBPs in SJF4422 (*S. aureus* SH1000 *pbp3::spec*), SJF4425 (*S. aureus* SH1000 *pbp4::Tn*) and SJF4423 (*S. aureus* SH1000 *pbp3::spec pbp4::Tn*) were investigated by a gel-based Bocillin FL labelling. Membrane fractions were isolated from each strain grown to an OD_{600} of ~1. The membrane proteins (~30 μg) were incubated with 25 μM Bocillin FL for 10 min at 37^{o}C and separated in a 10% (w/v) SDS-PAGE gel. As expected, no band of ~77 kDa, which represents PBP3, was detected in SJF4422. SJF4425 did not have a band of ~48 kDa for PBP4. Neither PBP3 nor PBP4 were present in SJF4423. This confirmed that PBP3 or PBP4 or both PBP3 and PBP4 were not produced in SJF4422, SJF4425 and SJF4423, respectively (Figure 5.10E).

Introduction of the Tn and the spectinomycin resistance cassette in the *pbp4* and *pbp3* genes, respectively, resulted in inactivation of these genes and interrupted protein

production. Localisation of the remaining PBPs in in SJF4422 (*S. aureus* SH1000 *pbp3::spec*), SJF4425 (*S. aureus* SH1000 *pbp4::Tn*) and SJF4423 (*S. aureus* SH1000 *pbp3::spec pbp4::Tn*) was visualised using Bocillin FL. Cells were grown to early-exponential phase and incubated with 1 μg ml^{-1} Bocillin-FL for 5 min at 37^{o}C. Fixed cells were examined by fluorescence microscopy. Labelling using Bocillin FL showed that in the absence of PBP3 or/and PBP4 remaining PBPs formed the localisation pattern similar to one observed in the wild type strain, that is more signal at midcell and less in the cell periphery (Figure 5.11A and B). Although the general localisation pattern did not change upon *pbp3* and/or *pbp4* interruption, the amount of signal observed for a particular strain changed depending on a batch of Bocillin FL used for labelling (Figure 5.11A and B). Utilisation of Bocillin FL batch 1 showed reduction of fluorescent signal in strains lacking PBP3, but deletion of *pbp4* did not result in reduced Bocillin FL binding (Figure 5.11A). By contrast Bocillin FL batch 2 showed no difference in the distribution and intensity of fluorescent signals between SH1000 and mutants SJF4422, SJF4425 and SJF4423 (Figure 5.11B). In SJF423 PBP1 and PBP2 localised to the midcell, suggesting that these two proteins do not require the presence of PBP3 and PBP4 for septal recruitment.

To check if Bocillin FL selectively bound PBPs and the obtained signal was not a result of nonspecific labelling of the cell surface by Bocillin FL a competition assay using penicillin G (PenG) was performed (Figure 5.11C). When *S. aureus* SH1000 reached early exponential phase, it was incubated with 0, 0.01, 0.1, 1, 10 and 100 μg ml^{-1} PenG for 5 min at 37^{o}C. Cells were washed by centrifugation, grown with 1 μg ml^{-1} Bocillin FL for 5 min and fixed cells were visualised by fluorescence microscopy. Pretreatment with 0.01-0.1 μg ml^{-1} PenG reduced Bocillin FL binding, while 1 μg ml^{-1} PenG and above prevented fluorescent labelling by competition (Figure 5.11C), indicating that Bocillin FL bound specifically PBPs and not other cell structures in *S. aureus*.

PBP4 is a LMW transpeptidase involved in production of highly cross-linked peptidoglycan in *S. aureus* and its deletion leads to a decrease in the level of peptidoglycan cross-linking (Wyke et al., 1981; Memmi et al., 2008; Loskill et al., 2014; Qiao et al., 2014). PBP3 is a transpeptidase of unknown function and localisation in *S. aureus* (Pinho et al., 2000, 2013). Incorporation of nascent peptidoglycan by *pbp3*

and *pbp4* mutants was investigated by HADA labelling. SH1000, SJF4422 (*S. aureus* SH1000 *pbp3::spec*), SJF4425 (*S. aureus* SH1000 *pbp4::Tn*) and SJF4423 (*S. aureus* SH1000 *pbp3::spec pbp4::Tn*) were grown to early exponential phase and incubated with 500 μM HADA for 5 min. Cells were fixed and examined by fluorescence microscopy. While SH1000 and SJF4422 showed strong HADA labelling mostly at the septum, fluorescent signal was decreased both in SJF4423 and SJF4425 (Figure 4.11A). Closer investigation of distribution of fluorescence in the mutants depleted of *pbp4* revealed that although they had reduced HADA incorporation when compared to SH1000, HADA was still present in the cross wall and in the off-septal wall (Figure 4.11A). Although there was a reduction in HADA fluorescent signal detected for each mutant: SJF4422 was ~85%, SJF4425 was ~40% and SJF4423 was ~7% of SH1000, the ratio between the septal and off-septal labelling in the mutants was comparable to the ratio in the wild type strain (Victoria Lund, unpublished). This was in contrast to work published for an *S. aureus* COL Δ*pbp4* strain, in which *pbp4* deletion resulted in absence of peripheral signal and in an increase of the ratio septal/off-septal signal from incorporated NADA, which is a green analogue of HADA (Monteiro et al., 2015).

Decreased HADA incorporation could be a result of a HADA toxic effect on the mutant strains. Thus SH1000, SJF4422 (*S. aureus* SH1000 *pbp3::spec*), SJF4425 (*S. aureus* SH1000 *pbp4::Tn*) and SJF4423 (*S. aureus* SH1000 *pbp3::spec pbp4::Tn*) were grown in the absence and presence of 500 μM HADA (Figure 4.11B), which was the HADA concentration used for labelling experiments. All strains were found to grow with the same rate regardless of HADA absence or presence (Figure 4.11B), showing that HADA did not affect cell growth and thus it was an unlikely reason for reduction in nascent peptidoglycan incorporation in the *pbp3* and *pbp4* mutants but it was due to the role PBPs in the cell. Moreover, Victoria Lund (unpublished) has shown that the uptake of radiolabelled Glc*N*Ac was comparable between the wild type strain and SJF4422 SJF4425, and SJF4423, showing that differences in HADA incorporation were not caused by a reduced rate of peptidoglycan synthesis in the mutants (Victoria Lund, unpublished).

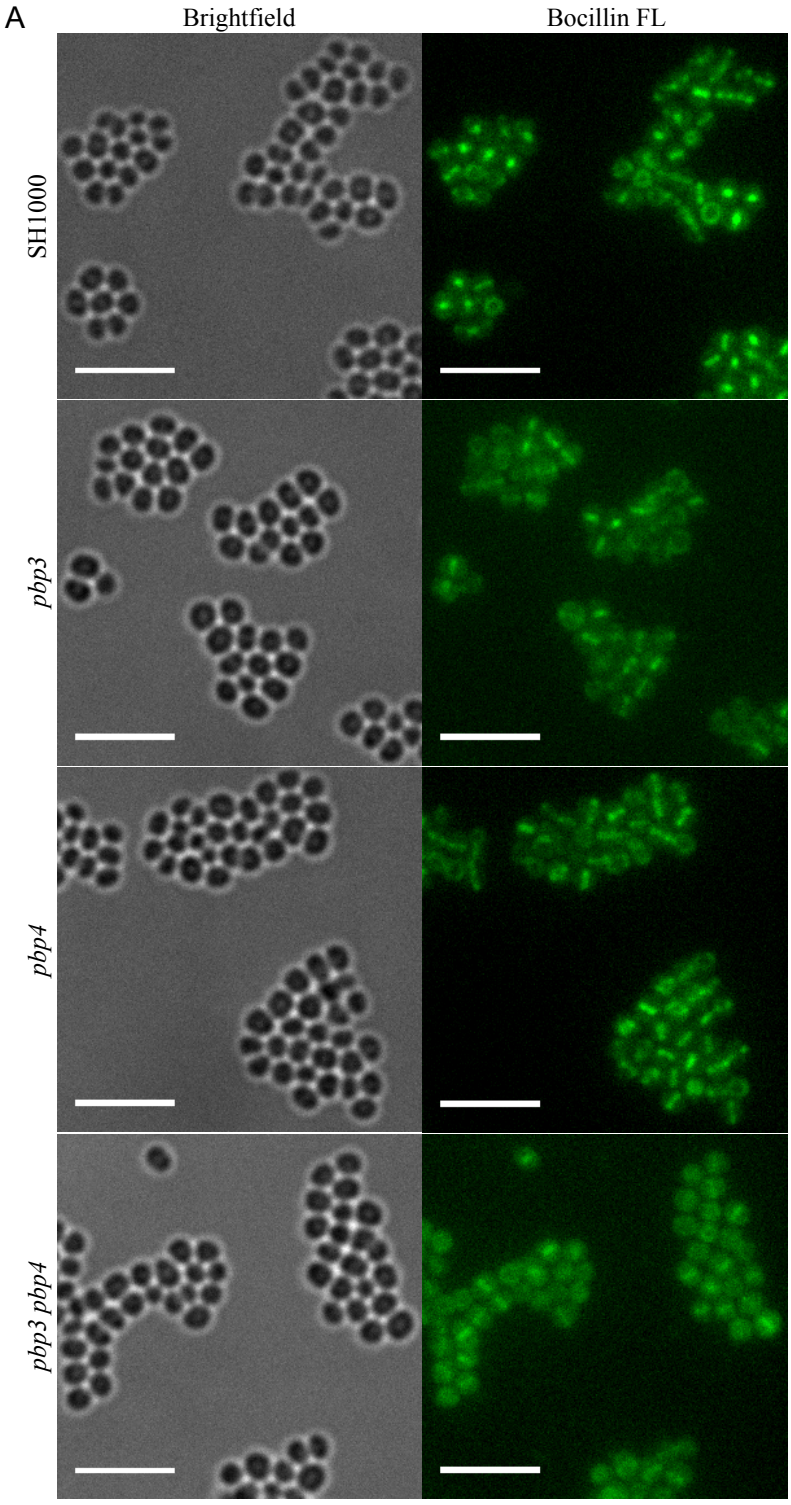
A
Brightfield
Bocillin FL
SH1000
pbp3
pbp4
pbp3 pbp4

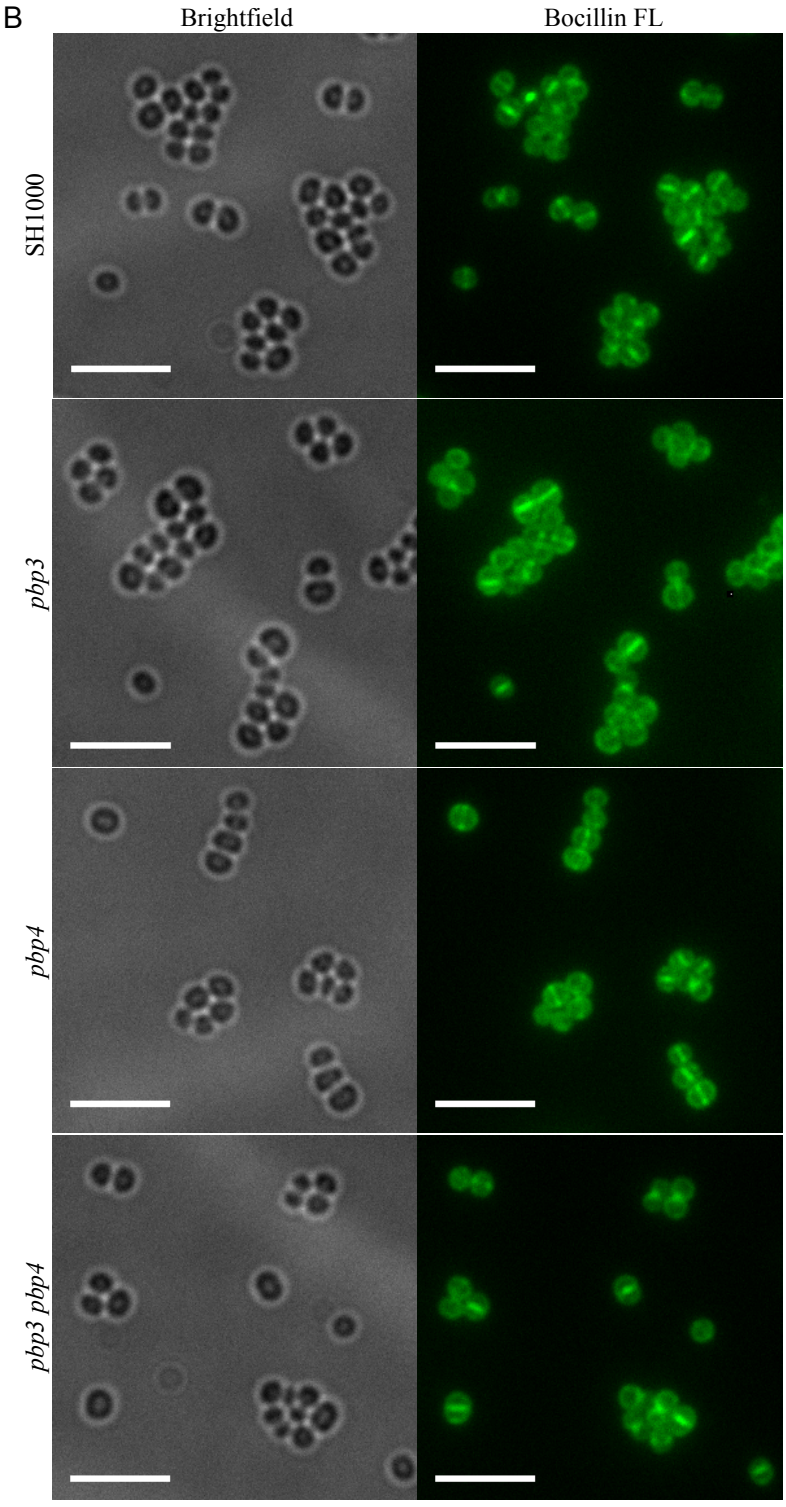
B
Brightfield
Bocillin FL
SH1000
pbp3
pbp4
pbp3 pbp4

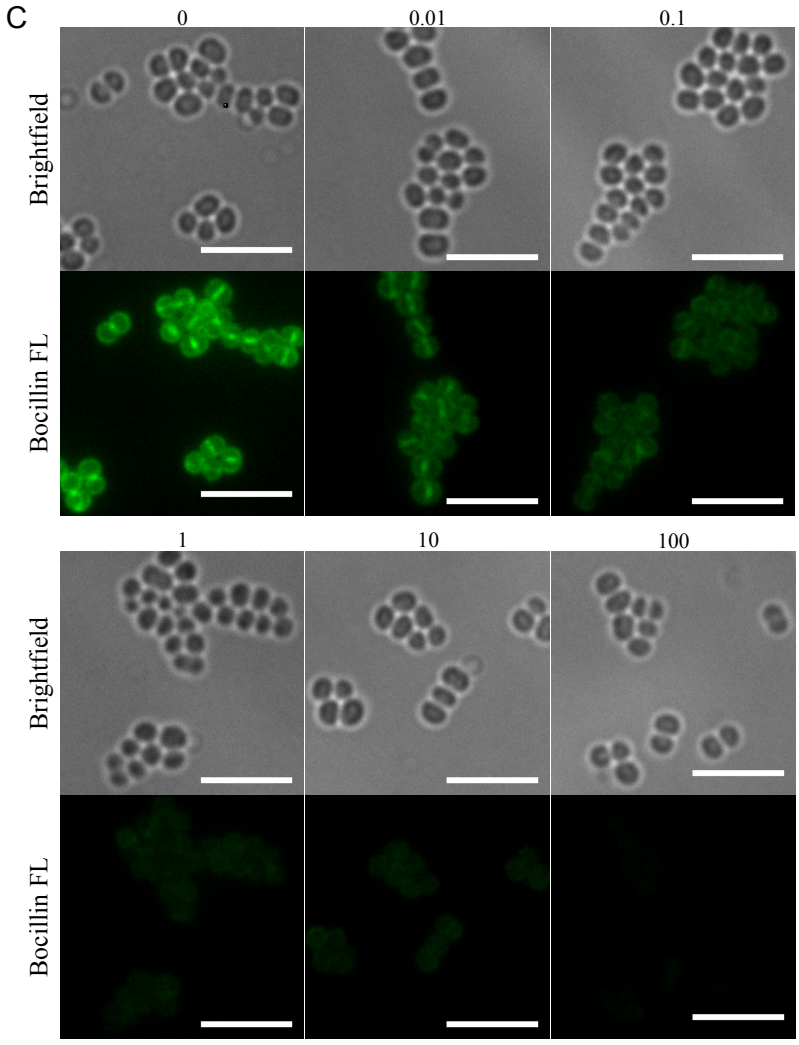

Figure 5.11. Localisation of PBPs in the *pbp3* and *pbp4* mutants using Bocillin FL

A. Bocillin FL, batch 1. *pbp3* - SJF4422 (*S. aureus* SH1000 *pbp3::spec*), *pbp4* - SJF4425 (*S. aureus* SH1000 *pbp4::Tn*) and *pbp3 pbp4* - SJF4423 (*S. aureus* SH1000 *pbp3::spec pbp4::Tn*) were stained with 1 μg ml^{-1} Bocillin FL (batch 1). Remaining PBPs localise to the septum, similar to all four PBPs in the wild type strain (SH1000). Mutants lacking PBP3 (*pbp3* and *pbp3 pbp4*) give a less defined pattern but overall it does not change. Fluorescence images are maximum intensity projections of z-stack images acquired at 200 nm z-intervals. The same contrast was adjusted to the fluorescence images. Scale bars 5 μm.

B. Bocillin FL, batch 2. *pbp3* - SJF4422 (*S. aureus* SH1000 *pbp3::spec*), *pbp4* - SJF4425 (*S. aureus* SH1000 *pbp4::Tn*) and *pbp3 pbp4* - SJF4423 (*S. aureus* SH1000 *pbp3::spec pbp4::Tn*) were stained with 1 μg ml^{-1} Bocillin FL (batch 2). Reduction of PBPs does not result in reduced signal from Bocillin FL. Fluorescence images are maximum intensity projections of z-stack images acquired at 200 nm z-intervals. The same contrast was adjusted to the fluorescence images. Scale bars 5 μm.

C. Competition of labelling between PenG and Bocillin FL in *S. aureus* SH1000. SH1000 was grown with 0, 0.01, 0.1, 1, 10 and 100 μg ml^{-1} PenG for 5 min, washed by centrifugation and incubated with 1 μg ml^{-1} Bocillin FL (batch 2) for 5 min. Pretreatment with PenG inhibited Bocillin FL binding. Fluorescence images are maximum intensity projections of z-stack images acquired at 200 nm z-intervals. The same contrast was adjusted to the fluorescence images Scale bars 5 μm.

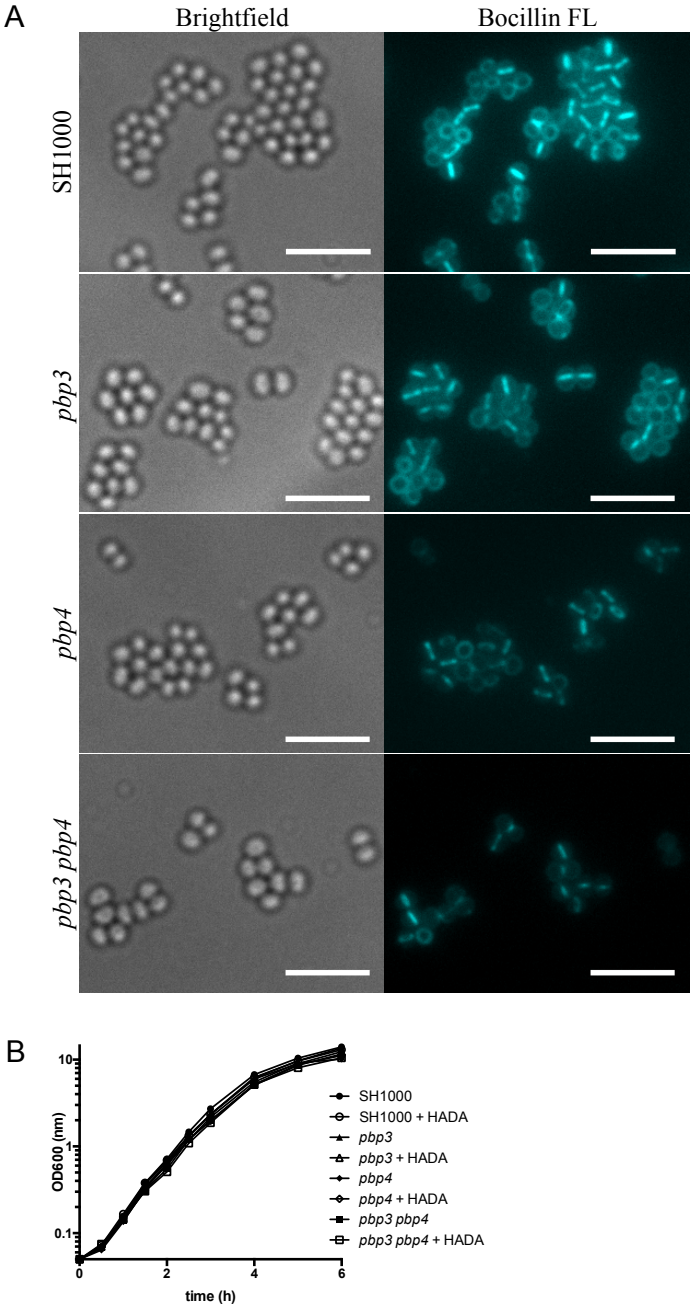

Figure 5.12. Incorporation of nascent peptidoglycan in the *pbp3* and *pbp4* mutants

A. *S. aureus* SH1000, *pbp3* - SJF4422 (*S. aureus* SH1000 *pbp3::spec*), *pbp4* - SJF4425 (*S. aureus* SH1000 *pbp4::Tn*) and *pbp3 pbp4* - SJF4423 (*S. aureus* SH1000 *pbp3::spec pbp4::Tn*) were grown to early-exponential phase and incubated with 500 µM HADA for 5 min at 37°C. Mutants lacking PBP4 (*pbp4* and *pbp3 pbp4*) showed reduction of fluorescent signal both in the cross wall and at peripheral cell wall. Fluorescence images are maximum intensity projections of z-stack images acquired at 200 nm z-intervals. The same contrast was adjusted to the fluorescence images. Scale bars 5 µm.

B. Growth of *S. aureus* SH1000, *pbp3* - SJF4422 (*S. aureus* SH1000 *pbp3::spec*), *pbp4* - SJF4425 (*S. aureus* SH1000 *pbp4::Tn*) and *pbp3 pbp4* - SJF4423 (*S. aureus* SH1000 *pbp3::spec pbp4::Tn*) in the absence and presence (+ HADA) of 500 µM HADA measured by optical density. HADA does not affect growth of the mutants and they grow with the similar rate as SH1000.

5.2.2.2 Construction of an *S. aureus pbp1** mutant

In SJF4423 (*S. aureus* SH1000 *pbp3::spec pbp4::Tn*) deletion of *pbp3* and *pbp4* did not cause any obvious morphological changes and it showed mostly septal associated signal when it was labelled with Bocillin FL, indicating the localisation of two remaining PBPs (PBP1 and PBP2). PBP1 is an essential enzyme, but it has been shown that cells with an inactivated PBP1 transpeptidase domain, that is Ser314Ala point mutation, were alive, suggesting that the physical presence of PBP1 is essential, not its activity (Pereira et al., 2009). An attempt to construct a triple *S. aureus* mutant, in which PBP3 and PBP4 are absent and PBP1 was inactivated (PBP1*), therefore allowing for localisation of PBP2, the only remaining active transpeptidase, using a fluorescent derivative of penicillin, was made.

A plasmid for allelic replacement of *pbp1* with nonfunctional *pbp1* (*pbp1**) was constructed. A ~1.3 kb fragment (up) covering an upstream region of *pbp1* (from -1 bp to -334 bp) and the 5' *pbp1* fragment (first 950 bp of the *pbp1* coding sequence), and a ~1.3 kb fragment (down) comprising the 3' fragment of *pbp1* (930-2235 bp region) were PCR amplified from *S. aureus* SH1000 genomic DNA using primer pairs pbp1*5'-F and pbp1*5'-R, and pbp1*3'-F and pbp1*3'-R, respectively (Figure. 5.13A and C). Primers pbp1*5'-R and pbp1*3'-F were designed to introduce a T to G point mutation resulting in a Ser314Ala substitution (Figure 5.13B). The PCR products were resolved on a 1% (w/v) agarose gel (Figure 5.13D), purified and ligated with the pMAD plasmid cut with *EcoRI* and *BamHI* by Gibson assembly (Figure 5.15C). The assembly products were transformed into chemically competent *E. coli* NEB5α cells with selection on LB plates containing ampicillin (100 μg ml^{-1}) at 28°. Positive clones were verified by plasmid extraction and restriction digestion with *SacI* (Figure 5.13E). Plasmids were sequenced by GATC Biotech to check for the introduction of the designed mutation. The resulting vector, pMAD-PBP1* (Figure 5.13C) had the expected sequence.

pMAD-PBP1* was transformed into electrocompetent *S. aureus* RN4220 with selection on BHI plates containing erythromycin (5 μg ml^{-1}), lincomycin (25 μg ml^{-1}) and X-Gal (80 μg ml^{-1}) at 28°C, resulting in dark blue colonies, indicating successful transformation.

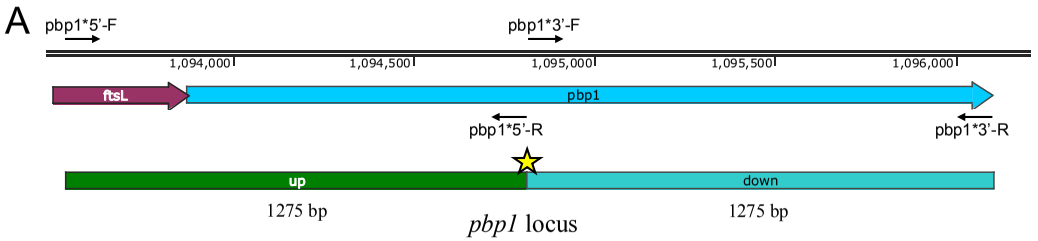
A
pbp1*5'-F
pbp1*3'-F
1,094,000
1,094,500
1,095,000
1,095,500
1,096,000
ftsL
pbp1
pbp1*5'-R
pbp1*3'-R
up
down
1275 bp
1275 bp
pbp1 locus

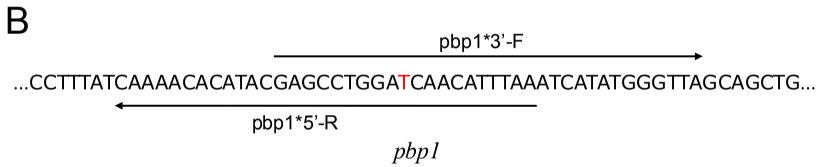
B
pbp1*3'-F
...CCTTTATCAAAACACATACGAGCCTGGATCAACATTTAAATCATATGGGTTAGCAGCTG...
pbp1*5'-R
pbp1

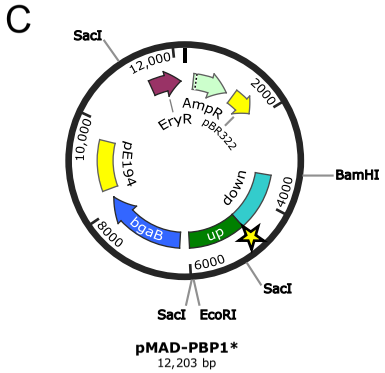
C
SacI
12,000
2000
AmpR
EryR
pBR322
10,000
pE194
down
BamHI
4000
8000
bgaB
up
6000
SacI
SacI
EcoRI
pMAD-PBP1*
12,203 bp

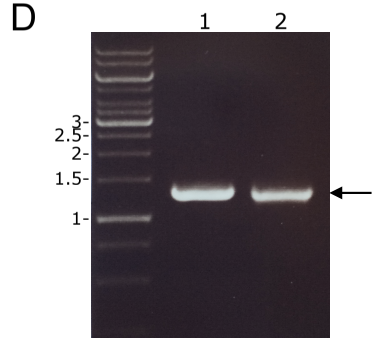
D
1
2
3
2.5
2
1.5
1

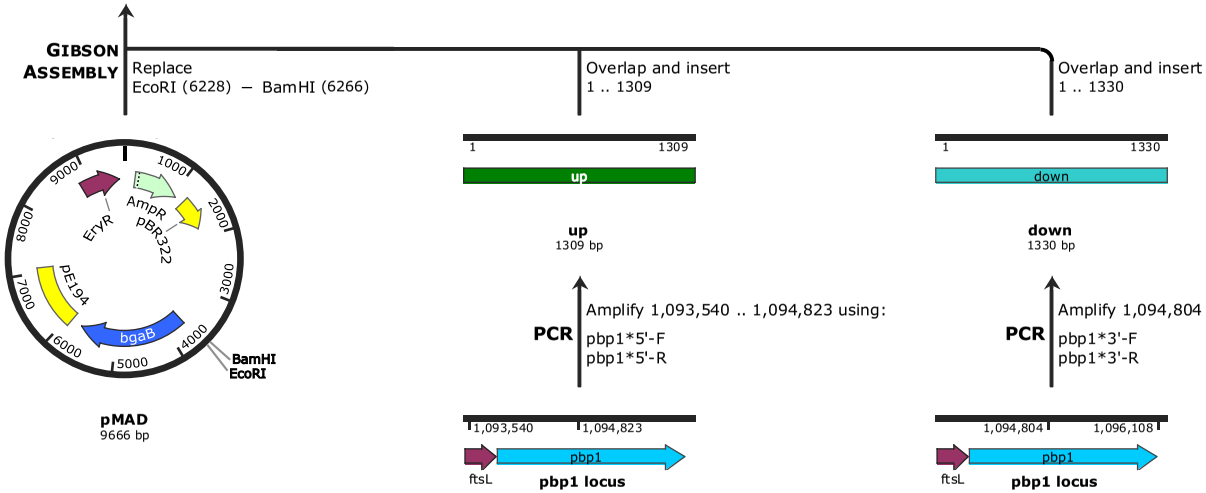
GIBSON ASSEMBLY
Replace
EcoRI (6228) – BamHI (6266)
Overlap and insert
1 .. 1309
Overlap and insert
1 .. 1330
9000
1000
AmpR
EryR
pBR322
2000
8000
pE194
3000
7000
bgaB
6000
4000
5000
BamHI
EcoRI
pMAD
9666 bp
1
1309
up
up
1309 bp
1
1330
down
down
1330 bp
PCR
Amplify 1,093,540 .. 1,094,823 using:
pbp1*5'-F
pbp1*5'-R
PCR
Amplify 1,094,804 .. 1,096,108 using:
pbp1*3'-F
pbp1*3'-R
1,093,540
1,094,823
pbp1
ftsL
pbp1 locus
1,094,804
1,096,108
pbp1
ftsL
pbp1 locus

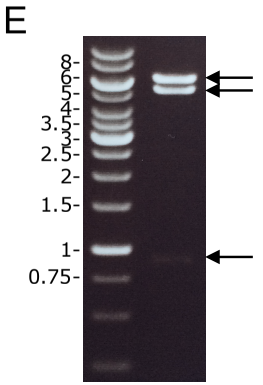
E
8
6
5
4
3.5
3
2.5
2
1.5
1
0.75

Figure 5.13. Construction of pMAD-PBP1*, a plasmid for PBP1 inactivation in *S. aureus*

A. Schematic representation of the chromosome region of *pbp1* in *S. aureus*. The coding sequence of *pbp1* overlaps with the 3' end of the *ftsL* gene. The locations of pbp1*5'-F, pbp1*5'-R, pbp1*3'-F and pbp1*3'-R annealing sites allowing for amplification of ~1.3 kb fragments (up and down) are indicated. The star indicates position of the Ser315Ala mutation within the *pbp1* gene.

B. A fragment of the nucleotide sequence of the *pbp1* gene. The T residue that is a part of the Ser314 codon and which was substituted for G is indicated in red. Primers pbp1*5'-R and pbp1*3'-F were used to introduce the Ser315Ala mutation and their annealing sites to the *S. aureus* chromosome are indicated.

C. Diagrammatic representation of pMAD-PBP1* construction. A ~ 1.3 kb fragment (up) covering the region from -1 bp to -334 bp upstream of the *pbp1* gene and the 5' end (1-950 bp) of the *pbp1* coding sequence, and a ~1.3 kb fragment (down) comprising the 3' fragment of *pbp1* (930-2235 bp) were PCR amplified from *S. aureus* SH1000 genomic DNA using primers pbp1*5'-F and pbp1*5'-R, and pbp1*3'-F and pbp1*3'-R, respectively. The up and down fragments were joined with *BamHI* and *EcoRI* cut pMAD by Gibson assembly. The resulting pMAD-PBP1* vector comprises an *E. coli* pBR322 origin of replication (pBR322), a staphylococcal pE194 thermosensitive origin of replication (pE194), a *bgaB* gene encoding a thermostable β-galactosidase from *Bacillus stearothermophilus* (BgaB), the ampicillin resistance (AmpR) and erythromycin resistance (EryR) cassettes and the up-down cassette for homologous recombination of *pbp1*. The star indicates position of the Ser315Ala mutation within the *pbp1* gene.

D. 1% (w/v) TAE agarose gel showing products of PCR amplification of the up (1) and the down (1) fragments using primer pairs pbp1*5'-F and pbp1*5'-R, and pbp1*3'-F and pbp1*3'-R, respectively. The expected DNA fragments of ~ 1.3 kb are indicated with a black arrow. Sizes of a DNA ladder are shown in kb. The products of the PCR reaction were used in the Gibson assembly (C).

E. Restriction enzyme analysis of the pMAD-PBP1* plasmid with *SacI*. The expected DNA bands of 6 kb, 5.3 kb and 0.9 kb are indicated with black arrows. Sizes of a DNA ladder are shown in kb.

pMAD-PBP1* was moved into *S. aureu*s SH1000 by phage transduction and incubation at 28°C in the presence of erythromycin (5 μg ml^{-1}), lincomycin (25 μg ml^{-1}) and X-Gal (80 μg ml^{-1}). One blue colony was selected and grown overnight in BHI erythromycin (5 μg ml^{-1}) and lincomycin (25 μg ml^{-1}) at 42°C to initiate plasmid integration into the *S. aureus* chromosome via a single crossover event (Figure 5.14). The overnight culture was serially diluted, spread on BHI plates containing erythromycin (5 μg ml^{-1}), lincomycin (25 μg ml^{-1}) and X-Gal (80 μg ml^{-1}) and cells were incubated at 42°C overnight. A light blue colony, SJF4430 (*S. aureus* SH1000 *pbp1::*pMAD-PBP1*), which was a single crossover recombinant, was grown in BHI without any antibiotic at 28°C in order to initiate a double crossover event (Figure 5.14). After several passages the culture was serially diluted and plated on BHI containing X-Gal and incubated overnight at 42°C. The white colonies were tested for erythromycin sensitivity. The *pbp1* gene region was PCR amplified on genomic DNA extracted from the erythromycin sensitive clones using up-pbp1-F and down-pbp1-R primers, which annealed 42 bp upstream of the *ftsL* gene and 70 bp downstream of the *pbp1* gene (Figure 5.14). PCR products were purified and sent for sequencing to screen for the Ser314Ala substitution in *pbp1*. Unfortunately, all 400 tested candidates had the wild type genotype (Figure 5.14).

The resolution of pMAD-PBP1* via homologous recombination led to recreation of wild type *pbp1,* indicating that the transpeptidase activity of PBP1 was crucial and creation of the *pbp1** mutant was impossible due to lethality of PBP1 inactivation. Therefore an ectopic copy of *pbp1* under the control of the Pspac promoter was introduced into SJF4430 (*S. aureus* SH1000 *pbp1::*pMAD-PBP1*) to resolve the *pbp1** mutation in the *pbp1* native locus and to examine if the PBP1 transpeptidase activity was required for *S. aureus* vitality.

A plasmid encoding functional PBP1 was constructed. The putative RBS and the full length *pbp1* gene were PCR amplified from *S. aureus* genomic DNA using pCQ-pbp1-F and pCQ-PBP1-R primers (Figure 5.15A and B). The expected DNA fragment of ~2.3 kDa was cloned into the *NheI* and *NcoI* cut pCQ11-FtsZ-SNAP plasmid (Fabien Grein, unpublished) by Gibson assembly, resulting in the pCQ11-PBP1-SNAP plasmid (Figure 5.15B). pCQ11-PBP1-SNAP was verified by digestion with *EcoRI* and *AscI* (Figure 5.15C) and confirmed to have the correct sequence by GATC Biotech sequencing.

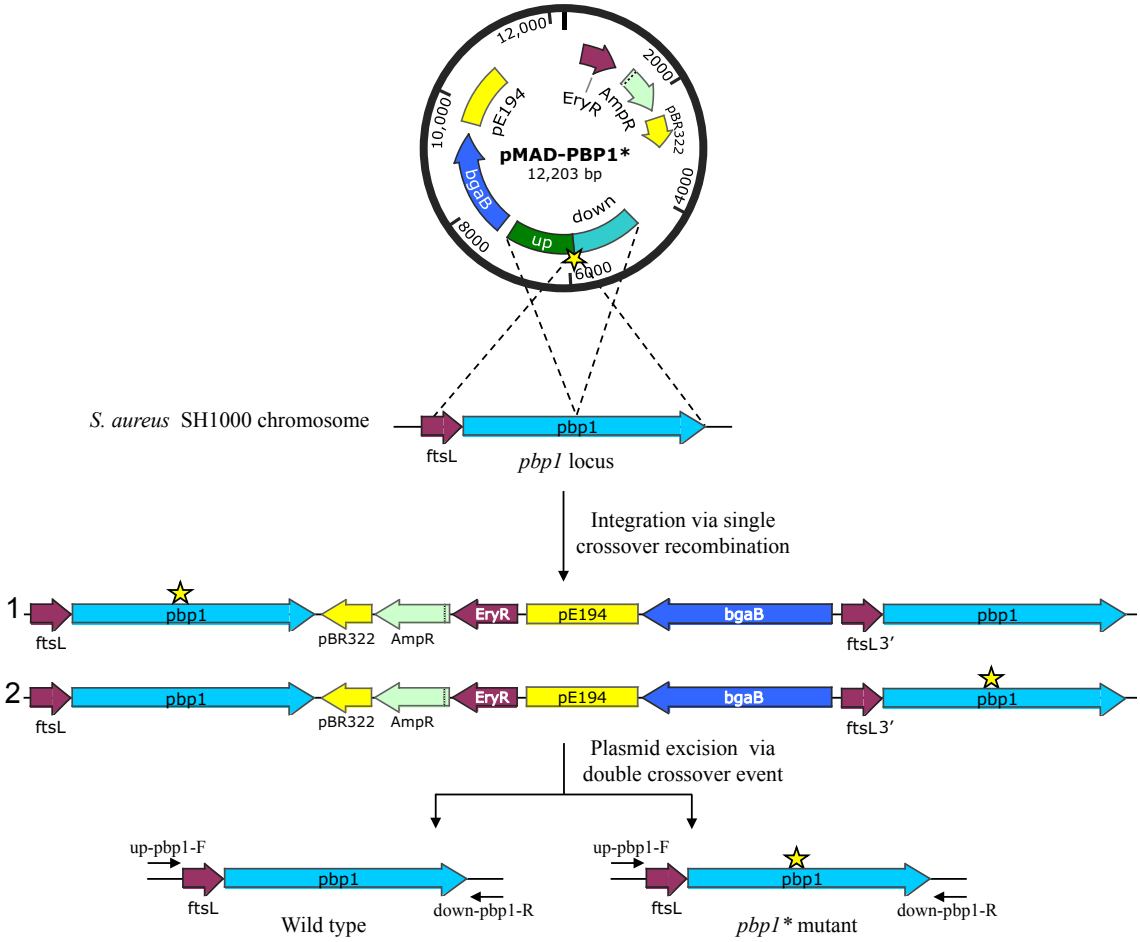

Figure 5.14. Homologous recombination of pMAD-PBP1* into the *S. aureus* chromosome

Diagrammatic representation of the likely recombination outcomes of pMAD-PBP1* into the *S. aureus* SH1000 chromosome. A single crossover can occur via either the up region (1) or the down region (2). The double crossover event either recreates the wild type *pbp1* locus or creates the *pbp1** mutant, in which Ser314 is substituted for Ala in the native *pbp1* gene. The star indicates position of the introduced Ser315Ala mutation. Annealing sites of up-pbp1-F and down-pbp1-R primers used to amplify the *pbp1* region to screen for the Ser314Ala substitution are indicated. Not to scale.

A fragment of ~2.4 kb containing the Pspac promoter, RBS and the complete coding sequence of *pbp1* was PCR amplified from the pCQ11-PBP1-SNAP plasmid using primers pKB-Pspac-pbp1-F and pKB-Pspac-pbp1-R and joined with *BamHI* and *EcoRI* cut pGM073 by Gibson assembly. pGM073 (Gareth McVicker, unpublished) is a tetracycline resistant analogue of pGM074, the pKASBAR derivative carrying *ezrA-psmorange* (section 3.2.1). The resulting plasmid, pKB-Pspac-PBP1 was confirmed to have the correct size by restriction enzyme digestion using *EcoRI* (Figure 5.15D) and to have the expected sequence by GATC Biotech sequencing. pKB-Pspac-PBP1 was transformed into electrocompetent SJF1332 (*S. aureus* RN4220 pYL112Δ19) with selection on BHI plates containing tetracycline (5 μg ml^{-1}). Integration of the plasmid into the RN4220 chromosome was confirmed by a loss of lipase activity by plating cells onto Baird-Parker agar (data not shown). The chromosome region containing the *pbp1* gene under the Pspac promoter was transferred by Φ11 transduction into SJF4430 (*S. aureus* SH1000 *pbp1::*pMAD-PBP1*) with selection using tetracycline (5 μg ml^{-1}) and erythromycin (5 μg ml^{-1}) at 42^{o}C. The resulting SJF4589 (*S. aureus* SH1000 *pbp1::*pMAD-PBP1* *geh::*Pspac-*pbp1*) strain had pMAD-PBP1* integrated within the *pbp1* gene and an ectopic copy of *pbp1* under the control of the Pspac promoter located at the lipase (*geh*) locus (Figure 5.16A).

The procedure of recombination was repeated but this time cells were incubated in the presence of 1 mM IPTG at 28^{o}C. After a few passages cells were serially diluted and grown on BHI X-Gal (80 μg ml^{-1}) and 1 mM IPTG plates at 42^{o}C. White colonies that appeared after a double crossover event were screened for erythromycin sensitivity and tetracycline resistance. Genomic DNA was extracted from the erythromycin sensitive colonies and the *pbp1* gene region was PCR amplified using up-pbp1-F and down-pbp1-R primers (Figure 5.16A). PCR products were purified and sent for sequencing. 12 out of 70 (~17%) screened candidates had the expected Ser314Ala mutation (Figure 5.16B). However the majority of the clones (11 out of 12) that had the Ser314Ala substitution had an extra single mutation within Glu292 that introduced a premature STOP codon in the *pbp1* gene (Figure 5.16B). SJF4590 (*S. aureus* SH1000 *pbp1::pbp1** *geh::*Pspac-*pbp1*) was the only positive clone that did not encode truncated PBP1 but full length inactivated PBP1 (PBP1*).

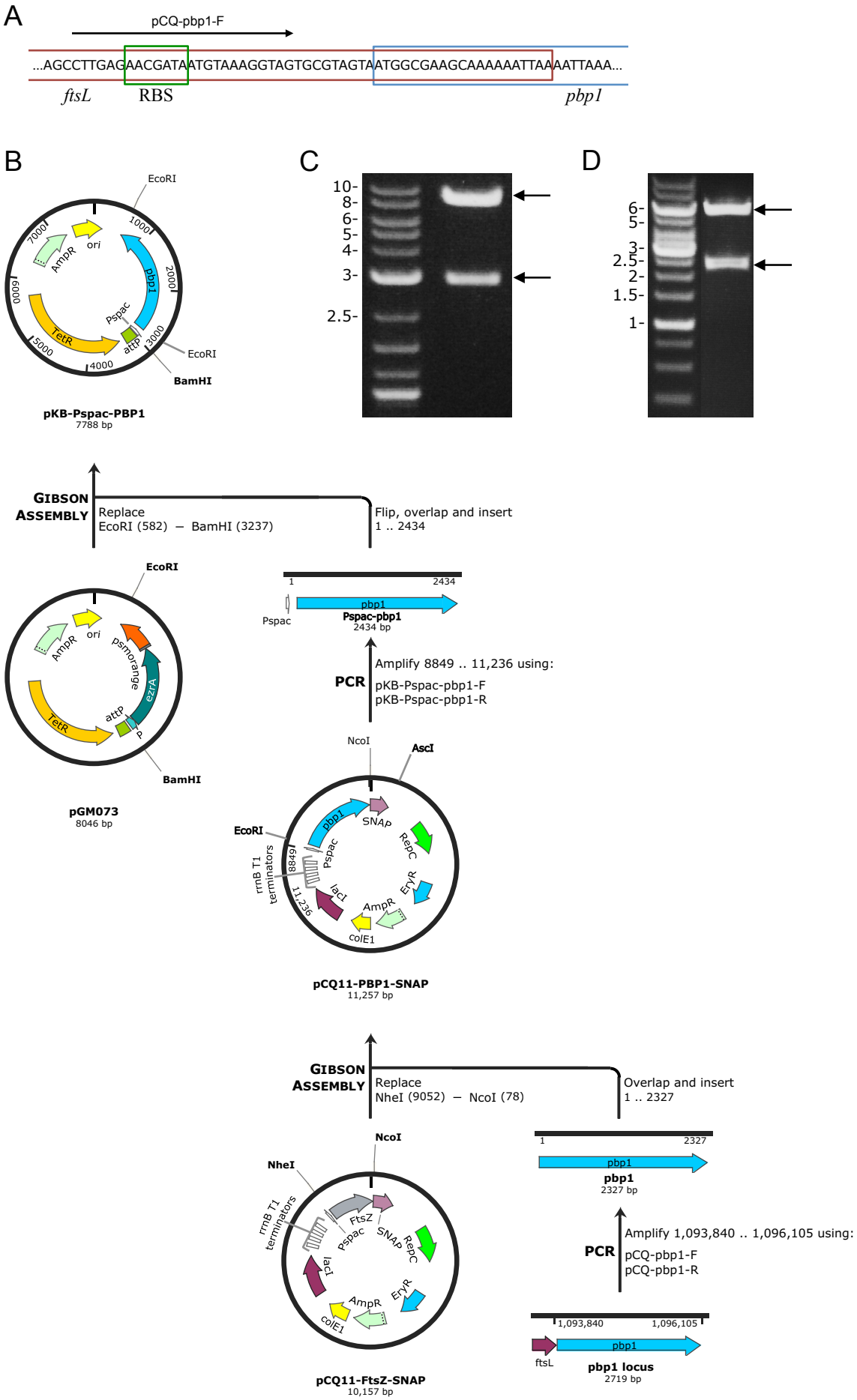
A
pCQ-pbp1-F
...AGCCTTGAGAACGATAATGTAAAGGTAGTGCGTAGTAATGGCGAAGCAAAAAATTAAAATTAAA...
ftsL
RBS
pbp1
B
EcoRI
ori
AmpR
pbp1
Pspac
attP
TetR
EcoRI
BamHI
pKB-Pspac-PBP1
7788 bp
C
10-
8-
6-
5-
4-
3-
2.5-
D
6-
5-
3-
2.5-
2-
1.5-
1-
GIBSON ASSEMBLY
Replace
EcoRI (582) – BamHI (3237)
Flip, overlap and insert
1 .. 2434
EcoRI
ori
AmpR
pspmorange
ezrA
attP
TetR
P
BamHI
pGM073
8046 bp
1
2434
pbp1
Pspac
Pspac-pbp1
2434 bp
PCR
Amplify 8849 .. 11,236 using:
pKB-Pspac-pbp1-F
pKB-Pspac-pbp1-R
NcoI
AscI
EcoRI
pbp1
SNAP
RepC
Pspac
rrnB T1 terminators
8849
11,236
lacI
EryR
AmpR
colE1
pCQ11-PBP1-SNAP
11,257 bp
GIBSON ASSEMBLY
Replace
NheI (9052) – NcoI (78)
Overlap and insert
1 .. 2327
NcoI
NheI
rrnB T1 terminators
FtsZ
Pspac
SNAP
RepC
lacI
EryR
AmpR
colE1
pCQ11-FtsZ-SNAP
10,157 bp
1
2327
pbp1
pbp1
2327 bp
PCR
Amplify 1,093,840 .. 1,096,105 using:
pCQ-pbp1-F
pCQ-pbp1-R
1,093,840
1,096,105
pbp1
ftsL
pbp1 locus
2719 bp

Figure 5.15. Construction of pKB-Pspac-PBP1, a plasmid to complement PBP1*

A. The chromosomal region of *pbp1* in *S. aureus* SH1000. Nucleotide sequence of the 3' end of the *ftsL* gene is indicated with a red box, the 5' fragment of the *pbp1* gene is in a blue box and the putative ribosome binding site (RBS) is highlighted in a green box. The annealing site of the pCQ11-pbp1-F primer to the SH1000 chromosome is indicated.

B. Construction of pKB-Pspac-PBP1. The putative RBS and the full length *pbp1* gene were PCR amplified from the genomic DNA of *S. aureus* using pCQ-pbp1-F and pCQ-pbp1-R primers. The PCR product was cloned into *NheI* and *NcoI* cut pCQ11-FtsZ-SNAP by Gibson assembly, resulting in pCQ11-PBP1-SNAP. The Pspac promoter, RBS and the complete coding sequence of *pbp1* were PCR amplified from the pCQ11-PBP1-SNAP plasmid using primers pKB-Pspac-pbp1-F and pKB-Pspac-pbp1-F and cloned into *BamHI* and *EcoRI* cut pGM073 by Gibson assembly, resulting in pKB-Pspac-PBP1. The pKB-Pspac-PBP1 plasmid comprises the high-copy-number ColE1 origin of replication (*ori*), the ampicillin resistance (AmpR) and the tetracycline resistance (TetR) cassettes, a phage attachment site (*attP*) and the putative *pbp1*RBS with the full length *pbp1*, placed under the control of the Pspac promoter.

C. Restriction enzyme digest of pCQ11-PBP1-SNAP with *EcoRI* and *AscI.* The expected DNA bands of 8.4 kb and 2.9 kb are indicated with black arrows. Sizes of a DNA ladder are shown in kb.

D. Restriction enzyme digest of pKB-Pspac-PBP1 with *EcoRI.* The expected DNA bands of 5.4 kb and 2.9 kb are indicated with black arrows. Sizes of a DNA ladder are shown in kb.

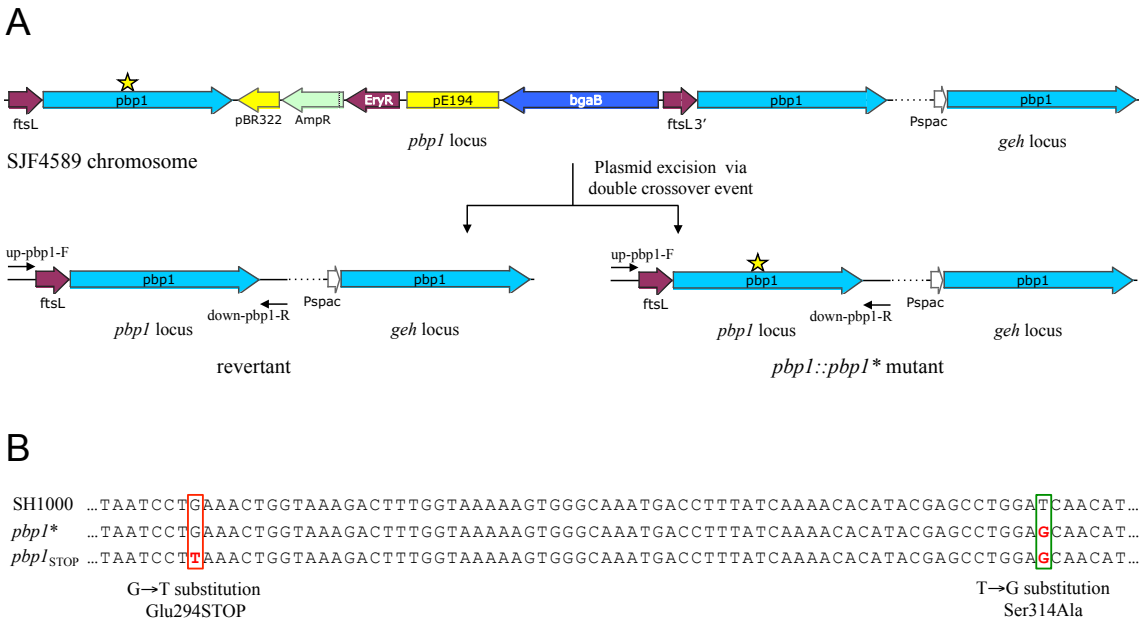

Figure 5.16. Construction of a complemented *S. aureus pbp1 mutant**

A. Diagrammatic representation of a double crossover event that leads to MAD-PBP1* excision from the SJF4589 (*S. aureus* SH1000 *pbp1::*pMAD-PBP1* *geh::*Pspac-*pbp1*) chromosome. The likely recombination outcomes are shown for pMAD-PBP1* integrated via the upstream region into the chromosome. The excision of the plasmid via a double crossover event can either recreate the wild type *pbp1* locus (revertant) or creates a mutant that encodes PBP1 with inactivated transpeptidase domain (*pbp1::pbp1** mutant). Both the revertant and the *pbp1::pbp1** mutant have a second copy of *pbp1* placed under the Pspac promoter in the lipase (*geh*) locus. The star indicates position of the introduced Ser315Ala mutation. Annealing sites of up-pbp1-F and down-pbp1-R primers used to amplify the *pbp1* region to screen for the Ser314Ala substitution are indicated. Not to scale.

B. Fragment of the nucleotide sequence of the *pbp1* gene in the *pbp1** mutants obtained by allelic exchange of pMAD-PBP1* in SJF4589 (*S. aureus* SH1000 *pbp1::*pMAD-PBP1* *geh::*Pspac-*pbp1*). SH100 - DNA sequence of the *pbp1* fragment in the wild type *S. aureus* SH1000 strain; *pbp1** - DNA sequence of the *pbp1* in SJF4589 (*S. aureus* SH1000 *pbp1::pbp1** *geh::*Pspac-*pbp1*) showing the T to G substitution at 940 bp position (indicated with a green box) that results in the Ser314Ala substitution; $pbp1_{STOP}$ - DNA sequence of *pbp1* in most of the mutants obtained after pMAD-PBP1* excision from the SJF4589 (*S. aureus* SH1000 *pbp1::*pMAD-PBP1* *geh::*Pspac-*pbp1*) chromosome, they have an additional G to T substitution at 874 bp position (indicated in a red box) that replaces Glu294 for a premature STOP codon.

The IPTG dependence of SJF4590 (*S. aureus* SH1000 *pbp1::pbp1* geh::*Pspac-*pbp1*) was tested. A single colony of SJF4590 was resuspended in 10 ml PBS and spread on BHI tetracycline (5 μg ml^{-1}) plates with or without 1 mM IPTG with a cotton swab and incubated for 16 h at 37°C (Figure 5.17A). No difference was observed in growth of SJF4590 in the presence or absence of IPTG (Figure 5.17A), indicating that either a functional PBP1 transpeptidase domain was not crucial in *S. aureus* or the Pspac promoter was leaky allowing for production of functional PBP1 in the absence of inducer. The IPTG dependence of SJF4390 was also investigated in a liquid medium (Figure 5.17B). SJF4590 was grown to early-exponential phase (OD_{600} ~0.5) in BHI medium containing 50 μM IPTG. Cells were washed by centrifugation in fresh BHI three times in order to remove IPTG. 50 ml of prewarmed BHI containing 0 or 1 mM IPTG was inoculated to an OD_{600} of 0.005 and growth of the cultures was measured by optical density (Figure 5.17B). No difference in growth between SJF4590 grown with and without inducer was seen (Figure 5.17B).

The pKB-Pspac-PBP1 plasmid, which was used to introduce a functional copy of *pbp1*, did not contain a *lacI* gene that would repress expression of *pbp1* placed under Pspac in the absence of IPTG. To allow for controlled *pbp1* expression, pGL485 a multi-copy plasmid carrying the *lacI* gene under the control of the constitutive *Bacillus licheniformis* penicillinase promoter (Ppcn) (Cooper et al., 2009) was introduced into SJF4590 (*S. aureus* SH1000 *pbp1::pbp1* geh::*Pspac-*pbp1*) by ϕ11 transduction using a lysate from VF17 (*S. aureus* SH1000 pGL485) in the presence of 1 mM IPTG and chloramphenicol (30 μg ml^{-1}). The resulting strain, SJF4656 (*S. aureus* SH1000 *pbp1::pbp1* geh::*Pspac-*pbp1* pGL485) was tested for its IPTG dependence. A single colony of SJF4656 was resuspended in 10 ml PBS and an equal volume was spread on solid medium containing chloramphenicol (30 μg ml^{-1}) and either no or 1 mM IPTG. After a 16 h incubation time at 37°C only a few colonies appeared in the absence of IPTG compared to the large amount of cells grown in the presence of IPTG (Figure 5.17C). After a prolonged incubation (40 h) more colonies appeared on the plate without IPTG and additionally two populations of cells could be observed, big and small colonies (Figure 5.17C). The IPTG dependence of SJF4656 was further investigated by its growth in liquid medium. SJF4656 and VF17 (*S. aureus* SH1000 pGL485), which was used as a control strain, were grown to an OD_{600} of 0.5 in BHI containing 50 μM IPTG and chloramphenicol (30 μg ml^{-1}). Cells were washed by

centrifugation in fresh BHI three times in order to remove IPTG and 50 ml of prewarmed BHI chloramphenicol (30 μg ml^{-1}) containing either no or 1 mM IPTG was inoculated to an OD_{600} of 0.005. Growth of SJF4656 and VF17 was measured by optical density (Figure 5.17D). As VF17 has been previously shown to grow with the same rate with and without IPTG (Steele et al., 2011) it was only grown in the absence of IPTG. No difference between VF17 and SJF4656 grown in the presence of IPTG was seen (Figure 5.17D). In the absence of IPTG SJF4656 grew slightly slower than the other two cultures for the first 6 hours (Figure 5.17D). When it reached an OD_{600} of ~1, its optical density was constant and did not change for the next for 2-3 hours. However SJF4656 incubated in the absence of IPTG started to grow again after 9 h and reached an optical density comparable to VF17 and SJF4656 grown with 1 mM IPTG after 24 hours.

In order to investigate the morphology of cells depleted of functional PBP1 SJF4656 and VF17 were grown as described above. After 5 hours of incubation at 37^{o}C cells were collected, fixed visualise by light microscopy. Cell morphology of SJF4656 grown in 1 mM IPTG was similar to VF17 (Figure 5.17E). Although some minor changes in morphology of single SJF4656 cells could be observed, this was probably a result of altered expression of functional *pbp1* from the Pspac promoter (Figure 5.17E). SJF4656 grown without IPTG showed severe morphological defects and cells had notably increased sizes. Occasionally cells displaying wild type morphology could be seen (Figure 5.17E). Examination of SJF4656 growth on solid and liquid media indicated that *S. aureus* growth and cell division were impaired when functional PBP1 was not present.

The above results showed that PBP1 transpeptidase activity was essential for growth and vitality of *S. aureus* and therefore construction of a triple *S. aureus* mutant, in which *pbp3* and *pbp4* were deleted, and PBP1 was produced but its transpeptidase domain was inactivated, was not possible.

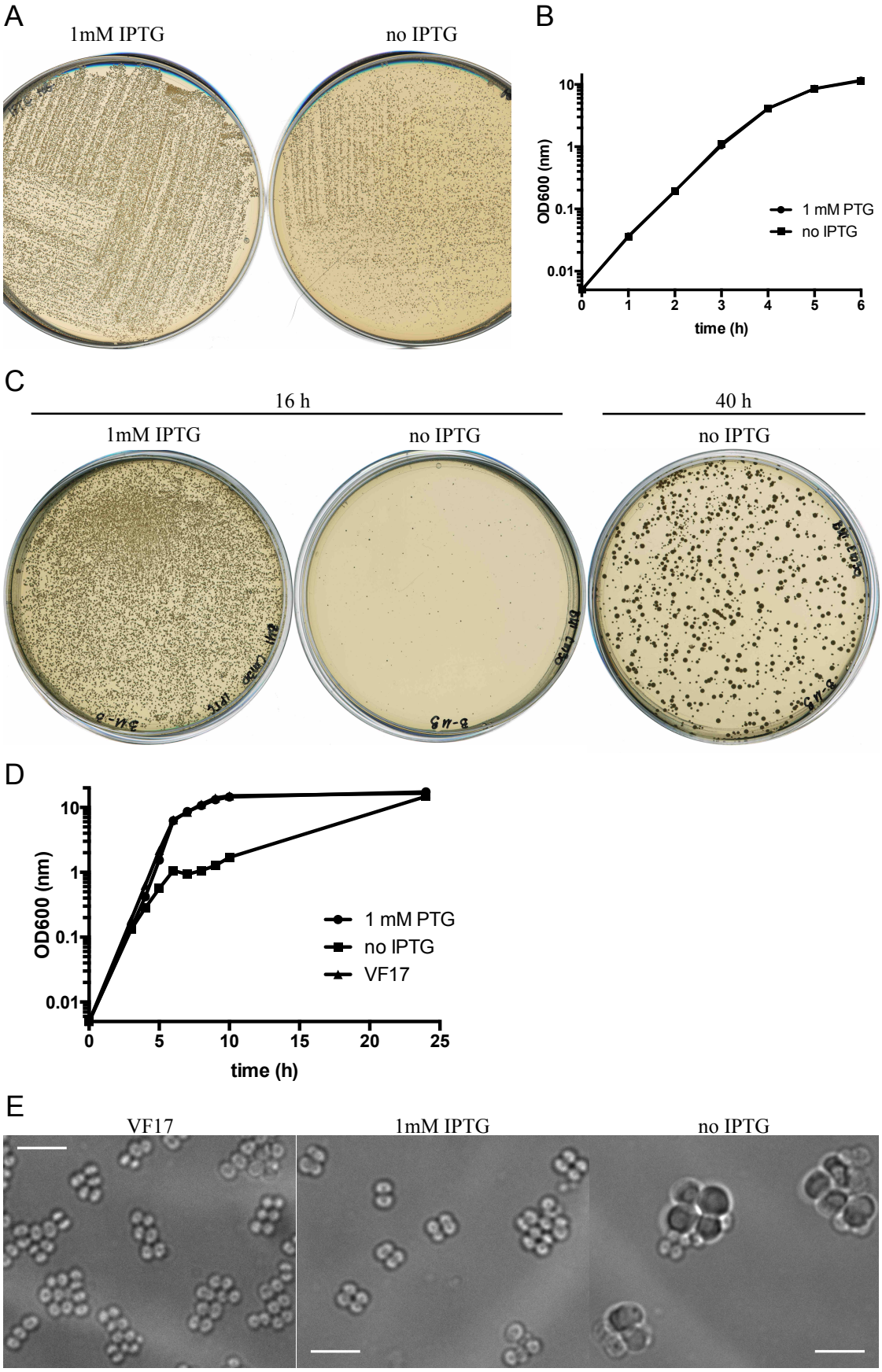

Figure 5.17. Role of the PBP1 transpeptidase domain in cell growth and morphology of *S. aureus*

A. Growth of SJF4590 (*S. aureus* SH1000 *pbp1::pbp1* geh::*Pspac-*pbp1*) on solid medium is not IPTG dependent. A single SJF4590 colony was resuspended in PBS and spread on BHI plates with (1 mM IPTG) or without (no IPTG) 1 mM IPTG followed by 16 h incubation at 37^{o}C.

B. SJF4590 (*S. aureus* SH1000 *pbp1::pbp1* geh::*Pspac-*pbp1*) was grown to OD_{600} 0.5 in BHI with 50 μM IPTG. Cells were washed with BHI three times to remove IPTG. 50 ml BHI without (no IPTG) or with 1 mM IPTG was inoculated to OD_{600} 0.005. Cell growth was measured by optical density. Bacterial cultures were prepared in triplicate and the error bars represent standard deviation from the mean.

C. Growth of SJF4656 (*S. aureus* SH1000 *pbp1::pbp1* geh::*Pspac-*pbp1* pGL485) on solid medium is IPTG dependent. A single SJF4656 colony was resuspended in PBS and spread on BHI chloramphenicol (30 μg ml^{-1}) plates with (1 mM IPTG) or without (no IPTG) 1 mM IPTG. After 16 h incubation at 37^{o}C few cells appeared on the plate without IPTG and prolonged incubation (up to 40 h) resulted in a population of small colonies and a population of big ones.

D. SJF4656 (*S. aureus* SH1000 *pbp1::pbp1* geh::*Pspac-*pbp1* pGL485) and VF17 (*S. aureus* SH1000 pGL485) were grown to an OD_{600} of 0.5 in BHI with chloramphenicol (30 μg ml^{-1}) and 50 μM IPTG. Cells were washed with BHI three times to remove IPTG. 50 ml BHI chloramphenicol (30 μg ml^{-1}) with no or 1 mM IPTG was inoculated to OD_{600} 0.005. VF17 was grown without IPTG. Cell growth was measured by optical density. Bacterial cultures were prepared in triplicate and the error bars represent standard deviation from the mean.

E. Morphology of SJF4656 (*S. aureus* SH1000 *pbp1::pbp1* geh::*Pspac-*pbp1* pGL485) grown in the presence or absence of IPTG. VF17 (*S. aureus* SH1000 pGL485) and SJF4656 were grown in the presence or absence of 1 mM IPTG as described in (D). After a 5 h incubation time cells were examined under a light microscope. VF19 and SJF4656 (1 mM IPTG) form cells of comparable morphology, while SJF4656 grown in the absence of IPTG (no IPTG) has abnormal morphology. Scale bar 5 μm.

5.2.2.3 PBP detection with a STORM-compatible labelled penicillin probe

Bocillin labelling of the double *pbp3 pbp4* mutant, SJF4423 (*S. aureus* SH1000 *pbp3::spec pbp4::Tn*) showed that the remaining PBP1 and PBP2 were detectable by Bocillin FL and their localisation resembled that observed when all four PBPs were present (Figure 5.11A and B). Bocillin FL is not STORM-compatible and could not be employed in localisation studies of PBP1 and PBP2 in *S. aureus* at a molecular level. Pen-AF647, a fluorescent β-lactam compatible with STORM was designed and synthesised by Bryony Cotterell (University of Sheffield). Pen-AF647 is a (+)-6-aminopenicillanic acid (APA) and Alexa Fluor 647 conjugate and is a far-red analogue of Bocillin FL. Pen-AF647 was successfully used for detection of PBPs in *S. aureus in vitro* (Figures 5.4E and 5.7D) and therefore it was tested if it could be used for microscopy visualisation of PBPs in *S. aureus*.

S. aureus SH1000 was grown to early-exponential phase, incubated with 1 μM Pen-AF647 for 5 min and fixed. No fluorescent signal from Alexa Fluor 647 was detected (Figure 5.18). Pen-AF647 did not label fixed cells either (Figure 5.18). Different Pen-AF647 concentrations and labelling times were tested but still no fluorescent signal could be observed. Pen-AF647 recognised and bound PBPs in a gel-based analysis and it selectivity was comparable to Bocillin FL (Figure 5.11A and B), indicating that Pen-AF647 did not label cells because of another reason than the lack of its affinity for PBPs. The charge of the cell surface and the probe could be the reason why Pen-AF647 could not penetrate the cell wall barrier and bind the PBPs. Alexa Fluor 647 is a negatively charged large molecule (molecular weight ~ 1250 g mol^{-1}) and the cell wall of Gram-positive bacteria has a negative net charge due to presence of wall teichoic acids (WTAs), anionic polymers covalently bound to peptidoglycan (Neuhaus and Baddiley, 2003). TarO (TagO) is the first protein in the biosynthesis pathway of WTAs and in *tarO* mutants the cell wall negative net charge is reduced due the absence of WTAs (Soldo et al., 2002). Therefore an *S. aureus* SA113 *tarO::erm* strain, which did not have WTAs, was labelled with Pen-AF647. Similar to SH1000, this mutant was not bound by Pen-AF647 (Figure 5.18), indicating that the cell wall charge was not the only reason for no Pen-AF647 labelling of *S. aureus* cells. As a result super-resolution microscopy of PBP1 and PBP2 localisation was not possible as

no β-lactam that would be both STORM-compatible and label proteins present in the cell was available.

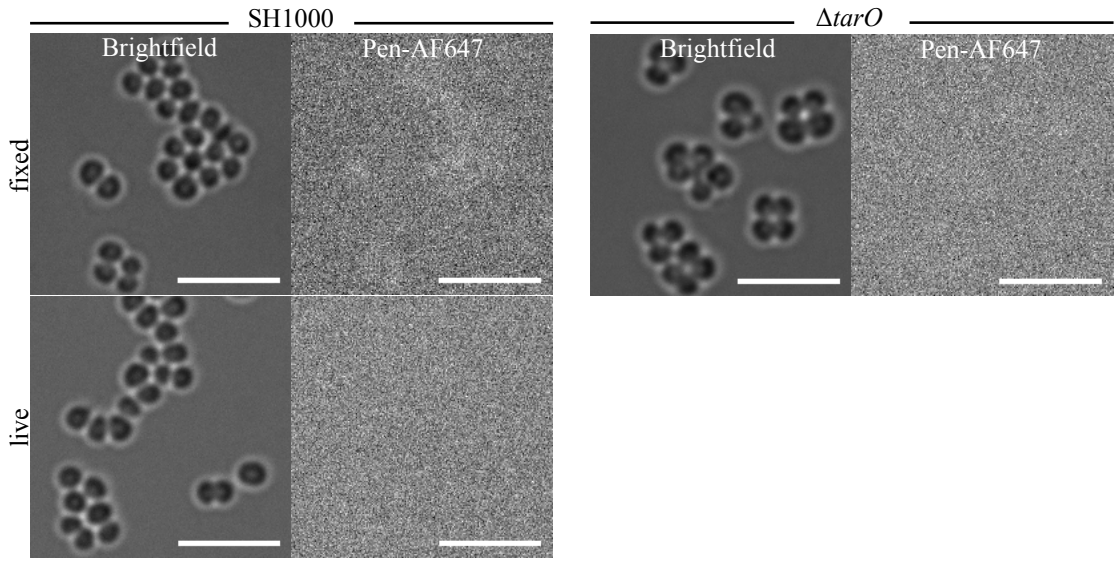

Figure 5.18. PBPs labelling with Pen-AF647

Pen-AF647 does not label PBPs in live and fixed *S. aureus in vivo*. *S. aureus* SH1000 was grown to early-exponential phase, labelled with 1 μM Pen-AF547 and fixed (SH1000, live) or it was first fixed and then labelled with 1 μM Pen-AF547 (SH1000, fixed). *S. aureus* SA113 *tarO*::*erm* (Δ*tarO*) grown to early-exponential phase and labelling with 1 μM Pen-AF547 was followed by fixation. No fluorescent signal was detected. Scale bars 5 μm.

5.2.3 Construction of an *S. aureus mgt sgtA* mutant

As labelling of the transpeptidase domain of PBPs was unsuccessful another approach was taken. PBP2 has two activities, a transpeptidase and a transglycosylase (Pinho et al., 2001b, 2013). Moenomycins are a relatively well characterised group of direct inhibitors of transglycosylases (Ostash and Walker, 2010). Moenomycin is classified as a phosphoglycolipid antibiotic (Ostash and Walker, 2010). It is a pentasaccharide chain attached via a phosphoglycerate linkage to a polyprenol chain and is thought to mimic a polymerised form of the substrate, lipid II and to bind the active site and inhibit the transglycosylation reaction (Lovering et al., 2007; Schneider and Sahl, 2010). PBP2 is the only PBP in *S. aureus* that has the transglycosylase activity and thus a fluorescent derivative of moenomycin could be used to specifically label PBP2. In *S. aureus* there are two additional proteins, Mgt and SgtA that possess transglycosylase activities but do not bind penicillins (Wang et al., 2001; Heaslet et al., 2009; Reed et al., 2011). Mgt and SgtA are not essential monofunctional transglycosylases and their deletion does not cause any defect in *S. aureus* growth and morphology (Reed et al., 2015). It was hoped to localise PBP2 using a fluorescent derivative of moenomycin therefore an *S. aureus* mutant, in which monofunctional transglycosylases were absent and therefore PBP2 was the only transglycosylase present in the cell, was prepared.

As *mgt* and *sgtA* are not crucial mutations are available in the Nebraska Transposon (Tn) Mutant Library of *S. aureus* JE2 (Fey et al., 2013). In NE596 (*S. aureus* JE2 *mgt::Tn*) and NE267 (*S. aureus* JE2 *sgtA::Tn*) the genes encoding monofunctional transglycosylases are inactivated due to transposon insertion at the 5' ends of the genes. The chromosomal regions containing the Tn insertions were transferred from NE596 and NE267 into *S. aureus* SH1000 by Φ11 transduction and selection using erythromycin (5 μg ml^{-1}), resulting in SJF4628 (*S. aureus* SH1000 *mgt::Tn*) and SJF4629 (*S. aureus* SH1000 *sgtA::Tn*). In order to construct a double mutant of monofunctional transglycosylases the Tn in SJF4629 was exchanged for a tetracycline resistance cassette (TetR) by allelic exchange using pTET. pTET is a tetracycline resistant analogue of thermosensitive pSPC (Figure 5.10A). SJF4629 was transduced with a phage lysate from SJF4313 (*S. aureus* RN4220 pTET) and transformants were selected using chloramphenicol (10 μg ml^{-1}) and tetracycline (0.5 μg ml^{-1}) at 28°C.

The process of homologous recombination of pTET in SJF4629 was performed in the same way as for pSPC in SJF4421 (*S. aureus* SH1000 *pbp3::Tn*) (Section 5.2.2.1). An SJF4643 (*S. aureus* SH1000 *sgtA::tet*) strain, which was tetracycline resistant and did not grow on erythromycin any longer, was obtained. SJF4643 was then transduced with a phage lysate from SJF4628 (*S. aureus* SH1000 *mgt::Tn*) and transformants were selected using tetracycline (0.5 μg ml^{-1}) and erythromycin (5 μg ml^{-1}). The resulting SJF4644 (*S. aureus* SH1000 *mgt::Tn sgtA::tet*) strain had both monofunctional transglycosylases inactivated. In SJF4628, SJF4629, SJF4643 and SJF4644 interruption of the *mgt* and *sgtA* genes by the Tn or the TetR cassette insertion was confirmed by PCR on extracted genomic DNA using Tn-mgt-F and Tn-mgt-R, and Tn-sgtA-F and Tn-sgtA-R primers (Figure 5.19A and B). Both primer pairs Tn-mgt-F and Tn-mgt-R, and Tn-sgtA-F and Tn-sgtA-R annealed ~250 bp upstream and downstream of site of the Tn/TetR cassette insertion in the *mgt* and *sgtA* genes, respectively.

Deletion of *mgt* and *sgtA* was shown to not affect growth of *S. aureus* COL (Reed et al., 2011). When growth of SJF4628 (*S. aureus* SH1000 *mgt::Tn*), SJF4643 (*S. aureus* SH1000 *sgtA::tet*) and SJF4644 (*S. aureus* SH1000 *mgt::Tn sgtA::tet*) was analysed in liquid medium, all mutants grew with the same rate (~25 min) as SH1000 (Figure 5.19C), indicating that mutations in *mgt* or/and *sgtA* did not cause any growth defect in the SH1000 background.

SJF4628 (*S. aureus* SH1000 *mgt::Tn*), SJF4643 (*S. aureus* SH1000 *sgtA::tet*) and SJF4644 (*S. aureus* SH1000 *mgt::Tn sgtA::tet*) did not have one or both monofunctional transglycosylases. Moenomycin, an inhibitor of transglycosylation was planned to be used as a reporter of transglycosylases localisation in *S. aureus*. Therefore how mutations in *mgtA* and *sgtA* influenced *S. aureus* SH1000 sensitivity to moenomycin was tested by determination of the MICs for SJF4628, SJF4643 and SJF4644. Overnight cultures of SH1000, SJF4628, SJF4643 and SJF4644 were adjusted to the same OD_{600} and serial dilutions (10^{0}-10^{-7}) prepared in PBS were plated on BHI agar containing 0, 0.1, 0.2, 0.4 and 0.5 μg ml^{-1} moenomycin A. No drastic reduction in the MIC of moenomycin A in the mutants was observed and they all had the same MIC as SH1000 strain (0.4 μg ml^{-1}) (Figure 5.19). Whilst SJF4628 and SH1000 had identical sensitivity to the increasing moenomycin A concentrations,

SJF4643 and SJF4644 showed a slight increase in sensitivity to 0.2 μg ml^{-1} moenomycin A. The observed effect of transglycosylase mutations was analogous to the one reported for *S. aureus* COL mutants (Reed et al., 2011).

Due to time constraints and the fact that no fluorescent derivative of moenomycin became available no microscopy examination on PBP2 localisation could be performed.

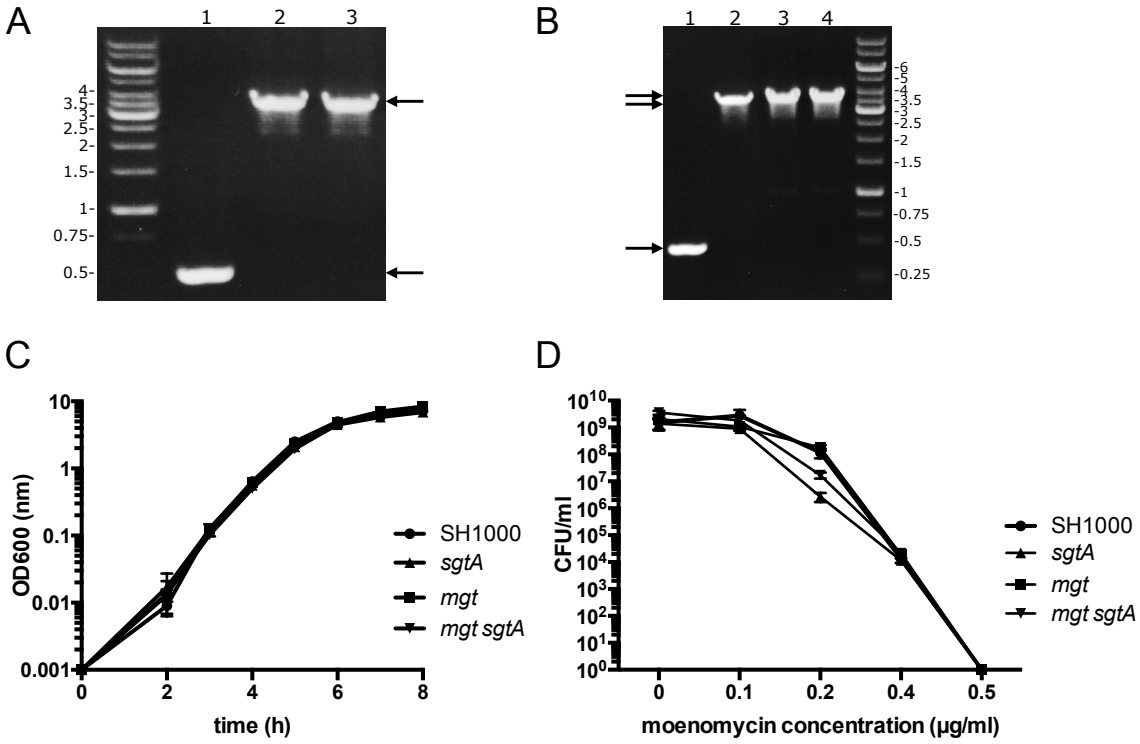

Figure 5.19. Construction of an *S. aureus mgt sgtA* mutant

A. Insertion of the Tn within the *mgt* gene was confirmed by PCR using Tn-mgt-F and Tn-mgt-R primers on extracted genomic DNA. Primers Tn-mgt-F and Tn-mgt-R anneal ~250 bp and ~ 240 bp upstream and downstream, respectively, of the Tn insertion site in the *mgt* gene. 1, *S. aureus* SH1000; 2, SJF4628 (*S. aureus* SH1000 *mgt::Tn*); 3, SJF4644 (*S. aureus* SH1000 *mgt::Tn sgtA::tet*). The expected DNA fragments of ~0.5 kb and ~3.7 kb are indicated with black arrows. Sizes of a DNA ladder are shown in kb.

B. Replacement of Tn for the tetracycline resistance cassette in the *sgtA* gene was confirmed by PCR of extracted genomic DNA using Tn-sgtA-F and Tn-sgtA-R primers. Tn-sgtA-F and Tn-sgtA-R anneal ~250 bp upstream and ~ 240 bp downstream of the Tn/TetR cassette insertion site in the *sgtA* gene, respectively. 1, *S. aureus* SH1000; 2, SJF4629 (*S. aureus* SH1000 *sgtA::Tn*); 3, SJF4643 (*S. aureus* SH1000 *sgtA::tet*); 4, SJF4644 (*S. aureus* SH1000 *mgt::Tn sgtA::tet*). The expected DNA fragments of ~0.5 kb, ~3.7 kb and ~4 kb are indicated with black arrows. Sizes of a DNA ladder are shown in kb.

C. Growth of: *sgtA*, SJF4643 (*S. aureus* SH1000 *sgtA::tet*); *mgt*, SJF4628 (*S. aureus* SH1000 *mgt::Tn*); *mgt sgtA*, SJF4644 (*S. aureus* SH1000 *mgt::Tn sgtA::tet*) was measured by optical density. The doubling times of the mutants are comparable to SH1000 (~25 min). Bacterial cultures were prepared in triplicate and the error bars represent standard deviation from the mean.

D. Moenomycin A population analysis profiles (MIC) of SJF4643 (*S. aureus* SH1000 *sgtA::tet*), SJF4628 (*S. aureus* SH1000 *mgt::Tn*) and SJF4644 (*S. aureus* SH1000 *mgt::Tn sgtA::tet*). All three mutants had the same MIC as SH1000 strain (0.4 µg ml^{-1}). Whilst SJF4628 (*mgtA*) showed the same sensitivity as the wild type SH1000 strain to tested moenomycin A concentrations, SJF4643 (*sgtA*) and SJF4644 (*mgt sgtA*) showed slightly higher sensitivity to 0.2 µg ml^{-1} moenomycin A.

5.3 Discussion

In the previous chapter colocalisation of EzrA with nascent peptidoglycan showed EzrA-eYFP 'patches' juxtapositioned to newly synthesised material of peptidoglycan, suggesting that in *S. aureus* peptidoglycan synthesis might be directed from EzrA 'patches'. This is further supported by positive EzrA interactions with other cell membrane proteins that show affinity toward peptidoglycan in *S. aureus* in a bacterial two hybrid system (Steele et al., 2011; Kent, 2013). Peptidoglycan is however the final product of the coordinated activity of the cell division components and studies on nascent peptidoglycan synthesis colocalisation with cell division components, as EzrA and FtsZ, did not show how, where and when penicillin binding proteins (PBPs), which are directly involved in making peptidoglycan, localise during cell division. *S. aureus* has four PBPs: PBP1, PBP2, PBP3 and PBP4 and two of them, PBP1 and PBP2, are essential, while PBP3 and PBP4 are redundant (Pinho et al., 2013; Reed et al., 2015). Since PBP2 is crucial and is the only bifunctional and the most abundant PBP (~400 molecules per cell) in *S. aureus* (Murakami et al., 1994; Pinho et al., 2001b, 2013; Pucci and Dougherty, 2002), it is considered to be the most important PBP among other PBPs in *S. aureus*.

PBP2 is a HMW class A PBP and as most of the PBPs in this group it consists of a short cytoplasmic tail, a transmembrane helix which is followed by a transglycosylase domain connected via a short β-rich linker to a transpeptidase domain (Goffin and Ghuysen, 1998; Lovering et al., 2007). Bifunctional PBPs are considered to be docked in a membrane by a non-cleavable signal peptide and the active domains to fold in the periplasm (Goffin and Ghuysen, 1998). N-terminal fusions of PBP2, in which the fluorescent tag is located in the cytoplasm, were shown to be produced and to localise to the septum in *S. aureus*. More recently a GFP-PBP2 fusion was shown to be functional in MRSA treated with oxacillin (Tan et al., 2012). Fluorescent proteins were reported to fail to fold in the periplasm (Feilmeier et al., 2000), therefore an *S. aureus* strain producing an N-terminal fusion of PBP2 was constructed in order to localise this bifunctional PBP in STORM.

In SJF4595 (*S. aureus* SH1000 *pbp2::eyfp-pbp2*) eYFP-PBP2 was the only PBP2 present. However the amount of produced eYFP-PBP2 was found to be drastically

reduced compared to the PBP2 levels in the wild type strain (Figure 5.4E). This number of eYFP-PBP2 molecules was enough for cells to stay alive, grow and divide but was not sufficient for cells to maintain wild type morphology (Figure 5.4A-D). Interestingly, the small size phenotype observed for SJF4595 was different from the one reported for a conditional *pbp2* mutant, in which PPB2 depletion resulted in enlarged cells with more than one septum (Pinho et al., 2001a). The addition of the fluorescent protein to PBP2 resulted in a longer peptide than native PBP2. This could alter transcription and/or translation leading to the lower amount of eYFP-PBP2 in the mutant strain compared to PBP2 levels in SH1000. Furthermore, fusing PBP2 with eYFP could perturb folding properties and functionality of the engineered protein. This was confirmed by Bocillin FL/Pen-AF647 labelling of PBPs *in vitro* and western blot analysis, which showed that eYFP-PBP2 was unstable and was truncated to a form of the same size as native PBP2 (Figure 5.4E and F). Addition of plasmid born *eyfp-pbp2* to SFJ4595 aimed to restore the wild type phenotype of the *eyfp-pbp2* mutant. SJF4596 (*S. aureus* SH1000 *pbp2::eyfp-pbp2* pCQ11-eYFP-PBP2) had a growth and morphology comparable to SH1000 (Figures 5.6 and 5.7A-C), suggesting that the concept of complementation was achieved. This strain produced also enough of the fluorescent protein fusion so that a fluorescent signal associated with the cell septa and the cell periphery could be observed (Figure 5.6). Complementation not only resulted in reconstitution of the wild type morphology and in the increase in the emitted fluorescent signal but also the amount of degraded eYFP-PBP2 became greater (Figure 5.7D and E). Western blot analysis, which allowed for a quantitative analysis of total protein in the cell, showed that SJF4596 produced comparable amounts of eYFP-PBP2, and the degraded form, to the level of PBP2 in the wild type strain (Figure 5.7E). Interestingly, Pen-AF647 labelling of PBPs revealed that the amount of eYFP-PBP2 was not equal to the amount of the truncated form (Figure 5.7D), suggesting that the full length fusion protein was not properly folded and therefore was not fully functional, which was manifested by its decreased affinity for the fluorescent penicillin. Presumably truncation of eYFP-PPB2 by cutting out eYFP allowed the trimmed protein to efficiently fold and have greater activity, demonstrated by more efficient binding of Pen-AF647 and restored growth of the complemented mutant (Figure 5.7C and D). Moreover, introduction of pCQ11-eYFP-PBP2 into SH1000 showed that the effectiveness of fusion production relies on the presence of native PBP2. When the native protein was present, SJF4597 (*S. aureus* SH1000 pCQ11-eYFP-PBP2) produced as little

eYFP-PBP2 as SJF4595 (*S. aureus* SH1000 *pbp2::eyfp-pbp2*), but SJF4596 (*S. aureus* SH1000 *pbp2::eyfp-pbp2* pCQ11-eYFP-PBP2) in the same growth conditions (1 mM IPTG) gave higher eYFP-PBP2 levels in the absence of the native protein (Figure 5.7D-F).

Utilisation of eYFP-PBP2 for localisation studies in super-resolution did not bring insight into PBP2 localisation in *S. aureus* (Figure 5.9). Although eYFP-PBP2 presented intrinsic blinking properties, the generated blinks were quite dim and not well separated preventing localisation of eYFP-PBP2 molecules with high precision. Localisation studies should rely on functional proteins. Despite the fact that eYFP-PBP2 was not stable or fully functional, it might have however had a localisation pattern reminiscent of native PBP2 in *S. aureus*. The other issue associated with this particular fusion was the signal detected in the cell cytoplasm (Figure 5.9). PBP2 is a membrane protein therefore its fluorescent derivative was also expected to be associated with the cell membrane. The cytoplasmic signal could come from eYFP that was cut out from the fusion protein and was released to freely float in the cytoplasm. Presence of free eYFP in the cytoplasm was not however confirmed, as only membrane fractions, where most of the protein was expected to be present, were analysed by western blot (Figure 5.7F).

Although PBP2 was not amenable for fluorescent fusions, the transpeptidase or transglycosylase activities could be used to target and label this protein. There are commercially available fluorescent derivatives of penicillin, which is a transpeptidase inhibitor, therefore fluorescent β-lactams were chosen to label and localise PBP2. *S. aureus* has four PBPs and all of them are transpeptidases (Murakami et al., 1994; Wada and Watanabe, 1998; Pinho et al., 2013; Qiao et al., 2014). Penicillin is not selective towards one particular PBP, therefore other transpeptidases (PBP1-PBP3) had to be deleted or their transpeptidase domains had to be inactivated. PBP3 and PBP4 are not essential and when both *pbp3* and *pbp4* were interrupted by the transposon or a resistance marker cassette insertion, resulting in SJF4423 (*S. aureus* SH1000 *pbp3::spec pbp4::Tn*) that had the wild type growth and morphology (Figures 5.10D, and 5.11A and B). This showed that together these two genes are not essential in *S. aureus* and this was also in agreement with other research report (Reed et al., 2015). Bocillin FL labelling of the *pbp3* and *pbp4 S. aureus* mutants showed that with the

reduction of the pool of available PBPs the amount of the signal from bound Bocillin FL changed (Figure 5.11A). Nevertheless the variations in the fluorescent signal between samples were found to be dependent on the batch of used Bocillin FL (Figure 5.11A and B). Therefore any quantitative analysis could not be performed, as detected emission was not necessarily an actual representation of an amount of PBPs in the cell. Regardless of Bocillin FL batch and intensity of the emitted signal, in SJF4423 the remaining PBP1 and PBP2 were mostly septally located and their localisation pattern resembled that in SH1000, which has all four PBPs (Figure 5.11A and B). Furthermore the competition assay using penicillin G and Bocillin FL (Figure 5.11C), showed the Bocillin FL binding to be specific.

Labelling of newly synthesised peptidoglycan in the *pbp3*, *pbp4* and *pbp3 pbp4* mutants, revealed a decreased incorporation of HADA (Figure 5.12A). This observation is in agreement with Victoria Lund's data, who estimated that the fluorescent signal was reduced by ~15%, ~60% and ~90% in the *pbp3, pbp4* and *pbp3 pbp4* mutants, respectively (Victoria Lund, unpublished). Moreover, the decreased HADA labelling was not caused by HADA toxicity as mutants grown in the presence of the fluorescent D-Ala had comparable growth rates to the wild type strain (Figure 5.12B). Additionally, incorporation of radiolabelled Glc*N*Ac showed that the amount of newly synthesised peptidoglycan was comparable between the mutants and SH1000 (Victoria Lund, unpublished). These results together with data published by Qiao et al. (2014) support the role of PBP4 in catalysing exchange of the terminal D-Ala in the peptidoglycan stem peptide. The massive reduction in HADA incorporation by the double *pbp3 pbp4* mutant (Figure 5.12A) may imply that PBP1 and PBP2 are not involved in the exchange of the terminal D-Ala in the stem peptide and the remaining signal comes form HADA that has been incorporated into dipeptide of the peptidoglycan precursor side chain, lipid II. The septal and off-septal labelling of Bocillin FL and HADA (Figures 5.11 and 5.12B) shows that all PBPs are present at the midcell and cell periphery but play different roles in peptidoglycan synthesis, its growth (PBP1 and PBP2) and remodelling (PBP3 and PBP4).

Construction of a triple *S. aureus* mutant strain was not possible. Whilst PBP3 and PBP4 together were not essential for *S. aureus* to grow and divide, inactivation the transpeptidase domain in the conditional *pbp1* mutant, SJF4656 (*S. aureus* SH1000

pbp1::pbp1 geh::*Pspac-*pbp1* pGL485) resulted in a severe growth defect, morphological changes and reduction in viability (Figure 5.17C-E), indicating that the functional transpeptidase domain of PBP1 is crucial in *S. aureus*. Sporadically, wild type looking cells for SJF4656 grown without IPTG could be observed (Figure 5.17E). These cells were presumably the ones that gained suppressor mutations within the Pspac promoter allowing for production of functional PBP1 in the absence of inducer.

Pen-AF647 seemed to be an excellent candidate for labelling of transpeptidases in *S. aureus*. It was STORM-compatible, bright and selectively labelled PBPs *in vitro* (Figures 5.4E and 5.7D). Unfortunately, it did not bind PBPs *in vivo* (Figure 5.18). The reason for not labelling PBPs present in the cell can be complex and utilisation of a *ΔtarO* mutant showed that the cell wall net charge was not the only or main cause (Figure 5.18). The size or charge of the Alexa Fluor 647 dye could prevent Pen-AF647 from getting through the peptidoglycan layer and reaching the PBPs. Pen-AF647 labelled PBPs present in isolated membrane fractions, indicating that the dye did not impair penicillin specificity against PBPs (Figures 5.4E and 5.7D). Conjunction of (+)-6-aminopenicillanic acid (APA) with Alexa Fluor 647 could have changed it antibacterial properties. However the amount of synthesised Pen-AF647 did not allow for the MIC determination.

Neither the STORM-compatible fluorescent fusion nor penicillin allowed for visualisation of PBP2 at the molecular level. The second activity of PBP2, transglycosylase is inhibited by a family of moenomycin antibiotics. In the prepared SJF4644 (*S. aureus* SH1000 *mgt::Tn sgtA::tet*) strain the *mgt* and *sgtA* genes encoding monofunctional transglycosylases were inactivated, making PBP2 the only transglycosylase present in the cell that could be targeted by a transglycosylase inhibitor. SJF4644 showed similar sensitivity to moenomycin A as SH1000 (Figure 5.19D). Thus the transglycosylase activity of PBP2 is the major growth function.

CHAPTER 6

General discussion

Staphylococcus aureus is an important human pathogen and increasing antibiotic resistance means new drug targets must be investigated. Cell division is a fundamental process of all bacteria. Therefore components of cell division are attractive targets for potential drugs (Lock and Harry, 2008). Cell division has been well studied in *B. subtilis* and *E. coli*, which are rod-shaped bacteria, but little is known about this process in *S. aureus*. Although there is a high level of homology between *B. subtilis* and *S. aureus,* and many essential *B. subtilis* cell division proteins are conserved in *S. aureus,* differences in the role of particular components are present (Steele et al., 2011; Bottomley et al., 2014). Moreover, these two organisms have different modes of peptidoglycan synthesis, elongation, division and sporulation in *B. subtilis* versus only an apparent division mode in *S. aureus* (Daniel and Errington, 2003; Pinho and Errington, 2003). This divergence is event more apparent in the number of penicillin binding proteins (PBPs), which from 16 PBPs in *B. subtilis*, is drastically reduced to 4 PBPs in *S. aureus* (Zapun et al., 2008b; Pinho et al., 2013). Therefore, development of efficient therapeutic agents to target *S. aureus* cell division components requires correct understanding of this process at the molecular level.

Cell division components of *S. aureus* were identified and their roles predicted based on their homology to *B. subtilis* (Steele et al., 2011). Bacterial two-hybrid assays have shown that there is a dense net of interactions between proteins involved in cell division and that one protein can have several interacting partners (Figure 6.1). Moreover, cross talk between components engaged in different cell processes such as division, peptidoglycan synthesis, wall teichoic acids synthesis, lipoteichoic acids synthesis and chromosome segregation was found (Figure 6.1) (Steele et al., 2011; Kent, 2013; Reichmann et al., 2014; Xing Ma, unpublished). This emphasises the correlation and interdependence between seemingly independent processes. In *S. aureus* EzrA, a membrane-associated protein, was identified as an essential cell division component that localises to the division site where it forms a ring-like structure (Steele et al., 2011). Additionally, EzrA was shown to interact both with cytoplasmic proteins and those with

periplasmic domains in the bacterial two-hybrid system (Figure 6.1) (Steele et al., 2011). Based on its interactions and the effect of its depletion on cell growth, peptidoglycan synthesis and localisation of other cell division components, EzrA was proposed to act as an interface between FtsZ, which is considered as a key component of the divisome, and PBPs, which mediate insertion of new peptidoglycan (Steele et al., 2011). The γ-proteobacteria have two FtsZ membrane tethering proteins, FtsA and ZipA required for the Z-ring stability (Pichoff and Lutkenhaus, 2002). *S. aureus* does not encode ZipA, however the membrane topology of EzrA resembles that of ZipA, indicating a possible scaffold function for EzrA (Hale and de Boer, 1997; Haeusser et al., 2004). Additionally, its role as a scaffolding protein is supported by a recently solved crystal structure, which revealed that the cytoplasmic domain of EzrA is a semi-circle with a spectrin-like motif (Cleverley et al., 2014). Therefore it could form an arch to trap FtsZ protofilaments inside the curve, bringing them closer to the cell membrane (Cleverley et al., 2014).

In order to further understand the role of EzrA in cell division and to correlate it with other cell division components, localisation of EzrA, FtsZ and PBPs, and peptidoglycan synthesis was studied using fluorescence microscopy approaches, including super-resolution microscopy.

Conventional fluorescence microscopy depicts cell division components localised to the division site where they form uniform ring-like structures (Ma et al., 1996; Pinho and Errington, 2003; Steele et al., 2011). Additionally, the known interactions between division proteins and the localisation dependence of one component on one another suggests that once all the proteins are present at the division site they form a 'fixed' complex, which is stabilised by multiple associations, and drives cell division (Addinall and Lutkenhaus, 1996; Weiss et al., 1999; Chen and Beckwith, 2001; Karimova et al., 2005). With the development of new fluorescence microscopy techniques the understanding of the cell division process has started to change. First of all, cell division components do not form static structures, as shown by FRAP experiments for FtsZ in *E. coli* and *B. subtilis* (Anderson et al., 2004). Moreover, there is accumulating evidence that division proteins are not uniformly distributed at the division site (Fu et al., 2010; Strauss et al., 2012; Holden et al., 2014; Rowlett and Margolin, 2014). The first super-resolution imaging of FtsZ in *S. aureus* by SIM revealed that this key protein is

heterogeneously distributed around division site and forms bead-like structures (Strauss et al., 2012). Two other proteins, EzrA and PBP2 were shown to resemble the pattern formed by FtsZ (Strauss et al., 2012).

In this study another super-resolution microscopy technique, STORM was utilised to provide information on EzrA and FtsZ localisation in *S. aureus*. A functional fluorescent fusion of EzrA with eYFP revealed, that similar to the SIM data, EzrA did not form homogenous rings, as the conventional fluorescence microscopy suggests (Strauss et al., 2012 and this study). Localisation of EzrA-eYFP at a single molecule level showed that EzrA did not form distinct 'beads' either. Its distribution can be defined as 'patchy', since no regular or well defined arrangement of EzrA molecules could be observed by STORM. The molecules were randomly, with some regions of increased local concentrations, distributed around the division site. Localisation of EzrA at super-resolution also revealed that it formed enveloping structures around developing septum, surprisingly wider (100-300 nm) than the ~5 nm width of the membrane (Suganuma, 1961). The heterogeneous distribution of EzrA was further confirmed by fusing it to the monomeric variant of eYFP (meYFP) and a SNAP tag labelled with the caged TMR-Star dye. This showed that the non-uniform EzrA pattern was not determined by self interactions of the fluorophore.

FtsZ is the first protein that localises to the midcell where it initiates cell division and recruits other proteins involved in the process (Adams and Errington, 2009). Several studies on FtsZ in different bacterial species showed that FtsZ does not form uniform rings but its distribution can be described as 'patchy' (Fu et al., 2010; Holden et al., 2014) Here, FtsZ-mEos2 was also revealed to be a heterogeneous and relatively wide ring. Additionally, localisation of FtsZ-mEos2 by STORM revealed that not all FtsZ molecules were recruited to the midcell, which is in agreement with other studies suggesting that less than half of cellular FtsZ forms the Z-ring (Anderson et al., 2004; Geissler et al., 2007).

Due to technical limitations EzrA and FtsZ were not visualised together by STORM. Conventional fluorescence microscopy however showed that FtsZ was accompanied by EzrA at every stage of cell division. Moreover, FtsZ rings were observed inside EzrA rings, showing that FtsZ is located further away from the membrane than EzrA. This

also suggests that EzrA could interact with FtsZ protofilaments through the outside of its curve, instead of trapping them between the inside of the curve and the cell membrane (Cleverley et al., 2014).

EzrA is required for peptidoglycan synthesis, whilst the presence of FtsZ is needed for septal localisation of the synthetic machinery (Pinho and Errington, 2003; Steele et al., 2011). This study showed that overproduction of FtsZ can lead to its own mislocalisation and in consequence to a delocalised peptidoglycan insertion. Interestingly, the altered patterns of FtsZ, PBPs and peptidoglycan correlated between one another. This showed that FtsZ not only marks division site but as long as it is active it guides cell division components and thus peptidoglycan synthetic machinery in any location. In agreement with FtsZ being an initiator of the cell division, utilisation of the FtsZ inhibitor PC190723 showed that in cells entering a new cycle of cell division EzrA localisation was disrupted and cells did not form division septa. This was presumably due to a reduced pool of free FtsZ monomers that could form the Z-ring at the new division site. Eventually, FtsZ suppression led to the same effect seen for FtsZ depletion, that is enlarged cells with dispersed peptidoglycan synthesis all around the cell surface (Pinho and Errington, 2003). Colocalisation of EzrA with peptidoglycan synthesis, and FtsZ with peptidoglycan showed that both EzrA and FtsZ are within surrounding cell wall. Their juxtaposition to newly synthesised peptidoglycan suggests that FtsZ and EzrA may form a framework that guides production of nascent peptidoglycan. Although insertion of new peptidoglycan may be directed from EzrA and FtsZ ‘patches’, they are not directly catalysing peptidoglycan formation. Peptidoglycan is a result of penicillin binding protein (PBP) activities, which mediates the latter stages of peptidoglycan formation, transglycosylation and transpeptidation (Typas et al., 2012).

S. aureus has only four PBPs (Pinho et al., 2013). PBP2 is the only class A PBP present in *S. aureus* (Pinho et al., 2001b, 2013). Attempts to label and localise PBP2 were not successful, as this protein was found not to be amenable for fluorescent fusions. Since PBP2 has two activities, transpeptidase and transglycosylase, fluorescently labelled antibiotics were incorporated into localisation studies of PBP2. All PBPs in *S. aureus* have transpeptidase activity, and thus utilisation of fluorescent derivatives of β-lactam antibiotics to label PBP2 required removal of the other PBPs (PBP1, PBP3 and PBP4).

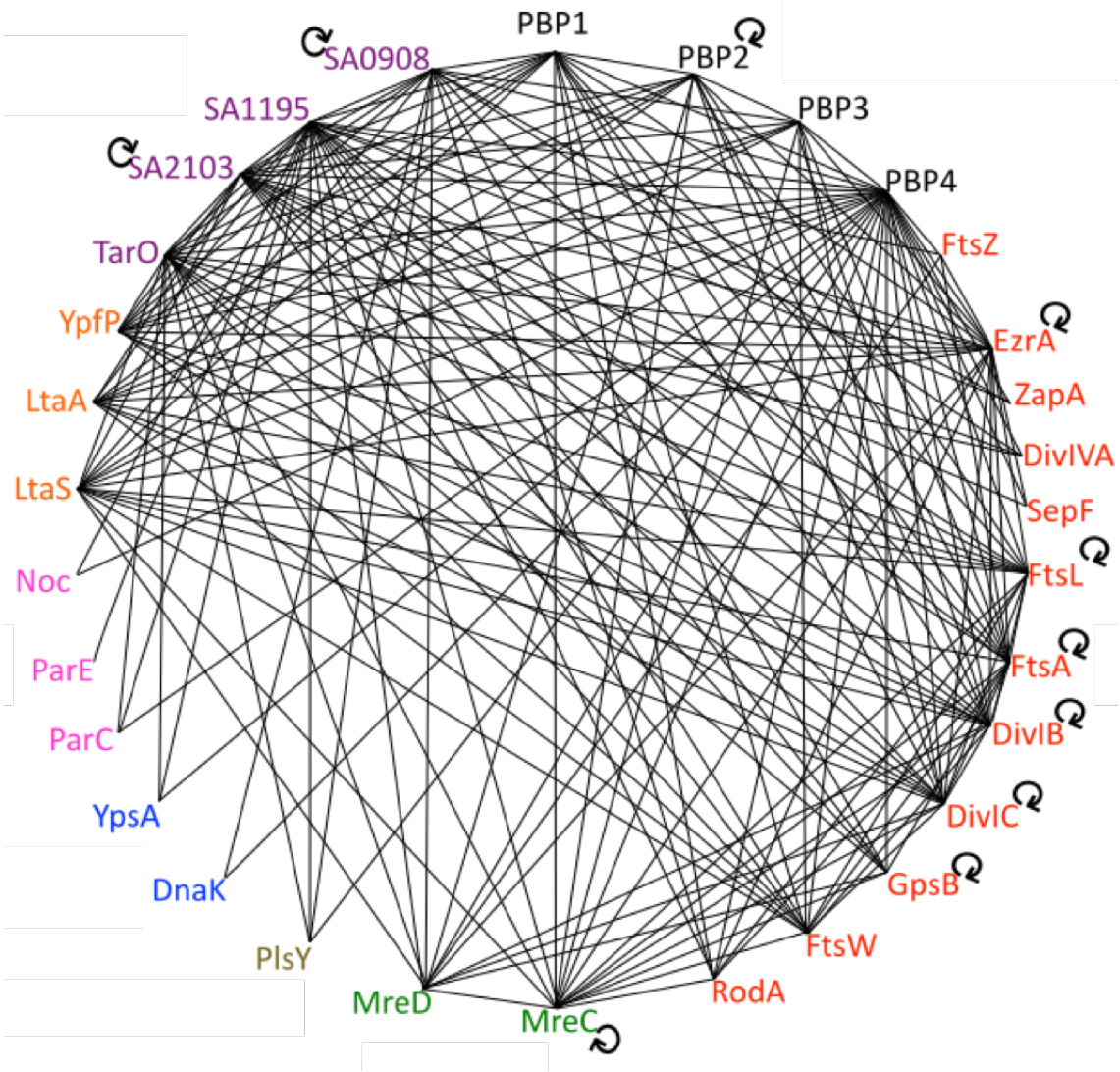

Figure 6.1. Interaction map of proteins in *S. aureus*

Interactions between *S. aureus* cell division (red), peptidoglycan biosynthesis (black), wall teichoic acids synthesis (purple), lipoteichoic acids synthesis (orange), chromosome segregation (pink), chaperones (blue), phospholipid biosynthesis (brown) and shape maintenance (green) proteins as determined by bacterial two-hybrid system are shown (Steele et al., 2011; Kent, 2013; Reichmann et al., 2014; Xing Ma, unpublished). Arrows indicate self interactions. The image courtesy of Victoria Lund.

This was however not possible. Although PBP3 and PBP4 are not essential and could be easily removed, PBP1 transpeptidase activity was found to be indispensable for cell viability, in contrast to a previous report (Pereira et al., 2009). Therefore, only PBP3 and PBP4 were shown to be together not crucial. This is in agreement with another research report, which showed that *S. aureus* cell division is not hampered when these two proteins are absent (Reed et al., 2015). Employment of Bocillin FL showed that in the absence of PBP3 and PBP4, PBP1 and PBP2 are mostly localised to the division site and give some minor peripheral signal, similar to when all four PBPs are present in the cell. Super-resolution imaging of PBP1 and PBP2 using fluorescent penicillin was not accomplished, since STORM-compatible penicillin Alexa Fluor 647 (Pen-AF647) did not bind PBPs *in vivo*. This was probably caused by the negative net charge of the cell wall (Neuhaus and Baddiley, 2003), and the large size and also negative charge of Pen-AF647, which together prevented penetration of the peptidoglycan by Pen-AF64, stopping it reach the PBPs.

What is more, STORM imaging of EzrA and FtsZ revealed that not all EzrA and FtsZ molecules were present at the division septa. Whilst FtsZ could be observed in the cytoplasm and peripheral membrane, EzrA gave a signal associated with the peripheral membrane. Pulse chase labelling of peptidoglycan using fluorescent derivatives of D-Ala showed that this off-septal signal was on a plane orthogonal to the current and previous cell division planes. This indicates that FtsZ together with EzrA may mark future division sites. How *S. aureus* selects the division site still remains unknown. Studies on *S. aureus* peptidoglycan suggested that local peptidoglycan architecture, a 'piecrust' and 'ribs' could act as 'signposts' of the next division plane (Turner et al., 2010). The selection of the division site could be guided by division components such as, DivIB and FtsL (Bottomley et al., 2014; Kabli, 2013). Both proteins interact with EzrA in the bacterial-two hybrid system (Figure 6.1) but their localisation patterns do not resemble that of EzrA or FtsZ (Bottomley et al., 2014; Kabli, 2013). DivIB and FtsL were shown to only transiently localise to the septum and mostly to the cell periphery (Bottomley et al., 2014; Kabli, 2013). The peripheral location was suggested to mark previous division sites by recognition of the peptidoglycan 'rib' structures, preventing their reuse (Turner et al., 2010; Bottomley et al., 2014). Contrary to previous studies, WTAs were shown to be non-uniformly distributed across the cell surface and septum, suggesting that the 'piecrust' and 'rib' features may be free of WTAs (Schlag et al.,

2010; Kent, 2013). DivIB affinity toward peptidoglycan is decreased in the presence of wall teichoic acids (WTAs) (Bottomley et al., 2014). Thus WTAs may direct DivIB to the WTAs free regions (Kent, 2013; Bottomley et al., 2014).

In *E. coli* FtsN, a cell division protein has a SPOR periplasmic domain that binds peptidoglycan (Ursinus et al., 2004; Müller et al., 2007). Recently, FtsN was suggested to trigger peptidoglycan synthesis by conformational changes in FtsA and the FtsLBQ complex, stimulating peptidoglycan synthesis by FtsI (Liu et al., 2015; Tsang and Bernhardt, 2015). FtsI is a class B HMW PBP crucial for cell division in *E. coli* (Spratt, 1975; Scheffers and Pinho, 2005). FtsN and FtsI also interact with PBP1B, a HMW class A PBP, which is involved both in cell elongation and division in *E. coli* and becomes essential when PBP1A, another HMW class A PBP, is absent (Suzuki et al., 1978; Scheffers and Pinho, 2005; Bertsche et al., 2006; Müller et al., 2007). *S. aureus* does not have FtsN but DivIB, DivIC and FtsL can bind peptidoglycan (Kabli, 2013; Bottomley et al., 2014). Additionally, DivIB is required for septum completion in *S. aureus* (Bottomley et al., 2014). Moreover, all these three proteins (DivIB, DivIC and FtsL) interact with EzrA, FtsA, and PBP1 and PBP2 (Figure 6.1). *S. aureus* PBP1 is homologue of *E. coli* FtsI, while PBP2 is bifunctional as is *E. coli* PBP1A/B (Scheffers and Pinho, 2005; Pereira et al., 2007; Steele et al., 2011). Therefore, in *S. aureus* DivIB together with DivC and FtsL may regulate peptidoglycan synthesis led by PBP1 and PBP2 through its temporal localisation in the septum and interactions with FtsA and EzrA.

The data gathered during this project leads to the following model of septum formation in *S. aureus* (Figure 6.2). FtsZ is the first protein localising to the division site, which promptly recruits EzrA, therefore these two components appear almost simultaneously at midcell. EzrA interacts and tethers FtsZ protofilaments to the membrane. FtsZ through EzrA recruits penicillin binding proteins (PBPs), whose arrival results in initiation of peptidoglycan synthesis (Figure 6.2 A-B). Cell division components form dynamic ‘patches’ (Figure 6.2C) that envelope the leading edge of the septum and extend down its sides (Figure 6.2D). The decreasing concentration gradient of molecules from the leading to the distal edge of the septum wraps around the septum and forms a framework for peptidoglycan synthesis (Figure 6.2D). Cryo-electron microscopy and STORM of nascent peptidoglycan insertion in *S. aureus* revealed that

septum is flared with a gap (a low density region), which separates the cross walls, and peptidoglycan is therefore not solely inserted at the leading edge of the septum, but in a gradient along the septum, forming a zone of synthesis (Matias and Beveridge, 2007; Victoria Lund, unpublished). Since peptidoglycan is the outcome of the collective activity of division components, the gradient insertion of peptidoglycan supports the distribution of FtsZ, EzrA and PBPs. FtsZ dynamics (polymerisation, depolymerisation, remodelling) are not sufficient for Z-ring constriction in *B. subtilis* (Strauss et al., 2012) and as peptidoglycan is incorporated into the septum it may mechanically push the leading edge together with cell division proteins inwards, leading to septal disc closure (Figure 6.2).

6.1 Future perspectives

This work provides information on localisation and organisation of crucial cell division components in *S. aureus*. The data presented here contribute to the growing evidence for a dynamic and heterogeneous distribution of cell division components.

The localisation and role of particular PBPs in cell division remains an unanswered question. Here preparation for localisation of PBP2 using probes targeting its transglycosylase activity were made. Utilisation of fluorescent Moenomycin A and moenomycin-like probes, such as recently described disaccharide based ACL19378 or monosaccharide derivatives as ACL20215 and ACL20965 (Zuegg et al., 2015), may allow for selective labelling and visualisation of PBP2 in *S. aureus*.

Cell division proteins do not form static structures but remain dynamic throughout the cell division cycle. FtsZ is a dynamic protein and it would be fascinating to find out if other cell division components present the same motions. This could be achieved by FRAP experiments to monitor cell division protein turnover. Single particle tracking PALM would not only give data about dynamics of proteins in live cells, but it would also reveal if the molecular motion is random or ordered.

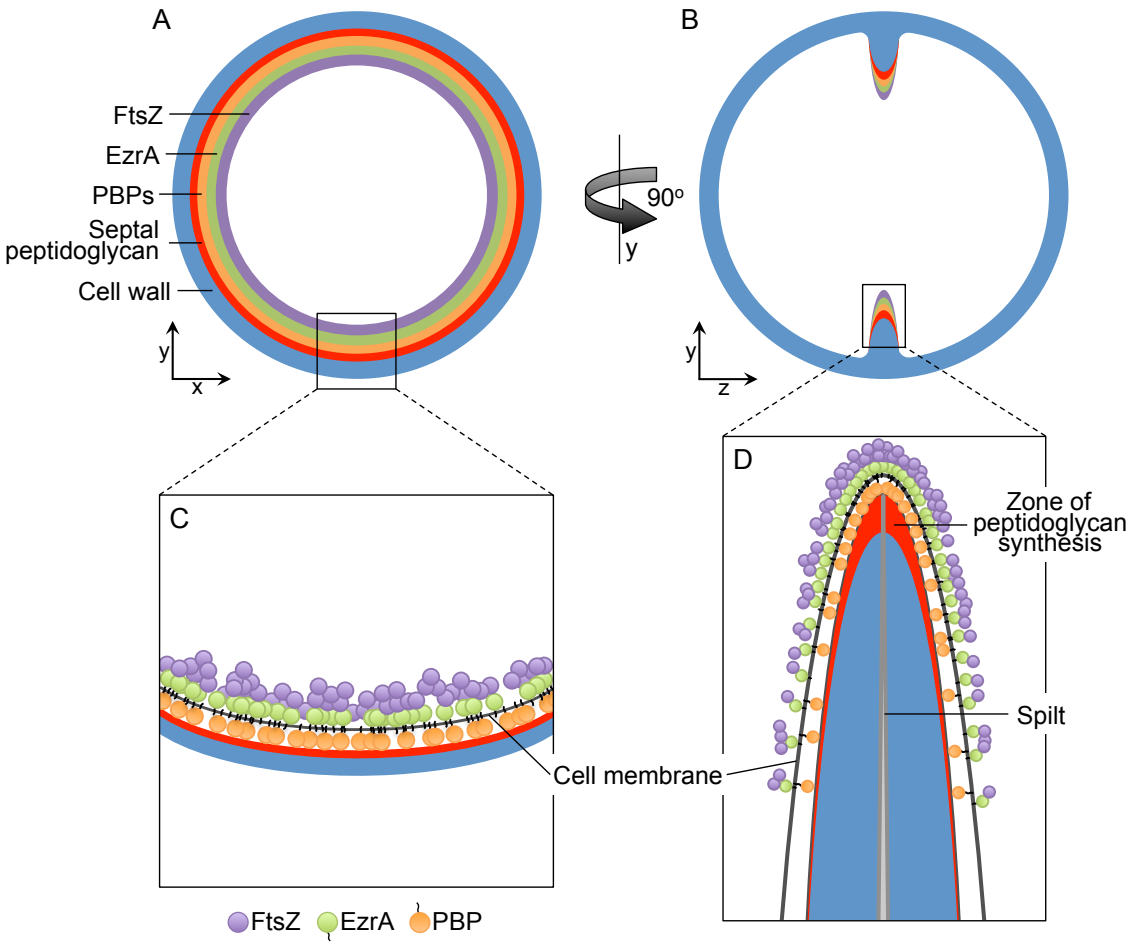

Figure 6.2. Schematic illustration of the organisation of *S. aureus* cell division components at the septum

In *S. aureus* cell division components FtsZ (purple), EzrA (green) and PBPs (yellow) are recruited to the division septum where they form structures observed as either enclosing rings (A) or a line (B) depending on the orientation of the division plane to the plane of the image when visualised by diffraction limited microscopy techniques. FtsZ forms the innermost ring that precedes all other components, while septal peptidoglycan (red) forms the outermost structure. (C) Super-resolution microscopy reveals that FtsZ and EzrA are heterogeneously distributed along the division site. In the cytoplasm non-uniform arrangement of EzrA molecules (green spheres) tethers heterogeneously spread FtsZ (purple spheres) to the cell membrane. In the membrane/periplasm EzrA interacts with PBPs (yellow spheres) that catalyse septal peptidoglycan synthesis (red). FtsZ indirectly leads peptidoglycan synthesis through its association with EzrA. (D) In *S. aureus* the incomplete septum is flared. The septal peptidoglycan synthesis occurs as a zone of synthesis (red). The septum is formed as two plates with a low density 'split' (grey) running between them. FtsZ, EzrA and PBPs envelope the septum forming a decreasing concentration gradient from the leading to the distal edge of the septum. Other cell division components are not shown.

Understanding the role of particular cell components is difficult in the whole-cell system due to the presence of all the other cell components. Reconstitution of cell division proteins, including PBPs, in liposomes or on supported lipid bilayers may identify important components that directly coordinate cell division and synthesis of peptidoglycan but also help to identify the required substrates for the process to occur.

Microscopy localisation studies and the bacterial two-hybrid system are not sufficient tools for studying protein interactions and colocalisations. Conclusions from the bacterial-two hybrid system can be obfuscated by false-positive interactions, whilst proteins located in close proximity do not necessarily have to interact with each other. These methods require further verification by such as pull down assays or FRET microscopy studies. Combining the power of biochemical and microscopy approaches will complement current understanding and shed more light on the mechanisms of *S. aureus* cell division.

References

Adams, D.W., and Errington, J. (2009). Bacterial cell division: assembly, maintenance and disassembly of the Z ring. Nat Rev Micro *7*, 642–653.

Adams, D.W., Wu, L.J., and Errington, J. (2015). Nucleoid occlusion protein Noc recruits DNA to the bacterial cell membrane. The EMBO Journal *34*, 491–501.

Addinall, S.G., and Lutkenhaus, J. (1996). FtsA is localized to the septum in an FtsZ-dependent manner. J. Bacteriol. *178*, 7167–7172.

Addinall, S.G., Bi, E., and Lutkenhaus, J. (1996). FtsZ ring formation in *fts* mutants. J. Bacteriol. *178*, 3877–3884.

Addinall, S.G., Cao, C., and Lutkenhaus, J. (1997). FtsN, a late recruit to the septum in *Escherichia coli*. Mol. Microbiol. *25*, 303–309.

Aish, J.L. (2003). Environmental regulation of virulence determinant expression in *Staphylococcus aureus*. University of Sheffield.

Anderson, D.E., Gueiros-Filho, F.J., and Erickson, H.P. (2004). Assembly dynamics of FtsZ dings in *Bacillus subtilis* and *Escherichia coli* and effects of FtsZ-regulating proteins. J Bacteriol *186*, 5775–5781.

Arbeloa, A., Segal, H., Hugonnet, J.-E., Josseaume, N., Dubost, L., Brouard, J.-P., Gutmann, L., Mengin-Lecreulx, D., and Arthur, M. (2004). Role of class A penicillin-binding proteins in PBP5-mediated beta-lactam resistance in *Enterococcus faecalis*. J. Bacteriol. *186*, 1221–1228.

Archer, G.L. (1998). *Staphylococcus aureus*: a well-armed pathogen. Clin. Infect. Dis. *26*, 1179–1181.

Arends, S.J.R., Kustusch, R.J., and Weiss, D.S. (2009). ATP-binding site lesions in FtsE impair cell division. J Bacteriol *191*, 3772–3784.

Arnaud, M., Chastanet, A., and Débarbouillé, M. (2004). New vector for efficient allelic replacement in naturally nontransformable, low-GC-content, Gram-positive bacteria. Appl Environ Microbiol *70*, 6887–6891.

Atilano, M.L., Pereira, P.M., Yates, J., Reed, P., Veiga, H., Pinho, M.G., and Filipe, S.R. (2010). Teichoic acids are temporal and spatial regulators of peptidoglycan cross-linking in *Staphylococcus aureus*. Proc. Natl. Acad. Sci. U.S.A. *107*, 18991–18996.

Aussel, L., Barre, F.X., Aroyo, M., Stasiak, A., Stasiak, A.Z., and Sherratt, D. (2002). FtsK is a DNA motor protein that activates chromosome dimer resolution by switching the catalytic state of the XerC and XerD recombinases. Cell *108*, 195–205.

Baba, T., Bae, T., Schneewind, O., Takeuchi, F., and Hiramatsu, K. (2008). Genome sequence of *Staphylococcus aureus* strain Newman and comparative analysis of staphylococcal genomes: Polymorphism and Evolution of Two Major Pathogenicity Islands. J. Bacteriol. *190*, 300–310.

Bailey, M.W., Bisicchia, P., Warren, B.T., Sherratt, D.J., and Männik, J. (2014). Evidence for divisome localization mechanisms independent of the Min system and SlmA in *Escherichia coli*. PLoS Genet. *10*, e1004504.

Barber, M. (1961). Methicillin-resistant staphylococci. J. Clin. Pathol. *14*, 385–393.

Barber, M., and Rozwadowska-Dowzenko, M. (1948). Infection by penicillin-resistant staphylococci. Lancet *2*, 641–644.

Bartual, S.G., Straume, D., Stamsås, G.A., Muñoz, I.G., Alfonso, C., Martínez-Ripoll, M., Håvarstein, L.S., and Hermoso, J.A. (2014). Structural basis of PcsB-mediated cell separation in *Streptococcus pneumoniae.* Nat Commun *5*, 3842.

Bates, M., Huang, B., and Zhuang, X. (2008). Super-resolution microscopy by nanoscale localization of photo-switchable fluorescent probes. Current Opinion in Chemical Biology *12*, 505–514.

Bath, J., Wu, L.J., Errington, J., and Wang, J.C. (2000). Role of *Bacillus subtilis* SpoIIIE in DNA transport across the mother cell-prespore division septum. Science *290*, 995–997.

Beall, B., and Lutkenhaus, J. (1989). Nucleotide sequence and insertional inactivation of a *Bacillus*

subtilis gene that affects cell division, sporulation, and temperature sensitivity. J. Bacteriol. *171*, 6821–6834.

Beall, B., and Lutkenhaus, J. (1991). FtsZ in *Bacillus subtilis* is required for vegetative septation and for asymmetric septation during sporulation. Genes Dev. *5*, 447–455.

Beall, B., and Lutkenhaus, J. (1992). Impaired cell division and sporulation of a *Bacillus subtilis* strain with the *ftsA* gene deleted. J Bacteriol *174*, 2398–2403.

Beall, B., Lowe, M., and Lutkenhaus, J. (1988). Cloning and characterization of *Bacillus subtilis* homologs of *Escherichia coli* cell division genes *ftsZ* and *ftsA*. J. Bacteriol. *170*, 4855–4864.

Beaufay, F., Coppine, J., Mayard, A., Laloux, G., De Bolle, X., and Hallez, R. (2015). A NAD-dependent glutamate dehydrogenase coordinates metabolism with cell division in *Caulobacter crescentus*. EMBO J. *34*, 1786–1800.

Begg, K.J., and Donachie, W.D. (1985). Cell shape and division in *Escherichia coli:* experiments with shape and division mutants. J. Bacteriol. *163*, 615–622.

Begg, K.J., Hatfull, G.F., and Donachie, W.D. (1980). Identification of new genes in a cell envelope-cell division gene cluster of *Escherichia coli*: cell division gene *ftsQ*. J. Bacteriol. *144*, 435–437.

Begg, K.J., Dewar, S.J., and Donachie, W.D. (1995). A new *Escherichia coli* cell division gene, *ftsK*. J. Bacteriol. *177*, 6211–6222.

Ben-Yehuda, S., and Losick, R. (2002). Asymmetric cell division in *B. subtilis* involves a spiral-like intermediate of the cytokinetic protein FtsZ. Cell *109*, 257–266.

van den Berg van Saparoea, H.B., Glas, M., Vernooij, I.G.W.H., Bitter, W., den Blaauwen, T., and Luirink, J. (2013). Fine-mapping the contact sites of the *Escherichia coli* cell division proteins FtsB and FtsL on the FtsQ protein. J Biol Chem *288*, 24340–24350.

Bernhardt, T.G., and de Boer, P.A.J. (2005). SlmA, a nucleoid-associated, FtsZ binding protein required for blocking septal ring assembly over chromosomes in *E. coli*. Mol. Cell *18*, 555–564.

Berscheid, A., Sass, P., Weber-Lassalle, K., Cheung, A.L., and Bierbaum, G. (2012). Revisiting the genomes of the *Staphylococcus aureus* strains NCTC 8325 and RN4220. Int. J. Med. Microbiol. *302*, 84–87.

Bertsche, U., Kast, T., Wolf, B., Fraipont, C., Aarsman, M.E.G., Kannenberg, K., von Rechenberg, M., Nguyen-Distèche, M., den Blaauwen, T., Höltje, J.-V., et al. (2006). Interaction between two murein (peptidoglycan) synthases, PBP3 and PBP1B, in *Escherichia coli*. Mol. Microbiol. *61*, 675–690.

Betzig, E., Patterson, G.H., Sougrat, R., Lindwasser, O.W., Olenych, S., Bonifacino, J.S., Davidson, M.W., Lippincott-Schwartz, J., and Hess, H.F. (2006). Imaging intracellular fluorescent proteins at nanometer resolution. Science *313*, 1642–1645.

Beuria, T.K., Mullapudi, S., Mileykovskaya, E., Sadasivam, M., Dowhan, W., and Margolin, W. (2009). Adenine nucleotide-dependent regulation of assembly of bacterial tubulin-like FtsZ by a hypermorph of bacterial actin-like FtsA. J. Biol. Chem. *284*, 14079–14086.

Bhattacharya, A., Ray, S., Singh, D., Dhaked, H.P.S., and Panda, D. (2015). ZapC promotes assembly and stability of FtsZ filaments by binding at a different site on FtsZ than ZipA. International Journal of Biological Macromolecules *81*, 435–442.

Bi, E.F., and Lutkenhaus, J. (1991). FtsZ ring structure associated with division in *Escherichia coli*. Nature *354*, 161–164.

Bigot, S., Corre, J., Louarn, J.-M., Cornet, F., and Barre, F.-X. (2004). FtsK activities in Xer recombination, DNA mobilization and cell division involve overlapping and separate domains of the protein. Mol. Microbiol. *54*, 876–886.

Bigot, S., Saleh, O.A., Cornet, F., Allemand, J.-F., and Barre, F.-X. (2006). Oriented loading of FtsK on KOPS. Nat Struct Mol Biol *13*, 1026–1028.

Bigot, S., Sivanathan, V., Possoz, C., Barre, F.-X., and Cornet, F. (2007). FtsK, a literate chromosome segregation machine. Mol. Microbiol. *64*, 1434–1441.

Bisicchia, P., Steel, B., Debela, M.H.M., Löwe, J., and Sherratt, D. (2013). The N-terminal membrane-spanning domain of the *Escherichia coli* DNA translocase FtsK hexamerizes at midcell. mBio *4*, e00800–

e00813.

Bismuth, R., Zilhao, R., Sakamoto, H., Guesdon, J.L., and Courvalin, P. (1990). Gene heterogeneity for tetracycline resistance in *Staphylococcus* spp. Antimicrob. Agents Chemother. *34*, 1611–1614.

Biteen, J.S., Thompson, M.A., Tselentis, N.K., Bowman, G.R., Shapiro, L., and Moerner, W. (2008). Super-resolution imaging in live *Caulobacter crescentus* cells using photoswitchable EYFP. Nat Methods *5*, 947–949.

de Boer, P.A.J. (2010). Advances in understanding *E. coli* cell fission. Curr. Opin. Microbiol. *13*, 730–737.

de Boer, P.A., Crossley, R.E., and Rothfield, L.I. (1989). A division inhibitor and a topological specificity factor coded for by the minicell locus determine proper placement of the division septum in *E. coli*. Cell *56*, 641–649.

de Boer, P.A., Crossley, R.E., Hand, A.R., and Rothfield, L.I. (1991). The MinD protein is a membrane ATPase required for the correct placement of the *Escherichia coli* division site. EMBO J. *10*, 4371–4380.

de Boer, P.A., Crossley, R.E., and Rothfield, L.I. (1992a). Roles of MinC and MinD in the site-specific septation block mediated by the MinCDE system of *Escherichia coli*. J. Bacteriol. *174*, 63–70.

de Boer, P., Crossley, R., and Rothfield, L. (1992b). The essential bacterial cell-division protein FtsZ is a GTPase. Nature *359*, 254–256.

Borek, F. (1961). The fluorescent antibody method in medical and biological research. Bull World Health Organ *24*, 249–256.

Bork, P., Sander, C., and Valencia, A. (1992). An ATPase domain common to prokaryotic cell cycle proteins, sugar kinases, actin, and hsp70 heat shock proteins. Proc. Natl. Acad. Sci. U.S.A. *89*, 7290–7294.

Bottomley, A.L. (2011). Identification and characterisation of the cell division machinery in *Staphylococcus aureus*. University of Sheffield.

Bottomley, A.L., Kabli, A.F., Hurd, A.F., Turner, R.D., Garcia-Lara, J., and Foster, S.J. (2014). *Staphylococcus aureus* DivIB is a peptidoglycan-binding protein that is required for a morphological checkpoint in cell division. Mol. Microbiol.

Bowler, L.D., and Spratt, B.G. (1989). Membrane topology of penicillin-binding protein 3 of *Escherichia coli*. Mol. Microbiol. *3*, 1277–1286.

Boyle, D.S., Khattar, M.M., Addinall, S.G., Lutkenhaus, J., and Donachie, W.D. (1997). *ftsW* is an essential cell-division gene in *Escherichia coli*. Molecular Microbiology *24*, 1263–1273.

Bramhill, D. (1997). Bacterial cell division. Annu. Rev. Cell Dev. Biol. *13*, 395–424.

Bramkamp, M., Emmins, R., Weston, L., Donovan, C., Daniel, R.A., and Errington, J. (2008). A novel component of the division-site selection system of *Bacillus subtilis* and a new mode of action for the division inhibitor MinCD. Mol. Microbiol. *70*, 1556–1569.

Breinbauer, R., and Köhn, M. (2003). Azide–alkyne coupling: a powerful reaction for bioconjugate chemistry. ChemBioChem *4*, 1147–1149.

Buddelmeijer, N., and Beckwith, J. (2004). A complex of the *Escherichia coli* cell division proteins FtsL, FtsB and FtsQ forms independently of its localization to the septal region. Mol. Microbiol. *52*, 1315–1327.

Buddelmeijer, N., Aarsman, M.E., Kolk, A.H., Vicente, M., and Nanninga, N. (1998). Localization of cell division protein FtsQ by immunofluorescence microscopy in dividing and nondividing cells of *Escherichia coli*. J. Bacteriol. *180*, 6107–6116.

Buddelmeijer, N., Judson, N., Boyd, D., Mekalanos, J.J., and Beckwith, J. (2002). YgbQ, a cell division protein in *Escherichia coli* and *Vibrio cholerae*, localizes in codependent fashion with FtsL to the division site. Proc. Natl. Acad. Sci. U.S.A. *99*, 6316–6321.

Busiek, K.K., and Margolin, W. (2014). A role for FtsA in SPOR-independent localization of the essential *Escherichia coli* cell division protein FtsN. Mol Microbiol *92*, 1212–1226.

Busiek, K.K., Eraso, J.M., Wang, Y., and Margolin, W. (2012). The early divisome protein FtsA interacts

directly through its 1c subdomain with the cytoplasmic domain of the late divisome protein FtsN. J. Bacteriol. *194*, 1989–2000.

Buske, P.J., and Levin, P.A. (2013). A flexible C-terminal linker is required for proper FtsZ assembly in vitro and cytokinetic ring formation in vivo. Molecular Microbiology *89*, 249–263.

Buss, J., Coltharp, C., Shtengel, G., Yang, X., Hess, H., and Xiao, J. (2015). A multi-layered protein network stabilizes the *Escherichia coli* FtsZ-ring and modulates constriction dynamics. PLoS Genet *11*.

Butler, E.K., Davis, R.M., Bari, V., Nicholson, P.A., and Ruiz, N. (2013). Structure-function analysis of murj reveals a solvent-exposed cavity containing residues essential for peptidoglycan biogenesis in *Escherichia coli*. J Bacteriol *195*, 4639–4649.

Cabré, E.J., Monterroso, B., Alfonso, C., Sánchez-Gorostiaga, A., Reija, B., Jiménez, M., Vicente, M., Zorrilla, S., and Rivas, G. (2015). The nucleoid occlusion slma protein accelerates the disassembly of the ftsz protein polymers without affecting their GTPase activity. PLoS ONE *10*, e0126434.

Carballido-López, R., and Formstone, A. (2007). Shape determination in *Bacillus subtilis*. Current Opinion in Microbiology *10*, 611–616.

Carson, M.J., Barondess, J., and Beckwith, J. (1991). The FtsQ protein of *Escherichia coli*: membrane topology, abundance, and cell division phenotypes due to overproduction and insertion mutations. J. Bacteriol. *173*, 2187–2195.

Cattoni, D.I., Thakur, S., Godefroy, C., Gall, A.L., Lai-Kee-Him, J., Milhiet, P.-E., Bron, P., and Nöllmann, M. (2014). Structure and DNA-binding properties of the *Bacillus subtilis* SpoIIIE DNA translocase revealed by single-molecule and electron microscopies. Nucl. Acids Res. *42*, 2624–2636.

Chambers, H.F., and DeLeo, F.R. (2009). Waves of Resistance: *Staphylococcus aureus* in the antibiotic era. Nat Rev Microbiol *7*, 629–641.

Chaudhuri, R.R., Allen, A.G., Owen, P.J., Shalom, G., Stone, K., Harrison, M., Burgis, T.A., Lockyer, M., Garcia-Lara, J., Foster, S.J., et al. (2009). Comprehensive identification of essential *Staphylococcus aureus* genes using Transposon-Mediated Differential Hybridisation (TMDH). BMC Genomics *10*, 291.

Chen, J.C., and Beckwith, J. (2001). FtsQ, FtsL and FtsI require FtsK, but not FtsN, for co-localization with FtsZ during *Escherichia coli* cell division. Mol. Microbiol. *42*, 395–413.

Chen, Y., and Erickson, H.P. (2005). Rapid in vitro assembly dynamics and subunit turnover of FtsZ demonstrated by Fluorescence Resonance Energy Transfer. J. Biol. Chem. *280*, 22549–22554.

Chien, A.-C., Zareh, S.K.G., Wang, Y.M., and Levin, P.A. (2012a). Changes in the oligomerization potential of the division inhibitor UgtP co-ordinate *Bacillus subtilis* cell size with nutrient availability. Molecular Microbiology *86*, 594–610.

Chien, A.-C., Hill, N.S., and Levin, P.A. (2012b). Cell size control in bacteria. Curr. Biol. *22*, R340–R349.

Cho, H., and Bernhardt, T.G. (2013). Identification of the SlmA active site responsible for blocking bacterial cytokinetic ring assembly over the chromosome. PLoS Genet *9*, e1003304.

Cho, H., McManus, H.R., Dove, S.L., and Bernhardt, T.G. (2011). Nucleoid occlusion factor SlmA is a DNA-activated FtsZ polymerization antagonist. PNAS *108*, 3773–3778.

Chung, K.-M., Hsu, H.-H., Govindan, S., and Chang, B.-Y. (2004). Transcription regulation of *ezrA* and its effect on cell division of *Bacillus subtilis*. J Bacteriol *186*, 5926–5932.

Chung, K.-M., Hsu, H.-H., Yeh, H.-Y., and Chang, B.-Y. (2007). Mechanism of regulation of prokaryotic tubulin-like GTPase FtsZ by membrane protein EzrA. J. Biol. Chem. *282*, 14891–14897.

Claessen, D., Emmins, R., Hamoen, L.W., Daniel, R.A., Errington, J., and Edwards, D.H. (2008). Control of the cell elongation–division cycle by shuttling of PBP1 protein in *Bacillus subtilis*. Molecular Microbiology *68*, 1029–1046.

Claessen, D., Rozen, D.E., Kuipers, O.P., Søgaard-Andersen, L., and van Wezel, G.P. (2014). Bacterial solutions to multicellularity: a tale of biofilms, filaments and fruiting bodies. Nat Rev Micro *12*, 115–124.

Clarke, S.R., and Foster, S.J. (2006). Surface adhesins of *Staphylococcus aureus*. Adv. Microb. Physiol. *51*, 187–224.

Cleverley, R.M., Barrett, J.R., Baslé, A., Bui, N.K., Hewitt, L., Solovyova, A., Xu, Z.-Q., Daniel, R.A., Dixon, N.E., Harry, E.J., et al. (2014). Structure and function of a spectrin-like regulator of bacterial cytokinesis. Nat Commun *5*, 5421.

Coltharp, C., and Xiao, J. (2012). Superresolution microscopy for microbiology. Cell Microbiol *14*, 1808–1818.

Considine, K.M., Sleator, R.D., Kelly, A.L., Fitzgerald, G.F., and Hill, C. (2011). Identification and characterization of an essential gene in *Listeria monocytogenes* using an inducible gene expression system. Bioeng Bugs *2*, 150–159.

Conti, J., Viola, M.G., and Camberg, J.L. (2015). The bacterial cell division regulators MinD and MinC form polymers in the presence of nucleotide. FEBS Lett. *589*, 201–206.

Coons, A.H., and Kaplan, M.H. (1950). Localization of antigen in tissue cells. J Exp Med *91*, 1–13.

Cooper, E.L., García-Lara, J., and Foster, S.J. (2009). YsxC, an essential protein in *Staphylococcus aureus* crucial for ribosome assembly/stability. BMC Microbiol. *9*, 266.

Corbin, B.D., Wang, Y., Beuria, T.K., and Margolin, W. (2007). Interaction between cell division proteins FtsE and FtsZ. J. Bacteriol. *189*, 3026–3035.

Crozat, E., and Grainge, I. (2010). FtsK DNA translocase: the fast motor that knows where it's going. Chembiochem *11*, 2232–2243.

Dai, K., and Lutkenhaus, J. (1991). *ftsZ* is an essential cell division gene in *Escherichia coli*. J. Bacteriol. *173*, 3500–3506.

Dai, K., and Lutkenhaus, J. (1992). The proper ratio of FtsZ to FtsA is required for cell division to occur in *Escherichia coli*. J. Bacteriol. *174*, 6145–6151.

Dai, K., Xu, Y., and Lutkenhaus, J. (1993). Cloning and characterization of *ftsN*, an essential cell division gene in *Escherichia coli* isolated as a multicopy suppressor of *ftsA12*(Ts). J. Bacteriol. *175*, 3790–3797.

Dai, K., Xu, Y., and Lutkenhaus, J. (1996). Topological characterization of the essential *Escherichia coli* cell division protein FtsN. J. Bacteriol. *178*, 1328–1334.

Dajkovic, A., Lan, G., Sun, S.X., Wirtz, D., and Lutkenhaus, J. (2008). MinC spatially controls bacterial cytokinesis by antagonizing the scaffolding function of FtsZ. Curr. Biol. *18*, 235–244.

Dajkovic, A., Pichoff, S., Lutkenhaus, J., and Wirtz, D. (2010). Cross-linking FtsZ polymers into coherent Z rings. Molecular Microbiology *78*, 651–668.

Dancer, S.J. (2008). The effect of antibiotics on methicillin-resistant *Staphylococcus aureus*. J. Antimicrob. Chemother. *61*, 246–253.

Daniel, R.A., and Errington, J. (2000). Intrinsic instability of the essential cell division protein FtsL of *Bacillus subtilis* and a role for DivIB protein in FtsL turnover. Mol. Microbiol. *36*, 278–289.

Daniel, R.A., and Errington, J. (2003). Control of cell morphogenesis in bacteria: two distinct ways to make a rod-shaped cell. Cell *113*, 767–776.

Daniel, R.A., Williams, A.M., and Errington, J. (1996). A complex four-gene operon containing essential cell division gene *pbpB* in *Bacillus subtilis.* J. Bacteriol. *178*, 2343–2350.

Daniel, R.A., Harry, E.J., Katis, V.L., Wake, R.G., and Errington, J. (1998). Characterization of the essential cell division gene *ftsL*(*yIID*) of *Bacillus subtilis* and its role in the assembly of the division apparatus. Mol. Microbiol. *29*, 593–604.

Daniel, R.A., Harry, E.J., and Errington, J. (2000). Role of penicillin-binding protein PBP 2B in assembly and functioning of the division machinery of *Bacillus subtilis*. Molecular Microbiology *35*, 299–311.

Daniel, R.A., Noirot-Gros, M.-F., Noirot, P., and Errington, J. (2006). Multiple interactions between the transmembrane division proteins of *Bacillus subtilis* and the role of FtsL instability in divisome assembly. J. Bacteriol. *188*, 7396–7404.

Dempsey, G.T., Vaughan, J.C., Chen, K.H., Bates, M., and Zhuang, X. (2011). Evaluation of fluorophores for optimal performance in localization-based super-resolution imaging. Nat Methods *8*, 1027–1036.

Den Blaauwen, T., Buddelmeijer, N., Aarsman, M.E.G., Hameete, C.M., and Nanninga, N. (1999).

Timing of FtsZ assembly in *Escherichia coli*. J Bacteriol *181*, 5167–5175.

Derouaux, A., Wolf, B., Fraipont, C., Breukink, E., Nguyen-Distèche, M., and Terrak, M. (2008). The monofunctional glycosyltransferase of *Escherichia coli* localizes to the cell division site and interacts with penicillin-binding protein 3, FtsW, and FtsN. J. Bacteriol. *190*, 1831–1834.

Di Lallo, G., Fagioli, M., Barionovi, D., Ghelardini, P., and Paolozzi, L. (2003). Use of a two-hybrid assay to study the assembly of a complex multicomponent protein machinery: bacterial septosome differentiation. Microbiology (Reading, Engl.) *149*, 3353–3359.

Din, N., Quardokus, E.M., Sackett, M.J., and Brun, Y.V. (1998). Dominant C-terminal deletions of FtsZ that affect its ability to localize in *Caulobacter* and its interaction with FtsA. Mol. Microbiol. *27*, 1051–1063.

Donachie, W.D. (1968). Relationship between cell size and time of initiation of DNA replication. Nature *219*, 1077–1079.

Donachie, W.D., and Begg, K.J. (1989). Cell length, nucleoid separation, and cell division of rod-shaped and spherical cells of *Escherichia coli*. J Bacteriol *171*, 4633–4639.

Dopazo, A., Palacios, P., Sánchez, M., Pla, J., and Vicente, M. (1992). An amino-proximal domain required for the localization of FtsQ in the cytoplasmic membrane, and for its biological function in *Escherichia coli*. Mol. Microbiol. *6*, 715–722.

Dowzicky, M., Talbot, G.H., Feger, C., Prokocimer, P., Etienne, J., and Leclercq, R. (2000). Characterization of isolates associated with emerging resistance to quinupristin/dalfopristin (Synercid) during a worldwide clinical program. Diagn. Microbiol. Infect. Dis. *37*, 57–62.

Draper, G.C., McLennan, N., Begg, K., Masters, M., and Donachie, W.D. (1998). Only the N-terminal domain of FtsK functions in cell division. J. Bacteriol. *180*, 4621–4627.

Du, S., and Lutkenhaus, J. (2014). SlmA antagonism of FtsZ assembly employs a two-pronged mechanism like MinCD. PLoS Genet *10*, e1004460.

Dubarry, N., Possoz, C., and Barre, F.-X. (2010). Multiple regions along *the Escherichia coli* FtsK protein are implicated in cell division. Mol. Microbiol. *78*, 1088–1100.

D'Ulisse, V., Fagioli, M., Ghelardini, P., and Paolozzi, L. (2007). Three functional subdomains of the *Escherichia coli* FtsQ protein are involved in its interaction with the other division proteins. Microbiology (Reading, Engl.) *153*, 124–138.

Duman, R., Ishikawa, S., Celik, I., Strahl, H., Ogasawara, N., Troc, P., Löwe, J., and Hamoen, L.W. (2013). Structural and genetic analyses reveal the protein SepF as a new membrane anchor for the Z ring. Proc Natl Acad Sci U S A *110*, E4601–E4610.

Duncan, T.R., Yahashiri, A., Arends, S.J.R., Popham, D.L., and Weiss, D.S. (2013). Identification of SPOR domain amino acids important for septal localization, peptidoglycan binding, and a disulfide bond in the cell division protein FtsN. J Bacteriol *195*, 5308–5315.

Durand-Heredia, J., Rivkin, E., Fan, G., Morales, J., and Janakiraman, A. (2012). Identification of ZapD as a cell division factor that promotes the assembly of FtsZ in *Escherichia coli*. J Bacteriol *194*, 3189–3198.

Durand-Heredia, J.M., Yu, H.H., De Carlo, S., Lesser, C.F., and Janakiraman, A. (2011). Identification and characterization of ZapC, a stabilizer of the FtsZ ring in *Escherichia coli*. J Bacteriol *193*, 1405–1413.

Ebersbach, G., Galli, E., Møller-Jensen, J., Löwe, J., and Gerdes, K. (2008). Novel coiled-coil cell division factor ZapB stimulates Z ring assembly and cell division. Mol. Microbiol. *68*, 720–735.

Edwards, D.H., and Errington, J. (1997). The *Bacillus subtilis* DivIVA protein targets to the division septum and controls the site specificity of cell division. Mol. Microbiol. *24*, 905–915.

Edwards, D.H., Thomaides, H.B., and Errington, J. (2000). Promiscuous targeting of *Bacillus subtilis* cell division protein DivIVA to division sites in *Escherichia coli* and fission yeast. EMBO J. *19*, 2719–2727.

Egan, A.J.F., and Vollmer, W. (2013). The physiology of bacterial cell division. Annals of the New York Academy of Sciences *1277*, 8–28.

Elsen, N.L., Lu, J., Parthasarathy, G., Reid, J.C., Sharma, S., Soisson, S.M., and Lumb, K.J. (2012).

Mechanism of action of the cell-division inhibitor PC190723: modulation of FtsZ assembly cooperativity. J. Am. Chem. Soc. *134*, 12342–12345.

Endesfelder, U., Malkusch, S., Flottmann, B., Mondry, J., Liguzinski, P., Verveer, P.J., and Heilemann, M. (2011). Chemically induced photoswitching of fluorescent probes--a general concept for super-resolution microscopy. Molecules *16*, 3106–3118.

van den Ent, F., and Löwe, J. (2000). Crystal structure of the cell division protein FtsA from *Thermotoga maritima*. EMBO J. *19*, 5300–5307.

van den Ent, F., Vinkenvleugel, T.M.F., Ind, A., West, P., Veprintsev, D., Nanninga, N., den Blaauwen, T., and Löwe, J. (2008). Structural and mutational analysis of the cell division protein FtsQ. Mol. Microbiol. *68*, 110–123.

Erickson, H.P. (1997). FtsZ, a tubulin homologue in prokaryote cell division. Trends Cell Biol. *7*, 362–367.

Erickson, H.P. (2007). Evolution of the cytoskeleton. Bioessays *29*, 668–677.

Erickson, H.P., Taylor, D.W., Taylor, K.A., and Bramhill, D. (1996). Bacterial cell division protein FtsZ assembles into protofilament sheets and minirings, structural homologs of tubulin polymers. Proc Natl Acad Sci U S A *93*, 519–523.

Erickson, H.P., Anderson, D.E., and Osawa, M. (2010). FtsZ in bacterial cytokinesis: cytoskeleton and force generator all in one. Microbiol Mol Biol Rev *74*, 504–528.

Errington, J. (2010). From spores to antibiotics via the cell cycle. Microbiology *156*, 1–13.

Espéli, O., Borne, R., Dupaigne, P., Thiel, A., Gigant, E., Mercier, R., and Boccard, F. (2012). A MatP–divisome interaction coordinates chromosome segregation with cell division in *E. coli*. EMBO J *31*, 3198–3211.

Eswaramoorthy, P., Erb, M.L., Gregory, J.A., Silverman, J., Pogliano, K., Pogliano, J., and Ramamurthi, K.S. (2011). Cellular architecture mediates diviva ultrastructure and regulates Min activity in *Bacillus subtilis*. mBio *2*, e00257–11.

Fairclough, V. (2009). Functional analysis of novel essential genes of *Staphylococcus aureus*. University of Sheffield.

Feilmeier, B.J., Iseminger, G., Schroeder, D., Webber, H., and Phillips, G.J. (2000). Green fluorescent protein functions as a reporter for protein localization in *Escherichia coli*. J Bacteriol *182*, 4068–4076.

Fernández-Suárez, M., and Ting, A.Y. (2008). Fluorescent probes for super-resolution imaging in living cells. Nat Rev Mol Cell Biol *9*, 929–943.

Ferrero, L., Cameron, B., and Crouzet, J. (1995). Analysis of *gyrA* and *grlA* mutations in stepwise-selected ciprofloxacin-resistant mutants of *Staphylococcus aureus*. Antimicrob. Agents Chemother. *39*, 1554–1558.

Feucht, A., Lucet, I., Yudkin, M.D., and Errington, J. (2001). Cytological and biochemical characterization of the FtsA cell division protein of *Bacillus subtilis*. Mol. Microbiol. *40*, 115–125.

Fey, P.D., Endres, J.L., Yajjala, V.K., Widhelm, T.J., Boissy, R.J., Bose, J.L., and Bayles, K.W. (2013). A genetic resource for rapid and comprehensive phenotype screening of nonessential *Staphylococcus aureus*. Genes. mBio *4*, e00537–12.

Fleming, T.C., Shin, J.Y., Lee, S.-H., Becker, E., Huang, K.C., Bustamante, C., and Pogliano, K. (2010). Dynamic SpoIIIE assembly mediates septal membrane fission during *Bacillus subtilis* sporulation. Genes Dev. *24*, 1160–1172.

Fleurie, A., Manuse, S., Zhao, C., Campo, N., Cluzel, C., Lavergne, J.-P., Freton, C., Combet, C., Guiral, S., Soufi, B., et al. (2014a). Interplay of the serine/threonine-kinase StkP and the paralogs DivIVA and GpsB in pneumococcal cell elongation and division. PLoS Genet *10*.

Fleurie, A., Lesterlin, C., Manuse, S., Zhao, C., Cluzel, C., Lavergne, J.-P., Franz-Wachtel, M., Macek, B., Combet, C., Kuru, E., et al. (2014b). MapZ beacons the division sites and positions FtsZ-rings in *Streptococcus pneumoniae*. Nature *516*, 259–262.

Foster, T.J. (2005). Immune evasion by staphylococci. Nat. Rev. Microbiol. *3*, 948–958.

Fournier, B., and Philpott, D.J. (2005). Recognition of *Staphylococcus aureus* by the innate immune system. Clin Microbiol Rev *18*, 521–540.

Fraipont, C., Adam, M., Nguyen-Distèche, M., Keck, W., Van Beeumen, J., Ayala, J.A., Granier, B., Hara, H., and Ghuysen, J.M. (1994). Engineering and overexpression of periplasmic forms of the penicillin-binding protein 3 of *Escherichia coli*. Biochem. J. *298 (Pt 1)*, 189–195.

Fraipont, C., Alexeeva, S., Wolf, B., van der Ploeg, R., Schloesser, M., den Blaauwen, T., and Nguyen-Distèche, M. (2011). The integral membrane FtsW protein and peptidoglycan synthase PBP3 form a subcomplex in *Escherichia coli*. Microbiology (Reading, Engl.) *157*, 251–259.

Fu, G., Huang, T., Buss, J., Coltharp, C., Hensel, Z., and Xiao, J. (2010). In Vivo structure of the *E. coli* FtsZ-ring revealed by photoactivated localization microscopy (PALM). PLoS ONE *5*, e12680.

de la Fuente, A., Palacios, P., and Vicente, M. (2001). Transcription of the *Escherichia coli dcw* cluster: evidence for distal upstream transcripts being involved in the expression of the downstream *ftsZ* gene. Biochimie *83*, 109–115.

Gahlmann, A., Ptacin, J.L., Grover, G., Quirin, S., von Diezmann, A.R.S., Lee, M.K., Backlund, M.P., Shapiro, L., Piestun, R., and Moerner, W.E. (2013). Quantitative multicolor subdiffraction imaging of bacterial protein ultrastructures in three dimensions. Nano Lett. *13*, 987–993.

Galli, E., and Gerdes, K. (2010). Spatial resolution of two bacterial cell division proteins: ZapA recruits ZapB to the inner face of the Z-ring. Molecular Microbiology *76*, 1514–1526.

Galli, E., and Gerdes, K. (2012). FtsZ-ZapA-ZapB interactome of *Escherichia coli*. J Bacteriol *194*, 292–302.

Gamba, P., Veening, J.-W., Saunders, N.J., Hamoen, L.W., and Daniel, R.A. (2009). Two-step assembly dynamics of the *Bacillus subtilis* divisome. J. Bacteriol. *191*, 4186–4194.

Gardete, S., and Tomasz, A. (2014). Mechanisms of vancomycin resistance in *Staphylococcus aureus*. Journal of Clinical Investigation *124*, 2836–2840.

Gardner, K.A.J.A., Moore, D.A., and Erickson, H.P. (2013). The C-terminal linker of *Escherichia coli* FtsZ functions as an intrinsically disordered peptide. Mol. Microbiol. *89*, 264–275.

Garti-Levi, S., Hazan, R., Kain, J., Fujita, M., and Ben-Yehuda, S. (2008). The FtsEX ABC transporter directs cellular differentiation in *Bacillus subtilis*. Molecular Microbiology *69*, 1018–1028.

Gautier, A., Juillerat, A., Heinis, C., Corrêa, I.R., Kindermann, M., Beaufils, F., and Johnsson, K. (2008). An engineered protein tag for multiprotein labeling in living cells. Chemistry & Biology *15*, 128–136.

Geissbuehler, S., Dellagiacoma, C., and Lasser, T. (2011). Comparison between SOFI and STORM. Biomed Opt Express *2*, 408–420.

Geissler, B., Elraheb, D., and Margolin, W. (2003). A gain-of-function mutation in *ftsA* bypasses the requirement for the essential cell division gene *zipA* in *Escherichia coli*. Proc. Natl. Acad. Sci. U.S.A. *100*, 4197–4202.

Geissler, B., Shiomi, D., and Margolin, W. (2007). The *ftsA** gain-of-function allele of *Escherichia coli* and its effects on the stability and dynamics of the Z ring. Microbiology (Reading, Engl.) *153*, 814–825.

Gelles, J., Schnapp, B.J., and Sheetz, M.P. (1988). Tracking kinesin-driven movements with nanometre-scale precision. Nature *331*, 450–453.

Gérard, P., Vernet, T., and Zapun, A. (2002). Membrane topology of the *Streptococcus pneumoniae* FtsW division protein. J Bacteriol *184*, 1925–1931.

Gerding, M.A., Liu, B., Bendezú, F.O., Hale, C.A., Bernhardt, T.G., and de Boer, P.A.J. (2009). Self-enhanced accumulation of FtsN at division sites and roles for other proteins with a SPOR domain (DamX, DedD, and RlpA) in *Escherichia coli* cell constriction. J Bacteriol *191*, 7383–7401.

Ghigo, J.M., and Beckwith, J. (2000). Cell division in *Escherichia coli*: role of FtsL domains in septal localization, function, and oligomerization. J. Bacteriol. *182*, 116–129.

Ghigo, J.M., Weiss, D.S., Chen, J.C., Yarrow, J.C., and Beckwith, J. (1999). Localization of FtsL to the *Escherichia coli* septal ring. Mol. Microbiol. *31*, 725–737.

Ghosal, D., Trambaiolo, D., Amos, L.A., and Löwe, J. (2014). MinCD cell division proteins form

alternating copolymeric cytomotive filaments. Nat Commun *5*, 5341.

Gibson, C.W., Daneo-Moore, L., and Higgins, M.L. (1983). Cell wall assembly during inhibition of DNA synthesis in *Streptococcus faecium*. J. Bacteriol. *155*, 351–356.

Gill, D.R., Hatfull, G.F., and Salmond, G.P. (1986). A new cell division operon in *Escherichia coli*. Mol. Gen. Genet. *205*, 134–145.

Glas, M., Saparoea, H.B. van den B. van, McLaughlin, S.H., Roseboom, W., Liu, F., Koningstein, G.M., Fish, A., Blaauwen, T. den, Heck, A.J.R., Jong, L. de, et al. (2015). The soluble periplasmic domains of *E. coli* cell division proteins FtsQ/FtsB/FtsL form a trimeric complex with sub-micromolar affinity. J. Biol. Chem. jbc.M115.654756.

Goehring, N.W., Gueiros-Filho, F., and Beckwith, J. (2005). Premature targeting of a cell division protein to midcell allows dissection of divisome assembly in *Escherichia coli*. Genes Dev *19*, 127–137.

Goffin, C., and Ghuysen, J.M. (1998). Multimodular penicillin-binding proteins: an enigmatic family of orthologs and paralogs. Microbiol. Mol. Biol. Rev. *62*, 1079–1093.

Goffin, C., Fraipont, C., Ayala, J., Terrak, M., Nguyen-Distèche, M., and Ghuysen, J.M. (1996). The non-penicillin-binding module of the tripartite penicillin-binding protein 3 of *Escherichia coli* is required for folding and/or stability of the penicillin-binding module and the membrane-anchoring module confers cell septation activity on the folded structure. J. Bacteriol. *178*, 5402–5409.

Gola, S., Munder, T., Casonato, S., Manganelli, R., and Vicente, M. (2015). The essential role of SepF in mycobacterial division. Molecular Microbiology *97*, 560–576.

Goley, E.D., Yeh, Y.-C., Hong, S.-H., Fero, M.J., Abeliuk, E., McAdams, H.H., and Shapiro, L. (2011). Assembly of the *Caulobacter cell* division machine. Mol. Microbiol. *80*, 1680–1698.

Gonzalez, M.D., and Beckwith, J. (2009). Divisome under construction: distinct domains of the small membrane protein FtsB are necessary for interaction with multiple cell division proteins. J. Bacteriol. *191*, 2815–2825.

González, J.M., Jiménez, M., Vélez, M., Mingorance, J., Andreu, J.M., Vicente, M., and Rivas, G. (2003). Essential cell division protein FtsZ assembles into one monomer-thick ribbons under conditions resembling the crowded intracellular environment. J. Biol. Chem. *278*, 37664–37671.

Gonzalez, M.D., Akbay, E.A., Boyd, D., and Beckwith, J. (2010). Multiple interaction domains in FtsL, a protein component of the widely conserved bacterial FtsLBQ cell division complex. J. Bacteriol. *192*, 2757–2768.

Gordon, R.J., and Lowy, F.D. (2008). Pathogenesis of methicillin-resistant *Staphylococcus aureus* infection. Clin Infect Dis *46*, S350–S359.

Graham, J.E., Sherratt, D.J., and Szczelkun, M.D. (2010). Sequence-specific assembly of FtsK hexamers establishes directional translocation on DNA. Proc. Natl. Acad. Sci. U.S.A. *107*, 20263–20268.

Grainge, I. (2010). FtsK-a bacterial cell division checkpoint? Mol. Microbiol. *78*, 1055–1057.

Grainge, I., Lesterlin, C., and Sherratt, D.J. (2011). Activation of XerCD-dif recombination by the FtsK DNA translocase. Nucleic Acids Res *39*, 5140–5148.

Grantcharova, N., Lustig, U., and Flärdh, K. (2005). Dynamics of FtsZ assembly during sporulation in *Streptomyces coelicolor* A3(2). J. Bacteriol. *187*, 3227–3237.

Gregory, J.A., Becker, E.C., and Pogliano, K. (2008). Bacillus subtilis MinC destabilizes FtsZ-rings at new cell poles and contributes to the timing of cell division. Genes Dev. *22*, 3475–3488.

Grotjohann, T., Testa, I., Leutenegger, M., Bock, H., Urban, N.T., Lavoie-Cardinal, F., Willig, K.I., Eggeling, C., Jakobs, S., and Hell, S.W. (2011). Diffraction-unlimited all-optical imaging and writing with a photochromic GFP. Nature *478*, 204–208.

Gu, B., Kelesidis, T., Tsiodras, S., Hindler, J., and Humphries, R.M. (2012). The emerging problem of linezolid-resistant *Staphylococcus*. J. Antimicrob. Chemother. dks354.

Gueiros-Filho, F.J., and Losick, R. (2002). A widely conserved bacterial cell division protein that promotes assembly of the tubulin-like protein FtsZ. Genes Dev *16*, 2544–2556.

Gündoğdu, M.E., Kawai, Y., Pavlendova, N., Ogasawara, N., Errington, J., Scheffers, D.-J., and Hamoen,

L.W. (2011). Large ring polymers align FtsZ polymers for normal septum formation: SepF rings align FtsZ protofilaments. The EMBO Journal *30*, 617–626.

Gustafsson, M.G. (2000). Surpassing the lateral resolution limit by a factor of two using structured illumination microscopy. J Microsc *198*, 82–87.

Guzman, L.M., Barondess, J.J., and Beckwith, J. (1992). FtsL, an essential cytoplasmic membrane protein involved in cell division in *Escherichia coli*. J. Bacteriol. *174*, 7716–7728.

Guzman, L.M., Weiss, D.S., and Beckwith, J. (1997). Domain-swapping analysis of FtsI, FtsL, and FtsQ, bitopic membrane proteins essential for cell division in *Escherichia coli*. J. Bacteriol. *179*, 5094–5103.

Haeusser, D.P., Schwartz, R.L., Smith, A.M., Oates, M.E., and Levin, P.A. (2004). EzrA prevents aberrant cell division by modulating assembly of the cytoskeletal protein FtsZ. Molecular Microbiology *52*, 801–814.

Haeusser, D.P., Garza, A.C., Buscher, A.Z., and Levin, P.A. (2007). The division inhibitor EzrA contains a seven-residue patch required for maintaining the dynamic nature of the medial FtsZ ring. J Bacteriol *189*, 9001–9010.

Haeusser, D.P., Rowlett, V.W., and Margolin, W. (2015). A mutation in *Escherichia coli ftsZ* bypasses the requirement for the essential division gene *zipA* and confers resistance to FtsZ assembly inhibitors by stabilizing protofilament bundling. Molecular Microbiology *97*, 988–1005.

Hale, C.A., and de Boer, P.A.J. (1997). Direct Binding of FtsZ to ZipA, an essential component of the septal ring structure that mediates cell division in *E. coli*. Cell *88*, 175–185.

Hale, C.A., and de Boer, P.A.J. (1999). Recruitment of ZipA to the septal ring of *Escherichia coli* is dependent on FtsZ and independent of FtsA. J Bacteriol *181*, 167–176.

Hale, C.A., and de Boer, P.A.J. (2002). ZipA is required for recruitment of FtsK, FtsQ, FtsL, and FtsN to the septal ring in *Escherichia coli*. J Bacteriol *184*, 2552–2556.

Hale, C.A., Rhee, A.C., and de Boer, P.A. (2000). ZipA-induced bundling of FtsZ polymers mediated by an interaction between C-terminal domains. J. Bacteriol. *182*, 5153–5166.

Hale, C.A., Meinhardt, H., and de Boer, P.A.J. (2001). Dynamic localization cycle of the cell division regulator MinE in *Escherichia coli*. EMBO J *20*, 1563–1572.

Hale, C.A., Shiomi, D., Liu, B., Bernhardt, T.G., Margolin, W., Niki, H., and de Boer, P.A.J. (2011). Identification of *Escherichia coli* ZapC (YcbW) as a component of the division apparatus that binds and bundles FtsZ polymers. J Bacteriol *193*, 1393–1404.

Hamoen, L.W., Meile, J.-C., De Jong, W., Noirot, P., and Errington, J. (2006). SepF, a novel FtsZ-interacting protein required for a late step in cell division. Molecular Microbiology *59*, 989–999.

Harris, L.G., Foster, S.J., and Richards, R.G. (2002). An introduction to *Staphylococcus aureus*, and techniques for identifying and quantifying *S. aureus* adhesins in relation to adhesion to biomaterials: review. Eur Cell Mater *4*, 39–60.

Harry, E.J. (2014). Microbiology: A beacon for bacterial tubulin. Nature *516*, 175–176.

Harry, E.J., and Wake, R.G. (1997). The membrane-bound cell division protein DivIB is localized to the division site in *Bacillus subtilis*. Mol. Microbiol. *25*, 275–283.

Harry, E., Monahan, L., and Thompson, L. (2006). Bacterial cell division: the mechanism and its precison. Int. Rev. Cytol. *253*, 27–94.

Harry, E.J., Stewart, B.J., and Wake, R.G. (1993). Characterization of mutations in *divIB* of *Bacillus subtilis* and cellular localization of the DivIB protein. Mol. Microbiol. *7*, 611–621.

Harry, E.J., Partridge, S.R., Weiss, A.S., and Wake, R.G. (1994). Conservation of the 168 *divIB* gene in *Bacillus subtilis* W23 and *B. licheniformis*, and evidence for homology to *ftsQ* of *Escherichia coli*. Gene *147*, 85–89.

Harry, E.J., Pogliano, K., and Losick, R. (1995). Use of immunofluorescence to visualize cell-specific gene expression during sporulation in *Bacillus subtilis*. J. Bacteriol. *177*, 3386–3393.

Hartman, B.J., and Tomasz, A. (1984). Low-affinity penicillin-binding protein associated with beta-lactam resistance in *Staphylococcus aureus*. J. Bacteriol. *158*, 513–516.

Hayden, M.K., Rezai, K., Hayes, R.A., Lolans, K., Quinn, J.P., and Weinstein, R.A. (2005). Development of daptomycin resistance in vivo in methicillin-resistant *Staphylococcus aureus*. J Clin Microbiol *43*, 5285–5287.

Haydon, D.J., Stokes, N.R., Ure, R., Galbraith, G., Bennett, J.M., Brown, D.R., Baker, P.J., Barynin, V.V., Rice, D.W., Sedelnikova, S.E., et al. (2008). An inhibitor of FtsZ with potent and selective anti-staphylococcal activity. Science *321*, 1673–1675.

Heaslet, H., Shaw, B., Mistry, A., and Miller, A.A. (2009). Characterization of the active site of *S. aureus* monofunctional glycosyltransferase (Mtg) by site-directed mutation and structural analysis of the protein complexed with moenomycin. Journal of Structural Biology *167*, 129–135.

Hell, S.W., and Wichmann, J. (1994). Breaking the diffraction resolution limit by stimulated emission: stimulated-emission-depletion fluorescence microscopy. Opt Lett *19*, 780–782.

Henriques, A.O., Glaser, P., Piggot, P.J., and Moran Jr, C.P. (1998). Control of cell shape and elongation by the rodA gene *in Bacillus subtilis*. Molecular Microbiology *28*, 235–247.

Henze, U.U., and Berger-Bächi, B. (1996). Penicillin-binding protein 4 overproduction increases beta-lactam resistance in *Staphylococcus aureus*. Antimicrob Agents Chemother *40*, 2121–2125.

Hess, S.T., Girirajan, T.P.K., and Mason, M.D. (2006). Ultra-high resolution imaging by fluorescence photoactivation localization microscopy. Biophys. J. *91*, 4258–4272.

Hill, N.S., Buske, P.J., Shi, Y., and Levin, P.A. (2013). A moonlighting enzyme links *Escherichia coli* cell size with central metabolism. PLoS Genet *9*, e1003663.

Hiramatsu, K., Aritaka, N., Hanaki, H., Kawasaki, S., Hosoda, Y., Hori, S., Fukuchi, Y., and Kobayashi, I. (1997a). Dissemination in Japanese hospitals of strains of *Staphylococcus aureus* heterogeneously resistant to vancomycin. The Lancet *350*, 1670–1673.

Hiramatsu, K., Hanaki, H., Ino, T., Yabuta, K., Oguri, T., and Tenover, F.C. (1997b). Methicillin-resistant *Staphylococcus aureus* clinical strain with reduced vancomycin susceptibility. J. Antimicrob. Chemother. *40*, 135–136.

Holden, S.J., Pengo, T., Meibom, K.L., Fernandez Fernandez, C., Collier, J., and Manley, S. (2014). High throughput 3D super-resolution microscopy reveals *Caulobacter crescentus* in vivo Z-ring organization. Proc Natl Acad Sci U S A *111*, 4566–4571.

Holečková, N., Doubravová, L., Massidda, O., Molle, V., Buriánková, K., Benada, O., Kofroňová, O., Ulrych, A., and Branny, P. (2015). LocZ Is a new cell division protein involved in proper septum placement in *Streptococcus pneumoniae*. mBio *6*, e01700–e01714.

Höltje, J.V. (1998). Growth of the stress-bearing and shape-maintaining murein sacculus of *Escherichia coli*. Microbiol. Mol. Biol. Rev. *62*, 181–203.

Hope, R., Mushtaq, S., James, D., Pllana, T., Warner, M., and Livermore, D.M. (2010). Tigecycline activity: low resistance rates but problematic disc breakpoints revealed by a multicentre sentinel survey in the UK. J. Antimicrob. Chemother. dkq370.

Hörger, I., Velasco, E., Rivas, G., Vélez, M., and Tarazona, P. (2008). FtsZ bacterial cytoskeletal polymers on curved surfaces: the importance of lateral interactions. Biophys J *94*, L81–L83.

Horsburgh, M.J., Wharton, S.J., Cox, A.G., Ingham, E., Peacock, S., and Foster, S.J. (2002a). MntR modulates expression of the PerR regulon and superoxide resistance in *Staphylococcus aureus* through control of manganese uptake. Molecular Microbiology *44*, 1269–1286.

Horsburgh, M.J., Aish, J.L., White, I.J., Shaw, L., Lithgow, J.K., and Foster, S.J. (2002b). *sigmaB* modulates virulence determinant expression and stress resistance: characterization of a functional *rsbU* strain derived from *Staphylococcus aureus* 8325-4. J. Bacteriol. *184*, 5457–5467.

Hoskins, J., Matsushima, P., Mullen, D.L., Tang, J., Zhao, G., Meier, T.I., Nicas, T.I., and Jaskunas, S.R. (1999). Gene disruption studies of penicillin-binding proteins 1a, 1b, and 2a in *Streptococcus pneumoniae*. J Bacteriol *181*, 6552–6555.

Hsieh, C.-W., Lin, T.-Y., Lai, H.-M., Lin, C.-C., Hsieh, T.-S., and Shih, Y.-L. (2010). Direct MinE-membrane interaction contributes to the proper localization of MinDE in *E. coli*. Mol. Microbiol. *75*, 499–512.

Hu, Z., and Lutkenhaus, J. (1999). Topological regulation of cell division in *Escherichia coli* involves rapid pole to pole oscillation of the division inhibitor MinC under the control of MinD and MinE. Mol. Microbiol. *34*, 82–90.

Hu, Z., and Lutkenhaus, J. (2000). Analysis of MinC reveals two independent domains involved in interaction with MinD and FtsZ. J. Bacteriol. *182*, 3965–3971.

Hu, Z., and Lutkenhaus, J. (2003). A conserved sequence at the C-terminus of MinD is required for binding to the membrane and targeting MinC to the septum. Mol. Microbiol. *47*, 345–355.

Hu, Z., Mukherjee, A., Pichoff, S., and Lutkenhaus, J. (1999). The MinC component of the division site selection system in *Escherichia coli* interacts with FtsZ to prevent polymerization. Proc. Natl. Acad. Sci. U.S.A. *96*, 14819–14824.

Hu, Z., Gogol, E.P., and Lutkenhaus, J. (2002). Dynamic assembly of MinD on phospholipid vesicles regulated by ATP and MinE. Proc. Natl. Acad. Sci. U.S.A. *99*, 6761–6766.

Huang, B., Wang, W., Bates, M., and Zhuang, X. (2008). Three-dimensional super-resolution imaging by stochastic optical reconstruction microscopy. Science *319*, 810–813.

Huang, K.C., Meir, Y., and Wingreen, N.S. (2003). Dynamic structures in *Escherichia coli*: Spontaneous formation of MinE rings and MinD polar zones. Proc Natl Acad Sci U S A *100*, 12724–12728.

Huber, J., Donald, R.G.K., Lee, S.H., Jarantow, L.W., Salvatore, M.J., Meng, X., Painter, R., Onishi, R.H., Occi, J., Dorso, K., et al. (2009). Chemical genetic identification of peptidoglycan inhibitors potentiating carbapenem activity against methicillin-resistant *Staphylococcus aureus*. Chem. Biol. *16*, 837–848.

Huecas, S., and Andreu, J.M. (2004). Polymerization of nucleotide-free, GDP- and GTP-bound cell division protein FtsZ: GDP makes the difference. FEBS Lett. *569*, 43–48.

Ikeda, M., Sato, T., Wachi, M., Jung, H.K., Ishino, F., Kobayashi, Y., and Matsuhashi, M. (1989). Structural similarity among *Escherichia coli* FtsW and RodA proteins and *Bacillus subtilis* SpoVE protein, which function in cell division, cell elongation, and spore formation, respectively. J. Bacteriol. *171*, 6375–6378.

Ikeda, M., Wachi, M., Ishino, F., and Matsuhashi, M. (1990). Nucleotide sequence involving *murD* and an open reading frame ORF-Y spacing *murF* and *ftsW* in *Escherichia coli*. Nucleic Acids Res. *18*, 1058.

Inoue, A., Murata, Y., Takahashi, H., Tsuji, N., Fujisaki, S., and Kato, J. (2008). Involvement of an essential gene, *mviN*, in murein synthesis in *Escherichia coli*. J. Bacteriol. *190*, 7298–7301.

Ishikawa, S., Kawai, Y., Hiramatsu, K., Kuwano, M., and Ogasawara, N. (2006). A new FtsZ-interacting protein, YlmF, complements the activity of FtsA during progression of cell division in *Bacillus subtilis*. Mol. Microbiol. *60*, 1364–1380.

Janeway, C.A., Travers, P., Walport, M., Shlomchik, M.J., Janeway, C.A., Travers, P., Walport, M., and Shlomchik, M.J. (2001). Immunobiology (Garland Science).

Jennings, P.C., Cox, G.C., Monahan, L.G., and Harry, E.J. (2011). Super-resolution imaging of the bacterial cytokinetic protein FtsZ. Micron *42*, 336–341.

de Jonge, B.L., Chang, Y.S., Gage, D., and Tomasz, A. (1992). Peptidoglycan composition in heterogeneous Tn551 mutants of a methicillin-resistant *Staphylococcus aureus* strain. J. Biol. Chem. *267*, 11255–11259.

Jorge, A.M., Hoiczyk, E., Gomes, J.P., and Pinho, M.G. (2011). EzrA contributes to the regulation of cell size in *Staphylococcus aureus*. PLoS ONE *6*, e27542.

Jusuk, I., Vietz, C., Raab, M., Dammeyer, T., and Tinnefeld, P. (2015). Super-resolution imaging conditions for enhanced yellow fluorescent protein (eYFP) demonstrated on DNA origami nanorulers. Scientific Reports *5*, 14075.

Kabli, A. (2013). Identification and characterisation of cell division proteins in *Staphylococcus aureus*. University of Sheffield.

Karimova, G., Dautin, N., and Ladant, D. (2005). Interaction network among *Escherichia coli* membrane proteins involved in cell division as revealed by bacterial two-hybrid analysis. J. Bacteriol. *187*, 2233–2243.

Katayama, Y., Ito, T., and Hiramatsu, K. (2000). A new class of genetic element, staphylococcus cassette chromosome mec, encodes methicillin resistance in *Staphylococcus aureus*. Antimicrob. Agents Chemother. *44*, 1549–1555.

Katis, V.L., Harry, E.J., and Wake, R.G. (1997). The *Bacillus subtilis* division protein DivIC is a highly abundant membrane-bound protein that localizes to the division site. Mol. Microbiol. *26*, 1047–1055.

Kent, V. (2013). Cell wall architecture and the role of wall teichoic acid in *Staphylococcus aureus*. University of Sheffield.

Keppler, A., Gendreizig, S., Gronemeyer, T., Pick, H., Vogel, H., and Johnsson, K. (2003). A general method for the covalent labeling of fusion proteins with small molecules in vivo. Nat. Biotechnol. *21*, 86–89.

Khadria, A.S., and Senes, A. (2013). The transmembrane domains of the bacterial cell division proteins FtsB and FtsL form a stable high-order oligomer. Biochemistry *52*, 7542–7550.

Kiekebusch, D., Michie, K.A., Essen, L.-O., Löwe, J., and Thanbichler, M. (2012). Localized dimerization and nucleoid binding drive gradient formation by the bacterial cell division inhibitor MipZ. Mol Cell *46*, 245–259.

Kjeldgaard, N.O., Maaloe, O., and Schaechter, M. (1958). The transition between different physiological states during balanced growth of *Salmonella typhimurium*. J. Gen. Microbiol. *19*, 607–616.

Klar, T.A., Jakobs, S., Dyba, M., Egner, A., and Hell, S.W. (2000). Fluorescence microscopy with diffraction resolution barrier broken by stimulated emission. PNAS *97*, 8206–8210.

Klein, T., Löschberger, A., Proppert, S., Wolter, S., van de Linde, S., and Sauer, M. (2011). Live-cell dSTORM with SNAP-tag fusion proteins. Nat Meth *8*, 7–9.

Kobayashi, K., Ehrlich, S.D., Albertini, A., Amati, G., Andersen, K.K., Arnaud, M., Asai, K., Ashikaga, S., Aymerich, S., Bessieres, P., et al. (2003). Essential *Bacillus subtilis* genes. Proc. Natl. Acad. Sci. U.S.A. *100*, 4678–4683.

Kohanski, M.A., Dwyer, D.J., and Collins, J.J. (2010). How antibiotics kill bacteria: from targets to networks. Nat Rev Microbiol *8*, 423–435.

Kozarich, J.W., and Strominger, J.L. (1978). A membrane enzyme from *Staphylococcus aureus* which catalyzes transpeptidase, carboxypeptidase, and penicillinase activities. J. Biol. Chem. *253*, 1272–1278.

Kreiswirth, B.N., Löfdahl, S., Betley, M.J., O'Reilly, M., Schlievert, P.M., Bergdoll, M.S., and Novick, R.P. (1983). The toxic shock syndrome exotoxin structural gene is not detectably transmitted by a prophage. Nature *305*, 709–712.

Król, E., van Kessel, S.P., van Bezouwen, L.S., Kumar, N., Boekema, E.J., and Scheffers, D.-J. (2012). *Bacillus subtilis* SepF binds to the C-terminus of FtsZ. PLoS ONE *7*, e43293.

Krupka, M., Cabré, E.J., Jiménez, M., Rivas, G., Rico, A.I., and Vicente, M. (2014). Role of the FtsA C terminus as a switch for polymerization and membrane association. mBio *5*, e02221–14.

Kuroda, M., Ohta, T., Uchiyama, I., Baba, T., Yuzawa, H., Kobayashi, I., Cui, L., Oguchi, A., Aoki, K., Nagai, Y., et al. (2001). Whole genome sequencing of meticillin-resistant *Staphylococcus aureus*. Lancet *357*, 1225–1240.

Kuru, E., Velocity Hughes, H., Brown, P.J., Hall, E., Tekkam, S., Cava, F., de Pedro, M.A., Brun, Y.V., and VanNieuwenhze, M.S. (2012). In situ probing of newly synthesized peptidoglycan in live bacteria with fluorescent D-amino acids. Angew Chem Int Ed Engl *51*, 12519–12523.

Lacey, R.W. (1975). Antibiotic resistance plasmids of *Staphylococcus aureus* and their clinical importance. Bacteriol Rev *39*, 1–32.

Lackner, L.L., Raskin, D.M., and de Boer, P.A.J. (2003). ATP-dependent interactions between Escherichia coli Min proteins and the phospholipid membrane in vitro. J. Bacteriol. *185*, 735–749.

Lambert, M.P., and Neuhaus, F.C. (1972). Mechanism of D-cycloserine action: alanine racemase from *Escherichia coli* W. J. Bacteriol. *110*, 978–987.

Land, A.D., Tsui, H.-C.T., Kocaoglu, O., Vella, S.A., Shaw, S.L., Keen, S.K., Sham, L.-T., Carlson, E.E., and Winkler, M.E. (2013). Requirement of essential Pbp2x and GpsB for septal ring closure in *Streptococcus pneumoniae* D39. Mol Microbiol *90*, 939–955.

Land, A.D., Luo, Q., and Levin, P.A. (2014). Functional domain analysis of the cell division inhibitor EzrA. PLoS One *9*.

Landgraf, D., Okumus, B., Chien, P., Baker, T.A., and Paulsson, J. (2012). Segregation of molecules at cell division reveals native protein localization. Nat. Methods *9*, 480–482.

LaPointe, L.M., Taylor, K.C., Subramaniam, S., Khadria, A., Rayment, I., and Senes, A. (2013). Structural organization of FtsB, a transmembrane protein of the bacterial divisome. Biochemistry *52*, 2574–2585.

Lara, B., and Ayala, J.A. (2002). Topological characterization of the essential *Escherichia coli* cell division protein FtsW. FEMS Microbiology Letters *216*, 23–32.

Lara, B., Rico, A.I., Petruzzelli, S., Santona, A., Dumas, J., Biton, J., Vicente, M., Mingorance, J., and Massidda, O. (2005). Cell division in cocci: localization and properties of the *Streptococcus pneumoniae* FtsA protein. Mol. Microbiol. *55*, 699–711.

Lee, C.Y., and Iandolo, J.J. (1986). Lysogenic conversion of staphylococcal lipase is caused by insertion of the bacteriophage L54a genome into the lipase structural gene. J. Bacteriol. *166*, 385–391.

Lee, S., and Price, C.W. (1993). The *minCD* locus of *Bacillus subtilis* lacks the *minE* determinant that provides topological specificity to cell division. Mol. Microbiol. *7*, 601–610.

Lee, C.Y., Buranen, S.L., and Ye, Z.H. (1991). Construction of single-copy integration vectors for *Staphylococcus aureus*. Gene *103*, 101–105.

de Leeuw, E., Graham, B., Phillips, G.J., ten Hagen-Jongman, C.M., Oudega, B., and Luirink, J. (1999). Molecular characterization of *Escherichia coli* FtsE and FtsX. Mol. Microbiol. *31*, 983–993.

Lenarcic, R., Halbedel, S., Visser, L., Shaw, M., Wu, L.J., Errington, J., Marenduzzo, D., and Hamoen, L.W. (2009). Localisation of DivIVA by targeting to negatively curved membranes. EMBO J. *28*, 2272–2282.

Lesterlin, C., Pages, C., Dubarry, N., Dasgupta, S., and Cornet, F. (2008). Asymmetry of chromosome replichores renders the DNA translocase activity of FtsK essential for cell division and cell shape maintenance in *Escherichia coli*. PLoS Genet *4*.

Levin, P.A., and Losick, R. (1994). Characterization of a cell division gene from *Bacillus subtilis* that is required for vegetative and sporulation septum formation. J. Bacteriol. *176*, 1451–1459.

Levin, P.A., and Losick, R. (1996). Transcription factor Spo0A switches the localization of the cell division protein FtsZ from a medial to a bipolar pattern in *Bacillus subtilis*. Genes Dev. *10*, 478–488.

Levin, P.A., Kurtser, I.G., and Grossman, A.D. (1999). Identification and characterization of a negative regulator of FtsZ ring formation in *Bacillus subtilis*. Proc Natl Acad Sci U S A *96*, 9642–9647.

Li, Y., Hsin, J., Zhao, L., Cheng, Y., Shang, W., Huang, K.C., Wang, H.-W., and Ye, S. (2013). FtsZ protofilaments use a hinge-opening mechanism for constrictive force generation. Science *341*.

Li, Z., Trimble, M.J., Brun, Y.V., and Jensen, G.J. (2007). The structure of FtsZ filaments in vivo suggests a force-generating role in cell division. EMBO J *26*, 4694–4708.

Liechti, G.W., Kuru, E., Hall, E., Kalinda, A., Brun, Y.V., VanNieuwenhze, M., and Maurelli, A.T. (2014). A new metabolic cell-wall labelling method reveals peptidoglycan in *Chlamydia trachomatis*. Nature *506*, 507–510.

Liew, A.T.F., Theis, T., Jensen, S.O., Garcia-Lara, J., Foster, S.J., Firth, N., Lewis, P.J., and Harry, E.J. (2011). A simple plasmid-based system that allows rapid generation of tightly controlled gene expression in *Staphylococcus aureus*. Microbiology *157*, 666–676.

Lim, D., and Strynadka, N.C.J. (2002). Structural basis for the beta lactam resistance of PBP2a from methicillin-resistant *Staphylococcus aureus*. Nat. Struct. Biol. *9*, 870–876.

Liu, B., Persons, L., Lee, L., and de Boer, P.A.J. (2015). Roles for both FtsA and the FtsBLQ subcomplex in FtsN-stimulated cell constriction in *Escherichia coli*. Molecular Microbiology *95*, 945–970.

Liu, G., Draper, G.C., and Donachie, W.D. (1998). FtsK is a bifunctional protein involved in cell division and chromosome localization in *Escherichia coli*. Mol. Microbiol. *29*, 893–903.

Liu, Z., Mukherjee, A., and Lutkenhaus, J. (1999). Recruitment of ZipA to the division site by interaction

with FtsZ. Mol. Microbiol. *31*, 1853–1861.

Lock, R.L., and Harry, E.J. (2008). Cell-division inhibitors: new insights for future antibiotics. Nat Rev Drug Discov *7*, 324–338.

Loose, M., and Mitchison, T.J. (2014). The bacterial cell division proteins FtsA and FtsZ self-organize into dynamic cytoskeletal patterns. Nat Cell Biol *16*, 38–46.

Loskill, P., Pereira, P.M., Jung, P., Bischoff, M., Herrmann, M., Pinho, M.G., and Jacobs, K. (2014). Reduction of the peptidoglycan crosslinking causes a decrease in stiffness of the *Staphylococcus aureus* cell envelope. Biophys. J. *107*, 1082–1089.

Lovering, A.L., Castro, L.H. de, Lim, D., and Strynadka, N.C.J. (2007). Structural insight into the transglycosylation step of bacterial cell-wall biosynthesis. Science *315*, 1402–1405.

Low, H.H., Moncrieffe, M.C., and Löwe, J. (2004). The crystal structure of ZapA and its modulation of FtsZ polymerisation. Journal of Molecular Biology *341*, 839–852.

Löwe, J., and Amos, L.A. (1998). Crystal structure of the bacterial cell-division protein FtsZ. Nature *391*, 203–206.

Löwe, J., and Amos, L.A. (2005). Helical tubes of FtsZ from *Methanococcus jannaschii*. Biological Chemistry *381*, 993–999.

Löwe, J., Ellonen, A., Allen, M.D., Atkinson, C., Sherratt, D.J., and Grainge, I. (2008). Molecular mechanism of sequence-directed DNA loading and translocation by FtsK. Molecular Cell *31*, 498–509.

Lowy, F.D. (1998). *Staphylococcus aureus* infections. N. Engl. J. Med. *339*, 520–532.

Lowy, F.D. (2003). Antimicrobial resistance: the example of *Staphylococcus aureus*. J Clin Invest *111*, 1265–1273.

Lu, C., Stricker, J., and Erickson, H.P. (1998). FtsZ from *Escherichia coli*, *Azotobacter vinelandii*, and *Thermotoga maritima*--quantitation, GTP hydrolysis, and assembly. Cell Motil. Cytoskeleton *40*, 71–86.

Lu, C., Reedy, M., and Erickson, H.P. (2000). Straight and curved conformations of FtsZ are regulated by GTP hydrolysis. J. Bacteriol. *182*, 164–170.

Lukinavičius, G., Umezawa, K., Olivier, N., Honigmann, A., Yang, G., Plass, T., Mueller, V., Reymond, L., Corrêa Jr, I.R., Luo, Z.-G., et al. (2013). A near-infrared fluorophore for live-cell super-resolution microscopy of cellular proteins. Nat Chem *5*, 132–139.

Lutkenhaus, J.F., Wolf-Watz, H., and Donachie, W.D. (1980). Organization of genes in the *ftsA-envA* region of the *Escherichia coli* genetic map and identification of a new *fts* locus (*ftsZ*). J. Bacteriol. *142*, 615–620.

Ma, X., and Margolin, W. (1999). Genetic and functional analyses of the conserved C-terminal core domain of *Escherichia coli* FtsZ. J. Bacteriol. *181*, 7531–7544.

Ma, L., King, G.F., and Rothfield, L. (2004). Positioning of the MinE binding site on the MinD surface suggests a plausible mechanism for activation of the *Escherichia coli* MinD ATPase during division site selection. Mol. Microbiol. *54*, 99–108.

Ma, X., Ehrhardt, D.W., and Margolin, W. (1996). Colocalization of cell division proteins FtsZ and FtsA to cytoskeletal structures in living *Escherichia coli* cells by using green fluorescent protein. PNAS *93*, 12998–13003.

MacDonald, L., Baldini, G., and Storrie, B. (2015). Does super resolution fluorescence microscopy obsolete previous microscopic approaches to protein co-localization? Methods Mol Biol *1270*, 255–275.

Machnicka, B., Czogalla, A., Hryniewicz-Jankowska, A., Bogusławska, D.M., Grochowalska, R., Heger, E., and Sikorski, A.F. (2014). Spectrins: A structural platform for stabilization and activation of membrane channels, receptors and transporters. Biochimica et Biophysica Acta (BBA) - Biomembranes *1838*, 620–634.

Madigan, M.T., Martinko, J.M., and Parker, J. (2002). Brock Biology of Microorganism (Upper Saddle River, NJ: Prentice Hall/Pearson Education).

Maggi, S., Massidda, O., Luzi, G., Fadda, D., Paolozzi, L., and Ghelardini, P. (2008). Division protein interaction web: identification of a phylogenetically conserved common interactome between

Streptococcus pneumoniae and *Escherichia coli*. Microbiology (Reading, Engl.) *154*, 3042–3052.

Malachowa, N., and DeLeo, F.R. (2010). Mobile genetic elements of *Staphylococcus aureus*. Cell. Mol. Life Sci. *67*, 3057–3071.

Malbruny, B., Canu, A., Bozdogan, B., Fantin, B., Zarrouk, V., Dutka-Malen, S., Feger, C., and Leclercq, R. (2002). Resistance to quinupristin-dalfopristin due to mutation of L22 ribosomal protein in *Staphylococcus aureus.* Antimicrob. Agents Chemother. *46*, 2200–2207.

Mani, N., Tobin, P., and Jayaswal, R.K. (1993). Isolation and characterization of autolysis-defective mutants of *Staphylococcus aureus* created by *Tn917-lacZ* mutagenesis. J Bacteriol *175*, 1493–1499.

Männik, J., Castillo, D.E., Yang, D., Siopsis, G., and Männik, J. (2016). The role of MatP, ZapA and ZapB in chromosomal organization and dynamics in *Escherichia coli*. Nucl. Acids Res. gkv1484.

Margolin, W. (2000). Themes and variations in prokaryotic cell division. FEMS Microbiol. Rev. *24*, 531–548.

Margolin, W. (2005). FtsZ and the division of prokaryotic cells and organelles. Nat. Rev. Mol. Cell Biol. *6*, 862–871.

Marrec-Fairley, M., Piette, A., Gallet, X., Brasseur, R., Hara, H., Fraipont, C., Ghuysen, J.M., and Nguyen-Distèche, M. (2000). Differential functionalities of amphiphilic peptide segments of the cell-septation penicillin-binding protein 3 of *Escherichia coli*. Mol. Microbiol. *37*, 1019–1031.

Marston, A.L., and Errington, J. (1999). Selection of the midcell division site in *Bacillus subtilis* through MinD-dependent polar localization and activation of MinC. Mol. Microbiol. *33*, 84–96.

Marteyn, B.S., Karimova, G., Fenton, A.K., Gazi, A.D., West, N., Touqui, L., Prevost, M.-C., Betton, J.-M., Poyraz, O., Ladant, D., et al. (2014). ZapE is a novel cell division protein interacting with FtsZ and modulating the Z-ring dynamics. mBio *5*.

Marty, F.M., Yeh, W.W., Wennersten, C.B., Venkataraman, L., Albano, E., Alyea, E.P., Gold, H.S., Baden, L.R., and Pillai, S.K. (2006). Emergence of a clinical daptomycin-resistant *Staphylococcus aureus* isolate during treatment of methicillin-resistant *Staphylococcus aureus* bacteremia and osteomyelitis. J Clin Microbiol *44*, 595–597.

Massey, T.H., Mercogliano, C.P., Yates, J., Sherratt, D.J., and Löwe, J. (2006). Double-stranded DNA translocation: structure and mechanism of hexameric FtsK. Molecular Cell *23*, 457–469.

Masson, S., Kern, T., Gouëllec, A.L., Giustini, C., Simorre, J.-P., Callow, P., Vernet, T., Gabel, F., and Zapun, A. (2009). Central domain of DivIB caps the C-terminal regions of the FtsL/DivIC coiled-coil rod. J. Biol. Chem. *284*, 27687–27700.

Matias, V.R.F., and Beveridge, T.J. (2007). Cryo-electron microscopy of cell division in *Staphylococcus aureus* reveals a mid-zone between nascent cross walls. Molecular Microbiology *64*, 195–206.

Mavrici, D., Marakalala, M.J., Holton, J.M., Prigozhin, D.M., Gee, C.L., Zhang, Y.J., Rubin, E.J., and Alber, T. (2014). *Mycobacterium tuberculosis* FtsX extracellular domain activates the peptidoglycan hydrolase, RipC. Proc Natl Acad Sci U S A *111*, 8037–8042.

McCormick, J.R., and Losick, R. (1996). Cell division gene *ftsQ* is required for efficient sporulation but not growth and viability in *Streptomyces coelicolor* A3(2). J. Bacteriol. *178*, 5295–5301.

McCormick, J.R., Su, E.P., Driks, A., and Losick, R. (1994). Growth and viability of *Streptomyces coelicolor* mutant for the cell division gene *ftsZ*. Mol. Microbiol. *14*, 243–254.

McKinney, S.A., Murphy, C.S., Hazelwood, K.L., Davidson, M.W., and Looger, L.L. (2009). A bright and photostable photoconvertible fluorescent protein. Nat Meth *6*, 131–133.

McPherson, D.C., and Popham, D.L. (2003). Peptidoglycan synthesis in the absence of class A penicillin-binding proteins in *Bacillus subtilis*. J. Bacteriol. *185*, 1423–1431.

Meisner, J., Llopis, P.M., Sham, L.-T., Garner, E., Bernhardt, T.G., and Rudner, D.Z. (2013). FtsEX is required for CwlO peptidoglycan hydrolase activity during cell wall elongation in *Bacillus subtilis*. Mol Microbiol *89*, 1069–1083.

Memmi, G., Filipe, S.R., Pinho, M.G., Fu, Z., and Cheung, A. (2008). *Staphylococcus aureus* PBP4 is essential for reusR., Pinho, M.G., Fu, Z., and Cheung, A. (2008). and Rudner, D.Z. (2. Antimicrob Agents Chemother *52*, 3955–3966.

Mercer, K.L.N., and Weiss, D.S. (2002). The *Escherichia coli* cell division protein FtsW is required to recruit its cognate transpeptidase, FtsI (PBP3), to the division site. J Bacteriol *184*, 904–912.

Migocki, M.D., Freeman, M.K., Wake, R.G., and Harry, E.J. (2002). The Min system is not required for precise placement of the midcell Z ring in *Bacillus subtilis*. EMBO Rep *3*, 1163–1167.

Milam, S.L., Osawa, M., and Erickson, H.P. (2012). Negative-stain electron microscopy of inside-out FtsZ rings reconstituted on artificial membrane tubules show ribbons of protofilaments. Biophys J *103*, 59–68.

Mistry, B.V., Del Sol, R., Wright, C., Findlay, K., and Dyson, P. (2008). FtsW is a dispensable cell division protein required for z-ring stabilization during sporulation septation in *Streptomyces coelicolor*. J Bacteriol *190*, 5555–5566.

Miyagishima, S., Nozaki, H., Nishida, K., Nishida, K., Matsuzaki, M., and Kuroiwa, T. (2004). Two types of FtsZ proteins in mitochondria and red-lineage chloroplasts: the duplication of FtsZ is implicated in endosymbiosis. J. Mol. Evol. *58*, 291–303.

Miyagishima, S.-Y., Wolk, C.P., and Osteryoung, K.W. (2005). Identification of cyanobacterial cell division genes by comparative and mutational analyses. Mol. Microbiol. *56*, 126–143.

Mohammadi, T., van Dam, V., Sijbrandi, R., Vernet, T., Zapun, A., Bouhss, A., Diepeveen-de Bruin, M., Nguyen-Distèche, M., de Kruijff, B., and Breukink, E. (2011). Identification of FtsW as a transporter of lipid-linked cell wall precursors across the membrane. EMBO J. *30*, 1425–1432.

Mohammadi, T., Sijbrandi, R., Lutters, M., Verheul, J., Martin, N.I., den Blaauwen, T., de Kruijff, B., and Breukink, E. (2014). Specificity of the transport of lipid II by FtsW in *Escherichia coli*. J. Biol. Chem. *289*, 14707–14718.

Möll, A., and Thanbichler, M. (2009). FtsN-like proteins are conserved components of the cell division machinery in proteobacteria. Molecular Microbiology *72*, 1037–1053.

Monahan, L. G., and Harry, E. J. (2013). Identifying how bacterial cells find their middle: a new perspective. Molecular Microbiology *87*, 231–234.

Monahan, L.G., Liew, A.T.F., Bottomley, A.L., and Harry, E.J. (2014a). Division site positioning in bacteria: one size does not fit all. Front Microbiol *5*.

Monahan, L.G., Hajduk, I.V., Blaber, S.P., Charles, I.G., and Harry, E.J. (2014b). Coordinating bacterial cell division with nutrient availability: a role for glycolysis. MBio *5*, e00935–00914.

Monteiro, J.M., Fernandes, P.B., Vaz, F., Pereira, A.R., Tavares, A.C., Ferreira, M.T., Pereira, P.M., Veiga, H., Kuru, E., VanNieuwenhze, M.S., et al. (2015). Cell shape dynamics during the staphylococcal cell cycle. Nat Commun *6*, 8055.

Mosyak, L. (2000). The bacterial cell-division protein ZipA and its interaction with an FtsZ fragment revealed by X-ray crystallography. The EMBO Journal *19*, 3179–3191.

Moy, F.J., Glasfeld, E., Mosyak, L., and Powers, R. (2000). Solution structure of ZipA, a crucial component of *Escherichia coli* cell division. Biochemistry *39*, 9146–9156.

Mukherjee, A., and Lutkenhaus, J. (1994). Guanine nucleotide-dependent assembly of FtsZ into filaments. J. Bacteriol. *176*, 2754–2758.

Mukherjee, A., and Lutkenhaus, J. (1998). Dynamic assembly of FtsZ regulated by GTP hydrolysis. EMBO J *17*, 462–469.

Mukherjee, A., Dai, K., and Lutkenhaus, J. (1993). *Escherichia coli* cell division protein FtsZ is a guanine nucleotide binding protein. Proc. Natl. Acad. Sci. U.S.A. *90*, 1053–1057.

Mukherjee, A., Saez, C., and Lutkenhaus, J. (2001). Assembly of an FtsZ mutant deficient in GTPase activity has implications for FtsZ assembly and the role of the Z ring in cell division. J. Bacteriol. *183*, 7190–7197.

Müller, P., Ewers, C., Bertsche, U., Anstett, M., Kallis, T., Breukink, E., Fraipont, C., Terrak, M., Nguyen-Distèche, M., and Vollmer, W. (2007). The essential cell division protein FtsN interacts with the murein (peptidoglycan) synthase PBP1B in *Escherichia coli*. J. Biol. Chem. *282*, 36394–36402.

Muntel, J., Fromion, V., Goelzer, A., Maaβ, S., Mäder, U., Büttner, K., Hecker, M., and Becher, D. (2014). Comprehensive absolute quantification of the cytosolic proteome of *Bacillus subtilis* by data

independent, parallel fragmentation in liquid chromatography/mass spectrometry (LC/MSE). Mol Cell Proteomics *13*, 1008–1019.

Murakami, K., Fujimura, T., and Doi, M. (1994). Nucleotide sequence of the structural gene for the penicillin-binding protein 2 of *Staphylococcus aureus* and the presence of a homologous gene in other staphylococci. FEMS Microbiology Letters *117*, 131–136.

Murray, I.A., and Shaw, W.V. (1997). O-Acetyltransferases for chloramphenicol and other natural products. Antimicrob Agents Chemother *41*, 1–6.

Murray, T., Popham, D.L., and Setlow, P. (1997). Identification and characterization of *pbpA* encoding *Bacillus subtilis* penicillin-binding protein 2A. J. Bacteriol. *179*, 3021–3029.

Murray, T., Popham, D.L., and Setlow, P. (1998). *Bacillus subtilis* cells lacking penicillin-binding protein 1 require increased levels of divalent cations for growth. J Bacteriol *180*, 4555–4563.

Naidoo, J., and Noble, W.C. (1978). Transfer of gentamicin resistance between strains of *Staphylococcus aureus* on skin. J. Gen. Microbiol. *107*, 391–393.

Nanninga, N. (1998). Morphogenesis of *Escherichia coli*. Microbiol. Mol. Biol. Rev. *62*, 110–129.

Navratna, V., Nadig, S., Sood, V., Prasad, K., Arakere, G., and Gopal, B. (2010). Molecular basis for the role of *Staphylococcus aureus* penicillin binding protein 4 in antimicrobial Resistance. J Bacteriol *192*, 134–144.

Neuhaus, F.C., and Baddiley, J. (2003). A continuum of anionic charge: structures and functions of D-alanyl-teichoic acids in Gram-positive bacteria. Microbiol. Mol. Biol. Rev. *67*, 686–723.

Neuhaus, F.C., and Lynch, J.L. (1964). The enzymatic synthesis of D-alanyl-D-alanine. 3. On the inhibition of D-alanyl-D-alanine synthetase by the antibiotic D-cycloserine. Biochemistry *3*, 471–480.

Ng, E.Y., Trucksis, M., and Hooper, D.C. (1996). Quinolone resistance mutations in topoisomerase IV: relationship to the *flqA* locus and genetic evidence that topoisomerase IV is the primary target and DNA gyrase is the secondary target of fluoroquinolones in *Staphylococcus aureus*. Antimicrob. Agents Chemother. *40*, 1881–1888.

Nicola, F.G., McDougal, L.K., Biddle, J.W., and Tenover, F.C. (1998). Characterization of erythromycin-resistant isolates of *Staphylococcus aureus* recovered in the United States from 1958 through 1969. Antimicrob Agents Chemother *42*, 3024–3027.

Nierman, W.C., Feldblyum, T.V., Laub, M.T., Paulsen, I.T., Nelson, K.E., Eisen, J., Heidelberg, J.F., Alley, M.R.K., Ohta, N., Maddock, J.R., et al. (2001). Complete genome sequence of *Caulobacter crescentus*. PNAS *98*, 4136–4141.

Nogales, E., Downing, K.H., Amos, L.A., and Löwe, J. (1998). Tubulin and FtsZ form a distinct family of GTPases. Nat. Struct. Biol. *5*, 451–458.

Noirclerc-Savoye, M., Le Gouëllec, A., Morlot, C., Dideberg, O., Vernet, T., and Zapun, A. (2005). In vitro reconstitution of a trimeric complex of DivIB, DivIC and FtsL, and their transient co-localization at the division site in *Streptococcus pneumoniae*. Mol. Microbiol. *55*, 413–424.

Oliva, M.A., Cordell, S.C., and Löwe, J. (2004). Structural insights into FtsZ protofilament formation. Nat Struct Mol Biol *11*, 1243–1250.

Osawa, M., and Erickson, H.P. (2005). Probing the domain structure of FtsZ by random truncation and insertion of GFP. Microbiology *151*, 4033–4043.

Osawa, M., and Erickson, H.P. (2013). Liposome division by a simple bacterial division machinery. Proc. Natl. Acad. Sci. U.S.A. *110*, 11000–11004.

Osawa, M., Anderson, D.E., and Erickson, H.P. (2008). Reconstitution of contractile FtsZ rings in liposomes. Science *320*, 792–794.

Ostash, B., and Walker, S. (2010). Moenomycin family antibiotics: chemical synthesis, biosynthesis, biological activity. Nat Prod Rep *27*, 1594–1617.

Paradis-Bleau, C., Sanschagrin, F., and Levesque, R.C. (2005). Peptide inhibitors of the essential cell division protein FtsA. Protein Engineering, Design and Selection *18*, 85–91.

Park, W., and Matsuhashi, M. (1984). *Staphylococcus aureus* and *Micrococcus luteus* peptidoglycan

transglycosylases that are not penicillin-binding proteins. J. Bacteriol. *157*, 538–544.

Park, K.-T., Wu, W., Battaile, K.P., Lovell, S., Holyoak, T., and Lutkenhaus, J. (2011). MinD-dependent conformational changes in MinE required for the Min oscillator to spatially regulate cytokinesis. Cell *146*, 396–407.

Pastoret, S., Fraipont, C., den Blaauwen, T., Wolf, B., Aarsman, M.E.G., Piette, A., Thomas, A., Brasseur, R., and Nguyen-Distèche, M. (2004). Functional analysis of the cell division protein FtsW of *Escherichia coli*. J Bacteriol *186*, 8370–8379.

Patrick, J.E., and Kearns, D.B. (2008). MinJ (YvjD) is a topological determinant of cell division in *Bacillus subtilis*. Mol. Microbiol. *70*, 1166–1179.

Peacock, S.J., Moore, C.E., Justice, A., Kantzanou, M., Story, L., Mackie, K., O'Neill, G., and Day, N.P.J. (2002). Virulent combinations of adhesin and toxin genes in natural populations of *Staphylococcus aureus*. Infect Immun *70*, 4987–4996.

Pereira, P.M., Veiga, H., Jorge, A.M., and Pinho, M.G. (2010). Fluorescent reporters for studies of cellular localization of proteins in *Staphylococcus aureus*. Appl Environ Microbiol *76*, 4346–4353.

Pereira, S.F.F., Henriques, A.O., Pinho, M.G., de Lencastre, H., and Tomasz, A. (2007). Role of PBP1 in cell division of *Staphylococcus aureus*. J. Bacteriol. *189*, 3525–3531.

Pereira, S.F.F., Henriques, A.O., Pinho, M.G., de Lencastre, H., and Tomasz, A. (2009). Evidence for a dual role of PBP1 in the cell division and cell separation of *Staphylococcus aureus*. Mol. Microbiol. *72*, 895–904.

Peters, P.C., Migocki, M.D., Thoni, C., and Harry, E.J. (2007). A new assembly pathway for the cytokinetic Z ring from a dynamic helical structure in vegetatively growing cells of *Bacillus subtilis*. Mol. Microbiol. *64*, 487–499.

Phillips, G.J. (2001). Green fluorescent protein--a bright idea for the study of bacterial protein localization. FEMS Microbiol. Lett. *204*, 9–18.

Pichoff, S., and Lutkenhaus, J. (2002). Unique and overlapping roles for ZipA and FtsA in septal ring assembly in *Escherichia coli*. EMBO J. *21*, 685–693.

Pichoff, S., and Lutkenhaus, J. (2005). Tethering the Z ring to the membrane through a conserved membrane targeting sequence in FtsA. Mol. Microbiol. *55*, 1722–1734.

Pichoff, S., and Lutkenhaus, J. (2007). Identification of a region of FtsA required for interaction with FtsZ. Mol. Microbiol. *64*, 1129–1138.

Pinho, M.G., and Errington, J. (2003). Dispersed mode of *Staphylococcus aureus* cell wall synthesis in the absence of the division machinery. Molecular Microbiology *50*, 871–881.

Pinho, M.G., and Errington, J. (2004). A *divIVA* null mutant of *Staphylococcus aureus* undergoes normal cell division. FEMS Microbiol. Lett. *240*, 145–149.

Pinho, M.G., and Errington, J. (2005). Recruitment of penicillin-binding protein PBP2 to the division site of *Staphylococcus aureus* is dependent on its transpeptidation substrates. Mol. Microbiol. *55*, 799–807.

Pinho, M.G., Ludovice, A.M., Wu, S., and De Lencastre, H. (1997). Massive reduction in methicillin resistance by transposon inactivation of the normal PBP2 in a methicillin-resistant strain of *Staphylococcus aureus*. Microb. Drug Resist. *3*, 409–413.

Pinho, M.G., de Lencastre, H., and Tomasz, A. (1998). Transcriptional analysis of the *Staphylococcus aureus* penicillin binding protein 2 gene. J Bacteriol *180*, 6077–6081.

Pinho, M.G., Lencastre, H. de, and Tomasz, A. (2000). Cloning, characterization, and inactivation of the gene *pbpc*, encoding penicillin-binding protein 3 of *Staphylococcus aureus*. J. Bacteriol. *182*, 1074–1079.

Pinho, M.G., Filipe, S.R., de Lencastre, H., and Tomasz, A. (2001a). Complementation of the essential peptidoglycan transpeptidase function of penicillin-binding protein 2 (PBP2) by the drug resistance protein PBP2A in *Staphylococcus aureus*. J Bacteriol *183*, 6525–6531.

Pinho, M.G., de Lencastre, H., and Tomasz, A. (2001b). An acquired and a native penicillin-binding protein cooperate in building the cell wall of drug-resistant staphylococci. Proc Natl Acad Sci U S A *98*, 10886–10891.

Pinho, M.G., Kjos, M., and Veening, J.-W. (2013). How to get (a)round: mechanisms controlling growth and division of coccoid bacteria. Nat. Rev. Microbiol. *11*, 601–614.

Poczopko, G. (2012). STORM-compatible EzrA fusions for *Staphylococcus aureus*.

Porthouse, A., Brown, D.F.J., Smith, R.G., and Rogers, T. (1976). Gentamicin resistance in *Staphylococcus aureus.* The Lancet *307*, 20–21.

Ptacin, J.L., Nöllmann, M., Bustamante, C., and Cozzarelli, N.R. (2006). Identification of the FtsK sequence-recognition domain. Nat Struct Mol Biol *13*, 1023–1025.

Pucci, M.J., and Dougherty, T.J. (2002). Direct quantitation of the numbers of individual penicillin-binding proteins per cell in *Staphylococcus aureus*. J Bacteriol *184*, 588–591.

Pucci, M.J., Thanassi, J.A., Discotto, L.F., Kessler, R.E., and Dougherty, T.J. (1997). Identification and characterization of cell wall-cell division gene clusters in pathogenic Gram-positive cocci. J Bacteriol *179*, 5632–5635.

Qiao, Y., Lebar, M.D., Schirner, K., Schaefer, K., Tsukamoto, H., Kahne, D., and Walker, S. (2014). Detection of lipid-linked peptidoglycan precursors by exploiting an unexpected transpeptidase reaction. J Am Chem Soc *136*, 14678–14681.

Radhakrishnan, S.K., Pritchard, S., and Viollier, P.H. (2010). Coupling prokaryotic cell fate and division control with a bifunctional and oscillating oxidoreductase homolog. Dev. Cell *18*, 90–101.

Raskin, D.M., and de Boer, P.A. (1997). The MinE ring: an FtsZ-independent cell structure required for selection of the correct division site in *E. coli*. Cell *91*, 685–694.

RayChaudhuri, D. (1999). ZipA is a MAP-Tau homolog and is essential for structural integrity of the cytokinetic FtsZ ring during bacterial cell division. EMBO J. *18*, 2372–2383.

RayChaudhuri, D., and Park, J.T. (1992). *Escherichia coli* cell-division gene *ftsZ* encodes a novel GTP-binding protein. Nature *359*, 251–254.

Real, G., and Henriques, A.O. (2006). Localization of the *Bacillus subtilis murB* gene within the *dcw* cluster is important for growth and sporulation. J. Bacteriol. *188*, 1721–1732.

Reddy, M. (2007). Role of FtsEX in cell division of *Escherichia coli*: viability of *ftsEX* mutants is dependent on functional SufI or high osmotic strength. J Bacteriol *189*, 98–108.

Reed, P., Veiga, H., Jorge, A.M., Terrak, M., and Pinho, M.G. (2011). Monofunctional transglycosylases are not essential for *Staphylococcus aureus* cell wall synthesis. J. Bacteriol. *193*, 2549–2556.

Reed, P., Atilano, M.L., Alves, R., Hoiczyk, E., Sher, X., Reichmann, N.T., Pereira, P.M., Roemer, T., Filipe, S.R., Pereira-Leal, J.B., et al. (2015). *Staphylococcus aureus* survives with a minimal peptidoglycan synthesis machine but sacrifices virulence and antibiotic resistance. PLoS Pathog. *11*, e1004891.

Reichmann, N.T., Piçarra Cassona, C., Monteiro, J.M., Bottomley, A.L., Corrigan, R.M., Foster, S.J., Pinho, M.G., and Gründling, A. (2014). Differential localization of LTA synthesis proteins and their interaction with the cell division machinery in *Staphylococcus aureus*. Mol. Microbiol. *92*, 273–286.

Reimold, C., Defeu Soufo, H.J., Dempwolff, F., and Graumann, P.L. (2013). Motion of variable-length MreB filaments at the bacterial cell membrane influences cell morphology. Mol Biol Cell *24*, 2340–2349.

Reynolds, P.E. (1989). Structure, biochemistry and mechanism of action of glycopeptide antibiotics. Eur. J. Clin. Microbiol. Infect. Dis. *8*, 943–950.

Rice, L.B. (2006). Antimicrobial resistance in Gram-positive bacteria. Am J Infect Control *34*, S11–S19; discussion S64–S73.

Rice, L.B., Carias, L.L., Rudin, S., Hutton, R., Marshall, S., Hassan, M., Josseaume, N., Dubost, L., Marie, A., and Arthur, M. (2009). Role of class A penicillin-binding proteins in the expression of beta-lactam resistance in *Enterococcus faecium*. J. Bacteriol. *191*, 3649–3656.

Rismondo, J., Cleverley, R.M., Lane, H.V., Großhennig, S., Steglich, A., Möller, L., Mannala, G.K., Hain, T., Lewis, R.J., and Halbedel, S. (2015). Structure of the bacterial cell division determinant GpsB and its interaction with penicillin binding proteins: *Listeria monocytogenes* GpsB. Molecular Microbiology *99*, 978-998.

Rittweger, E., Han, K.Y., Irvine, S.E., Eggeling, C., and Hell, S.W. (2009). STED microscopy reveals crystal colour centres with nanometric resolution. Nat Photon *3*, 144–147.

Roach, E.J., Kimber, M.S., and Khursigara, C.M. (2014). Crystal structure and site-directed mutational analysis reveals key residues involved in *Escherichia coli* ZapA function. J Biol Chem *289*, 23276–23286.

Robert, L., Hoffmann, M., Krell, N., Aymerich, S., Robert, J., and Doumic, M. (2014). Division in *Escherichia coli* is triggered by a size-sensing rather than a timing mechanism. BMC Biol. *12*, 17.

Robichon, C., Karimova, G., Beckwith, J., and Ladant, D. (2011). Role of leucine zipper motifs in association of the *Escherichia coli* cell division proteins FtsL and FtsB. J Bacteriol *193*, 4988–4992.

Robson, S.A., and King, G.F. (2006). Domain architecture and structure of the bacterial cell division protein DivIB. Proc. Natl. Acad. Sci. U.S.A. *103*, 6700–6705.

Robson, S.A., Michie, K.A., Mackay, J.P., Harry, E., and King, G.F. (2002). The *Bacillus subtilis* cell division proteins FtsL and DivIC are intrinsically unstable and do not interact with one another in the absence of other septasomal components. Mol. Microbiol. *44*, 663–674.

Rodrigues, C.D.A., and Harry, E.J. (2012). The Min system and nucleoid occlusion are not required for identifying the division site in *Bacillus subtilis* but ensure its efficient utilization. PLoS Genet *8*.

Rowland, S.L., Katis, V.L., Partridge, S.R., and Wake, R.G. (1997). DivIB, FtsZ and cell division in *Bacillus subtilis*. Molecular Microbiology *23*, 295–302.

Rowland, S.L., Wadsworth, K.D., Robson, S.A., Robichon, C., Beckwith, J., and King, G.F. (2010). Evidence from artificial septal targeting and site-directed mutagenesis that residues in the extracytoplasmic β domain of DivIB mediate its interaction with the divisomal transpeptidase PBP 2B. J Bacteriol *192*, 6116–6125.

Rowlett, V.W., and Margolin, W. (2013). The bacterial Min system. Curr. Biol. *23*, R553–R556.

Rowlett, V.W., and Margolin, W. (2014). 3D-SIM super-resolution of FtsZ and its membrane tethers in *Escherichia coli* cells. Biophysical Journal *107*, L17–L20.

Rowlett, V.W., and Margolin, W. (2015a). The bacterial divisome: ready for its close-up. Phil. Trans. R. Soc. B *370*, 20150028.

Rowlett, V.W., and Margolin, W. (2015b). The Min system and other nucleoid-independent regulators of Z ring positioning. Front. Microbiol. 478.

Ruiz, N. (2008). Bioinformatics identification of MurJ (MviN) as the peptidoglycan lipid II flippase in *Escherichia coli*. Proc. Natl. Acad. Sci. U.S.A. *105*, 15553–15557.

Rust, M.J., Bates, M., and Zhuang, X. (2006). Sub-diffraction-limit imaging by stochastic optical reconstruction microscopy (STORM). Nat. Methods *3*, 793–795.

Sánchez, M., Valencia, A., Ferrándiz, M.J., Sander, C., and Vicente, M. (1994). Correlation between the structure and biochemical activities of FtsA, an essential cell division protein of the actin family. EMBO J. *13*, 4919–4925.

Sánchez-Pulido, L., Devos, D., Genevrois, S., Vicente, M., and Valencia, A. (2003). POTRA: a conserved domain in the FtsQ family and a class of beta-barrel outer membrane proteins. Trends Biochem. Sci. *28*, 523–526.

Sauvage, E., Kerff, F., Terrak, M., Ayala, J.A., and Charlier, P. (2008). The penicillin-binding proteins: structure and role in peptidoglycan biosynthesis. FEMS Microbiology Reviews *32*, 234–258.

Sauvage, E., Derouaux, A., Fraipont, C., Joris, M., Herman, R., Rocaboy, M., Schloesser, M., Dumas, J., Kerff, F., Nguyen-Distèche, M., et al. (2014). Crystal structure of penicillin-binding protein 3 (PBP3) from *Escherichia coli*. PLoS One *9*.

Schaechter, M., Maaloe, O., and Kjeldgaard, N.O. (1958). Dependency on medium and temperature of cell size and chemical composition during balanced grown of *Salmonella typhimurium*. J. Gen. Microbiol. *19*, 592–606.

Schaefler, S. (1989). Methicillin-resistant strains of *Staphylococcus aureus* resistant to quinolones. J Clin Microbiol *27*, 335–336.

Scheffers, D.-J., and Driessen, A.J.M. (2001). The polymerization mechanism of the bacterial cell division protein FtsZ. FEBS Letters *506*, 6–10.

Scheffers, D.-J., and Pinho, M.G. (2005). Bacterial cell wall synthesis: new insights from localization studies. Microbiol. Mol. Biol. Rev. *69*, 585–607.

Scheffers, D.J., de Wit, J.G., den Blaauwen, T., and Driessen, A.J. (2001). Substitution of a conserved aspartate allows cation-induced polymerization of FtsZ. FEBS Lett. *494*, 34–37.

Scheffers, D.-J., de Wit, J.G., den Blaauwen, T., and Driessen, A.J.M. (2002). GTP hydrolysis of cell division protein FtsZ: evidence that the active site is formed by the association of monomers. Biochemistry *41*, 521–529.

Scheffers, D.-J., Robichon, C., Haan, G.J., Blaauwen, T. den, Koningstein, G., Bloois, E. van, Beckwith, J., and Luirink, J. (2007). Contribution of the FtsQ transmembrane segment to localization to the cell division site. J. Bacteriol. *189*, 7273–7280.

Schermelleh, L., Heintzmann, R., and Leonhardt, H. (2010). A guide to super-resolution fluorescence microscopy. J Cell Biol *190*, 165–175.

Schlag, M., Biswas, R., Krismer, B., Kohler, T., Zoll, S., Yu, W., Schwarz, H., Peschel, A., and Götz, F. (2010). Role of staphylococcal wall teichoic acid in targeting the major autolysin Atl. Mol. Microbiol. *75*, 864–873.

Schmidt, K.L., Peterson, N.D., Kustusch, R.J., Wissel, M.C., Graham, B., Phillips, G.J., and Weiss, D.S. (2004). A predicted ABC transporter, FtsEX, is needed for cell division in *Escherichia coli*. J Bacteriol *186*, 785–793.

Schmidt, M., Schwarzwaelder, K., Bartholomae, C., Zaoui, K., Ball, C., Pilz, I., Braun, S., Glimm, H., and von Kalle, C. (2007). High-resolution insertion-site analysis by linear amplification–mediated PCR (LAM-PCR). Nat Meth *4*, 1051–1057.

Schmidt, R., Wurm, C.A., Punge, A., Egner, A., Jakobs, S., and Hell, S.W. (2009). Mitochondrial cristae revealed with focused light. Nano Lett. *9*, 2508–2510.

Schneider, T., and Sahl, H.-G. (2010). An oldie but a goodie – cell wall biosynthesis as antibiotic target pathway. International Journal of Medical Microbiology *300*, 161–169.

Schneider, J., Klein, T., Mielich-Süss, B., Koch, G., Franke, C., Kuipers, O.P., Kovács, Á.T., Sauer, M., and Lopez, D. (2015). Spatio-temporal remodeling of functional membrane microdomains organizes the signaling networks of a bacterium. PLoS Genet *11*, e1005140.

Schumacher, M.A., Zeng, W., Huang, K.-H., Tchorzewski, L., and Janakiraman, A. (2016). Structural and functional analyses reveal insights into the molecular properties of the *Escherichia coli* Z ring stabilizing protein, ZapC. J. Biol. Chem. *291*, 2485–2498.

Seligman, S.J., and Pincus, M.R. (1987). A model for the three-dimensional structure of peptidoglycan in staphylococci. J. Theor. Biol. *124*, 275–292.

Sham, L.-T., Barendt, S.M., Kopecky, K.E., and Winkler, M.E. (2011). Essential PcsB putative peptidoglycan hydrolase interacts with the essential FtsXSpn cell division protein in *Streptococcus pneumoniae* D39. Proc Natl Acad Sci U S A *108*, E1061–E1069.

Sham, L.-T., Tsui, H.-C.T., Land, A.D., Barendt, S.M., and Winkler, M.E. (2012). Recent advances in pneumococcal peptidoglycan biosynthesis suggest new vaccine and antimicrobial targets. Curr. Opin. Microbiol. *15*, 194–203.

Sham, L.-T., Jensen, K.R., Bruce, K.E., and Winkler, M.E. (2013). Involvement of FtsE ATPase and FtsX extracellular loops 1 and 2 in FtsEX-PcsB complex function in cell division of *Streptococcus pneumoniae* D39. mBio *4*.

Sham, L.-T., Butler, E.K., Lebar, M.D., Kahne, D., Bernhardt, T.G., and Ruiz, N. (2014). Bacterial cell wall. MurJ is the flippase of lipid-linked precursors for peptidoglycan biogenesis. Science *345*, 220–222.

Sharpe, M.E., Hauser, P.M., Sharpe, R.G., and Errington, J. (1998). *Bacillus subtilis* cell cycle as studied by fluorescence microscopy: constancy of cell length at initiation of DNA replication and evidence for active nucleoid partitioning. J Bacteriol *180*, 547–555.

Shih, Y.-L., Kawagishi, I., and Rothfield, L. (2005). The MreB and Min cytoskeletal-like systems play

independent roles in prokaryotic polar differentiation. Mol. Microbiol. *58*, 917–928.

Shiomi, D., and Margolin, W. (2007). The C-terminal domain of MinC inhibits assembly of the Z ring in *Escherichia coli*. J. Bacteriol. *189*, 236–243.

Sieradzki, K., and Tomasz, A. (1997). Suppression of beta-lactam antibiotic resistance in a methicillin-resistant *Staphylococcus aureus* through synergic action of early cell wall inhibitors and some other antibiotics. J. Antimicrob. Chemother. *39*, 47–51.

Sievers, J., Raether, B., Perego, M., and Errington, J. (2002). Characterization of the *parB*-like *yyaA* gene of *Bacillus subtilis*. J. Bacteriol. *184*, 1102–1111.

Singh, J.K., Makde, R.D., Kumar, V., and Panda, D. (2007). A membrane protein, EzrA, regulates assembly dynamics of FtsZ by interacting with the C-terminal tail of FtsZ. Biochemistry *46*, 11013–11022.

Singh, J.K., Makde, R.D., Kumar, V., and Panda, D. (2008). SepF increases the assembly and bundling of FtsZ polymers and stabilizes FtsZ protofilaments by binding along its length. J Biol Chem *283*, 31116–31124.

Singh, P., Makde, R.D., Ghosh, S., Asthana, J., Kumar, V., and Panda, D. (2013). Assembly of *Bacillus subtilis* FtsA: effects of pH, ionic strength and nucleotides on FtsA assembly. Int. J. Biol. Macromol. *52*, 170–176.

Small, E., Marrington, R., Rodger, A., Scott, D.J., Sloan, K., Roper, D., Dafforn, T.R., and Addinall, S.G. (2007). FtsZ polymer-bundling by the *Escherichia coli* ZapA orthologue, YgfE, involves a conformational change in bound GTP. Journal of Molecular Biology *369*, 210–221.

Söderström, B., Skoog, K., Blom, H., Weiss, D.S., von Heijne, G., and Daley, D.O. (2014). Disassembly of the divisome in *Escherichia coli*: evidence that FtsZ dissociates before compartmentalization. Molecular Microbiology *92*, 1–9.

Soldo, B., Lazarevic, V., and Karamata, D. (2002). *tagO* is involved in the synthesis of all anionic cell-wall polymers in *Bacillus subtilis* 168. Microbiology (Reading, Engl.) *148*, 2079–2087.

Song, J.-H., Ko, K.S., Lee, J.-Y., Baek, J.Y., Oh, W.S., Yoon, H.S., Jeong, J.-Y., and Chun, J. (2005). Identification of essential genes in *Streptococcus pneumoniae* by allelic replacement mutagenesis. Mol. Cells *19*, 365–374.

Spratt, B.G. (1975). Distinct penicillin binding proteins involved in the division, elongation, and shape of *Escherichia coli* K12. Proc. Natl. Acad. Sci. U.S.A. *72*, 2999–3003.

Spratt, B.G. (1977). Temperature-sensitive cell division mutants of *Escherichia coli* with thermolabile penicillin-binding proteins. J Bacteriol *131*, 293–305.

Stadler, C., Rexhepaj, E., Singan, V.R., Murphy, R.F., Pepperkok, R., Uhlén, M., Simpson, J.C., and Lundberg, E. (2013). Immunofluorescence and fluorescent-protein tagging show high correlation for protein localization in mammalian cells. Nat Meth *10*, 315–323.

Steele, V.R., Bottomley, A.L., Garcia-Lara, J., Kasturiarachchi, J., and Foster, S.J. (2011). Multiple essential roles for EzrA in cell division of *Staphylococcus aureus*. Mol. Microbiol. *80*, 542–555.

Stefani, S., Chung, D.R., Lindsay, J.A., Friedrich, A.W., Kearns, A.M., Westh, H., and MacKenzie, F.M. (2012). Meticillin-resistant *Staphylococcus aureus* (MRSA): global epidemiology and harmonisation of typing methods. International Journal of Antimicrobial Agents *39*, 273–282.

von Stetten, D., Noirclerc-Savoye, M., Goedhart, J., Gadella, T.W.J., and Royant, A. (2012). Structure of a fluorescent protein from *Aequorea victoria* bearing the obligate-monomer mutation A206K. Acta Crystallogr. Sect. F Struct. Biol. Cryst. Commun. *68*, 878–882.

Stokes, K.D., and Osteryoung, K.W. (2003). Early divergence of the FtsZ1 and FtsZ2 plastid division gene families in photosynthetic eukaryotes. Gene *320*, 97–108.

Stouf, M., Meile, J.-C., and Cornet, F. (2013). FtsK actively segregates sister chromosomes in *Escherichia coli*. Proc Natl Acad Sci U S A *110*, 11157–11162.

Strauss, M.P., Liew, A.T.F., Turnbull, L., Whitchurch, C.B., Monahan, L.G., and Harry, E.J. (2012). 3D-SIM super resolution microscopy reveals a bead-like arrangement for FtsZ and the division machinery: implications for triggering cytokinesis. PLoS Biol *10*, e1001389.

Stricker, J., Maddox, P., Salmon, E.D., and Erickson, H.P. (2002). Rapid assembly dynamics of the *Escherichia coli* FtsZ-ring demonstrated by fluorescence recovery after photobleaching. Proc. Natl. Acad. Sci. U.S.A. *99*, 3171–3175.

Subach, F.V., Patterson, G.H., Manley, S., Gillette, J.M., Lippincott-Schwartz, J., and Verkhusha, V.V. (2009). Photoactivatable mCherry for high-resolution two-color fluorescence microscopy. Nat Methods *6*, 153–159.

Subach, O.M., Patterson, G.H., Ting, L.-M., Wang, Y., Condeelis, J.S., and Verkhusha, V.V. (2011). A photoswitchable orange-to-far-red fluorescent protein, PSmOrange. Nat Meth *8*, 771–777.

Suganuma, A. (1961). The plasma membrane of *Staphylococcus aureus*. J Biophys Biochem Cytol *10*, 292–298.

Sun, Q., and Margolin, W. (1998). FtsZ dynamics during the division cycle of live *Escherichia coli* cells. J. Bacteriol. *180*, 2050–2056.

Sundararajan, K., Miguel, A., Desmarais, S.M., Meier, E.L., Casey Huang, K., and Goley, E.D. (2015). The bacterial tubulin FtsZ requires its intrinsically disordered linker to direct robust cell wall construction. Nat Commun *6*, 7281.

Suzuki, H., Nishimura, Y., and Hirota, Y. (1978). On the process of cellular division in *Escherichia coli*: a series of mutants of *E. coli* altered in the penicillin-binding proteins. PNAS *75*, 664–668.

Swulius, M.T., and Jensen, G.J. (2012). The helical MreB cytoskeleton in *Escherichia coli* MC1000/pLE7 Is an artifact of the N-Terminal yellow fluorescent protein tag. J. Bacteriol. *194*, 6382–6386.

Szwedziak, P., Wang, Q., Freund, S.M.V., and Löwe, J. (2012). FtsA forms actin-like protofilaments. EMBO J. *31*, 2249–2260.

Szwedziak, P., Wang, Q., Bharat, T.A.M., Tsim, M., and Löwe, J. (2014). Architecture of the ring formed by the tubulin homologue FtsZ in bacterial cell division. eLife *3*.

Tamames, J., González-Moreno, M., Mingorance, J., Valencia, A., and Vicente, M. (2001). Bringing gene order into bacterial shape. Trends Genet. *17*, 124–126.

Tan, C.M., Therien, A.G., Lu, J., Lee, S.H., Caron, A., Gill, C.J., Lebeau-Jacob, C., Benton-Perdomo, L., Monteiro, J.M., Pereira, P.M., et al. (2012). Restoring methicillin-resistant *Staphylococcus aureus* susceptibility to β-lactam antibiotics. Sci Transl Med *4*, 126ra35.

Taschner, P.E., Huls, P.G., Pas, E., and Woldringh, C.L. (1988). Division behavior and shape changes in isogenic *ftsZ, ftsQ, ftsA, pbpB,* and *ftsE* cell division mutants of *Escherichia coli* during temperature shift experiments. J. Bacteriol. *170*, 1533–1540.

Tavares, J.R., Souza, R.F. de, Meira, G.L.S., and Gueiros-Filho, F.J. (2008). Cytological characterization of YpsB, a novel component of the Bacillus subtilis divisome. J. Bacteriol. *190*, 7096–7107.

Thanassi, J.A., Hartman-Neumann, S.L., Dougherty, T.J., Dougherty, B.A., and Pucci, M.J. (2002). Identification of 113 conserved essential genes using a high-throughput gene disruption system in *Streptococcus pneumoniae*. Nucleic Acids Res. *30*, 3152–3162.

Thanbichler, M., and Shapiro, L. (2006). MipZ, a spatial regulator coordinating chromosome segregation with cell division in *Caulobacter*. Cell *126*, 147–162.

Thanedar, S., and Margolin, W. (2004). FtsZ exhibits rapid movement and oscillation waves in helix-like patterns in *Escherichia coli*. Curr. Biol. *14*, 1167–1173.

Tonthat, N.K., Arold, S.T., Pickering, B.F., Van Dyke, M.W., Liang, S., Lu, Y., Beuria, T.K., Margolin, W., and Schumacher, M.A. (2011). Molecular mechanism by which the nucleoid occlusion factor, SlmA, keeps cytokinesis in check. EMBO J. *30*, 154–164.

Tonthat, N.K., Milam, S.L., Chinnam, N., Whitfill, T., Margolin, W., and Schumacher, M.A. (2013). SlmA forms a higher-order structure on DNA that inhibits cytokinetic Z-ring formation over the nucleoid. PNAS *110*, 10586–10591.

Traag, B.A., and van Wezel, G.P. (2008). The SsgA-like proteins in actinomycetes: small proteins up to a big task. Antonie Van Leeuwenhoek *94*, 85–97.

Treuner-Lange, A., Aguiluz, K., van der Does, C., Gómez-Santos, N., Harms, A., Schumacher, D., Lenz,

P., Hoppert, M., Kahnt, J., Muñoz-Dorado, J., et al. (2013). PomZ, a ParA-like protein, regulates Z-ring formation and cell division in *Myxococcus xanthus*. Molecular Microbiology *87*, 235–253.

Trueba, F.J. (1982). On the precision and accuracy achieved by *Escherichia coli* cells at fission about their middle. Arch. Microbiol. *131*, 55–59.

Tsang, M.-J., and Bernhardt, T.G. (2015). A role for the FtsQLB complex in cytokinetic ring activation revealed by an *ftsL* allele that accelerates division. Molecular Microbiology *95*, 925–944.

Tsiodras, S., Gold, H.S., Sakoulas, G., Eliopoulos, G.M., Wennersten, C., Venkataraman, L., Moellering, R.C., and Ferraro, M.J. (2001). Linezolid resistance in a clinical isolate of *Staphylococcus aureus*. Lancet *358*, 207–208.

Tsui, H.-C.T., Boersma, M.J., Vella, S.A., Kocaoglu, O., Kuru, E., Peceny, J.K., Carlson, E.E., VanNieuwenhze, M.S., Brun, Y.V., Shaw, S.L., et al. (2014). Pbp2x localizes separately from Pbp2b and other peptidoglycan synthesis proteins during later stages of cell division of *Streptococcus pneumoniae* D39. Molecular Microbiology *94*, 21–40.

Turner, R.D., Ratcliffe, E.C., Wheeler, R., Golestanian, R., Hobbs, J.K., and Foster, S.J. (2010). Peptidoglycan architecture can specify division planes in *Staphylococcus aureus*. Nat Commun *1*, 26.

Turner, R.D., Hurd, A.F., Cadby, A., Hobbs, J.K., and Foster, S.J. (2013). Cell wall elongation mode in Gram-negative bacteria is determined by peptidoglycan architecture. Nat Commun *4*, 1496.

Tuson, H.H., and Biteen, J.S. (2015). Unveiling the inner workings of live bacteria using super-resolution microscopy. Anal. Chem. *87*, 42–63.

Typas, A., Banzhaf, M., Gross, C.A., and Vollmer, W. (2012). From the regulation of peptidoglycan synthesis to bacterial growth and morphology. Nat. Rev. Microbiol. *10*, 123–136.

Tzagoloff, H., and Novick, R. (1977). Geometry of cell division in *Staphylococcus aureus*. J Bacteriol *129*, 343–350.

Uehara, T., Parzych, K.R., Dinh, T., and Bernhardt, T.G. (2010). Daughter cell separation is controlled by cytokinetic ring-activated cell wall hydrolysis. EMBO J. *29*, 1412–1422.

Uphoff, S., Reyes-Lamothe, R., Garza de Leon, F., Sherratt, D.J., and Kapanidis, A.N. (2013). Single-molecule DNA repair in live bacteria. Proc. Natl. Acad. Sci. U.S.A. *110*, 8063–8068.

Ursinus, A., van den Ent, F., Brechtel, S., de Pedro, M., Höltje, J.-V., Löwe, J., and Vollmer, W. (2004). Murein (peptidoglycan) binding property of the essential cell division protein FtsN from *Escherichia coli*. J. Bacteriol. *186*, 6728–6737.

Varma, A., de Pedro, M.A., and Young, K.D. (2007). FtsZ directs a second mode of peptidoglycan synthesis in Escherichia coli. J. Bacteriol. *189*, 5692–5704.

Vaughan, J.C., Jia, S., and Zhuang, X. (2012). Ultrabright photoactivatable fluorophores created by reductive caging. Nat. Methods *9*, 1181–1184.

Veiga, H., Jorge, A.M., and Pinho, M.G. (2011). Absence of nucleoid occlusion effector Noc impairs formation of orthogonal FtsZ rings during *Staphylococcus aureus* cell division. Molecular Microbiology *80*, 1366–1380.

Vicente, M., Gomez, M.J., and Ayala, J.A. (1998). Regulation of transcription of cell division genes in the *Escherichia coli dcw* cluster. Cell. Mol. Life Sci. *54*, 317–324.

Vollmer, W. (2008). Structural variation in the glycan strands of bacterial peptidoglycan. FEMS Microbiology Reviews *32*, 287–306.

Vollmer, W., and Seligman, S.J. (2010). Architecture of peptidoglycan: more data and more models. Trends in Microbiology *18*, 59–66.

Voskuil, M.I., and Chambliss, G.H. (1998). The −16 region of *Bacillus subtilis* and other Gram-positive bacterial promoters. Nucl. Acids Res. *26*, 3584–3590.

Wada, A., and Watanabe, H. (1998). Penicillin-binding protein 1 of *Staphylococcus aureus* is essential for growth. J. Bacteriol. *180*, 2759–2765.

Wadenpohl, I., and Bramkamp, M. (2010). DivIC stabilizes FtsL against RasP cleavage. J Bacteriol *192*, 5260–5263.

Wadsworth, K.D., Rowland, S.L., Harry, E.J., and King, G.F. (2008). The divisomal protein DivIB contains multiple epitopes that mediate its recruitment to incipient division sites. Molecular Microbiology *67*, 1143–1155.

Wang, H.C., and Gayda, R.C. (1990). High-level expression of the FtsA protein inhibits cell septation in *Escherichia coli* K-12. J Bacteriol *172*, 4736–4740.

Wang, X., and Lutkenhaus, J. (1996). FtsZ ring: the eubacterial division apparatus conserved in Archaebacteria. Mol. Microbiol. *21*, 313–319.

Wang, L., Khattar, M.K., Donachie, W.D., and Lutkenhaus, J. (1998). FtsI and FtsW are localized to the septum in *Escherichia coli*. J. Bacteriol. *180*, 2810–2816.

Wang, Q.M., Peery, R.B., Johnson, R.B., Alborn, W.E., Yeh, W.-K., and Skatrud, P.L. (2001). Identification and characterization of a monofunctional glycosyltransferase from *Staphylococcus aureus*. J. Bacteriol. *183*, 4779–4785.

Wang, S.C.E., West, L., and Shapiro, L. (2006). The bifunctional Ftsk protein mediates chromosome partitioning and cell division in *Caulobacter*. J. Bacteriol. *188*, 1497–1508.

Wang, W., Li, G.-W., Chen, C., Xie, X.S., and Zhuang, X. (2011). Chromosome organization by a nucleoid-associated protein in live bacteria. Science *333*, 1445–1449.

Wang, X., Huang, J., Mukherjee, A., Cao, C., and Lutkenhaus, J. (1997). Analysis of the interaction of FtsZ with itself, GTP, and FtsA. J. Bacteriol. *179*, 5551–5559.

Warsa, U.C., Nonoyama, M., Ida, T., Okamoto, R., Okubo, T., Shimauchi, C., Kuga, A., and Inoue, M. (1996). Detection of *tet*(K) and *tet*(M) in *Staphylococcus aureus* of Asian countries by the polymerase chain reaction. J. Antibiot. *49*, 1127–1132.

Weart, R.B., Lee, A.H., Chien, A.-C., Haeusser, D.P., Hill, N.S., and Levin, P.A. (2007). A metabolic sensor governing cell size in bacteria. Cell *130*, 335–347.

Webb, C.D., Decatur, A., Teleman, A., and Losick, R. (1995). Use of green fluorescent protein for visualization of cell-specific gene expression and subcellular protein localization during sporulation in *Bacillus subtilis*. J. Bacteriol. *177*, 5906–5911.

Weigel, L.M., Clewell, D.B., Gill, S.R., Clark, N.C., McDougal, L.K., Flannagan, S.E., Kolonay, J.F., Shetty, J., Killgore, G.E., and Tenover, F.C. (2003). Genetic analysis of a high-level vancomycin-resistant isolate of *Staphylococcus aureus*. Science *302*, 1569–1571.

Weiss, D.S., Chen, J.C., Ghigo, J.M., Boyd, D., and Beckwith, J. (1999). Localization of FtsI (PBP3) to the septal ring requires its membrane anchor, the Z ring, FtsA, FtsQ, and FtsL. J. Bacteriol. *181*, 508–520.

Werner, G., Cuny, C., Schmitz, F.-J., and Witte, W. (2001). Methicillin-resistant, quinupristin-dalfopristin-resistant *Staphylococcus aureus* with reduced sensitivity to glycopeptides. J Clin Microbiol *39*, 3586–3590.

Wheeler, R., Mesnage, S., Boneca, I.G., Hobbs, J.K., and Foster, S.J. (2011). Super-resolution microscopy reveals cell wall dynamics and peptidoglycan architecture in ovococcal bacteria. Molecular Microbiology *82*, 1096–1109.

Wheeler, R., Turner, R.D., Bailey, R.G., Salamaga, B., Mesnage, S., Mohamad, S.A.S., Hayhurst, E.J., Horsburgh, M., Hobbs, J.K., and Foster, S.J. (2015). Bacterial cell enlargement requires control of cell wall stiffness mediated by peptidoglycan hydrolases. MBio *6*, e00660.

Willemse, J., Borst, J.W., Waal, E. de, Bisseling, T., and Wezel, G.P. van (2011). Positive control of cell division: FtsZ is recruited by SsgB during sporulation of *Streptomyces*. Genes Dev. *25*, 89–99.

Willig, K.I., Harke, B., Medda, R., and Hell, S.W. (2007). STED microscopy with continuous wave beams. Nat Meth *4*, 915–918.

Wissel, M.C., Wendt, J.L., Mitchell, C.J., and Weiss, D.S. (2005). The transmembrane helix of the *Escherichia coli* division protein FtsI localizes to the septal ring. J Bacteriol *187*, 320–328.

Wu, L.J., and Errington, J. (1994). *Bacillus subtilis* SpoIIIE protein required for DNA segregation during asymmetric cell division. Science *264*, 572–575.

Wu, L.J., and Errington, J. (2004). Coordination of cell division and chromosome segregation by a nucleoid occlusion protein in *Bacillus subtilis*. Cell *117*, 915–925.

Wu, L.J., Ishikawa, S., Kawai, Y., Oshima, T., Ogasawara, N., and Errington, J. (2009). Noc protein binds to specific DNA sequences to coordinate cell division with chromosome segregation. EMBO J. *28*, 1940–1952.

Wyke, A.W., Ward, J.B., Hayes, M.V., and Curtis, N.A. (1981). A role in vivo for penicillin-binding protein-4 of *Staphylococcus aureus*. Eur. J. Biochem. *119*, 389–393.

Yan, K., Pearce, K.H., and Payne, D.J. (2000). A conserved residue at the extreme C-terminus of FtsZ is critical for the FtsA-FtsZ interaction in *Staphylococcus aureus*. Biochemical and Biophysical Research Communications *270*, 387–392.

Yang, D.C., Peters, N.T., Parzych, K.R., Uehara, T., Markovski, M., and Bernhardt, T.G. (2011). An ATP-binding cassette transporter-like complex governs cell-wall hydrolysis at the bacterial cytokinetic ring. Proc Natl Acad Sci U S A *108*, E1052–E1060.

Yanouri, A., Daniel, R.A., Errington, J., and Buchanan, C.E. (1993). Cloning and sequencing of the cell division gene *pbpB*, which encodes penicillin-binding protein 2B in *Bacillus subtilis*. J. Bacteriol. *175*, 7604–7616.

Yoshida, H., Kawai, F., Obayashi, E., Akashi, S., Roper, D.I., Tame, J.R.H., and Park, S.-Y. (2012). Crystal structures of penicillin-binding protein 3 (PBP3) from methicillin-resistant *Staphylococcus aureus* in the apo and cefotaxime-bound forms. J. Mol. Biol. *423*, 351–364.

Yu, X.-C., and Margolin, W. (1999). FtsZ ring clusters in min and partition mutants: role of both the Min system and the nucleoid in regulating FtsZ ring localization. Molecular Microbiology *32*, 315–326.

Yu, X.C., Tran, A.H., Sun, Q., and Margolin, W. (1998). Localization of cell division protein FtsK to the *Escherichia coli* septum and identification of a potential N-terminal targeting domain. J. Bacteriol. *180*, 1296–1304.

Zacharias, D.A., Violin, J.D., Newton, A.C., and Tsien, R.Y. (2002). Partitioning of lipid-modified monomeric GFPs into membrane microdomains of live cells. Science *296*, 913–916.

Zapun, A., Vernet, T., and Pinho, M.G. (2008a). The different shapes of cocci. FEMS Microbiology Reviews *32*, 345–360.

Zapun, A., Contreras-Martel, C., and Vernet, T. (2008b). Penicillin-binding proteins and beta-lactam resistance. FEMS Microbiol. Rev. *32*, 361–385.

Zawadzki, P., May, P.F.J., Baker, R.A., Pinkney, J.N.M., Kapanidis, A.N., Sherratt, D.J., and Arciszewska, L.K. (2013). Conformational transitions during FtsK translocase activation of individual XerCD-dif recombination complexes. Proc. Natl. Acad. Sci. U.S.A. *110*, 17302–17307.

Zhang, J., Campbell, R.E., Ting, A.Y., and Tsien, R.Y. (2002). Creating new fluorescent probes for cell biology. Nat. Rev. Mol. Cell Biol. *3*, 906–918.

Zhao, G., Meier, T.I., Kahl, S.D., Gee, K.R., and Blaszczak, L.C. (1999). Bocillin FL, a sensitive and commercially available reagent for detection of penicillin-binding proteins. Antimicrob Agents Chemother *43*, 1124–1128.

Zhou, X., Halladin, D.K., Rojas, E.R., Koslover, E.F., Lee, T.K., Huang, K.C., and Theriot, J.A. (2015). Mechanical crack propagation drives millisecond daughter cell separation in *Staphylococcus aureus*. Science *348*, 574–578.

Zhuang, X. (2009). Nano-imaging with STORM. Nat Photonics *3*, 365–367.

Zuegg, J., Muldoon, C., Adamson, G., McKeveney, D., Le Thanh, G., Premraj, R., Becker, B., Cheng, M., Elliott, A.G., Huang, J.X., et al. (2015). Carbohydrate scaffolds as glycosyltransferase inhibitors with in vivo antibacterial activity. Nat Commun *6*, 7719.

Appendix I

DNA fragments selected for generation of translational EzrA fluorescent fusions

Putative *ezrA* promoter and the *ezrA* gene sequence (the promoter region is shown in lowercase, *ezrA* coding sequence in uppercase):

gtcatatttaaaacctcttattttcatagattttataatagtatagaatttcgaaaatattatggcaataaatt
cattttataatttatccttaagcaaaattacgttataatagtaatgataaattaggaggagaagcatATGGTGT
TATATATCATTTTGGCAATAATTGTGATTATATTGATTGCTGTAGGTGTATTATTCTATTTACGTTCAAATAAA
CGACAAATTATTGAAAAAGCAATCGAACGTAAAAATGAAATTGAGACGTTACCTTTTGATCAAAACCTTGCACA
ATTATCTAAGTTGAATTTAAAAGGTGAAACAAAAACGAAATACGATGCAATGAAAAAGGACAACGTAGAAAGTA
CAAATAAGTATCTAGCTCCTGTGGAAGAAAAAATCCATAATGCTGAGGCTTTATTAGATAAATTTAGTTTCAAC
GCATCTCAAAGTGAAATTGATGATGCAAATGAGTTGATGGATAGTTACGAACAAAGCTATCAGCAACAATTAGA
AGATGTAAATGAAATTATTGCGTTATACAAAGATAATGATGAATTATATGACAAATGTAAGGTTGATTATCGTG
AAATGAAACGTGATGTTTTAGCAAATCGTCATCAATTTGGTGAGGCAGCAAGTCTACTTGAAACTGAAATTGAA
AAATTTGAGCCAAGGTTAGAGCAATATGAAGTACTAAAAGCTGATGGTAATTATGTACAAGCGCACAACCATAT
AGCTGCCTTGAATGAACAAATGAAACAGCTAAGATCTTATATGGAAGAAATACCAGAATTAATTAGAGAAACTC
AAAAAGAATTACCTGGTCAATTCCAAGATTTAAAATATGGTTGCCGTGATCTTAAAGTTGAAGGGTATGATCTG
GATCACGTGAAAGTAGACAGTACATTACAAAGCTTAAAAACAGAGCTTAGTTTCGTTGAACCATTAATTAGCCG
CTTAGAATTAGAAGAAGCTAATGATAAACTAGCTAATATCAATGATAAGTTAGATGACATGTATGATTTAATTG
AACATGAAGTTAAAGCTAAAAATGATGTCGAAGAAACAAAAGATATCATTACGGATAACTTATTCAAAGCTAAA
GACATGAATTATACATTGCAAACAGAAATTGAATATGTACGTGAAAACTACTATATAAATGAATCTGATGCTCA
GAGTGTTCGTCAATTTGAAAATGAAATTCAAAGTTTAATTTCTGTATATGATGATATTTTAAAAGAAATGTCTA
AATCTGCTGTGCGATATAGCGAGGTTCAGGATAATTTACAATATTTAGAAGATCATGTCACAGTTATTAATGAC
AAACAAGAAAAGCTACAAAATCATCTGATTCAATTGCGTGAAGATGAAGCAGAAGCAGAAGACAATCTGCTACG
AGTACAATCGAAGAAAGAAGAAGTGTATCGTCGATTACTTGCTTCTAACTTAACAAGCGTTCCTGAAAGGTTTA
TCATCATGAAAAATGAAATTGATCATGAAGTTCGTGATGTTAACGAACAATTTAGTGAACGTCCAATACACGTT
AAACAGTTAAAAGATAAAGTGTCTAAAATTGTGATTCAAATGAATACATTTGAAGATGAAGCAAATGATGTTCT
TGTTAATGCTGTTTATGCAGAGAAATTAATTCAATATGGAAATAGATATCGTAAGGACTATAGCAATGTTGATA
AGAGCTTAAATGAAGCTGAACGATTATTTAAAAATAATCGCTATAAGCGTGCGATTGAAATTGCAGAGCAAGCT
CTTGAAAGTGTTGAGCCAGGTGTTACTAAACATATTGAAGAAGAAGTTATTAAGCAA

Linker joining *ezrA* with *meos2*:

TCAGGTTCAGGTTCAGGTTCAGGTTCAGGTTCAGGT

Linker joining *ezrA* with *psmorange/eyfp/meyfp/pamcherry1/gfp/snap*:

TCAGGTTCAGGTTCAGGTGGGCGCGCCTCAGGTTCAGGTTCAGGT

meos2

ATGAGTGCGATTAAGCCAGACATGAAGATCAAACTCCGTATGGAAGGCAACGTAAACGGGCACCACTTTGTGAT
CGACGGAGATGGTACAGGCAAGCCTTTTGAGGGAAAACAGAGTATGGATCTTGAAGTCAAAGAGGGCGGACCTC
TGCCTTTTGCCTTTGATATCCTGACCACTGCATTCCATTACGGCAACAGGGTATTCGCCAAATATCCAGACAAC
ATACAAGACTATTTTAAGCAGTCGTTTCCTAAGGGGTATTCGTGGGAACGAAGCTTGACTTTCGAAGACGGGGG
CATTTGCATTGCCAGAAACGACATAACAATGGAAGGGGACACTTTCTATAATAAAGTTCGATTTTATGGTACCA
ACTTTCCCGCCAATGGTCCAGTTATGCAGAAGAAGACGCTGAAATGGGAGCCCTCCACTGAGAAAATGTATGTG
CGTGATGGAGTGCTGACGGGTGATATTCATATGGCTTTGTTGCTTGAAGGAAATGCCCATTACCGATGTGACTT
CAGAACTACTTACAAAGCTAAGGAGAAGGGTGTCAAGTTACCAGGCTACCACTTTGTGGACCACTGCATTGAGA
TTTTAAGCCATGACAAAGATTACAACAAGGTTAAGCTGTATGAGCATGCTGTTGCTCATTCTGGATTGCCTGAC
AATGCCAGACGATAA

psmorange

ATGGTGAGCAAGGGCGAGGAGAATAATATGGCCATCATCAAGGAGTTCATGCGCTTCAAGGTGCGCATGGAGGG
CACCGTGAACGGCCACGAGTTCGAGATCGAGGGCGAGGGCGAGGGCCGCCCCTACGAGGGCTTTCAGACCGCTA
AGCTGAAGGTGACCAAGGGCGGCCCCCTGCCCTTCGCCTGGGACATCCTGTCCCCTCTCTTCACCTACGGCTCC

AAGGCCTACGTGAAGCACCCCGCCGACATCCCCGACTACTTCAAGCTGTCCTTCCCCGAGGGCTTCAAGTGGGA
GCGCGTGATGAACTACGAGGACGGCGGCGTGGTGACCGTGACCCAGGACTCCTCACTGCAGGACGGCGAGTTCA
TCTACAAGGTGAAGATGCGCGGCACCAACTTCCCCTCCGACGGCCCCGTGATGCAGAAGAAGACCATGGGCTGG
GAGGCCTCCTCCGAGCGGATGTACCCCGAGGACGGCGCCCTGAAGGGCGAGATCAGGATGAGGCTGAAGCTGAA
GGACGGCGGCCACTACACCTCCGAGGTCAAGACCACCTACAAGGCCAAGAAGTCCGTGCAGCTGCCCGGCGCCT
ACATCGTCGGCATCAAGCTGGACATCACCTCCCACAACGAGGACTACACCATCGTGGAACAGTACGAACGCGCC
GAGGGCCGCCACTCCACCGGCGGCATGGACGAGCTGTACAAGTAA

eyfp

ATGGTGAGCAAGGGCGAGGAGCTGTTCACCGGGGTGGTGCCCATCCTGGTCGAGCTGGACGGCGACGTAAACGG
CCACAAGTTCAGCGTGTCCGGCGAGGGCGAGGGCGATGCCACCTACGGCAAGCTGACCCTGAAGTTCATCTGCA
CCACCGGCAAGCTGCCCGTGCCCTGGCCCACCCTCGTGACCACCTTCGGCTACGGCCTGCAGTGCTTCGCCCGC
TACCCCGACCACATGAAGCAGCACGACTTCTTCAAGTCCGCCATGCCCGAAGGCTACGTCCAGGAGCGCACCAT
CTTCTTCAAGGACGACGGCAACTACAAGACCCGCGCCGAGGTGAAGTTCGAGGGCGACACCCTGGTGAACCGCA
TCGAGCTGAAGGGCATCGACTTCAAGGAGGACGGCAACATCCTGGGGCACAAGCTGGAGTACAACTACAACAGC
CACAACGTCTATATCATGGCCGACAAGCAGAAGAACGGCATCAAGGTGAACTTCAAGATCCGCCACAACATCGA
GGGCGGCAGCGTGCAGCTCGCCGACCACTACCAGCAGAACACCCCCATCGGCGACGGCCCCGTGCTGCTGCCCG
ACAACCACTACCTGAGCTACCAGTCCGCCCTGAGCAAAGACCCCAACGAGAAGCGCGATCACATGGTCCTGCTG
GAGTTCGTGACCGCCGCCGGGATCACTCTCGGCATGGACGAGCTGTACAAG

meyfp

ATGGTGAGCAAGGGCGAGGAGCTGTTCACCGGGGTGGTGCCCATCCTGGTCGAGCTGGACGGCGACGTAAACGG
CCACAAGTTCAGCGTGTCCGGCGAGGGCGAGGGCGATGCCACCTACGGCAAGCTGACCCTGAAGTTCATCTGCA
CCACCGGCAAGCTGCCCGTGCCCTGGCCCACCCTCGTGACCACCTTCGGCTACGGCCTGCAGTGCTTCGCCCGC
TACCCCGACCACATGAAGCAGCACGACTTCTTCAAGTCCGCCATGCCCGAAGGCTACGTCCAGGAGCGCACCAT
CTTCTTCAAGGACGACGGCAACTACAAGACCCGCGCCGAGGTGAAGTTCGAGGGCGACACCCTGGTGAACCGCA
TCGAGCTGAAGGGCATCGACTTCAAGGAGGACGGCAACATCCTGGGGCACAAGCTGGAGTACAACTACAACAGC
CACAACGTCTATATCATGGCCGACAAGCAGAAGAACGGCATCAAGGTGAACTTCAAGATCCGCCACAACATCGA
GGGCGGCAGCGTGCAGCTCGCCGACCACTACCAGCAGAACACCCCCATCGGCGACGGCCCCGTGCTGCTGCCCG
ACAACCACTACCTGAGCTACCAGTCCaagCTGAGCAAAGACCCCAACGAGAAGCGCGATCACATGGTCCTGCTG
GAGTTCGTGACCGCCGCCGGGATCACTCTCGGCATGGACGAGCTGTACAAGTAA

pamcherry1

ATGGTGAGCAAGGGCGAGGAGGATAACATGGCCATCATTAAGGAGTTCATGCGCTTCAAGGTGCACATGGAGGG
GTCCGTGAACGGCCACGTGTTCGAGATCGAGGGCGAGGGCGAGGGCCGCCCCTACGAGGGCACCCAGACCGCCA
AGCTGAAGGTGACCAAGGGTGGCCCCCTGCCCTTCACCTGGGACATCCTGTCCCCTCAATTCATGTACGGCTCC
AATGCCTACGTGAAGCACCCCGCCGACATCCCCGACTACTTTAAGCTGTCCTTCCCCGAGGGCTTCAAGTGGGA
GCGCGTGATGAAATTCGAGGACGGCGGCGTGGTGACCGTGACCCAGGACTCCTCCCTGCAGGACGGTGAGTTCA
TCTACAAGGTGAAGCTGCGCGGCACCAACTTCCCCTCCGACGGCCCCGTAATGCAGAAGAAGACCATGGGCTGG
GAGGCCCTCTCCGAGCGGATGTACCCCGAGGACGGCGCCCTGAAGGGCGAGGTCAAGCCGAGAGTGAAGCTGAA
GGACGGCGGCCACTACGACGCTGAGGTCAAGACCACCTACAAGGCCAAGAAGCCCGTGCAGCTGCCCGGCGCCT
ACAACGTCAACCGCAAGTTGGACATCACCTCACACAACGAGGACTACACCATCGTGGAACAGTACGAACGTGCC
GAGGGCCGCCACTCCACCGGCGGCATGGACGAGCTGTACAAGTAA

gfp

ATGGCTAGCAAAGGAGAAGAACTTTTCACTGGAGTTGTCCCAATTCTTGTTGAATTAGATGGTGATGTTAATGG
GCACAAATTTTCTGTCAGTGGAGAGGGTGAAGGTGATGCTACATACGGAAAGCTTACCCTTAAATTTATTTGCA
CTACTGGAAAACTACCTGTTCCATGGCCAACACTTGTCACTACTTTGACCTATGGTGTTCAATGCTTTTCCCGT
TATCCGGATCATATGAAACGGCATGACTTTTTCAAGAGTGCCATGCCCGAAGGTTATGTACAGGAACGCACTAT
ATCTTTCAAAGATGACGGGAACTACAAGACGCGTGCTGAAGTCAAGTTTGAAGGTGATACCCTTGTTAATCGTA
TCGAGTTAAAAGGTATTGATTTTAAAGAAGATGGAAACATTCTCGGACACAAACTCGAGTACAACTATAACTCA
CACAATGTATACATCACGGCAGACAAACAAAAGAATGGAATCAAAGCTAACTTCAAAATTCGCCACAACATTGA
AGATGGATCCGTTCAACTAGCAGACCATTATCAACAAAATACTCCAATTGGCGATGGCCCTGTCCTTTTACCAG
ACAACCATTACCTGTCGACACAATCTGCCCTTTCGAAAGATCCCAACGAAAAGCGTGACCACATGGTCCTTCTT
GAGTTTGTAACTGCTGCTGGGATTACACATGGCATGGATGAGCTCTACAAATAA

Appendix II

SIM data analysis

Section 3.2.4.2.2

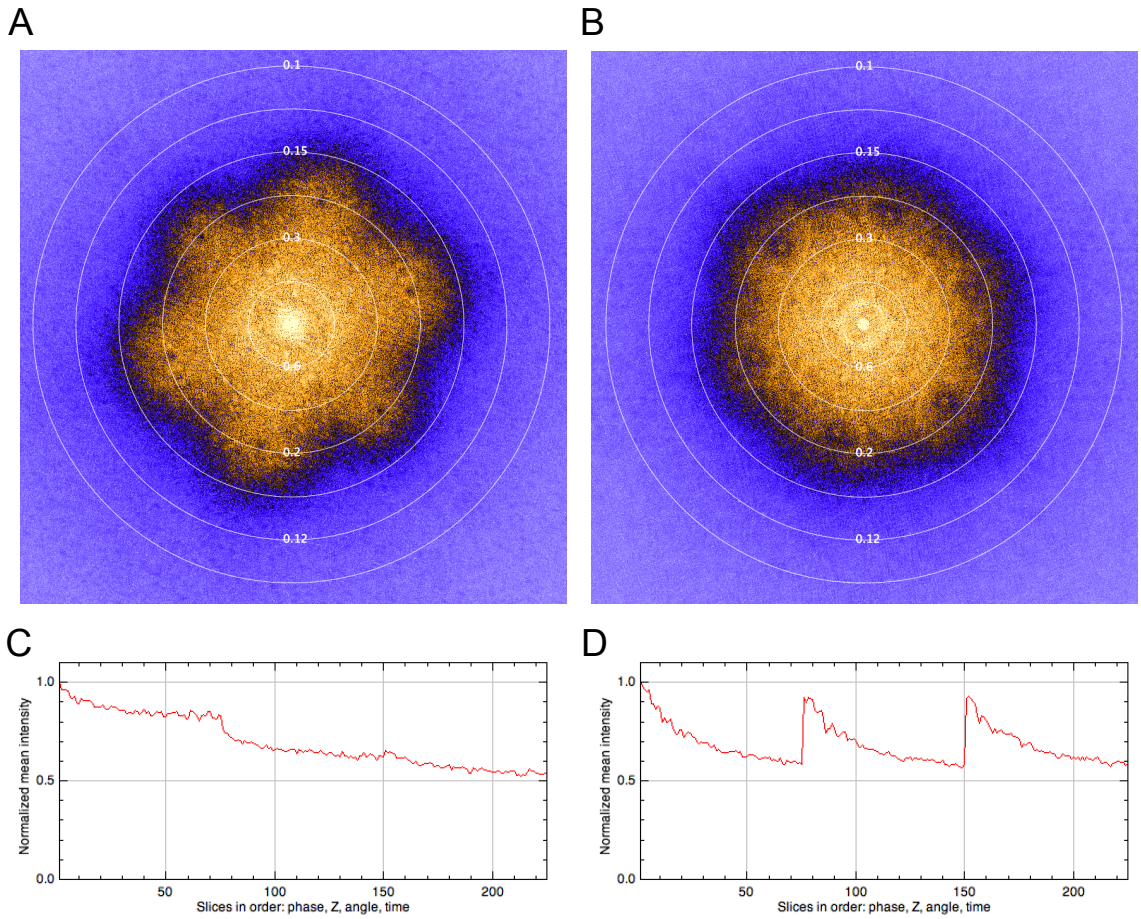

Figure A1. Fourier transforms of SIM reconstruction images for EzrA-GFP (A) and EzrA-SNAP TMR-Star (B) presented in Figures 3.30A and 3.31A, respectively. The fluorescence intensity profiles show a drop in fluorescence by ~40% and ~25% for EzrA-GFP(C) and EzrA-SNAP TMR-Star (D), respectively.

Section 4.2.2.2

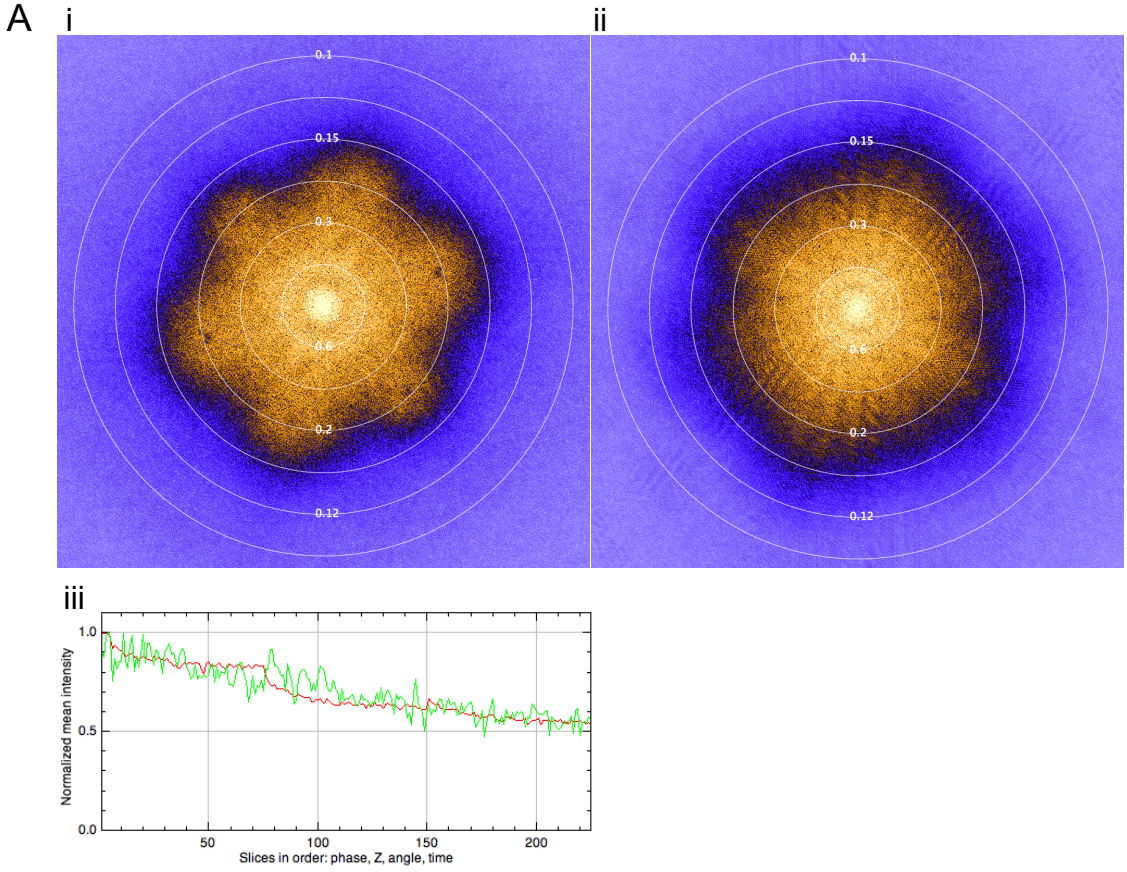

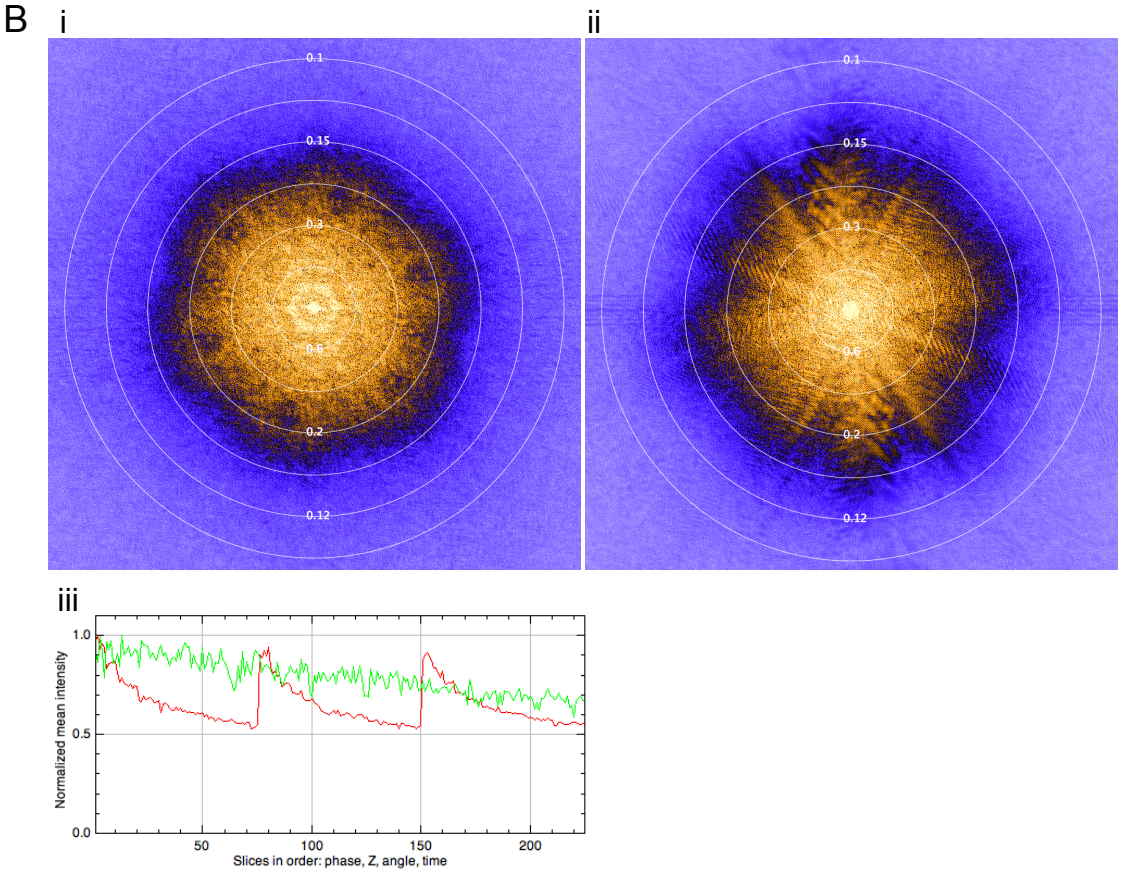

Figure A2. Fourier transforms of SIM reconstruction images for HADA labelled cells producing EzrA-GFP (A) and EzrA-SNAP (B) presented in Figures 4.10 and 4.11, respectively. The

A. i, Fourier transform for EzrA-GFP; ii, Fourier transform of HADA labelled peptidoglycan, iii, fluorescence intensity profiles show a drop in the fluorescence by ~40% and ~52% for EzrA-GFP (red) and HADA (green), respectively.
B. i, Fourier transform for EzrA-SNAP TMR-Star; ii, Fourier transform of HADA labelled peptidoglycan, iii, fluorescence intensity profiles show a drop in fluorescence by ~36% and ~41% for EzrA-SNAP TMR-Star (red) and HADA (green), respectively.

Section 4.2.5

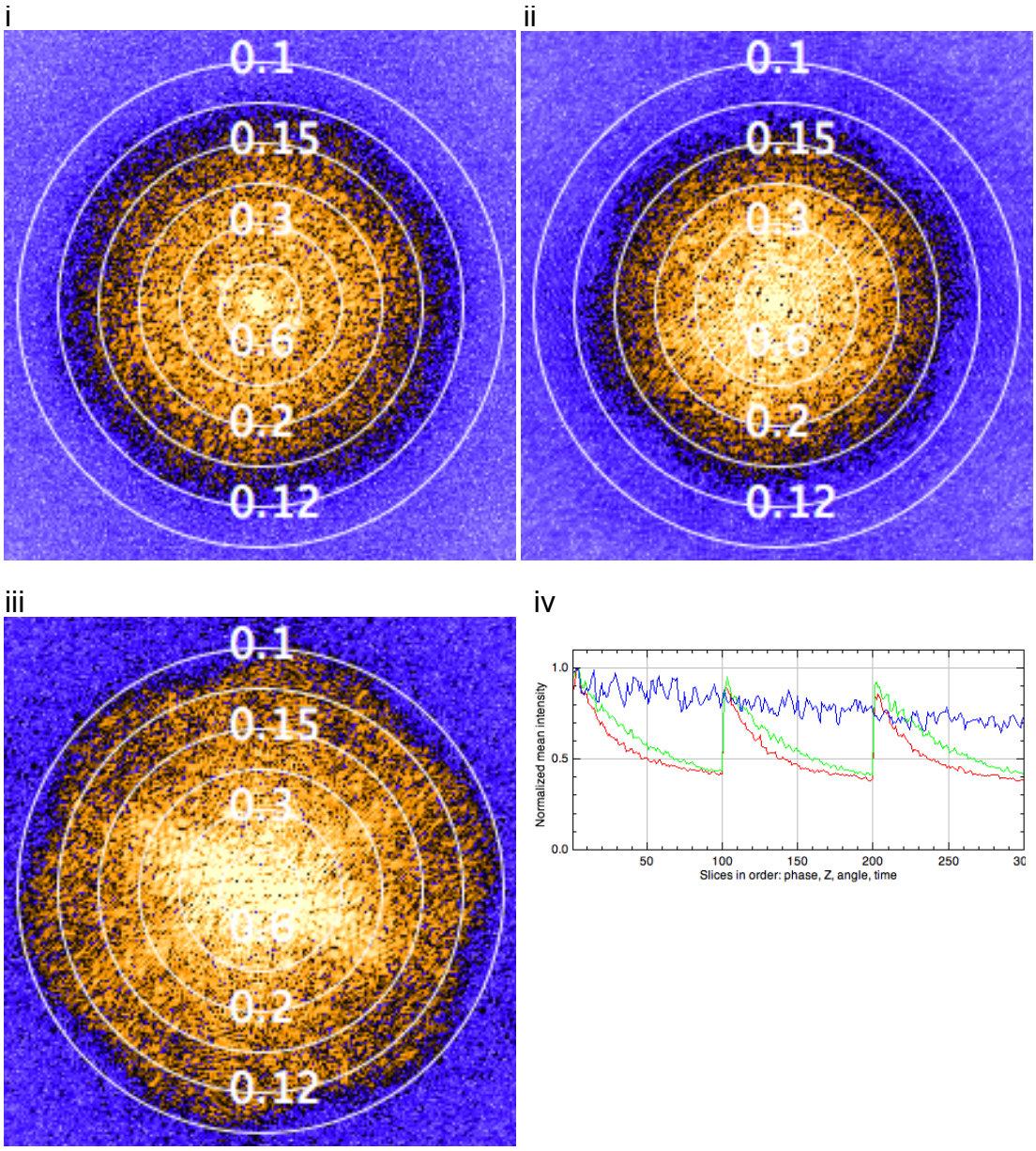

Figure A3. Fourier transforms of SIM reconstruction images for HADA and Bocillin labelled cells producing EzrA-SNAP presented in Figure 4.22

i. Fourier transform for Bocillin FL

ii. Fourier transform for EzrA-SNAP TMR-Star

iii. Fourier transform for HADA labelled peptidoglycan

iv. Fluorescence intensity profiles show a drop in fluorescence by 31%, 35% and 32% for Bocillin FL (red), EzrA-SNAP TMR-Star (green) and HADA (blue), respectively.